T70-27033
N 70 31050

NASA CONTRACTOR REPORT

NASA CR-66945
·GDC-DBD70-003

NASA CR-66945
GDC-DBD70-003

CASE FILE
COPY

FINAL REPORT
GRAVITY-SENSITIVITY ASSESSMENT CRITERIA STUDY
"The Life Support System Zero-G Study"

RECEIVED
JUL 1970
NASA STI FACILITY
INPUT BRANCH

Prepared by
CONVAIR DIVISION OF GENERAL DYNAMICS CORPORATION
San Diego, California
for Langley Research Center

NATIONAL AERONAUTICS AND SPACE ADMINISTRATION · WASHINGTON, D. C. · JUNE 1970

NASA CR-66945
GDC-DBD70-003

FINAL REPORT

GRAVITY-SENSITIVITY ASSESSMENT CRITERIA STUDY

"The Life Support System Zero-G Study"

Prepared under Contract No. NAS1-8494 by
CONVAIR DIVISION OF GENERAL DYNAMICS
San Diego, California

for Langley Research Center

NATIONAL AERONAUTICS AND SPACE ADMINISTRATION

FOREWORD

This report was prepared by the Convair division of General Dynamics under Contract NAS 1-8494 to the National Aeronautics and Space Administration, for the Langley Research Center. The report documents the work performed from the inception of the Mod 1 version of the contract through the completion of the first phase of the analytical and experimental work being conducted in the synthesis of the six analytical models relating to gravity-sensitive phenomena involved in typical life support systems of the near-term future.

Technical monitors for the NASA/LRC were Messrs. F. W. Booth, principal; G. Hausch, P. M. Jackson, and W. Piland, assistants. The principal members of the Convair study team were J. Burnett, Project Leader; E. Evans, R. Bradshaw, K. Burton, D. Heppner, Analytical Model Development and Evaluation; and G. Wood and F. Rivinius, Experimental Test.

The period of performace for the work described here-in was October 1968 through June 1970 and covered all tasks defined under modifications 1, 2, and 3 for the NAS1-8494 contract.

CONTENTS

	Page
SUMMARY	1
INTRODUCTION	4
PROGRAM OBJECTIVES	4
TASK DEFINITIONS	5
PROGRAM TASK ORGANIZATION	6
SELECTION OF ANALYTICAL SYSTEMS	11
DEFINITION OF TERMS	11
EXPERIENCE WITH LSS DESIGNS	12
CRITIQUE OF AVAILABLE DATA	13
THE LIFE SUPPORT SYSTEM INVENTORY DEFINED	13
THE DEGENERATIVE ANALYSIS	23
THE ANALYTICAL SYSTEMS	26
DEVELOPMENT AND TEST OF ANALYTICAL MODELS	28
GENERAL APPROACH	28
ANALYTICAL MODEL NO. 1 – "NUCLEATE BOILING"	31
DESCRIPTION OF THE MODEL	34
Single-Bubble Dynamics	34
Bubble Energy Equation for a Single Bubble	38
Wake Effects	39
Agglomeration and Container - Wall Interaction	41
Vaporization	42
Liquid Energy Conservation and Level Determination	43
Summary	43
THE COMPUTER PROGRAM	43
APPLICATION TO LSS DESIGN STUDIES	44
EXPERIMENTAL EVALUATION	47
Requirements	47
Description of the Experiment	47
Major Goals	47
Primary	47
Secondary	48
Tertiary	48
Principal Observations	48
Test Apparatus	48
Waterjacket and boiler assembly	49
Nucleation site assembly	51
Nucleation site heater control assembly	53
Instrumentation	53
Working fluid	53

Page

Test Procedures 53
Chronology 54
Test Data Summary 54
Critique of the Test Design 57
Instrumentation 57
Process Apparatus 58
Procedures 58
Correlation of Analytical and Experimental Data 58
Velocity Observations 58
Frequency Observations 61
Bubble-Volume Observations 61
Agglomeration Observations 63
Qualitative Observations 63
REFERENCES 65
ANALYTIC MODEL NO. 2 — "DIFFUSION CONVECTION" 66
DESCRIPTION OF THE MODEL 67
THE COMPUTER PROGRAM 74
GENERAL INFLUENCE OF INERTIAL FIELDS 74
APPLICATION TO LSS DESIGNS 78
EXPERIMENTAL EVALUATION 79
Requirements 79
Description of the Experiment 80
Major Goals 80
Primary 80
Secondary 80
Tertiary 80
Principal Observations 80
Criteria for Test Model Design 80
Test Apparatus 81
Air stream control assembly 83
Flow-channel and test section assembly 83
Heat-and-water exchange circuit 85
Instrumentation 85
Test Procedures 88
Test Data Summary 89
Trial data runs 89
Condensation mode 89
Evaporation mode 89
Critique of the Test Design 89
Instrumentation 93
Humidity measurement technology review 94

Page

Process apparatus 99
Procedures 100
Correlation of Analytical and Experimental Data 100
Predictive Data 100
Channel thickness parameter 100
Diffusion coefficient parameter 101
Experimental Data 108
Data Correlation 118
Results of the Experimental Evaluation 120
The analytical model 120
The experimental evaluation 120
The supra-efficiency anomaly 121
REFERENCES 123
ANALYTICAL MODEL NO. 3 — "FILM STABILITY AND TRANSPORT" . . . 123
DESCRIPTION OF THE MODEL 124
Case 1 - Flat Plate Surfaces 124
Case 2 - Conical Surfaces 130
THE COMPUTER PROGRAM 136
APPLICATION TO LSS DESIGNS 138
EXPERIMENTAL EVALUATION 138
Requirements 138
Laboratory Experiments 140
Reduced-Gravity Experiments 140
Description of the Case 1 Experiment 140
Major Goals 140
Primary 140
Secondary 140
Principal Observations 140
Criteria for Test Model Design 141
Test Apparatus 142
Air-stream control assembly 144
Flow-channel and test-section assembly 144
Instrumentation 146
Liquid-circulation circuit 147
Test Procedures 147
Test Data Summary 150
Calibration and trial data runs 150
Formal data runs 161
Critique of Test Design 161
Instrumentation 162
Film plate length 163

Page

CORRELATION OF ANALYTICAL AND EXPERIMENTAL OBSERVABLES . 163
Predictive Data 163
Experimental Data 163
Data Correlation 166
Film Thickness Characteristics 166
Film Thickness Correlation 173
Film Stability 174
Results of the Experimental Evaluation 180
Impact on the Analytical Model 180
Recommendations for Further Experimental Evaluation 185
Laboratory experiments 185
Reduced-gravity experiments 185
REFERENCES 185
ANALYTICAL MODEL NO. 4 — "INERTIAL SEPARATION" 186
DESCRIPTION OF THE MODELS 190
Case 1 — Hydrophobic Screen Liquid/Gas Separation 192
Droplet Adhesion 192
Liquid Droplet Size in a Turbulent Gas Stream 194
Droplet Deformation at Impact 195
Entrainment of Liquid Drops in a Moving Gas 195
Pressure Loss in Flow Through Screens 196
Drop Behavior on the Screen 197
An Alternate Configuration 200
Case 2 — Vortex Separator 201
The Cylindrical Section 201
Particles in Suspension 206
The Conical Section 206
Taylor's swirl problem 206
Inclusion of gravity force 208
Numerical analysis and results 211
THE COMPUTER PROGRAMS 214
APPLICATION TO LSS DESIGNS 214
EXPERIMENTAL EVALUATION 214
Requirements 214
Laboratory Experiments 216
Reduced Gravity Experiments 216
Description of the Case 1 Experiment 216
Major Goals 218
Principal Observations 218
Criteria for Test Model Design 218
Test Apparatus 219

Page

Air stream control assembly 219
Flow channel and working section assembly 222
Screen assemblies 222
Droplet generator circuit 223
Instrumentation 223
Test Procedures 230
Test level I - analytical component tests 230
Test A - screen configuration 230
Test B - adhesion force test 230
Test C - screen penetration test - static 230
Test D - screen penetration - drop distance 230
Test level II - analytical system tests 231
Test A - vertical orientation 231
Test B - horizontal orientation 231
Test Data Summary 232
Manually recorded data 232
Photographically recorded data 232
Critique of the Test Design 232
Instrumentation 242
Droplet generation 242
Screen types, configurations, and materials 242
Procedures 244
CORRELATION OF ANALYTICAL AND EXPERIMENTAL OBSERVABLES . 244
Predictive Data 245
Experimental Data 245
Droplet Adhesion 245
Pressure Loss in Flow-Through Screens 247
Penetration Due to Screen Pressure Drop 247
Penetration Due to Impact Velocity 248
Penetration Under Combined Conditions 251
Droplet Movement Under Combined Conditions 255
Data Correlation 259
Impact on the Analytical Model 259
Recommendation for Further Experimental Evaluation 260
Laboratory experiments 260
Screen separator 260
Vortex separator 260
Reduced gravity experiments 260
Screen separator 260
Drop tower tests 260
KC-135 261

Page

Orbital experiments 261
Vortex Separator 261
REFERENCES 261
ANALYTICAL MODEL NO. 5 — "CONVECTION HEAT TRANSPORT 262
DESCRIPTION OF THE MODEL 262
General Approach 264
The Model Defined 266
Physical Description of Stability/Instability and Higher Order Transitions 271
THE COMPUTER PROGRAM 275
APPLICATION TO LSS DESIGNS 275
EXPERIMENTAL EVALUATION 277
Requirements 277
Description of the Experiment 277
Major Goals 277
Primary 277
Secondary 277
Principal Observations 277
Criteria for Test Model Design 278
Test Apparatus 278
Air stream control assembly 278
Flow channel and test section assembly 281
Test Procedures 285
Test Data Summary 287
Exploratory data runs 287
Resolution of test uncertainties and calibration 287
Calibration and trial data 288
Formal data runs 288
Critique of the Test Design 304
Instrumentation 304
Process apparatus 304
Procedures 305
Correlation of Analytical and Experimental Observables 305
Predictive Data 305
Experimental Data Analysis 306
Data Correlation 312
Results of the Experimental Evaluation 319
Critique of the Experimental Design Concept 319
Impact on the Analytical Model 321
Recommendations for Further Experimental Evaluation 321
Laboratory Experiments 321
Reduced-Gravity Experiments 322
REFERENCES 322

Page

ANALYTICAL MODEL NO. 6 — "FLOW REGIME CHARACTERISTICS" . . . 323
DESCRIPTION OF THE MODEL 324
Identification of the Flow Regimes 324
Characteristics of Two-Phase Flow 324
APPLICATION TO LSS DESIGNS 333
EXPERIMENTAL EVALUATION 335
Requirements 335
Potentials of Laboratory Experiments 335
Potentials of the Experiments Under Reduced Gravity 335
Description of the Experiments 335
Experimental Test Summary 335
Major Goals 336
Primary 336
Secondary 336
Principal Observations 336
Criteria for Test Model Design 337
Test Apparatus 337
Liquid supply circuit 337
Flow-control circuit 337
Working section 340
Instrumentation 340
Test Procedures 342
Summary of Test Data 347
Exploratory data runs 347
Calibration 347
Trial data runs 347
Formal data runs 352
Glycol/air system data 352
Water/air system data 366
Critique of the Test Design 366
Instrumentation 366
Process Apparatus 388
Procedures 388
Correlation of Predictive and Experimental Data 388
Effects of Fluid Physical Properties 390
Effects of Flow Channel Orientation 392
Characteristics of the Pressure Profile 392
Qualitative Correlation of the Analytical Model and Experimental Evidence 396
Significance of Motion Picture Data 396
REFERENCES 397

Page

DESIGN PARAMETRICS 398
ANALYTICAL MODEL NO. 1 — 'NUCLEATE BOILING" 398
ANALYTICAL MODEL NO. 2 — 'DIFFUSION CONVECTION" 401
ANALYTICAL MODEL NO. 3 — 'FILM STABILITY AND TRANSPORT" . . . 403
ANALYTICAL MODEL NO. 4 — 'INERTIAL SEPARATION" 403
ANALYTICAL MODEL NO. 5 — "CONVECTION HEAT TRANSPORT". . . . 405
ANALYTICAL MODEL NO. 6 — 'FLOW REGIME CHARACTERISTICS" . . . 405
REQUIREMENTS BEYOND THE SCOPE OF THE NAS1-8494 MOD 1 CONTRACT . 410
GENERAL REQUIREMENTS 410
NEW AREAS FOR INVESTIGATION 411
ANALYTICAL MODEL NO. 1 — 'NUCLEATE BOILING" 411
Experimental 411
Analytical 411
ANALYTICAL MODEL NO. 2 — 'DIFFUSION CONVECTION" 411
Experimental 411
Analytical 412
ANALYTICAL MODEL NO. 3 — 'FILM STABILITY AND TRANSPORT" . . 412
Experimental 412
Analytical 412
ANALYTICAL MODEL NO. 4 — 'INERTIAL SEPARATION" 412
Experimental 412
Analytical 413
ANALYTICAL MODEL NO. 5 — "CONVECTION HEAT TRANSPORT". . . 413
Experimental 413
Analytical 413
ANALYTICAL MODEL NO. 6 — 'FLOW REGIME CHARACTERISTICS" . . 413
Experimental 413
Analytical 414
DEFINITION OF A PROGRAM TO COMPLETE THE DEVELOPMENT OF
THE ANALYTICAL MODELS 415
INTERACTIONS WITH OTHER NASA PROGRAMS 415
EXPERIMENTAL PROGRAM SUMMARY 416
LABORATORY TESTS 416
GROUND-BASED REDUCED-GRAVITY EXPERIMENTS 417
Tower and Balloon Drops 417
Rockets 419
Unmanned Satellites 419
KC-135 Flights 419
MANNED ORBITAL-FLIGHT EXPERIMENTS 420
FLIGHT-EXPERIMENT-PACKAGE DESIGN CONCEPTS 420
Characterization of Package 420
Type 1 - Integrated Experiment Package 420
Type 2 - Nonintegrated Experiment Package 421

Page

Preliminary Design Concepts for Type 1 Experiment Packages 421
General Instrumentation Requirements 421
Package A 421
Package B 421
Installation Concepts 425
PROGRAM TASK SUMMARY 425
PROGRAM AND EXPERIMENT DEFINITION — PHASE I 425
PROTOTYPE DEVELOPMENT AND GROUND-BASED TESTS — PHASE II . 425
SPACEFLIGHT EXPERIMENT PACKAGE DEVELOPMENT — PHASE III . . 427
SPACE DATA ACQUISITION AND MODEL UPDATE — PHASE IV 427
GENERAL REFERENCES 429
APPENDIX A 431
APPENDIX B 434
LIBRARY CARD ABSTRACT

LIST OF TABLES

		Page
1.	Analytical Model Development - NAS1-8494 Mod 1 Summary	2
2.	Process Analysis Summary	21
3.	Phenomenologically Oriented Processes	24
4.	Analytically Oriented Process Systems	25
5.	Nomenclature for Nucleate Boiling Calculations	32
6.	Test Conditions Data - Experimental Test No. 1	55
7.	Bubble Volume Calculations from Photographic Data	62
8.	Nomenclature for Diffusion-Convection Calculations	67
9.	Trial Data Run - 23 September 1969	90
10.	Catch Weight Accuracy Tests - 26 September 1969	92
11.	Condensation Test Reduced Data	109
12.	Evaporation Test Reduced Data	110
13.	Efficiency Data for All Test Runs	112
14.	Results of Correlation Analysis	119
15.	Nomenclature for Film Stability and Transport Calculations	125
16.	Examples of LSS Equipment Designs for which the Analytical Model Has Relevance	139
17.	X-Y Plotter Calibration Data	159
18.	Movies — Set 1, Water/Air System	160
19.	Movies — Set 2, Glycol/Air System	160
20.	Channel Orientation	164
21.	Comparison Runs for Effects of Channel Slope	165
22.	Nomenclature for Inertial Separation Calculations	186
23.	Examples of LSS Equipment Designs for Which the Analytical Model has Relevance	215
24.	Screen Pore Configuration Summary	228
25.	Test IB - Adhesion Force Roll Angle	233
26.	Test IC - Screen Penetration - ΔP	234
27.	Test ID - Screen Penetration - Fall Distance	235
28.	Test IE - Screen ΔP	239
29.	Test IIA - Vertical Orientation	240
30.	Test IIB - Horizontal Orientation	241
31.	Convection Heat Transport Model Nomenclature	263
32.	Examples of LSS Equipment Designs for which the Analytical Model has Relevance	276
33.	Initial Trial Data Run Design	287
34.	Thermistor Calibration Data	289
35.	Trial Data Runs - Sample Data	293
36.	Manually Recorded Data	295
37.	Summary of Data Runs	307

Page

38. Reduced Experimental Data 308
39. Values of Normalized Reynolds Numbers 310
40. Thermistor Condition Matrix 311
41. Examples of LSS Equipment Designs for which the Analytical Model has Relevance 334
42. Valve Position Combinations Selected for Vertical Orientation 344
43. Valve Position Combinations Selected for Horizontal Orientation . . . 345
44. Candidate Valve Positions 346
45. Set Point Schedule for Trial Data Runs 351
46. Comparative Tests - Identical Readings Versus Identical Flows 353
47. Glycol/Air System Manual Data Runs. 354
48. Movie Data Summary - Glycol/Air System 360
49. Water/Air System Manual Data Runs. 367
50. Movie Data Summary - Water/Air System 372
51. (Part 1) P_3 Trace Selections and Documentation Groupings 377
52. Comparison of Flow Characteristics for Identical Mass Flow Rates in Each of Three Flow Directions for the Water/Air System 393
53. Ground-Based Reduced-Gravity Test Facilities 418

LIST OF FIGURES

		Page
1.	NASA-LRC Long-Range LSS Technology Development Program	5
2.	Program Task Sequence NAS1-8494	7
3.	Program Schedule	9
4.	System Diagram	18
5.	Process Identification Sheet - Condenser/Separator 59(c)	19
6.	Process Identification Sheet - Water Recovery 42	20
7.	Analytical Systems Designation Process - Task Sequence	22
8.	Model-Oriented System Schematics and Experimental Concepts	30
9.	Typical Model Predictions	45
10.	Boiler and Water Jacket Assembly	49
11.	Nucleation Site Design	50
12.	Experimental Test 1 - Test Apparatus	51
13.	Typical Bubble Patterns	52
14.	Predicted Versus Experimental Data - Effect of Wakes	59
15.	Predicted Versus Experimental Data — Velocity Versus Frequency Under 1g	60
16.	Predicted Versus Experimental Data — Velocity Versus Separation Distance Under 1g	60
17.	Bubble Frequency Versus Power Input	61
18.	Photographic Data - Measurement of Wake Effect	64
19.	Test Rig Schematic	81
20.	Test Apparatus	82
21.	Channel Assembly	84
22.	Waterbox Assembly	85
23.	Water Circulation and Heat Exchange Circuit	86
24.	Comparative Estimates of Condensation Rate for Five Measurement Techniques	91
25.	Predictive Performance for Rate of Water Exchange for Humidification/ Dehumidification Process	102
26.	Influence of Mean Stream Velocity on Rate of Water Exchange	103
27.	Effect of Channel Height on Efficiency	104
28.	Pseudo Channel Height/Efficiency Product Variation with Velocity	105
29.	Diffusion Coefficient as a Function of Temperature	106
30.	Effect of Diffusion on Process Efficiency	107
31.	Predicted Efficiency and Measured Condensation Data Efficiency from Wet/Dry Bulb Readings	113
32.	Predicted Efficiency and Measured Condensation Data Efficiency from Casella Dew Points	114
33.	Predicted Efficiency and Measured Condensation Data Efficiency from Catch Basin	115

Page

34. Predicted Efficiency and Measured Evaporation Data Efficiency from Catch Basin 116
35. Predicted Efficiency and Data Comparison for Deep Channel 117
36. Predicted Stability Boundary 129
37. Zero-Gravity Performance Prediction - Conical Surface 137
38. Test Apparatus — Film Stability and Transport Flat-Plate Configuration . 142
39. Test Apparatus Photograph 143
40. Channel Assembly 145
41. Liquid Plenum and Knife Injector 145
42. Instrumentation Schematic 148
43. Predicted Stability Region for Defining Test Variables 149
44. Flow Meter Calibration 151
45. Air Flow Calibration 152
46. Photocell Calibration 153
47. Typical X-Y Plotter Scale Calibration 154
48. Shadowgraph Photographs 155
49. Photocell Traces of Movie Runs, Set 2 156
50. Typical Wave Patterns — Photoelectric Trade, Single Versus Average Sweep 157
51. Waveform Perturbation Effects 158
52. Sample Data Recorded by X-Y Plotter 161
53. Effect of Water Flow Rate on Film Thickness 168
54. Effect of Water Flow Rate and Concurrent Air Drag on Film Thickness . 169
55. Film Height Comparison for Level and Down Slope Channel 170
56. Relationship of Film Height and Gas Reynolds Number 171
57. Comparison of Hanratty Stability Correlations with Marginal Stability Film Data 172
58. Test Data Comparison with Nusselt Film Thickness Parameter 175
59. Channel Slope Effect on Liquid Film Thickness 176
60. Comparison of Predicted and Experimental Data for Film Thickness . . 177
61. Correlation of Predictive Versus Experimental Data for Stability Criteria - Horizontal Channel 178
62. Correlation of Predictive Versus Experimental Data for Stability Criteria - Sloping Channel 179
63. Stability Regions Defined 182
64. Stability Data Correlation for Gas/Liquid Velocities 183
65. Effect of Channel Slope on Stability Criteria 184
66. Case 1, Analytical System Schematic — Two-Stage Screen Separation . . 191
67. Case 2, Analytical System Schematic — Cone Centrifuge Separation . . 191
68. Drop Penetration 199
69. Drop Movement Parallel to Screen 200
70. Screen Separation Device, Alternate Configuration 201
71. Cylindrical Section Length 205

		Page
72.	Taylor's Swirl Problem Nomenclature	207
73.	Boundary Layer Thickness - Vortex Separation	212
74.	Boundary Layer Mass Flow Rates - Vortex Separation	213
75.	Characteristic Predictive Data	217
76.	Test Apparatus - Schematic	220
77.	Test Apparatus — Photograph	221
78.	Test Apparatus Drawing	224
79.	Microphotographs, Uncoated Versus Coated Screens	225
80.	Microphotographs, Uncoated Versus Coated Screens	226
81.	Microphotographs, Uncoated Versus Coated Screens	227
82.	Instrument Schematic, Test Level II	229
83.	Typical Droplet Behavior - Movie Frame Prints	243
84.	Droplet Adhesion	246
85.	Penetration Due to Screen Pressure Drop	249
86.	Droplet Penetration Due to Impact	252
87.	Droplet Penetration	254
88.	Impact Droplet Extrusion	256
89.	Droplet Movement on Screens	258
90.	Stability Defined-Critical Rayleigh Number	270
91.	Stability Boundary	271
92.	Streamlines [for stable, forced convection primary flow (steady in time)]	272
93.	Streamlines and Stationary Vortices [for unstable, natural and forced convection, primary plus secondary flow (steady in time)]	272
94.	Stability Boundaries of Natural Convection/Forced Convection System	273
95.	Vortex Distribution (being convected past an observer illustrating unsteady, unstable, natural and forced convection)	274
96.	Test Apparatus Schematic	279
97.	Test Apparatus Photograph	280
98.	Flow Channel and Test Section Components	282
99.	Instrument Schematic	283
100.	Experiment Design Guidelines	286
101.	Turbulence Indicator Calibration, V_1 and V_5	290
102.	Turbine Flow Meter Calibration	291
103.	Mass Flow Meter Calibration	291
104.	Turbulence Indicator Data Samples	292
105.	Effect of Inlet Screen on Stream Turbulence	294
106.	Turbulence Indicator Data Samples Formal Data Runs 150-165	297
107.	Turbulence Indicator Data Samples	298
108.	Turbulence Indicator Data Samples	299
109.	Turbulence Indicator Data Samples	300
110.	Turbulence Indicator Data Samples (Photo Runs)	301
111.	Turbulence Indicator Data Samples (Inverted Channel)	302
112.	Smoke Stream Visualization of Channel Flow	303

Page

113. Stability Boundaries 306
114. Experimentally Determined Stability Boundary for Thermistor 2 . . . 313
115. Experimentally Determined Stability Boundary for Thermistor 3 . . . 314
116. Experimentally Determined Stability Boundary for Thermistor 4 . . . 315
117. Experimentally Determined Stability Boundary for Thermistor 5 . . . 316
118. Composite Stability Boundaries. 317
119. Composite Stability Boundaries (Rayleigh vs Normalized Reynolds Number) 318
120. Correlation of Experimental and Predictive Data 320
121. Two-Phase Flow Patterns - Vertical 325
122. Two-Phase Flow Patterns - Horizontal 326
123. Baker Flow Correlation 327
124. Test 6 Apparatus Schematic 338
125. Test Apparatus Photograph 339
126. Working Section Drawing 341
127. Instrumentation Schematic 342
128. Test Protocol Guidelines 343
129. Flow Meter Calibration, Liquid 348
130. Flow Meter Calibration, Air 349
131. Pressure Transducer (P_3) Calibration 350
132. Observed Flow Regimes - Sample Frames from Movie Data 365
133. Experimental Data Correlation, Horizontal Flow 389
134. Effects of Fluid Properties 391
135. Effects of the Liquid/Gas Mass Ratio on Pressure Profile Characteristics 394
136. Correlation of the Liquid/Gas Volume Ratio with the Magnitude of the Maximum Variation within the Pressure Profile 395
137. Typical Utilization of NAS1-8494 Analytical Models 399
138. Example Design Parametric - Void Fraction Versus Heat Flux 400
139. Parametric Design Data for Dehumidification Process 402
140. Predesign Representation for Gravity Field Effect on Interface Velocity 404
141. Effects of Droplet Velocity on Penetration 406
142. Typical Design Parametric 407
143. Example Design Parametrics 408
144. Integration Concepts Relative to Flight Experiment Package Type 1 Designs 422
145. Design Concepts for Type 1 Flight Packages 423
146. Swing-out Module Installation Package 424
147. Program Schedule 426

SUMMARY

This report presents the status of the "Gravity-Sensitivity Assessment Criteria Study," more popularly referred to as the "Life Support System Zero-G Study," at the conclusion of the tasks defined by the Mod 1 work statement. This 21-month study, funded under Contract NAS1-8494 through the Langley Research Center, was organized to produce:

a. A set of experimentally verified analytical models which predict the behavior of the various phenomenological processes which are basic to the life support equipment of the near-term future and which can be affected by the expected range of inertial acceleration field forces characteristic of manned space missions.

b. A set of graphically displayed parametric data which, insofar as is possible, relates phenomenological process characteristics to equipment design variables. The objective of this information is to aid in bridging the traditional gap between the information available in the analytical models and the practical world of the life support system designer.

c. Definitions of the additional experimental work required to completely test the validity of the analytical models, if such is required beyond the scope of the present contract. Assumptions are made that such may be required, especially under "reduced gravity" conditions including the use of R&D orbital space stations.

Six analytical models have been developed following an analysis of some 80 life support system (LSS) equipments and a laboratory experimental program has been completed. Analysis of the experimental data obtained from the test of each analytical model has shown, 1) that the approaches followed were generally sound, 2) that the experiment produced data which could be employed to improve the analytical model, and 3) that the predictive capability of the model (and computer program) has significant potential to the design of life support systems. A summary of the developments of the Mod 1 contract is given by table 1.

Two sets of documentation have been initiated — one consisting of the formal documents, the other of informal documents. The first has resulted in the publication of a monthly letter progress report, a mid-term, and this, the final report; the second results in reports released for restricted distribution which describe each analytical model and each experimental test.

Table 1. — Analytical Model Development - NAS1-8494 Mod 1 Summary

Model Characteristics / Model Identity, Documentaion & Classification	A General Orientation	B Mathematical Development	C Nature of Computer Utilization	D Place in the "State of the Art" (SA)	E Relevance to LSS Design	F State of Analytical Development	G Potentials of Additional Experimental Investigation
No. 1 — Nucleate Boiling AMR 1[1] Dec. 1969 ETR 1[2] GDC-DBD70-002 vol. I[3] Class IIA2c[4]	Bubble dynamics and energetics-agglomeration, wake effects, container interactions, gravity field effects, bubble geometry, & fluid characteristics are described.	Ordinary differential equations, numerically solved, describe the complex interactions of bubble motion under various conditions.	Program EVOLVE is a detailed and rigorous simulation of bubble motion and interactions of populations up to 1000 bubbles in a time and space domain. Run-time-to-real-time ratio is very high.	Advances the SA in the prediction of the effects on the geometry and quality of a host liquid in the presence of bubble evolution.	Provides insight into and means of predicting volume changes, liquid/gas configurations, bubble transport characteristics etc. for designs of reservoirs, boilers, storage vessels, electrolysis chambers, etc.	Verified at 1g with partial verification at reduced-g. Interface with models dealing with nucleation site and heat flux characteristics is desirable. Effect of pool temperature gradient needs attention.	Observations relative to variations of bubble behavior with variations in level of reduced-g, pool-temperature gradient, and container configuration will both evaluate and augment present model.
No. 2 — Diffusion Convection AMR 2 Jan. 1970 ETR 2 Oct. 1969 GDC-DBD70-002 vol. II Class IIID2a	Diffusion of a second component in a carrier gas is described. The mechanisms of dehumidification and humidification are explicitly examined.	The model precisely describes a binary diffusion process employing a system of differential equations. A process efficiency prediction model is developed.	A Fourier series boundary value solution was applied to the descriptive equation.	Development of the model was accomplished by adapting data from the literature to the specific form required.	Provides an insight into and means of evaluating various design solutions for mechanization of systems dependent upon the control of the humidification/dehumidification process.	Further work is required to resolve apparent anomalies in the correlation of experimental and analytical data. Integration with developments under model No. 5 is indicated.	Experimental investigations are primarily associated with management of the liquid-phase interface accompanying the humidification/dehumidification process.
No. 3 — Film Stability & Transport Case 1 - Flat Surface AMR 3 March 1970 ETR 3A Jan. 1970 GDC-DBD70-002 vol. III Class IID2c	The characteristics of thin liquid layers during transport along a flat surface by gas stream shear forces are examined. A stability criterion is developed.	A combination of partial differential and algebraic equations is employed. System simulation is not attempted.	Restricted to the adaptation of standard computational programs in the area of predictions of film thickness, film velocity, and general data reduction. Programs are SHEAR, RECRIT, & REDATA.	Initiates a new approach to film transport analysis at the micro-system level as opposed to the conventional modeling of ocean wave phenomena.	Provides insight into the mechanisms involved in moving liquid films along such surfaces as duct and shower bath walls, condensing heat exchanger fins, etc.	Partially verified at 1g. Additional investigation into development of alternate stability criteria indicated.	Experiments at both 1g & reduced-g will provide needed insight to complete model and verify approach.
Case 2 - Conical Surface AMR 3 March 1970 GDC-DBD70-002 vol. IV Class IIB2b	Motion of a thin liquid layer which uniformly wets the wall of a conical surface is described. Evolution of the liquid layer by both phase change and in-flow is included.	A combination of partial differential and algebraic equations is employed. System simulation is not attempted.	A partial simulation model is developed providing performance predictions under various g-levels. Program provides for numerical solution of transcendental equation.	Re-orients existing analytical treatments to the system involved and thus provides a new solution technique.	Helps to clarify the potential of a multiplicity of proposed designs for the collection and transport of liquid, especially as related to the stream condensate.	Verification under 1g is marginal at best. Model has been developed to the extent that low-g data is required as a next step.	The low-g experiments will both evaluate and produce data for added maturation of the model.

No. 4 — Inertial Separation Case 1 - Screen AMR 4 April 1970 ETR 4A March 1970 Class IVD2b	Behavior of a liquid droplet upon impact with a hydrophobic screen slanted across the transport duct is described.	Oriented to discreet elements of the process, principally restricted to the development of algebraic equations.	No simulation or computational programs are developed.	Advances the SA in the specific areas involved; i.e., the behavior at the micro-structure level.	Direct benefit to the analysis and design of liquid droplet capture and transport for several proposed systems.	Sufficient to directly undertake reduced-gravity verification.	Could include interface with prior stream transport of droplet and post-collection outflow as a gas-free liquid stream.
Case 2 - Vortex AMR 4 April 1970 Class IIC2b	Describes the process of separation of the components of two-phase media in a cyclonic flow path with subsequent outflow of the liquid phase along a conical surface.	Nonlinear, second-order, ordinary differential equations solved by conventional Runge-Kutta methods.	Computer programs were written for the numerical solution of each of the two separation stages; cylinder and exit cone.	Advances the SA by explicitly including the effect of gravity and by adapting current solutions to this specific problem.	Of direct application to the analysis and synthesis of cylindrical and or cone separator designs.	Additional development is desirable relevant to inlet flow characteristics especially as they may effect cylinder dimensions.	1g experiments could aid in low-g experiment designs. Low-g experiments needed for verification and augmentation.
No. 5 — Convection Heat Transport AMR 5 April 1970 ETR 6 March 1970 Class IID2c	Describes the convective phenomena in a fluid stream as influenced by variations in the temperature gradient across the stream, stream velocity, and in the inertial field.	A thermal stability/instability criterion is developed. Modifications of the Boussinesq approximation are employed. A sixth-order, linear ordinary differential equation is developed to describe the stable/unstable boundary.	Standard computational programs only for numerical solutions.	Model advances the SA by modifying existing analytical approaches to convective heat transport to more precisely describe the micro-mechanism involved, uniquely required for LSS design optimization.	Provides an aid to the analysis & synthesis of heat exchange & transport designs involving thermally controlled catalytic reactions, dehumidification, humidification, and other thermal processes.	Relatively mature as initially conceived but additional work needed to include higher order transitions thus providing more complete coverage of the thermal character of the stream.	Investigation of low-velocity streams and explitation of "thermal photography" for visualization of stream flow patterns are required at various reduced-gravity levels.
No. 6 — Flow Regime Characteristics AMR 6 March 1970 ETR 6 Feb. 1970 Class IIIc	Both the physical and dynamic aspects of two-phase flow are described, the former oriented to definitions of flow regimes, the later oriented to the dynamics of the mechanisms operating in the transport stream.	Flow-regime definitions by Baker correlations adopted as the initial model. A series of equations are formulated relative to such transport parameters as inertia, turbulence, eddy diffusion.	None at this point.	Translates Baker correlations into an approach for the low-g condition & through the suggested transport model promises a significant advance in SA.	Potentially provides insight into the two-phases flow condition sufficient to permit transport designs to be approached as rigorously as presently possible with "Newtonian" fluids.	The development of the transport model is embryonic and requires significant expenditure of additional study effort.	Experiments at various levels of reduced gravity are essential to the continued development of the suggested model.

[1] Analytical Model Report (AMR).
[2] Experimental Test Report (ETR).
[3] See footnote, page 29. A general bibliography for this program is given in APPENDIX A.
[4] Details of Classification System in APPENDIX B.

INTRODUCTION

This report describes the objectives, organization, method of execution, and results of the study program conducted by Convair under modification 1, 2, 3 of the NAS1-8494 contract* to the NASA-Langley Research Center.

The introduction describes the nature of the program, its objectives, execution, intended outputs, and status at this interim point. The remaining sections summarize and present examples of approaches being followed in the execution of the program with illustrations of the initial results being attained. Details of these results have been documented in a series of sequentially updated informal working papers which have been edited and published as an integral part of the documentation requirements specified under the contract.

PROGRAM OBJECTIVES

The objectives of the NAS1-8494 (Mod 1) program relating to the work being reported can be characterized by the following:

a. Provide a single source bank of information concerning, 1) the nature of the physiochemical processes basic to the overall inventory of life support equipment which is being considered for operational application in the near-term future, with particular emphasis on the 1970-80 time period, and 2) an indication of the degree to which these processes might be affected by variations in the local inertial acceleration field forces, i.e., their relative "g sensitivities."

b. Design, develop, and initiate the experimental evaluation of a set of analytical models which can be utilized to predict the behavior of the phenomena basic to these g-sensitive processes when operated under the range of inertial acceleration force levels expected for manned space flight.

c. Produce a set of "design parametrics" which, over a range of conditions, graphically defines the relationship of the parameters which control the actions characteristic of these phenomena to the equipment design variables which may be involved.

d. Identify and grossly define the requirements which may exist for additional experimental evaluation of the analytical models beyond the scope of the present program with particular emphasis on those evaluations which may be possible only under reduced gravitational conditions.

---

* Referred to hereafter as the Mod 1 contract.

Prior to the Mod 1 change, which essentially doubled the magnitude of the original task, the program objectives were more narrowly oriented and were centered on the development of a handbook as a guide to life support system designers relative to the analysis and design of equipments for operation in zero gravity. Initially the program was developed essentially as an extension of the previous NASA-LRC study program (ref. 1). The Mod 1 change reflected both the increased confidence attained through the demonstrated feasibility and practicality of manned orbital R&D space stations and the documentation of their potential value as an integral part of the overall manned space program (ref. 2).

As viewed by Convair, at the outset of the program, the orientation of the revised contract in the longrange space technology development program being conducted by NASA-LRC is illustrated by figure 1.

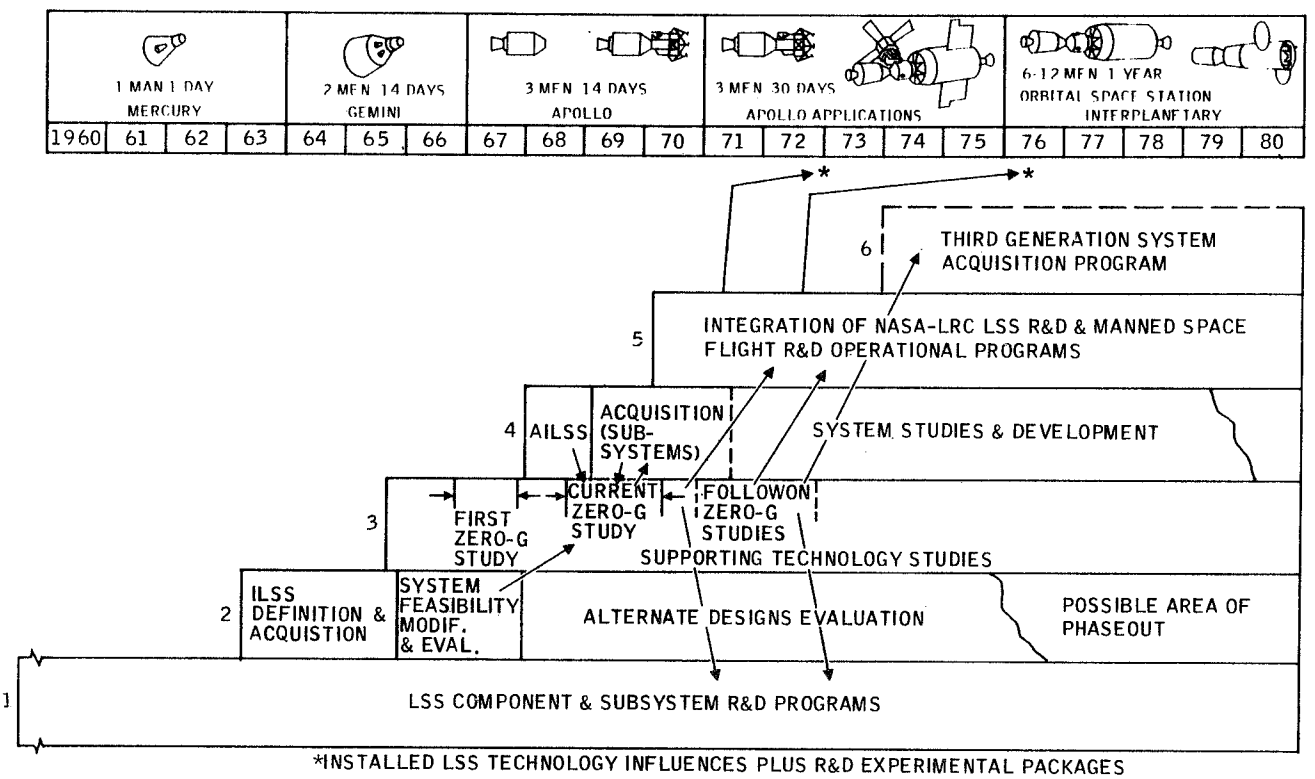


Figure 1. - NASA-LRC Long-Range LSS Technology Development Program

TASK DEFINITIONS

The program to date has been organized around the execution of four major tasks. The contractual definition of these tasks can be summarized as follows:

Task 1 - LIFE SUPPORT SYSTEM COMPONENT/PROCESS IDENTIFICATION AND SELECTION. Review the present LSS processes and their operational characteristics involved in both the existing integrated life support system (ILSS) and the processes used in the tradeoff analyses for the future advanced integrated life support system (AILSS). A list of the gravity-sensitive basic physical phenomena involved in these processes will be generated and submitted to the LRC with recommendations for detailed gravity-sensitivity analysis.

Task 2 - PROCESS ANALYSIS. Analyze those processes selected by the LRC to determine the effects of varying gravity environments on the performance of each process. These effects, or g sensitivities, shall be developed parametrically, with the parameters representing design variables where possible, and presented in parametric chart form having maximum utility and convenience for the LSS designer.

Task 3 - VERIFICATION TESTING. Conduct laboratory experimentation to support all the analytical prediction techniques derived in Task 2. These tests shall involve laboratory techniques such as reorientation, centrifugation, and balanced density (liquid/liquid) to vary gravity loads on the experiment. As a part of this task, the requirements for testing beyond the scope of this contract needed to completely evaluate and upgrade the analyses of Task 2 will be identified, and information which will be necessary to develop a preliminary program plan to accomplish the required experiment program will be provided.

Task 4 - DOCUMENTATION.

MID-TERM REPORT - At the midpoint of this contractual effort a mid-term report will be submitted which documents and summarizes the results of the first half of this study.

FINAL REPORT - At the conclusion of the analytical and experimental work a written report will be presented summarizing the full results of the study to date and shall include tables, graphs, diagrams, sketches, photographs, and drawings in sufficient detail to comprehensively explain the results achieved under the contract.

MONTHLY PROGRESS LETTERS - Program progress will be reported in monthly letters giving accomplishments during the period, significant problems encountered, and plans for the following period.

PROGRAM TASK ORGANIZATION

The program tasks were organized and operated along the lines illustrated by figure 2. Of major significance to the visualization of progress were the informal documents flowing into the In-Progress Monitoring Channel (B). Principal documents in this category were the Analytical Model Reports (AMR), the Experimental Test Plans

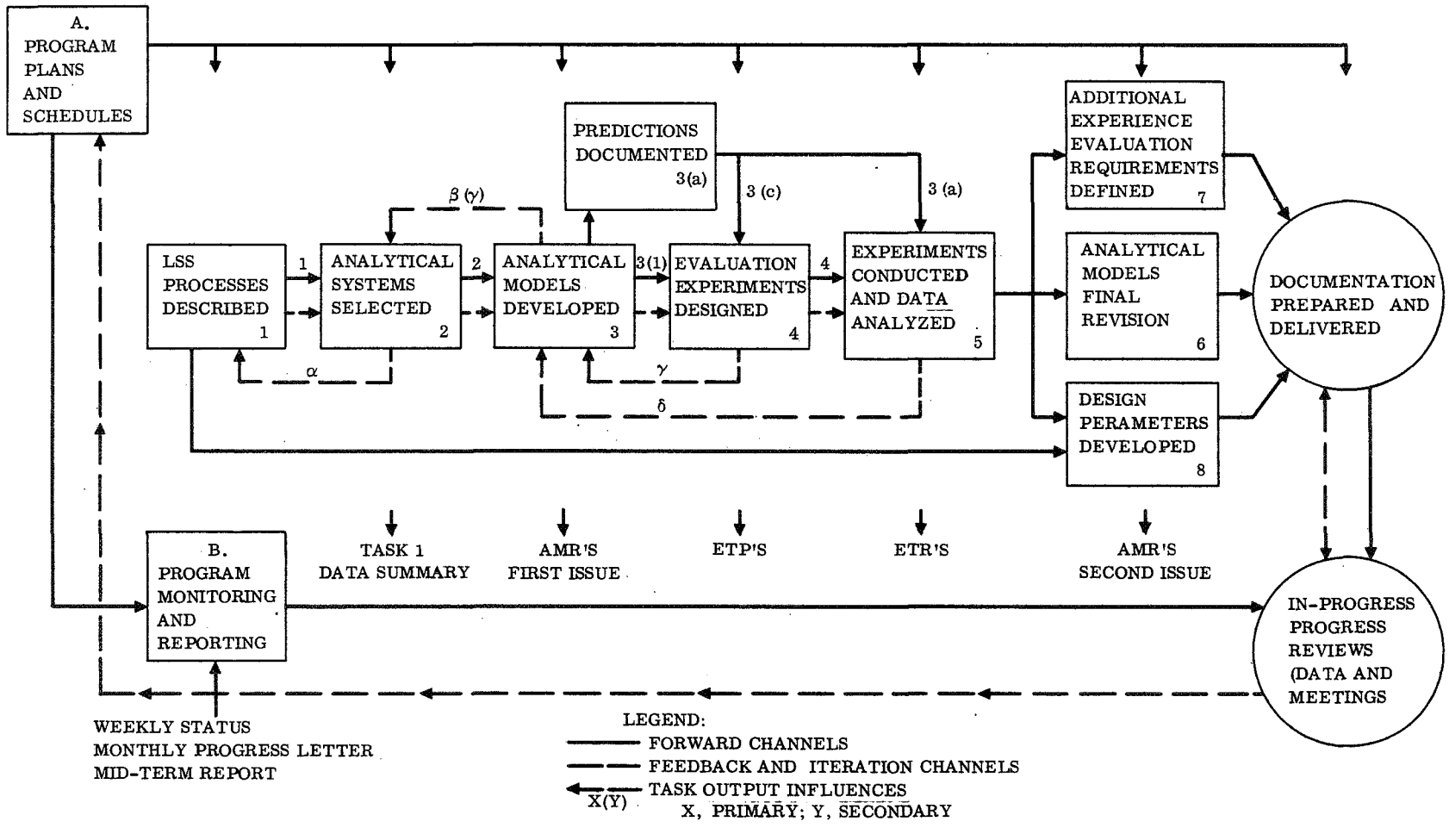
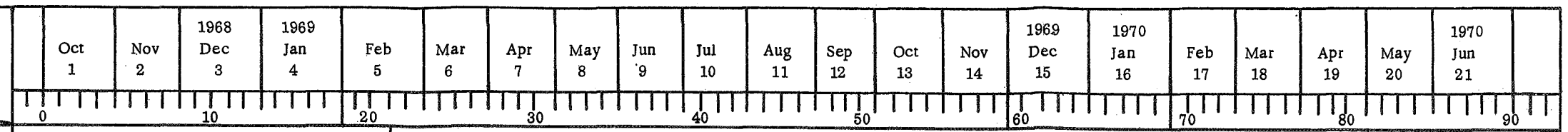


Figure 2. - Program Task Sequence NAS1-8494

(ETP), and the Experimental Test Reports (ETR) described in detail in subsequent sections of this report. The schedule against which these tasks were planned and performed is shown in figure 3. All tasks under the Mod 1 version of the NAS1-8494 program were completed as of 30 June, 1970.

PROGRAM TASKS	TASK DURATION AND MONITORING MILESTONES BY CALENDER TIME PERIOD(S) / WEEK(S)



TASK 1 — PROCESS IDENTIFICATION AND SELECTION

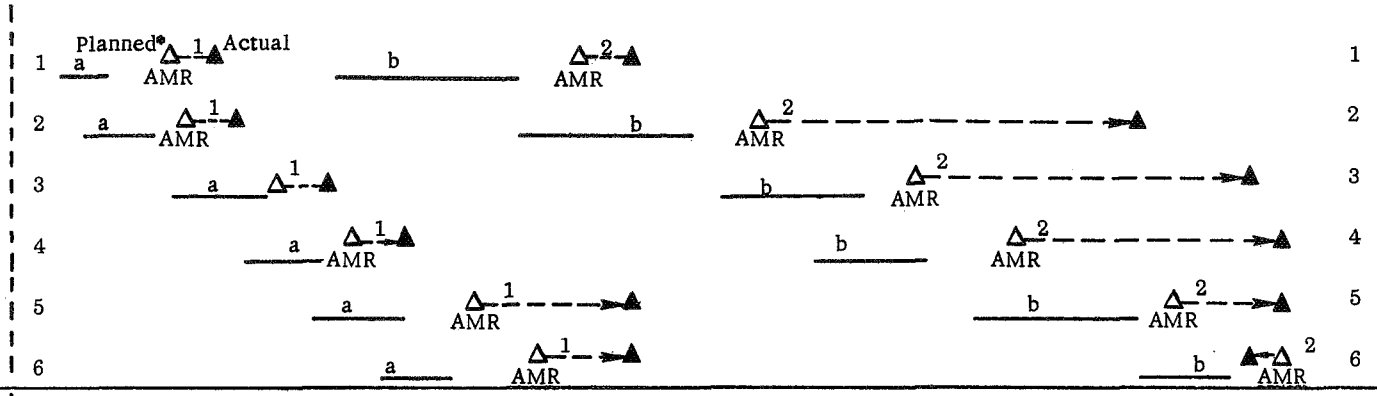
- A. Component and Process Description
- B. Preliminary "g" Sensitivity Screening
- C. Phenomenological System Design
- D. Analytical Model Studies
- E. Test Design Studies
- F. Data Summary Issued and Task Reviewed

TASK 2 — PROCESS ANALYSIS

- System 1 Nucleate Boiling
- System 2 Diffusion Convection
- System 3 Film Transport and Stability
- System 4 Inertial Separation
- System 5 Convection Heat Transport
- System 6 Flow Regime Characteristics

Legend:

- a = Formulate model
- b = Modify model (per test data) and develop parametrics
- Δ^{1}_{AMR} = Analytical Model Report, first iteration
- Δ^{2}_{AMR} = Analytical Model Report, second iteration
- ◭ = Contractually required milestone

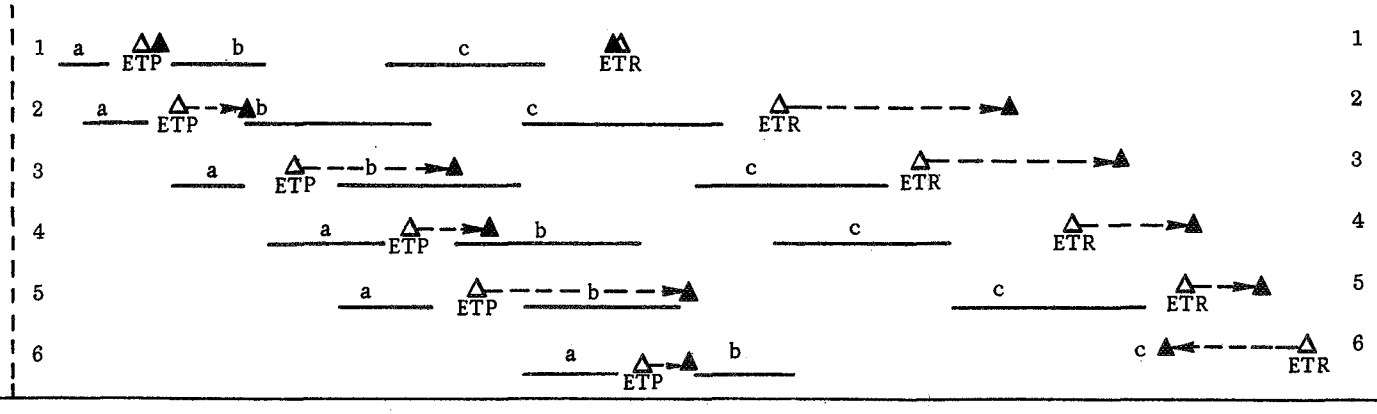


TASK 3 — VERIFICATION TESTING

- System 1 Nucleate Boiling
- System 2 Diffusion Convection
- System 3 Film Transport and Stability
- System 4 Inertial Separation
- System 5 Convection Heat Transport
- System 6 Flow Regime Characteristics

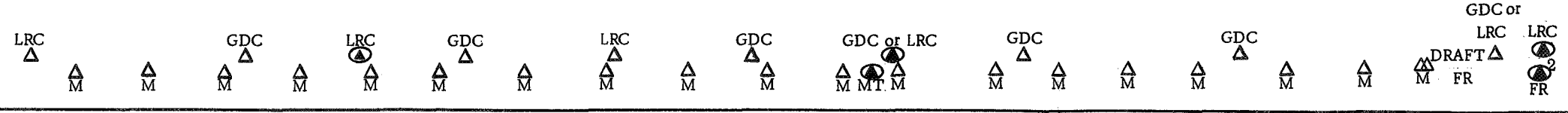
Legend:

- a = Test design study
- b = Detail equipment design and fabricate
- c = Execute test and analyse data
- Δ_{ETP} = Experimental Test Plan
- Δ_{ETR} = Experimental Test Report



TASK 4 — PROGRAM DIRECTION AND CONTRACTUAL DOCUMENTATION

- A. Review Meetings
- B. Contractual Reports



*EFFECTIVITY DATE - 10 APRIL 1969

EFFECTIVITY DATE - 10 APRIL 1969

Figure 3. — Program Schedule

SELECTION OF ANALYTICAL SYSTEMS

One of the problems experienced in the development of machine systems "producing" physio-chemical processes, such as those of the current life support systems, has been their lack of compatibility with the requirement to operate both where the local inertial acceleration field forces are essentially in equilibrium, such as that found in the "coast" phases of space flight (referred to as "zero gravity"), and also where the magnitude of the resultant forces is equivalent to at least one terrestrial gravitational unit (1g). Future systems development will require that increasing emphasis be placed on the assurance that this capability be achieved (ref. 3). The task undertaken by this study was the selection of analytical systems which would clearly encompass the area in which such problems exist.

DEFINITION OF TERMS

The term "g sensitivity" is widely used to denote the characteristic of a dynamic process to be influenced by variations in the magnitude of the resultant forces applied by the local inertial acceleration field(s). Quite often the term "g sensitive" is used to denote that the process (system) is so influenced to the extent that the process can be degraded sufficiently to create performance problems requiring some form of operational accommodation or corrective action or, in an a priori sense, would require that special attention be given this characteristic in the creation and test of the equipment system involved.

Several other terms were identified at the outset of the program and assigned a specific definition in an effort to minimize problems in communication. These terms included the following:

a. Phenomenon (Physical) - an observable event or manifestation involving the physical or material aspects of matter, usually associated with a mass, momentum, and/or energy transfer.

b. Process - a series of observable events or physical phenomena so ordered and controlled as to produce a desired result.

   1. Equipment-oriented process - the process system is identified at a level which uniquely includes physical portions of a specific machine system in its structure which is characteristically composed of a multiplicity of phenomenological actions.

2. Phenomenologically oriented process - the process system is identified at a level which minimizes unique interdependence with specific machine configurations and is characteristically composed of a limited number of phenomenological actions.

c. Mechanism - the fundamental constitutive property exchange involved in the phenomenon.

d. System (Machine) - an ordered association of machine elements which can support a given process or set of processes and which, in turn, can be controlled to produce a predictable result under a given set of conditions in response to a given set of inputs.

e. Subsystem (Machine) - a portion of a system which can produce a definable function within the system process usually is physically separable from other elements of the system and which, in turn, usually possesses the characteristics of a system if so viewed.

f. Mechanization - the material elements of a machine structure created in accordance with a specific design and intended to support a desired process.

EXPERIENCE WITH LSS DESIGNS

Throughout the current manned space program, operational problems have been experienced with various LSS processes. Liquid/gas phase separation problems have persisted throughout, starting with Mercury and continuing with the Apollo Lunar Landing missions. Mercury experienced problems relating to condensation collection and transport, while Gemini added the problems of phase continuity in the cryogenic gas storage and delivery system, along with those of personal hygiene and sanitation. Apollo 11 continued to experience problems with condensate collection, separation, and transport, with both an "improved design" for primary mode separation and its back-up. In addition, operational systems have yet to be designed and tested which satisfactorily provide fecal collection, solid waste processing, or bathing.

Examination of proposed designs for future systems reveals that there is still a high probability that these characteristic problems will continue until sufficient attention is focused on these problems during design and sufficient information is available to obviate their appearance.

CRITIQUE OF AVAILABLE DATA

At least two problems exist with the data available to design functions throughout the industry. One is the paucity of detail data made available to them by the operating agencies concerning the technical realities of the experience, both developmental and operational, relating to these problems. The other is the paucity of usable technical information concerning the characteristics of the processes and mechanisms involved which is available to the engineering functions of design and system selection. Most of the information which is available is either too closely tied to the design of a specific configuration to be of general value, or too highly generalized or esoteric to be readily usable by the design engineer.

THE LIFE SUPPORT SYSTEM INVENTORY DEFINED

Task 1 objectives called for the development of a "list of gravity-sensitive basic physical physical phenomena involved in these... (life support system) ... processes... with recommendations for detailed gravity-sensitivity analysis." To accomplish this primary objective, it was contractually required that, as an initial step, a review would be made of "present LSS processes and their operational characteristics...to include the existing...ILSS and those processes used in the tradeoff analysis for the AILSS."

The first step in the descriptive analysis of the LSS processes was to establish the exact identity of the equipments to be so analyzed. This was accomplished through the combined inputs from the LRC technical monitor and study team personnel. This series of communications, combined with a system-subsystem organization study, resulted in the following listing of equipment items.

	Reference* Number
I. Atmospheric Supplies	
A. Bulk Storage	
1. Gaseous State Storage (Hi Press)	1
2. Cryogenic "State" Storage	
a. Supercritical	2
b. Subcritical	3

* The reference number is used throughout the study documentation to specifically identify each proprietary equipment set.

	Reference Number
B. Dissociation of Stored Liquids	
1. Water Electrolysis	
General Electric	4
Ionics	5
Hamilton Standard	6
Allis Chalmers	7
Pratt & Whitney	8
TRW	9
Lockheed	10
Battelle (Special Case - Atmospheric Water Vapor Electrolysis)	(33)
2. Nitrogen Tetroxide and Hydrazine (Johns Hopkins)	11
3. Hydrogen Peroxide	12
II. CO_2 Removal	
A. Sorption Techniques	
1. Solid Adsorbents	
Hamilton Standard (4 bed)	13
GATCO (1 and 2 bed)	14
MSA (1 and 2 bed)	15
2. Liquid Absorbents	
General Dynamics	16
B. Electrochemical	
1. Electrodialysis (Ionics)	17
2. Electrolysis	
TRW (Carbonization Cell)	18
TRW (H_2 Depolarization Cell)	19
C. Freeze Out (Hamilton Standard)	20
III. Oxygen Recovery	
A. CO_2 Reduction-Forming H_2O	
1. Bosch Reaction	
Battelle	21
GATCO	22
TRW	23
General Dynamics	24
2. Sabatier Reaction (Methane Dump and Cracking)	
Boeing	25
Engelhard	26
Garrett	27
Hamilton Standard	28
Isomet	29
Lockheed	30
McDonnell-Douglas	31
TRW	32

	Reference Number
B. CO_2 Electrolysis-Forming O_2 (Solid Electrolysis)	
GATCO	34
Isomet	35
Lockheed	36
Westinghouse	37
C. Water Vapor Electrolysis	
Battelle (Special Case - Atmospheric Water Vapor Electrolysis)	(33)
IV. Water Reclamation	
A. Distillation	
1. Vacuum Distillation - Vapor Compression Condensation	
GATCO	38
Marquardt	39
2. Vacuum Distillation - Ambient Condensation	
General Electric (Pryolysis)	40
Whirlpool	41
3. Air Evaporation	
Hamilton Standard	42
McDonnell-Douglas	43
AiResearch	44
4. Flash Evaporation (AiResearch)	45
5. Vapor Membrane Diffusion (Hamilton Standard)	46
B. Electrochemical	
1. Electrodialysis	
Ionics	47, 47(a)
McDonnell-Douglas	48
C. Filtration	
1. Charcoal Adsorption	
General Dynamics	49, 49(a)
Pall	50
2. Ion Exchange Resin Beds	
General Dynamics	51, 51(a)
Pall	52
3. Mechanical Particulate	
Pall	53
D. Chemical Sterilization	
1. Electrochemical	
Ionics	54
McDonnell-Douglas	55
2. Mechanical Injection	
Hamilton Standard	56

	Reference Number
V. Humidity and Thermal Control	
A. Mass Effects - Inertial Separators	
1. Rotating Bowl (Hamilton Standard, GATCO)	57(a),(b)
2. Curvilinear Flow Path (Hamilton Standard)	58(a),(b)
B. Surface Effects Separators	
General Electric	59(a),(b) (c)
Lockheed	60
TRW	61
Langley Research Center	62
Hamilton Standard	63
C. Intermolecular Effects	
Hamilton Standard - Membrane Diffusion	64
VI. Solid Waste Processing	
A. Bacterial Stabilization	
1. Gamma Irradiation (Rad. Mach.)	65
2. Liquid Germicide (Hamilton Standard)	66
3. Vacuum Drying	
GATCO	67(a),(b) (c)
General Electric	68
Marquardt	69
B. Material Decomposition	
1. Incineration	
GATCO	70
Lockheed	71
2. Vacuum/Thermal	
GATCO	72
GATCO/Hamilton Standard	73
3. Wet Oxidation	
Whirlpool	74
VII. Sanitation and Hygiene	
A. Feces Collection	
GATCO	75
General Electric	76
Hamilton Standard and Rad. Mach.	77
B. Urine Collection	
GATCO	78
General Electric	79

	Reference Number
C. Bathing	
1. Body Wipe (Hamilton Standard)	80
2. "Automatic" Sponge (Hamilton Standard)	81
3. Shower (Hamilton Standard)	82
D. Clothes Washing (Hamilton Standard)	83

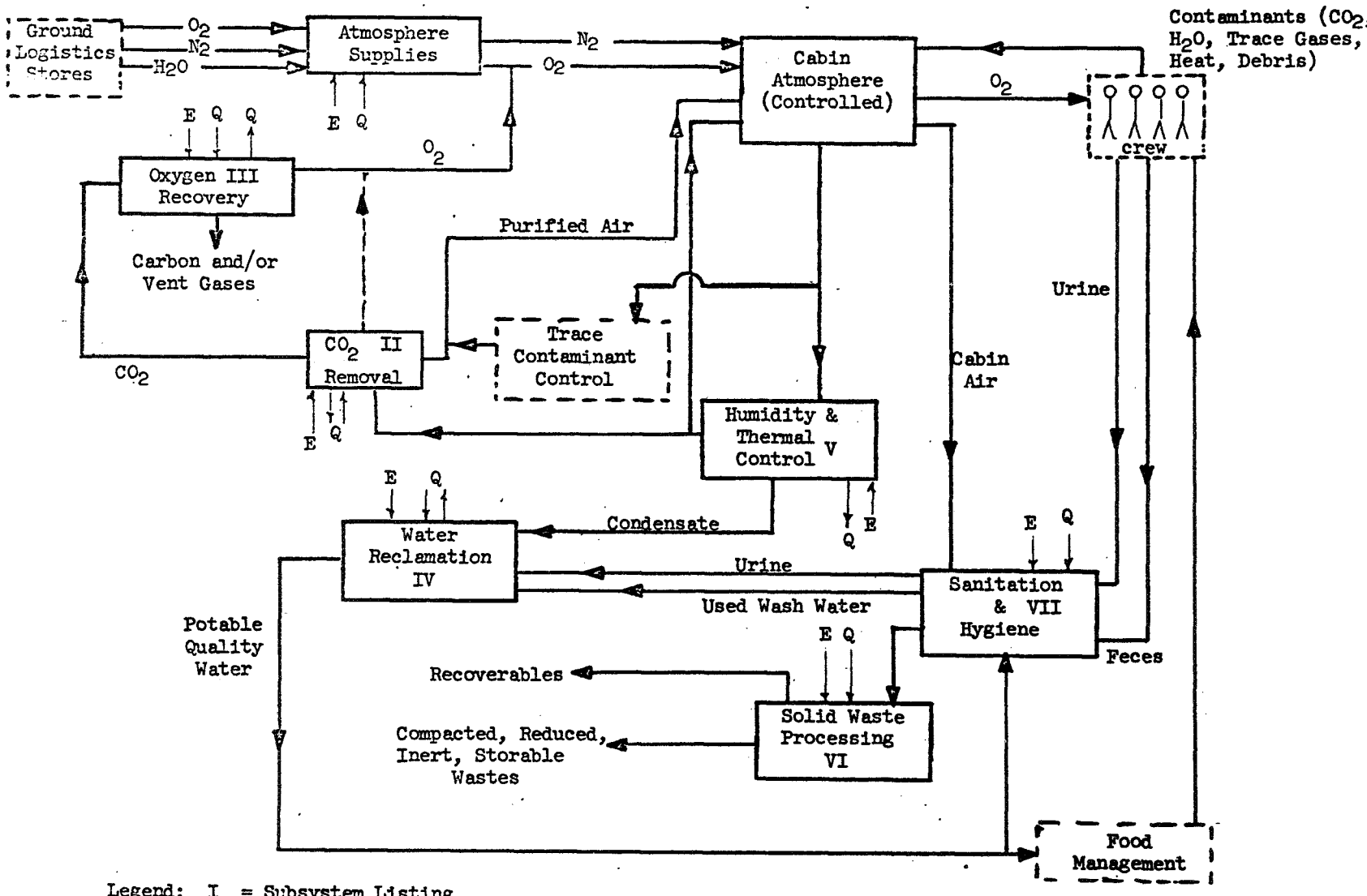
The results of the system organization study are diagramatically illustrated by figure 4.

The next step involved the detail descriptive analysis of each item listed, including the intuitive identification of potential gravity-sensitive processes. Figures 5 and 6 are examples of the documentation prepared to describe each of the equipment items considered to have a sufficiently unique functional or configurational characteristic as to warrant separate consideration. The system organization study and the preliminary process analyses formed the points of reference for all continuing work.

Some 80 LSS equipments were studied in these two steps, resulting in the identification of approximately 200 equipment-oriented processes considered to be potentially g sensitive. The principal processes identified as potentially g sensitive are listed by subsystem under four basic phenomenological groupings, table 2.

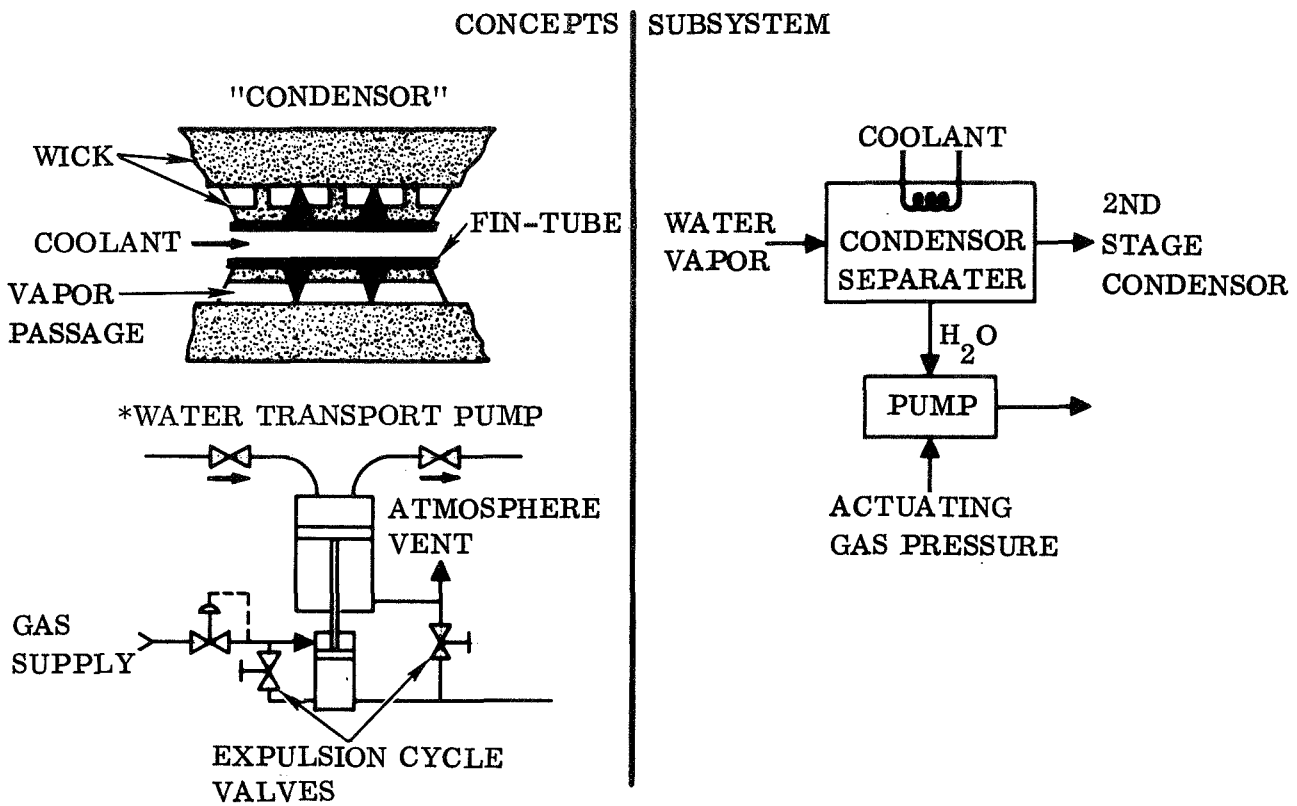
It was next required that this large number of specific equipment-oriented processes be reduced to the fewest number of basic analytical system models which, as a group, would encompass essentially all of the processes reported in the original set. However, in so doing, it was desirable to maintain visibility of as much of each of the phenomenological actions as possible in the analyses to be performed. To attain this goal, the concept of the analytical system, a traditional approach which permits the analyst to schematically represent the processes to be included in the analyses and a framework for defining its boundaries, was introduced. Such an approach requires that an iterative procedure be followed which sequentially reduces the large number of hardware systems models with many similarities to a small number of analytical system models. These, as a group, encompass at least the majority of the processes represented by the original set, but with a minimum of repetition between systems and yet with as wide an analytical application as possible.

This analytical process, then, is one of degeneration and the systems so amenable are typically referred to as "degenerate systems." These tasks are diagramatically represented as part of Steps 1, 2, and 3 of figure 7.



Legend: I = Subsystem Listing
E = Electrical Power
Q = Thermal Control Subsystem Heat Flux
= Subsystem Not Explicitly Included in Studies

Figure 4. - System Diagram

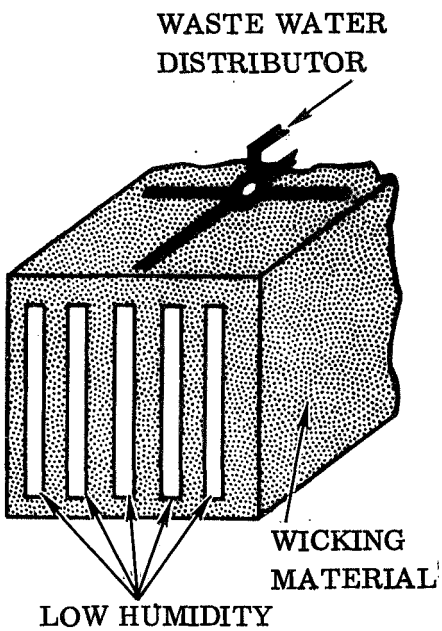


Process Technique: Fin Tube HX - Wick Collector and Transport
Mechanization & Mfg.: Condenser/Separator - General Electric 59(c)
LSS Function: L/G Separation - Water Recovery
Data Reference: N-40219, "Waste Management...", April 1965.

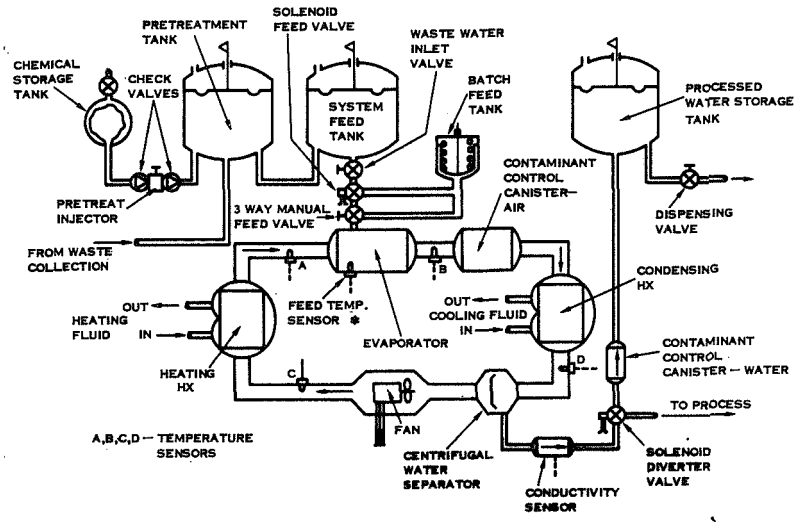
Processes Involved	Mechanism(s) Employed	Degree of g Sensitivity*
Condensing	Liquid-solid-gas H.T.	4
L/G Separation and Transport	1. Liquid/metal - surface tension	1
	2. Initial transport by fin energy gradient	2
	3. Secondary transport by wick capillarity	2
	4. Tertiary transport by pumping action	3

* 1 = Highly sensitive, 5 = essentially insensitive.

Figure 5. - Process Identification Sheet - Condenser/Separator 59(c)



EVAPORATOR
WICK PRINCIPLE



SUBSYSTEM

*Waste water feed control parameter

Process Technique: Air Evaporation - Wick - Closed Circuit Distillation
Mechanization & Mfg.: Air Evaporation Unit - Hamilton Standard 42
LSS Function: Water Recovery
Data Reference: #131268, "Air Evaporation Water Recovery System," 1968.

Processes Involved	Mechanism(s) Employed	Degree of g Sensitivity
Liquid/gas separation - liquid storage	Pressure bladder	4
Liquid/liquid injection and mixing	Displacement injector	3
Liquid/gas separation	Centrifugal separator	4
Liquid transport	Displacement	2
Wick saturation	Wick capillarity	4
Waste water evaporation	Evaporation H.T. at ambient pressures	2
Fluid management, L/G interface stability control	Wick capillarity	4
Gas transport	Inertial, blower	1
Liquid dispersoid transport	Air drag	1
Liquid evolution (condenser) and flow control	Condensation H.T. and gas drag	2

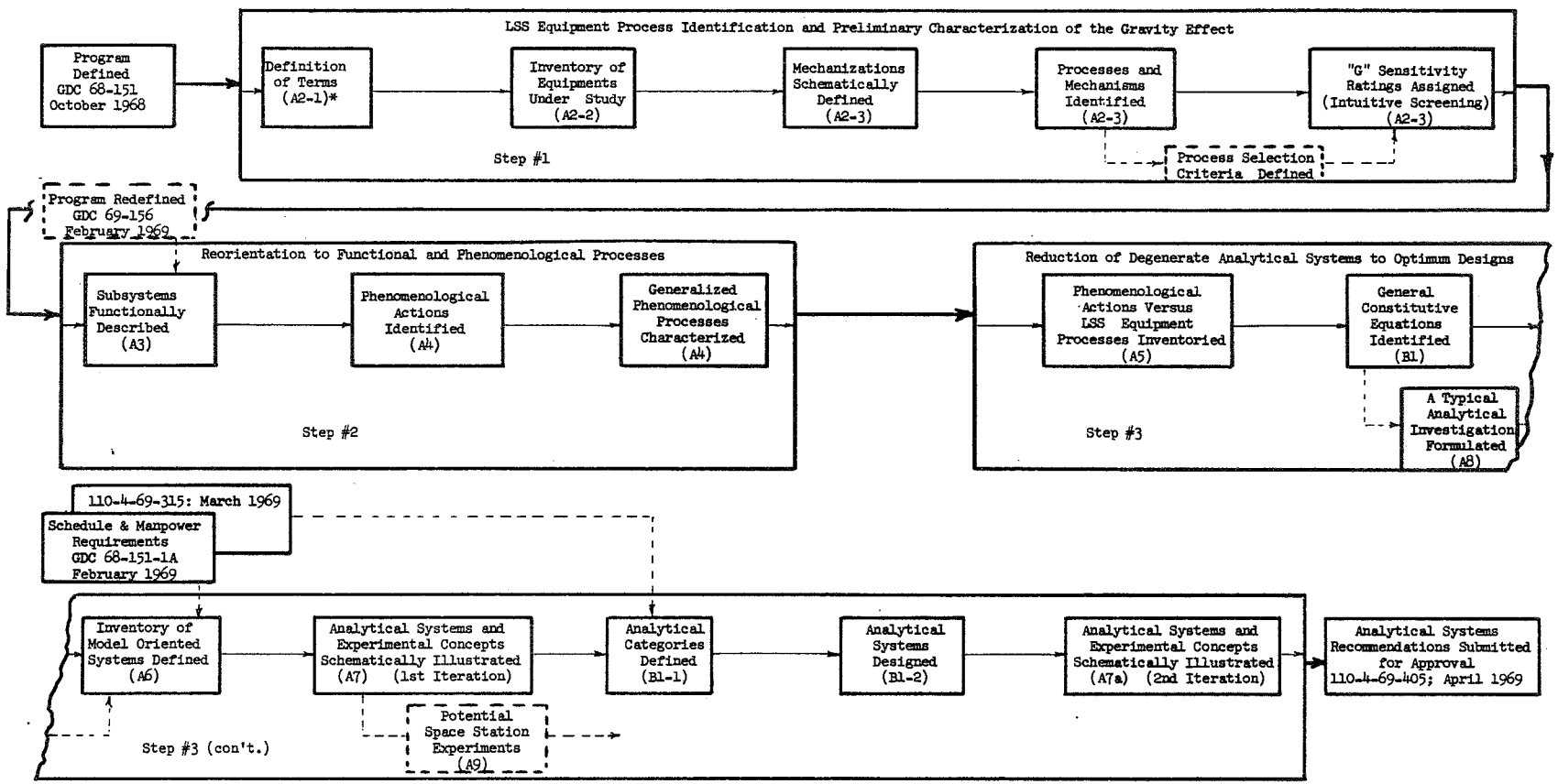
Figure 6. - Process Identification Sheet - Water Recovery 42

Table 2. - Process Analysis Summary

Subsystem \ Potential "G" Sensitive Processes	Materials Transport	Phase Change	Materials Separation	Conductive/ Convective Heat Transfer
I. Atmospheric Supply				
A. Storage	Gases	Evaporation	Liquid-Gas	Liquid & Gas
B. Chemical	Gases, Liquid/Liquid Liquid/Gas(1)	Dissociation Condensation	Liquid Dispersoid	Liquid & Gas
II. CO_2 Removal				
A. Sorption	Liquids, Gases, Liquid/Gas, Gas/Liquid	Evaporation Dissociation Absorption	Liquid Dispersoid L/G Mixture Gas-Gas (Solvent)	Gas, Liquid
B. Electro-Chemical	Liquids, Gases, Gas/Gas Gas Dispersoid in Liquid, Gas-Liquid Mixing	Dissociation Condensation Absorption	L/G (Dispersoid) L/G (Mixture) Gas-Gas (Solvent)	Liquid
III. Oxygen Recovery				
A. CO_2 Reduction	Solid (Dispersoid in Gas) Liquid Film Gas, Liquids, Gas-Gas (Mixing)	Condensation Crystallization	L/G Mixture G/Solid (Dispersoid)	Gas, Liquid
B. CO_2 Electrolysis	Gas	Dissociation Precipitation	Liquid (Solvent)	Gas, Liquid Plastic
C. H_2O Vapor Electrolysis	Gas	---	---	Liquid
IV. Water Reclamation				
A. Distillation	Liquids, Gases, L-L Mixing, G-G Mixing, Liquid Dispersoid, Liquid Film	Evaporation, Condensation	Liquid Dispersoids L/G Mixture Gas-Gas (Solvent) L-L (Solvent)	Liquid, Gas
B. Electro-Chemical	Liquid, Liquid Film	Dissociation Precipitate	Liquid (Solvent)	---
C. Filtration	Liquid	---	L/Solid (Dispersoid) Liquid (Solvent)	---
D. Sterilization	Liquid, L-L Mixing	---	---	---
V. Humidity Control(2)				
A. Mass Effects	Liquids, L-G Mixture, G/L Dispersoid, Liquid Film	---	L/G Mixture G/L Dispersoids	---
B. Surface Effects	Liquids, Gases, Liquid Film	---	L/G Mixture G/L Dispersoids	---
C. Inter-Molecular Effects	Liquids, Gases, Liquid Film	Diffusion (Membrane)	L/G Mixture	Liquid, Gas
VI. Solid Waste Processing				
A. Bacterial Stabilization	Liquids, Gases, Solid-Liquid Mixing	---	L/G Mixture G/Solid (Dispersoid) Gas (Solvent)	Gas, Liquid
B. Material Decomposition	Liquids, Gases Liquid/Gas Mixture, L-G and G-L Mixing	Dissociation Condensation Sublimation	L/G Mixture	Gas, Liquid
VII. Sanitation & Hygiene				
A. Feces Collection	Gas, Liquid, L-G Mix Gas/Solid (Dispersoid) G-L Mixing Solid-L Mixing	---	Gas/Solid Dispersoid Gas (Solvent)	---
B. Urine Collection	Liquids, Gases, L-G Mixture	---	L/G Mixture Gas (Solvent)	---
C. Bathing	Liquids, Gases, L-L Mixing, L-G Mixture	---	L/G Mixture L/Solid (Suspended)	---
D. Clothes Washing	Liquids	---	L/G Mixture L/Solid (Suspended)	---

Note: (1) Where applicable L = Liquid, G = Gas, S = Solid, L-G = Liquid introduced into Gas, L/G = Liquid & Gas, etc.

(2) Restricted primarily to the phase separation functions.



* Refers to data item identity as listed in the request for "Approval of Recommendations for Analysis" (in this case A2 Attachment 1).

Figure 7. — Analytical Systems Designation Process - Task Sequence

THE DEGENERATIVE ANALYSIS

The descriptive analysis had resulted in the identification of some 200 specific equipment-oriented processes. Reducing these equipment-oriented processes to a more generalized form and eliminating repetition followed and resulted in the identification of 44 phenomenologically oriented processes in six major categories as shown in table 3.

Continuation of the degenerative analysis transformed the 44 phenomenologically oriented processes into 13 highly generalized, analytically oriented process systems of phenomena which, in turn, were grouped under four major categories with the final results shown in table 4. This series of analyses was conducted under the following set of selection criteria:

a. The phenomena is basic to a process appearing on a process identification sheet.

b. The process appears to be inherently affected by inertial acceleration forces in the range of 10^{-6} to 2g (equivalent), or in certain cases the process presents a potential design problem with respect to the gravitational vector in at least one of the following:

   1. Research and/or operational experience to date indicates uncertainties in the design of equipment to support the processes involved.

   2. Analysis indicates that potential design problems may occur.

   3. Uncertainties exist in traditional design practices concerning the nature of the mechanisms involved and/or the analytical approaches to adopt to relate these mechanisms to the controlling design variables.

c. The process has a significant probability of being considered for LSS designs application in the 1970-1980 time period.

d. The process is amenable to theoretical and/or experimental analysis in a manner relatable to the attainment of design solutions.

Interim results are shown in the following listing with final results in table 4.
Interim results:

a. Material Transport Systems

   1. Fluid Transport (closed conduit): Single phase, homogeneous fluids (gas and liquid), bulk transfer through a closed conduit.

   2. Fluid Transport (open matrix): Single phase, homogeneous fluids, bulk transfer of liquid through a matrix capillary (wick) in the presence of a gas.

Table 3. - Phenomenologically Oriented Processes

A. Material Transport
- 1. Single Phase
  - a. Bulk Transfer
    - 1. Liquid
    - 2. Gas
  - b. Fluid Mixing
    - 1. Liquid-Liquid
    - 2. Gas-Gas
- 2. Multiple Phase
  - a. Bulk Transfer
    - 1. Liquid-Gas Mixture
    - 2. Liquid Dispersoids (Gas)
    - 3. Gas "Dispersoids" (Liquid)
    - 4. Solid Dispersoids (Gas)
    - 5. Solid "Dispersoids" (Liquid)
    - 6. Liquid Film (Solid-Gas)
  - b. Phase Mixing
    - 1. Gas in Liquid
    - 2. Solids in Liquid

B. Phase Change
- 1. Liquid to Gas
  - a. Evaporation
  - b. Dissociation
  - c. Desorption
- 2. Gas to Liquid
  - a. Condensation
  - b. Absorption
- 3. Gas to Solid
  - a. Crystallization
- 4. Solid to Gas
  - a. Sublimation

C. Materials Separation
- 1. Phase Separation
  - a. Liquid/Gas
    - 1. Liquid Dispersoid
    - 2. Gas "Dispersoids"
    - 3. Liquid/Gas Mixture
  - b. Solid/Gas
    - 1. Solid Dispersoids
  - c. Solids/Liquid
    - 1. Solid "Dispersoids"
- 2. Solute/Solvent Separation
  - a. Gas Phase
  - b. Liquid Phase

D. Heat Transfer
- 1. Conductive
  - a. Liquid → Solid
  - b. Gas → Solid
  - c. Liquid(Gas) → Solid → Liquid(Gas)
- 2. Convective
  - a. Liquid
  - b. Gas
- 3. Radiative
  - a. Solid → Liquid
  - b. Solid → Plastic

E. Chemical Reaction
- 1. Dissociation
  - a. Gases
  - b. Liquids
- 2. Reduction
  - a. Gases
- 3. Oxidation
  - a. Gases
  - b. Liquids (Organic Materials)
  - c. Micro-biological Materials

F. Materials Containment
- 1. Fluids Storage
  - a. Gases
  - b. Liquids
  - c. Vapor-Liquid Mixtures
- 2. Phase Interface Management
  - a. Liquid to Gas
  - b. Solid (Plastic) to Gas
- 3. Positional Stability (Maintain Relative Position)
  - a. Liquids
  - b. Solids
  - c. Plastics

Table 4. - Analytically Oriented Process Systems

I. Multiphase Flow A. One-Phase Continuum 1. Nucleate Boiling 2. Transport of Dispersoids 3. Inertial Separation 4. Mixing of Dispersoids and Carrier (Homogenation) B. Mixture Continuum (Non-Newtonian) 1. Transport 2. Separation 3. Mixing (Homogenation)	II. Multi-component Gas Flow A. Diffusion of One Component 1. Humidification 2. Dehumidification III. Motion of Thin Liquid Layers A. Films 1. Conical Surfaces 2. Flat Plate Surfaces IV. Thermal Energy Transport A. Convection 1. Natural 2. Forced

3. Fluid Transport (mixing): Single phase, heterogeneous fluids (liquid and gas), mixing within a closed conduit or vessel.

4. Fluid Transport (dispersoids and their suspending media): Multiphase, bulk transfer through closed conduit: a) liquid dispersoids, b) gas dispersoids.

5. Fluid Transport (liquid/gas mixtures): Multiphase, bulk transfer through closed conduit.

6. Solid Dispersoid Transport: Multiphase, bulk transfer through closed conduit, gas and liquid medium.

7. Fluid Transport (liquid film): Multiphase, interface with solid surface and gas: a) flat plate - surface effects and gas shear with interface stability and film-droplet transition as major concerns, and b) conical "plate" - general transport mechanism.

b. State Change

1. Vaporization: Physical and thermal aspects, particularly for the nucleate boiling case.

2. Condensation: Physical and thermal aspects, cold plate HX, solid and porous plate.

c. Material Separation

1. Phase Separation Liquid/Gas: Coalescence of liquid dispersoids in a gas stream and formation of a single liquid/gas interface employing a) surface effects, and b) inertial mechanisms.

2. Phase Separation Gas/Liquid: Gas dispersoids in a low-pressure liquid stream removed by surface effect mechanism (hydrophobic membrane).

3. Phase Separation Liquid/Gas: Separation of the liquid and gas components of a mixture being transported through closed circuit, inertial and surface effects mechanisms.

4. Phase Separation Solid/Gas: Concentration and retention of solid and gas stream (closed conduit). Inertial mechanisms.

d. Heat Transport — Convective Heat Transfer: Free and forced convection plus diffusion of a single phase fluid for a liquid and gas.

It can be noted that process categories E and F of table 3 were added to provide clearer visability to several actions not clearly identified by table 2. As a result of this examination these actions were not explicitly included in the analytical orientation of table 4 as only the material transport processes involved in chemical reactions are sufficiently affected by inertial forces to be of interest and, similarly, the containment processes are essentially special conditions of material transport and, as such, implicitly treated under the four analytical categories.

THE ANALYTICAL SYSTEMS

Six systems of analytically oriented processes were selected from those listed in table 4 as representing, at least in their final analytical form, virtually all of the basic phenomena which could be noticeably affected by variations in the local inertial field forces, i.e., are "g sensitive." These analytical systems, identified by their descriptive titles, were so defined as to include at least the following areas of interest:

a. Nucleate Boiling - Primarily defined by the parameters relating to bubble behavior and the characteristics of the liquid/vapor mass when enclosed in a rigid container and subjected to various forces and energy exchange rates. I A1 (I A2, IV A1 & 2)*

b. Diffusion Convection - Primarily defined by the parameters relating to the evolution of diffusion in a convection medium where co-current and counter-current diffusion may exist with single or two-component diffusion as an uncertainty. II A1 & 2

c. Film Stability and Transport - Primarily defined by the parameters relating to the transport of liquid films on solid surfaces and the influence of interfacial shear forces, surface temperature gradients, and gravity field effects with special

* Refers to listings under table 4; references in brackets are examples of implied relationships.

emphasis placed on the film behavior in the transition from stable to unstable transport regimes. III A1 & 2

d. Inertial Separation - Primarily defined by the parameters relating to the transport of liquid dispersoids in a gas stream and their eventual separation and single phase transport. Included are, 1) the effects of inertial and liquid surface forces on droplet size and, in turn, on transport drag forces and velocity, 2) the behavior of droplets impacting on various surfaces, and 3) the behavior of droplets and films reacting to various surface, interfacial shear, and inertial forces associated with the liquid phase transport functions. I A3 (I A2, I B2, III A1 & 2)

e. Convection Heat Transport - Primarily defined by the parameters relating to the process of transport of component fluid particles within a fluid body as a result of buoyancy (density) differences created by a nonuniform transfer of heat to or from the fluid mass. Of special interest are the effects of turbulent mixing, variations in the inertial acceleration field, and the conditions leading to and accompanying the transition from laminal to turbulent flow. IVA 1 & 2 (II A1 & 2, I A2)

f. Flow Regime Characteristics - Primarily defined by the parameters relating to the process of transport of various forms of a mixture continuum exhibiting non-Newtonian flow characteristics. Of particular interest is the transport of nonhomogeneous liquid/gas mixtures through a closed conduit. I B1 (I B2 & 3, III A2)

DEVELOPMENT AND TEST OF ANALYTICAL MODELS

GENERAL APPROACH

The first major step in the development of the analytical models was the selection of the general constitutive equations which specify the temporal and spatial history of the variables involved. Examination of the principal processes associated with life support systems indicates that elements of two phenomena are subject to alterations due to variations in the inertial fields, namely 1) multiphase transport and 2) heat transfer. Particularly involved are phase separation in the former set, with convection and boiling in the latter. The equations determined to apply were those dealing with the conservation of mass, momentum, and energy. Analytical prediction of sensitivity to the inertial acceleration field is explicitly considered in the general equations of motion, with solutions which are only peculiar to the applied boundary conditions.

A unique aspect of this study program was the requirement to test the validity of each predictive model with a physical model of the processes under study. Each test model was a simple and straightforward mechanization of the analytical model configured in such a way as to be relatable as possible to typical life support equipment designs, yet sufficiently general to permit a wide range of application of the results. All experiments were conducted under laboratory conditions, i.e., at 1g levels. Requirements for experimental evaluation of the analytical models under reduced-gravity conditions were identified and described.

Following the establishment of these basic guidelines, the six analytical models were developed under these criteria:

a. The level of treatment should be sufficiently general to ensure that its predictive aspects would have as wide an application as possible, yet be readily relatable to the equipment-oriented processes as identified.

b. Maximum use be made of prior analyses and analytical tools existing in 1) both the proprietary and nonproprietary inventories of Convair, 2) government documents, and 3) the open literature.

c. The model should be oriented to describe the behavior relative to the phenomenological actions identified in the "design" of the analytical systems under varying conditions, with emphasis on the effects of specified variations in the local inertial acceleration vector.

d. The level of detail for any given model should be such that it supports the development of maximum descriptive coverage of the full range of equipment processes

identified, yet is accomplishable within the schedule, manpower, and dollar allocations of the contract.

e. The model can be readily tested and augmented through relatively simple and economical experiments capable of significant yield, both when initially performed under typical ground-based laboratory conditions and, if subsequently found necessary, performed under the low-gravity conditions of space flight.

f. The model and its evaluation will be described in an informal working paper under the title of Analytical Model Report.[†]

The following guidelines were used in the design of each experimental test model and the corresponding set of procedures:

a. Each design will be such that the model and set of experiments can be completed within a specified cost and schedule allocation.

b. Experiments need not be conducted against certain facets of the analytical model if:

   1. Information is available in the literature concerning prior experiments.

   2. Expenditures in cost, manpower, schedule, would be excessive.

   3. Results are considered to be trivially obvious.

   4. The mechanization would complicate the apparatus to the extent that the collection of other data might be seriously impaired.

c. Test model and experiments design may include avenues of investigation not specifically required in the evaluation of the analytical models if it appears that such will produce information of value to the life support system design task and it can easily be accomplished without compromising the basic objectives of the experiment.

d. The design and fabrication of apparatus will be such as to demonstrate the capability to integrate the experiments into a minimal number of multijunction flight experiment packages.

e. The documentation of the preliminary design of each experimental test will be compiled in an informal working paper under the title of Experimental Test Plan.

f. The description of each experimental test as conducted will appear in a second informal working paper under the title of Experimental Test Report.

A schematic representation of the initial concepts employed in this developmental process is shown in figure 8.

[†] Additional documentation can be found in Evans, E. A.: Computer Program Documentation for the NAS1-8494 Mod 1 Contract. GDC-DBD70-002 (a set of three documents, vol. I, II, and III), Convair division of General Dynamics, June 1970.

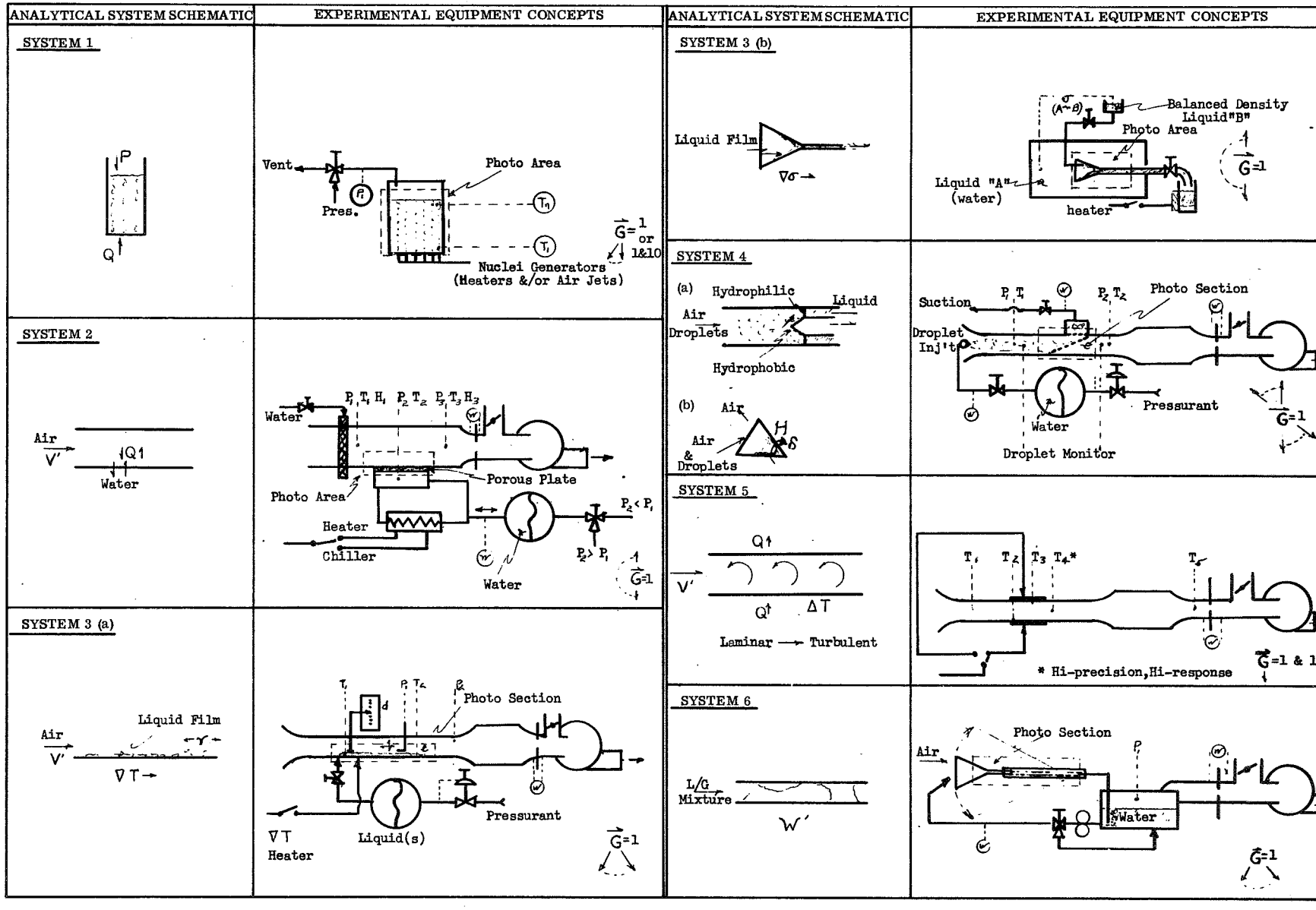


Figure 8. — Model-Oriented System Schematics and Experimental Concepts

ANALYTICAL MODEL NO. 1 — "NUCLEATE BOILING"

An analytical model has been developed which predicts both the evolution (temporal and spacial) of a bubble distribution in a nucleate boiling process and the resulting alteration of the pool configuration within the container. The predicted behavior is centered in the low-gravity case but correlations with behavior across a range of inertial acceleration forces experienced during prelaunch, boost, and orbital phases of space flight become possible.

The phenomenological considerations embodied in the model are:

a. Bubble generation with time- and spatial-dependent radii and frequencies.

b. Kinematics and energetics of a single bubble moving in temperature and inertial acceleration fields in three dimensions.

c. Time- and spatial-dependent temperature and inertial acceleration fields.

d. The effect of bubble wake on following bubbles.

e. Bubble agglomeration.

f. Interaction with container walls (slip or no slip) and with screens (escape).

g. Vaporization (two ways):

   1. Nucleate boiling.

   2. "Bulk" boiling.

      (This vapor generation is partitioned between the liquid/ullage interface and the existing bubble population in proportion to relative surface areas.)

h. Liquid energy conservation, outflow, and level determination.

i. Convective heat transfer to liquid phase, which is dependent on liquid level.

The model can be considered to predict the behavior of vapor bubbles moving in a pool of the vapor-forming liquid and specifically assesses the effects of variations in the forces, including those of inertial acceleration, which control this behavior. Phenomena associated with this behavior have been identified as appearing in the normal mode of operation for at least one equipment type in each of the LSS functions studied and in many equipment types for major degraded modes of operation (ref. 1).

Table 5. — Nomenclature for Nucleate Boiling Calculations

NOMENCLATURE

F	force
X	position coordinate
V	velocity
ρ	density
R_B	bubble radius
g	inertial acceleration (e.g., gravity)
$\hat{e}$	unit vector
$\delta( )$	variation in ( )
τ	shear stress
$\vec{n}_T$	surface tangent
$\hat{\theta}$	unit vector in polar angle direction (positive in direction of increasing angle)
dS	increment of surface
θ	polar angle
σ	surface tension
T	temperature
Z	axis of symmetry of bubble
$\vec{\nabla}$	gradient operator
C_D	drag coefficient
Re	Reynolds number $\frac{2 V R_B}{\mu}$
μ	viscosity
m	mass
u	specific internal energy
P	pressure

Table 5. — Nomenclature for Nucleate Boiling Calculations (Contd)

$\tilde{v}$	specific volume
h	specific enthalpy
$<\phi>^{ji}$	integrated average of ϕ over the wake shadow region of a lead (j) bubble projected on a following (i) bubble
$\lvert\vec{A}\rvert$	magnitude of vector $\vec{A}$

SUBSCRIPTS

ℓ	liquid parameter
g	gas parameter
B	bubble parameter
w	wake parameter
g	inertial field parameter
A	actual (with corrections)
o	defines the surface tension and radius values at the bubble equator
v	velocity parameter
D	drag parameter
∞	infinite spatial region

SUPERSCRIPTS

B	buoyant
D	drag
ST	surface tension
i	following bubble in wake consideration
j	lead bubble in wake consideration

DESCRIPTION OF THE MODEL

Single-Bubble Dynamics

The motion of a bubble moving in a liquid with noncolinear gravitational and temperature fields is considered by summing the body and surface forces acting on the bubble, neglecting the bubble inertia.

$$\vec{F}^{B} + \vec{F}^{ST} + \vec{F}^{D} = 0 \tag{1}$$

$\vec{F}^{B}$ ≡ buoyant force

$\vec{F}^{ST}$ ≡ surface tension force resultant

$\vec{F}^{D}$ ≡ liquid/bubble momentum exchange (drag)

The equation of motion for a bubble, neglecting inertia (implies terminal velocity), is written as the difference form of the time integral of velocity,

$$\delta \vec{x} = \bar{\vec{v}}_{B}\, \delta t$$

$\delta \vec{x}$ ≡ change in position

$\bar{\vec{v}}_{B}$ ≡ average velocity

δt ≡ time increment

The buoyant force is given by (for nearly spherical bubbles),

$$\vec{F}^{B} = \left[\frac{4}{3}\pi R_{B}^{3}\, g\, (\rho_{\ell} - \rho_{g})\right] \hat{e}_{g} \tag{2}$$

Consideration of the effect of a surface tension gradient on bubble motion requires conceptual investigation of the "grundlagen" of interfacial phenomena. The interface is a thin film which is elastic but not plastic (it may not flow) (ref. 2) for no circulation within the bubble. The bubble is treated as an inertialess void. The normal traction, therefore, establishes the surface topology and has no accelerative effect on the bubble. A confined liquid segment, on the other hand, would have an induced pressure gradient corresponding to the surface tension gradient and would cause the liquid to flow. The tangential tractions will accelerate the bubble since the interfacial surface cannot flow. The result for a spherical surface is given by, (ref. 3)

$$\vec{F}^{ST} = -\iint \Delta \underline{\underline{\tau}} \cdot \vec{n}_T \, dS \equiv \text{acceleration due to surface effects} \tag{3}$$

$\Delta \underline{\underline{\tau}} \equiv$ net surface traction tensor

$\vec{n}_T \equiv$ unit tangent vector to surface

For an azimuthally symmetric surface and surface tension gradient,

$$\Delta \underline{\underline{\tau}} \cdot \vec{n}_T = (\vec{\nabla}\sigma \cdot \vec{n}_T)\, \vec{n}_T$$

For small changes in bubble radius with polar angle,

$$\Delta \underline{\underline{\tau}} \cdot \vec{n}_T \cong \left[\frac{\partial \sigma}{\partial R_B} \left(\frac{1}{R_B} \frac{\partial R_B}{\partial \theta} \right) + \frac{1}{R_B} \frac{\partial \sigma}{\partial \theta} \right] \hat{\theta} \tag{4}$$

The bubble radius is given by the normal surface traction difference; this is constant since the surface is not growing,

$$\frac{\sigma}{R_B} = \frac{\sigma_o}{R_{Bo}} = \text{constant} \tag{5}$$

which defines the bubble radius or topology. For an axial temperature field,

$$\sigma = \sigma_o + R_B \cos\theta \frac{\partial \sigma}{\partial T} \frac{\partial T}{\partial Z} \tag{6}$$

$$\frac{\partial \sigma}{\partial R_B} = \cos\theta \frac{\partial \sigma}{\partial T} \frac{\partial T}{\partial Z} \tag{7}$$

from equation (5)

$$\frac{1}{R_B} \frac{\partial R_B}{\partial \theta} = \frac{R_{Bo}}{\sigma_o R_B} \frac{\partial \sigma}{\partial \theta} \tag{8}$$

Equation (4) becomes

$$\Delta \underline{\underline{\tau}} \cdot n_T \cong \frac{1}{R_B} \frac{\partial \sigma}{\partial \theta} \left[\cos\theta \frac{\partial \sigma}{\partial T} \frac{\partial T}{\partial Z} \frac{R_{Bo}}{\sigma_o} + 1 \right] \hat{\theta} \tag{9}$$

From symmetry, only the axial component of force survives,

$$F_Z^{ST} = \iint (\nabla \sigma \cdot \vec{n}_T) \sin\theta \, ds$$

$$\frac{1}{R_B} \frac{\partial \sigma}{\partial \theta} \cong - \sin\theta \frac{\partial \sigma}{\partial T} \frac{\partial T}{\partial Z}$$

$$F_Z^{ST} = - 2\pi \int_o^{\pi} R_B^2 \sin^3\theta \frac{\partial \sigma}{\partial Z} \left[\cos\theta \frac{\partial \sigma}{\partial T} \frac{\partial T}{\partial Z} \frac{R_{Bo}}{\sigma_o} + 1 \right] d\theta \tag{10}$$

To first order, equation (10) yields,

$$F_Z^{ST} = - \frac{8\pi}{3} \frac{\partial \sigma}{\partial T} \frac{\partial T}{\partial Z} R_{Bo}^2 \tag{11}$$

Equation (1) is for a nearly spherical gas volume with a single surface (bubble). The vector form of (11) is,

$$\vec{F}^{ST} = - \frac{8\pi}{3} \frac{\partial \sigma}{\partial T} R_{Bo}^2 \vec{\nabla} T \tag{12}$$

The drag force is given by,

$$\vec{F}_D = - C_D \rho_\ell \frac{v_B^2}{2} (\pi R_B^2) \hat{e}_v \tag{13}$$

The velocity vector direction is given by the vector sum of forces, equation (1),

$$\hat{e}_v = \frac{\{\vec{F}^{ST} + \vec{F}^B\}}{|\vec{F}^{ST} + \vec{F}^B|}$$

To define the drag coefficient, it is necessary to review the kinematics of bubble drag. Three regions of interest are considered,

I Spherical particle
II Nearly spherical particle
III Deformable body and the transition region

Region I is commonly known as Stokes drag region for spheres; the Reynolds number interface for Regions I and II occurs at Re = 2, (ref. 4). Region II is for nearly spherical particles and is the same functional relationship as Region I with different constants. The Reynolds number interface for Regions II and III is a function of fluid parameters

and is defined by the intersection of the drag function in Region II with the functional relationship in Region III. Typical values of Re at the intersection are 80 to 400. The evaluation of the region separation and functional dependences in each region are based on extensive study and comparison of data contained in references 4 and 5. Considerable scatter and conflict in data preclude a more definitive evaluation. In Regions I and II, the drag coefficient is a simple function of Reynolds number,

$$C_D \equiv a\,Re^n \tag{15}$$

The velocity is defined by

$$v_B = \left[\frac{\mu_\ell}{2R_B\rho_\ell}\right]\left[-\frac{64R_B^2\rho_\ell\frac{\partial\sigma}{\partial T}(\vec{\nabla}T\cdot e_v)}{3a\mu_\ell^2} + \frac{32R_B^3\rho_\ell g(\rho_\ell-\rho_g)(\hat{e}_g\cdot\hat{e}_v)}{3a\mu_\ell^2}\right]^{\frac{1}{2+n}} \tag{16}$$

The value for "a_1" of 24 provides reasonable data correlation for Region I, with $n_1 = -1$. For Region II, $a_2 = 19.7$ and $n_2 = -0.725$ are appropriate.

Region III is associated with the onset and growth of surface deformation due to tangential shear stresses. The region embodies both the initial oblate deformation and the final "hemispherical cap" configuration. The drag coefficient is a function of the ratio of accelerative forces ($\vec{F}^B + \vec{F}^{ST}$) to normal surface tension traction; for only buoyant forces, this is the Eötvös or Bond number

$$N_E \equiv \frac{3\left|\vec{F}^B + \vec{F}^{ST}\right|}{\pi R_B \sigma}$$

$$C_D = C_\infty\,(1 - e^{-\lambda N_E}) \tag{17}$$

The exponential relaxation of equation (17) accommodates the transition to the totally deformed hemispherical cap state. Values of $C_\infty = 2.64$ and $\lambda = 0.13$ were found to give the best correlation with references 4 and 5. Using $n = 0$ and $a = C_D$ in equation (16), the velocity is prescribed for Region III.

In Region III, the acceleration due to surface tension gradient (temperature field) is reduced because the topological deformation alters the surface integral and traction in equation (3) and introduces anisotropic components. However, this force is only important in low-buoyancy situations; therefore, the alteration for region dependence is neglected.

The effect of finite medium on the velocity is approximately treated by considering the mass conservation equation of the liquid surrounding the bubble in the limited region. The increased relative velocity around the bubble increases the drag and results in a reduced velocity for the bubble in the confined region.

$$\frac{v_{B_A}}{v_{B_\infty}} = \left[1 - \left(\frac{R_B}{R_T}\right)^2\right]$$

$R_T \equiv$ finite region radius

Reference 5 shows that this result is approximately correct (it is obviously self-consistent). The velocity, actually, falls off somewhat faster for bubbles in Region III.

For a medium containing many bubbles, the velocity is defined by,

$$v_{B_A} \cong v_{B_\infty} (1 - \alpha) \tag{18}$$

where α is the local area fraction of bubbles.

Bubble Energy Equation for a Single Bubble

Thermodynamic evolution of a bubble is described by a differential form of the first law energy equation. The gaseous phase inside the bubble is considered to be saturated at the pressure corresponding to the external pressure plus the surface traction. Energy transport (heat and/or mass transfer) between the bubble and liquid phase is considered.

$$0 = m_2 u_2 - m_1 u_1 + \delta m_c \bar{h}_T + \delta m_Q \bar{h}_T - \delta m_V \bar{h}_T + \delta(P\tilde{v}) \tag{19}$$

for time 1 to time 2, where,

$m \equiv$ bubble mass

$u \equiv$ bubble internal energy (specific)

$\delta m_c \equiv$ mass transfer due to change in state of bubble

$\delta m_Q \equiv$ mass transfer due to heat transfer to liquid phase

$\delta m_V \equiv$ mass transfer due to change in liquid state (vaporization)

$P \equiv$ bubble internal pressure

$\tilde{v} \equiv$ bubble specific volume

$$\bar{h}_T \equiv \begin{cases} \bar{h}_g \sim \delta m_c < 0, \ \delta m_Q < 0, \ \delta m_V > 0 \\ \bar{h}_{fg} \sim \delta m_c > 0, \ \delta m_Q > 0, \ \delta m_V < 0 \end{cases}$$

$\bar{h}_g \equiv$ average bubble enthalpy (specific)

$\bar{h}_{fg} \equiv$ average heat of vaporization

$P \equiv P_\ell + 2\sigma/R_B$

$P_\ell \equiv$ local liquid phase pressure

Continuity of bubble mass yields,

$$m_2 - m_1 = \delta m_V - \delta m_Q - \delta m_c \tag{20}$$

It is assumed that the bubble remains at saturated gas conditions.

Wake Effects

In the study of bubble populations, the velocity field behind a bubble (wake) must be considered in the velocity prescription of bubbles rising in succession. As an approximate approach, a superposition of wake velocities which interfere with a particular bubble is used. This is quite reasonable for moderately dense populations because the wake relaxes as $(x/D)^{-2/3}$ for axisymmetric bubbles.

The velocity of bubble "i" is given by,

$$\vec{v}_B^{\,i} = \vec{v}_{B_A}^{\,i} + \sum_{j \neq i} < \vec{v}_w^{\,ji} > \tag{21}$$

where

$\vec{v}_w^{\,ji} \equiv$ wake velocity which interacts with bubble "i" from bubble "j."

The velocity field in the wake of axisymmetric bodies is expressed (this is a vector representation of the wake velocity) as

$$\vec{v}_w^{\,ji} = f_1^{ji} \vec{v}_{B_A}^{\,j} + f_2^{ji} \left[\frac{\vec{R}_{ji}}{|\vec{R}_{ji}|} - \frac{(\vec{R}_{ji} \cdot \vec{v}_{B_A}^{\,j})}{|\vec{R}_{ji}| \, |\vec{v}_{B_A}^{\,j}|} \vec{v}_{B_A}^{\,j} \right] \tag{22}$$

where

$\vec{R}_{ji} \equiv \vec{x}^{j} - \vec{x}^{i} \equiv$ relative vector coordinate of bubble (j) with respect to bubble (i)

$\vec{x} \equiv$ position vector of bubble

$f_1^{ji} \equiv$ functional dependence of axial† velocity in wake on the relative distance $|\vec{R}_{ji}|$

$f_2^{ji} \equiv$ functional dependence of radial† velocity in wake on the relative distance $|\vec{R}_{ji}|$

The velocity field behind a single body with axial symmetry has been investigated (ref. 6) for turbulent wakes. The consideration of only turbulent wakes is reasonable since laminar wakes occur only for very small bubbles or low velocities where wakes are not important; also, the laminar wake is similar to turbulent wake in its attenuation, $(x/D)^{-1}$, references 2 and 7.

The functions f_1^{ji} and f_2^{ji} are,

$$f_1^{ji} = |\vec{v}^{\,j}_{B_A}| \left[0.202\, C^{-0.8}\right] \left[\frac{C_D \pi R_B^{j2}}{x_{ji}^2}\right] \left[1 - \eta_{ji}^{3/2}\right]^2$$

$$f_2^{ji} = |\vec{v}^{\,j}_{B_A}| \left[0.0825\, C^{-1.067}\right] \left[\frac{C_D \pi R_B^{j2}}{x_{ji}^2}\right]^{2/3} \eta_{ji} \left[1 - \eta_{ji}^{3/2}\right]^2$$

where

$x_{ji} \equiv \dfrac{\vec{R}_{ji} \cdot \vec{v}^{\,j}_{B_A}}{|\vec{v}^{\,j}_{B_A}|} \equiv$ projection of relative position vector on velocity direction of lead bubble.

$\eta_{ji} \equiv |\vec{R}_{ji} - x_{ji} \vec{v}^{\,j}_{B_A}| / b \equiv$ normalized projection of relative position vector on direction normal to velocity of lead bubble.

$b \equiv 1.222\, C^{-0.267} (C_D \pi R_B^{j2} x_{ji})^{1/3}$

The constant "C" is determined by experimental correlation. A value of C = 0.288 was obtained using data in reference 8.

†Axial and radial are defined by the velocity vector of the lead bubble (j).

Agglomeration and Container-Wall Interaction

Interbubble agglomeration (coalescence) and bubble, liquid/ullage surface coalescence is represented by two equations,

$$|\vec{R}_{ji}| \leq (R_B^i + R_B^j) + \delta_{IMP} \tag{23}$$

δ_{IMP} ≡ impact parameter for bubble collisions

$$|\vec{R}_{is}| \leq R_B^i + \delta_{IMP}^s \tag{24}$$

δ_{IMP}^s ≡ impact parameter for bubble/surface collision

$\vec{R}_{is}$ ≡ vector from bubble center normal to liquid/ullage surface

Equations (23) and (24) define conditions for agglomeration to occur: for interbubble collision, the resulting bubble is positioned at the center of mass of the two original bubbles. Observation of coalescence indicates that

$$\delta_{IMP}^s = \delta_{IMP} = 0$$

Bubble collisions with the confining walls of the container result in one of two possible situations: free slip, no slip.

$$\text{Free Slip} \sim \vec{v}_B \cdot \vec{n} \,|_{WALL} = v_{B_n}|_{WALL} = 0$$

$$\text{No Slip} \sim \vec{v}_B \,|_{WALL} = 0$$

In the first situation, the bubble hits the wall and travels along a geodesic of the surface; for the second situation, the bubble strikes the wall and remains at the point of impact.

Another consideration is that the wall may be porous and the bubble could possibly escape; this is determined by the relation of the normal force of the bubble at the container wall to the surface tension retardation force provided by the wall pores. If the normal force is greater than the combined surface tension forces of all involved pores, then the bubble "escapes" and is lost forever; if the normal force is less, the bubble is retained.

Vaporization

There are two mechanisms for vapor generation: nucleate boiling and "bulk" boiling. For nucleate boiling, the site, the time-dependent initial radius, and the time-dependent frequency of production are input to the program. The mass of vapor produced is subtracted from the liquid phase and a new bubble is born.

Boiling which is the result of change in thermodynamic state of the liquid (bulk), e.g., pressure decay and convective heat transfer, is added to the existing voids, including the ullage space, in proportion to liquid/gas interfacial areas.

$$\delta m_V^i = \frac{C_A \left(4\pi R_B^{i2}\right) \delta m_{LV}}{\left[A_s + 4 C_A C_{DEG} \sum_j \left(\pi R_B^{j2}\right)\right]} \tag{25}$$

where

δm_{LV} = liquid phase mass change due to vaporization

A_s = liquid ullage interface area

δm_V^i = mass addition to i^{th} bubble

C_A ≡ arbitrary weighing factor

C_{DEG} ≡ degeneracy factor for considering only a sector

The parameter C_A permits alteration in the partitioning of vapor production between bubbles and the ullage space. The degeneracy factor is an artifact which represents an axisymmetric container and void distribution as a degenerate sector of the cross section. In other words, only the evolution of voids in one degenerate sector needs to be considered if all forces obey the same symmetry rules as the container and the voids do not outgrow this sector. The program uses C_{DEG} to keep track of gas, liquid phase, and volume changes to insure the satisfaction of conservation requirements.

$$C_{DEG} = \frac{2\pi}{\text{Sector Angle (Radians)}} \equiv \text{Integer quantity}$$

Observations of boiling due to pressure reduction indicate that existing voids increase appreciably in size and that some nucleation sites appear on the walls; however, there is no evidence that new bubbles are created internal to the liquid phase providing that no incipients are present, e.g., gases in solution, solid particles, and other contaminants. The latter could be inputed as additional nucleation sites.

Liquid Energy Conservation and Level Determination

The liquid phase energy conservation is defined by a differential first law energy equation. The pressure history is a given function of time (input).

$$\delta Q_{\ell} = m_{\ell_2} u_{\ell_2} - m_{\ell_1} u_{\ell_1} + \bar{h}_{\ell} \delta m_o + \bar{h}_{fg} \delta m_{LV} \tag{26}$$

where

δQ_{ℓ} ≡ convective or conductive heat transfer to liquid (input per unit liquid height)

$\delta m_o \equiv \delta m_{FO} - \delta m_c - \delta m_Q$

δm_{FO} ≡ liquid outflow (input)

Mass conservation yields,

$$m_{\ell_2} - m_{\ell_1} = \delta m_o + \delta m_{LV} \tag{27}$$

Because of the arbitrary surface angle (function of time) and the various axisymmetric container configurations, the liquid level is calculated every time step by an iterative method. The convective or conductive heat transfer to liquid is input per unit liquid height; therefore, the program explicitly calculates the feedback effect of changing heat input with liquid level.

Summary

Equations (1) through (27) and attendant equations are coupled together in Program EVOLVE to calculate each bubble lifetime and total liquid conservation for the axisymmetric container. The utility of the model is such that it has been applied to small life support system containers and to the large S-IVB propellant tanks.

THE COMPUTER PROGRAM

The computer program EVOLVE was initially developed under Convair IRAD funding (ref. 9) and provides predictive time-dependent definitions of the geometry of a gas (vapor)/liquid mixture in which bubble evolution is operating. In so doing, the program is designed to consider 1) populations of up to 1000 bubbles, 2) three-dimensional transport, 3) bubble generation from up to 100 sites at varying bubble radii and frequencies, 4) time-dependent surface orientation, and 5) time-dependent pressure history.

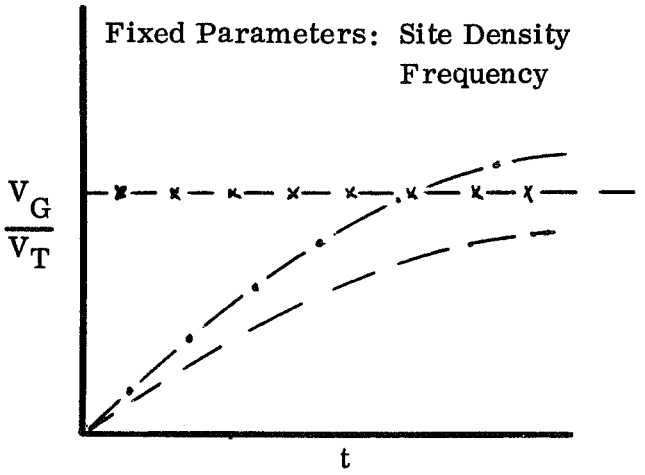
Input to computer program EVOLVE consists of five principal types: property data, liquid environment site data, geometry and thermal environment, and constants. The liquid property data includes the temperature/vapor pressure relationship, temperature-dependent properties of surface tension, viscosity, liquid and gas density, and liquid and gas specific energy. The pressure and gravity fields are specified as well as the liquid heating rate, liquid outflow rate, and plane angle of the surface. For each site the x-y-z coordinates are required, the time that the site becomes active, and the size and frequency of bubbles generated as a function of time. A two-dimensional asymmetric time-dependent temperature field can be specified. The vessel geometry is specified by a radius-height table. Constants include the drag relation specifications, initial liquid conditions, bubble wake and impact parameters, as well as other program factors.

Operationally the program considers the time-dependent interactions of the bubbles with all others in the population in the three-dimensional environment representing the liquid. These interactions necessitate small time steps to model the discrete bubble interactions. The ability to consider 1000 bubbles from 100 sites produced as prescribed at time-dependent frequency adds to both versatility and complexity in the program. The consideration of wall or screen interactions in variable geometry asymmetric containers offers increased utility. Precise modeling results from the inclusion of surface tension forces due to temperature fields. Energy balances account for transport processes during bubble transient.

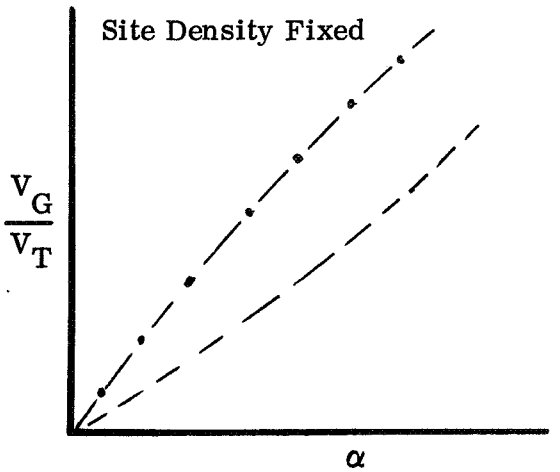
The computer simulation EVOLVE has been used for simulation of the laboratory experiment using Freon 11 as the liquid. It has previously been used for the sample case of the S-IVB at 3×10^{-4} g. Running times for the low-g level cases increase appreciably since the time for an equivalent number of bubbles to leave the system significantly increases. Typical computer time for a 150-second low-g problem with one site was 1/2 hour of CDC 6400. The program runs at one-tenth real time for a population of 10 to 20 bubbles.

APPLICATION TO LSS DESIGN STUDIES

Examples of the predictions of the macroscopic phenomena operating in bubble behavior which can be expected from the computer outputs are illustrated by figure 9. Additional predictions can be related to "microscopic" (implicit) phenomena correlation (e.g., bubble velocities, trajectories, and interactions) of a particular bubble. These outputs relate specifically to the "Nucleate Boiling" experimental test model (ref. 1) and thus served as a guide to test planning but, as with the analytical model, the test model has addressed itself to phenomena, the understanding of which is basic to the analysis and, thus, design of many LSS processes.

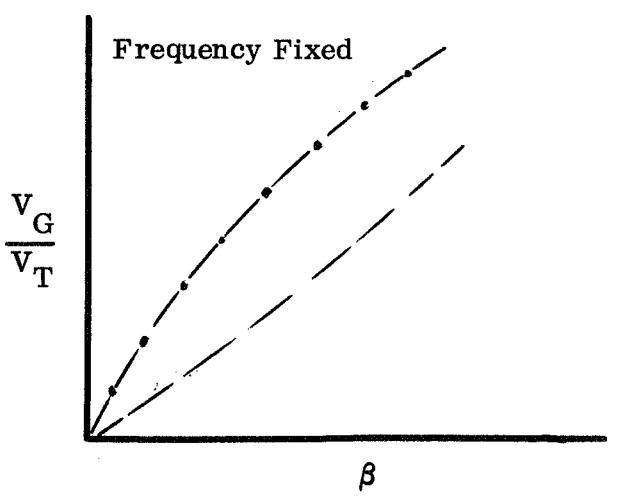


Example A. Transient Void Fraction $\frac{V_G}{V_T}$ versus Time (t)



Example B. Steady State Void Fraction versus Volume-Frequency Parameter (α)





Example C. Steady State Void Fraction versus Site Density-Volume Parameter (β)

Figure 9. - Typical Model Predictions

In spite of the fact that most designs attempt to avoid producing a multiphase fluid state flow whenever practicable because of problems inherent with its management under zero-g, there are many processes in the current and near-term future inventory which must accommodate phenomena in this category, either in their normal or degraded performance (failure) modes of operation. Examples of the existence of the phenomena explicitly or implicitly (dispersoid transport ~ bubble transport) treated by the analytical model can be found in the following applications:

	Operating Modes	
LSS Function	Normal	Degraded
Oxygen Supply	3*	4, 11, 12
CO_2 Removal	15, 17	18
O_2 Recovery		22, 23, 24, 27, 32
Water Reclamation	40, 47	38, 39, 41, 42, 43, 45
Waste Management	74	68
Urine Collection	78	79
Bathing	80, 81, 82	

*Note: Refers to LSS Inventory Reference Number serial numbers of the LSS Process Identification Sheet specifically identifying the application.

A specific example of the potential application of these phenomena can be given by an examination of design problems posed by the equipment concepts illustrated by the LSS/PIS equipment schematics for numbers 15 (Regenerable Sorption CO_2 Removal Unit) and 17 (Electrochemical CO_2 Scrubber). The design of item 15 must examine the method for steam generation (desorb cycle) and evaluate the applicability of the nucleate boiling mode, both as a primary mode and as an off-design contingency. The analysis would require that the designer be able to predict whether manageable bubble behavior could be anticipated or whether the behavior would approach a homogeneous frothing configuration throughout the pool. The design of item 17 must determine the behavior of the product gas entrained in the water (scrubber) loop. Item 40 employs nucleate boiling in the primary evaporation mode and thus is in direct correlation with both the analytical and experimental data. Introduction of air to and/or evolution of gases within the various storage tanks of the water management systems resulting either from normal or degraded performance, requires an understanding of bubble behavior to adequately provide for its management in the resulting designs.

Additionally, there are many elements of the study, both analytical and experimental, which have the potential of directly relating to phenomenological processes in other categories. One such process is that of separation of the liquid and gas phases. Unsymmetrical heating (an experimental requirement for this model) within the vessel can give rise to swirl patterns producing centrifugation and an accelerated bubble agglomeration, a major step in the inertial separation process.

EXPERIMENTAL EVALUATION

Requirements

An evaluation of the accuracy of the predictive aspects of the analytical model must include observations recorded against time, temperature, pressure and vessel orientation:

a. Bubble population and size versus number and patterns of active nucleation sites.

b. Bubble velocity variations for various wake conditions (generation frequencies).

c. Bubble path variations with respect to variations in active nucleation sites.

d. Agglomeration rate changes with variations in nucleation site patterns and bubble production rates.

To increase the effectiveness of the experimental observations, the experiment design criteria should include the following considerations:

a. Bubbles be of sufficient size that their shapes, volumes, and interactions effects can be realistically assessed by both direct observation and photographic examination.

b. Bubble generation frequency be controlled.

c. Bubble rise (liquid) column height be such that the full scope of their interactions phenomena can be attained.

d. Vessel to bubble(s) diameter ratio be such that bubble rise dynamics produce minimal disturbance in the overall pool volume.

e. A liquid be used which minimizes the heat input requirements, thus minimizing temperature gradients within the pool.

These criteria are intended in part to provide high visualization of the phenomena under study, and in part to more nearly approximate bubble behavior in the prevalent LSS liquids (most often water) under reduced-gravity conditions.

Description of the Experiment

Major Goals

Primary. — To determine if the analytical predictions satisfactorily approximate the actual behavior of the liquid/vapor interfaces in a boiling pool.

Secondary. — To add sufficient understanding of the actual behavior to correct and/or augment the analytical model as originally developed.

Tertiary. — To determine the differences between the behavior of bubbles formed by vaporization of the liquid medium and those formed by injection of a "noncondensable" gas.

Principal Observations

The patterns of behavior to be investigated and the characteristics to be experimentally assessed included:

a. The configurations and the velocities, both vertical and horizontal, of bubbles rising through a pool at a considerable distance from each other and from the wall of the container. Of particular interest were those bubbles large enough to be heavily distorted by the forces acting on them.

b. The effects of proximity and bubble wakes on the configurations and velocities of bubbles rising with small separations:

   1. Between bubble and wall.

   2. Vertically between bubbles.

   3. Horizontally between bubbles.

   4. Combinations of these.

c. The bubble population character with respect to:

   1. Number and volume.

   2. Effects on the large (top) liquid/vapor interface.

   3. Liquid circulation in the pool for the conditions under b.

d. The experimental variance, if any, which might be introduced by simulating bubble formation in the nucleate boiling process by controlled gas injection at the nucleation sites.

e. The effects of higher levels of inertial acceleration than those imposed on the initial laboratory experiments if such appears necessary and feasible as a result of the experimental evidence in the initial observations of a through d. (Such a requirement did not materialize.)

Test Apparatus

The concepts relative to test apparatus requirements as illustrated in ETP 1 were subsequently modified in response to interactions between the on-going maturation of the

analytical and accompanying test design studies. The apparatus used in this experiment is shown schematically by figures 10 and 11 and pictorially by figure 12. Typical bubble patterns are shown by figure 13.

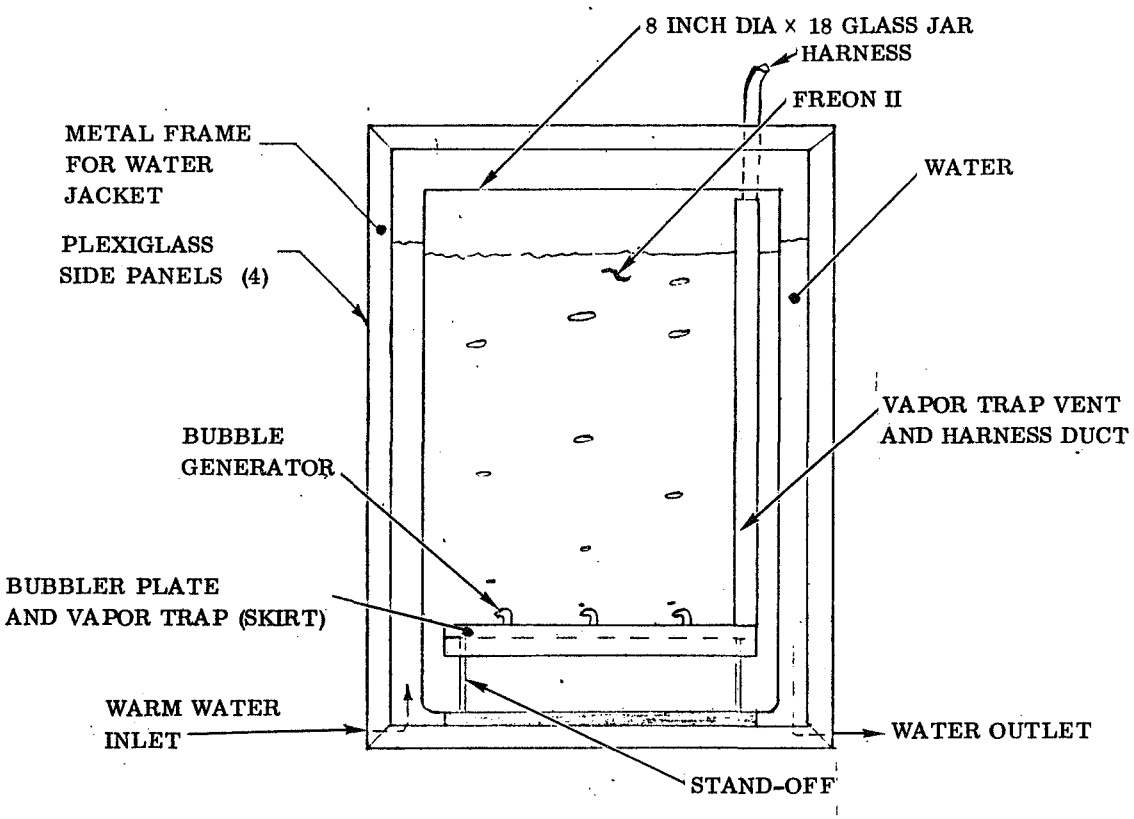
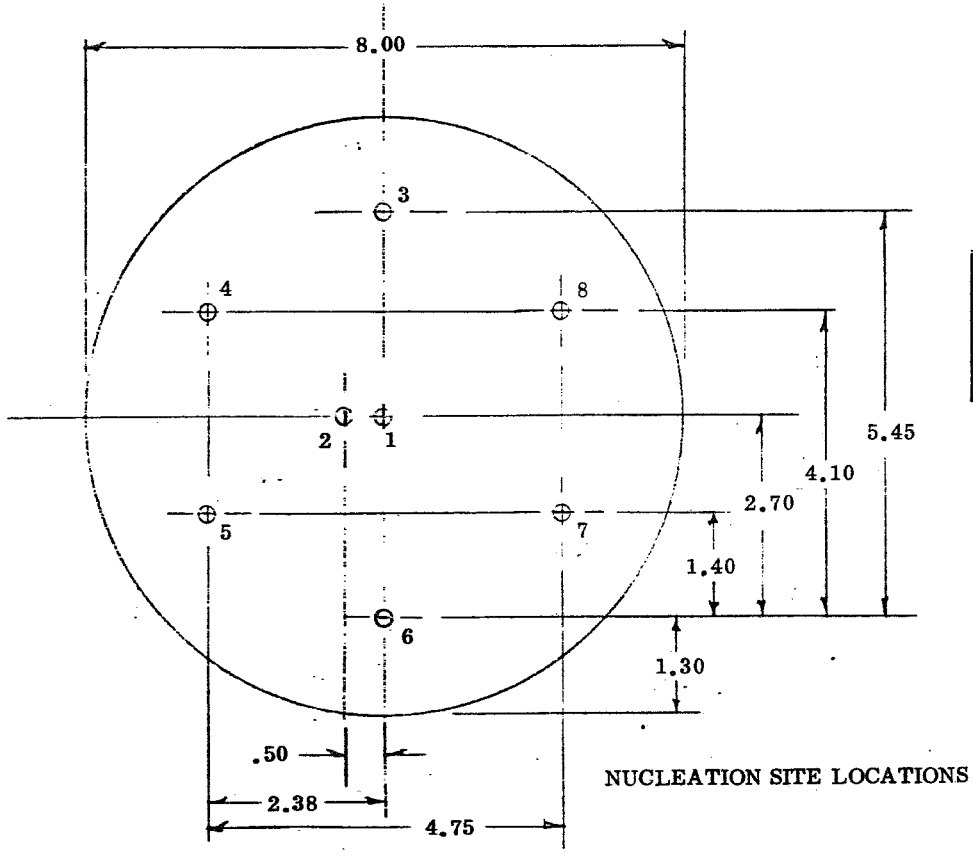
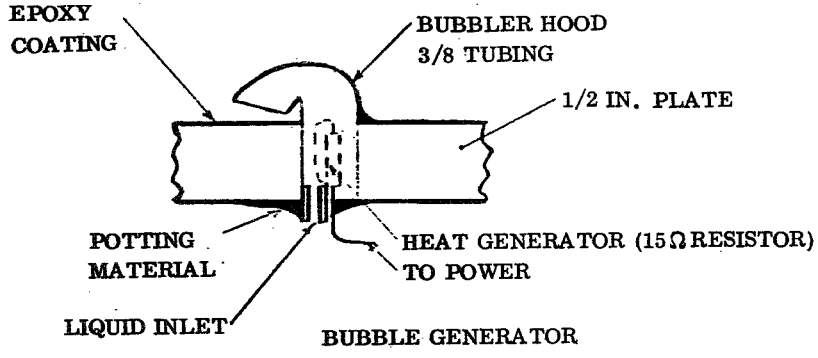


Figure 10. – Boiler and Water Jacket Assembly

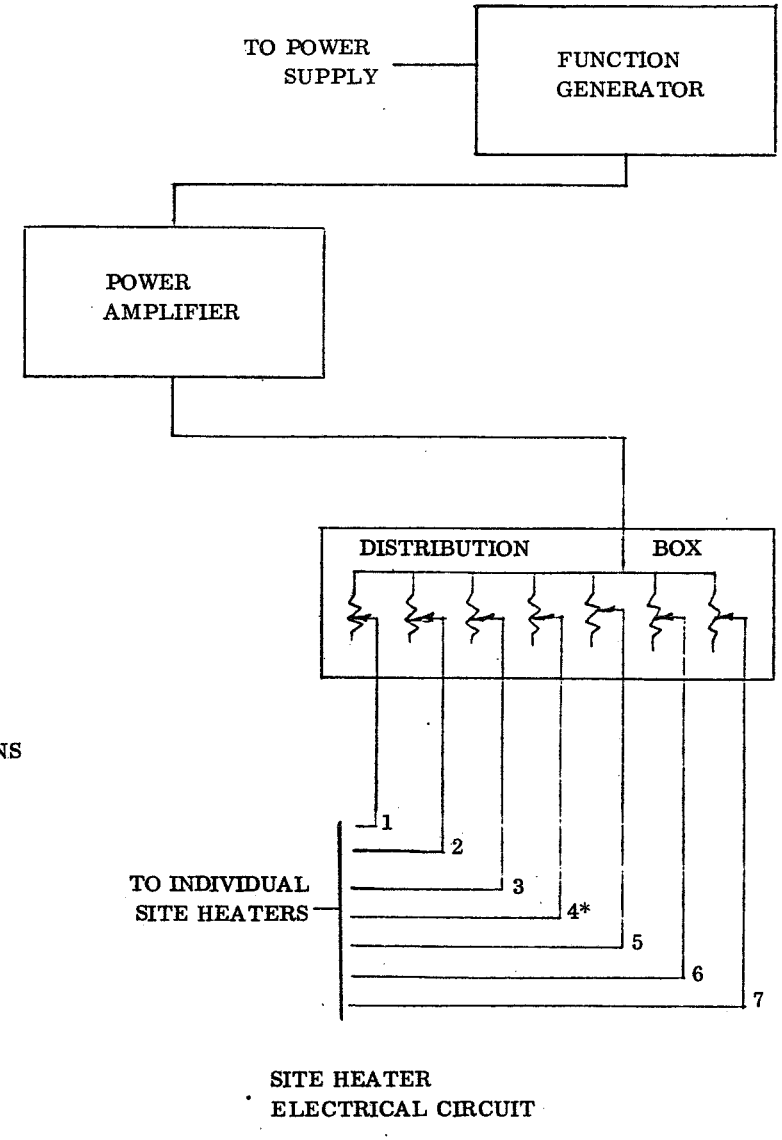
Water jacket and boiler assembly. — The boiler assembly was a standard laboratory cylindrical Pyrex jar approximately 8-1/4 inches in diameter and 18 inches high. The water jacket in which the boiler was installed served two basic functions. First, it provided a stable, uniform, controllable heat source for the boiler. Boiler fluid temperature was controllable within ±0.05°C with a top-to-bottom temperature difference of no more than 0.1°C with very low convective circulation present. Secondly, its rectangular cross section provided a means of reducing the problems of obtaining reliable photographic data by providing a flat plate surface at each of the four plexiglass side panels. The water jacket was approximately 12 by 12 by 20 inches, with the side panel frames constructed of 1-inch aluminum angle mounted on an aluminum sheet stock base approximately 1 inch thick. The latter was plumbed to provide for the controlled circulation of the heating water. Frame-to-panel and base sealing was accomplished by fabricated rubber gaskets augmented by a silicone RTV.



NUCLEATION SITE LOCATIONS



BUBBLE GENERATOR



SITE HEATER ELECTRICAL CIRCUIT

*Site No. 4 Operated as Noncondensable Gas Injector, Heater Element Not Installed.

Figure 11. – Nucleation Site Design

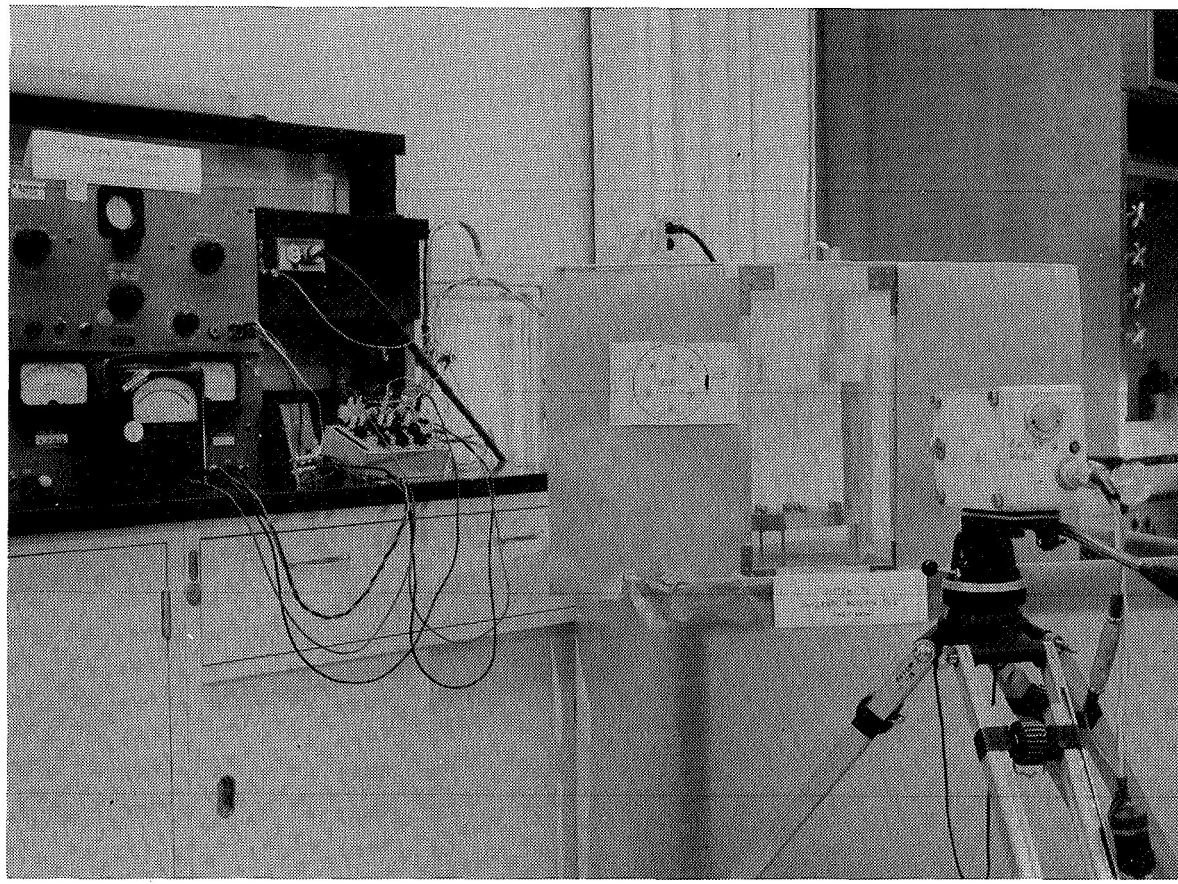


Figure 12. – Experimental Test 1 - Test Apparatus

Nucleation site assembly. — The nucleation site or bubble generator assembly included:

a. A circular base of aluminum sheet stock approximately 1/2-inch thick and 8 inches in diameter, the latter dimension allowing for clearance with the boiler wall.

b. A set of eight nucleation sites, seven of which incorporated an individually controlled resistance heater (15 ohm), with the remaining site plumbed for introduction of a gas from an external source (routed through the vapor vent tube).

c. A vapor vent system comprised of, 1) an aluminum strip extending around and protruding below the edge of the base, and 2) a metal vapor vent tube connecting the skirted area on the under side of the base to the atmosphere above the boiler pool.

d. A nucleation site heater harness which grouped the seven heater leads and provided routing through the vapor vent tube to the power source distribution box.

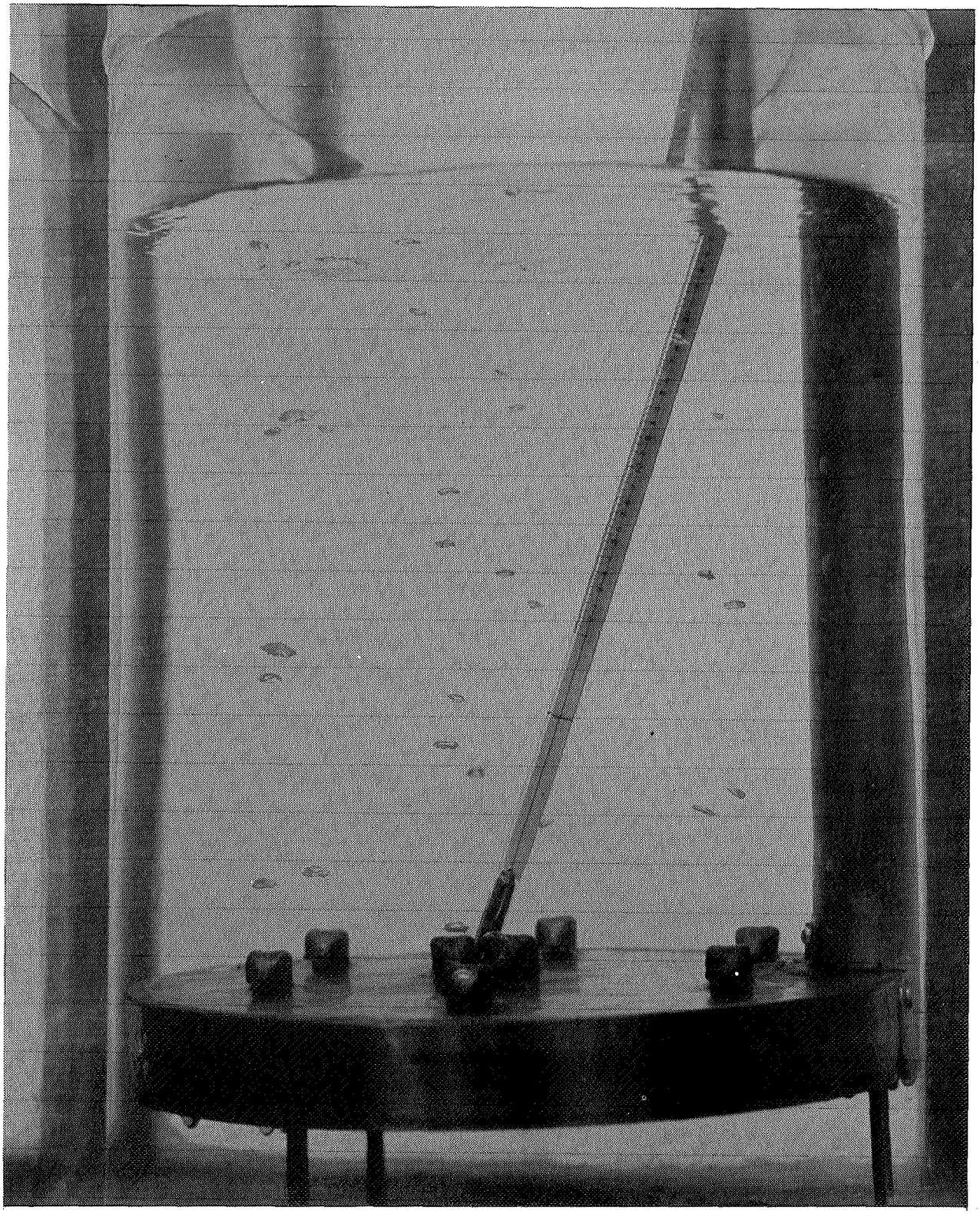


Figure 13. – Typical Bubble Patterns

Nucleation site heater control assembly. — The heater control assembly consisted of a distribution box, power amplifier, and function generator.

The distribution box included eight 25-ohm variable resistors and bayonet junctions for each heater lead. The power amplifier was an emitter-follower current amplifier incorporating a 30-Vdc regulated power supply. The function generator was a Hewlett-Packard 202A low-frequency function generator whose output had been modified with a half-wave rectifier.

Instrumentation. – Instrumentation for this experiment was not extensive and included:

a. Laboratory thermometer (mercury, 0 to 100°C, graduated 0.1°C).

b. High-speed movie camera (Milliken, DB-4 Pin Registered, 16mm) and film analyzer (Vanguard, M-16).

c. Scale:

   1. Copper screen 2 by 18 inches, 18 openings/inch.

   2. 18-inch steel drafting scale.

   3. Perforated metal, holes on 3/16-inch centers.

d. Mercury barometer.

e. Graduated cylinders, 10 and 25 ml.

f. Stopwatch.

Working fluid. – Freon 11 was chosen as the working fluid rather than the somewhat more attractive Freon 114 as initially intended, based principally on the fact that more complete characteristics data were available thus providing higher confidence computer inputs earlier in the schedule. It should be noted that conventional sealing materials such as the silicone RTV's are soluble in the Freon fluids; however, epoxy conformal coating, Convair Specification 0-73040-1 (Hysol Company, El Monte, California, PC12-007) was found satisfactory and was used throughout the nucleation site assembly both as a sealer and to provide smoother (increased radius) contours which minimize vapor traps and thus unwanted nucleation sites.

Test Procedures

The unpressurized boiler (pressurization was eliminated as it was considered marginally productive in view of its complexity) combined with the precise controllability of the pool temperature afforded by the water jacket assembly, greatly simplified

the test procedures. Test conditions were varied by changing any combination of the following experimental variables:

a. Pool height.

b. Pool temperature.

c. Sites active.

d. Heater current levels and pulse frequencies.

Still further simplification resulted from the decision not to conduct tests at g levels greater than unity. This decision came about as a result of continued consideration of its value against the early indications of the excellent results being obtained from the exploratory runs under 1g.

Twenty-five data recording test runs were designed in which one or more of the following experimental variables was altered for each run in the range indicated:

a. Fluid temperature (23.5 to 24.0° C).

b. Sites active (1 to 7 + 1, activation of the "noncondensable gas" site).

c. Liquid column height, above sites (7.9 to 8.5 inches).

d. Heater power (1.4 to 1.8 volts/site).

Chronology

Test equipment design, fabrication, exploratory tests, and equipment improvements were completed in the period 1 May to 1 July. Data runs were initiated on 8 July and completed on 17 July.

Test Data Summary

Test conditions data recorded against the 25 runs are summarized by table 6. The films for these and previous exploratory runs are identified as follows:

a. Photo Lab job number - 9078MP.

b. Photo Lab job title - Nucleate Boiling.

c. Photo Lab vault location - E-3-56.

d. Photo Lab job date - 6/12/69.

e. Individual reel numbers and information content.

Table 6. – Test Conditions Data - Experimental Test No. 1

Run	Pool Temp. (°C)	Clock Time	Active Sites	Liquid Height Above Plate (Inches)	Heater Power (Volts)	Vapor Vol.(Ml)	Collection Time(Sec.)	Bubble Frequency (No./sec)	Remarks
									8 July
1	23.9	1100	1	8.7	1.75			1	
2	23.9	1112	1	8.7	2.75			3	
3	23.9	1115	1	8.7	3.20			5	
4	23.8	1120	1	8.7	4.80			~11	
5	23.8	1122	1&2	8.7	1.82,1.72				
6	23.9	1126	1&2	8.7	2.74,2.65				
7	23.9	1130	1&2	8.6	3.50,3.40				
8	23.7	1140	3-8	8.6	2.04,2.02,2.02, 2.04,2.02				#4 = Air
9A	23.7	1142	3-8	8.6	2.04,2.02,2.02, 2.04,2.02				#4 = Air
9	23.7	1145	3-8	8.6	2.90,2.90,2.87, 2.90,2.90				#4 = Air
10	23.6	1145	3-8	8.6	4.78,4.78,4.78, 4.78,4.78				#4 = Air
11	23.6	1150	4	8.5	--				
12	23.6	1151	4	8.5	--				
13	23.6	1152	4	8.5	--				
14	23.6	1155	1-8	8.5	4.02 → 4.05				
									17 July
15	23.7	0920	1	8.5	1.41	0.9	82.3	0.121	10 bubbles
						1.3	89.5	0.112	10 "
						1.4	94.8	0.105	10 "
						0.9	98.2	0.102	10 "
15A	24.0		1	8.5	1.41				
16	23.6	1010	1	8.5	1.41			0.167	Lighting heat errors

Table 6. – Test Conditions Data - Experimental Test No. 1 (Cont.)

Run	Pool Temp. (°C)	Clock Time	Active Sites	Liquid Height Above Plate (Inches)	Heater Power (Volts)	Vapor Vol.(Ml)	Collection Time(Sec.)	Bubble Frequency (No./sec)	Remarks
17	23.6	1011	1	8.5	1.41			0.333	Lighting heat errors
18	23.8	1028	1	8.4	1.41			0.200	" " "
19	23.8	1029	1	8.4	1.41			0.200	" " "
20	23.6	1047	2	8.4	1.76			>Site #1	" " "
20A	23.6	1047	2	8.4	1.76	0.7	39.8	0.250	10 bubbles
	23.6	1047	2	8.4	1.76	0.7	41.8	0.240	10 "
	23.6	1047	2	8.4	1.76	0.6	53.5	0.187	10 "
21	23.5	1055	2	8.3	2.75	25.0	--		See film for time
22	23.5	1057	2	8.3	2.75	10.0	--		" "
23	23.5	1115	2	8.3	2.75				Velocity study
24	23.6	1118	2	8.2	2.75	4.0	20.8		See film for bubbles
25	23.9	1125	2	8.2	1.4			0.40	
--	23.9	1130	2	8.2	1.4				Calibration run

Constants:

1) Barometric pressure: Runs 1 - 14 @ 29.54, Runs 15 - 25 @ 29.55.

2) Camera location: 36" water jacket face-to-film plane, 1" focal length.

3) Calibration scale: a) 18" drafting ruler
   b) 11.25" with holes on 3/16" centers, perforated metal
   c) Screen mesh, 18 openings per inch @ 3/64" x 3/64" openings.

4) Camera speed: 200 fps @ 1/500 except runs 22 and 24 at 64 fps.

5) Heater resistance (Ω): #1 = 15.2, #2 = 16, #3 = 16, (#4 N/A), #5 = 15.4, #6 = 15.6, #7 = 15.6, #8 = 15.3 (all values include 0.4 Ω lead resistance).

Reel # 1. 6/16/69 - Preliminary investigations - system characteristics.

Reel # 2. 6/19/69 - Preliminary investigations - boiling phenomena.

Reel # 3. 6/19/69 - Preliminary investigations - miscellaneous.

Reel # 4. 7/8/69 - Test data runs 1 to 14.

Reel # 4a. 7/8/69 - Test data runs 1 to 14.

Reel # 5. 7/17/69 - Test data runs 15 to 25.

Reel 2 shows several cases of boiling phenomena in a superheated pool. The boiling is shown originating at the end of a glass rod inserted into the pool where temperatures ranged from 0.4 to 1.7° C in the superheat region. A small bubble initiated in this manner at the bottom of the boiler developed and fractured with almost explosive quality as the vapor mass rose through the pool. Development of such a superheat in a "clean" container was thus shown to be both possible and potentially useful or damaging depending on the circumstances.

Critique of the Test Design

In general, the test was very satisfactory and can be recommended as a guide to future test designs in the area of bubble-behavior studies. However, several pros and cons of the major elements of the test design are worth discussing.

Instrumentation

The concept of reproducing the image of the bubble behavior on high-speed motion-picture film and subsequently obtaining measurements data directly from the films greatly simplified the design of the test apparatus, particularly its instrumentation and the execution of the test. However, unless at least two synchronized cameras (90 degrees apart) or an equivalent are employed, problems are introduced in estimating the fully developed, three-dimensional characteristic of the behavior. Additionally, a significant probability of measurements data inaccuracies relative to the dynamic aspects of the bubble behavior is introduced by the refractive characteristics of the liquid and the boiler walls combined with the view angle error produced by the length of the vertical path through which the bubble moves. However, with adequate reference scales designed into the boiler, the magnitude of the measurements errors can be greatly reduced and maintained well within the accuracy requirements of the experiment.

Care should be taken to minimize the unwanted boiler heating which can be produced by the flood lighting required by the photography. Low-heat-producing lighting should be used wherever possible.

Problems were experienced in arriving at consistent estimates of bubble volume through film analysis. This was mainly due to the rolling oscillations of the spherical-cap bubbles in their rise through the pool. To overcome this difficulty, direct measurements of bubble volume were taken by inverting a temperature-stabilized 10-ml graduate in the path of a column of rising bubbles and averaging the resulting vapor void volume over the number of bubbles "captured."

Process Apparatus

The nucleation site and heater input control assemblies were satisfactory and would be considered for any future laboratory testing. No problems other than those related to sealant compatibility were experienced with the choice of Freon 11.

Procedures

Care needs to be taken to assure that the fluid is essentially free of contaminants to avoid producing bubble behavior which is not characteristic. Ten to 15 minutes of gentle boiling was found sufficient to produce a steady-state boiling characteristic as a result of vaporizing the fluid contaminants present following a boiler refill. It is advisable not to return the boiler fluid to the new-fluid-supply vessel, although it can be stored in a separate vessel and reused as determined satisfactory.

Correlation of Analytical and Experimental Data

Data evaluation and correlation were accommodated by program EVOLVE. A set of observables was established prior to the experiment which represented the physical characteristics of the experiment and which were included in the program. Bubble velocity, production frequency, volume, and agglomeration were required. In addition, qualitative evaluation of the effects of electrical power input, condensable or noncondensable wall proximity, and pool turbulence was observed.

The experimental objectives which were derived from the previously mentioned observables were defined a priori and included various particularized parametric investigations; these were the magnitude and character of the bubble wake, the merit of existing drag coefficient data, and agglomeration evaluation. Such parameters represent the "micro" structure of the physical problem of bubble population evolution.

Velocity Observations

Bubble velocities were determined using the Vanguard M-16 film analyser. Figure 14 illustrates this technique. The spatial history of a bubble from evolution until breaking the surface can be traced. The time derivative results in bubble velocities. Results for bubble velocities were sufficiently reproducible to support the analytical investigation.

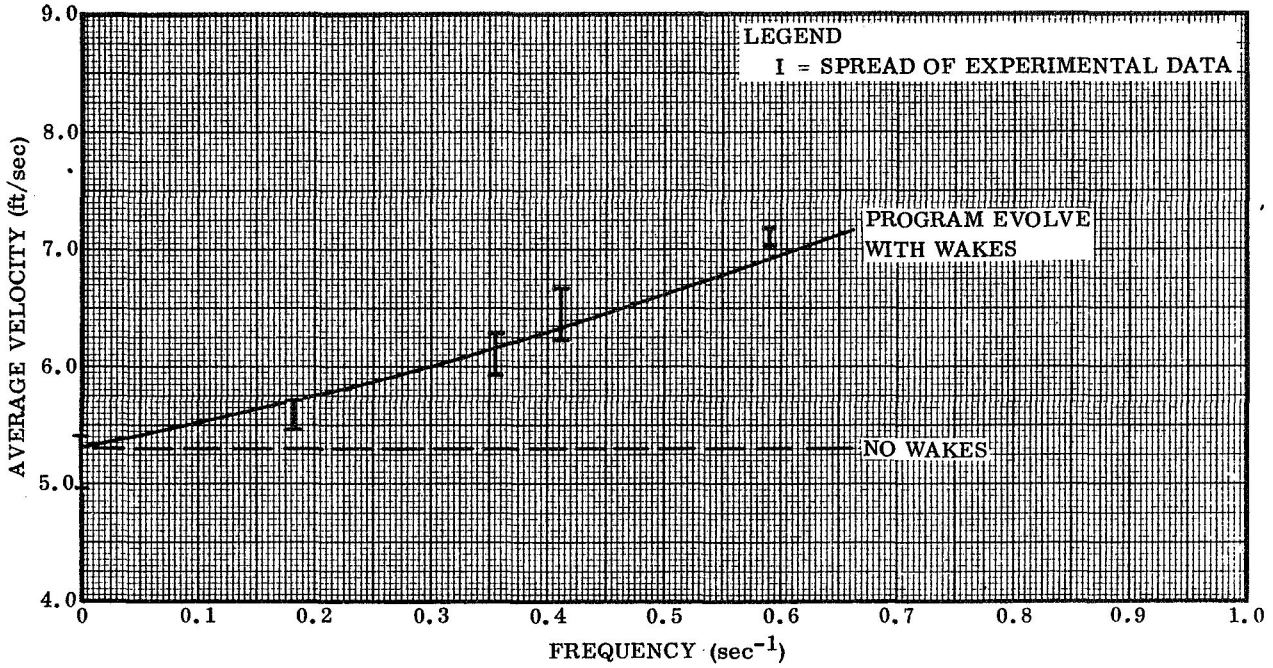


Figure 14. — Predicted Versus Experimental Data - Effect of Wakes

Bubbles originating from a single site at various frequencies formed the data spectrum. Tests 1 through 4 provided frequency data in the 1.85 to 12.2 sec^{-1} range. To establish a responsible representation of data, several bubble-velocity measurements were taken for each test run. A particular measurement is the average of the individual bubble's velocity during its total traverse to the surface. Data scatter is illustrated in figure 14 as a bracket relative to the predicted value from EVOLVE. No attempt was made to establish statistical averages and deviations since the total sampling was small (<10 per frequency). Each film evaluation is extremely time consuming.

Velocity was a monatonically increasing function of frequency up to the point of agglomeration. The velocity range, 0.5 to 0.75 ft/sec, is illustrated. If the liquid medium were an ideal fluid, no viscosity, the bubble velocity would be independent of frequency. The strong velocity dependence is due to the viscous nature of the liquid, i.e., the wake effect.

In the velocity correlation using program EVOLVE, it was discovered that the initial drag coefficient specification was not appropriate. A reinvestigation of the current literature supported this presumption and resulted in the new drag coefficient definitions previously discussed under Single-Bubble Dynamics. The transition region was not adequately considered in a reference previously used and an empirical fit to data in ref. 5 was developed. The result was excellent correlation with the experimental data obtained in the Freon 11 test. Correlations for the situations of wake and no-wake effects are illustrated. Figures 15 and 16 show the wake velocity with experiment correlation. This obviously important aspect of group bubble motion has not been considered in the past.

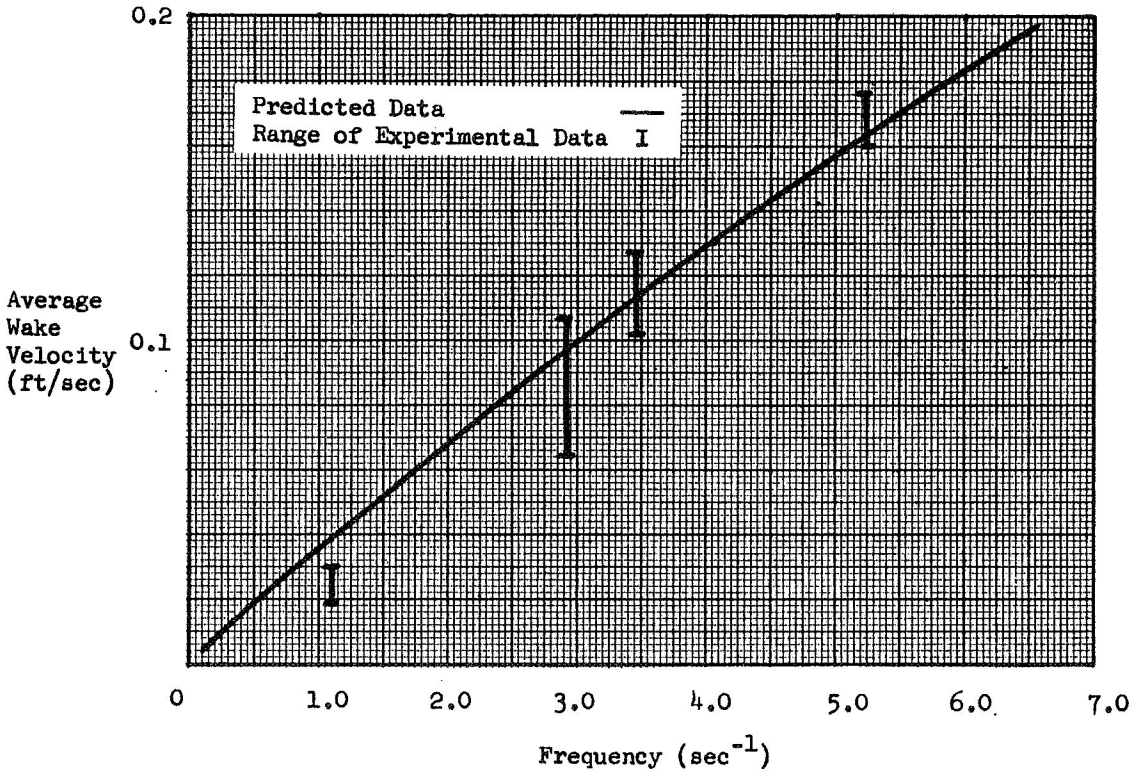


Figure 15. — Predicted Versus Experimental Data — Velocity Versus Frequency Under 1g

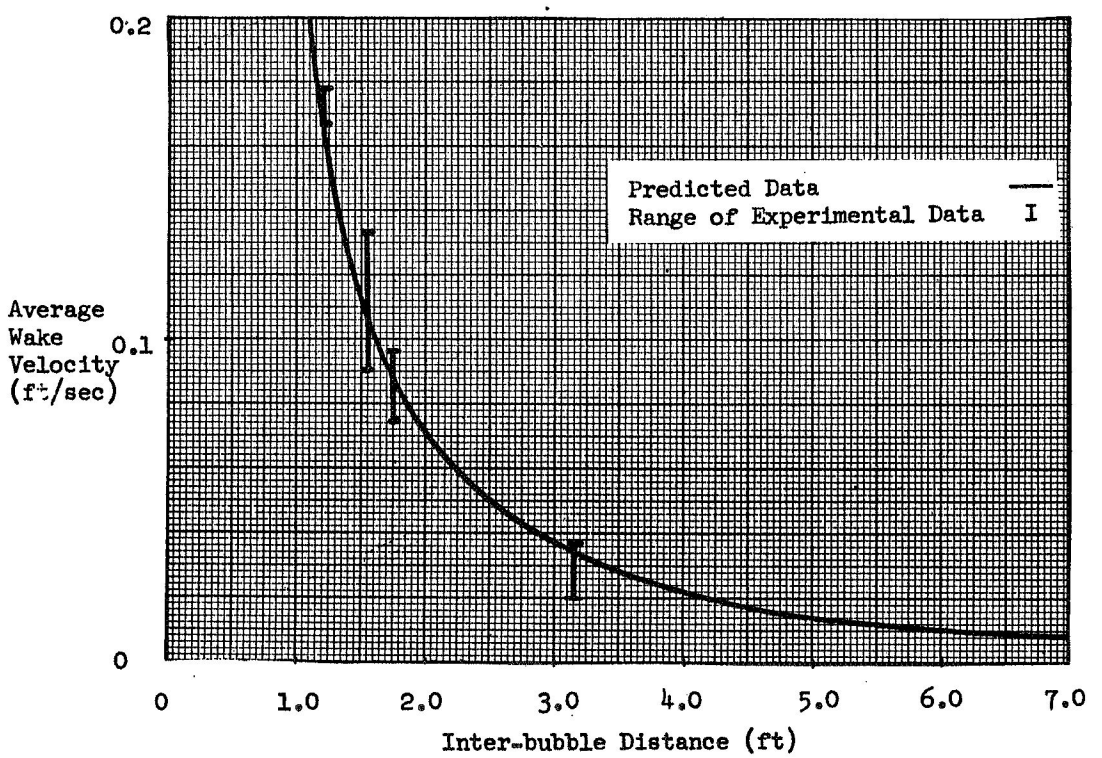


Figure 16. — Predicted Versus Experimental Data — Velocity Versus Separation Distance Under 1g

The frequency coordinate is a measure of the interbubble distance ($\sim\frac{\text{average velocity}}{\text{frequency}}$). Figure 16 illustrates the strong change in wake velocity with interbubble distance. The cutoff at frequency of about 0.6 corresponds to a height of about 0.8 feet which was the liquid level above the bubble generator; below the cutoff only a single bubble existed in the pool at any time. Frequencies above 7 sec^{-1} resulted in agglomeration.

Frequency Observations

Bubble-production frequency was also established using the film analyzer. Several production periods were used in obtaining the final value for each run. The frequency was remarkably constant for the total run time. Correlation of frequency versus electrical power input was excellent except for low frequencies (<1 sec^{-1}) as is illustrated in figure 17.

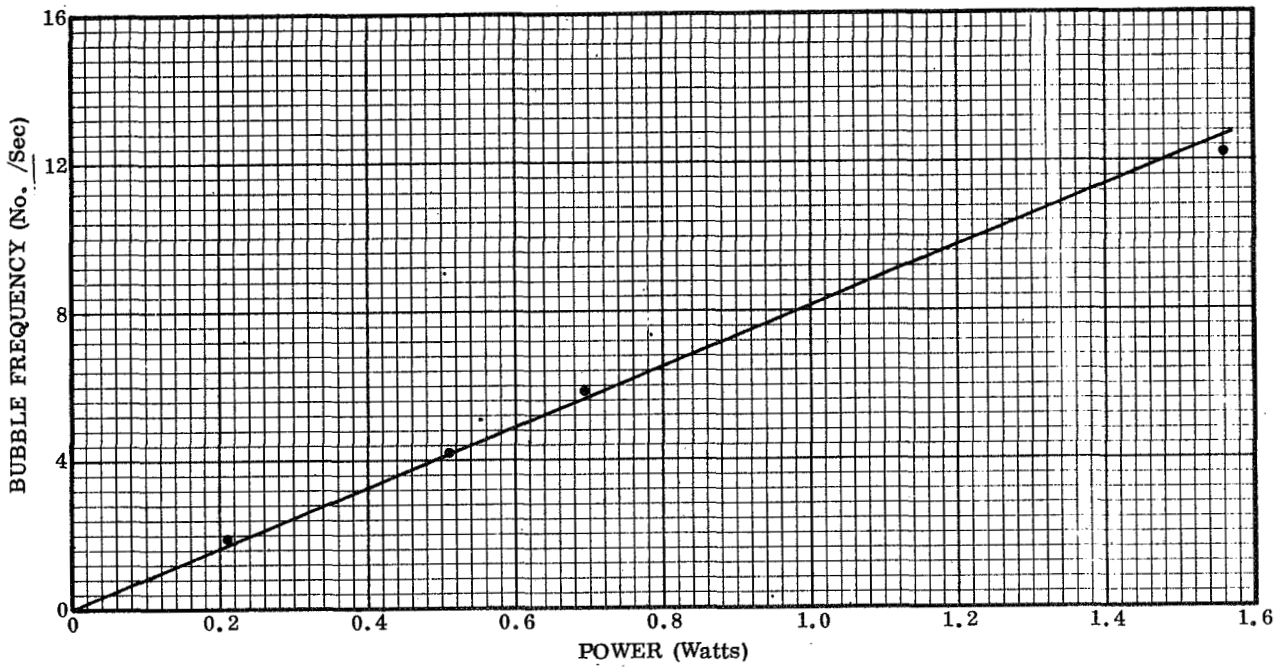


Figure 17. — Bubble Frequency Versus Power Input

Bubble-Volume Observations

Bubble-volume measurement was a difficult and critical item to obtain. The effective diameter of the bubble is an important parameter entering into all dynamic calculations. Therefore, three distinct methods were used: electrical power dissipation (carbon resistor element), film analysis, and bubble collection.

The first method appeared to be useful after observing the reasonable frequency/power correlation. However, at low frequencies the relationship deteriorates, and it

did not agree with other more reliable measurements. The effective diameter was 0.0197 feet.

The second method, better than the first, was tedious and suffered from two major anachronisms. The bubbles were not spheres and, therefore, had multiple dimensions; the resolution of the photography at that level was in doubt. Table 7 illustrates the variations obtained with this method. Also, it is evident that only two-place accuracy is available (from columns 2 and 3). The range in effective diameter was 0.0113 to 0.0196 feet.

The third method was chosen to determine the bubble volume, crude in nature but totally reliable. Separate samples of 106 and 66 bubbles collected in an inverted 10-ml graduated cylinder yielded identical results of 0.0158-foot effective diameter. The rapid evolution rate required the sample size to be determined from film data. This result was used as input to EVOLVE.

Table 7. — Bubble Volume Calculations from Photographic Data

Desig.	Height Units	Width Units	Volume cu.ft. x 10^6	Diameter feet
1-1	37	79	1.29	.0135
1-1A	33	70	.99	.0124
1-2	41	68	1.24	.0133
1-2A	26	90	1.29	.0135
1-3	57	103	3.72	.0192
1-3A	33	140	3.97	.0196
3-1	36	89	1.76	.0150
3-2	26	68	.75	.0113
3-3	34	88	1.61	.0145
3-4	39	78	1.46	.0141
3-4A	34	90	1.69	.0148
3-5	36	71	1.11	.0128
3-5A	27	74	.91	.0120
3-6	23	84	1.06	.0126

Notes: 1. 1 and 1A, et cetera, are same bubble at two times.

2. Three bubbles were observed at one frame in Run 1, six in Run 3.

3. 100 units = .0245 feet.

Agglomeration Observations

Agglomeration was investigated by activating two sites, 1/2 inch apart, at slightly different frequencies. The effects of the two-dimensional character of the bubble wake were thusly observed. Film analysis of Run 5 provided the single-event data for program correlation. The two columns of bubbles were in a steady-flow configuration with a relative distance phase between columns. The sequence of agglomeration is illustrated with two selected frames from Run 5, figure 18. The lead bubble is in advance of the trailing second column bubble by 0.135 second, the two moving at 0.530 ft/sec and 0.643 ft/sec respectively. After 0.74 second, the agglomeration occurs.

The program simulation gave a velocity range of 0.533 ft/sec to 0.644 ft/sec for leading and trailing bubbles. An agglomeration did not occur for direct simulation; however, the two bubbles came within a bubble diameter of each other. Applying a flattening correction to simulate actual deformed bubble geometry causes an agglomeration to occur since the bubbles are not spherical. Flattening and slight bubble trajectory oscillations enhance the agglomeration process. Program EVOLVE accommodates this correction in the impact parameter input.

Experimental evidence and visual observation support the program model for agglomeration and the two-dimensional nature of the bubble wake; e.g., it is observed that the trailing bubble moves into the shadow of the wake and accelerates toward the lead bubble resulting in coalescence. (Reference film record of Run 5.)

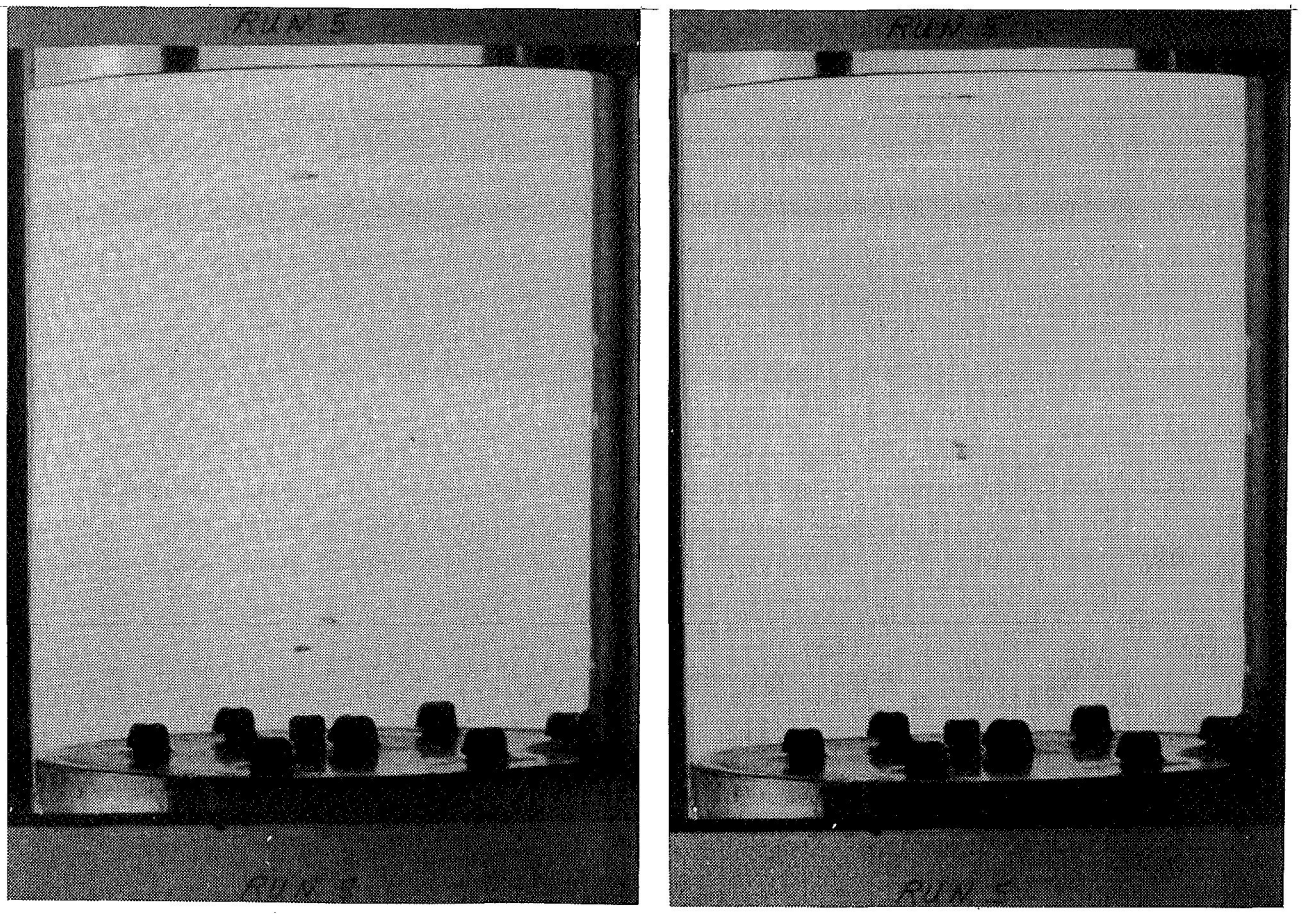
Qualitative Observations

Various qualitative observations were noted during experimental operation. The phenomena provide possible areas for future investigation but were not within the scope of the present study.

The condensable/noncondensable relation was modeled by a single air-injected site. It was not possible to obtain bubble sizes comparable to the condensable site generation; the noncondensable air site provided larger bubbles. Therefore, a velocity comparison was not possible.

Activating all sites at high frequencies developed major convection paths in the liquid and increased turbulence levels. Turbulence affected the individual bubble stability, tending to fraction and mutate the larger bubbles. The large convection modes disturbed bubble motions in the vicinity of the container wall. The indication is that for active pool populations, liquid velocity fields should be considered and an input to EVOLVE is currently available for these data.

No bubble adherence to the wall was observed and bubbles appeared to be unaffected by wall proximity except in the large convection situation.



Frame A Frame B

Frame A shows two bubbles rising from adjacent sites. Frame B illustrates the effect of the lead bubble wake on the rise path of the second bubble, subsequently resulting in agglomeration.

Figure 18. — Photographic Data - Measurement of Wake Effect

Conclusions which can be drawn from the correlation of predictive and experimental data include (see ref. 10):

a. Program EVOLVE provided excellent data correlation and contains the physical essentials necessary to model the process.

b. An adequate drag model has been incorporated in EVOLVE; however, additional correlation with various fluids is warranted.

c. The inclusion of wake consideration is necessary and quite important; the EVOLVE wake model gives excellent correlation.

d. Agglomeration and two-dimensional aspects of wakes are significant; the EVOLVE program provides excellent correlation and description.

e. Additional work is required in investigating the condensable/noncondensable problem and large convection-motion fields.

f. Low-gravity testing is absolutely necessary to provide general technical confidence in the applicability of existing dynamic data, e.g., drag coefficient. Program EVOLVE provides an immediate and capable instrument for data correlation of low-g experiments.

REFERENCES

1. Anon.: Experimental Test Plan — NAS1-8494, Test No. 1, Nucleate Boiling. Convair division of General Dynamics, 15 April 1969.

2. Landau, L.D.; Lifshitz, E. M.: Fluid Mechanics. Addison Wesley, 1959.

3. Aris, R.: Vectors, Tensors and the Basic Equations of Fluid Mechanics. Prentice-Hall, Inc., 1962.

4. Peebles, F. N.; Farber, J. H.: Studies on Motion of Gas Bubbles in Liquids. Chemical Engineering Progress, vol. 49, no. 2, February 1953.

5. Harmathy, T. Z.: Velocity of Large Drops and Bubbles in Media of Infinite or Restricted Extent. A.I.Ch.E. Journal, vol. 6, no. 2, June 1960.

6. Swain, L. M.: On the Turbulent Wake Behind a Body of Revolution. Proc. Royal Society London, series A, vol. 125, 1929, p. 647.

7. Schlichting, H.: Boundary Layer Theory. McGraw-Hill, Inc., 1960.

8. Gibson, C. H.; Chen, C. C.; Lin, S. C.: Measurements of Turbulent Velocity and Temperature Fluctuations in the Wake of a Sphere. Journal of AIAA, vol. 6, no. 4, April 1968, p. 642.

9. Anon.: Temporal and Spatial Evolution of Bubble Distribution in Low-Gravity Environments. GDC-ERR-1333, Convair division of General Dynamics, section 3.

10. Evans, E.; Bradshaw, R.; Burnett, J.: Analytical Model Report No. 1, Nucleate Boiling. Second issue, February 1970.

ANALYTICAL MODEL NO. 2 — "DIFFUSION CONVECTION"

An analytical model has been developed which describes the phenomenological behavior which characterizes a process stream in which diffusive and convective mechanisms dominate a humidification/dehumidification process. The model considers the effects on the predicted "performance" resulting from variations in such parameters as:

a. Gravitational field.

b. Concentration field.

c. Velocity field.

d. Diffusion coefficient for the vapor present.

e. Temperature.

f. Physical dimensions of the system.

Solutions for two conditions are presented, one where the concentration varies over a small portion of the channel width (herein called Case 1) and another where the concentration varies over a large portion of the channel width (herein called Case 2). Case 1 utilizes a similarity solution to incorporate velocity variations and is appropriate only to boundary layer changes, e.g., systems with very low efficiencies, $\left(\frac{C_{initial} - C_{final}}{C_{initial} - C_{surface}}\right)$. Case 2 employs separation of variables and an eigenvalue solution series to give a description of major concentration variations and to cover the total efficiency spectrum. Additionally a discussion is presented of closely related phenomena involving gravitational effects on dispersoid or suspension flows, e.g., water droplets in air, carbon particles in air.

The model is so designed as to be of potential value in the analytical phases of the design of LSS equipments which either directly involve or interface with the humidification/dehumidification process. In one form or another the humidification/dehumidification process is the most prevalent of all processes in the current and near-term LSS designs. Prior analyses have shown that the process appears at least once in more than 50% of the LSS equipments involved. In addition, principally due to the inherent existence of the liquid/gas interface accompanying this process, it has proven to be one of the most difficult to manage in the "absence" of a significant (resultant) gravitational field typical of the major portion of the flight regime for manned spacecraft.

Table 8 gives the nomenclature with subscripts for the diffusion-convection calculations.

Table 8. — Nomenclature for Diffusion-Convection Calculations

NOMENCLATURE

K	Boltzmann constant
h	channel height
c	concentration field
ρ	density
D	diffusion coefficient
x	direction normal to flow
y	flow direction
ℓ	length in flow direction
g	magnitude of inertial acceleration
p	pressure
T	temperature
v	velocity of bulk flow field

SUBSCRIPTS

E	exit
o	initial
w	surface or wall

DESCRIPTION OF THE MODEL

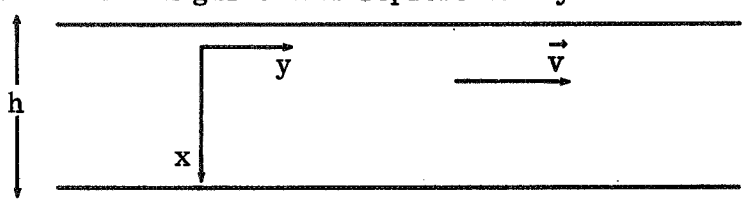
The two-dimensional humidification/dehumidification problem is a balance of diffusive and convective mechanisms. Many effects complicate the attempt at an analytical solution: turbulence, multicomponent diffusion, multiprocess diffusion (thermal diffusion), and gravitational separation. In turbulent flow, normal diffusion no longer exists and turbulent (eddy) diffusion occurs. Multicomponent diffusion is considered when the components have concentrations of the same order of magnitude. Thermal diffusion is important only for very large temperature differences as the coefficient for gases is about two orders smaller than the molecular diffusion coefficient alone. Gravitational separation is related to the ratio of gravitational potential energy to kinetic energy of the gas, $(\Delta\rho)g/KT$.

For life support systems, single components may be considered (concentration of water vapor <10%); also, laminar flow is usually present. Temperature gradient and magnitude are such that thermal diffusion and concentration stratification are negligible. The major gravitation effect for diffusing gas systems is the onset of turbulent instability due to adverse temperature gradients. The forced-to-free convection transition is treated in AMR No. 5 and is applicable to the problem being considered here. The secondary problem of separation is not important for air/water-vapor mixtures, but is of interest when droplets are present. A subsequent section titled GENERAL INFLUENCE OF INERTIAL FIELDS contains an analytical discussion concerning suspension flows and explicitly incorporates inertial field effects.

Diffusion in a convective medium is given by

$$D\nabla^2 c = (\vec{v} \cdot \nabla)c \tag{1}$$

The two-dimensional configuration is represented by



Equation (1) becomes,

$$D\left(\frac{\partial^2 c}{\partial x^2} + \frac{\partial^2 c}{\partial y^2}\right) = v(x)\,\frac{\partial c}{\partial y} \tag{2}$$

In most situations, co-current and counter-current diffusion may be neglected; this is determined by

$$\frac{D}{\ell v} \ll 1$$

where

$\ell \equiv$ characteristic length in y direction.

The diffusion coefficient for water vapor in air is given by, (ref. 1)

$$D = 4.4 \times 10^{-7} \left(\frac{T^{2.334}}{p}\right) \text{cm}^2/\text{s}$$

where the temperature is in °K and pressure in atmospheres.

Equation (2) reduces to,

$$D \frac{\partial^2 c}{\partial x^2} = v(x) \frac{\partial c}{\partial y} \tag{3}$$

Solution to equation (3) for a semi-infinite medium can be obtained by similarity methods (ref. 1) with the convective velocity a function of x; this approach is reasonable when the concentration gradient occurs over a dimension which is small with respect to the channel width, h (Case 1), i.e., boundary layer diffusion.

Define a new variable, η, and dependent variable, $f(\eta)$, such that,

$$\frac{C - C_w}{C_o - C_w} \equiv f(\eta) \tag{4}$$

$$\eta \equiv \beta^{1/3} x y^{-1/3} \tag{5}$$

$C_w \equiv$ concentration at wall

$C_o \equiv$ initial stream concentration

$v(x) \equiv$ a x linear velocity distribution (next to wall).

Equation (4) satisfies equation (3),

$$\frac{\partial^2 f}{\partial x^2} = \frac{v(x)}{D} \frac{\partial f}{\partial y}$$

$$\frac{d^2 f}{d\eta^2} \left(\frac{\partial \eta}{\partial x}\right)^2 = \frac{ax}{D} \frac{df}{d\eta} \frac{\partial \eta}{\partial y} \tag{6}$$

Equations (5) and (6) combine to give,

$$\frac{d^2 f}{d\eta^2} + 3 \eta^2 \frac{df}{d\eta} = 0 \tag{7}$$

$$\beta = \frac{a}{9D} \tag{8}$$

The boundary conditions are,

$$f(\infty) = 1 \text{ at } \eta = \infty$$

$$f(0) = 0 \text{ at } \eta = 0$$

$$\frac{C - C_w}{C_o - C_w} = \frac{\int_0^{\eta} e^{-\tau^3} d\tau}{\int_0^{\infty} e^{-\tau^3} d\tau}$$

The mass flow rate for the entire surface is given by,

$$\dot{M} = +\rho D B \int_0^L \left(\frac{\partial c}{\partial x}\right)_{x=0} dy$$

$$\dot{M} = 1.68D (C_o - C_w) (BL)\rho \left(\frac{a}{9 DL}\right)^{1/3} \tag{9}$$

where

B ≡ depth of surface

L ≡ length of surface

$a = \frac{-h}{2\mu} \frac{dP}{dy}$ for laminar flow (fully developed) between parallel plates

μ ≡ viscosity

$\frac{dP}{dy}$ ≡ pressure gradient

For general $v = ax^n$, equation (7) holds with

$$\eta = (\beta)^{1/m} (x)^{\frac{n+2}{m}} (y)^{-1/m}$$

$$\beta = \frac{a}{(n+2)^2 D}$$

The exponent $\left(\frac{1}{m}\right)$ is restricted by the existence of the first derivative of η with respect to x,

$$m = n+2$$

$$\frac{d^2f}{d\eta^2} + m\eta^{m-1}\frac{df}{d\eta} = 0 \tag{10}$$

The concentration field is given by,

$$C = \frac{(C_o - C_w)}{\Gamma\left(\frac{m+1}{m}\right)} \int_0^{\eta} e^{-\tau^m}\, d\tau + C_w \tag{11}$$

The surface mass flow rate is,

$$\dot{M} = \left(\frac{m+1}{m-1}\right) \frac{D(C_o - C_w)}{\Gamma\left(\frac{2m+1}{m}\right)} (BL)\,\rho \left(\frac{a}{m^2 DL}\right)^{1/m} \tag{12}$$

where

Γ ≡ gamma function

$$\Gamma(n) = \int_0^{\infty} x^{n-1} e^{-x}\, dx$$

The solution for Case 1 has limited applicability since it is appropriate only to very low efficiency situations. It was developed, however, to describe the boundary layer diffusion process.

For situations where the concentration varies over a major portion of the channel width (h), herein referred to as Case 2, equation (3) becomes a boundary value problem and is solved by separation of variables and an eigenfunction series in the eigenvalue λ_n

$$C = \sum_{n=0}^{\infty} e^{-\lambda_n y} A_n \Phi_n(x) \tag{13}$$

$$D\frac{d^2\Phi_n}{dx^2} + \lambda_n v(x)\,\Phi_n = 0 \tag{14}$$

with boundary conditions

$$y = 0 \quad C = C_o \quad h \le x < 0$$
$$C = C_w \quad x = 0$$
$$y \to \infty \quad C = C_w \quad h \le x \le 0$$

The second boundary condition implies

$$C = C_w + 2 \sum_{n=1}^{\infty} e^{-\lambda_n y} A_n \Phi_n(x) \tag{15}$$

The first boundary condition is represented by

$$C_o = C_w + 2 \sum_{n=1}^{\infty} A_n \Phi_n(x) \tag{16}$$

Equation (14) is readily solved only for $v(x) = v_o$, a constant. Functions $\Phi_n(x)$ are periodic about $x = 0$ with fundamental wave length $2h$.

$$\Phi_n(x) = \operatorname{Sin} \frac{n\pi x}{2h} \qquad n = 1, 3, 5 \ldots$$

Equation (14) implies,

$$\lambda_n = \frac{D\, n^2\, \pi^2}{4\, h^2\, v_o}$$

Using the orthonormality property of the sine function and equation (16), the following equation results

$$A_n = \frac{\int_0^h (C_o - C_w) \operatorname{Sin} \frac{n\pi x}{2h}\, dx}{\int_{-h}^{h} \operatorname{Sin}^2 \frac{n\pi x}{2h}\, dx}$$

$$A_n = \frac{2(C_o - C_w)}{n\pi} \left[1 - \operatorname{Cos} \frac{n\pi}{2}\right]$$

$$A_n = \frac{2(C_o - C_w)}{n\pi} \qquad n = 1,\ 3,\ 5,\ \ldots.$$

$$\frac{C(x,y) - C_w}{C_o - C_w} = \frac{4}{\pi} \sum_{n=1,\ 3,\ 5,\ \ldots}^{\infty} \frac{e^{-\frac{Dn^2\pi^2}{4h^2 v_o} y} \ \mathrm{Sin}\ \frac{n\pi x}{2h}}{n} \tag{17}$$

Mass flow rate is given by

$$\dot{M} = -\rho DB \int_0^L \left(\frac{\partial C}{\partial x}\right)_{x=0} dy$$

$$\frac{\partial C}{\partial x}\Big|_{x=0} = \frac{2(C_o - C_w)}{h} \sum_{n=1,\ 3,\ 5\ldots}^{\infty} e^{-\frac{Dn^2\pi^2 y}{4h^2 v_o}}$$

$$\dot{M} = 8\rho \frac{Bh\,(C_o - C_w) v_o}{\pi^2} \sum_{n=1,\ 3,\ 5\ldots}^{\infty} \frac{\left(1 - e^{-\frac{D\pi^2 n^2 L}{4h^2 v_o}}\right)}{n^2} \tag{18}$$

The average exit concentration is given by

$$\bar{C}_E = \frac{8}{\pi^2} (C_o - C_w) \sum_{n=1,\ 3,\ 5}^{\infty} \frac{e^{-\frac{Dn^2\pi^2 L}{4h^2 v_o}}}{n^2} + C_w \tag{19}$$

The efficiency is defined by

$$\epsilon = \frac{C_o - \bar{C}_E}{C_o - C_w} \left(\frac{C_{Initial} - C_{Final}}{C_{Initial} - C_{Surface}}\right)$$

$$\epsilon = 1 - \frac{8}{\pi^2} \sum_{n=1,3,5}^{\infty} \frac{e^{-\frac{Dn^2\pi^2 L}{4h^2 v_o}}}{n^2} \tag{20}$$

Equations (18) through (20) are solutions for equation (3) with constant velocity. A variable velocity profile, e.g., parabolic laminar, could be used with equation (3) to generate another solution set by using Green's function integral methods to solve the Sturm-Liouville system of equations; however, this is somewhat complicated and the test results indicate that this correction is not required.

THE COMPUTER PROGRAM

A computer program has been developed to provide a tool for economical execution of the computational tasks associated with use of the model. The program is based on equations (17) through (20) (Fortran IV) and designed for the CDC 6400 computer.

GENERAL INFLUENCE OF INERTIAL FIELDS

A particular form of two-phase flow is that of a solid particulate suspension in a gas. The term suspension is related to the small-volume fraction of solid and to the characteristic of spatial evolution which is statistically influenced (influenced by collisional ineractions). For isotropic-kinetic velocity distributions, the spatial evolution of the suspension is prescribed by the diffusion equation.

In many instances the particles are of macroscopic dimensions and, therefore, affected by inertial fields. The flux of particles is given by

$$\vec{j} = -\rho D \nabla c + \rho c b \vec{f} \tag{21}$$

where

$b\vec{f}$ ≡ velocity due to inertial acceleration (assumed terminal)

$\vec{f}$ ≡ inertial field, e.g., gravity, centrifugal

b ≡ mobility coefficient

The conservation of mass for the particle population is written

$$\frac{\partial c}{\partial t} + \vec{v} \cdot \nabla c = - \frac{\nabla \cdot \vec{j}}{\rho} \tag{22}$$

Equation (22) contains explicit dependence of the distribution on the carrier (gas) stream velocity, $\vec{v}$. Equations (21) and (22) combine to give the constitutive relation for the time-dependent, spatial distribution of particles (since the gas stream in most cases is subsonic, the fluid is considered incompressible).

$$\frac{\partial c}{\partial t} = D \nabla^2 c - (b \vec{f} + \vec{v}) \cdot \nabla c \tag{23}$$

For the situation of steady flow, equation (23) is

$$D \nabla^2 c = (b \vec{f} + \vec{v}) \cdot \nabla c \tag{24}$$

A classical physics problem is contained in equation (24) without carrier velocity. The equation $\nabla^2 c = (b/D) \vec{f} \cdot \nabla c$ is used to obtain the Einstein relation, $D = KTb$, for the diffusion constant. Solution to this equation is

$$c = c_o \, e^{-(bU/D)} \tag{25}$$

where

$$-\nabla U \equiv \vec{f}$$

For a Maxwellian velocity distribution, thermal equilibrium, the exponential coefficient in equation (25) is the Boltzmann factor

$$e^{-(U/KT)} = e^{-(bU/D)}$$

which implies the Einstein relation

$$D = KTb \tag{26}$$

where

$K \equiv$ Boltzmann constant

$b \equiv \dfrac{1}{6 \pi \eta R}$ for low diffusion velocity (Stokes flow past a sphere)

$\eta \equiv$ gas viscosity

$R \equiv$ particle radius

Equation (24) is re-written

$$\nabla^2 c = \left(\frac{\vec{f}}{KT} + \frac{\vec{v}}{bKT}\right) \cdot \nabla c \tag{27}$$

The relative importance of inertial field (e.g., gravity) diffusion over convection is represented by

$$N_I = \frac{|\vec{f}|\, b}{|\vec{v}|}$$

The extent of inertial field stratification is indicated by

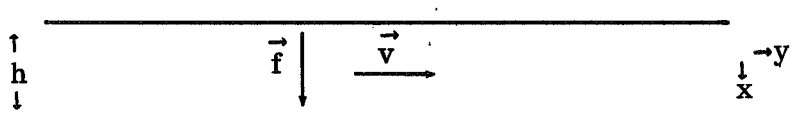
$$N_S = \frac{|\vec{f}|h}{KT}$$

For water droplets in air at 15°C and earth's gravity

$$N_S \sim R^3 \, (4 \times 10^{16})$$

$$N_S \sim 1 \text{ for } R \sim 3 \times 10^{-6} \text{ cm}$$

A two-dimensional example illustrates a method of solution. Consider the flow in a two-dimensional channel with the inertial normal to flow.



$$\frac{\partial^2 c}{\partial x^2} + \frac{\partial^2 c}{\partial y^2} = \frac{f}{KT}\frac{\partial c}{\partial x} + \frac{v}{bKT}\frac{\partial c}{\partial y} \tag{28}$$

In most convection problems

$$\frac{\partial^2 c}{\partial y^2} \ll \frac{v}{bKT}\frac{\partial c}{\partial y}$$

which states that diffusion in the flow direction is negligible, resulting in

$$\frac{\partial^2 c}{\partial x^2} - \frac{f}{KT}\frac{\partial c}{\partial x} = \frac{v}{bKT}\frac{\partial c}{\partial y} \tag{29}$$

Solution to equation (29) is of the form

$$c(x,y) = \sum_{n=1}^{\infty} e^{-\lambda_n^2 [(bKT/v)y]} \Gamma_n(x) A_n \tag{30}$$

where

$$\frac{d^2 \Gamma_n}{dx^2} - \frac{f}{KT} \frac{d \Gamma_n}{dx} + \lambda_n^2 \Gamma_n = 0$$

The functions, Γ_n, are of the type

$$\Gamma_n \sim e^{\alpha x}$$

where α is in general complex

$$\alpha^2 - \frac{f\alpha}{KT} + \lambda_n^2 = 0$$

$$\alpha = \frac{f}{2KT} \pm \sqrt{\left(\frac{f}{2KT}\right)^2 - \lambda_n^2}$$

The coefficients, A_n, and exponents, λ_n, are obtained through integral transformations of the boundary conditions

$c(x, 0) = \bar{c}(x)_o$ steady state, initial

$c(x, \infty) = \bar{c}(x)_\infty$ steady state, final

The steady state solution is obtained from

$$\frac{d^2 c}{dx^2} = \frac{f}{KT} \frac{dc}{dx}$$

$$\bar{c}(x)_o = c_o e^{\frac{fx}{KT}} \tag{31}$$

$$\bar{c}(x)_\infty = c_w e^{\frac{fx}{KT}}$$

An application of this approach is the water droplet transport and separation system.

Flow through a straight conduit with an inertial field has been discussed two-dimensionally (the three-dimensional problem associated with rotating flow in a cylinder is similar but algebraically more difficult). The flow around a corner can be handled easily considering the radial dependence of the velocity (gas) field and the inertial field including the centripetal acceleration. Flow in the heat exchanger region will be perturbed due to the local temperature gradients

$$D = KTb$$

$$\nabla \cdot (D \nabla c) = D \nabla^2 c + \nabla c \cdot \nabla D$$

$$\nabla \cdot (D \nabla c) = D (\nabla^2 c + \nabla c \cdot \nabla \ell n\ T) \tag{32}$$

Equation (27) becomes,

$$\nabla^2 c = \left(\frac{\vec{f}}{KT} + \frac{\vec{v}}{bKT} - \nabla \ell n\ T \right) \cdot \nabla c \tag{33}$$

APPLICATION TO LSS DESIGNS

The analytical model relates directly to several LSS processes and indirectly to most, the principal exception being those processes employed for Subsystem VII - Sanitation and Hygiene.

Although the model or portions of it are relatable to virtually all processes involving the mechanisms of humidification/dehumidification, possibly the most directly recognizable relationship exists with a system similar to that described by reference 2.

The subtle but inextricable relationship between the basic mechanisms of dehumidification and the characteristics of the mechanizations for their execution are emphasized by a comparison of the nature of the analytical model and the equipment concept for the experimental model (ref. 3). The analytical model treats the diffusive-convective mechanisms, the humidity and velocity profiles, and the mass flow rate(s) — the essential elements of the process, and does so with respect to the influences of variations in the forces involved. However, full mechanization of the process for operation under zero-g has added the liquid/gas interface control and separation-transport processes in the form of the capillarity of the porous cold plate and water transport circuit. The stabilizing mechanisms for the liquid/gas interface provided by the porous plate, unlike the diffusive-convective mechanisms, are highly sensitive to the magnitude of the inertial acceleration vector and thus, potentially at least, may result in alterations in the mass flow rate, essentially an alteration to the process itself. The examination of the exact nature of this interaction is considered more appropriate to the experimental portion of the investigation,

at least in the initial stages. Specific examples of their appearance as relatable phenomena can be found in the following applications which have been identified by their LSS Process Identification Sheet number. Additionally, the processes have been listed (somewhat arbitrarily) under one of two categories relating to the degree to which the process under investigation related to the primary process functions of equipment.

LSS Function	Process Identity	
	Principal	Supplemental
Oxygen Supply (and Recovery)	7, 8, 9, 10, 11, 12, 22, 23*, 24*, 27, 28, 32	4, 21, 36
CO_2 Removal	14*, 15*	13*, 16*, 18, 19, 20*
Water Reclamation	38, 39, 40, 41, 42*, 43*, 45, 46	
Humidity Control	61, 62, 63	
Waste Management	67(a), 67(c), 68, 69, 70, 71, 72, 73, 75	66*, 67(b)*
Bathing		82*

*Process varies from that described by the analytical model but not necessarily from the experimental investigation -- example: most CO_2 removal humidification and/or dehumidification occurs under turbulent flow (eddy diffusion) conditions.

EXPERIMENTAL EVALUATION

Requirements

An evaluation of the accuracy of the predictive aspects of the analytical model should include the following observations against each condition in a set of steady state conditions:

a. Temperature and humidity profiles.

b. Static pressures.

c. Stream velocity profiles.

d. Water exchange rates.

The experiment design should be such to include an examination of the potential effect on the model parameters of various levels of inertial acceleration on the nature of the liquid/gas interface being maintained by the porous-plate capillarity and gas-to-liquid stream-pressure differential. Analysis of the experimental data may lead to altering and/or augmenting the analytical model in this area.

Description of the Experiment

Major Goals

Primary. — To determine if the analytical predictions satisfactorily approximate the actual characteristics of the diffusive and convective mechanisms operating in the humidification-dehumidification process within a controlled gas stream.

Secondary. — To add sufficient understanding of the actual characteristics to correct and/or augment the analytical model as originally developed.

Tertiary. — To determine the effects, if any, on water removal rate of changes in the pressure differential across the porous plate.

Principal Observations

The experimental observations required included:

a. Humidity content of the air stream.

b. Water-exchange rates.

The experimental variables to be programmed against these observations included:

a. Air-flow rate.

b. Porous-plate pressure differential.

c. Plate temperature.

d. Air-flow characteristic.

e. Porous-plate (channel) orientation to the local gravity vector.

Criteria for Test Model Design

The test model and its supporting apparatus were designed under the following criteria.

a. Produce an air flow within a channel with a range of steady-state-flow set points in both the laminar and turbulent regions.

b. Produce a means of controlled heat exchange between a given length of one wall of the channel and the air stream required to support either humidification or dehumidification of the stream under varying stream inlet conditions.

c. Provide a means of directly measuring both condensation and evaporation rate in the heat exchange section.

d. Provide a means of measuring humidity concentrations both upstream and downstream of the heat exchange section.

e. Provide a means of varying the humidity concentrations at the inlet to the heat exchange section.

f. Construct the channel-installed, humidification/dehumidification water exchange component(s) in a configuration which provides as high a probability of successful operation in the zero-g environment as is possible.

g. Provide a means of visually monitoring as many of the potentially observable characteristics of the humidification/dehumidification as possible.

h. Provide for maximum utilization of the test equipments in subsequent experiments as an aid in experiment integration during the flight experiment phases of model evaluation.

Test Apparatus

The apparatus is shown schematically by figure 19 and pictorially by figure 20.

1. Blower & Flow Controls
2. Plenum Chamber
3. Humidifying Maze
4. Humidifying Mixing Circuit
5. Flow Channel
6. Porous Plate & Water Box
7. Water Circulation Circuit
8. Temperature Control
9. Instrumentation Chamber
10. Instrumentation

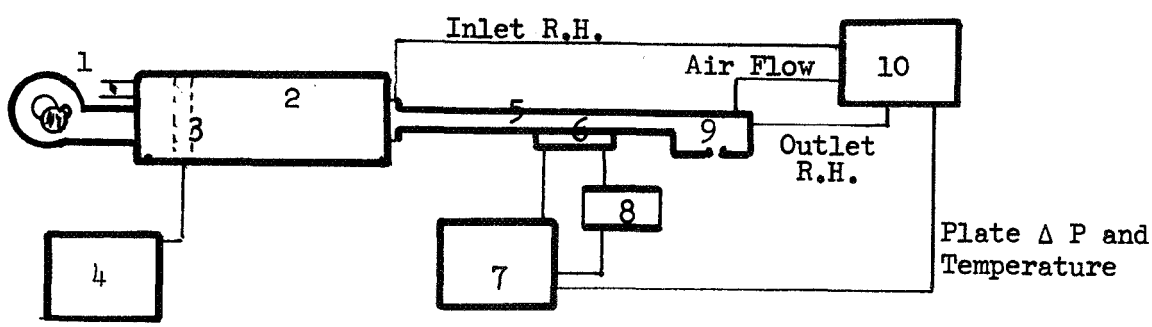


Figure 19. — Test Rig Schematic

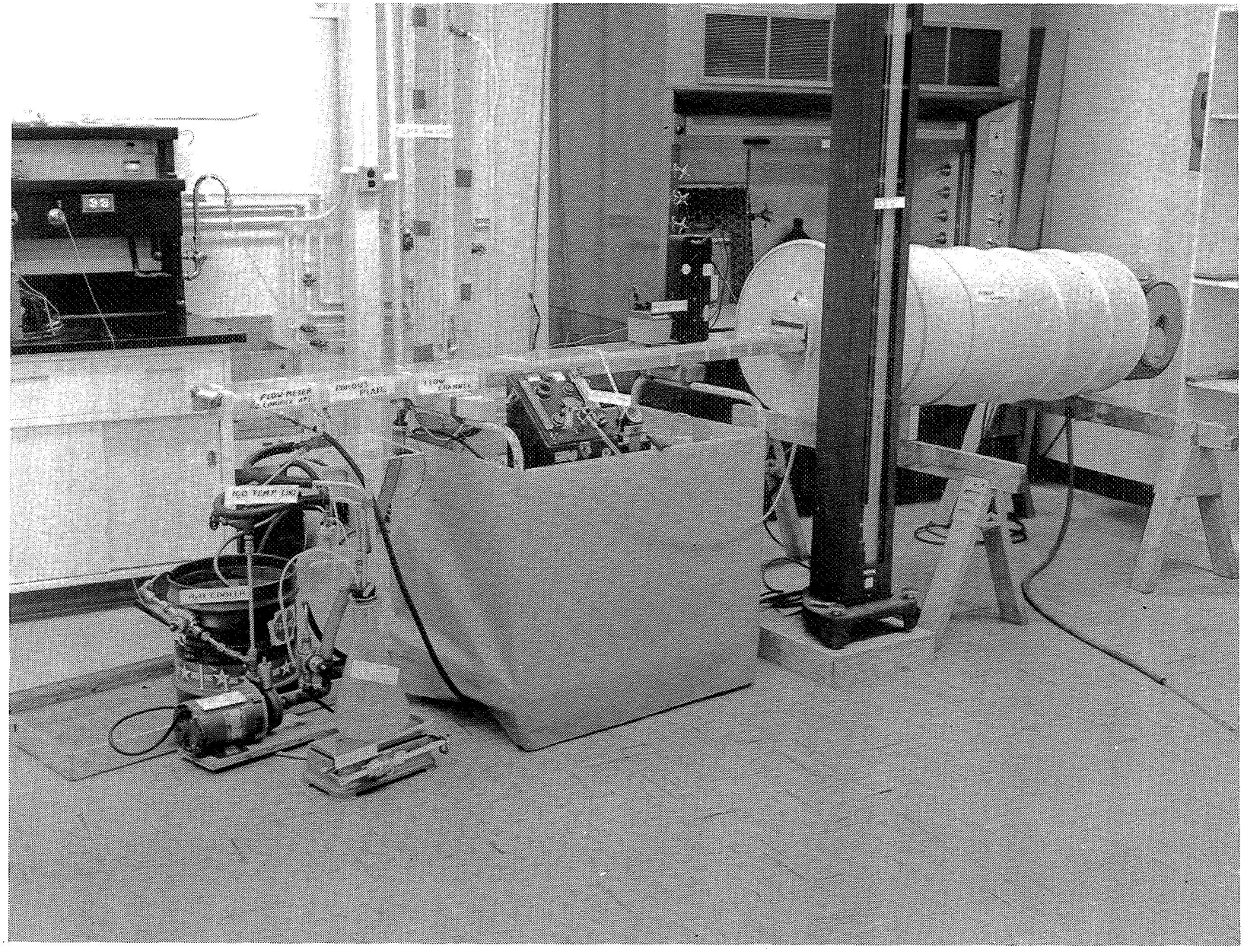


Figure 20. — Test Apparatus

Air-stream control assembly. — The air-stream control assembly consisted of the following components:

a. Blower.

b. Plenum chamber.

c. Humidifier.

d. Air-flow control.

The blower was a Dayton, Model 2C570, with a modified (restricted) single side inlet.

The plenum chamber was fabricated from two metal drums attached end-to-end and coated with corrosion-resistant paint. This provided a chamber volume of approximately 13.3 ft^3 over an inlet-to-outlet distance of approximately 5.7 feet. The exit end of the chamber was removable (typical drum top peripheral-over-center compression-ring clamp). An adapter section was incorporated into the exit end of the chamber to facilitate 1) channel inlet instrumentation mounting, 2) channel attachment, and 3) minimum disturbance in the transition from plenum to channel stream velocities.

The humidifier assembly consisted of a wetted maze covering the full cross section of the plenum chamber in a plane normal to the longitudinal axis of the chamber. The maze material was Scott Industrial Foam (97% void open cell, 20 cell/inch, urethane) configured as a circular disc approximately 2 inches thick with a diameter matching the ID of the chamber. The disc was supported across the chamber by several plastic-coated wires extending through the walls of the chamber fore and aft of the maze. Warm tap water was metered to the maze at a temperature and rate set by the operator. A drain was provided for maze overflow.

Air-flow control capability was provided by 1) restriction of the blower inlet with a plate which could vary the effective inlet area from 0 to 12.6 $in.^2$, and by 2) altering the setting on a butterfly valve in a 12.6 $in.^2$ circular cross section vent pipe mounted on the inlet end of the plenum chamber.

Air flow was provided in a controllable range from less than 1 ft/sec to well above 100 ft/sec with the 1 $in.^2$ cross-section channel.

Flow-channel and test-section assembly. — The detail configuration of the flow-channel assembly was influenced by a requirement that it be usable for subsequent tests; however, no major functional limitations resulted from this requirement. The flow channel was formed by two 6- by 84-inch parallel plates, one aluminum and the other lucite, attached at the sides by a 0.2- by 0.5- by 84-inch lucite strip for one series of runs and a 1.0- by 0.5- by 84-inch strip for a comparative series. A smooth

transition from the plenum chamber to channel was accomplished as shown in figure 21. Also shown is the instrumentation (expansion) chamber at the channel outlet and the two porous plate/waterbox cutouts. The two cutouts for the porous plate provide a potential for test under two levels of flow development, one close to the inlet and the other sufficiently downstream from the inlet to provide a high degree of flow development.

The test section comprised the porous plate/waterbox assembly and the area of the channel in the vicinity of the porous plate installation. The porous plate/waterbox assembly was mounted in the channel cutout with the exposed surface of the porous plate flush with the surface of the metal plate which formed the base of the channel. Sealing of the clearance between the channel and the porous plate/waterbox was accomplished with nonhardening plastic sealing compound (Johns-Manville DUXSEAL). A metal coverplate was placed in the unused channel cutaway.

The porous plate material was the Union Carbide Corporation, Stellite Division, NR-30 porous metal stock (nickel, 0.007-inch thick, 0.30-void fraction, and 2.9-micron mean pore diameter). An initial stock of the material was obtained from surplus at NASA-LRC with supplemental purchase from Union Carbide.

The waterbox was constructed of plexiglass to provide visual observation of both the quality of flow from the water-flow circuit and the quality of "operation" of the porous plate. The details of the structure are illustrated by figure 22. Water-flow velocity at the surface of the porous plate was approximately 4 to 6 ft/sec to provide sufficient heat transfer rates under the limitations imposed by the ice bath cooler chosen for its economy to the program.

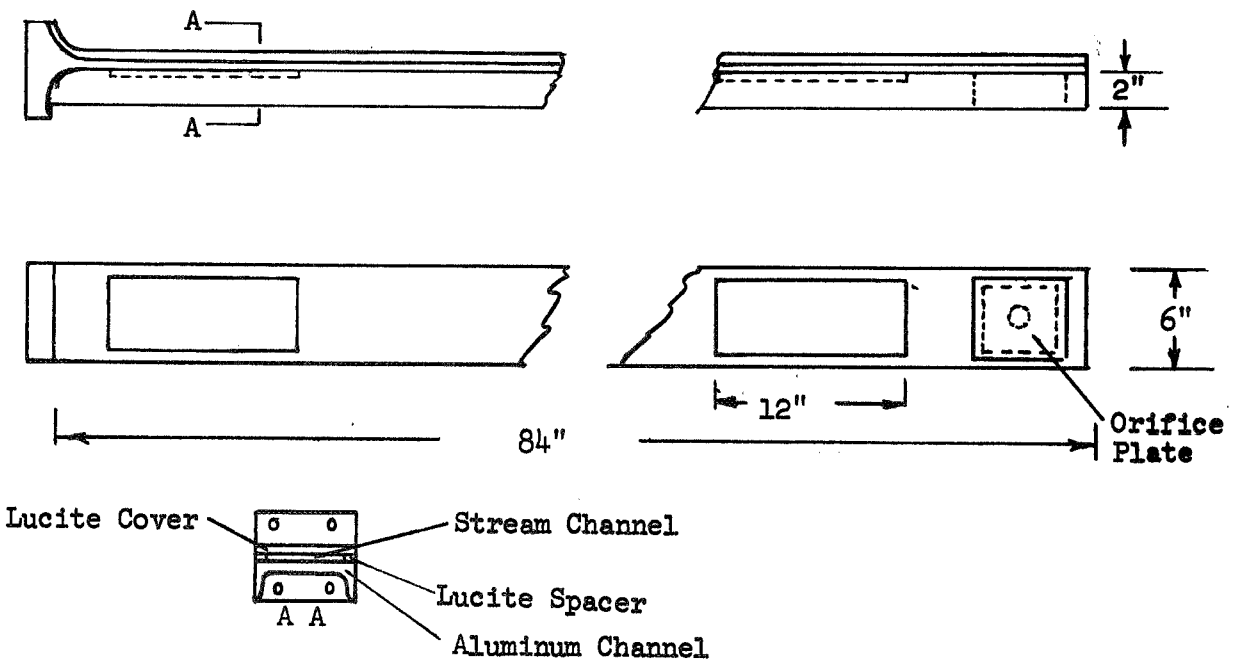


Figure 21. — Channel Assembly

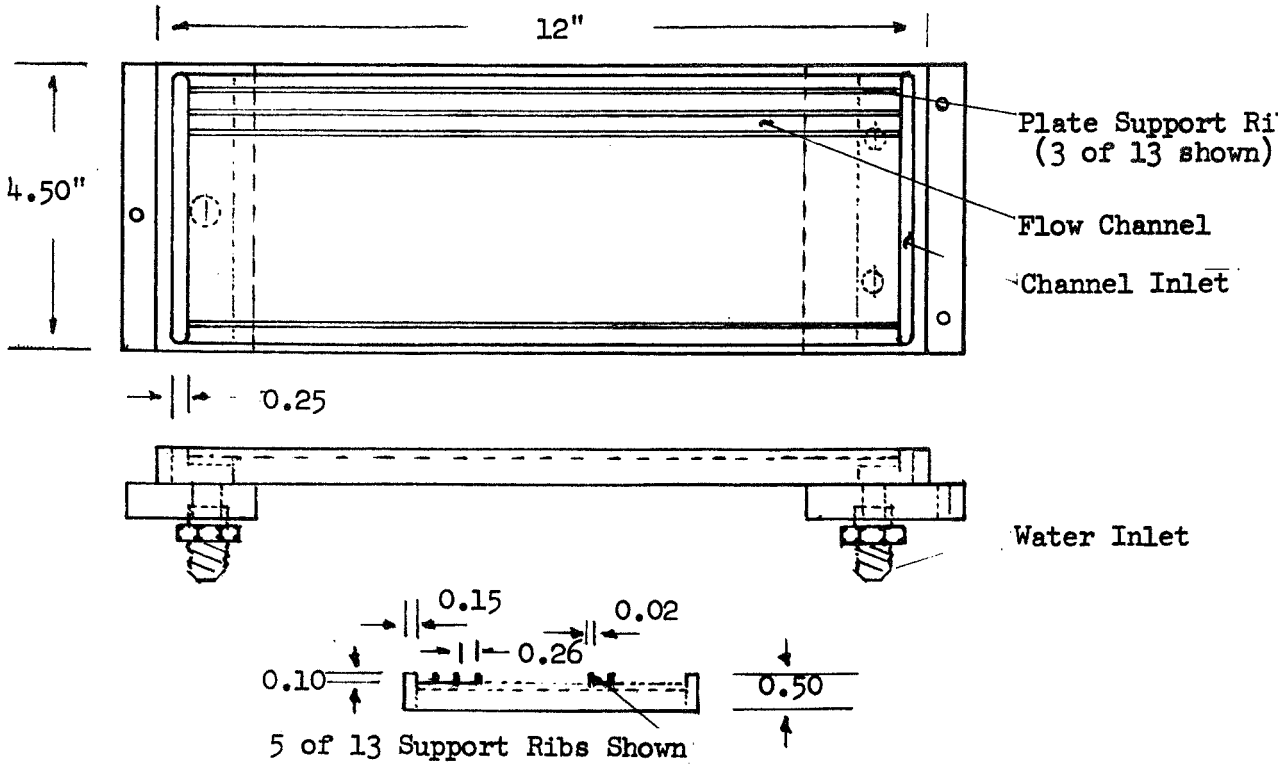


Figure 22. — Waterbox Assembly

Several methods were investigated for attaching the porous plate to the waterbox and providing the necessary air (water) seal. Although various permanent attaching methods were investigated, including silver solder, heliarc, and electron-beam weld, the latter found by NASA-LRC to be most satisfactory, it was decided that a rapid remove-and-replace capability was highly desirable for an experimental program; thus a temporary attachment method was employed. Zinc chromate "Duct Seal" was found entirely satisfactory once a good seal was formed and a hold-down force provided by a waterbox pressure lower than channel pressure, a condition attainable with water-circulation circuit in operation.

Heat-and-water exchange circuit. — The heat-and-water exchange circuit shown in figure 23 provided both the cooling flow for the condensing mode and the heated flow for the evaporating mode. In addition, the circuit was so constructed as to both continuously collect and measure the condensate being drawn through the porous cold plate or provide a continuous and measurable flow of water to the porous plate during evaporation. Major components of the circuit were:

a. Waterbox (previously discussed).

b. Water circulating pump.

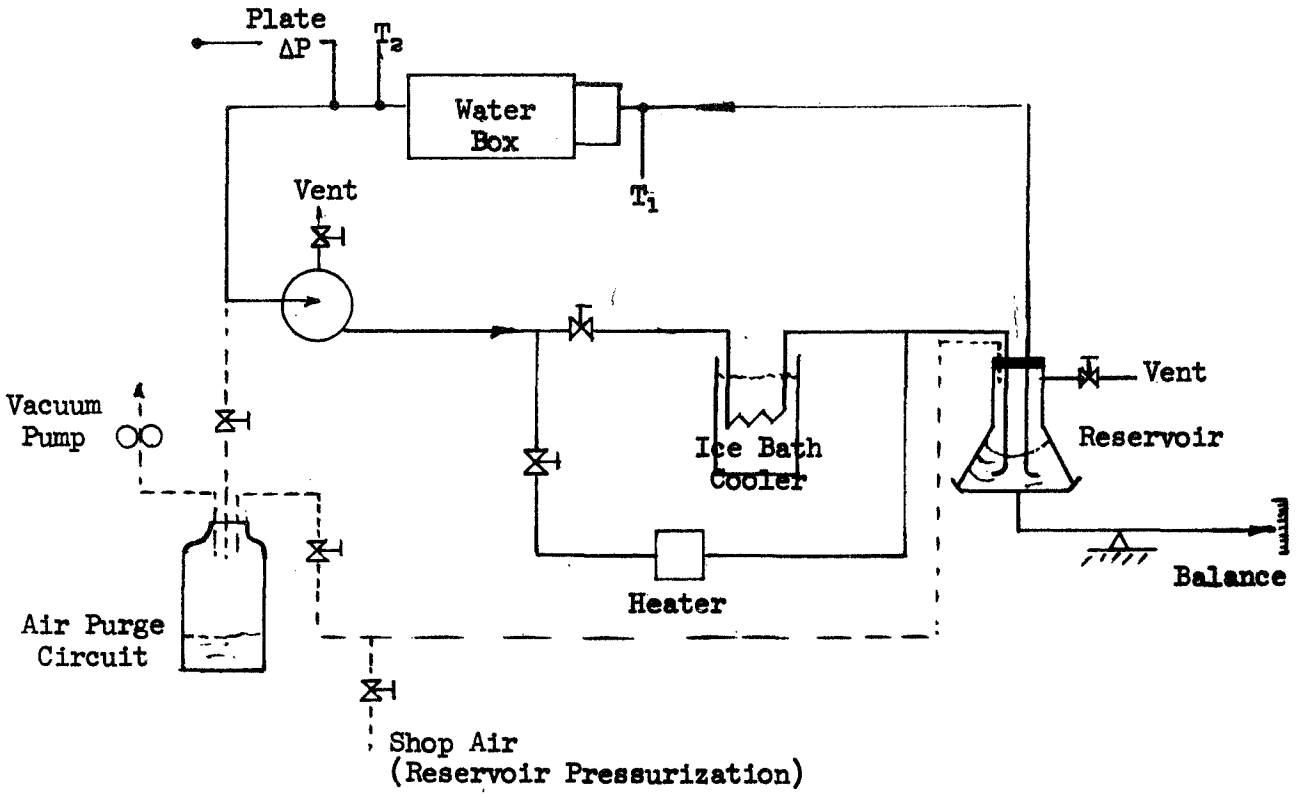


Figure 23. — Water Circulation and Heat Exchange Circuit

c. Reservoir.

d. Cooler.

e. Heater.

f. Instrumentation and controls.

g. Miscellaneous valves.

h. Air-purge pump.

i. Purge water/air separator.

Water circulation was maintained by a centrifugal pump (Oberdarfer Model 5168, 2.5-inch impeller, 3/4-inch inlet modified for reduced pressure drop, 1/2-inch outlet, carbon face seal, 3450 rpm). The reservoir was a 4000-cc Erlenmeyer filtering flask with two standpipes extending through a secured stopper and well below the reservoir water level. The inlet pipe discharge was bent to maintain rapid rotation of the water to promote entrained air separation. The output pipe inlet was bent into the flow of the swirl to promote smooth pickup.

Reservoir atmospheric venting was effected through the filtration fitting. Reservoir pressures below atmospheric were effected by a crossover circuit to the air-purge

vacuum circuit and above atmospheric pressure by a tie-in to the shop air supply. The reservoir provided for both air/water separation prior to circulation through the porous plate waterbox and measurement of the weight changes of the reservoir water, i.e., weight loss during evaporation and weight gain during condensation.

Plate cooling was provided by directing the circulating pump output through a copper tubing coil immersed in an icewater bath. Plate heating was provided by directing a portion of the pump output through an in-line heater constructed from two rod heaters (1 kW each) in either end of a 1-inch pipe.

An air-purge circuit comprised a heavy-wall laboratory bottle, vacuum pump, and valving and provided an air-purge capability for the water circulation system as might be needed at start-up following circuit modification or as a result of plate breakthrough.

Instrumentation. — The major components of the instrumentation employed for the data runs included:

a. Laboratory mercury thermometers (including wet bulb wicks).

b. Casella dew point apparatus (modified).

c. Water manometer and orifice set.

d. Mercury manometer.

e. Triple beam balance (modified).

The mercury thermometers were used to measure channel inlet and outlet dry-bulb/wet-bulb temperatures and waterbox-outlet temperature. The latter was permanently installed in a water line fitting, while the former were inserted into the air stream through holes drilled immediately upstream of the channel inlet and at the instrumentation expansion chamber at the channel outlet. The thermometers were held in place and holes sealed with nonhardening plastic sealing compound.

The Casella dew point apparatus, a manually operated, visual dew point hygrometer, was selected due to its relatively consistent correlation with the dry/wet bulb technique. The instrument was modified for increased accuracy and response by substituting a resistance thermometer attached to the back of the condensing plate for its original mercury thermometer. Sample ports for the instrument were located adjacent to the mercury thermometer ports.

Channel air flow was calculated from pressure drop measurements obtained with a water manometer (Charles Meriam Company, Model 34EH10TM, scale vernier in 0.0001 psi) and the appropriate sharp-edge orifice from a set with individual orifices ranging in size from 0.1 to 1.0-inch diameter.

Waterbox pressure was determined from a locally fabricated mercury manometer which registered "pump suction" in inches of mercury at the outlet of the waterbox as sensed through a water column to the manometer. Changes in reservoir weight due to increases in water volume during condensing and decreases during evaporation were measured with a modified (balance weighted) triple-beam balance reading in 0.1 gram.

Test Procedures

The individual test runs were conducted by establishing a specified air-stream velocity and, for the condensation mode runs, by adjusting the in-flow of warm water to the humidifying maze. The appropriate air-flow measurement orifice was selected for each flow range to assure maximum possible accuracy.

Initially, porous plate waterbox pressure (pump suction), the control parameter for porous plate ΔP, was considered an experimental variable. But, when it was determined that process rate changes could not be detected for even wide variations in ΔP, a procedural set (circuit state) was initiated and continued for the remainder of the tests.

Steps were taken to assure that no unwanted condensation was present throughout the system which would introduce errors in the data being recorded. Test conditions were varied by changing any combination of the following experimental variables in the approximate ranges shown:

a. Air-flow velocity (1 to 30 ft/sec).

b. Plate temperature (35 to 48° F and 124 to 134° F).

c. Channel height (0.22 and 1.0 inch).

d. Orientation to the local gravitational vector (plate at top and plate at bottom of channel).

e. Inlet humidity (dew point) (48 to 73° F).

f. Plate ΔP (initial runs only).

As indicated by the test data displayed herein, several evaporation runs were repeated when a dropoff in evaporation rate was noted and plate-plugging was suspected.

Test equipment design, fabrication, exploratory tests, and equipment improvements were completed in the period 1 June to 20 September 1969.

Official data runs were initiated on 23 September and completed on 29 October 1969.

Test Data Summary

Data was recorded against three sets of experiments, namely:

a. Trial Data Runs — essentially instrumentation and test mode evaluation and modification.

b. Condensation Mode Runs — the major experimental variables were mass flow rate and channel height.

c. Evaporation Mode Runs — the major variables were mass flow rate, orientation to the gravity vector, and channel height.

The data produced from these runs were summarized and recorded on Test Data Summary Sheets and included in the Test Report (ref. 4).

Trial data runs. — Table 9 is a typical set of data recorded during the pretest exploratory runs. Figure 24 illustrates the degree of variation experienced. Data obtained from wet/dry bulb and Casella techniques were retained for formal data acquisition. Table 10 records data obtained to investigate the accuracy of the catch weight measurements. Modifications subsequent to this investigation reduced the apparent variations.

Condensation mode. — Fourteen condensation mode runs were conducted with the cold plate both on the bottom and top of the channel, with a channel height of 0.22 and 1.0 inch.

Evaporation mode. — Eighteen test runs were conducted in the evaporation mode. These runs were also conducted with the channel oriented with the porous plate on the bottom and at the top of the channel. Two channel heights were also used, one at the original 0.22 inch and the second at 1.0 inch.

Critique of the Test Design

With the exception of the problems associated with the inherent inaccuracies of the commercially available hygrometric instruments and uncertainties relating to measurement of channel air flow, the general approach to the test design appeared to be sound, tests were easy to manage, and construction costs were low. The approaches followed and the instrumentation information compiled can be recommended as a guide to future test designs for experimental studies involving diffusion-convection/condensation-evaporation phenomena.

Table 9. — Trial Data Run - 23 September 1969

A. Catch reading: (1410) 76.5 (gms)

			Assumed Catch (gms)	Rate (gms/min)	
Time Period I	(1435)	(25 min)	81.5	5.0	0.200
	(1507)	(32 min)	87.5	6.0	0.188
					0.190 (Rate #1)
Time Period II	(1530)	(23 min)	90.8	3.3	0.144
	(1602)	(32 min)	95.8	5.0	0.156
					0.149 (Rate #2)

B. Air flow: 0.0470 ft^3/sec. (2.820 ft^3/min. ≅ 0.216 lbs/min)
6.38 ft/sec.

C. Comparative calculations of humidity (grams/lb. air) from four measurement techniques:

	Wet-Dry Bulb		Alnor		Honeywell Dry Bulb		Honeywell Wet Bulb		Casella	
Inlet:	(1400)*	109.1	(1355)	88.8	(1357)	129.3	(1400)	115.0	(1400)	94.8
	(1440)	101.6	(1425)	87.1	(1429)	139.0	(1445)	109.6	(1418)	91.5
	(1515)	100.4	(1455)	87.1	(1452)	146.7	(1515)	110.5	(1500)	94.8
	(1535)	101.4			(1600)	130.8	(1535)	109.6	(1530)	95.2
Outlet:	(1400)	90.4	(1400)	86.0	(1350)	97.2	(1400)	92.6	(1350)	75.8
	(1420)	85.3	(1420)	84.2	(1425)	97.8	(1420)	89.8	(1427)	75.0
	(1522)	85.6	(1450)	82.5	(1530)	97.2	(1522)	89.8	(1510)	81.6
	(1543)	84.2			(1550)	98.0	(1543)	88.8	(1535)	79.4
Δ:	(1400)**	18.7	(1400)	2.8	(1400)	32.1	(1400)	22.4	(1400)	19.0
	(1430)	17.6	(1425)	2.9	(1430)	32.2	(1445)	20.8	(1430)	17.0
	(1520)	15.1	(1455)	4.6	(1530)	39.0	(1520)	20.7	(1505)	13.2
	(1540)	17.4			(1550)	32.8	(1540)	20.8	(1535)	15.8

D. Calculated removal rates (gms/min) averaged for time periods I and II:

	I		II	
	Rate	Variation***	Rate	Variation
Wet-dry bulb =	0.233	-18.4	0.214	-30.4
Casella =	0.210	- 9.6	0.201	-25.7

* Clock time (actual)
** Clock time, assumed for calculation
*** Catch to calculated (%)

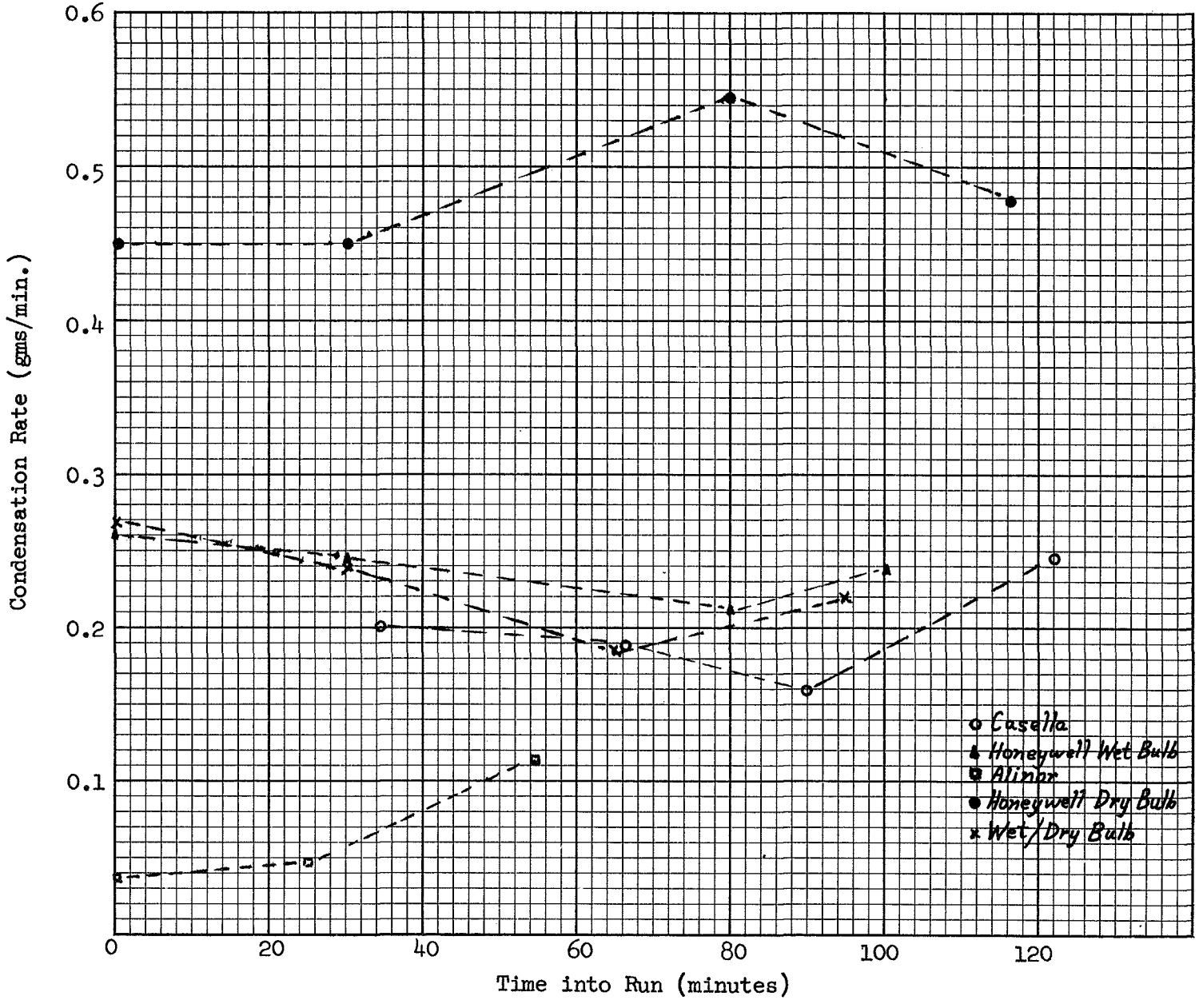


Figure 24. — Comparative Estimates of Condensation Rate for Five Measurement Techniques

Table 10. — Catch Weight Accuracy Tests - 26 September 1969

Conditions:
1. Water circulating in the condensate withdrawal circuit, fully purged.
2. Air flow channel cover removed.
3. Water inserted at porous plate with 5 cc syringe.
4. Catch weight obtained on modified triple beam balance; unmodified capacity 2610 gms, fine scale in 0.1 gms.*

Trial	Water Added	Catch Vessel Weight (gms)	Observed Catch Weight (gms)	Δ Weight (gms) (Catch to Added)	Trial Variation (%)	Cumulative Variation (%)
		40.6				
1.	3.0	43.7	3.1	+0.1	+3.3	+3.3
2.	4.0	47.5	3.8	-0.2	-0.5	-1.4
3.	2.2	49.8	2.3	+0.1	+4.5	0
4.	1.7	50.7 (beam scale change)	0.9	-0.8	-47.0	-7.3
5.	4.2	54.3	3.6	-0.6	-14.2	-9.3
6.	3.2	58.0 (beam scale change)	3.7	+0.5	+15.6	-5.1
7.	4.6	63.4	5.4	+0.8	+17.4	-0.4
Σ	22.9		22.8	-0.1	- 0.4	

Weight following shutdown 58.5 - 7.8%**

Weight following restart 62.0 (restart) - 2.2%**

* Modification consisted of adding balance weight to beam to offset reservoir structural weight.

** Apparent weight loss from Trial #7 due to shutdown and restart cycle.

Note: A modification of the counterweight configuration subsequent to this test reduced the variation potential to at least 50% of that implied by these seven trials.

Instrumentation. — It became apparent during the trial data runs for the condensing mode tests that major uncertainties existed relevant to obtaining accurate and precise measurements data required for the analytical determination of air-stream water-vapor content and for the explicit weight measurements of condensate removed from the condensing surfaces of the cold plate. In an attempt to minimize both the uncertainties and the apparent inaccuracies of these measurements, a series of exploratory condensing runs was initiated. One phase of the investigation involved comparative performance of several types of hygrometric instrumentation simultaneously on-line in a series of trial data runs.

Another phase of the investigation involved tests on the accuracy of the water-catch measurements.

It was concluded from these studies that determination of dew point by the conventional wet-bulb technique backed up by the modified Casella unit would provide the best accuracy with a sufficiently high confidence to warrant proceeding with the formal data runs. This decision was based on analysis of trial run data showing an extremely close similarity between estimates of condensate production rate based on the wet/dry bulb and on the Casella dew point determinations. Both, in turn, were reasonably close to the catch weight values as illustrated by figure 24. (A second modification of the balance subsequent to these trial runs improved the correlation between catch weight values and calculated values.)

Analysis of the results obtained from initial data runs indicated that the level of accuracy being attained was probably sufficient to adequately evaluate at least the relevancy and characteristics of the analytical predictions, if not the degree of accuracy of the predicted values.

Improvements in the accuracy of the wet-bulb temperature values might have been effected with a more rigorous approach to system design to assure that ventilation rates and wick configuration were consistent with recent findings of the influence of the instrument Reynolds number as described by Morrison in volume 1 of reference 5. Future test designs should take full account of this source of measurements error.

Air flow and pump suction measurements were considered highly accurate and precise, with no apparent variations or inconsistencies during and between runs.

Provisions for accurate measurement of inlet air and water volumes provide a significant potential for these experiments but add a high degree of complexity. Such require both a zero-leakage-to-ambient throughout and an input of dry air or other dehumidified gas.

Humidity measurement technology review: A survey of humidity measurement technology was undertaken both to provide information against which to evaluate the appropriateness of the hygrometric instrumentation chosen for this test and to provide a first step in the determination of instrumentation for the flight experiment package(s). A summary of this survey follows.

The information base for this survey is principally found in the 102 technical papers contained in volumes 1 and 3 of the four-volume set of over 200 papers delivered to the International Symposium on Humidity and Moisture held in Washington, D.C., in May 1963, under the combined sponsorship of the National Bureau of Standards; U.S. Weather Bureau; American Soceity of Heating, Refrigerating and Air-Conditioning Engineers; American Meteorological Society; and the Instrument Society of America. Arnold Wexler of the National Bureau of Standards was the program chairman and editor-in-chief of the four volumes.

Supplementation of this information base was provided by standard texts, product brochures, additional technical papers, and personal conversations with instrumentation engineers associated with the Convair Standards Laboratory and with staff scientists of the Space Sciences department working in the development of qualitative and quantitative measurements techniques for atmospheric constituents.

a. Categorization of hygrometric techniques. — The term hygrometric instrumentation as used herein applies to any technique which results in the estimate of the amount of vapor (water) in a stream of air. Each of the many hygrometric techniques can be conveniently, although not exclusively, grouped under one of six categories.

   1. Psychometric hygrometry — determination of the temperature drop caused by the evaporative cooling effect set up by a wetted wick surrounding a thermometer which has been placed in the air mass of interest. Principal measurements involved are the sensible temperature (dry bulb) of the air mass and the lowest temperature recorded in the drying cycle of the wick (wet bulb).

   2. Dew point hygrometry — determination of the temperature at which the air mass becomes completely saturated with a vapor (water) as measured by observing the temperature at which condensation initially appears on an optical surface which has been progressively lowered to a temperature below that of the air mass of interest.

   3. Electric hygrometry — determination of the value of a specific electrical characteristic of a humidity-sensitive resistive or capacitive device exposed to the humidity effects of the air mass of interest. A calibration chart is typically employed showing a range of RH curves for various values of the specific electrical resistance versus values of the sensible temperature of the air mass of interest.

4. Spectroscopic hygrometry — determination of the degree to which various radiation phenomena are absorbed by the amount of water vapor present in a specific column length of the air mass of interest. The degree of absorption observed across the molecular spectra of the radiation phenomena is relatable to a specific vapor density with the sample. Various radiation phenomena are practical, with infrared and ultraviolet being the most commonly employed.

5. Coulometric hygrometry — determination of the current required to electrolyze the water present in a sample air stream of known mass flow. A linear relationship exists between current flow and humidity concentration.

6. Miscellaneous hygrometric methods — there are several methods of hygrometry which are of interest in the type of experiments under consideration but which are neither clearly classifiable under the foregoing nor sufficiently widespread in application to warrant a specific additional classification.

   a) Thermal conductivity: determination of the resistivity of a heated element whose temperature is influenced by the rate of heat transfer to a sample of the air mass of interest as compared with that of a reference cell. The effect of vapor concentration on thermal conductivity is established which, in turn, is relatable to the temperature and, thus, resistivity of the heated elements.

   b) Gravimetric: determination of the weight of water vapor absorbed by a desiccant which has been exposed to a known quantity of the air mass of interest. A variation of this technique determines the difference in pressure drop across a set of matched orifices between a dehydrated and nondehydrated sample of the air mass of interest. The difference is relatable to the water vapor concentration in the nondehydrated sample. Both methods are best suited for instrumentation standards; however, the latter is employed by the NBS.

   c) Piezoelectric sorption: determination of the oscillatory frequency of a humidity-sensitive, radio-frequency quartz crystal when immersed in a sample of the air mass of interest where flow rate, pressure, and temperature are controlled. The observed frequency is relatable to humidity concentration.

b. Operational characteristics by hygrometric category. —

1. Psychometric hygrometry —

   a) Accuracy: ±2% (±5%), theoretical and expected values.

   b) Response: low (2 to 10 minutes).

   c) Problems: wet bulb temperatures are subject to "reading" error unless great care is taken and/or mechanization is provided to assure that the

lowest temperature value is taken. Additional errors are introduced by variations in ventilation rate and wick configuration. Inaccuracies and imprecision of psychrometric charts add to the expected error band.

d) Application comments: simplicity is attractive for laboratory tests. Special designs, such as Peltier effect thermocouples, are flight candidates.

2. Dew point hygrometry —

a) Accuracy: ±1% (±3%).

b) Response: varies widely, highly automated range from 1 to 30 seconds.

c) Problems: deterioration or contamination of condensing surfaces combined with reading errors can produce high orders of inaccuracy. Minimization of reading error by photoelectric sensing is practical.

d) Application comments: simple, visually read instruments are ideal for laboratory use. Flight instruments, both aircraft and radiosonde, have been extensively and successfully deployed although somewhat complex. Apollo telemeters dew-point temperature. The most advanced designs employ thermoelectric sensors; volume approximately 125 $in.^3$ (exclusive of power supply); weight approximately 2 pounds.

3. Electric hygrometry —

a) Accuracy: ±2% (±5%).

b) Response: high, 10 to 30 seconds.

c) Problems: storage degradation and in-use contamination of sensors can result in major inaccuracies.

d) Application comments: extensive radiosonde flight experience has been compiled during the past 10 years. This approach has been used for the Apollo systems. Packaging potential for flight systems is generally superior to typical dew point hygrometric techniques.

4. Spectroscopic hygrometry —

a) Accuracy: 2 to 10 ppm (0.1 to 0.5%).

b) Response: very high, $\ll$ 1 to 1 second.

c) Problems: absorption path length can be a function of measurement range requirements and may be as high as 3.5 feet, a problem to flight design for the wide range which can be required of certain experiment packages. Cabin atmosphere monitoring is not a problem.

d) Application comments: the Naval Research Laboratory has successfully flown an aircraft R&D model for atmospheric soundings, and the U.S. Weather Bureau hurricane hunting aircraft have included instruments of this type. Recent developments under contract to NASA-LRC have produced prototypes for spacecraft atmosphere sensing.

5. Coulometric hygrometry —

a) Accuracy: can be as high as ±0.2% in low-humidity range.

b) Response: varies significantly with moisture content — high for high-humidity streams, 1 to 10 seconds; fair for low-humidity streams, 50 to 150 seconds.

c) Problems: the problems associated with water vapor electrolysis are inherent and include degradation of both the structural material and the electrolyte.

d) Application comments: aircraft flight tests have been conducted successfully. Packaging can be simple and very compact.

6. Miscellaneous hygrometric methods —

a) Thermal conductivity: accuracy is similar to that of dew point hygrometry but response, essentially that of a hot-wire anemometer, can be virtually instantaneous, i.e., in milliseconds, for some designs. Development for flight systems has not been extensive but appears to have considerable potential.

b) Gravimetric hygrometry: the manual weighing of an absorbing canister to determine humidity can produce exceptionally high accuracy under equally high confidence but is extremely slow, taking from 15 to 45 minutes for a single measurement. This is, however, fairly competitive with manual wet/dry bulb readings. Variations, such as the pneumatic bridge (matched orifices in a bridge circuit), produce very high response ($\ll$ 0.1 to 0.5 seconds). Accuracies are essentially determined by the quality of the pressure-measuring instrumentation employed and, typically, can attain values within ±0.5% of the theoretical RH. Applications have been primarily for the laboratory, but it presents at least a limited potential for flight application. Desiccant management would be a significant design and operational problem.

c) Piezoelectric sorption hygrometry: the inherent accuracy is excellent, being of the order of 0.1 ppm, with response at least that of the electrical humidity-sensitive sensors. The piezoelectric sorption sensor may be somewhat more sensitive to gas composition changes than the electric sensors. This approach has many things in its favor for both operational systems and flight experiment packages. These advantages include the

nature of the sensor output signal (radio frequency), the extreme simplicity of both components and circuitry, life characteristics of the sensor, and the inherent potential for miniaturization of the entire system.

c. Hygrometry for experimental test No. 2. — The performance of four hygrometric techniques were experimentally investigated and compared during the trial data runs for the condensing mode tests. Condensing rate estimates for each of the four were compared and, in turn, checked against condensate catch weights. Figure 24 illustrates the variations in the data. Unquestionably, further work with the Alinor and Honeywell instruments would have produced better results but the psychometric and Casella dew point techniques were chosen for continued use on the basis of the initial investigations, thus no further work was undertaken in an attempt to improve results being obtained from the other two. Although the Casella (modified) and wet/dry bulb techniques frequently did not agree on absolute humidity level, the changes in humidity across the test section with the two methods were in much closer agreement and were considered adequate for this test program. The nature of the four hygrometric techniques can be summarized as follows:

1. Psychometric — wet/dry bulb technique determines two points on the psychometric chart (Carrier) leading to estimates of humidity concentration of the air stream.

2. Casella dew point apparatus — manually operated, visually observed dew formation on the surface of a mirror, the temperature of which can be varied by the operator. The temperature at which moisture from the stream sample starts to form or disappears is recorded as the dew-point temperature. Estimates of humidity concentration are again taken from the psychometric chart.

3. Honeywell RH meter — a semiautomated, portable unit producing a direct readout of RH. The device operates on signals from a stream-mounted, humidity-sensitized resistive sensor and a thermistor. Manually adjusted dials on the panel produce a nulled bridge circuit which, in turn, produces a temperature-compensated readout of RH. Accuracies of $\pm 1 - \pm 2\%$ are claimed as possibilities for new sensors; an expected value might be closer to $\pm 5\%$. Since relative humidity is read from the meter, it must be used in combination with either a stream wet or dry bulb reading to yield absolute humidity.

4. Alinor dew pointer — a manually operated, visually observed fog behavior in a drawn stream sample when the sample is subjected to a pressurization-depressurization-repressurization cycle. Temperature and pressure data are noted at the point at which the fog disappears from the sample chamber in the repressurization cycle. A rotary disc calculator indicates the dew-point temperature for the observed data. The psychometric chart is used for estimates of concentration.

d. Recommendations. — It is recommended that the piezoelectric sorption and capacitive sensor techniques be given high priorities in the development of both flight systems and experiment packages.

Process apparatus: The simplicity, ease of management, and economy of the process apparatus when viewed against the excellent process control achieved indicates that a similar approach should be considered for future laboratory testing. Improvements could be readily attained by providing for monitoring and control of the plenum chamber humidifying water in-flow rate and temperature. The precision of this control is not critical; thus any one of several readily available, inexpensive, commercial flow meters could be employed, and manual control of hot-cold tap water mixing would suffice. Temperature pick-up could be easily accomplished by a resistive thermometer attached to the exterior of a short length of insulated thin-wall, high-thermal conductivity tubing inserted as a section of the in-flow circuit.

The formation of condensate at several points in the system required special attention. Although the design was such that dew points in the channel upstream and down of the cold plate were below ambient during the condensing mode, unwanted condensation occurred in two places, namely, on the wall of the channel working section and on the exterior of the inlet to the water reservoir. The former leads to inaccuracies in the calculated efficiency of the process, while the latter produces inaccuracies in the catch weight measurements. A low-energy heat lamp can be used to raise the working section wall temperature during condensing mode runs to that of the average value along the nonworking portion of the channel, and to levels above dew point during evaporation. Intermittent area heating of the aluminum channel base downstream of the working section is also effective for the latter. A laboratory Meker burner was found satisfactory. A transparent plastic enclosure was placed around the reservoir section of the water circulation circuit and its enclosed atmosphere purged and maintained with dry nitrogen. Condensation occurring in the reservoir during evaporation does not produce a measurement problem.

Problems were experienced with the porous plate/waterbox assembly when the test mode was changed from condensation to evaporation. The installation clearances between the plate/waterbox assembly and the channel base were designed for minimum leakage at condensing temperatures and were too close for the higher evaporating temperatures, causing buckling of the plexiglass waterbox resulting in bowing the porous plate above the channel base, i.e., into the channel. Clearances were increased to accommodate this condition and presented no problems; however, for tests where transition from one mode to another must be made without the opportunity for rework or seal adjustments, the problems of installation clearances and dissimilar material fits and bonds must be thoroughly resolved prior to initiation of test.

During evaporation runs problems were experienced with an apparent dropoff in evaporation rate. It was thought that this might have resulted from contamination of the

porous plate from rust particles in the water circulation/heat transport circuit originating from the commercial fittings and heater housing. A new porous plate appeared to correct the problem. Although a rather obvious point, it is imperative that flight experiment and operational systems avoid this pitfall by employing both noncontaminant generating materials and submicron filtration.

Procedures: The technique for initially establishing air-free water loading of the porous plate recommended by NASA-LRC (that of placing the plate in a pan of water which is subsequently brought to a boil and, following a prolonged boiling "soak," returned to ambient temperature) was found convenient and effective.

In that there is no significant interaction between consecutive test runs or modes, no special care need be taken in the mode sequence except as the effective use of time dictates.

Correlation of Analytical and Experimental Data

Statistical correlation of analytical with experimental data was employed primarily as an evaluation of the technique. It is apparent that the test design was such that the data were neither sufficiently numerous nor appropriately distributed to meaningfully support such an analysis solely from an intrinsic point of view. The effort did serve, however, to sharpen the critique of the test design and as such is considered worthwhile.

Predictive Data

The analytical model computer program was used to predict the performance of the test apparatus for humidification and dehumidification processes. Predictive values which can be verified experimentally are the mass removal or addition rate of water and the efficiency of the process compared to maximum water exchange performance. For the latter comparison, equilibrium with the porous plate vapor pressure at the plate section outlet constitutes 100% efficiency.

Primary variables in the analysis result from an inspection of equation (18). Identifying the variables, the mass removal rate is proportional to the plate length along the channel (contact time) and a more complex function of the channel thickness and the gas flow velocity. The length of the plate was physically constrained; however, channel thickness was a variable and flow velocity was the prime variable. Control of inlet humidity and plate temperature at specific levels was not attempted; moreover, relatively constant inlet conditions existed.

Channel thickness parameter. — In predicting performance for this process, the effects of channel thickness on water exchange rate and efficiency were investigated.

The computer model of equations (18) and (20) was utilized to define the possible water exchange rates for a channel thickness of 0.22 inch. The concentration change factor is the initial driving force between the gas and the porous-plate wall. The concentration change factor is the initial driving force between the gas and the porous-plate wall. The concentration change involves plate temperatures from approximately 40 to 145° F. The removal rate is observed in figure 25 to be linear with concentration change for a fixed geometrical condition; i.e., the rate, r, is a function of $|C_i - C_o|$ and the efficiency, ϵ, is independent of the driving force. An alternate manner to consider the same data is to enter with the parameter of stream velocity. Results for this parametric evaluation are shown in figure 26.

It was indicated earlier that the efficiency of the process, $\Delta C_{io}/\Delta C_{iw}$, is dependent only on geometry, diffusion coefficient, and velocity; therefore, this variable was used to predict and compare test performance. A primary working plot was developed to determine efficiency for various stream velocities at set channel thickness. Most of the tests were to be performed at an arbitrarily selected channel height of 0.22 inch, although some tests were conducted at a height of 0.98 inch. The parametric height versus efficiency relationships are shown in figure 27. One hundred percent efficiency is a saturated air stream at the plate temperature. In using figure 27, it was noted that for velocities in excess of 2 feet per second, the efficiency was halved when the channel thickness was doubled for a constant velocity. This suggested the use of an effective or pseudo channel height, ϵh, to reduce the data range on figure 27 to a single curve. The results of this are shown in figure 28 where for velocities above 2 feet per second, the data converges to a single line.

The above analysis provided sufficient direction to select the velocities and channel heights for the test investigation.

Diffusion coefficient parameter. — The use of the diffusion coefficient for the air/water system is used explicitly in the solution for efficiency of the process. Although theoretical formulations are available for this quantity, they have been determined to be low by 5 to 12% (volume 3, ref. 5). Wexler presents values for the temperature range of interest; these values are plotted in figure 29. A difficulty arises in the selection of the temperature to evaluate this property; the temperature is somewhere between a plate temperature and entrance temperature of 41 and 80° F, respectively, for condensation and 132 and 76° F, respectively, for evaporation.

The effect of the diffusion coefficient on the predicted efficiency is shown in figure 30. The effect is not so pronounced as the channel thickness, but is enters numerically in the same exponential matter. Initially, the efficiencies were evaluated parametrically for channel depth at a mean temperature for the condensation process, 63° F. It is apparent that a considerably higher temperature, near 100° F, would be more suitable for theoretical prediction of runs E1 to E17.

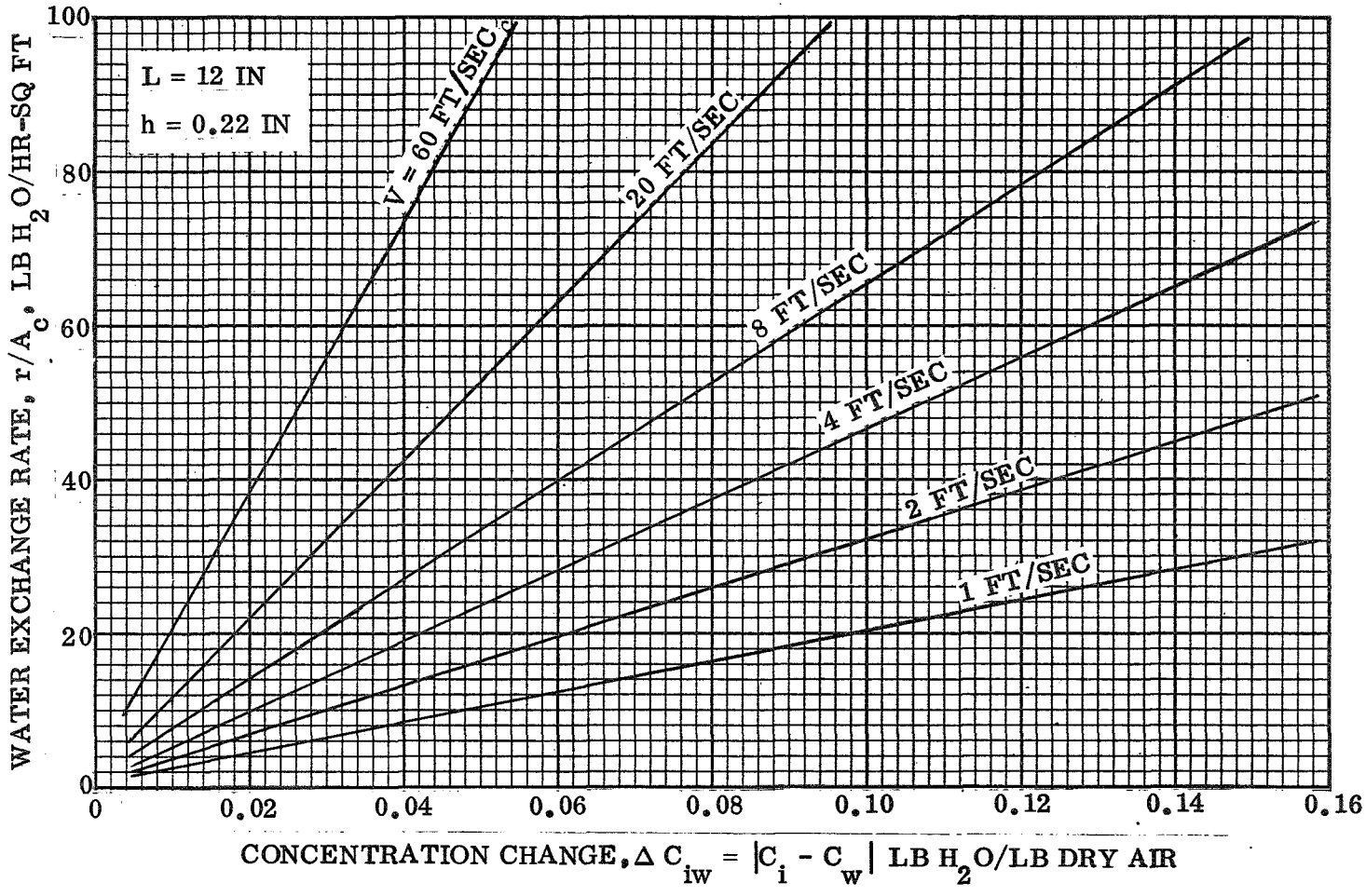


Figure 25. — Predictive Performance for Rate of Water Exchange for Humidification/Dehumidification Process

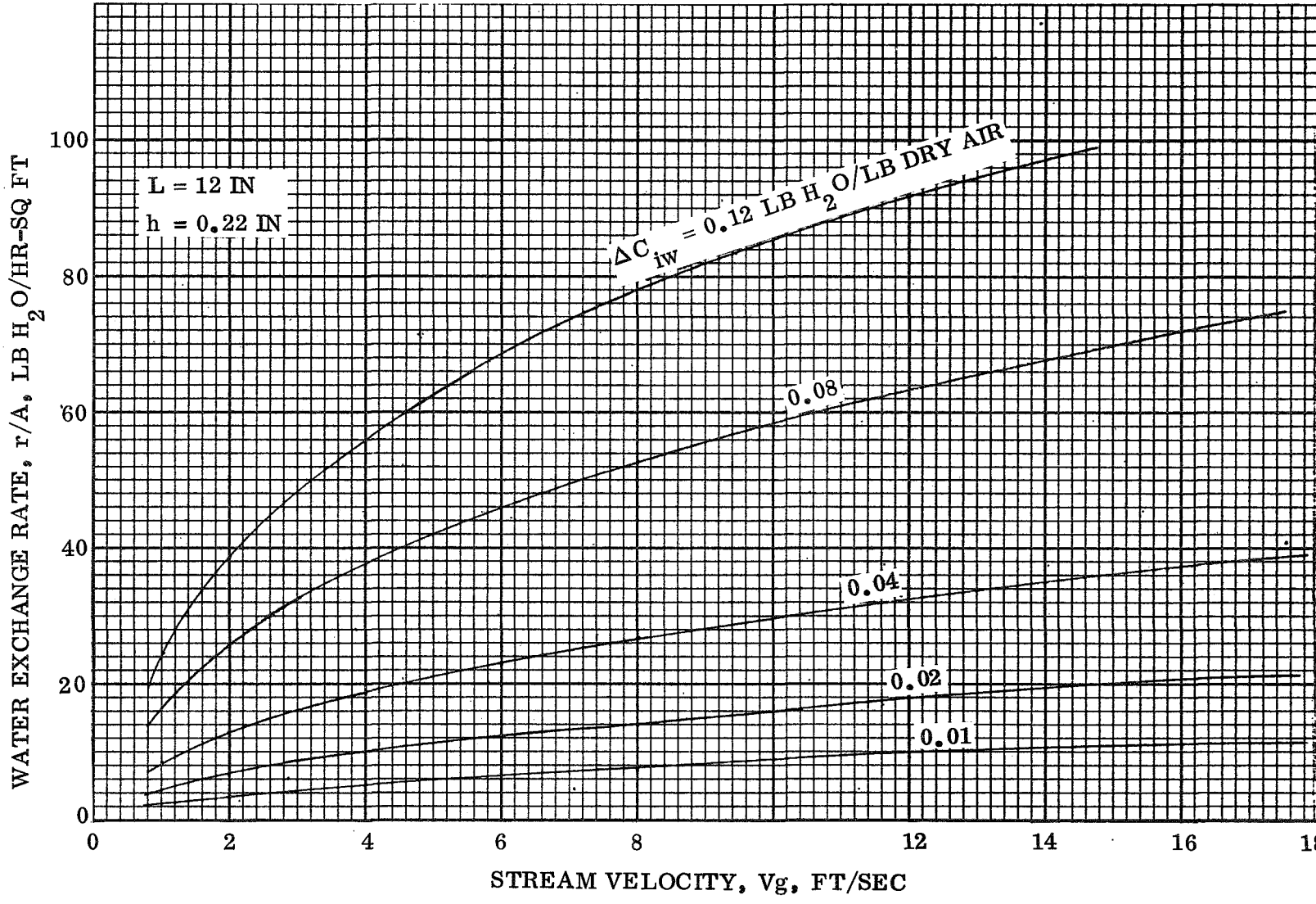


Figure 26. — Influence of Mean Stream Velocity on Rate of Water Exchange

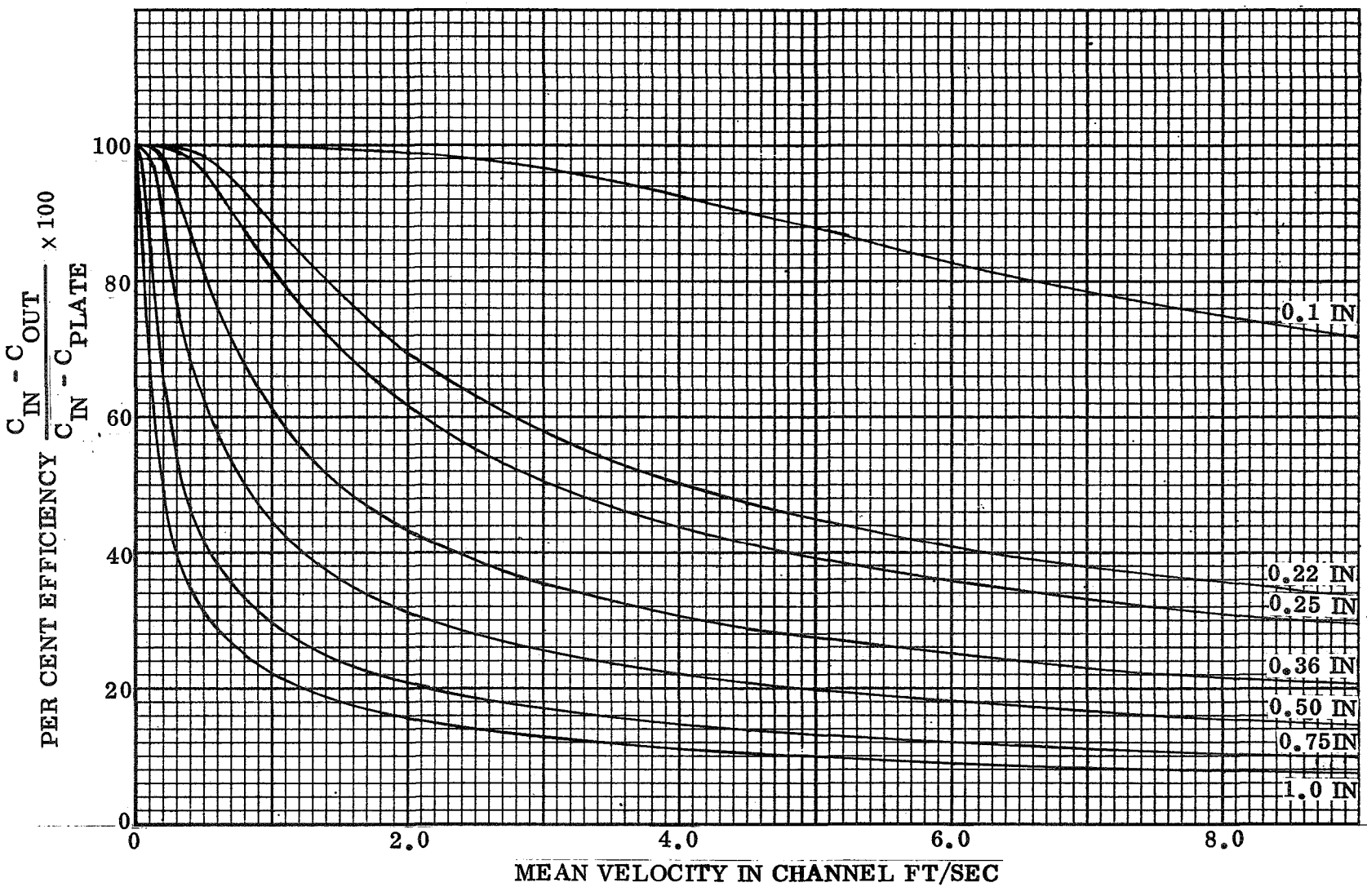


Figure 27. — Effect of Channel Height on Efficiency

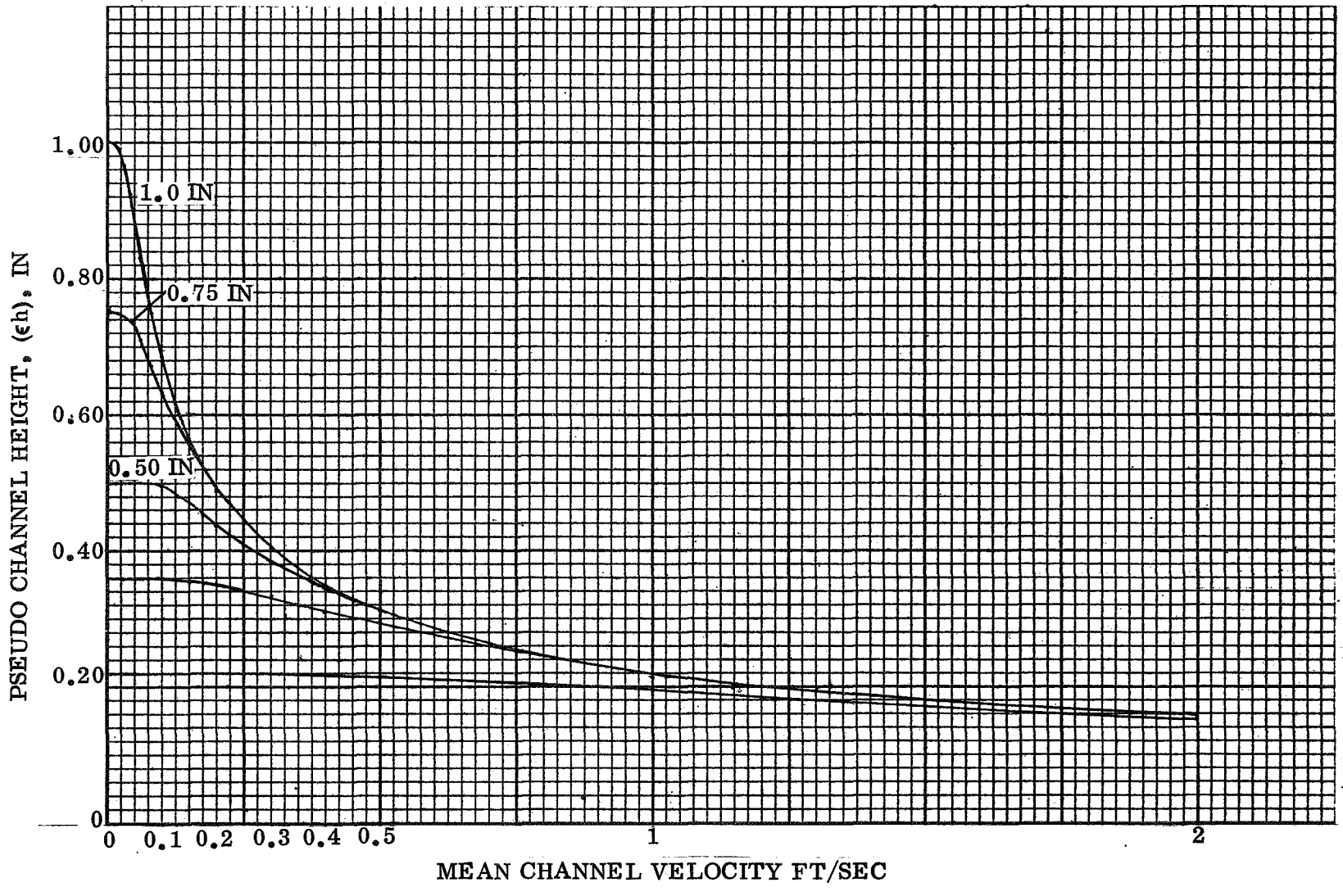


Figure 28. — Pseudo Channel Height/Efficiency Product Variation with Velocity

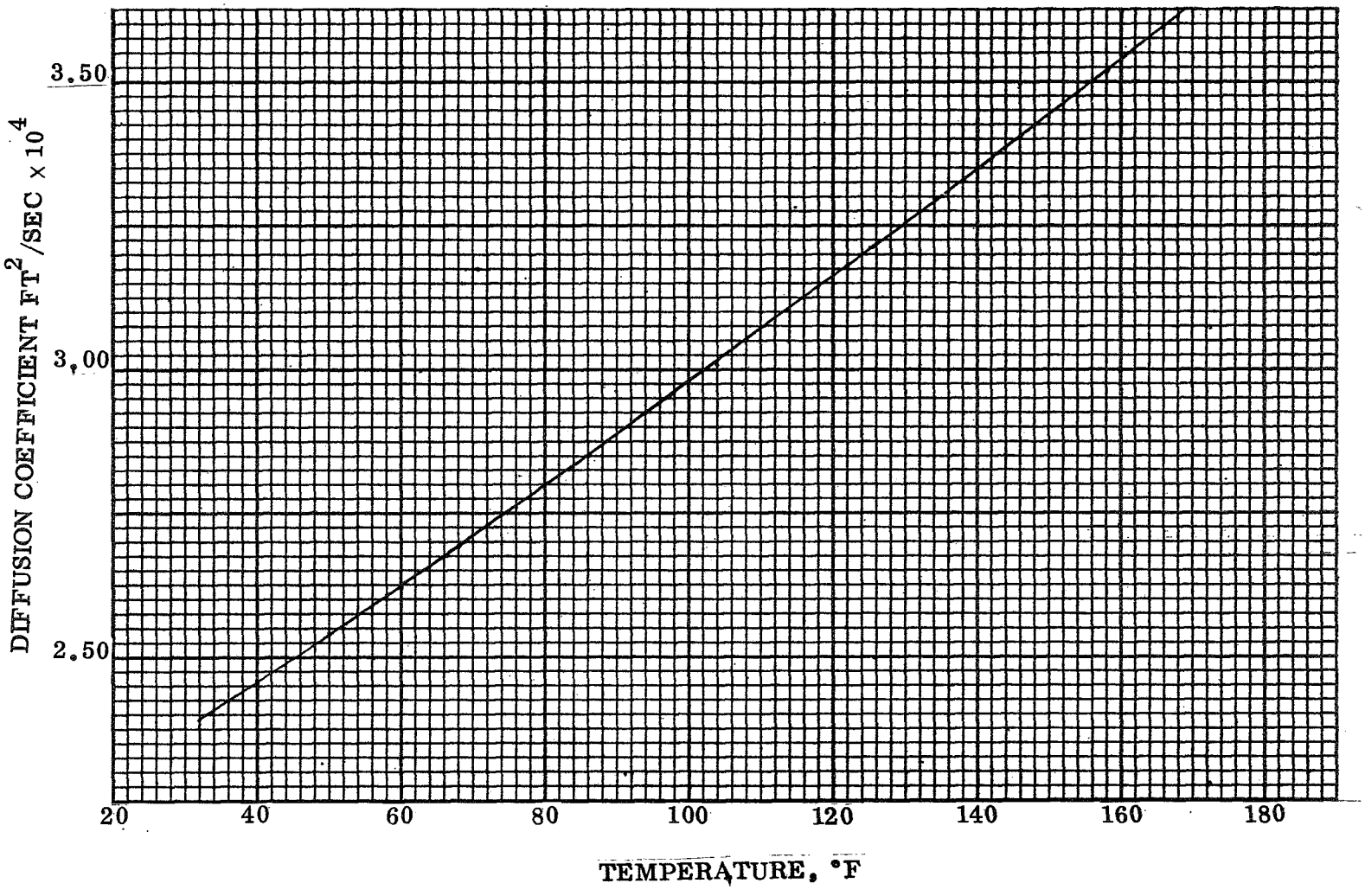


Figure 29. — Diffusion Coefficient as a Function of Temperature

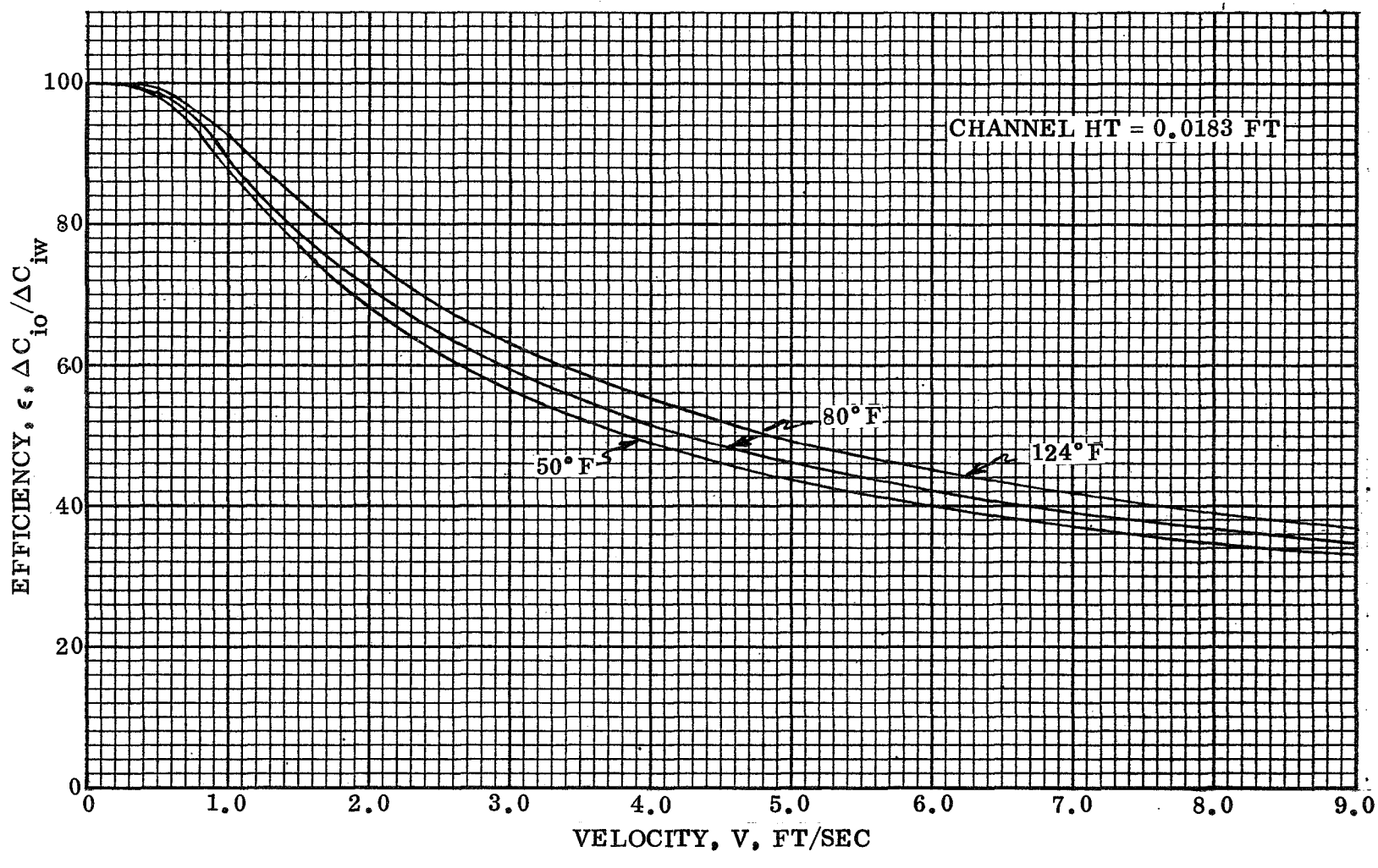


Figure 30. — Effect of Diffusion on Process Efficiency

A statistical analysis of the data will suggest the most suitable value for the diffusion coefficient.† These values for the coefficient will be applicable only to the temperature range and this hardware; however, the effects of diffusion coefficient cannot be separated from channel height which enters to the square power and may be in error by as much as 5%.

Experimental Data

The experimental data obtained in this investigation were presented in the experimental test report (ref. 4). The wet/dry bulb temperatures and the Casella dew point temperature measurements were reduced to obtain the humidity change in the flowing stream and ultimately the exchange rate. On condensation runs, the above two methods of humidity measurement can be compared with a catch basis removal rate. For evaporation runs, condensation and temperature problems resulted in only the catch rate measurement for most runs. Details of the calculations from the raw data are presented in Appendix A of reference 8.

Measurement of the gas flow rate was made at the outlet of the test section with an orifice measurement. These data were reduced to mean velocity over the porous plate, mass flow in the channel, and a channel Reynolds number using moist air properties applicable to outlet conditions.

With a known dry air flow rate and a water exchange rate from the catch tank, an equivalent ΔH change can be calculated for this measurement method. These are presented in tables 11 and 12 in units of grains for easy comparison (7000 grains equal one pound). Table 11 also points up the disparity between measurement techniques, i.e., wet/dry bulb and the dew point method. The latter consistently indicated lower humidity. The tolerances on the measurements reflect changes in conditions during a run as well as measurement error. Since conditions at inlet were not constant, ΔH was determined at several times during a typical 1- to 2-hour run. Although no well-defined data pattern appears, closer agreement generally exists between wet/dry bulb and Casella methods than either of these with the catch basin results. Since only catch basin data were available for the evaporation runs, these data suffer from the apparent limitations of the technique. However, as it will be shown later, the evaporation data exhibited the highest correlation coefficient and least scatter, at least for the correlation approach which has been utilized.

Reduced data similar to table 11 are presented for the evaporation runs in table 12. Only two attempts are shown for dew point and wet/dry bulb determination of humidity. These two cases did result in reasonable agreement with the catch basin evaluation. Inlet humidities were required to evaluate the saturation condition of the outlet stream after the porous plate.

† A value of the lumped parameter $D\,\pi^2 L/4\,h^2$ will be determined.

Table 11. — Condensation Test Reduced Data

	Humidity, Grains wet-dry bulb inlet	Humidity, Grains wet-dry bulb outlet	Humidity, Grains Casella inlet	Humidity, Grains Casella outlet	ΔH wet-dry grains	ΔH Casella grains	ΔH catch (calc) grains	$\dot{w}$ lb m gas / sec.	V ft / sec.	N_{Re}	Plate Suction in Hg
C1	112.0 ± 4	82 ± 4	98 ± 1	76 ± 2	30 ± 3	22 ± 2	33.9	.00203	3.7	392	11
C2a	105 ± 3	87 ± 2	93 ± 2	75.4 ± .4	18 ± 5	18 ± 2	14.3	.00345	6.4	667	11
C2b	100.9 ± .5	84.9 ± .7	95 ± .2	81.5 ± 1	16.0 ± 1.2	15 ± 1	11.1	.00345	6.4	667	11
C3	109.0 ± 1.0	95.0 ± 2	108.8 ± 2	95.2 ± 4	14.0 ± 3	13.6 ± 6	18.8	.00342	6.3	660	11
C4	83.5 ± 3	69 ± 2	80 ± 5	52.5 ± 1	14.5 ± 5	27.5 ± 6	22.2	.00068	1.3	132	11
C5	92.4 ± 3	74 ± 2	84.5 ± 10	63 ± 4	18.4 ± 5	21.5 ± 10	24.1	.00160	2.9	308	11
C6	106.4 ± .3	84.0 ± 1.2	95.0 ± 1	72.4 ± 3	22.4 ± 1.5	22.6 ± 4	26.2	.00204	3.7	396	11
C7	95.2 ± 1	61.0 ± 1	89 ± 2	59 ± 2	34.0 ± 1	30 ± 1.5	55	.00067	1.2	129	11
C8	95.6 ± .7	62.2 ± .3	86 ± 6	60 ± 2	33.4 ± .9	26 ± 6	55	.00067	1.2	129	3
C9	93 ± 2	85 ± 3	90.4 ± 4	77.2 ± 4	7.4 ± 1.5	13.2 ± 2	19.7	.00450	7.9	872	11
$C12_i$	85.2 ± 4	---	81 ± 5	70 ± 2	---	10 ± 3	12.6	.00378	6.47	737	---
$C13_i$	117 ± 10	---	122 ± 3	79 ± 4	---	43 ± 1	103	.00079	1.37	155	---
$C14_i$	133	---	125	92.2	---	32.8	65	.00165	2.86	323	---
$C16_t$	124 ± 1	---	117 ± 3	110 ± 1	---	7 ± 2	5.4	.0133	5.40	2580	---
$C17_t$	114	---	124 ± 3	110 ± 3	---	13.7 ± .3	10.5	.0068	2.75	1320	---
$C18_t$	146	---	135 ± 1	127	---	8 ± 1	8.7	.0193	7.88	3740	---

NOTE: For the tolerance on humidity, grains do not indicate measurement error necessarily, but change in conditions during test period. The ΔH measurements are a better indication of measurement accuracy but also reflect changing conditions.

i inverted t thicker channel

Table 12. — Evaporation Test Reduced Data

	Humidity, Grains wet-dry bulb inlet	outlet	Humidity, Grains Casella inlet	outlet	ΔH wet-dry grains	ΔH Casella grains	ΔH catch (calc) grains	$\dot{\omega}$ lb m gas / sec.	V ft sec.	N_{Re}
E1	65	--	59	--			242	.00321	6.52	580
E2	64.5	--	54	--			595	.00065	1.32	117
E3	60	--	51	--			406	.00146	2.94	264
$E4_R$	71	--	61	--			119	.01650	30.5	3270
$E5_i$	57.5	--	57	--			416	.00142	2.76	246
$E6_{Ri}$	58	--	57	--			850	.00057	1.12	98
$E7_{Ri}$	72	--	59	--			212	.00421	7.91	724
$E8_{Ri}$	74	--	57	--			252	.00325	6.22	562
$E9_{Ri}$	71	--	61	--			370	.00202	3.90	348
$E10_{Ri}$	67	--	59	--			888	.00091	1.78	163
$E11_{Ri}$	80	--	68	--			275	.00364	6.86	626
$E12_i$	71	--	69	--			324	.00259	5.00	433
$E14_{ti}$	67	112	61	100	45	39	46	.01790	8.11	3500
$E15_{ti}$	59	117	56	110	58	54	52	.00971	4.40	1900
$E16_{ti}$	69	--	55	--			59	.00655	2.96	1280
$E17_{ti}$	69	--	57	--			452	.00421	1.90	820

The prime correlation variable, the efficiency of the process, has been evaluated for each run from the available data. Each measurement method resulted in a separate evaluation for that run. The results of these evaluations are presented in table 13. One significant feature of this evaluation is the identification of calculated efficiencies greater than 100% for five low-gas velocity runs with a sixth run calculated at 98%. It can be noted that these catch basin results are not confirmed by the other measurement methods on runs C7, C8, and C13. For further discussion, refer to a subsequent section headed The supra-efficiency anomaly.

The data are presented in figures 31, 32, and 33 for the condensation runs C1 to C13 for the three respective measurement techniques. The theoretical prediction for an 0.22-inch channel thickness is also shown. The data fall significantly below prediction using the wet/dry bulb evaluations. The dotted lines reflect least squares correlation discussed in the section headed Data Correlation. It was earlier considered the theoretical prediction should be lowered by 10% to account for the fact that the porous plate is only 4.5 inches wide versus 5 inches for the actual channel width. Lateral diffusion probably negates this disparity when the distance is small and less than channel thickness. Therefore, for this work, the plate is assumed equal to channel width when considering the theoretical efficiency model, although this may have tended to result in producing some of the discrepancy between calculated and predicted efficiencies.

The reduced data obtained from the Casella dew point measurements is presented in figure 32. The improvement over the wet/dry bulb technique in reducing scatter is not readily apparent. Noteworthy in figure 32 are the three runs for condensation where the channel was inverted with the plate above. From those three points, no effect can be predicted. Theoretically, the model predicts the same efficiency for both cases.

The efficiencies determined from measured catch basin rates are shown in figure 33. In this instance, the measurements for the inverted channel do exhibit a trend; nonetheless, from three measurements it is difficult to discern if it is significant.

The efficiency data from measured catch basin data on the evaporation runs E1 to E12 appear in figure 34. At velocities above 2 ft/sec, these data exhibit the least scatter of any measured data. A slight trailing off from the prediction is observed at higher velocities. This was also detected in some condensation runs. The supra-efficiency data are indicated above 100%, but these values must be in error.

In evaluating the influence of channel thickness, a different theoretical efficiency curve results for each height. With a 0.98-inch channel thickness, very low efficiencies result. The calculated values from all three measurement techniques exhibit little scatter and are well predicted by theory (figure 35). One outlying point at a velocity of 1.9 ft/sec exists which appears to be experimentally in error although it is possibly related to the general trend of supra efficiencies below velocities of 2 ft/sec. It is below this velocity that efficiency moves rapidly upward toward 100%.

Table 13. — Efficiency Data for All Test Runs

Run	Efficiency %			Exchange Rate	Velocity
	wet-dry	Casella	Catch	gm/min	ft/sec
C1	43.5	49	49	.267	3.7
C2a	31.1	41.3	25.2	.190	6.4
C2b	31.4	40.5	21.4	.148	6.4
C3	23.7	23.1	31.9	.25	6.3
C4	36.3	74	55.5	.059	1.3
C5	37.6	51.3	49.2	.15	2.9
C6	34.4	42	40.3	.208	3.7
C7	61	60	98	.143	1.2
C8	62.5	59	102	.143	1.2
C9	13.9	25.8	36.6	.343	7.9
$C12_i$	--	24.5	28.7	.185	6.5
$C13_i$	--	49.4	116	.319	1.4
$C14_i$	--	73.7	72.2	.42	2.9
$C16_{ti}$	--	8	6.1	.281	5.4
$C17_{ti}$	--	14.6	11.1	.276	2.8
$C18_{ti}$	--	7.6	8.3	.65	7.9
E1	--	--	32.8	2.93	6.5
E2	--	--	106	1.51	1.3
E3	--	--	56.4	2.31	2.9
$E4_r$	--	--	15.8	7.6	30.5
$E5_i$	--	--	58.3	2.3	2.8
$E6_{ri}$	--	--	126	1.9	1.1
$E7_{ri}$	--	--	28.6	3.33	7.9
$E8_{ri}$	--	--	33.5	3.14	6.2
$E9_{ri}$	--	--	47.9	2.77	3.9
$E10_{ri}$	--	--	106	2.96	1.8
$E11_{ri}$	--	--	37	3.73	6.9
$E12_i$	--	--	43.7	3.09	5.0
$E14_{ti}$	5.7	5.0	6.0	3.18	8.11
$E15_{ti}$	7.5	6.9	6.7	1.93	4.4
$E16_{ti}$	--	--	7.6	1.45	3.0
$E17_{ti}$	--	--	78	7.15	1.9

r ≡ R = repeat

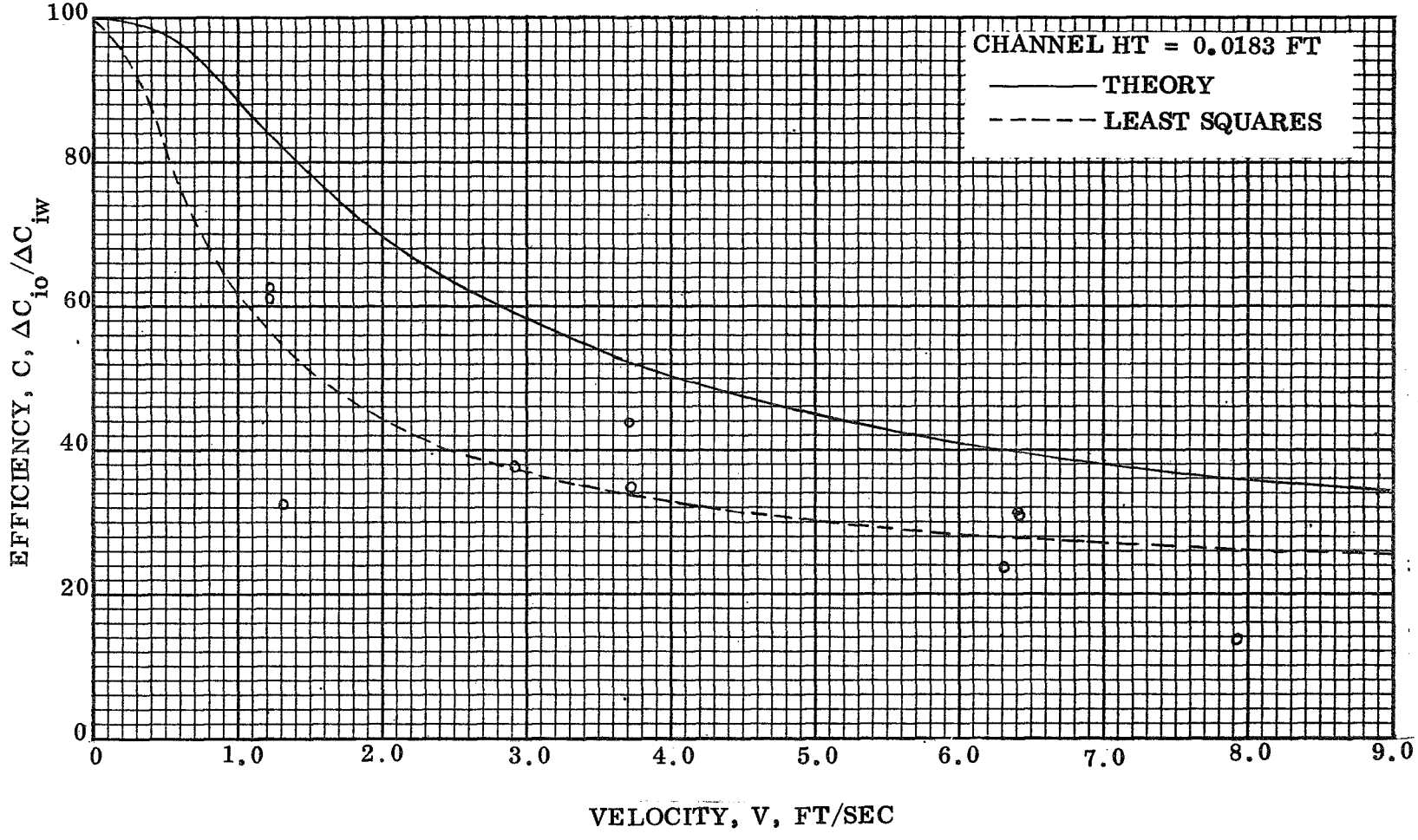


Figure 31. — Predicted Efficiency and Measured Condensation Data Efficiency from Wet/Dry Bulb Readings

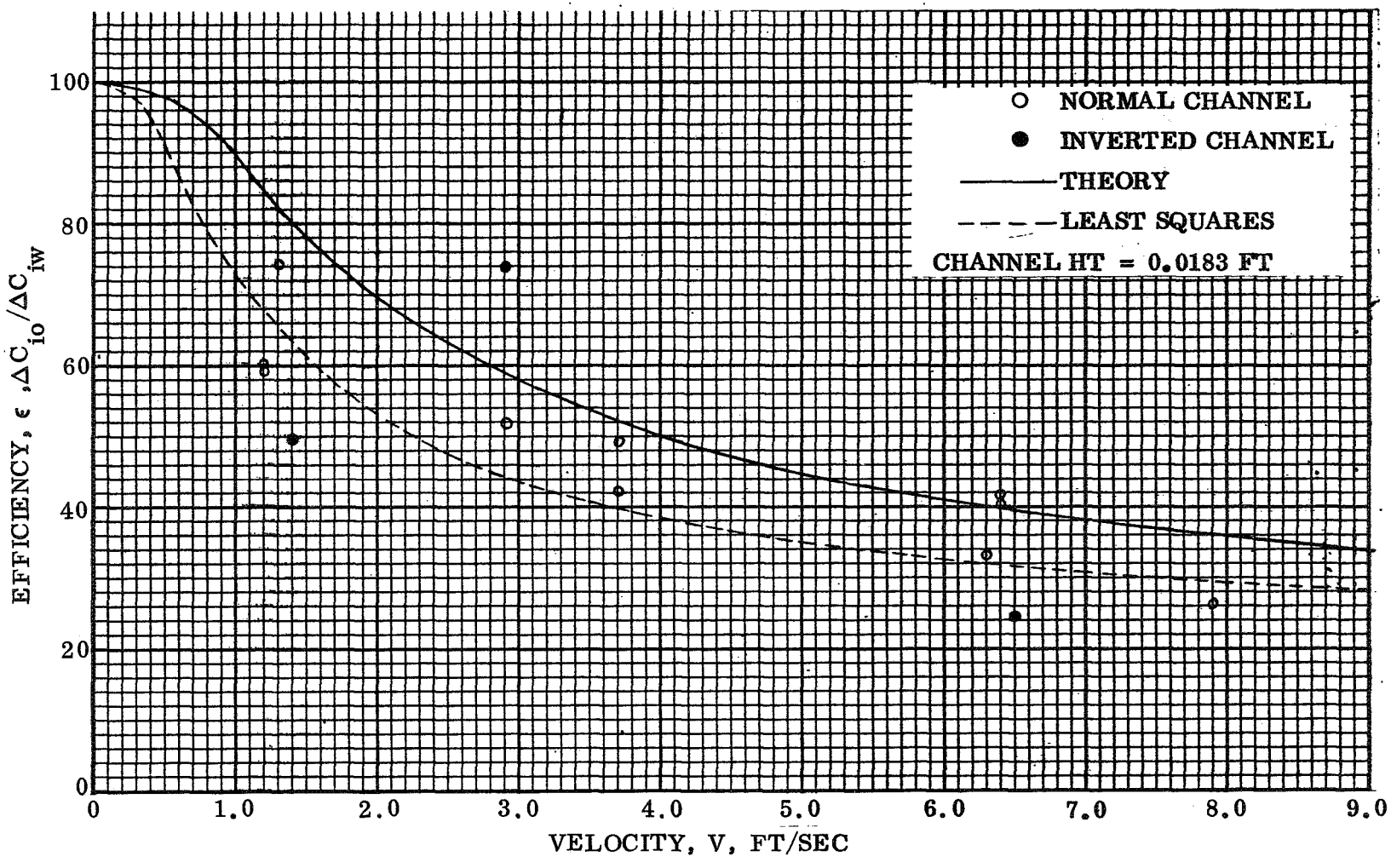


Figure 32. — Predicted Efficiency and Measured Condensation Data Efficiency from Casella Dew Points

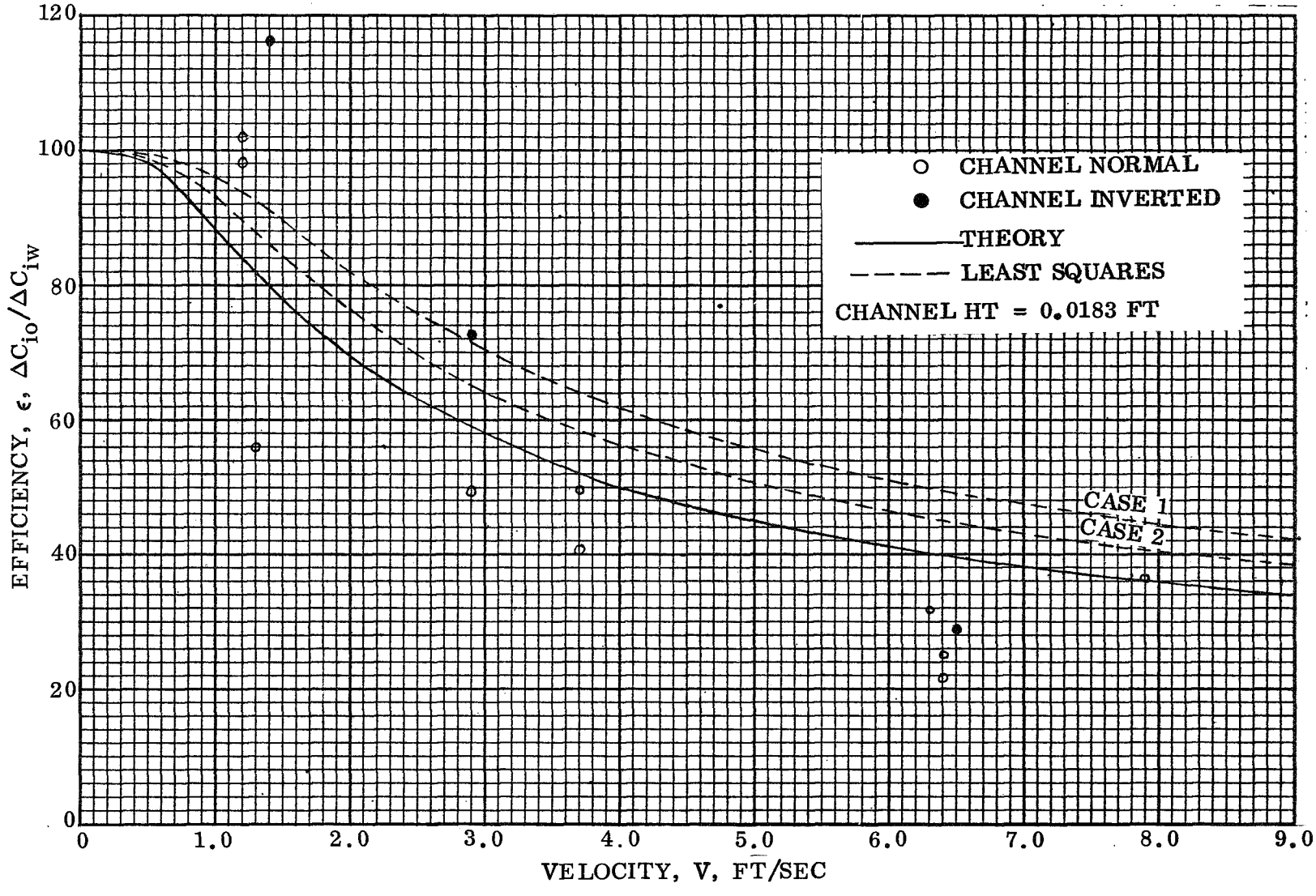


Figure 33. — Predicted Efficiency and Measured Condensation Data Efficiency from Catch Basin

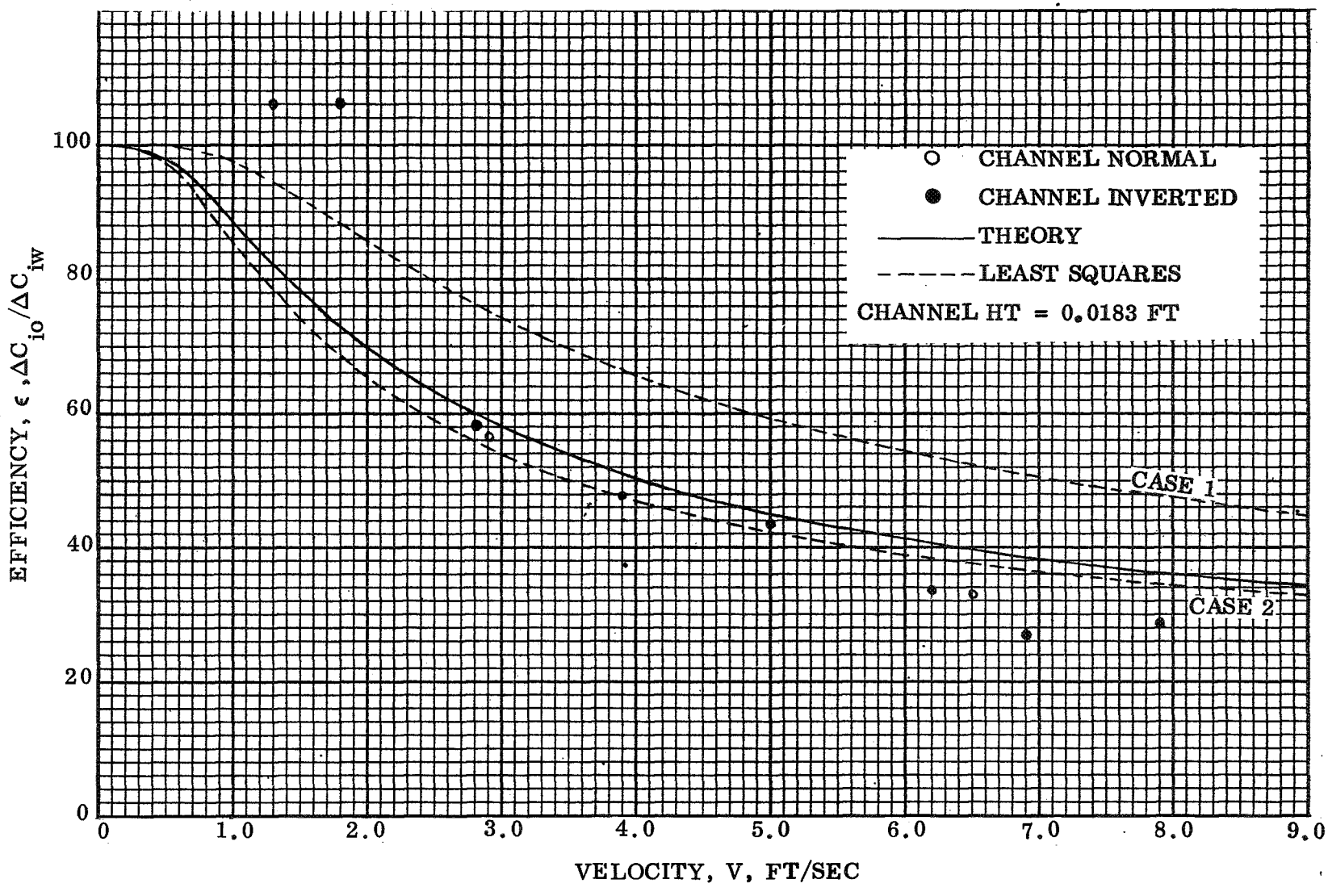


Figure 34. — Predicted Efficiency and Measured Evaporation Data Efficiency from Catch Basin

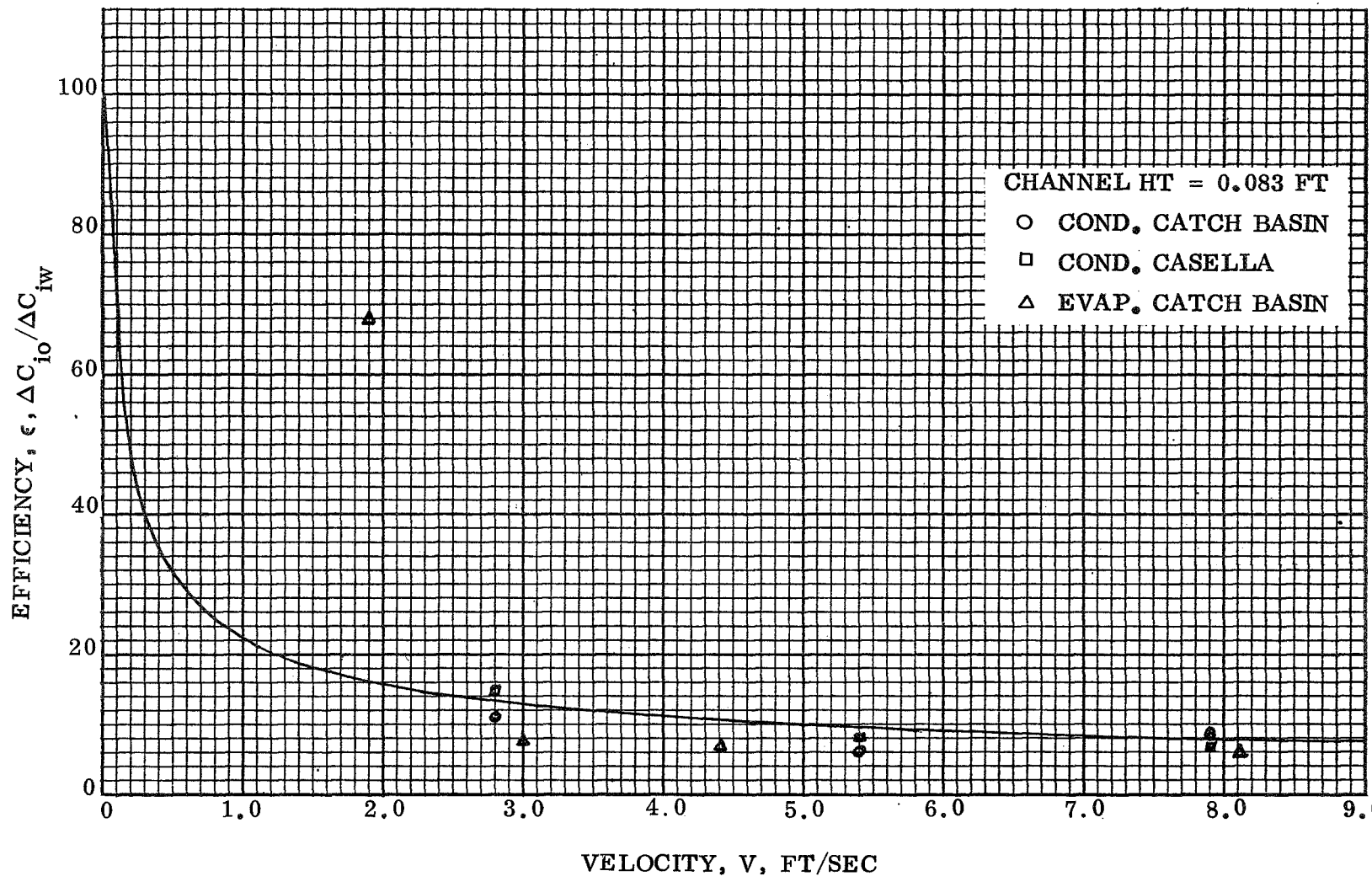


Figure 35. — Predicted Efficiency and Data Comparison for Deep Channel

Data Correlation

The experimental data have been reduced to efficiency values. The efficiency is a basic dimensionless parameter which yields the removal rate for a given initial driving force inlet humidity to porous plate. (Note that the term humidity is often used interchangeably with the term concentration.) The theory was derived for concentration units of lb H_2O/ft^3; thus, the density factor of moist air at various percent saturation enters into the efficiency. This simplification is not significant in this analysis. In summary, calculated efficiencies are based on humidities, theoretical predications on concentrations.

The data correlation was based on an expression with the same functional representation as the theoretical model. For velocities below 10 ft/sec and channel heights below 1/2 inch, little error is introduced if terms beyond the first in the summation in equation (20) are neglected. Therefore

$$\epsilon = 1 - \frac{8}{\pi^2} e \frac{-D \pi^2 L}{4 h^2 v_o}$$

Rearranging to a more suitable form for correlation

$$\text{en} \frac{\pi^2}{8} (1 - \epsilon) = - \frac{D \pi^2 L}{4 h^2 v_o}$$

Allowing y_i to take on values of $\text{en} \frac{\pi^2}{8} (1 - \epsilon)$ and $x_i = v_o^{-1}$, a least squares correlation through the origin results

$$y_i = A x_i$$

The solution for least squares with intercept of zero has only minor differences from standard least squares procedures (ref. 6, 7). The slope is defined by

$$A = E\, x\, y / E\, x^2$$

The variance of the estimate, S^2yx, has only one degree of freedom and is defined

$$S^2yx = \frac{E\, \hat{y}_o}{n-1} = \frac{E\, y^2 - b_o E\, xy}{n-1}$$

The correlation coefficient r is the measure of the correlation and its value approaches ±1 as the fit improves. It explains the deviation which can be explained by the x value, in this instance the gas velocity.

The correlation lines through the data are presented with dotted lines on figures 31 through 34. Some difficulty occurred for the catch basin runs with supra efficiencies. Values greater than 100% could not be considered since the value of $en(1-\epsilon)$ approaches minus infinity even for near 100% efficiency. Two correlation cases are shown: case 1 where 96% efficiency was substituted, and case 2 where these points are neglected. It is apparent the case 2 values represent all the data more reliably. Because of the nature of the en function, particularly large weight is given to the low-velocity values which unfairly bias the higher velocity data fit. Since the correlation line is forced to 100% at zero velocity, the case 2 coefficients are preferred.

The values for the coefficients, variance, and correlation coefficients for the data in figures 31 through 34 are presented in table 14.

Table 14. — Results of Correlation Analysis

Measurement	n	A	S	r
Condensation wet-dry bulb	10	-0.743	.989	.941
Condensation Casella	13	-1.096	.962	.900
Condensation catch basin 1	13	-3.023	.700	.900
Condensation catch basin 2	11	-2.455	.733	.832
Evaporation catch basin 1	12	-3.448	.880	.951
Evaporation catch basin 2	9	-1.703	.998	.990

Since A is equal to $-D\ \pi^2\ L/4\ h^2$, the only variable in all the above values of A is the diffusion coefficient since the remainder of the physical variables were held constant. There is no apparent explanation for the wide variation in A; consequently, one is led to conclude that the data are not of the same population, and the measurement technique is significantly influencing the coefficient A. The results further suggest the correlation value for slope A is not suitable for evaluating the effective diffusion coefficient. In evaporation case 2 above, a value of $D_V = 2.31 \times 10^{-4}\ ft^2/sec$ results, a slightly lower

than acceptable value (see figure 29). The range of D_v from table 14 above is 0.95×10^{-4} to 4.67×10^{-4} ft^2/sec, far exceeding the temperature range of figure 29 and this experimental evaluation.

It should be noted that two factors relative to the design of the experiment limit the value of a rigorous correlation analysis. First, the correlation is a statistical technique and, as such, is dependent upon relatively large quantities of data points and, secondly, that the data be dispersed throughout the range of the experimental observation rather than grouped as is the case for this experiment. The design of the experiment on the other hand was highly influenced by uncertainties relating to instrument accuracies and correlation between various measurement techniques which led to much grouping of data through attempts at replication.

Additionally, correlation analysis might be somewhat more effective if a more general function were employed instead of the particular exponential relation chosen which is not representative of the total range of physical behavior as the analytical model indicates. Indeed, the analytical model may itself be a more appropriate correlation mechanism even though not a simple functional form.

Results of the Experimental Evaluation

The execution of the experiment, analysis of the data, and examination of the correlative models have led to several changes both in the analytical model and the concepts relating to the utility and future design of the model and its experimental evaluation. Several of these changes appear to be of sufficient significance to warrant discussion.

The analytical model. — The analytical model results from the solution of the convective-diffusion equation (3). Solutions to this equation were obtained with similarity methods and Fourier boundary value solution. For a bounded channel, only the Fourier boundary value solution is appropriate. The model proved very beneficial in an examination of channel height effects and in the investigation of the effect of the diffusion coefficient. Changes in the analytical model resulting from the test were limited to an evaluation of the diffusion coefficient and an extension of the efficiency concept, equations (19) and (20).

The experimental evaluation. — In the analysis of the data, the wide variation in the data obtained in successive trials with the same instrumentation and between various measurement methods points out a need for more accurate and repeatable measurement techniques before proceeding with additional data acquisition. Although each of the three techniques employed in the experimental program is sufficiently dependable to evaluate the model in general terms, more precise evaluation is desirable. Other experimental procedures, potentially at least, add to the inaccuracies and possibly the scatter. For example, the use of external heaters or lamps to avoid condensation is in suspect and should be minimized or eliminated. Since the plate temperature is such an important

parameter in the efficiency evaluation, it probably should be measured more accurately. Any plate heating due to the lamps would introduce error. Similarly, very hot walls could permit more moisture to be carried in the stream than plate saturation temperature would indicate. The results of the evaporation catch basin data show the high degree of accuracy required in the results if meaningful evaluation of the diffusion coefficient is to be attained. The catch basin results are based on the gas flow rate in determining the efficiency whereas the other two evaluations are independent of mass flow of air. Any system leaks are more pronounced at low velocities where small flow orifices are used. Leaks occurring downstream of the plate but prior to the orifice lead to apparent high efficiencies and must be avoided.

The experimental approach was simple and is proven a highly valuable method for verifying the analytical model. The effectiveness of the experimental evaluation is only slightly degraded by the humidity measurement difficulties. Experimental control is simple and the efficiency evaluation eliminates necessity for precise control of inlet humidity conditions.

The supra-efficiency anomaly. — As can be seen from the data presented on figures 33 and 34, efficiencies calculated from water exchange rates (referred to as "catch basin") are generally below the model predictions for stream velocities above 2 ft/sec and higher than predicted below that value. For the lowest stream velocities the calculated efficiencies are above 100%. This apparent anomaly could arise from any one or combination of errors both experimental and computational. Errors must be expected in the determination of stream temperatures, velocities, and dew points. When these experimental errors are combined with the imprecision and, in some cases, inaccuracies of the psychometric tables (equations) on which most of the calculations depend, the errors can be quite significant. Likewise, transport of suspended liquid by the air stream could easily produce the apparent anomaly, as could errors in measurement of the water exchange rate. The appearance of this anomaly in the experiment was accompanied by increased interest due to similar experiences in tests being conducted by the LRC.

If one were to attempt to explain the apparent anomaly by assuming that whatever problem exists affects only the calculations involving the water exchange rates, one could logically show that any one or combination of several errors could be present as previously pointed out. Examples can be given to show that even small errors (1 to 2° F) in determining stream temperature could prove significant. Another error could be introduced by the transfer of liquid in droplet form, or a condensing of droplets, which allows the gas stream to pick up more moisture without reaching saturation. Still another, although less likely, could be introduced by the heating of the porous plate by radiation such that the plate temperature was somewhat higher than the water temperature in the reservoir below the plate. For Run 6R, the worst case, an increase in measured plate temperature from 135 to 141° F would decrease the efficiency from 126 to 100%.

However, if one were to view the possibility that the apparent anomaly results from a single mechanism or set of mechanisms which operates to provide observable error to the efficiency calculations for all three measurement techniques, a somewhat different set of conclusions results.

As one compares the calculated efficiencies derived from each of the three instrumentation techniques (figures 31, 32, and 33), it can be asserted that the calculated efficiencies for the psychometric method (wet/dry bulb) and the dew-point method (Casella) tend to be depressed throughout but somewhat more pronounced at the lowest stream velocities, while the calculated efficiencies employing the values attained by direct measurement of the water exchange rates tend to be increased. If such a characteristic were to be verified by the existence of more abundant data, it would lead one to question the accuracy of the stream velocity measurement for if the indicated velocity were lower than the true velocity, just such a combination of apparent characteristics would be in evidence.

Examination of the velocity measurement system reveals that several sources of error could have been present. Three of the more obvious of these potential error sources are:

a. Incorrect orifice coefficient employed in the velocity calculations.

b. Air leakage in the working section.

c. Phase change (condensation) phenomena at the orifice, especially during the evaporation runs.

Although it was not feasible to run a leak check and phase-change check following the final analysis of the test data (channel had been dismantled), a check on the 0.15-inch-diameter orifice coefficient was determined feasible and, thus, performed by the Standards Laboratory. A positive displacement air source was employed with flows scheduled in the range represented by channel velocities of 0 to 2 ft/sec. However, the results of this check indicated that lower rather than higher flow rates might well have been operating for the experiment than those calculated. (The check produced flow measurements lower than those which would have been calculated for identical orifice ΔP's, also a questionable finding.) However, if such were actually true during the experiments, it would have operated to reduce the magnitude of the apparent anomaly and simultaneously increased the apparent dropoff of efficiency for the estimates derived from the hygrometric measurements. However, duct leakage and phase change at the orifice are still suspect and stand as the mechanisms most logically producing the divergence of the calculation data based on catch and hygrometric techniques. Further experimentation is required to fully define the causative factors.

REFERENCES

1. Bird, R. B.; Stewart, W. E.; Lightfoot, E. N.: Transport Phenomena. John Wiley & Sons, New York, 1960.

2. Booth, F.: A Non-Aerosol Forming Zero Gravity Condenser/Separator Concept. LRC-LWP-575, April 1968.

3. Anon : Task #1 Data Summary, Item #7, System #2. Convair division of General Dynamics, 26 March 1969.

4. Burnett, J.: Experimental Test Report - Test #2, Diffusion Convection. NAS1-8494, Convair division of General Dynamics 29 October 1969.

5. Wexler, A. (editor): Humidity and Moisture, Measurement and Control in Science and Industry. A collection of papers presented at the1963 International Symposium on Humidity and Moisture, Washington, D.C. sponsored by NBS, U.S. Weather Bureau ASHRAE, AMS, ISA. Reinhold Publishing Corp. N.Y. 1965. Vol. 1, Principles and Methods of Measuring Humidity in Gases. R. E. Ruskin, editor. Vol. 3, Fundamentals and Standards, A. Wexler and W. Wildhack, editors.

6. Volk, William: Applied Statistics for Engineers. McGraw-Hill, New York, 1958, p. 256.

7. Bennett, C. A.; Franklin, N. L.: Statistical Analysis in Chemistry and the Chemical Industry. John Wiley & Sons, New York, 1954, p. 232.

8. Evans, E. A.; Bradshaw, R.; Burnett, J.: Analytical Model Report — Diffusion-Convection. NAS-1-8494, Second Issue, Convair division of General Dynamics, January 1970.

ANALYTICAL MODEL NO. 3 — "FILM STABILITY AND TRANSPORT"

The analytical model describes the behavior of thin liquid films which are reacting to the various forces applied in the interfaces between the film and the gaseous environment in which it exists.

The model is primarily oriented to the problem of film transport along the solid surface, with secondary interest in the transition from stable to unstable film configurations. The analysis has addressed itself to transport phenomena under two relatively dissimilar conditions, one involving film transport along flat surfaces where the film-to-gas stream interfacial shear may provide the major transport force, the other involving film transport on conical surfaces where the liquid surface effects may provide the major transport force.

The model considers the effects on the predicted behavior in each of the two cases resulting from variations in such system parameters as:

a. Gravitational field strength and orientation.

b. Surface temperature gradient.

c. Liquid characteristics as influenced by

   1. Mass density.

   2. Dynamic viscosity.

   3. Surface tension.

d. Gas stream characteristics as influenced by

   1. Velocity.

   2. Density.

   3. Pressure.

e. System boundary characteristics as influenced by

   1. Gas-film interface stability.

   2. Physical dimensions of the film and the solid surfaces.

Special attention is centered on both the conditions producing and the behavior during the transition from a stable to an unstable film/gas interface. The influence of the local gravity vector is explicitly examined.

The model is so designed as to be of potential value in the development or analysis of LSS equipments where film stability and transport phenomena can be expected. These phenomena are present in the on-design modes of operation in a high percentage of the LSS functions under study; thus the control of their behavior is critical. Additionally, when these phenomena are unintentionally produced as a result of off-design modes, the understanding of their behavior can be even more critical as, for instance, might be the case with a humidified breathing gas line choke resulting from unwanted condensation.

Table 15 gives the nomenclature used in the film stability and transport calculations.

DESCRIPTION OF THE MODEL

Case 1 - Flat Plate Surfaces

Motion of a thin liquid layer on a flat plate is described by the conservation of mass and momentum with two boundary conditions (steady flow, incompressible),

Table 15. — Nomenclature for Film Stability and Transport Calculations

NOMENCLATURE	
b	channel thickness, in.
d	channel width, in.
D_n	hydraulic radius, 4 A/P, ft
Fr	Froude number, $u_i/g\ h$
g	acceleration field, ft/sec
g_o	earth's gravity; 32.2 ft/sec
g_c	conversion constant, 32.17 lbm-ft/lbf-sec^2
h	film thickness, in.
$\bar{h}$	average film height, up and downstream, in.
N_T	Nusselt film thickness, n.d.
R	ratio of waveheight, δ_{dwm}/δ_{up}
Re_c	critical Reynolds number hu_i/ν
Re_ℓ	liquid Reynolds number, hu_i/ν
u_ℓ	liquid velocity, ft/sec
u_i	interface velocity, ft/sec
$\bar{u}_i$	average interface velocity, up and downstream, ft/sec
V_a	gas velocity ft/sec
We	Weber number, $u_i^2\ g\ h/\sigma\ g_c$
ϕ	empirical factor for shear, n.d.
θ	channel slope from horizontal, deg
ν_ℓ	kinematic viscosity for liquid
δ	wave height, in.
γ	surface tension

Mass Conservation

$$v_{i,i} = 0 \tag{1}$$

Momentum Conservation

$$v_j v_{i,j} = f_i - \frac{p,_i}{\rho} + \frac{\eta}{\rho} v_{i,jj} \tag{2}$$

where

v_i ≡ velocity field

f_i ≡ body force (e.g., gravity)

p ≡ pressure

ρ ≡ density

η ≡ dynamic viscosity

Boundary Conditions

@ Plate

$$v_i^{\ell} = 0 \tag{3}$$

@ Free Surface

$$\sigma_{ij}^{\ell} n_{s_j} = \sigma_{ij}^{g} n_{s_j} + \gamma,_i \tag{4}$$

where

Superscripts denote: $(\,)^{\ell}$ liquid, $(\,)^{g}$ gas

γ ≡ surface tension

σ_{ij}^{ℓ} ≡ stress tensor in liquid

σ_{ij}^{g} ≡ stress tensor in gas

n_{s_j} ≡ normal to free surface

$$\sigma_{ij}^{g} = - p^{g}\, \delta_{ij} + \eta^{g}\, (v_{i,j} + v_{j,i})_{s}^{g} \tag{5}$$

$$(\ )_{,i} \equiv \frac{\partial (\ )}{\partial x_i} \text{ or } \nabla(\ )$$

δ_{ij} = Kronecker Delta

$$\sigma_{ij}^{\ell} = - p^{\ell}\, \delta_{ij} + \eta^{\ell}\, (v_{i,j} + v_{j,i})_{s}^{\ell} \tag{6}$$

Equations (4) - (6) yield

$$(p^{g} - p^{\ell})\, n_{s_i} + \left[\eta^{\ell}\, (v_{i,j} + v_{j,i})_{s}^{\ell} - \eta^{g}\, (v_{i,j} + v_{j,i})_{s}^{g}\right] n_{s_j} - \gamma_{,i} = 0 \tag{7}$$

For the flat plate, laminar problem, the equations (1), (2), (3), and (7) reduce to

Mass Conservation

$$\frac{\partial u}{\partial x} = 0 \tag{8}$$

Momentum Conservation (using equation (8))

$$0 = g_x - \frac{1}{\rho^{\ell}} \frac{dp^{\ell}}{dx} + \frac{\eta^{\ell}}{\rho^{\ell}} \frac{d^2 u}{dy^2} \tag{9}$$

Boundary Conditions

@ Plate

$$u = 0$$

@ Free Surface

$$(y = h)$$

$$(p^{g} - p^{\ell})\, \hat{e}_y + \left[\eta^{\ell} \left(\frac{\partial u}{\partial y}\right)_{s}^{\ell} - \eta^{g} \left(\frac{\partial u}{\partial y}\right)_{s}^{g}\right] \hat{e}_x - \frac{\partial \gamma}{\partial x} \hat{e}_x = 0 \tag{10}$$

$\hat{e}_i \equiv$ unit vectors

which implies

$$p^g = p^\ell \tag{11}$$

$$\eta^\ell \left(\frac{\partial u}{\partial y}\right)_s^\ell - \eta^g \left(\frac{\partial u}{\partial y}\right)_s^g - \frac{\partial \gamma}{\partial x} = 0 \tag{12}$$

Define:

$$\tau \equiv \eta^g \left(\frac{\partial u}{\partial y}\right)_s^g + \frac{\partial \gamma}{\partial x}$$

$$a \equiv \left(\frac{dp^g}{dx} - \rho^\ell g_x\right)$$

Using the boundary conditions (equations (11) and (12)), equation (9) becomes

$$u = \frac{1}{\eta^\ell}\left[\frac{a y^2}{2} + (\tau - ah)\, y\right] \tag{13}$$

Normally, surface tension gradient is due to temperature gradient

$$u = \frac{1}{\eta^\ell}\left[\frac{a y^2}{2} + \left(\eta^g \left(\frac{\partial u}{\partial y}\right)_s^g + \frac{\partial \gamma}{\partial T}\,\frac{\partial T}{\partial x} - ah\right) y\right] \tag{14}$$

where

T ≡ temperature

$$\frac{\text{Flow Rate}}{\text{Width}} = \int_0^h \rho u\, dy = \frac{\rho h^2}{\eta^\ell}\left(\frac{\tau}{2} - \frac{ah}{3}\right)$$

Films experiencing interfacial shear acceleration become unstable and eventually disintegrate for a range of dynamic parameters (represented by Reynolds, Froude, and Weber numbers). Reference 1 is an extensive and comprehensive treatment of instability, an adaptation of which was employed for a numerical solution to the definition of the transition boundary.

The problem considered is that of a film with a linear velocity profile; equation (14) implies the following condition

$$\left[\eta^g\left(\frac{\partial u}{\partial y}\right)_s^g + \frac{\partial \gamma}{\partial T}\frac{\partial T}{\partial x} - ah\right] \gg \frac{ah}{2}$$

or

$$\left[\eta^g\left(\frac{\partial u}{\partial y}\right)_s^g + \frac{\partial \gamma}{\partial T}\frac{\partial T}{\partial x}\right] \gg \frac{3ah}{2} \tag{15}$$

Equation (15) represents an interfacial shear dominated film (the case of interest in life support systems). The stabilizing influence of gravity (resists perturbation) and of surface tension are considered in the boundary condition. Figure 36 defines the predicted stability boundary.

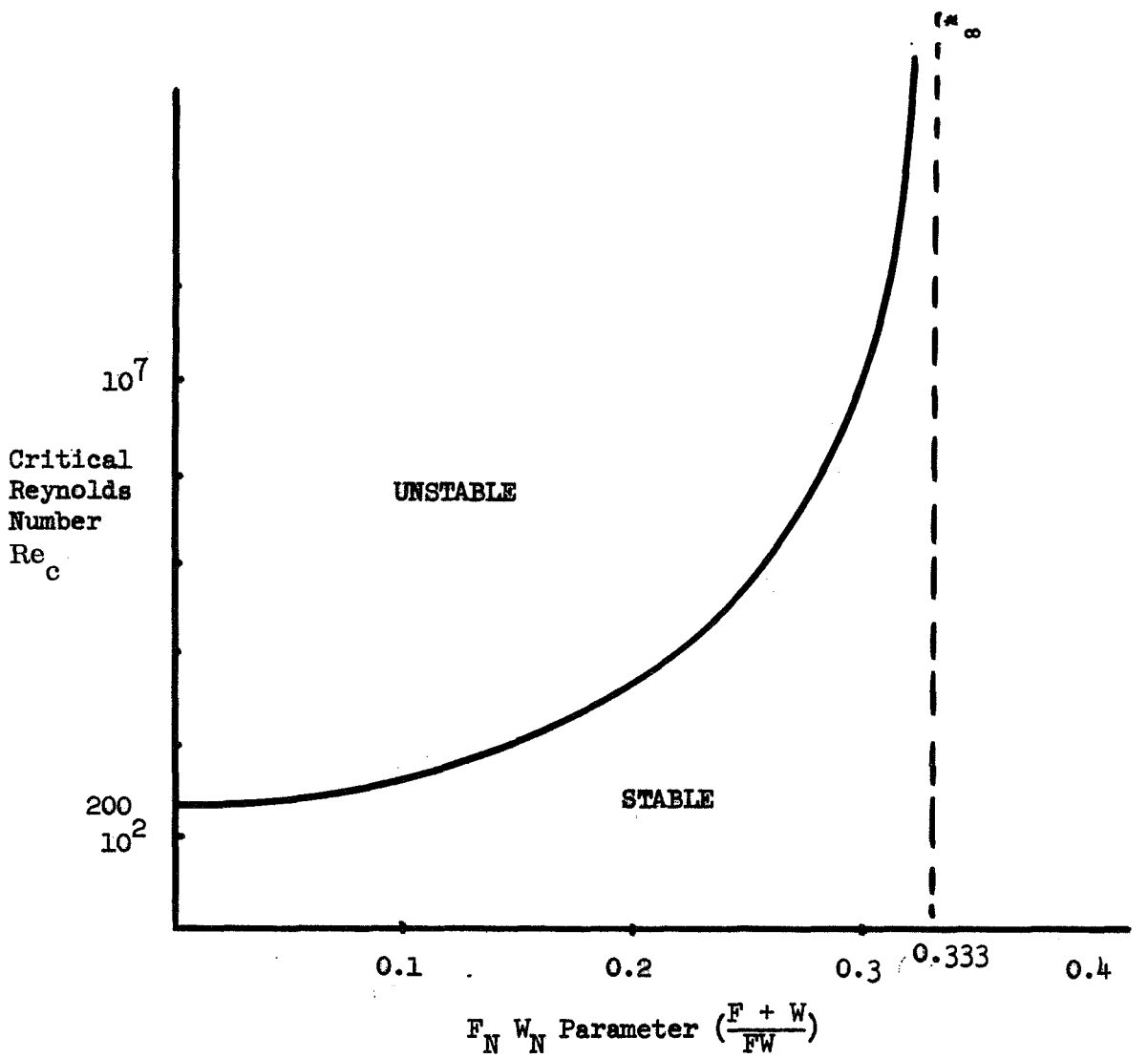


Figure 36. — Predicted Stability Boundary

For the situation of gas stream accelerating a liquid film, the critical Reynolds number is approximately given by

$$Re_c \cong 200\left[1 - 3\left(\frac{F+W}{FW}\right)\right]^{-4} \tag{16}$$

where

Re_c = critical Reynolds number

Fr = Froude number

We = Weber number

$$Re = \frac{\rho^{\ell} uh}{\eta^{\ell}}$$

$$Fr = \frac{u^2}{g_y h}$$

$$We = \frac{\rho^{\ell} u^2 h}{\gamma}$$

Note: This equation can be related to the graphical representation of "Film Stability Criteria" as shown by figure 3 of reference 2 which was based on work by Reynolds et al of Stanford University in 1964. However, equation (16) contains an inertial field dependence missing in the representation of the treatment by Reynolds.

Extremes of equation (16) are evident,

$$Re_c \cong 200 \quad \text{for} \quad \alpha = 0$$

$$Re_c \to \infty \quad \text{for} \quad \alpha \geq \frac{1}{3}$$

where

$$\alpha = \frac{\gamma + \rho^{\ell} g_y h^2}{u^2 h \rho^{\ell}} = \frac{F+W}{FW} \tag{17}$$

Stability is given by $Re < Re_c$.

$$Re < Re_c \cong 200\,(1-3\alpha)^{-4} \text{ STABLE}$$

Case 2 - Conical Surfaces

Motion of a thin liquid layer which uniformly wets the wall of a conical surface is described by equations (1), (2), (3), and a modified equation (4)

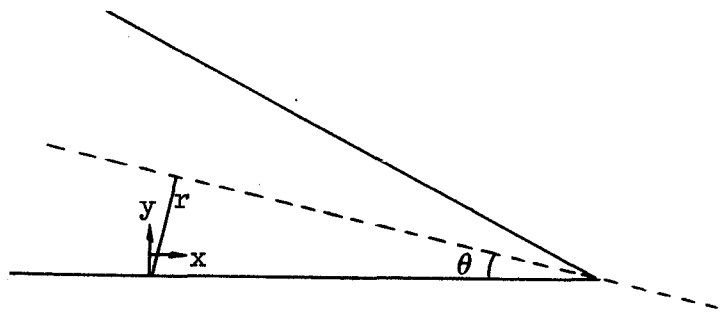
$$\sigma_{ij}^{\ell} n_{s_j} = \sigma_{ij}^{g} n_{s_j} + \gamma_{,i} + \gamma n_{s_i} (K_1 + K_2) \tag{18}$$

where

K_1 = principal curvature of surface

K_2 = principal curvature of surface

For this analysis, the fluid will be assumed to have no azimuthal velocity. The following coordinate system will be assumed.



Equations (1) and (2) become

Mass Conservation

$$\frac{1}{r}\frac{d}{dx}(r\,u) = \frac{\dot{m}\,\zeta(x)}{\rho^{\ell}} \tag{19}$$

where

$\dot{m}$ ≡ mass condensation flux (from gas interior to the liquid interface)

$\zeta(x)$ ≡ ratio of the circular perimeter of the interface at x to the film cross-sectional area at the coordinate x

$$\zeta(x) = \frac{(L-X)(\sin\theta) - h(\cos\theta)}{(L-X)(\sin\theta)\,h - \frac{h^2}{2}(\cos\theta)} \tag{20}$$

Momentum Conservation

$$u\frac{\partial u}{\partial x} = g_x - \frac{1}{\rho^{\ell}}\frac{\partial p^{\ell}}{\partial x} + \frac{\eta^{\ell}}{\rho^{\ell}}\frac{\partial^2 u}{\partial y^2} \tag{21}$$

It is assumed that gravity acts in the direction of the cone axis in order to preserve circular symmetry; however, the magnitude is variable.

$$g_x = g \cos \theta$$

Equations (19) and (21) combine to give,

$$\frac{u^2}{r}\frac{dr}{dx} - \frac{\dot{m}\, u\, \zeta}{\rho^{\ell}} + \frac{\eta^{\ell}}{\rho^{\ell}}\frac{\partial^2 u}{\partial y^2} = \frac{1}{\rho^{\ell}}\frac{\partial p^{\ell}}{\partial x} - g_x$$

$$\frac{1}{r}\frac{dr}{dx} \simeq \frac{1}{(L-X)}$$

$$-\frac{u^2}{(L-X)} - \frac{\dot{m}\, u\, \zeta}{\rho^{\ell}} + \frac{\eta^{\ell}}{\rho^{\ell}}\frac{\partial^2 u}{\partial y^2} = \frac{1}{\rho^{\ell}}\frac{\partial p^{\ell}}{\partial x} - g_x \qquad (22)$$

where

L ≡ length along surface of cone.

The boundary conditions become

@ plate

$$u = 0$$

@ free surface

$$(y \equiv h)$$

$$(p^g - p^{\ell})\,\hat{e}_y + \left[\eta^{\ell}\left(\frac{\partial u}{\partial y}\right)_s^{\ell} - \eta^g\left(\frac{\partial u}{\partial y}\right)_s^{g}\right]\hat{e}_x - \frac{\partial \gamma}{\partial x}\,\hat{e}_x - \gamma\,\hat{e}_y\,(K_1 + K_2) = 0$$

which implies

$$p^{\ell} = p^g - \gamma\,(K_1 + K_2)\ (\hat{e}_y \text{ component}) \qquad (23)$$

$$\eta^{\ell}\left(\frac{\partial u}{\partial y}\right)_s^{\ell} - \eta^g\left(\frac{\partial u}{\partial y}\right)_s^{g} - \frac{\partial \gamma}{\partial x} = 0\ (\hat{e}_x \text{ component})$$

$$\left(\frac{\partial u}{\partial y}\right)^{\ell}_{s} \equiv \frac{\tau}{\eta^{\ell}} = \frac{1}{\eta^{\ell}}\left[\eta^{g}\left(\frac{\partial u}{\partial y}\right)^{g}_{s} + \frac{\partial \gamma}{\partial x}\right] \tag{24}$$

Using equation (23)

$$\frac{\partial p^{\ell}}{\partial x} = \frac{\partial p^{g}}{\partial x} - \gamma \frac{\partial}{\partial x}(K_1 + K_2) - (K_1 + K_2)\frac{\partial \gamma}{\partial x}$$

For conical surface,

$$K_2 \cong 0$$

$$K_1 \cong \frac{1}{(L-x)(\tan\theta) - h}$$

$$\frac{\partial h}{\partial x} \cong 0, \text{ since } K_2 = 0$$

$$\frac{\partial K_1}{\partial x} \cong \left[(L-x)\tan\theta - h\right]^{-2}(\tan\theta)$$

$$\frac{\partial p^{\ell}}{\partial x} = \frac{\partial p^{g}}{\partial x} - \frac{1}{\left[(L-x)\tan\theta - h\right]^{2}}\left[\gamma \tan\theta + \left((L-x)\tan\theta - h\right)\frac{\partial \gamma}{\partial x}\right] \tag{25}$$

Equation (25) does not assume that the film is thin; however, it only neglects the curvature in the x direction (which is usually an order of magnitude smaller than that in the azimuthal direction).

Define

$$\Delta p \equiv -\rho^{\ell} g_x + \frac{\partial p^{\ell}}{\partial x} \tag{26}$$

Equation (22) becomes

$$\frac{d^2u}{dy^2} - \frac{\rho^{\ell} u^2}{\eta^{\ell}(L-x)} - \frac{\dot{m}\,\zeta\, u}{\eta^{\ell}} = \frac{\Delta p}{\eta^{\ell}} \tag{27}$$

Solution to the nonlinear equation (27) is of the form,

$$y = \int_o^u \frac{d\theta}{(C_4 + 2C_1\,\theta + C_3\,\theta^2 + 2/3\,C_2\,\theta^3)^{1/2}} \tag{28}$$

where

$C_4 \equiv$ integration constant

$$C_1 \equiv \frac{\Delta p}{\eta^{\ell}}$$

$$C_2 \equiv \frac{\rho^{\ell}}{\eta^{\ell}(L-x)}$$

$$C_3 \equiv \frac{\dot{m}\,\zeta}{\eta^{\ell}}$$

Since equation (28) is not readily inverted, it is of interest to linearize equation (27) and integrate (this is quite reasonable since the fluid inertia, ρu^2, is small in most situations).

$$u = u_o + \delta u$$

$$\frac{d^2(\delta u)}{dy^2} - \frac{2\,u_o\,\rho^{\ell}(\delta u)}{\eta^{\ell}(L-x)} - \frac{\dot{m}\,\zeta\,(\delta u)}{\eta^{\ell}} = \frac{p}{\eta^{\ell}} + \frac{u_o^2\,\rho^{\ell}}{\eta^{\ell}(L-x)} + \frac{\dot{m}\,\zeta\,u_o}{\eta^{\ell}}$$

$$\frac{d^2(\delta u)}{dy^2} - \frac{2u_o\,\rho^{\ell}}{\eta^{\ell}(L-x)}\left(1 + \frac{\dot{m}\,\zeta\,(L-x)}{2\,\rho^{\ell}\,u_o}\right)(\delta u) = \frac{\Delta p}{\eta^{\ell}} + \frac{u_o^2\,\rho^{\ell}}{\eta^{\ell}(L-x)}\left(1 + \frac{\dot{m}\,\zeta\,(L-x)}{\rho^{\ell}\,u_o}\right) \tag{29}$$

Solution to equation (29) is,

$$u = A_1\,e^{\lambda y} + A_2\,e^{-\lambda y} - \left[\frac{\Delta p(L-x)}{\rho^{\ell}\,u_o(2+\beta)} - u_o\left(\frac{1}{2+\beta}\right)\right] \tag{30}$$

$$\lambda = \sqrt{\frac{2\, u_o\, \rho^{\ell} \left(1+\frac{\beta}{2}\right)}{\eta^{\ell}\,(L-x)}} \tag{31}$$

$$\beta = \frac{\dot{m}\ \zeta\ (L-x)}{\rho^{\ell}\, u_o} \tag{32}$$

Boundary conditions yield,

$$A_1 + A_2 = \left[\frac{\Delta p(L-x)}{\rho^{\ell}\, u_o (2+\beta)} - u_o \left(\frac{1}{2+\beta}\right)\right]$$

$$A_1\, e^{\lambda h} - A_2\, e^{-\lambda h} = \frac{\tau}{\eta^{\ell}\,\lambda}$$

which imply,

$$A_1 = \frac{\left[\frac{\tau}{\eta^{\ell}\,\lambda} + \left(\frac{\Delta p(L-x)}{u_o\, \rho^{\ell}} - u_o\right) \frac{e^{-\lambda h}}{(2+\beta)}\right]}{(e^{\lambda h} + e^{-\lambda h})} \tag{33}$$

$$A_2 = \frac{-\left[\frac{\tau}{\eta^{\ell}\lambda} - \left(\frac{\Delta p(L-x)}{u_o\, \rho^{\ell}} - u_o\right) \frac{e^{\lambda h}}{(2+\beta)}\right]}{(e^{\lambda h} + e^{-\lambda h})} \tag{34}$$

The value for u_o is given by,

$$u_o = \frac{\int_o^h u\,(2\pi r)dy}{\int_o^h (2\pi r)dy} \tag{35}$$

$$r = (L-x)(\sin\theta) - y(\cos\theta)$$

Equation (35) is transcendental in u_o and must be solved iteratively. The equation for the iteration procedure is represented by

$$u_o = \left\{ A_1 \left[\frac{(L-x)\sin\theta}{\lambda} (e^{\lambda h} - 1) - \frac{\cos\theta}{\lambda^2} \left(e^{\lambda h} (\lambda h - 1) + 1 \right) \right] \right.$$

$$\left. + A_2 \left[\frac{(L-x)\sin\theta}{\lambda} (1 - e^{-\lambda h}) + \frac{\cos\theta}{\lambda^2} \left(e^{-\lambda h} (\lambda h + 1) - 1 \right) \right] \right\} \Big/$$

$$\left[(L-x)(\sin\theta) h - \frac{h^2}{2} (\cos\theta) \right] - \left\{ \frac{\Delta p (L-x)}{\rho^{\ell} u_o (2+\beta)} - \frac{u_o}{(2+\beta)} \right\} \tag{36}$$

To find $u_o = f(x)$, u_o is found at $x = 0$ and the mass conservation equation (19) is integrated to give u_o at any x

$$\int_o^x \frac{1}{r} \frac{d}{dx} (ru) A(x)\, dx = \int_o^x \frac{\dot{m} \zeta(x) A(x)}{\rho^{\ell}} dx \tag{37}$$

where

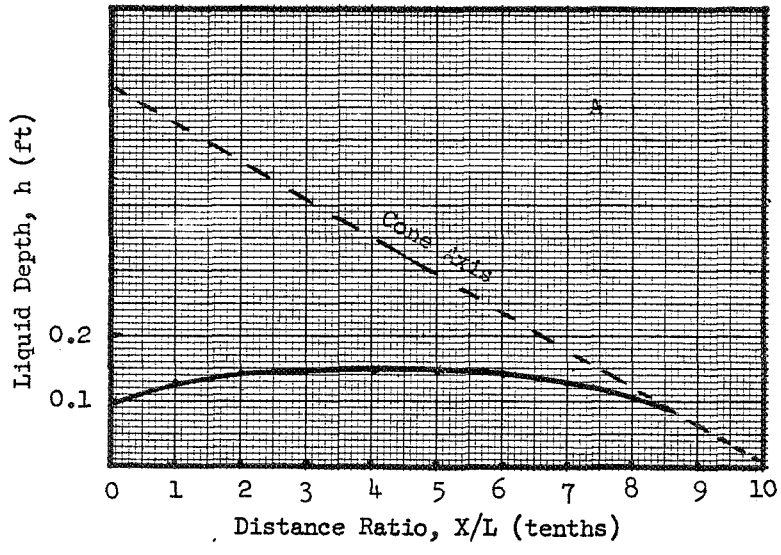
$A(x) \equiv$ film cross-sectional area, i.e., flow area.

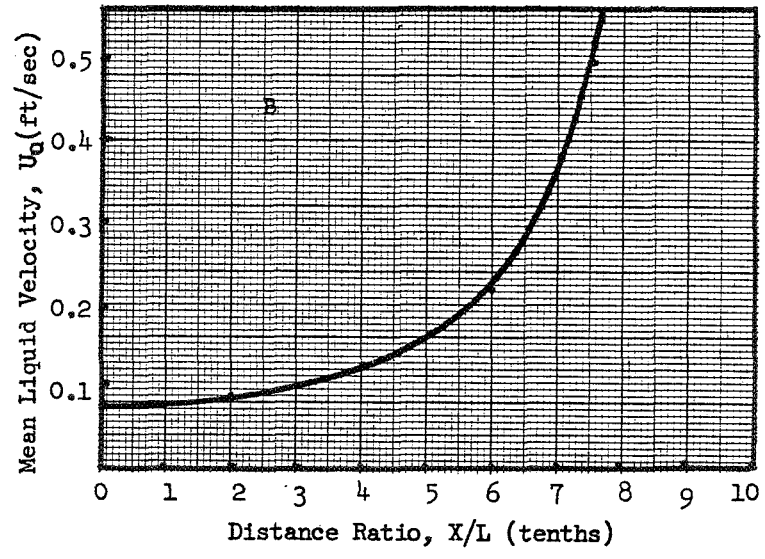
Figure 37 illustrates output from the computer program which solves equations (36) and (37) for liquid depth, mean velocity, and mass flow rate.

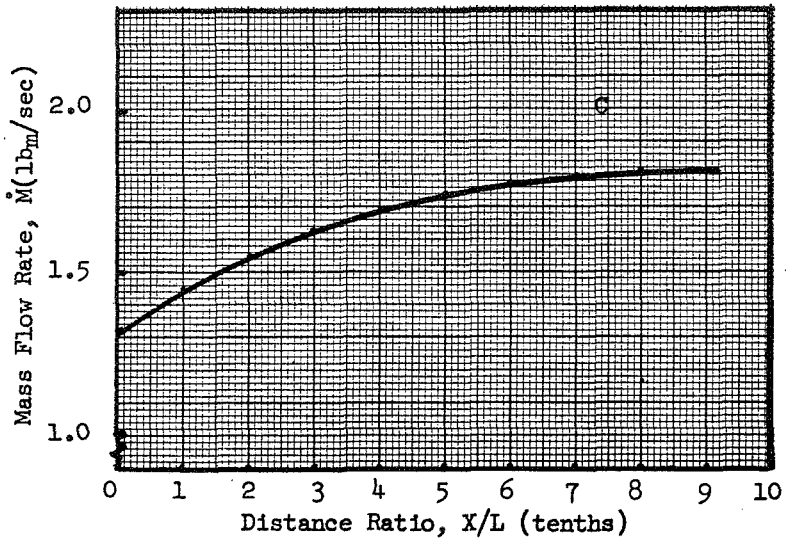
THE COMPUTER PROGRAM

A computer program was developed to provide a tool for economical computation of analytical parameters for experimental correlation and predesign utilization. Equations (36) and (37) form the nucleus of a FORTRAN IV CDC 6400 computer program.

In addition, three short computer programs were developed for the CDC 6400 in FORTRAN IV to conveniently reduce the large bulk of experimental data collected against the Case 1 model. These programs are reported in the appendices of reference 4. A program RECRIT solves equation (16) for interface velocity and calculates the critical Reynolds number, Froude number, and Weber number. Four roots of equation (16) exist; however, the region of valid values can be defined and imposed as a solution







Conditions:

Water Temp.: 540° R

Cone Dimensions: 1 ft, 1/2 ∠ = 30°

Gravity: Zero

Condensation Flux: 0.4 $lb_m/ft^2 sec.$

Air Flow: None

Figure 37. — Zero-Gravity Performance Prediction - Conical Surface

constraint. A Regala Falsi convergence technique is the primary scheme of this program. With this program, the line of neutral stability can be defined.

A second program, SHEAR, solves the empirical frictional relationships for the gas-phase drag on the liquid film. The flow rates and velocities of the two phases are determined as well as the film height. This tool has definite predesign application in that evaluation of film thickness is a prime requirement in any film transport problem.

The data reduction program, REDATA, converts voltages to film thicknesses, and with flow data, evaluates velocities, dimensionless numbers, and stability criteria.

APPLICATION TO LSS DESIGNS

The generalized nature of the analytical model provides a relatively high probability that the model can be directly applied to the development of several LSS design approaches. Table 16 identifies examples of the type of LSS equipment which, potentially at least, will be so designed that the model can be profitably applied to the analysis of primary or "on-design" modes of operation. However, possibly one of the major applications of the model may be in the analysis of the behavior of liquid films which might exist when systems operate under "off-design" conditions. Such conditions have existed when unwanted condensation or "spills" produced liquid films either on atmospherically exposed cabin walls and installed equipment surfaces or on the inner walls of ducts transporting "hi-humidity air" or liquid vapors such as might be the case with cabin air and certain water and oxygen reclamation system ducts. In the early phases of a system design study, the model might be employed in the comparative analysis of competing designs, one or more of which are either designed to transport liquid films or have the potential for formation of liquid films under off-design conditions.

Analysis of the transport characteristics of liquid films forming on the surfaces of condensing heat exchangers is perhaps the most likely on-design condition. The two surfaces explicitly examined by the model permit direct application to such equipments with both conical and flat plate surfaces, as might be the case with equipment items 40 and 42 respectively.

EXPERIMENTAL EVALUATION

Requirements

An experimental evaluation of the accuracy of the predictive aspects of the analytical model should include the following observations against each condition in both a set of steady state and transitory operating regimes:

Table 16. — Examples of LSS Equipment Designs for which the Analytical Model Has Relevance

Equipment Type by Degree of Relevance by Mode / LSS Function	Model Relevance			
	On-Design		Off-Design	
	A*	B	A	B
Oxygen Supply & Recovery	11**,12		2,3	1
CO_2 Removal	16		14	15
Water Reclamation	40,42, 43,59(b)			
Humidity Control***	58(a) & (b), 59(c)	60		
Hygiene		78,79, 80,81, 82		

* Degree of relevance: "A" implies a high degree of relevance both as to similarity of the model to the equipment processes produced under the designated mode combined with a high probability that the process will be extended into similar designs in updated systems, while "B" implies a lower degree of similarity and/or probability of extension to similar designs.

** Equipment type identified by LSS equipment reference number.

*** Many areas of the humidity control function were not included in the equipments for analysis, thus the paucity of entries especially in the off-design mode.

a. Liquid-film thickness profile.

b. Liquid/gas interface geometry.

c. Gas and film velocity (average).

d. Gas and film temperature profiles.

e. Gas superficial velocity profile.

The design of the experiments should be such that they include an examination of the potential effect on the model parameters of various values of the local inertial acceleration vector, especially with respect to film stability and transport rate.

Laboratory Experiments

Laboratory experiments designed to examine the validity of the Case 1 (flat-plate) analytical model should prove to be highly productive. The Case 2 Model (conical-surface system) as designed by the study is such that experimental evaluation under the influence of inertial acceleration field forces approaching or greater than 1g will produce minimal information; thus, emphasis under normal laboratory techniques should probably be directed to the flat-plate surface only. Such experiments can logically include observations of the previously listed film properties as they appear under the influence of various forces, including multiple orientation to the local gravitational vector.

Reduced-Gravity Experiments

Both the flat-plate and conical systems will require experimental evaluation under conditions where the values associated with the local gravity vector are sufficiently low to observe the film behavior when dominated by various combinations of the other forces involved. This is particularly true with the conical surface case where gas/liquid shear forces are by necessity essentially nonexistent; thus, a design where the liquid film/solid surface effects are dominant and, as such, a system which cannot be readily controlled by a dynamical equipment process controller. However, simulation of the reduced-gravity situation under laboratory conditions through the use of balanced density fluid techniques and/or scale models of the system may be of value as aids in the design of experiments under reduced gravity through both short-duration (drop tower or KC-135) and long-duration (orbital space station) observations.

Description of the Case 1 Experiment

Major Goals

Primary. — To determine if the analytical predictions satisfactorily delineate the actual characteristics of a thin liquid film forming on a solid surface and being transported by the various forces involved, including those resulting from interfacial shear and surface tension at the gas-liquid interface and the local inertial acceleration vector. Special attention is directed to the conditions producing a transition from a stable to unstable film-gas interface.

Secondary. — To examine various experimental test techniques, both for their applicability to laboratory testing and for their potential in the design of apparatus for experimental tests under reduced gravity.

Principal Observations

The experimental observations required included:

a. Liquid-film thickness.

b. Liquid/gas interface geometry.

c. Gas and film velocity.

d. Gas and film temperature.

e. Gas superficial velocity.

The experimental variables to be programmed against these observations included:

a. Air flow rate.

b. Liquid flow rate.

c. Channel orientation.

Criteria for Test Model Design

The test model and its supporting apparatus were designed under the following criteria:

a. Transport air velocity controllable to support the development air flow profiles ranging from laminar to turbulent.

b. Air flow velocity sufficient to produce instability at the gas/liquid film interface.

c. Liquid in-flow control sufficient to produce a continuous film under all conditions up to instability.

d. Liquid in-flow control providing an initial velocity in the direction of the gas flow ranging from zero to slightly above that of the gas flow.

e. Instrumentation to record the data required to define:

    1. Transport rate.

    2. Critical film conditions as defined by

        a) Reynolds number.

        b) Weber number.

        c) Froude number.

        d) Stability criteria.

f. Gravity effects on film transport characteristics can be observed.

g. Capability for visual observations and photographic data collection maximized.

h. Maximum utilization of previously employed test apparatus.

Test Apparatus

The apparatus used in this experiment is shown schematically by figure 38 and pictorially by figure 39.

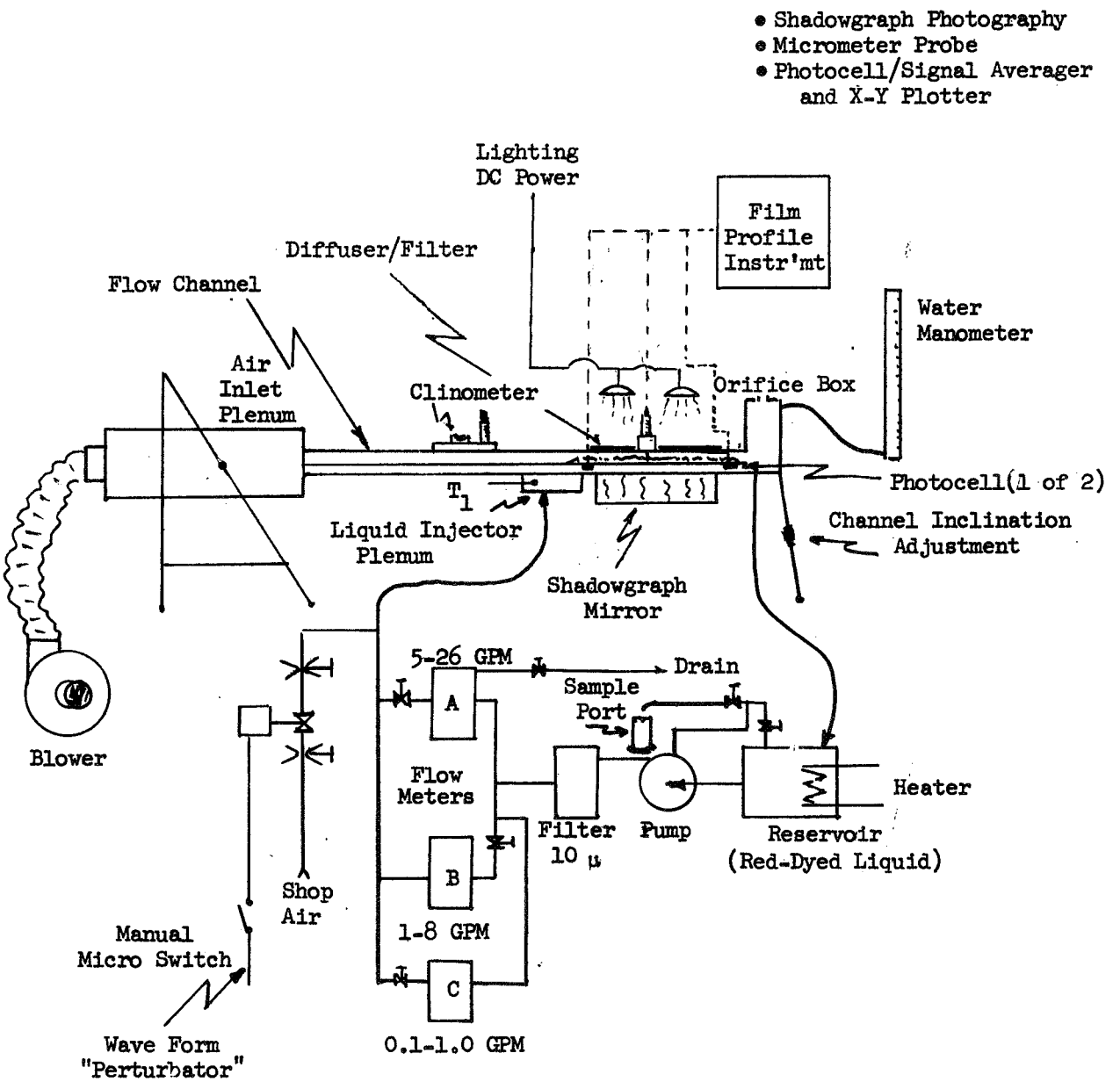
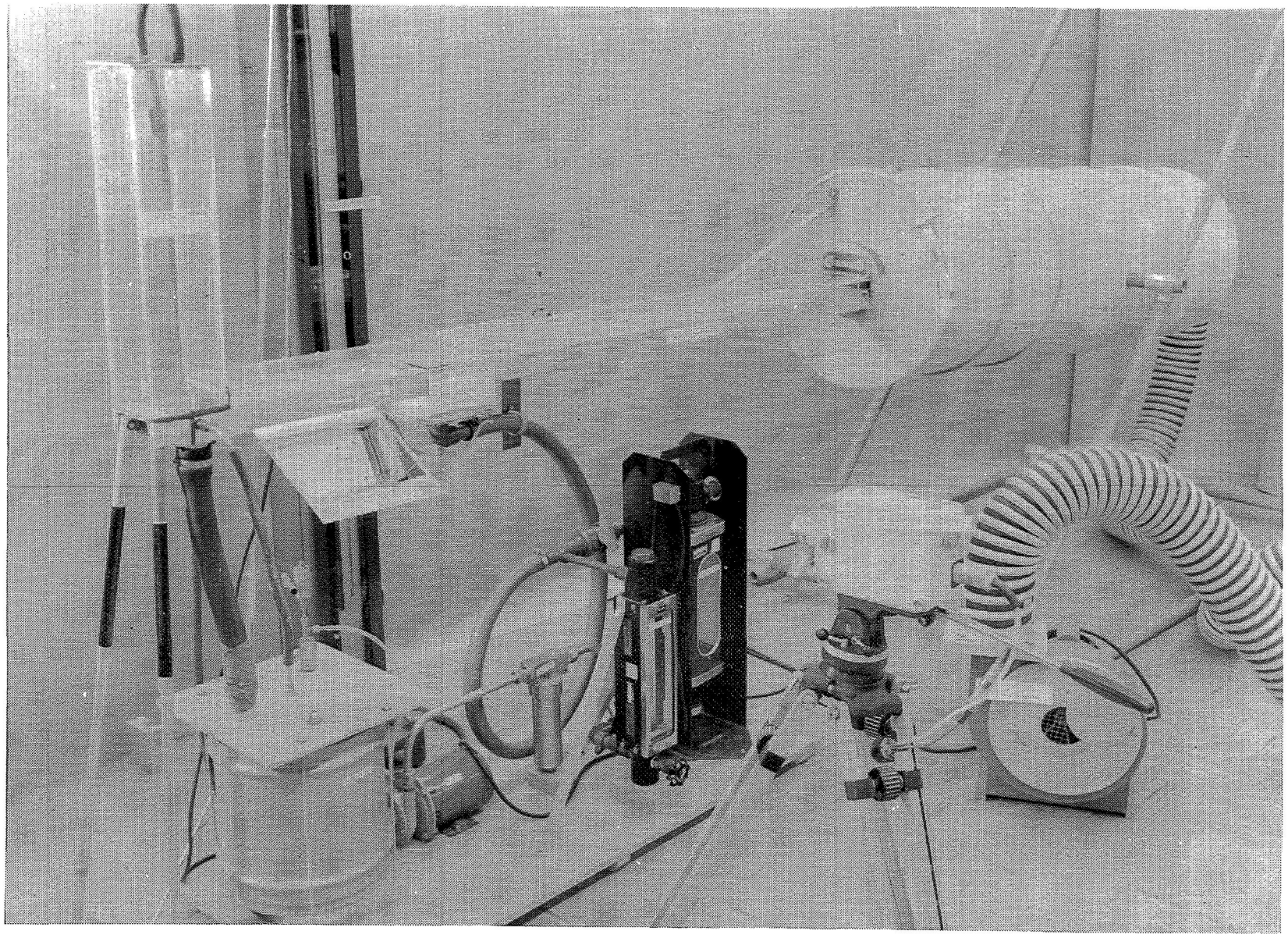


Figure 38. — Test Apparatus — Film Stability and Transport Flat-Plate Configuration



Note: Hooded Light and Photocell Data Processor Not Shown

Figure 39. — Test Apparatus Photograph

Air-stream control assembly. — The air-stream control assembly, essentially unmodified from Test 2, consisted of the following components:

a. Blower.

b. Plenum chamber.

c. Inclination pivot axis suspension.

d. Air flow control.

The plenum chamber provided a volume of approximately 13.3 ft^3 over an inlet-to-outlet distance of approximately 5.7 feet. The exit end of the chamber was removable (typical over center compression ring clamp). An adapter section was incorporated into the exit end of the chamber to facilitate 1) channel inlet instrumentation mounting, 2) channel attachment, and 3) minimum disturbance in the transition from plenum to channel stream velocities.

The inclination pivot axis suspension was a simple double A-frame construction fabricated from 1.5-inch commercial pipe and Nu-Rail fittings. Air flow was provided in a controllable range from less than 1 ft/sec to well above 60 ft/sec in the 4.5 $in.^2$ cross-section channel.

Flow-channel and test-section assembly. — The detail configuration of the flow-channel assembly was influenced by a requirement that it be merely a simple modification of the Test 2 assembly. The flow channel was formed by two 6- by 84-inch parallel plates, one aluminum and the other lucite, attached at the sides by a 1.0- by 0.5- by 84-inch lucite strip. A smooth transition from the plenum chamber to channel was accomplished as shown in Figure 40. Also shown are the air flow orifice box at the channel outlet, and the flow plate. The injector plenum and knife injector are shown in figure 41.

The test section was comprised of the injector and film plate assemblies. The lucite film plate was mounted in the channel cutout with the working surface of the plate flush with the surface of the metal plate which formed the base of the channel. Sealing of the clearance between the channel and the plate was accomplished with nonhardening plastic sealing compound (Johns-Manville DUXSEAL). A metal coverplate was placed in the unused channel cutaway. The under surface of the plate was sanded to produce a "frosted" condition required by the shadowgraph.

The film injector plenum was constructed of aluminum plate providing a 148 $in.^3$ capacity. It was mounted 1 inch upstream of the lucite film plate as shown in figure 40. Free-pivoting adjustable legs were attached to the channel to support the channel through a range of inclination angles both above and below the horizontal.

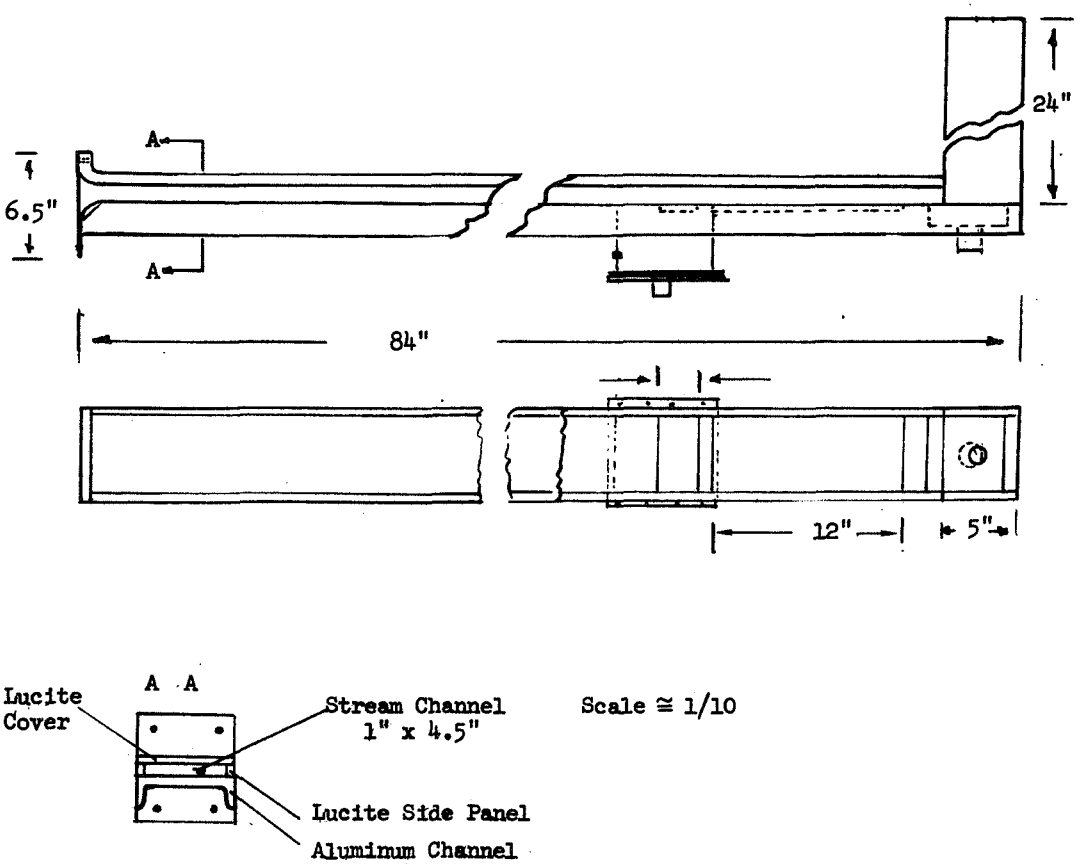


Figure 40. — Channel Assembly

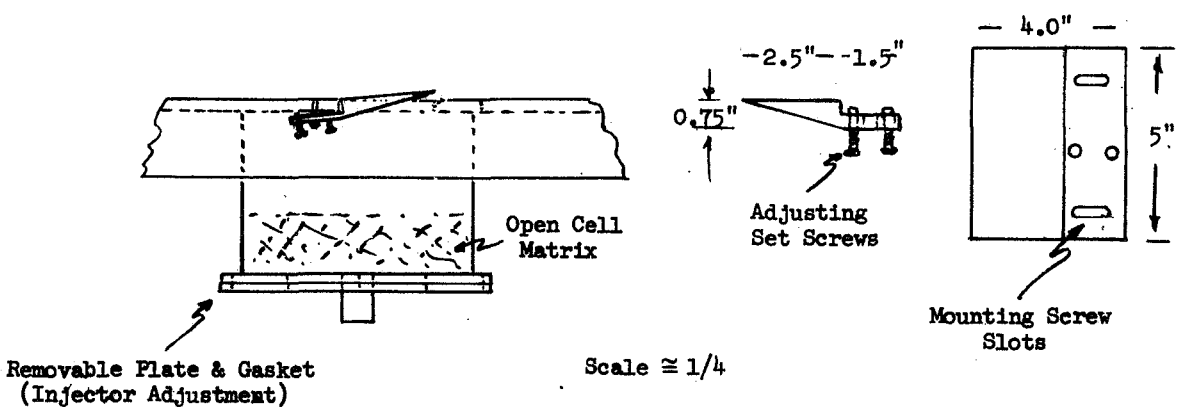


Figure 41. — Liquid Plenum and Knife Injector

Three film injector configurations were explored; namely, the knife, porous media, and open pool injectors. The knife injector illustrated by figure 41 produced a controlled smooth injection at a rate matching the channel air flow. The open pool injector was attained by merely removing the knife. In this configuration the initial acceleration of the liquid was attained through air stream drag forces, thus providing a straightforward means of observing its effects. The porous media injector was a modification of the open pool attained by placing an open matrix sponge material in the injector opening. Addition of the porous media reduced the disturbance of the liquid surface caused by the accelerating shear forces combined with impact with the channel base at the exit of the plenum chamber. Only the knife injector was used during the formal data runs.

A 1-inch layer of the porous media was placed in the bottom of the plenum to reduce turbulence caused by liquid in-flow from the recirculation pump. An air injector was installed in the fitting at the inlet to the plenum chamber to produce a perturbation on the liquid in-flow. Triggering of the injection was interlocked with initiation of the signal averager sweep.

The water and glycol were dyed red with Schilling (2.5%) vegetable dye at approximately 1 ounce to 8 gallons of liquid.

Instrumentation. — The major components of the instrumentation employed for the data runs included:

a. Air flow orifice set and water manometer.

b. Photographic and shadowgraph components.

c. Electromechanical wave height micrometer probe.

d. Photocell film profile recorder.

e. Photocell output voltmeters.

Channel air flow was calculated from pressure drop measurements obtained with a water manometer (Charles Meriam Company, Model 34EH10TM, scale vernier in 0.0001 psi) and the appropriate sharp-edge orifice from a set with individual orifices ranging in size from 0.1- to 1.0-inch diameter.

The shadowgraph wave forms appearing on the mirror suspended below the translucent working section plate were photographically recorded. Motion pictures were taken with the Milliken, DB-4 Pin-Registered, Hi-Speed, 16mm camera.

Wave height measurements were taken with a combination of devices. The electromechanical micrometer probe took measurements at four points along the centerline of

the plate, while the photocells recorded the wave forms in a band across the leading and trailing edges of the film plate.

The photocell measurements were attained with two selenium photovoltaic cells feeding into a parallel circuit, one branch of which contained a 545 oscilloscope with a specifically designed amplifier and bias/gain adjustment unit, and the other branch contained an FT-1050 Signal Averaging Memory Unit and an HP-7035A X-Y Recorder.

The diffused light source for the photocell sensors was supplied by two 35-watt dc lamps held approximately 14 inches above the channel working section. A lucite panel, the upper surface of which had been sanded and the lower surface coated with a green pliofilm filter, was placed on the upper cover plate of the channel immediately below the light source.

In-progress monitoring of the two photocell outputs, providing an indication of average steady-state film thickness, was made possible with two Triplett Model 630-NA Volt-Ohmmeters.

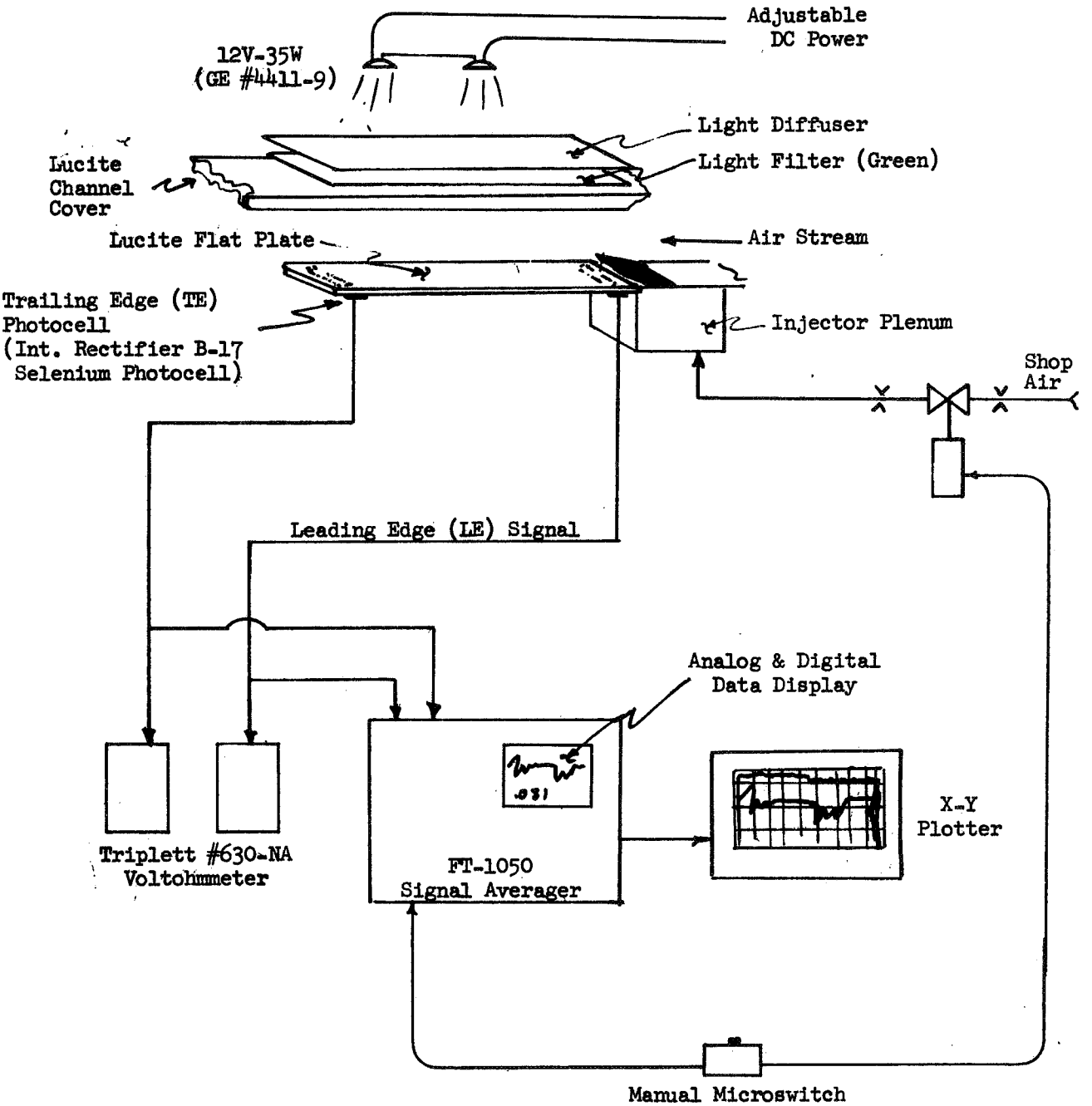
Details of this instrumentation are shown in figure 42.

Liquid circulation circuit. — The liquid circulation circuit was assembled from the heat and water exchange circuit of Test 2. The entire circuit is skid mounted. All components are inherently corrosion resistant, i.e., bronze, stainless steel, plastic, or plastic-coated except for flow meter A, which is isolated from the circuit except for the extreme high-flow runs. A flush drain has been incorporated to permit flushing the meter prior to use; it is considered desirable to minimize both dissolved and suspended salts which can alter both the physical and optical characteristics of the liquid and thus introduce experimental errors. A sample port was provided to permit in-progress liquid characteristics analysis and a 10-micron filter was added at the pump outlet. Two liquids were sequentially used for comparative purposes, namely, water and industrial quality propylene glycol, providing approximately a 1 to 20 ratio of viscosity.

Test Procedures

The concepts presented in the Test Plan were found to be generally applicable throughout. The guidelines for the test protocol were provided by data displayed in figure 43. Definition of the stability/instability transition points was adopted as the principal investigation. The stability parameter was the change in wave depth along the plate with an increasing depth indicating an unstable condition and a decreasing depth indicating a stable condition.

For the most part the individual test runs were conducted by establishing both a specified liquid flow and a specified air flow. When a change from a stable to unstable



Note: Working section and lighting system are hooded, both to provide a "no-light" reference point and to assure consistent control of the light intensity entering the working section.

Figure 42. — Instrumentation Schematic

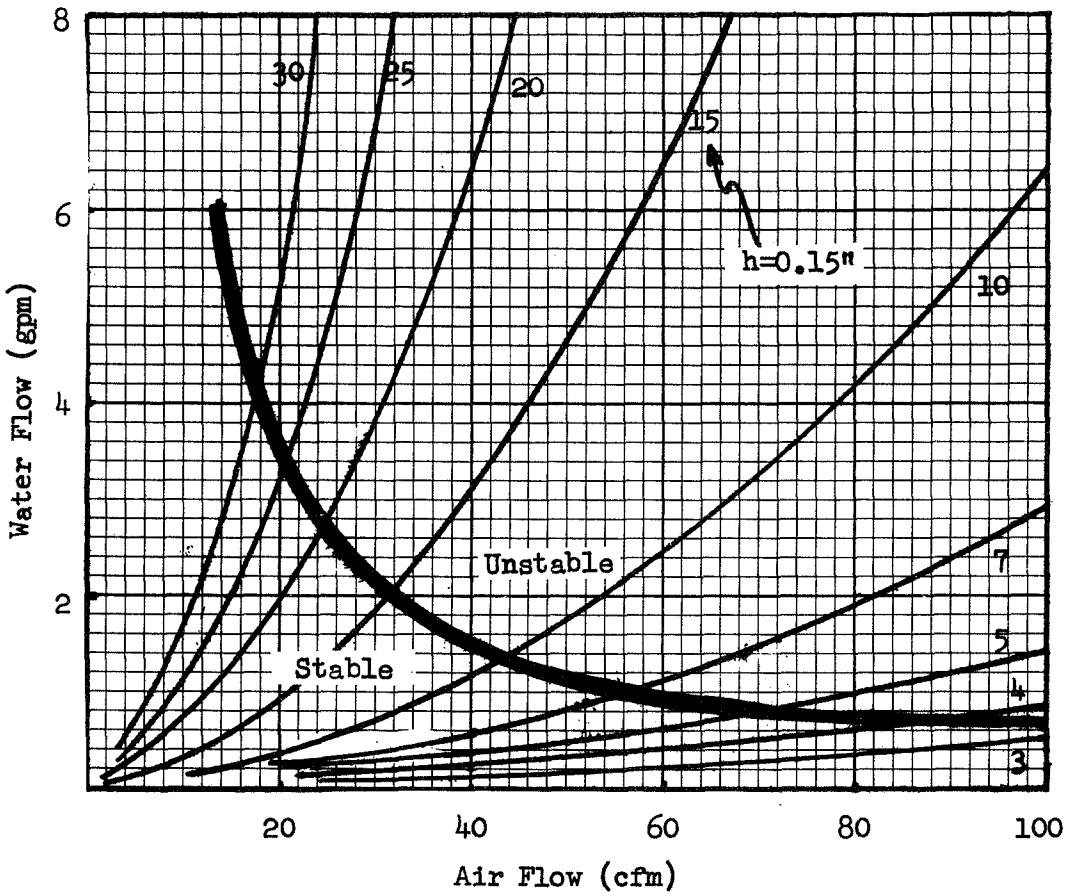


Figure 43. — Predicted Stability Region for Defining Test Variables

film was noted, a series of small changes in air velocity or liquid injection rate, whichever was determined applicable, was effected to more accurately locate the transition point.

Each data run was conducted as follows:

a. Record photocell voltage output with the channel in dry condition to provide a baseline for film thickness measurement (adjust light power if required). Manually record voltmeter reading with Signal Averager (SA) in memory storage mode.

b. Establish test conditions according to protocol (channel inclination, air flow, and liquid flow). Record all set points and volt-ohmmeter readings. Maintain SA in memory mode.

c. If flow perturbation required, switch SA to external sweep activation signal and activate manual perturbation switch. Repeat to produce three to five trial wave form perturbations.

d. Set SA to deliver to the X-Y plotter both baseline data and a typical sweep from the several trial wave forms previously stored in SA memory and individually viewed on the SA scope. Activate X-Y plotter and annotate the graphically displayed data with all state and condition data as previously recorded manually.

Note: Changes from baseline values in either the light source intensity or the light absorption characteristics of the liquid due to changes in dye concentration (mainly) will alter the measurements data accuracy.

Test conditions were varied by changing any combination of the following experimental variables in the approximate ranges shown:

a. Air flow velocity - 0 to 32 ft/sec.

b. Liquid injection rate - 1.1 to 5.5 gal/min.

c. Channel inclination - ±15°.

The calibration and trial runs were initiated on 14 November 1969. Formal data runs for the water/air system were initiated on 23 December 1969 and terminated on 6 January 1970. Runs for the glycol/air system were initiated on 7 January 1970 and terminated on 12 January 1970.

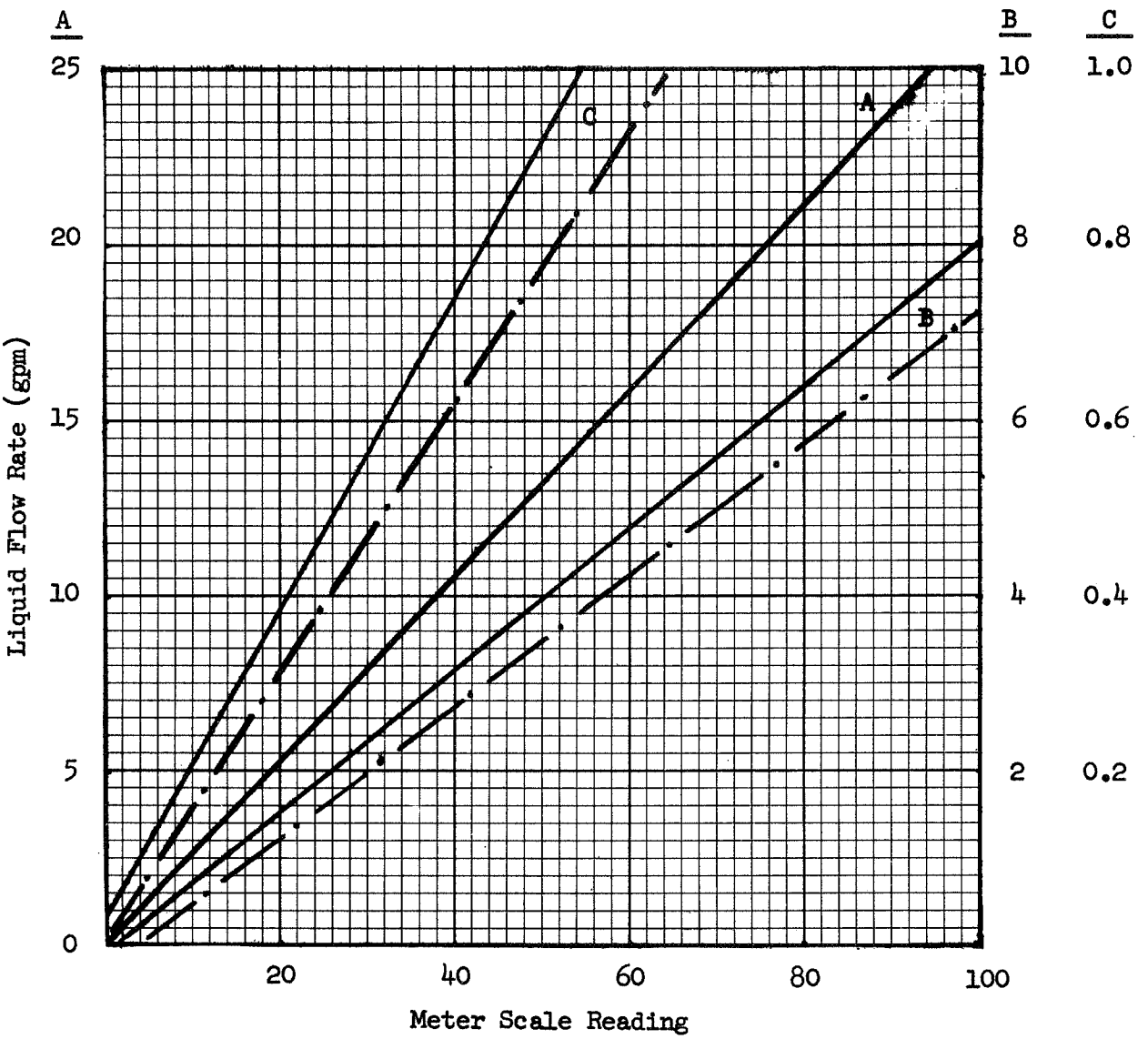
Test Data Summary

Data was recorded against two sets of experiments, namely:

a. Calibration and trial data runs — essentially instrumentation and test mode evaluation, modification, and calibration.

b. Formal data runs — the major experimental variables were liquid mass flow rate, air stream velocity, channel inclination, and liquid characteristics. The principal observable was film thickness while the principal determinant was change in wave height along the channel.

Calibration and trial data runs. — A series of experiments involving various approaches to shadowgraph (refractive, absorptive) photoanalysis (light intensity) in the determination of wave form and film thickenss indicated that severe problems were inherent, not the least of which was the long delay time in obtaining the results of the analysis. Reduction of this delay time is possible but requires on-line computer analysis which is beyond the scope of this contract. The nature of the experiment called for a directly interpretable and essentially instantaneous readout. As previously discussed, the investigation led to the adoption of the photocell system employing the Signal Averager (SA) and X-Y plotter. The results of the major calibration and trial data runs for the final system are summarized by figures 44 through 51 and tables 17, 18, and 19. All test procedures were investigated and determined workable.



Legend:

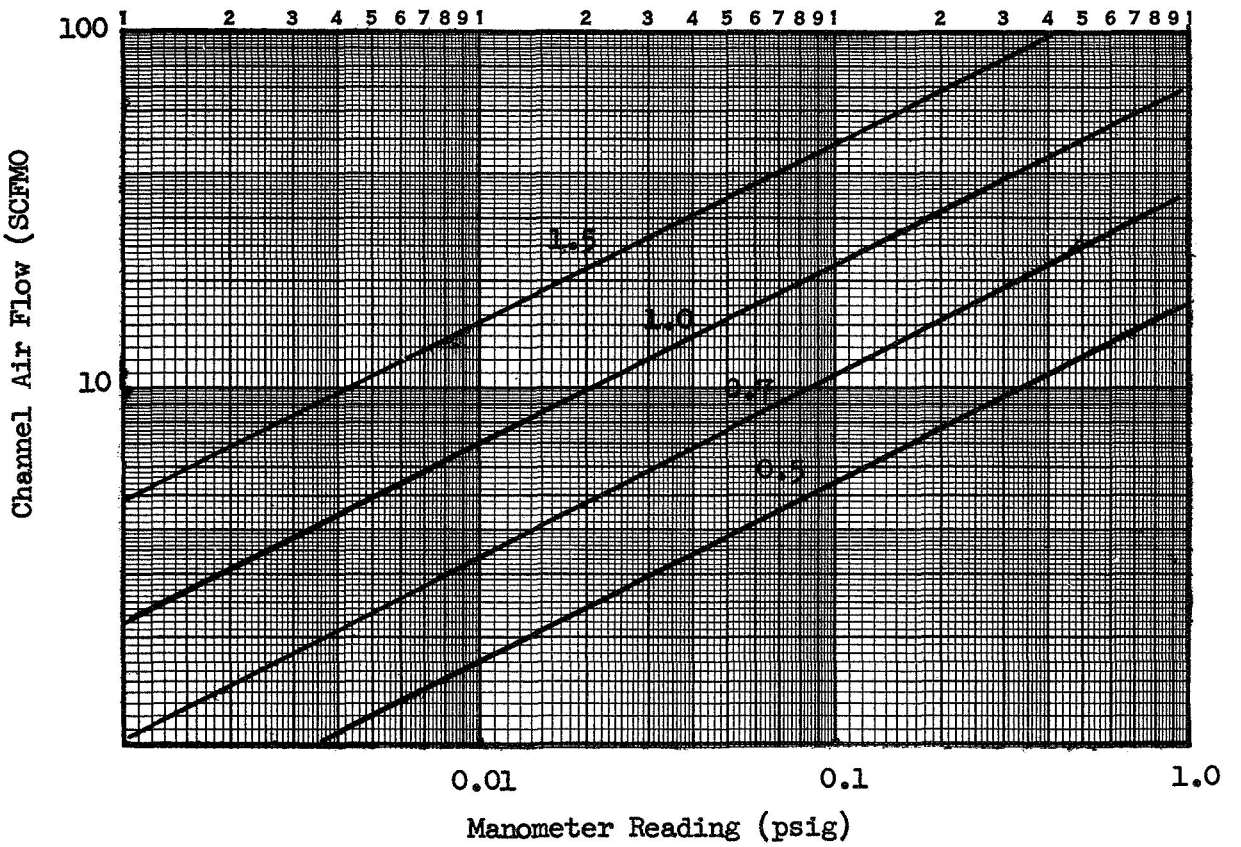
Water ————————

Glycol —— · (B & C only) ——·——

Note: 1. Water @ 69° F.

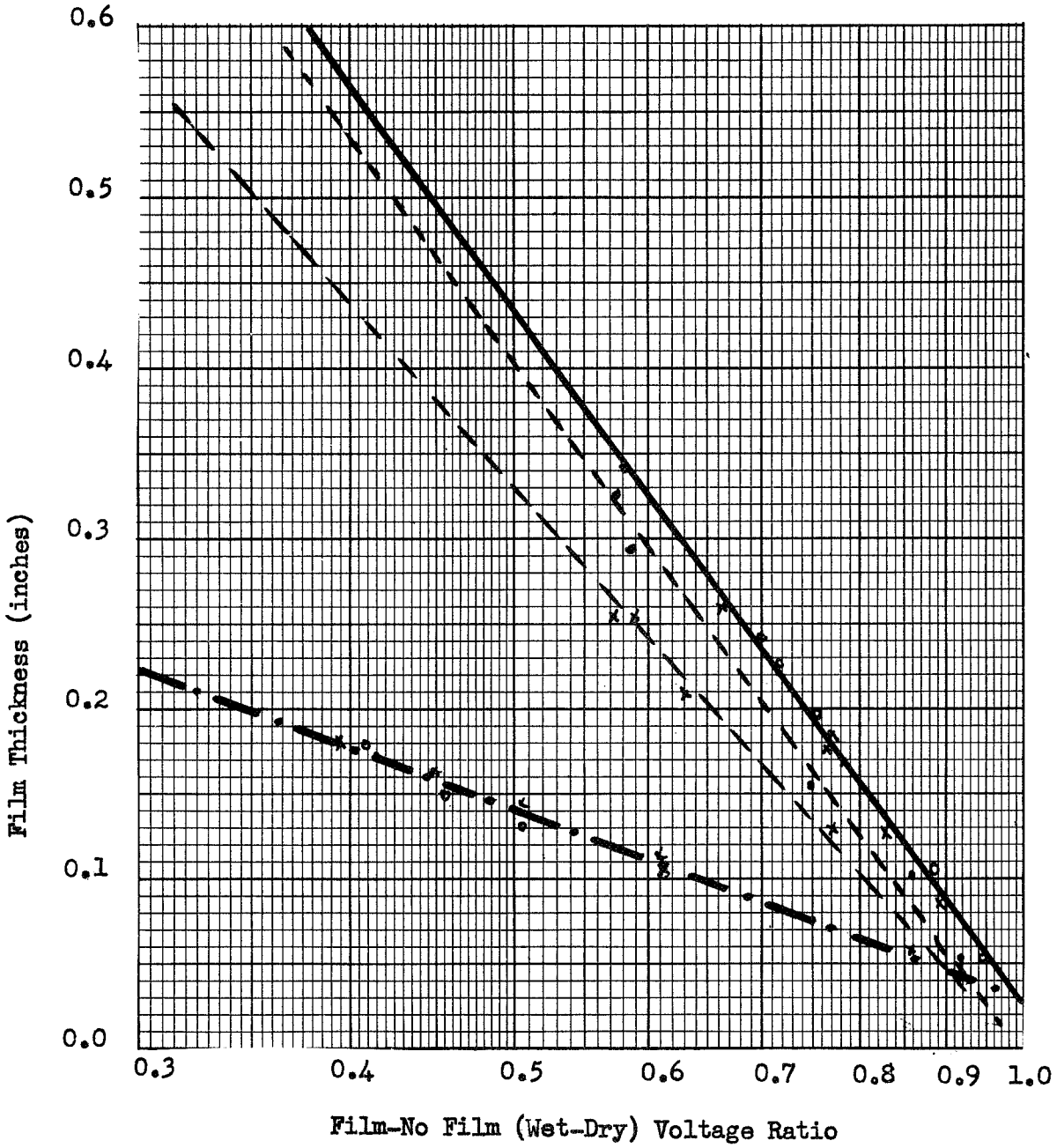
2. Letter designations identify corresponding graph scale and flow meter (see system schematic, figure 38).

Figure 44. — Flow Meter Calibration



Note: Plot notations are orifice diameters in inches.

Figure 45. Air Flow Calibration



Legend:

First Set of Cells	- - - - -	Water-Air System (prior 1-5-70)
Second Set of Cells	———	Water-Air System (1-5-70)
Second Set of Cells	—·—	Glycol-Air System (1-8-70)
Leading Edge Cell	o & ●	(Upstream)
Trailing Edge Cell	×	(Downstream)

Figure 46. — Photocell Calibration

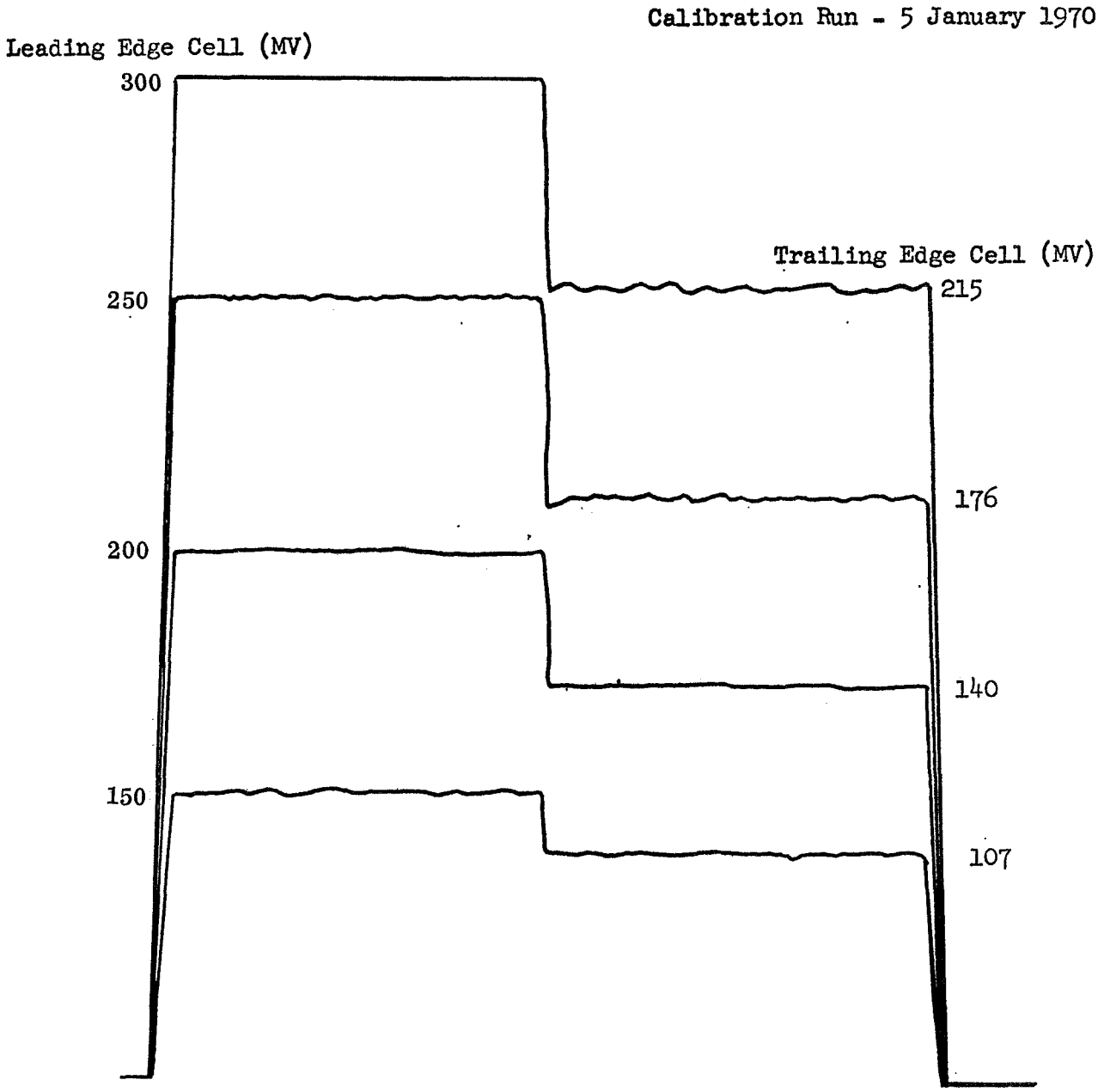
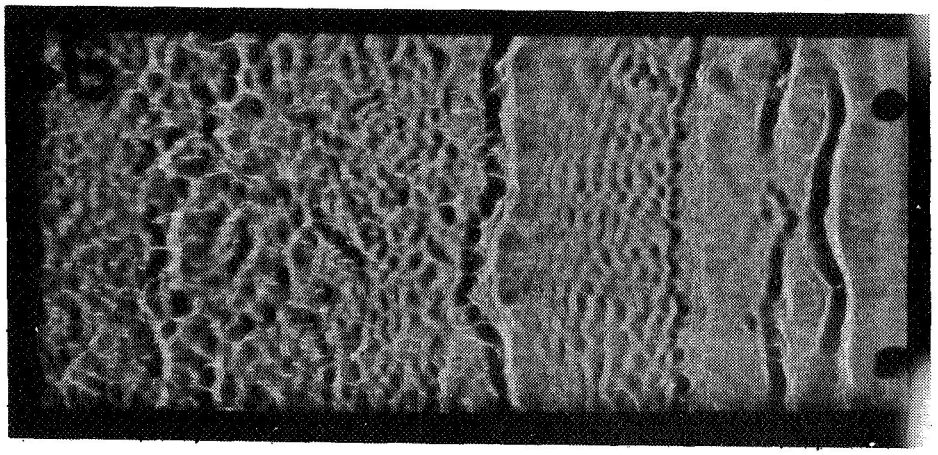
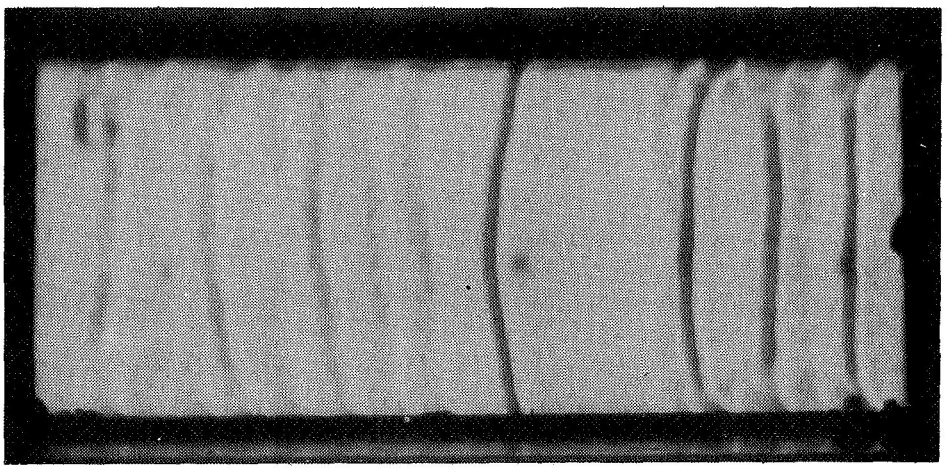


Figure 47. — Typical X-Y Plotter Scale Calibration



A. Water-Air System (Refractive Technique)



B. Glycol-Air System (Absorption Technique)

Note: Photographs are taken from high-speed motion pictures; A is Run #6 from Set #1, B is Run #6 from Set #2.

Figure 48. — Shadowgraph Photographs

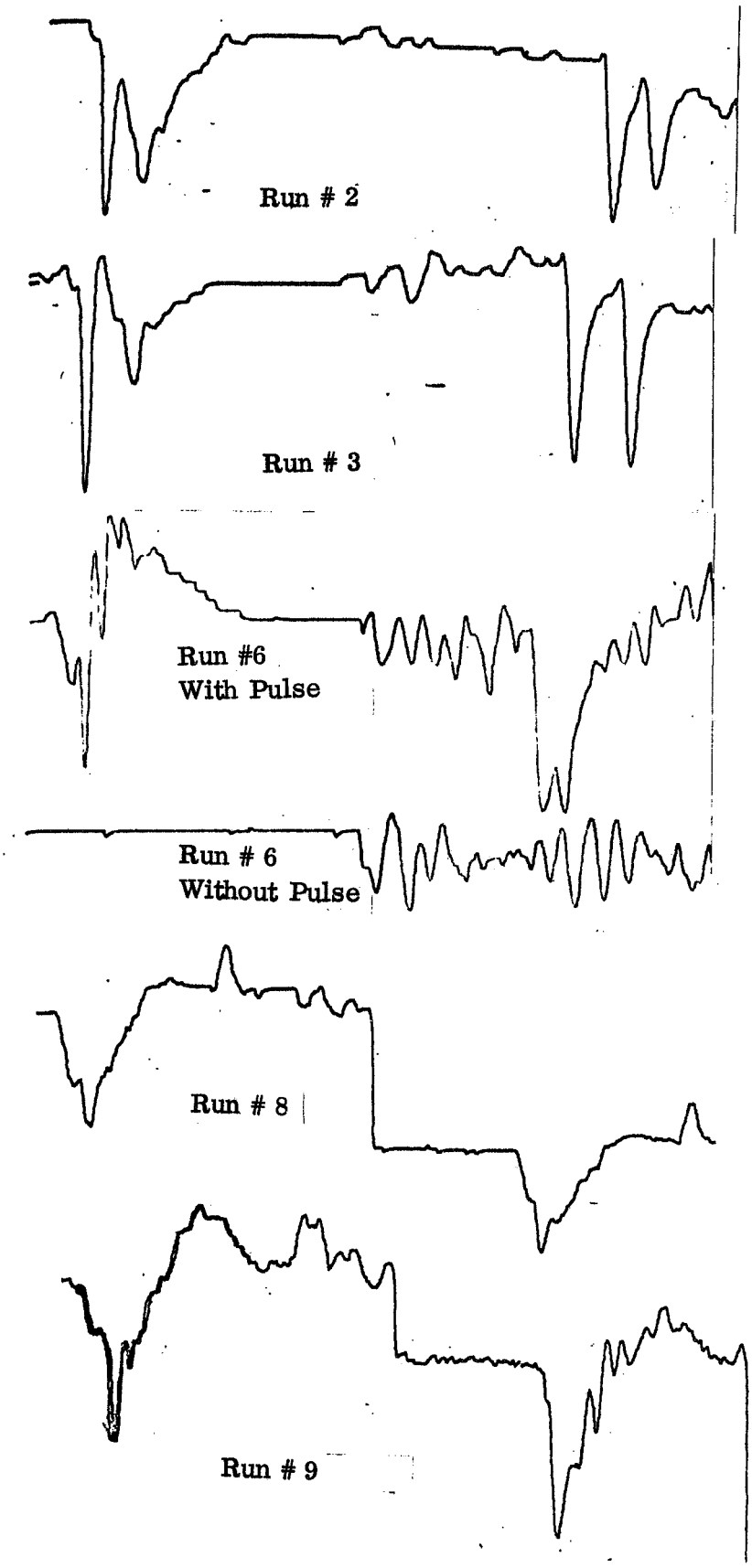
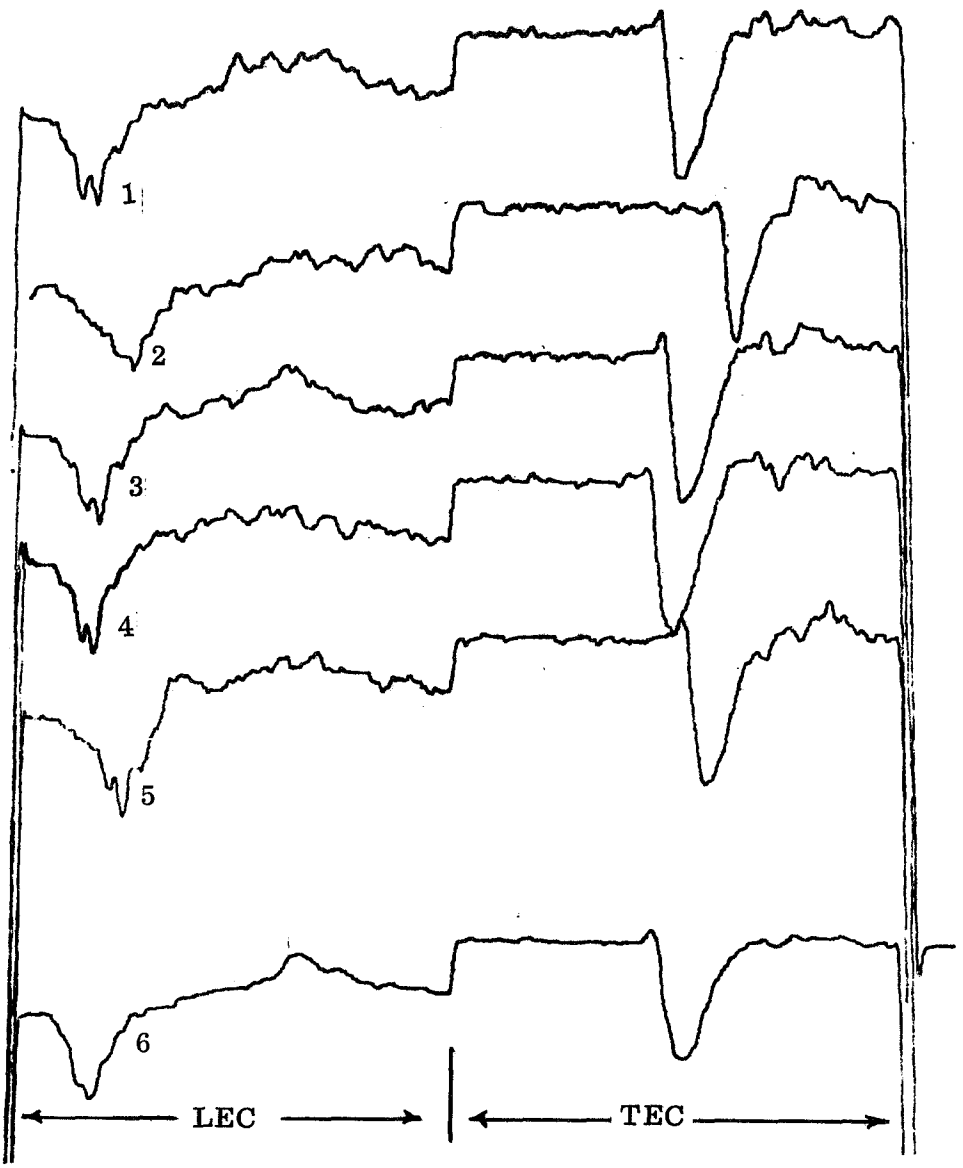
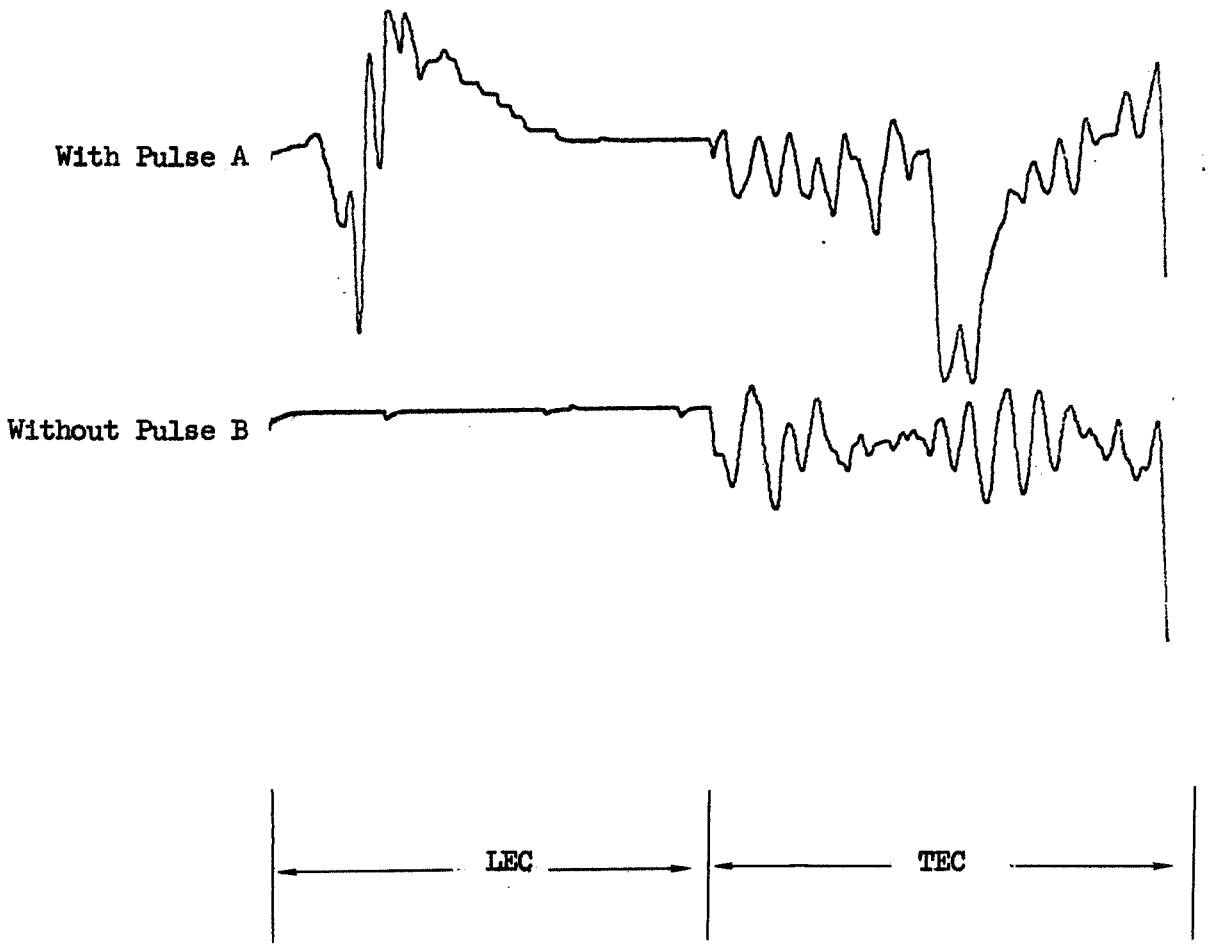


Figure 49. — Photocell Traces of Movie Runs, Set 2



Note: 1. Traces #1 - #5 are single sweep traces; Trace #6 is an average of 8 similar sweeps.
2. Fluid = Proplyene glycol, Δ P = .125 psi, 1.0" orifice, date 9 January 1970.

Figure 50. — Typical Wave Patterns — Photoelectric Trace, Single Versus Average Sweep



Note: Both runs were made with:
455 (0.72 gpm)
1.5" x .050 (35 SCFM)
Glycol-Air System
Channel Horizontal

Figure 51. — Waveform Perturbation Effects

Table 17. — X-Y Plotter Calibration Data

Date	Trace Sequence	Photocell Output (MV)		Trace Scale (MV/Inch)	
		LEC*	TEC*	LEC	TEC
12/24/69	1	300	268	-	-
	2	239	202	34.8	38.6
	3	177	143	32.2	32.8
	4	122	91	33.9	34.9
1-5-70	1	300	215	-	-
	2	250	176	38.5	31.2
	3	200	140	33.3	32.6
	4	150	107	35.7	33.0
1-6-70	1	300	217	-	-
	2	250	177	37.0	31.5
	3	200	141	34.0	31.3
	4	150	106	35.3	31.7
	5	100	72	33.4	32.3
1-7-70	1	300	217	-	-
	2	250	175	37.8	31.1
	3	200	136	34.0	32.7
	4	150	101	34.0	33.3
	5	100	-	33.4	-
1-8-70	1	300	236	-	-
	2	250	197	37.3	35.1
	3	200	159	34.5	31.6
	4	150	120	34.1	32.5
	5	100	81	35.7	34.8
	6	80	66	31.7	35.0
1-9-70	1	300	248	-	-
	2	250	203	38.4	34.5
	3	200	161	35.6	32.7
	4	150	120	32.2	32.5
	5	100	82	35.6	34.5

* LEC = Leading Edge Cell (Upstream)
TEC = Trailing Edge Cell (Downstream)

Table 18. — Movies — Set 1, Water/Air System

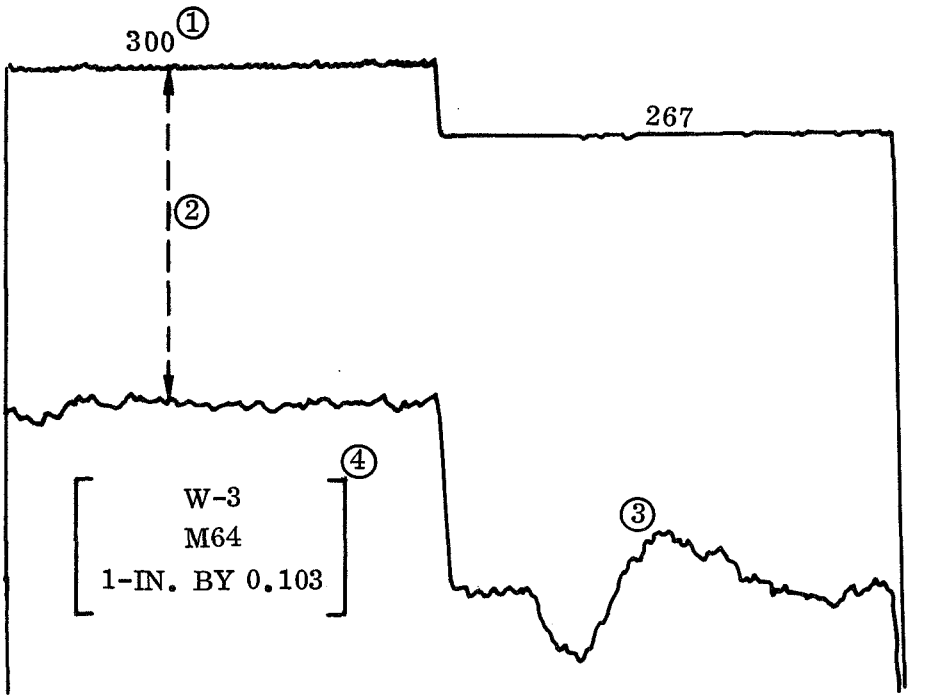
Run #	Meter	Orifice	ΔP
1	15M	-	0 (no air)
2	15M	1.5"	.0287
3	15M	1.5"	.0515
4	15M	1.5"	.0737
5	15M	1.5"	.1062
6	15M	1.5"	.1428
7	15M	1.5"	.1719
8	30M	1.5"	0
9	30M	1.5"	.0221
10	30M	1.5"	.0582
11	30M	1.5"	.0854
12	30M	1.5"	.1240
13	30M	1.5"	.1726
14	30M	2.2"	.0757
15	30M	2.2"	.0757
16	30M	1.5"	.1725
17	30M	1.5"	.1248
18	30M	1.5"	.0836

Table 19. — Movies — Set 2, Glycol/Air System*

Run #	Meter	Orifice	ΔP
1	12S	1.5"	.044
2	12S	1.5"	.054
3	12S	1.5"	.064
4	12S	1.5"	.081
5	45S	1.5"	.040
6	45S	1.5"	.050
7	45S	1.5"	.030
8	28M	1.0"	.070
9	28M	1.0"	.128
10	28M	1.0"	.170
11	5S	1.5"	.080
12	5S	1.5"	.120
13	5S	1.5"	.050
14	12S	1.5"	.054
15	21S	1.5"	.054

*Note: Set 2 run with channel inclined 0.264" down.

Formal data runs. — The formal data runs were conducted against each of two fluid systems, namely, water/air and propylene glycol/air. The principal means of wave form data recording was with the X-Y recording of the output of the two photocells. A secondary means was shadowgraph photography. Full scale copies of the actual X-Y traces were made (ref. 3), a sample of which is shown by figure 52.



① Dry Channel Baseline Sensor Voltage (mV) Leading Edge Sensor.

② Film Thickness Indicator — Values obtained from calibration scale.

③ Sensor Voltage Trace for Flow Condition, Trailing Edge Sensor

④ Test Run W-3 (Water/Air), Liquid Flow at 64 on B rotometer, with air flow indicated at a ΔP of 0.103 with 1-inch orifice.

Figure 52. — Sample Data Recorded by X-Y Plotter

Critique of Test Design

With the exception of the problems associated with the inherent difficulties with measurement accuracies of the film profile, the general approach to the test design appeared to be straightforward, tests were easy to manage, and construction costs were low. The approaches followed and the instrumentation information compiled can be recommended as a guide to future test designs for experimental studies involving film stability and transport phenomena.

Instrumentation. — It became apparent during the trial data runs that the instrumentation required to define the characteristics of the film profiles with sufficient detail and certainty to adequately examine the principal thrust of the experiment (that of the accuracy of the stability criteria developed as part of the analytical model) would require considerably more experimental investigation than had been anticipated. The need to determine not only the general wave form along the working section but, more importantly, to accurately determine the change in the wave form, the critical parameter of the stability criteria, required precise and essentially in-progress data interpretation. The initial concept that the mechanical micrometer probe and high-speed motion pictures would be adequate was seen as incomplete. Several techniques were examined to increase the precision and accuracy of the measurements.

Following a series of experiments, a refractive shadowgraph technique was developed which significantly increased the value of the photographic data. The shadowgraph image appearing on a mirror suspended below the channel was photographed. Subsequently, shadowgraph analysis relative to the determination of wave velocity, wave length, and wave height indicated that light absorption techniques were superior to the light refraction techniques originally employed. In the latter, a point light source above the stream is used to project the wave pattern on the pickup mirror. In that case the bottom of the film plate is "frosted."

The absorption technique, on the other hand, operates with a diffused/filtered light source above the channel with the liquid dyed to increase absorption. One method of interpretation might use a chart relating various wave photo shades to wave (film) thicknesses as calibrated by other measurement techniques employed.

Modification of the micrometer depth gauge from a purely mechanical probe to an electromechanical probe greatly increased its utility.

The third method of determining change in wave height along the plate found to be most practicable was the dual photocell pickup. Several other techniques had been examined, including the use of a capacitance sensor suspended above the film, and several variations on the shadowgraph technique.

Initially the output of the dual photocells, as modified by the amplifier stage, was fed to separate channels of an oscilloscope where the data from each sensor was observed and compared. It soon became apparent that although this approach could supply the measurements required, it left much to be desired in terms of both the recording and retention of data for evaluation and the precision of readout. To overcome these problems the Fabri-Tek FT-1050 Signal Averager and HP-7035A X-Y Recorder were examined. This made it possible to obtain a scope sweep readout representing a single wave form or average (essentially noiseless) trace of several wave forms. Additionally, the unit makes it possible to obtain a digital readout for any selected portion of the trace. Finally, the data can be stored for subsequent scope display and/or recording

by the X-Y plotter. Numerous variations of these basic capabilities are available. The major problem encountered involved the development of a workable calibration technique. The technique finally developed and described herein proved to be reasonably straightforward and would be followed in future laboratory tests if such were to be undertaken.

Film plate length. — Measurements of the film wave characteristics, particularly as associated with the investigations of the stability criteria, could have been made easier if the length of the film plate was greater than the 12 inches provided. During the trial runs serious consideration was given to modification of the working section to provide a plate of at least 24 inches, and possibly as much as 36 inches. However, the decision to design and install a highly sensitive measurements device was followed, principally because so doing would provide a greater contribution to the design of apparatus for the reduced-gravity tests.

CORRELATION OF ANALYTICAL AND EXPERIMENTAL OBSERVABLES

Correlation of film stability and thickness predictions with the evidence obtained from the analysis of experimental data will be graphically presented. Functional similarity is the criterion for correlation.

Predictive Data

Figure 36 has illustrated the type of predictive data characteristic of the analytical model under development for the Case 1 application. In addition, programs SHEAR and RECRIT were developed to formulate guidelines for experiment design (Appendix B of ref. 3).

Program SHEAR provided graphical relations of gaseous shear and liquid shear as a function of flow rate with film thickness as a parameter. By equating the shear at the interface for the two phases, a plot was developed in the form of figure 43. This plot predicts a specific film thickness for gaseous and liquid flow rates which are test variables. Program RECRIT results in a liquid interface velocity of neutral stability for each selected film thickness. Thus, RECRIT defines a line of stability on figure 43. This working plot provided the set points for obtaining data with an intent to establish the validity of the neutral line location.

Experimental Data

A total of 135 runs, 100 with air/water and 35 with air/proplyene glycol, were performed in evaluation of the stability of films flowing concurrent with an air stream

in a horizontal and slightly inclined channel. Details of the test configuration and raw test data are presented in reference 3. Film thickness, flowrates, and stability data were obtained. The complete listing of reduced data is presented in Appendix A of reference 4. A brief listing of the runs conducted with various channel elevations is presented in table 20. Small change in channel elevation had notable effect on film thickness, but less direct effect on the stability evaluation. Air velocities ranged from 0 to 36 ft/sec, bulk water velocities 0.14 to 3.2 ft/sec, and propylene glycol 0.05 to 0.63 ft/sec.

Table 20. — Channel Orientation

RUN	ELEVATION	ANGLE	g_y/g_o
W-1-33A	Level		
W-34-42	Up 0.167 in.	+0°57'	0.99986
W-43-51	Level		
W-52-63	Down 1.0 in.	-5°45'	0.99497
W-64-73	Down 0.06 in.	-0°20'	0.99998
W-74-83	Down 0.264 in.	-1°31'	0.99965
W-84-99	Up 0.06 in.	+0°20'	0.99998
G-1-14	Level		
G-15-35	Down 0.264 in.	-1°31'	0.99965

The raw data include voltage traces for photo cells at two locations along the channel for no liquid present and with liquid flowing with a pulse superimposed on the flowing liquid. From the traces made on the X-Y plotter, the voltages of the upstream and downstream locations for level flow and for the pulse are determined from calibration data of the plotter. These ratios of wet to dry voltage provide a measure of film thickness from calibration data obtained with a micrometer on a quiescent film.

Film stability has been defined as a disturbance (wave) which amplifies (unstable) or decays (stable) as it moves downstream from its source. Thus, a comparison of wave heights at two stream locations defines stability of the flow. Criterion established rather arbitrarily here is R, the ratio of wave height downstream to upstream, < 0.8 is stable, >1.2 is unstable, and $0.8 \leq R \leq 1.2$ is marginal stability. Questions relative to the selection of this criterion are discussed subsequently in the section headed "Impact on the Analytical Model." Values of R were computed for all runs with the computer program REDATA.

The raw data were reduced to provide an evaluation of α as defined in equation (17), where all velocities refer to interface values. Since upstream and downstream film heights vary, dimensionless Fr We numbers are evaluated at average liquid interface velocity and film height. Note that Re has the product $U_i h$ which is independent

of location; h increases as U decreases for constant flow rate. Throughout the analysis, some comparisons were made for film conditions while others are at bulk liquid rates. Where film height is used independently, the downstream value has been selected, and similarity U downstream is plotted rather than average values.

Small changes in channel elevation were made to evaluate the effect of this variable on the data. As indicated in table 20, the change resulted in only the smallest variation in g/go, the latter being proportional to the cosine of the slope. For each elevation, runs were conducted at similar flow rates to provide a comparison for film height and stability analysis. These comparison runs are tabulated in table 21. Similarily, repetitive runs were made to evaluate reproducibility of stability and film thickness data. These are also included at the bottom of table 21.

Table 21. — Comparison Runs for Effects of Channel Slope

Liquid gpm	Gas sctm	-5°45'	-1°31'	-0°20'	Level	+0°20'	+0°57'
0.80	37.0	W-56	W-78	W-70	W-18	W-89	W-37
0.80	43.0	W-56	W-79	W-71	W-16,17	W,90,91	W-38
0.80	56.0	W-54	W-80	W-73	W-14	W-92	W-39
1.60	37.0	---	W-74	W-67	W-31	W-96	---
1.60	40.0	---	W-75	W-68	W-32	---	---
1.60	44.0	---	W-76	W-69	---	---	---
1.60	48.0	W-63	W-77	---	---	---	---
3.50	13.0	W-59	W-83	W-65	W-10	W-99	---
0.32	34.0	---	G-19	---	G-3	---	---
0.71	22.0	---	G-24,25	---	G-8	---	---

Replicate runs: W-16,17; W-20,21; W-49,50; W-90,91;
G-4,9; G-24,25; G-33,35

Of the seven series of repetitive runs, only one set resulted in producing reproducible data on film stability. In several other instances, one case appears to be stable while the other appears as unstable. This points out one of the difficulties in obtaining quantitative data in this area. Heights of films without the pulse indicate good reproducibility and suggest the stability analysis may suffer from characteristics of the pulse or disturbance.

The movie coverage at 200 frames per second provides a good working tool for analysis of wave (disturbance) patterns and provides a measure of disturbance velocity. The light absorption characteristics of the fluid further provide a visual observation of wave decay which can be used to evaluate stability. This decay occurred too rapidly to visually detect during the experiment. The movie provides data on film surface characteristics for various flow rates, without the pulse superimposed. Improvement in technique could be achieved by a visual indication of the initiation of the disturbance. Program schedule constraints precluded a fully developed analysis of the movie data. Further exploitation of the movie data is required prior to subsequent experiment design.

The physical properties of the water and propylene glycol varied significantly in viscosity (0.00063 and 0.01413 lbm/ft/sec) respectively for a 22-fold change while surface tension varied only two fold (0.004 and 0.0024 lbf/ft). From analysis of the data, it appears that it may have been desirable to vary surface tension independent of viscosity by adding surface tension depressant to water achieving a two-to-three-fold reduction in surface tension while only slightly changing viscosity. Surface tension and gravity influences on stabilizing the film were a test objective; however, the radical change in viscosity may have masked the surface tension effects. This difficulty is emphasized when one considers that the Reynolds numbers for the propylene glycol runs lie below the so-called critical Reynolds number of 200 for which all flows are stable. Most of the propylene glycol runs were judged as being unstable, and are further discussed in the data correlation section.

Data Correlation

The two variables correlated are determined from raw data describing thin film flow in a nearly horizontal channel. A stability model defines a relationship between dimensionless numbers, Reynolds, Froude, and Weber. Regions of stable and unstable films are defined on a graphical presentation of the relationship as shown by figure 36. The stability of the films are judged from the value R, the ratio of wave heights at two points along the stream flow. The other liquid film under the correlation is the film height, h, during steady-state flow for a liquid film under the influence of drag by a concurrent air stream. Although the ultimate purpose of this study is the stability criterion of film under varying gravity and surface tension forces, the thickness of the film must be investigated as an initial step.

Film Thickness Characteristics

Program SHEAR was prepared from an amplification of the analytical model and equates interface shear for the two phases. The liquid phase shear is based on liquid viscosity and a linear velocity profile in the liquid. The gas phase interface shear is based on friction factors for turbulent stream gas flows. Predicted results in this data correlation section were obtained from SHEAR.

During exploratory checkout of the experimental equipment, preliminary data were obtained on liquid film thickness for various experimental conditions of flow and channel slope. In figure 53, data are presented for several liquid rates with zero air flow in a horizontal channel. As expected, this leads to a piling up of fluid near the inlet slit which runs along toward the outlet. This data reflected the thickest film to be expected at even the lowest airflow rates. A second test evaluated the film thickness in a closed horizontal channel for various water rates at a constant air rate of 29.6 scfm (18 ft/sec). In figure 54 an interesting behavior is found for low liquid flow, i.e., comparatively thin films. Thin films have a high shear rate; thus, for films of different heights under equal air stream shear, it is reasonable to assume that the very thin films will tend to thicken. As the thick films are accelerated by shear, they decrease in height. A more lengthy period of observation in a longer channel would contribute to a more complete analysis of this phenomenon. However, in that a constraint was placed on the design of the experiment requiring that the experimental apparatus be a reasonable approximation of or at least relatable to space flight experiments, the short channel was mandatory.

Data on this subject in the open literature are limited. When the channel was slanted downward one percent, slightly more than 1/2 degree, considerable effect on film thickness was noted for constant air drag. The comparisons are presented in figure 55 for several water flow rates. The increase in downstream liquid height at low flow rates is less significant for down sloping channels as would be anticipated. For only this slight change in channel slope, a change in physical appearance of the film for identical flow rates was observed. The thinner films in the sloping channel were notably more stable.

Excellent agreement is shown in the correlation of liquid film height with the Reynolds number of the gas phase (figure 56). Hanratty and Engen (ref. 5) had determined a correlation for film thicknesses of 0.15 to 0.20 inch. This work extended the same correlation line to films as thin as 0.015 inch. Although the data have some scatter, the correlation appears valid.* This type of correlation obviously is dependent on some observed characteristic of liquid flow or behavior. Hanratty describes his correlation applicable to a first transition, one from a smooth surface to a pebbled appearance. He defined second and third transitions as changes to squalls and roll waves on the surface respectively. These three qualitative observations are not directly relatable to our stability criterion. The data points of this work which were marginally stable, $0.8 < R < 1.2$, lie close to the correlation line in figure 56. These workers also developed correlations for the three transitions described for the liquid and gas Reynolds numbers. The marginal stability data of this work do not satisfactorily correlate with any of the figure 57 correlations by Hanratty (ref. 5, 6).

---

* Note that the propylene glycol data is a significantly different data set and is not correlated well by the water correlation.

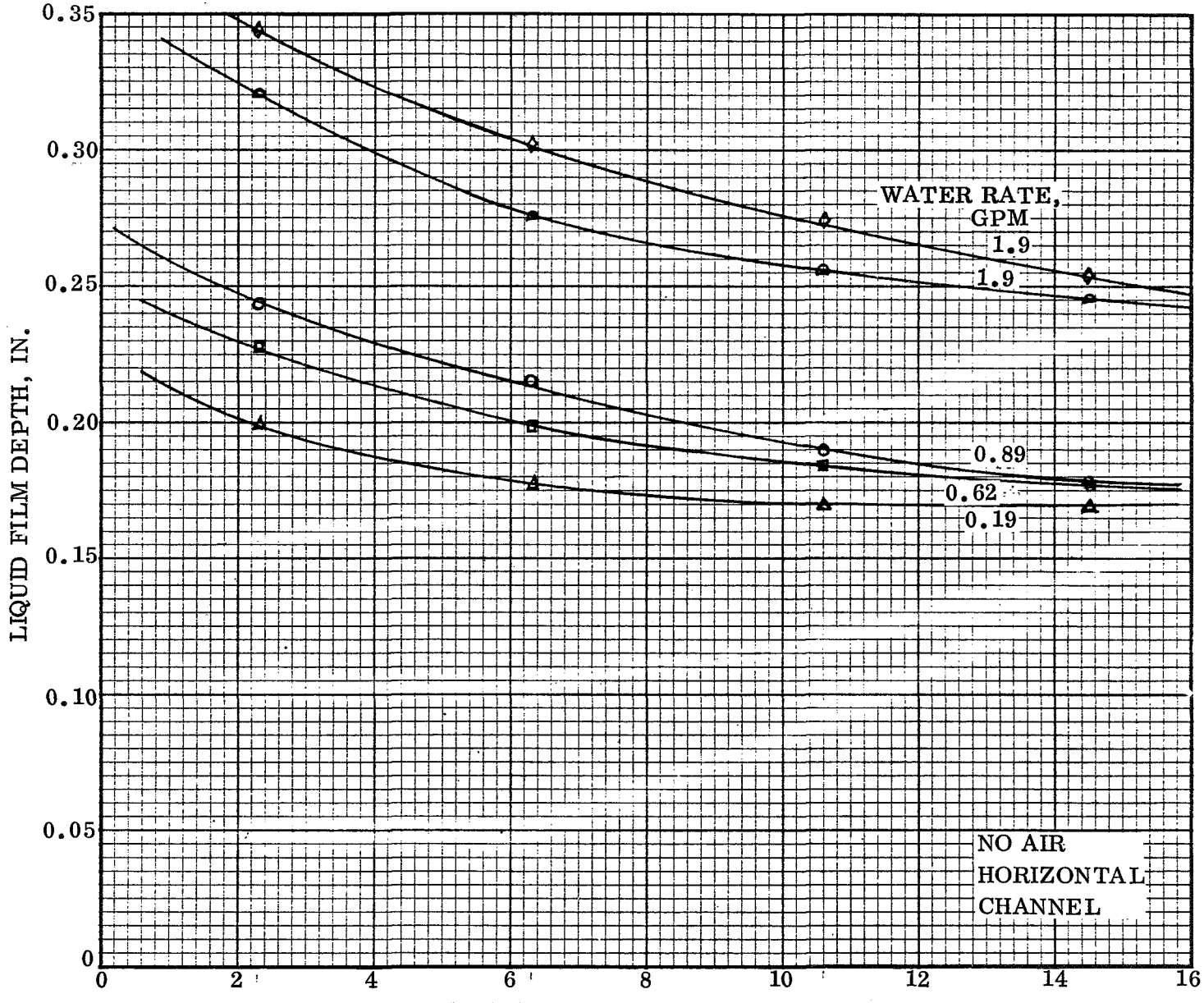


Figure 53. — Effect of Water Flow Rate on Film Thickness

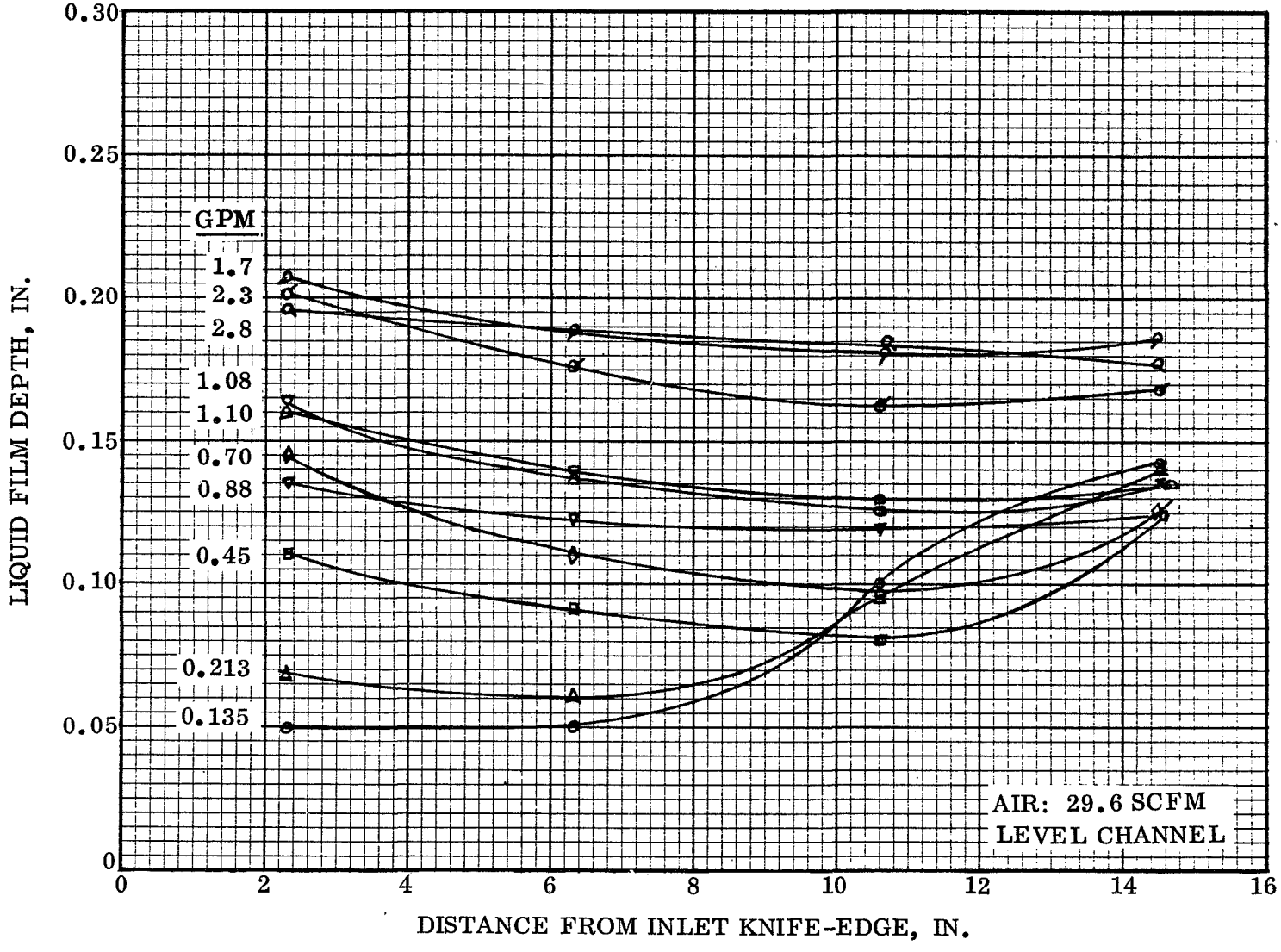


Figure 54. — Effect of Water Flow Rate and Concurrent Air Drag on Film Thickness

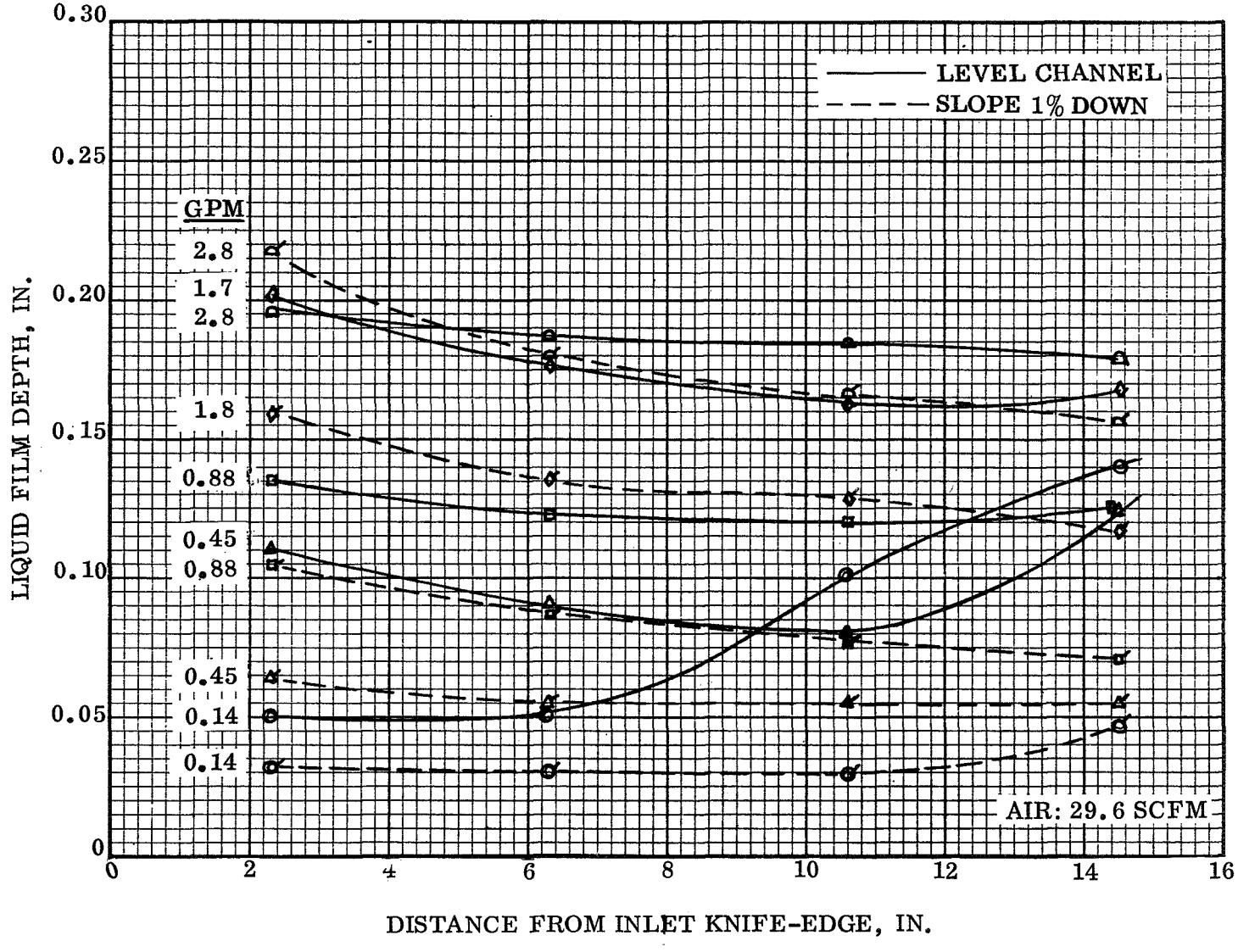


Figure 55. — Film Height Comparison for Level and Down Slope Channel

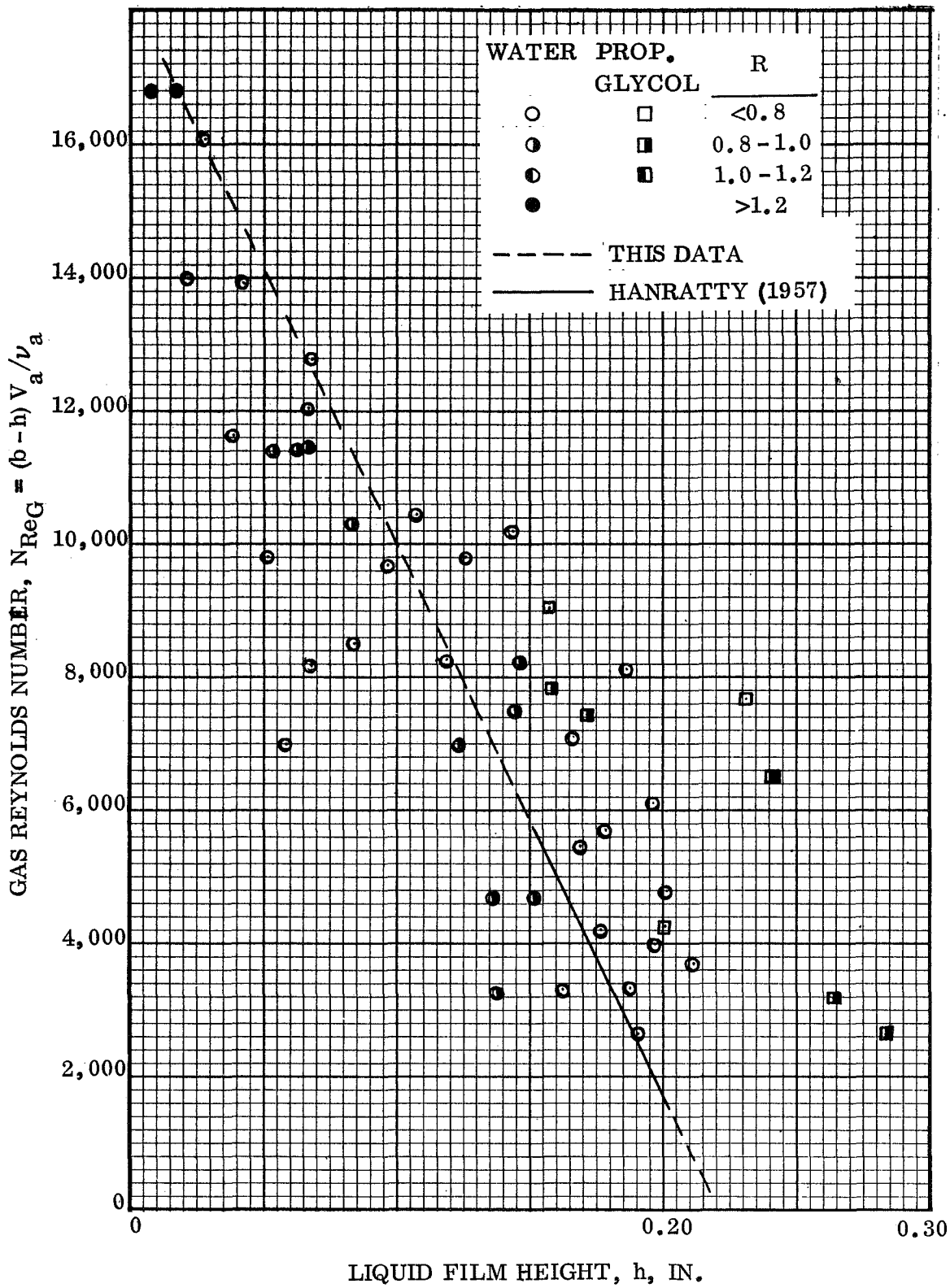


Figure 56. — Relationship of Film Height and Gas Reynolds Number

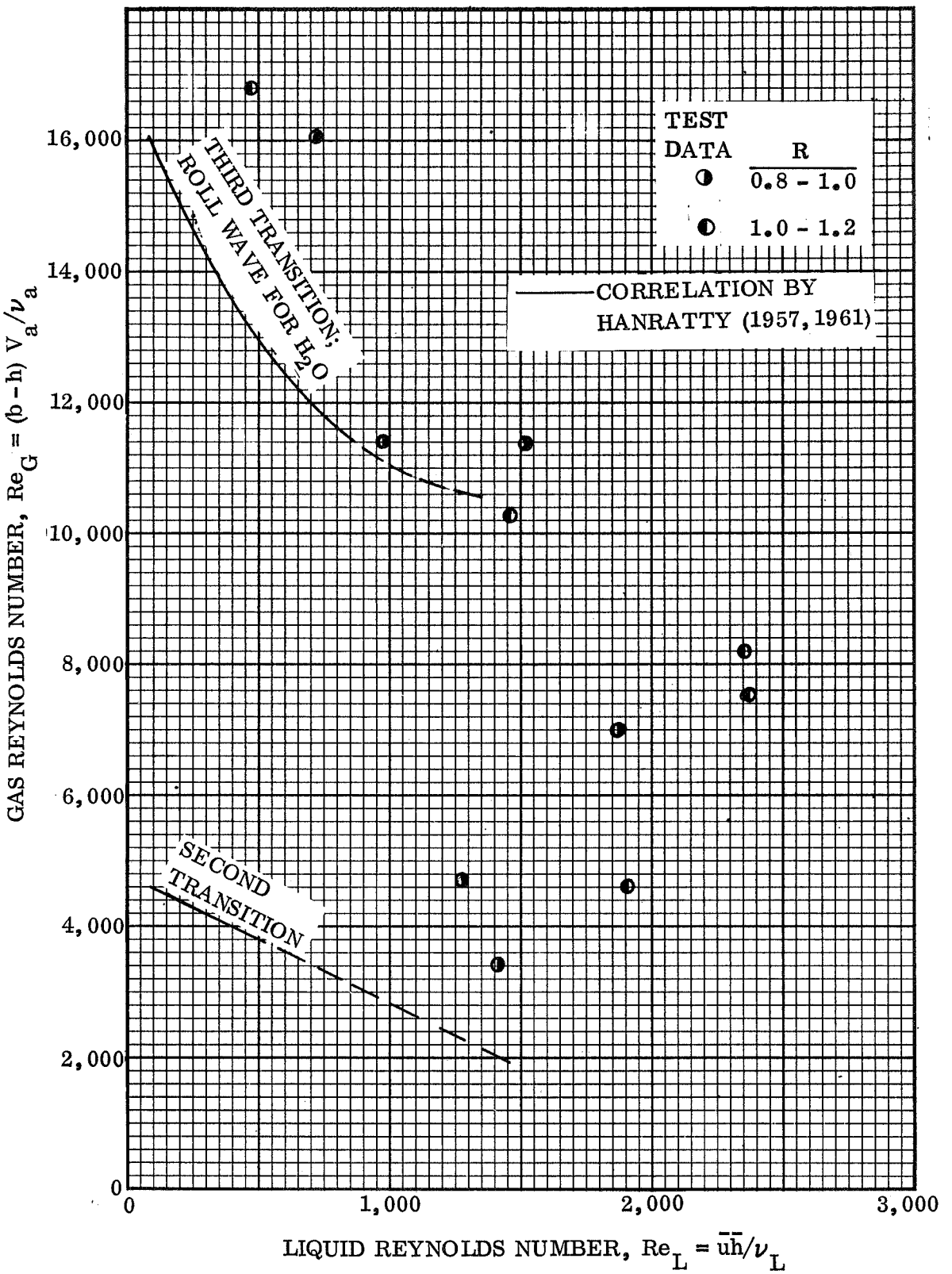


Figure 57. — Comparison of Hanratty Stability Correlations with Marginal Stability Film Data

Fulford (ref. 7) discusses many correlations of film thickness with the Nusselt film thickness, N_T, as a function of liquid Reynolds number

$$N_T = h\,(g \sin \theta/\nu_\ell)^{1/3}$$

This has applicability to sloping channels but with horizontal channels, $\sin \theta$ goes to zero. Results for sloping channel runs of this test series are compared with theory in figure 58. Agreement is good over a wide range of values, and film thickness is predicted within 15 percent. Correlations with gas stream drag present were not available in the literature for other than vertical channels.

The importance of changes in channel slope on film thickness is of immediate interest since film stability is influenced by film thickness, and it is unrealistic to attribute stability changes to channel slope which actually are only the result of thinner films. The experimental design set points of table 21 afford the data to examine effects of slope at several flow conditions. The data are presented in figure 59. The influence of slope is more prominent for plus degree or slope up, but down sloping channel runs do posses somewhat thinner films. The lower values at level than at -20 minutes slope are most probable data error in the former readings. Those points represent some of the earlier test data.

Film Thickness Correlation

In figure 60, the predicted liquid heights are presented as a function of liquid and gas bulk velocities. The predicted values are determined from program SHEAR using standard shear stress/friction factor relationships for smooth surfaces. These relationships with program SHEAR are presented in Appendix B of reference 3. As expected, considerably higher gaseous shear is expended in dragging the rough surface film. Comparing the predicted air velocity with that observed for a given run, a predicted gaseous shear velocity requirement two-fold or three-fold higher is not uncommon for the horizontal channel water data. Hanratty (ref. 6) refers to a distortion factor of the gas velocity profile which may result in gas shear 2.5 higher than predicted; this phenomenon is in accord with experimental results here. The factor for each test data point can be found from the ratio of predicted required air velocity versus observed at each point for a constant liquid depth, i.e., for run W-25, 13.0 ft/sec versus 9.0 ft/sec is a 1.4 higher shear force measured than predicted.

An excellent survey of the characteristics of film flow has been prepared by Fulford (ref. 7). His discussions served as an excellent guide to the literature in specific areas. A continuing investigation of films has been conducted by Hanratty and others (ref. 5, 6, 8) at the University of Illinois. His findings on channel length for good observations and methods for introducing the liquid film confirm the findings of this

work. Dukler (ref. 9) has conducted extensive investigations on films and heat transfer. His remarks are pertinent in the considerations for condenser design.

Film Stability

The experimental data was processed to provide the necessary variables for comparison with Miles Model (equation 16) (ref. 10). The data was reduced with REDATA to provide the variables α, a function of Froude and Weber number, and the variable of the critical Reynolds number based on interface velocity. The steps in the data reduction process to define these quantities as well as the program source listing and sample output are presented in Appendix B of reference 3. With a film thickness ranging from 0.008 to 0.219 inch in the horizontal channel with water, Froude number was varied from 1.4 to 4000 and Weber number from 3.3 to 130. This wide range of independent variables resulted in values for α of 0.025 to 1.0 for water in the horizontal channel.

The results of this correlation are presented in figure 61. The agreement with the model is considered to be excellent. As expected, points of marginal stability, $0.8 < R < 1.2$, bracket the theoretical correlation line while stable and unstable values depart from the line of neutral stability. The preponderance of unstable points in the stable region suggests the curves should be displaced to the right or downward. The manner in which Miles derived the theoretical model as a locus of minima of neutral stability curves would suggest some stable points could lie in the unstable region, but not the converse as observed. To complete the presentation of this data, points for all runs other than W-1 to 33A and W-13 to 51, which are horizontal water data, are presented on figure 62. These data are not conclusive as the horizontal channel data but the same comments on unstable points are valid. All glycol runs lie to the right of $\alpha = 0.35$ and below R_e of 100, but were not judged as exhibiting the stable nature suggested by their location with respect to the neutral stability line.

The "R" criterion as applied to the analysis of data obtained from the glycol runs indicated that errors existed in one or more or a combination of the following areas:

a. Incompatibility of the model with highly viscous fluids

b. Predictive location of the neutral stability line

c. Application of the R criterion in the analysis of data

d. Experimental error or bias imposed by

    1. Wave pulse dynamics

    2. Channel form interactions

Further discussion of this can be found in the section headed "Impact on the Analytical Model."

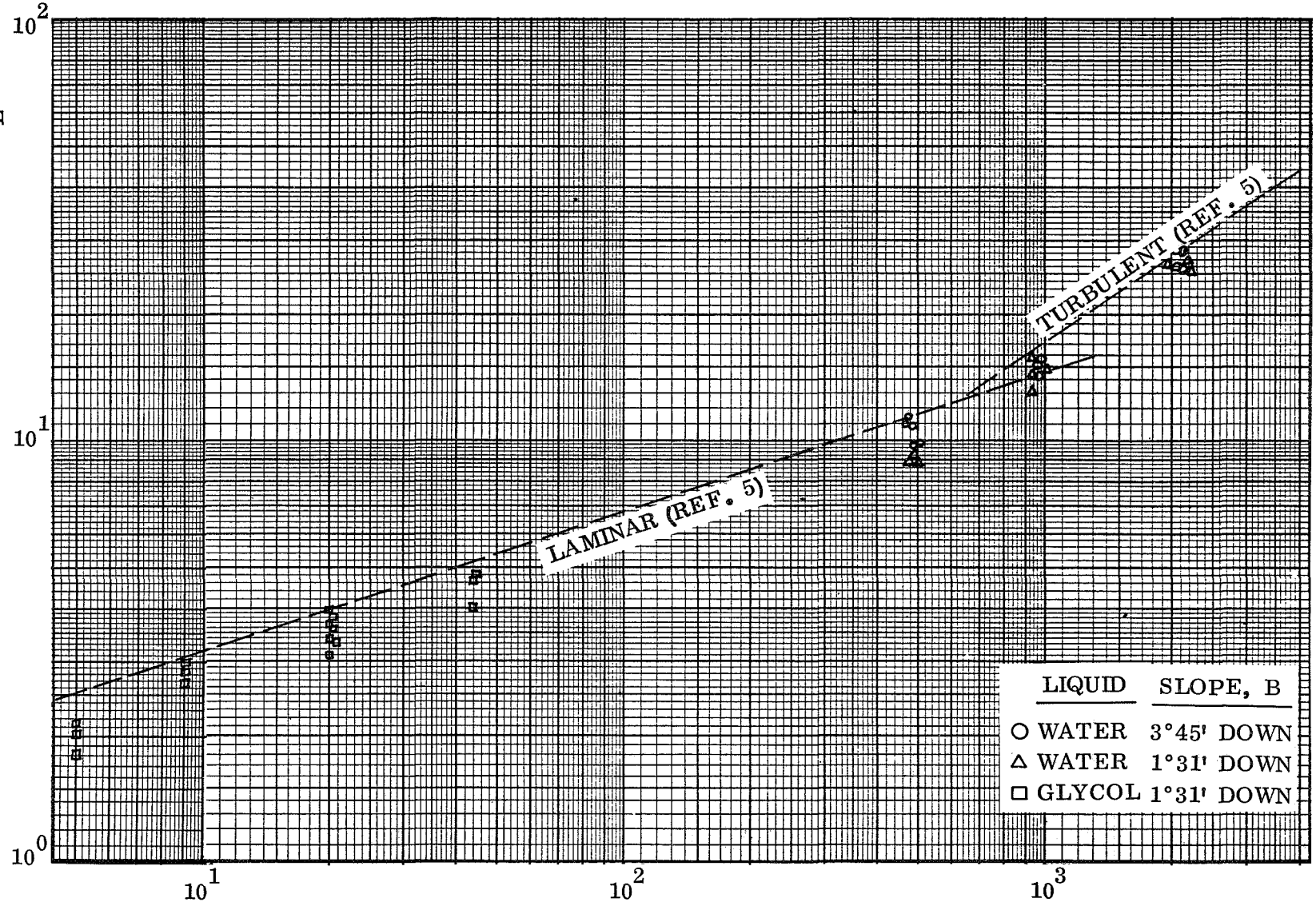


Figure 58. — Test Data Comparison with Nusselt Film Thickness Parameter

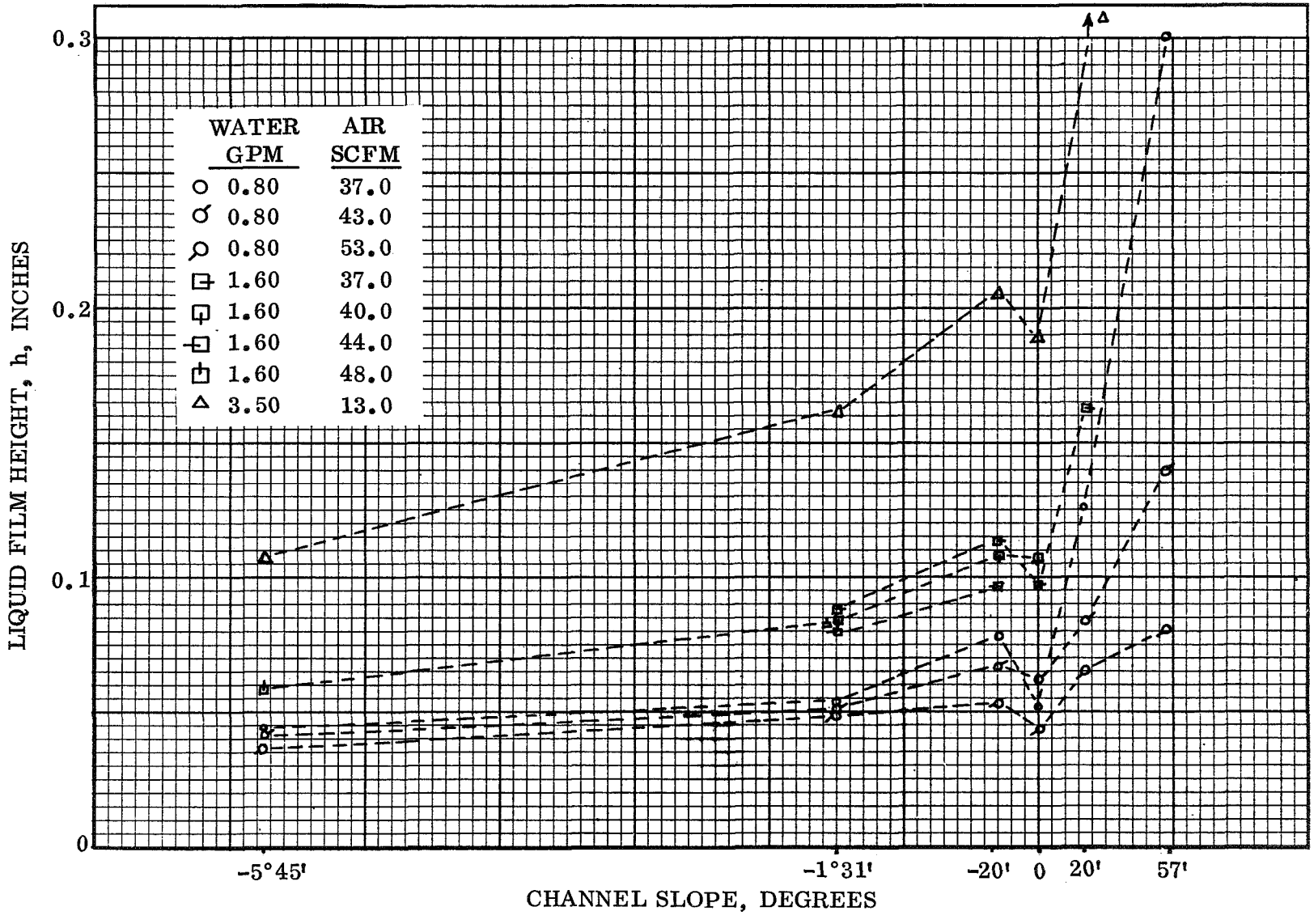


Figure 59. — Channel Slope Effect on Liquid Film Thickness

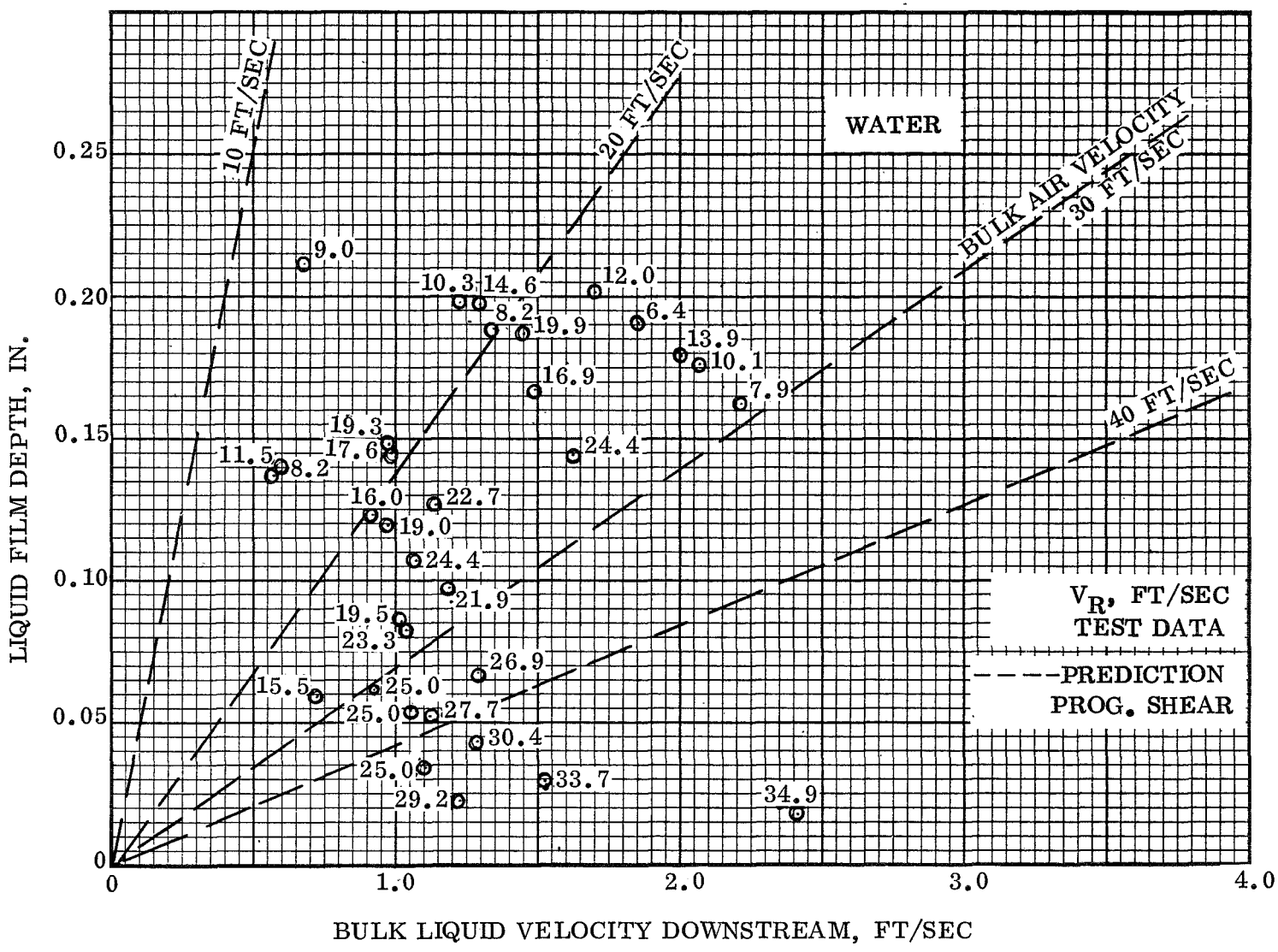


Figure 60. — Comparison of Predicted and Experimental Data for Film Thickness

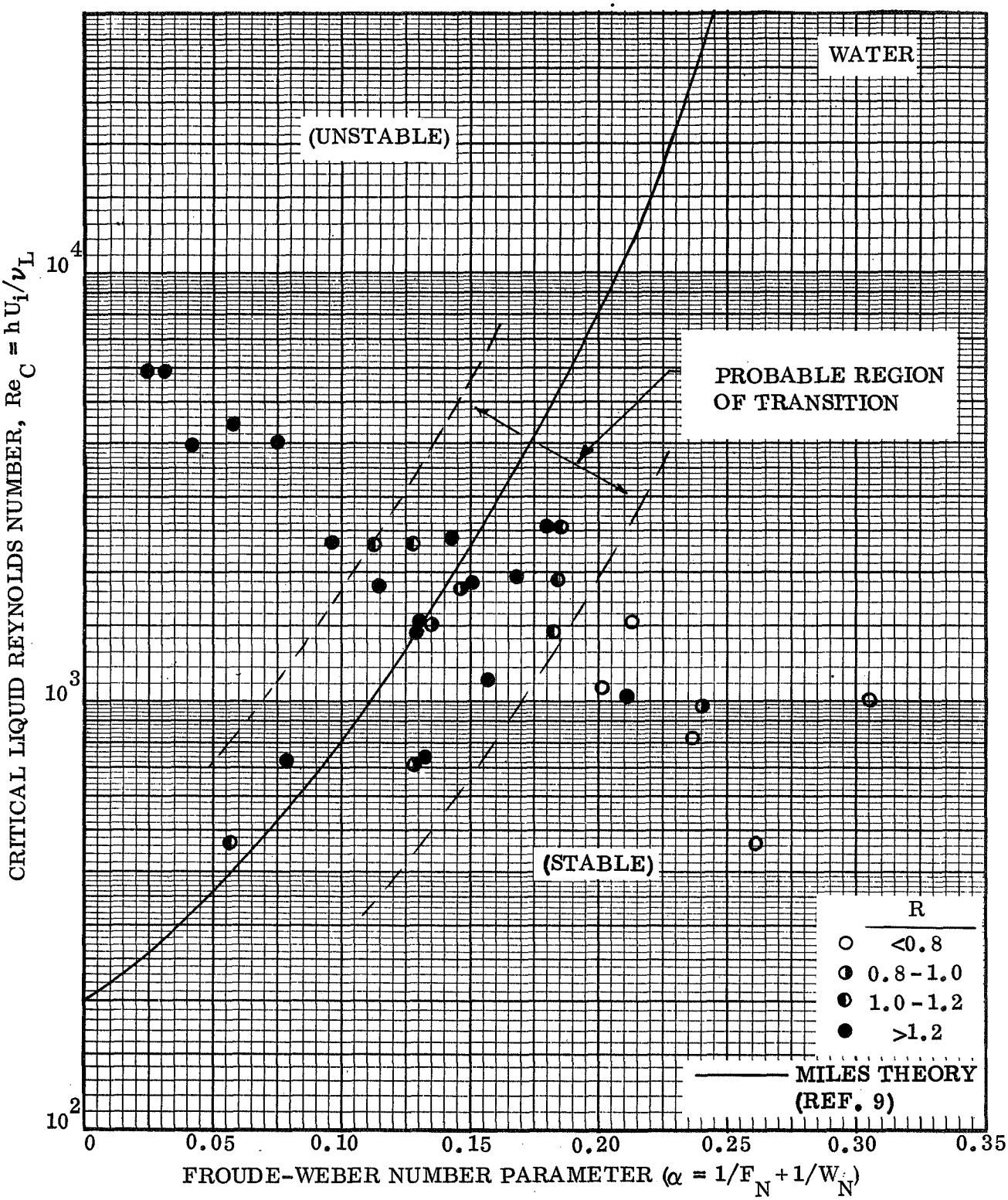


Figure 61. — Correlation of Predictive Versus Experimental Data for Stability Criteria - Horizontal Channel

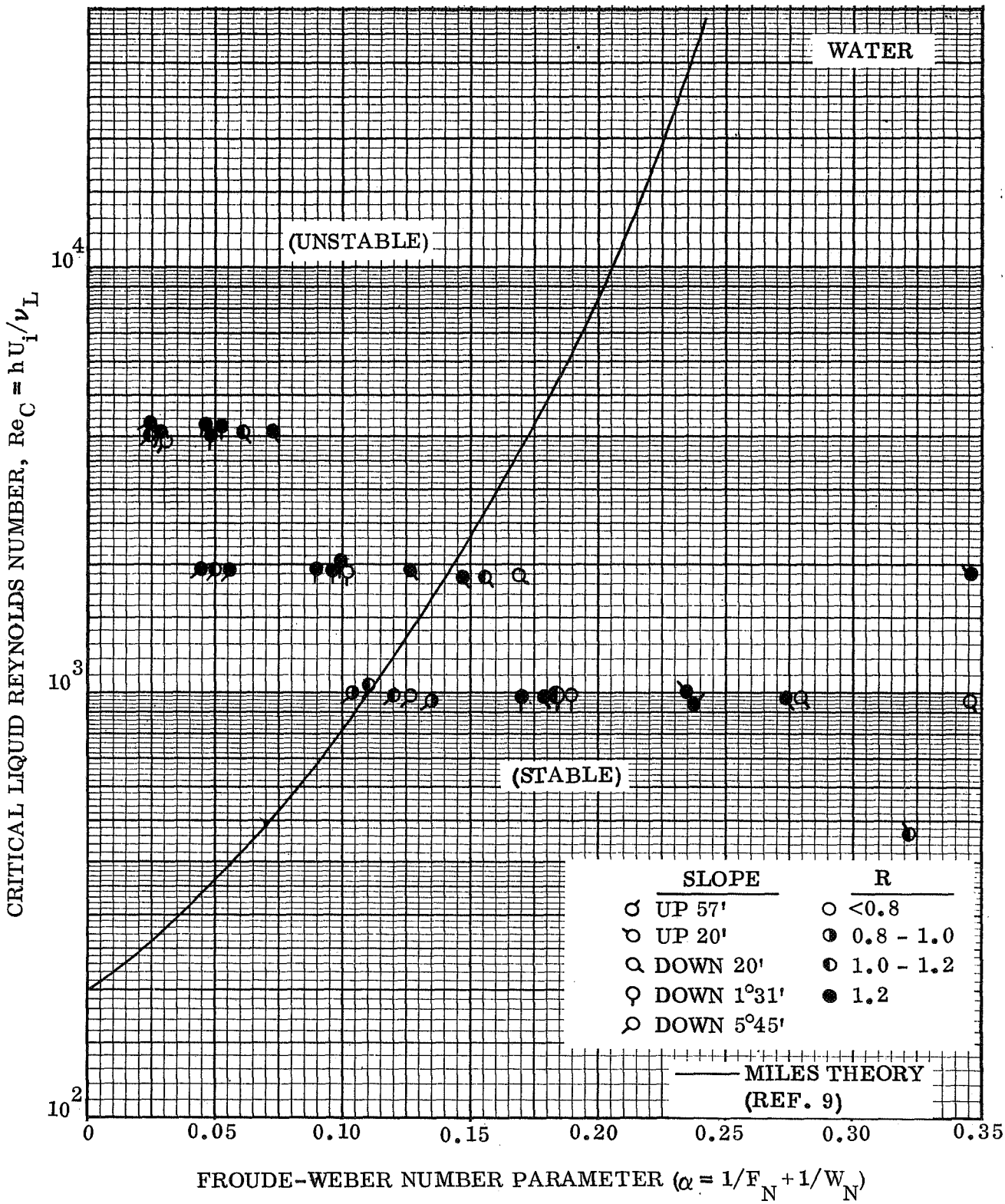


Figure 62. Correlation of Predictive Versus Experimental Data for Stability Criteria - Sloping Channel

An alternate, useful form of data presentation results from a combination of predictions from SHEAR with the liquid velocity/film height data obtained from RECRIT. The bulk liquid velocity for a given film height and its stability characteristic for a given gas velocity can be defined from figure 63. Since interface shear factor was considered to be unity, the predictive lines for film height would move to the left as interface shear is doubled to account for surface roughness. Only random data points were selected from the horizontal water data. Figure 63 is a generalized representation of figure 43. Similar data are shown for the proplyene glycol system in figure 64, but the neutral stability prediction is absent as per the discussion of figure 62. Similar comments to figure 63 on the film height predictions hold true.

The effect of channel slope of film stability is represented in figure 65. This graph must be intrepreted in light of the changes in film thickness shown in figure 59. Within the scope of this effort, it is not possible to separate these effects. It is significant to point out that film thickness varied more than two-fold, while gravity level affecting stability varied only 1.2 percent. Thus, when the influence of gravity field is considered alone, one might expect little influence on the stability variable, R. Such results were reflected in the comparison of data for various slopes with that of a level channel, figures 61 and 62.

Results of the Experimental Evaluation

Impact on the Analytical Model

Impact on the analytical model for film height, SHEAR, and the correlation by Miles for film stability were both noted from experimental results. It became quite obvious when results for film height were compared with predictions that the predicted film heights were too thick. As indicated by other investigators, rougher films under the drag of an air stream have a high interface shear. The model was changed to account for this with inclusion of an empirical factor, ϕ, which increases the gas shear by a factor of 2.0. A difficulty here is that some data points indicated the factor to be 1.5 while others suggested 2.5. Thus, 2.0 is a compromise value to bring more of the data closer to the prediction.

For the stability model, the water results for the horizontal channel did bracket the theoretical prediction and did not afford sufficient disagreement to suggest a change in the model. The model appears quite adequate for water under 1g conditions. The experimental data lying within the marginally stable area give confidence in the sensitivity to stability.

The propylene glycol provided some very interesting results in that the high viscosity of the fluid caused all liquid Reynolds numbers to lie below 200, which is the minimum Re for instability. Most of the runs were defined as unstable according to the R

criteria as applied, similarly many runs were defined as unstable with values of $\alpha > 0.33$.

At the conclusions of the data analysis and correlation, the movie data were again reviewed by the authors in a specific attempt to provide an insight into the problems relative to the analysis of the glycol/air system data against the stability predictions. Several observations are considered pertinent to the development of an understanding of the apparent anomaly. Although it has not been possible to attempt a quantitative analysis of the observations and thereby form the basis for re-evaluation of the correlation of data, it is believed that such is practicable. The observations can be summarized as follows and illustrated by references to the shadowgraph photos of figure 48.

a. Parabolic wave front patterns were typical of the glycol/air system but not observed for the water/air system. The parabolic pattern undoubtedly results from the viscous sidewall drag. It is estimated that the resulting sidewall boundary layer extends to 20 to 30% of the channel width. The curvature illustrated by figure 48 is less severe than that observed for the majority of runs.

b. The curvature of the waves appeared to be increased as they moved along the channel resulting in positive wave interference or coalescence which in effect appeared as increasing wave height.

c. The influence of the wave pulse generator was pronounced with the glycol runs. Although the movies for the water/air system runs were taken prior to the installation of the pulse generator and thus no direct comparison could be made, the observers agree that observations during the course of the experiment indicated that the pulse generation effects appeared to be less significant in terms of wave build-up for the water/air system.

d. The water waves rather than forming a parabolic front and eventually coalescing, degenerated into random frequency disturbances.

An intuitive analysis of the implications of these observations would tend to indicate that the following tentative conclusions are appropriate:

a. The behavior of glycol-air system was highly distorted by the channel interaction and pulse generation effects creating apparent instability as initially judged by the R criterion when in fact the film was fundamentally operating in a stable mode as correctly predicted by the analytical model.

b. A more experimentally manageable stability criterion may be indicated such as one based on wave frequency characteristics.

c. With this increased understanding a re-examination of the data might well indicate an acceptable degree of correlation between predicitive and experimental observations relative to the glycol/air system stability without altering the criterion.

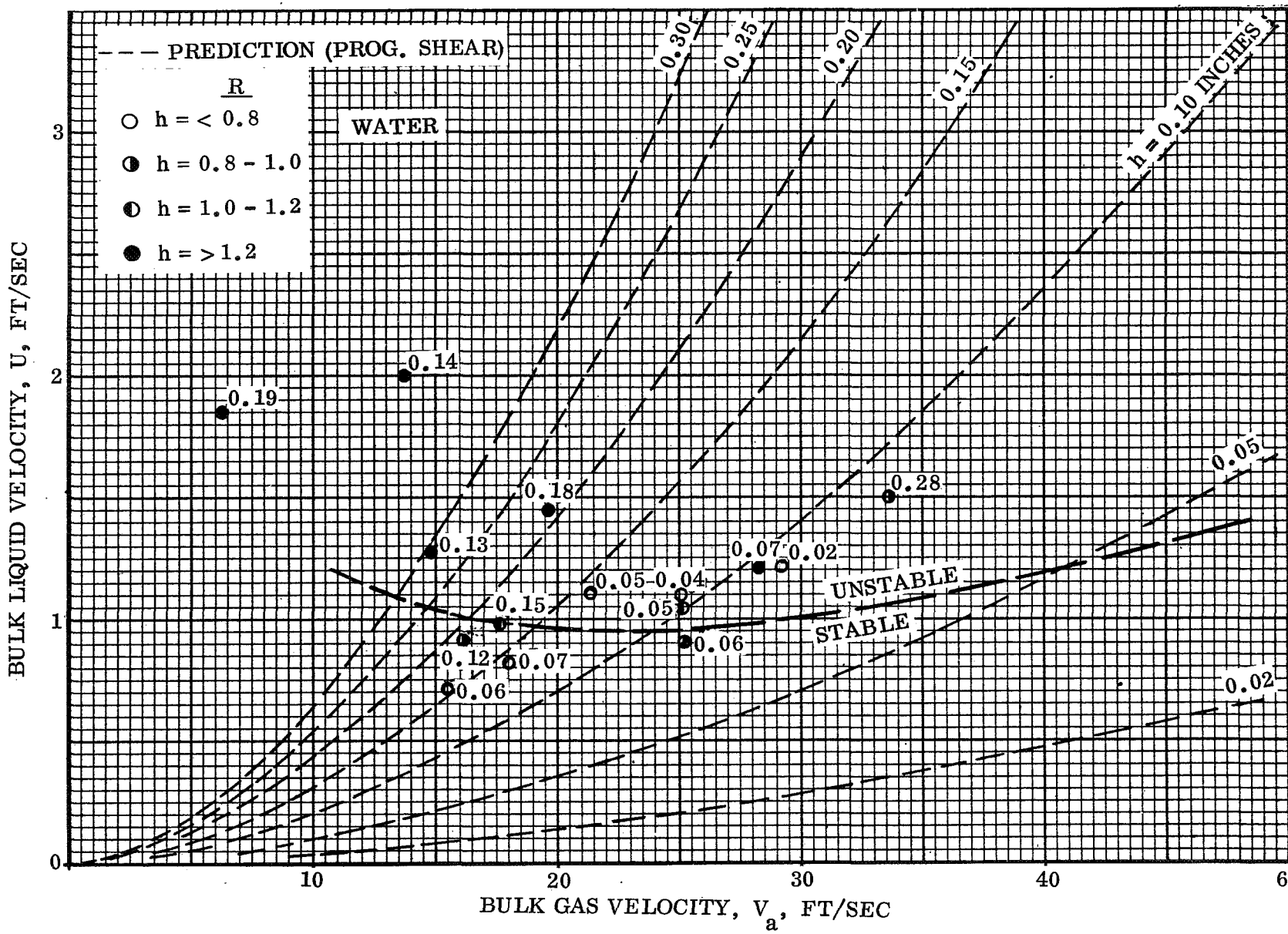


Figure 63. — Stability Regions Defined

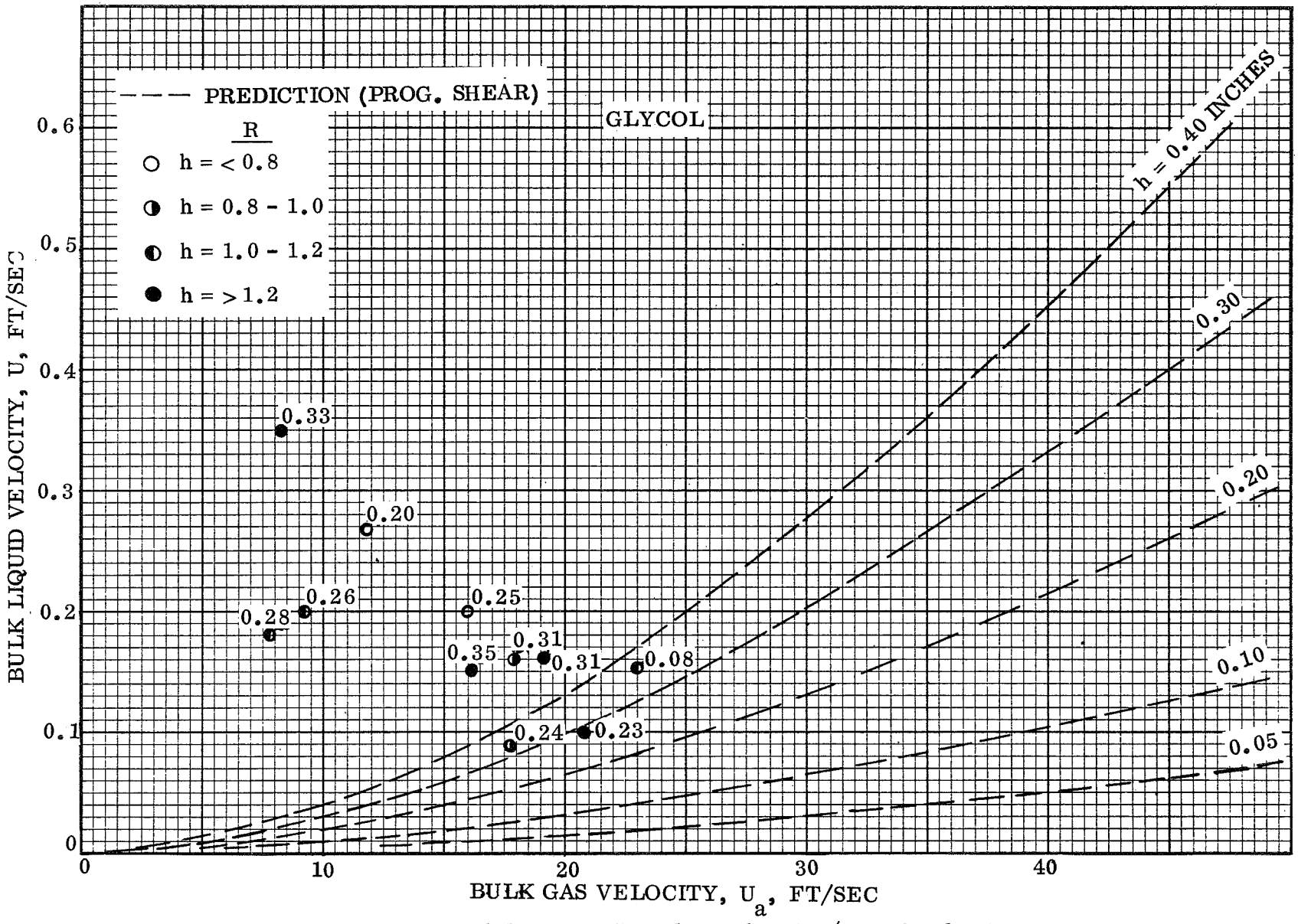


Figure 64. — Stability Data Correlation for Gas/Liquid Velocities

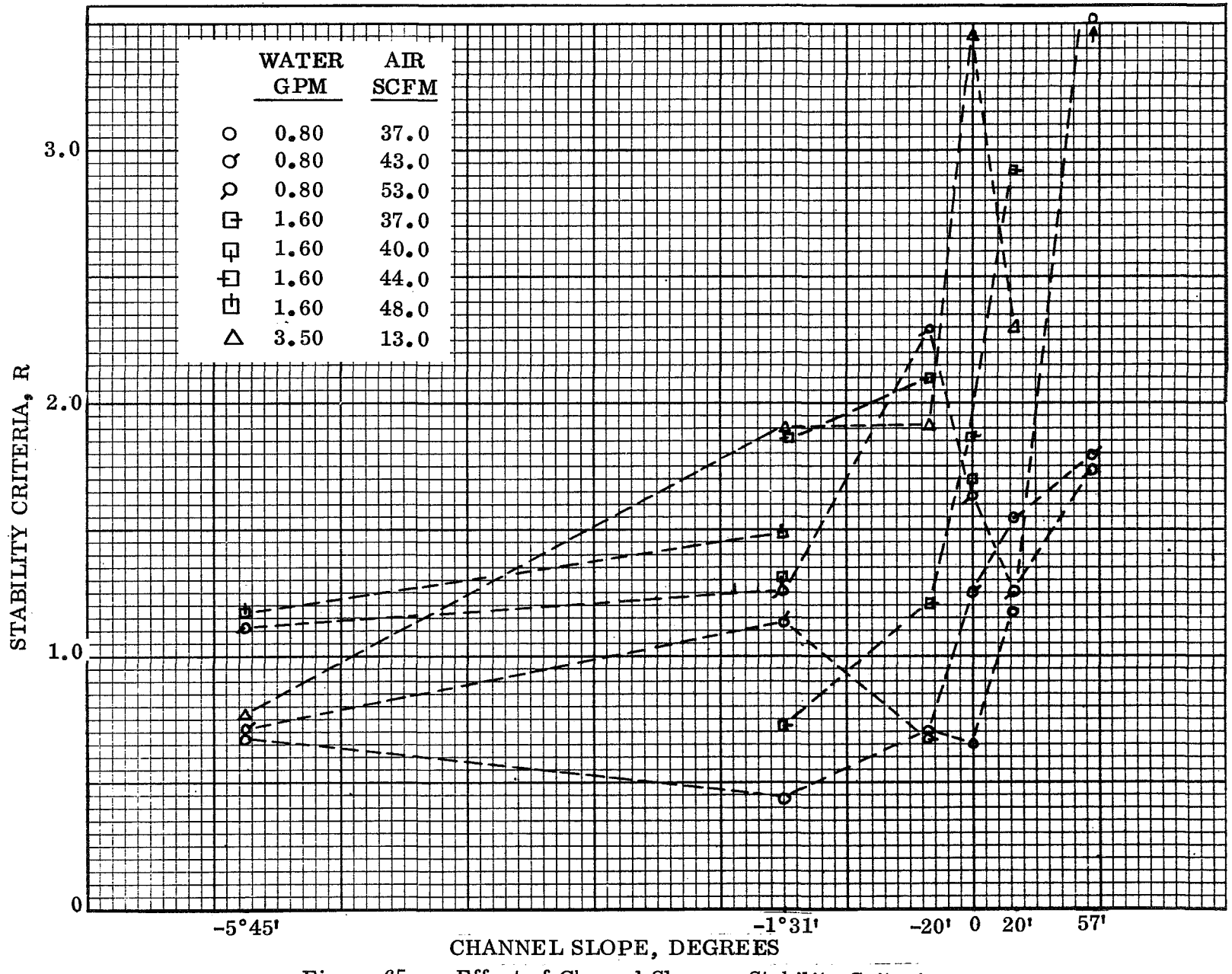


Figure 65. — Effect of Channel Slope on Stability Criteria

Recommendations for Further Experimental Evaluation

Laboratory experiments. — This laboratory experiment verified techniques highly suited for this type of analysis. Two areas could have been improved upon and should be the subject of further laboratory investigation. The length of channel to obtain good stability data and achieve film of relatively constant height should be determined. Further work should be done in the investigation of the effect of variations in surface tension with viscosity and density held constant. This work indicated that at high Froude numbers, variations in surface tension could result in a two-fold variation in the range of α, the independent variable in the stability correlation.

Reduced-gravity experiments. — Although the period required for attaining process stabilization following a change in g-level is relatively short; i.e., in the range of a few seconds, and the steady-state observation periods are likewise relatively short, also in the range of a few seconds, the overall stabilization period is in excess of that available for most ground-based facilities. The KC-135 may provide sufficient dwell time at a sufficiently low and stable g-level to be of potential value. However, it is considered that the manned orbital space station is ultimately required and thus should be considered the prime source of data.

REFERENCES

1. Miles, John W.: The Hydrodynamic Stability of a Thin Film. Journal of Fluid Mechanics, 8, 2960, p. 593.

2. Ballinger, J.C.; et al.: Study of Zero Gravity Capabilities of Life Support System Components and Processes — Final Technical Report. NASA CR-66534, NAS 1-6939, GDC-DBD67-004, Convair division of General Dynamics, February 1968.

3. Burnett, J.: Experimental Test Report - Test No. 3A, "Film Stability and Transport. NAS 1-8494, 12 January 1970.

4. Evans, E.; Bradshaw, B.; Burnett, J. R.: Analytical Model Report No. 3, Film Stability and Transport. Second Issue, NAS 1-8494, March 1970.

5. Hanratty, T. J.; Engen, J.M.: Interaction Between a Turbulent Air Stream and a Moving Water Surface. AIChEJ. 3 299 (1957).

6. Hanratty, T. J.; Hershman, A.: Initiation of Roll Waves. AIChEJ. 7 488 (1961).

7. Fulford, G. D.: The Flow of Liquids in Thin Films. Advances in Chemical Engineering, Editor T. B. Drew, vol. 5, pp. 151-236, Academic Press, New York, 1964.

8. Lilleleht, L. U.; Hanratty, T. J.: Relation of Interfacial Shear Stress to the Wave Height for Concurrent Air-Water Flow. AIChEJ. 7 548 (1961).

9. Dukler, A. E.: Fluid Mechanics and Heat Transfer in Vertical Falling-Film Systems. Chem. Engr. Progr. Symp. Ser. 30, 1 (1960).

10. Miles, J. W.: The Hydrodynamic Stability of a Thin Film of Liquid in Uniform Shearing Motion. J. Fluid Mech. 8, 593 (1960).

ANALYTICAL MODEL NO. 4 — "INERTIAL SEPARATION"

Nomenclature including subscripts for the inertial separation calculations is given in table 22. Note that a separate list is given for case 1 screen separator, and two separate lists are given for case 2 vortex separator.

Table 22. — Nomenclature for Inertial Separation Calculations

Case 1 Screen Separator

A	area - cm^2
C	drag coefficient - dimensionless
D	energy loss coefficient for droplet deformation - dimensionless
d	pore characteristic length (diameter) - cm
F	force - dyne
f	friction (adhesion coefficient) - dyne/cm
g	acceleration of gravity - cm/sec^2
k	slip ratio - dimensionless
L	system characteristic length - cm
ℓ	length - cm
n	number of screen pores covered by drop - dimensionless
P	pressure - $dyne/cm^2$
P_t	penetration parameter - $dyne/cm^2$
Re	Reynolds number - dimensionless

Table 22. — Nomenclature for Inertial Separation Calculations, Contd

s	solidity - dimensionless
t	time - sec
u	air stream velocity - cm/sec
V	volume - cm^3
v	droplet velocity - cm/sec
We	Weber number - dimensionless

Greek

α	surface tension force constant - dimensionless
β	angle between impacting drop and gravity vector - degrees
γ	screen angle in drop tests - degrees
ϵ	turbulence energy dissipation - cm^2/sec^3
θ_1	angle impacting droplet makes with screen - dimensionless
θ_2	angle air flow makes with screen - dimensionless
λ	droplet characteristic length (diameter) - cm
μ	dynamic viscosity - gm/cm-sec
υ	kinematic viscosity - cm^2/sec
ρ	mass density - gm/cc
σ	surface tension coefficient - dynes/cm
ϕ	porosity - dimensionless
ψ	contact angle - degrees

Subscripts

a	adhesion	p	pressure
c	capillary	st	surface tension
d	drag	t	total
g	gravity	v	inertia (velocity)
i	internal	1	upstream
ℓ	liquid	2	downstream

Table 22. — Nomenclature for Inertial Separation Calculations, Contd

Case 2 Vortex Separator — Cylindrical Section

A	dimensionless parameter
B	dimensionless parameter
c	vortex strength - cm^2/sec
F	momentum transfer parameter - 1/sec
g	acceleration of gravity - cm/sec^2
m	particle flux - gm/sec
r	radial coordinate from cylinder axis - cm
r_*	dimensionless radial coordinate
u	radial velocity - cm/sec
v	azmuthal velocity - cm/sec
w	axial velocity - cm/sec
z	axial coordinate - cm
z_*	dimensionless axial coordinate
ρ	mass density - gm/cc
ψ	stream function - gm/sec

Subscripts

o	at z = o or at r = o
1	initial position
w	cylinder wall

Table 22. — Nomenclature for Inertial Separation Calculations, Contd

Case 2 Vortex Separator — Conical Section

E	dimensionless parameter
Fr	Froude number - dimensionless
g	acceleration of gravity - cm/sec^2
K	dimensionless parameter
M	dimensionless mass flow rate
m	mass flow rate - gm/sec
P	pressure - dynes/cm
R	distance from vertex along cone surface - cm
r	distance perpendicular to axial planes - cm
u	radial velocity - cm/sec
v	velocity perpendicular to R - cm/sec
w	velocity perpendicular to axial planes - cm/sec

Greek

α	vertex half-angle - radians
Δ	dimensionless length increment
δ	boundary layer thickness - cm
η	dimensionless coordinate
θ	angle a radius vector makes with cone axis - radians
μ	dynamic viscosity - gm/cm-sec
υ	kinematic viscosity - cm^2/sec
ρ	mass density - gm/cc
Ω	circulation (vortex strength) - cm^2/sec

Subscripts

h	heavy fluid (liquid)
ℓ	light fluid (gas)
o	length of side of cone
1	dimensionless

DESCRIPTION OF THE MODELS

Two analytical models have been developed which describe the behavior of a liquid and a transport gas stream reacting to the forces applied in each of two approaches to liquid/gas (water/air) separation. These are Case 1, hydrophobic screen separation, and Case 2, vortex separation (ref. 1).

In both cases the water/air mixture is moved through the system initially as a liquid dispersoid transported in the gas stream and terminally as separated and independently transported streams: one channel operating to transport an "air-free" liquid stream, the other a "liquid-free" air stream. In additionto the inertial forces involved in the processes, gas stream interfacial shear and liquid/solid surface effects are treated. Figures 66 and 67 schematically illustrate the nature of the two systems.

The model considers the effects on the predicted behavior in each of the two cases resulting from variations in a broad range of parameters such as:

a. Gravitational field strength and orientation (the local g vector).

b. Dispersoid velocity.

c. Dispersoid size.

d. Gas stream velocity.

e. Dispersoidal impact angle.

f. Solid surface(s) characteristics (physical).

g. Fluid characteristics (physical).

h. Interfacial shear.

i. Droplet adhesion.

j. Gas pressure drop.

k. Liquid outflow rate.

Special emphasis was placed in each of the two cases on the behavior of the liquid in its transition from a distribution of impacting dispersoids to the controlled movement of a droplet or liquid film.

The models are so designed as to be of potential value in the development or analysis of LSS equipments where phase separation is required. The two cases treated herein can be related to a broad spectrum of separation techniques spanning, at least in part, essentially all of those being proposed for the near term future. The models should

help in solutions to such design questions as appropriate screen configuration, dispersoid impact velocity and angle, required "centrifugal field strength," and optimum or expected flow field distributions.

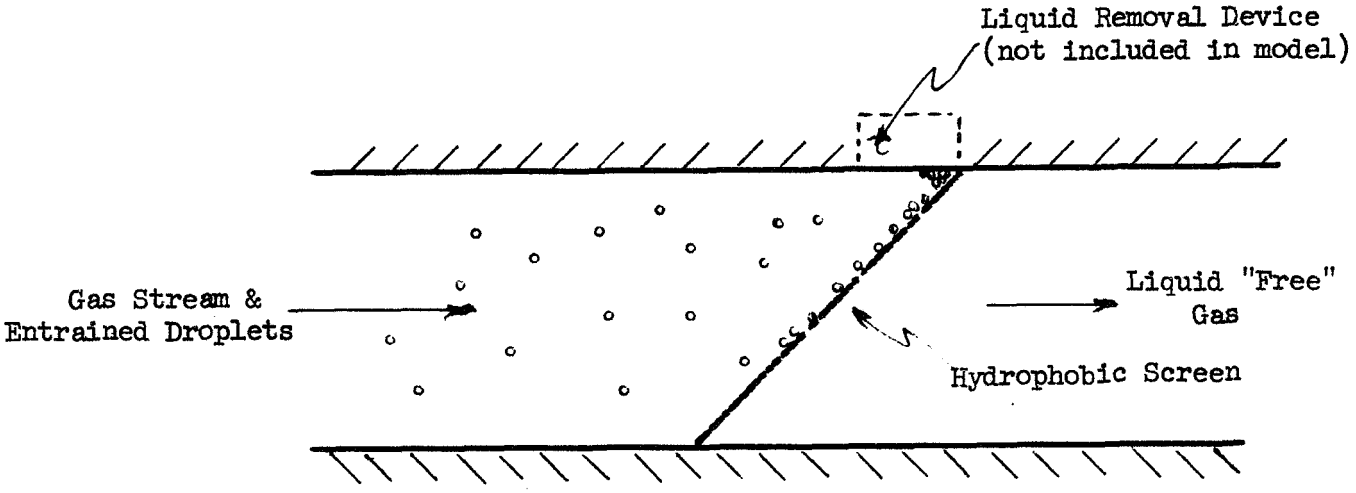


Figure 66. — Case 1, Analytical System Schematic — Two-Stage Screen Separation

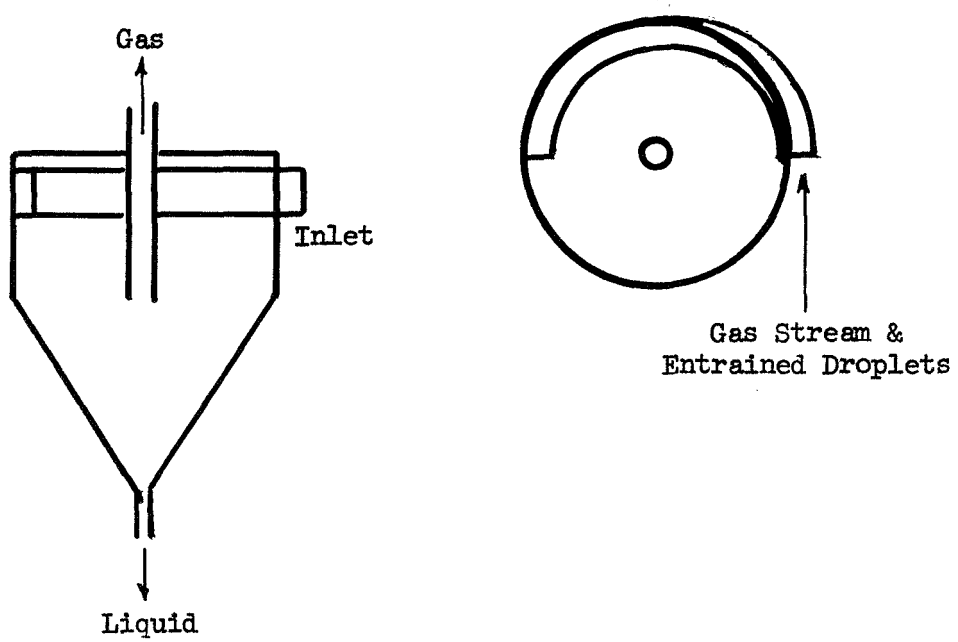


Figure 67. — Case 2, Analytical System Schematic — Cone Centrifuge Separation

Case 1 — Hydrophobic Screen Liquid/Gas Separation

Behavior of droplets on hydrophobic, i.e., "non-wetting" porous materials, is the consideration of central importance for evaluation of the effectiveness of the liquid/gas separation system shown in figure 66.

To properly determine this behavior, several features of the flow of gas with entrained liquid droplets must be known. These are:

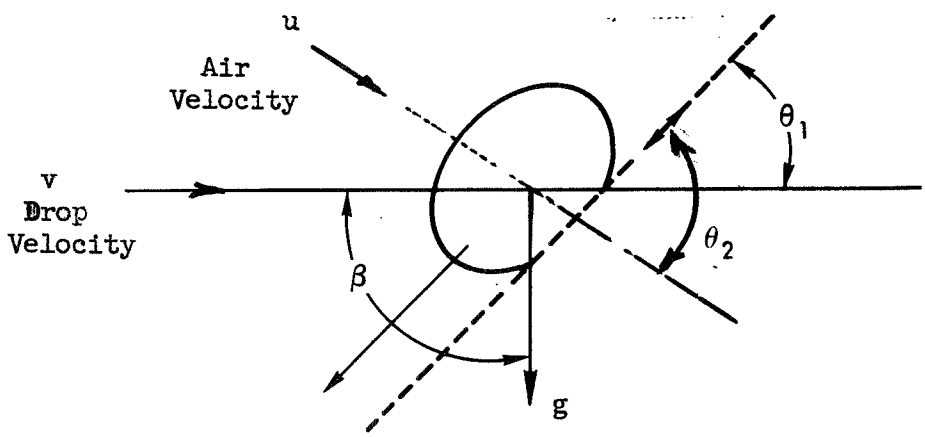
a. Droplet adhesion on surfaces.

b. Entrained drop velocities and sizes.

c. Gas pressure loss through the basic porous medium.

These problem areas will be analyzed separately and the resulting relationships will then be used to determine droplet behavior on the porous material.

Angle conventions and terminology used in the hydrophobic screen liquid/gas separation model are presented in the sketch.



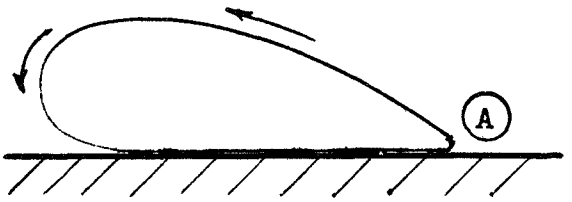
Droplet Adhesion

The adhesive forces between a liquid and a solid surface account for a variety of droplet phenomena including the "sticking" tendencies of small droplets on hydrophobic materials and the rolling action of larger drops on these "non-wetting" surfaces.

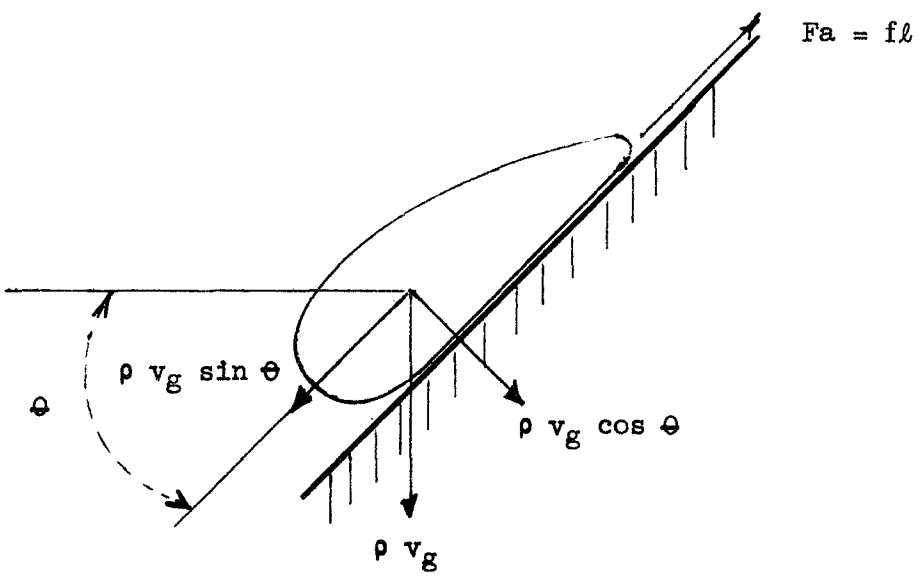
On horizontal surfaces the shape of liquid drops will be influenced by liquid surface cohesion, attempting to reduce the surface area and attain a spherical shape. Gravity forces will cause the bottom of the drop, where the pressure exerted by the column of liquid is greatest, to try to expand. Adhesion forces between the drop and the solid establish the angle of intersection of the liquid and solid surfaces. A very small drop,

for example, will be drawn into a nearly spherical shape because liquid head is dominated by liquid surface cohesion. For any size drop, however, the contact angle will not change.

An heuristic model of a rolling drop can be easily created with a loop of sticky tape as shown in the sketch.



As the tape is rolled over a surface, resistance occurs only at the trailing edge (A) where the surface contact is being continuously broken. When a body force is applied to a liquid drop, the force component applied to breaking the trailing edge adhesion is parallel to the surface. Thus for a drop on an inclined surface, in a gravity field, the next sketch describes the motion.



To simplify the development of a criterion for drop motion on a hydrophobic surface, a two-dimensional fluid drop will be considered. This drop has a volume per unit depth which can be represented, in order of magnitude, by λ^2. If the adhesion coefficient is f, then the adhesion force is

$$Fa = f\ell = \rho\ell\,\lambda^2\, g \sin\theta \qquad (1)$$

From the preceding discussion it is apparent that the larger drops in a given force field will roll more easily.

Liquid Droplet Size in a Turbulent Gas Stream

Deformation of the surface of a liquid droplet in a gas stream will occur when forces due to inertia no longer are dominated by liquid surface forces. Consider a liquid droplet with characteristic length λ. Velocity variation over this length will be specified as v_λ with liquid density ρ and surface tension coefficient σ. From these quantities, two force relationships can be formed:

a. Inertia force $\sim \rho \lambda^2 v_\lambda^2$

b. Surface force $\sim \lambda \sigma$

Dividing the inertia force parameter by the surface force parameter gives a Weber number

$$We = \frac{\rho \lambda v_\lambda^2}{\sigma} \tag{2}$$

When the Weber number is small, the shape of the drops will be spherical and stable. At large Weber numbers, however, the liquid surface will deform easily and drop break-up will occur. Of the four parameters above only one, v_λ, is unknown.

Velocity variation over small distances in a fully developed turbulent fluid is given by Kolmogorov and Obukhov's law (ref. 2), valid for $L >> \lambda >> \lambda_o$

$$v_\lambda \sim (\epsilon \lambda)^{1/3} \tag{3}$$

Distances L and λ_o are the characteristic length of the system and the Kolmogorov scale respectively.

The energy dissipation ϵ can be found from the quantities which characterize the large scale turbulent motion, the length L, and the variation of the mean velocity over L, Δu. If we take $\Delta u \sim u$, the average duct velocity, we have

$$\epsilon \sim \frac{u^a}{L} \tag{4}$$

The Weber number then becomes

$$We = \rho u^2 \lambda^{5/3} \sigma^{-1} L^{-2/3} \tag{5}$$

and the average liquid droplet size ($We \sim 1$) can be estimated by

$$\lambda \sim (\sigma L^{2/3} \rho^{-1} u^{-2})^{3/5} \tag{6}$$

Droplet Deformation at Impact

To determine whether drop deformation or fragmentation occurs upon impact with the screen we again relate inertia forces to surface forces. This time, however, the inertia force is determined by the velocity variation Δu. To determine Δu, we assume that the droplets do not stick to the screen but travel along parallel to the screen after impact. The velocity variation would then be $\Delta u = u(1-\cos\theta)$.

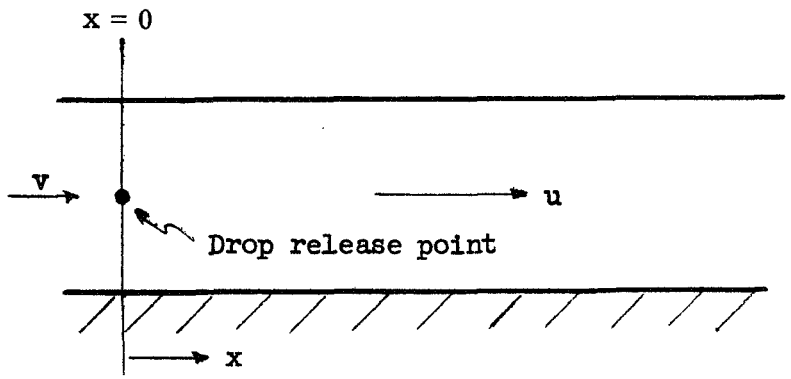
A range of Weber numbers

$$We = \frac{\rho \lambda u^2 (1-\cos\theta)^2}{\sigma} \tag{7}$$

has been determined for the phenomena of deformation and fragmentation and will be covered in the discussion entitled "EXPERIMENTAL EVALUATION."

Entrainment of Liquid Drops in a Moving Gas

Assume that in a duct, at position $x = 0$, a liquid droplet is released with initial velocity $v = 0$. The gas flow in the duct has a uniform and steady velocity u.



If the drop is spherical and the Reynolds number $\rho(u-v)\lambda/\mu$ of the drop is large, the drag law, assuming that the gas flow is nonturbulent, is independent of viscosity and proportional to the square of the characteristic dimension λ:

$$F = (\text{constant})\ \rho\,(u-v)^2\,\lambda^2 \tag{8}$$

The drop will be accelerated in accordance with Newton's second law of motion

$$F \sim \rho\lambda^3 \frac{dv}{dt} \tag{9}$$

If the gravity force is small compared to F, substituting equation (8) into (9) and integrating, we have (since $v=0$ at $t=0$):

$$t = \frac{\lambda}{u-v} - \frac{\lambda}{u} \tag{10}$$

Defining a slip ratio as $k = v/u$, we can specify that the length of duct L_* required to bring the droplet up to velocity v is

$$L_* \sim \frac{k}{1-k}\lambda \tag{11}$$

Of course the drag law which is valid only for high Reynolds numbers will no longer be applicable when $u-v$ is small. However, for the order of magnitude estimates derived here, the turbulent wake drag relationship should be sufficiently accurate.

If the gas flow is slow enough so that $x = 0$ the droplet Reynolds number is less than 1, say, the drag force is due almost entirely to viscous shear and

$$F \sim 12\,\mu\,\lambda\,(u-v) \tag{12}$$

Performing the substitutions as before and integrating, we have

$$L \sim -\lambda^2\, u \ln (u-ku)/(12\nu) \tag{13}$$

For this case the drag law will be valid over the entire region $0 \le x \le L$.

To determine whether a droplet will be entrained in the gas stream or will be pulled out by the gravity field, we can examine the relative manitudes of the forces involved. The drop will be entrained if F(drag) >> F(gravity). For entrainment, then, if $v = 0$,

$$\left.\begin{aligned} 12\,\mu\,\lambda\,u &\gg \rho\lambda^3\, g \quad (\mathrm{Re} < 1) \\ \rho\, u^2\lambda^2 &\gg \rho\,\lambda^3\, g \quad (\mathrm{Re} > 100) \end{aligned}\right\} \tag{14}$$

Pressure Loss in Flow Through Screens

Pressure losses in flow through screens (ref. 3) can be described by

$$\left.\begin{aligned} \Delta P &\sim L\,\mu\,u\,a^2\,\phi^{-2} \quad \mathrm{Re} < 1 \\ \Delta P &\sim \rho\, u^2 \left(\frac{s}{1-s}\right)^2 \quad \mathrm{Re} > 100 \end{aligned}\right\} \tag{15}$$

where

a = screen surface to volume ratio

μ = dynamic viscosity

ϕ = porosity (i.e., screen flow area divided by total area normal to flow direction)

s = solidity ($s = 1 - \phi$)

L = screen depth

$Re = \rho u d/\mu$ where d = average pore diameter.

Stainless steel wire mesh screens, in general, are hydrophilic with most liquids and must be coated to make them hydrophobic. This process will change the flow characteristics in the material, especially with regard to the pore diameter, d.

Solidity and porosity are dependent on the amount of liquid residing on the screen. If the surface area of this liquid is A_ℓ and the screen total area is A_t, then the effective solidity s is

$$s = s' + \frac{A_\ell}{A_t} \phi' \tag{16}$$

where the primes denote the basic (dry) screen properties.

Drop Behavior on the Screen

Several forces will be at work on a liquid droplet when it strikes (or as it is resting on) the screen. These forces can act together to produce two kinds of movement: parallel to the screen, or through the screen. The discussion will begin with a review of the important forces, some of which have previously been defined.

Surface tension force, F_{st}:

$$F_{st} = \alpha n d \sigma |\cos \Psi| \tag{17}$$

Ψ is the surface contact angle, d is the hole diameter, σ is the surface tension coefficient, α is a proportionality constant depending on the hole shape, and n is the number of screen pores covered by the drop. For round holes $\alpha = \pi$. For Dutch twill screens $\alpha \sim \pi/2$ (ref. 4).

Gravity force, F_g:

$$F_g = \rho V g \sim \rho \lambda^3 g \tag{18}$$

ρ is the mass density of the drop, g is the local acceleration of gravity, and λ is the drop diameter when the drop is spherical.

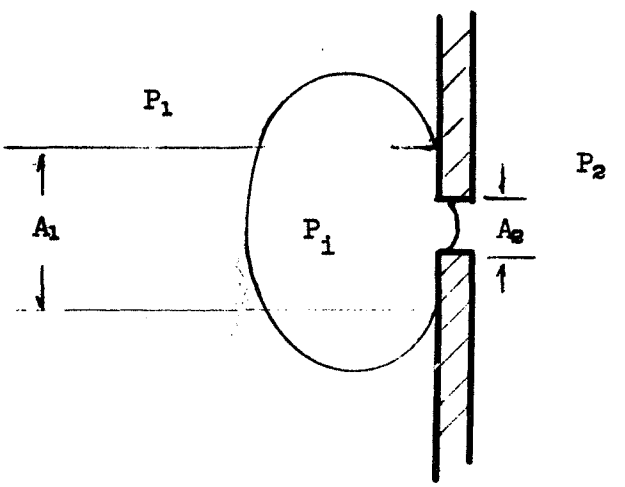
Inertia force, F_v:

$$F_V = 1/2\ D\ \rho \lambda^2\ v^2 \tag{19}$$

v is the droplet velocity (parallel to the duct axis) at impact, and D is a coefficient to account for energy lost in droplet deformation.

Pressure forces connected with the drop can be determined with the aid of the sketch.

$P_1 - P_2$ is the pressure difference due to the gas flow, and $P_i - P_1 \sim \frac{4\sigma}{\lambda}$ is the pressure difference across the drop surface.



The net force F_p is

$$F_p = P_i A_i - P_2 A_2$$

$$\sim \left(\frac{4\sigma}{\lambda} + P_1\right) A_1 - P_2 A_2$$

$$\sim \left(\frac{4\sigma}{\lambda} + P_1\right) \lambda^2 - P_2\, n\, d^2$$

For the case (as in the tests described) of $P_2 = 0$ these relations reduce to

$$F_p \sim \left(\frac{4\sigma}{\lambda} + \Delta P\right) \lambda^2 \tag{20}$$

This is the pressure force which holds the drop to the surface.

The pressure force trying to cause flow through the screen capillaries is

$$F_c = (P_1 - P_2)\ A_2$$

$$\sim \left(\frac{4\sigma}{\lambda} + P_1 - P_2\right) n\, d^2 \tag{21}$$

d is the hole diameter (assumed round), ΔP is the pressure loss across the screen as a result of the gas flow, n is the number of holes covered by the drop, λ is the drop diameter, P_1 is the upstream (high) pressure, P_2 is the downstream pressure, and σ is the surface tension coefficient.

The droplet adhesion force $F_a = f\lambda$ has already been discussed, and finally

Drag force, F_d:

$$F_d = c\,\rho\,\lambda^2\,u^2 \tag{22}$$

where c is a drag coefficient.

Force diagrams can now be set up for the two cases of interest; namely, drop penetration (figure 68) and drop movement parallel to the screen (figure 69).

For the drop to remain on the upstream side of the screen

$$\left[F_g \sin(\beta - \theta) + F_d \sin\theta_2 + F_v \sin\theta_1\right] \frac{n\,d^2}{\lambda^2} + F_c \leq F_{st} \tag{23}$$

To assure parallel movement

$$F_a < \left| F_g \cos(\beta - \theta) - F_v \cos\theta_1 - F_d \cos\theta_2 \right| \tag{24}$$

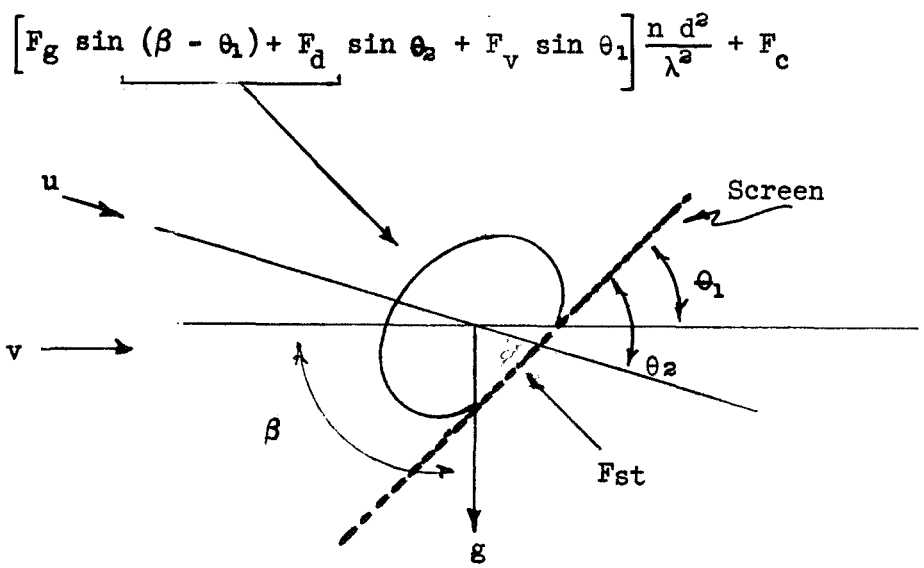


Figure 68. — Drop Penetration

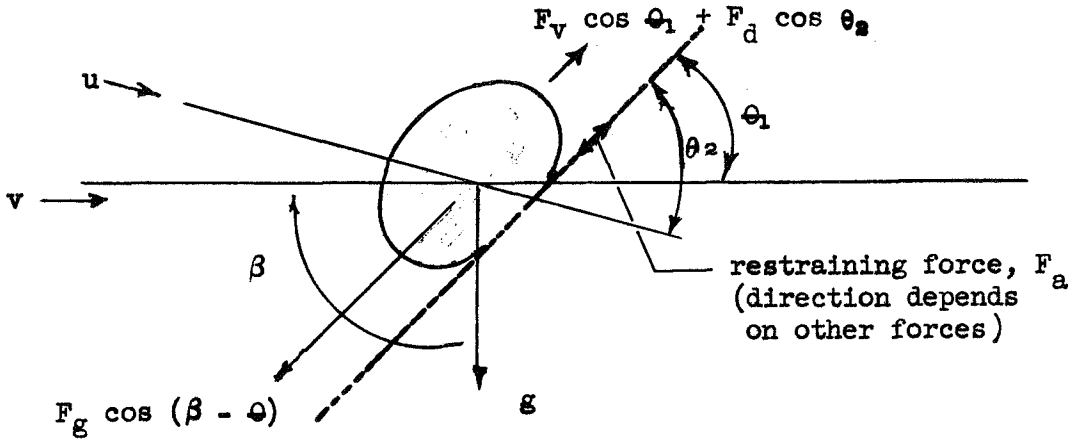


Figure 69. — Drop Movement Parallel to Screen

Penetration should not occur when equation (23) is respected. Substituting in the expressions used for evaluating the present test data, equation (23) becomes

$$\rho \lambda g \sin (\beta - \theta_1) + c \rho u^2 + 1/2 D \rho v^2 + \frac{4\sigma}{\lambda} + P \leq \frac{\alpha \sigma}{d} \left| \cos \psi \right| \qquad (25)$$

Drop motion parallel to the screen is assured when the following equation, obtained by substitution into equation (24), is respected.

$$\frac{f}{\rho \lambda} < \left| \lambda g \sin (\beta - \theta_1) - 1/2 D v^2 \cos \theta_1 - c u^2 \cos \theta_2 \right| \qquad (26)$$

The force F_p, equation (20), was found to be negligible in the range of the test design and thus can most probably be neglected when predicting the resistance of drops to parallel movement.

Note that equations (25) and (26) include the expressions in references 4 and 5 which were derived for pressure differences and impact velocities. The development herein, however, is more broadly generalized in that it additionally includes 1) the effects of gravity field strength and orientation, 2) liquid/solid adhesion, 3) screen angle, 4) dispersoid size prior to impact, and 5) dispersoid velocity, i.e., slip ratio.

An Alternate Configuration

The previous analysis shows that it is possible to find conditions where the system as shown in figure 66 will not work; namely, when the drops are too big to pass through the screen pores and yet small enough so that they stick when they hit the screen. If gravity and inertia forces are not sufficient to cause the drops to roll off, then impacting drops will combine until either the drops grow large enough to roll off or until they occupy

such a large portion of the screen area that they are pulled through by the increasing pressure drop across the screen.

If drops stick to the screen, the device in figure 66 is extremely gravity sensitive, both in direction and magnitude. A device that is much less gravity sensitive (ref. 7, 8) is shown in figure 70.

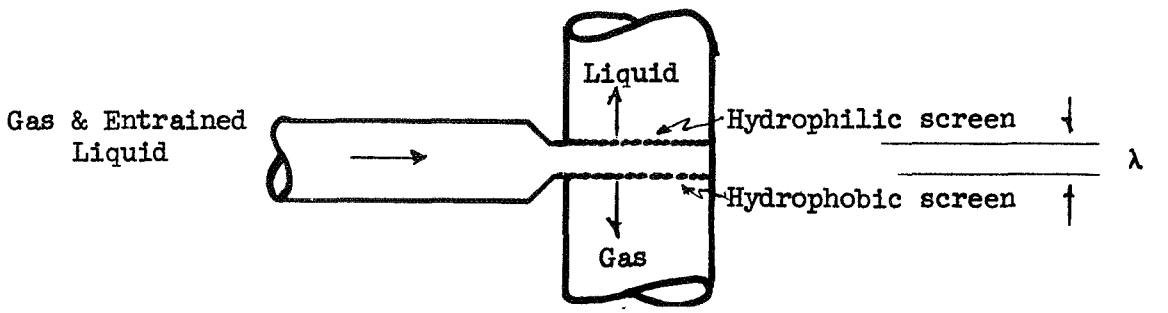


Figure 70. — Screen Separation Device, Alternate Configuration

Analysis of the efficiency of the alternate system is essentially the same as for the slanted screen except that direct droplet impingement on the screens does not occur. The screen separation (λ) is of the order of magnitude of a large droplet. Thus, with a high probability, droplets will be absorbed onto the hydrophilic screen before they reach the end of the passage between the screens, and there is little velocity sensitivity.

To keep the hydrophilic screen from drying out or flowing back into the two-phase channel, the pressure requirement is

$$0 \leq P_1 - P_2 \leq \alpha \frac{\sigma}{d} \tag{27}$$

Case 2 — Vortex Separator

The analytical model of the vortex separator has been developed in two parts — one dealing with liquid/gas separation functions, and the other with the outflow of the separated components. Separation is assumed to occur in the cylindrical section of the device pictured in figure 67, so that the outflow in the conical section is assumed to occur independent of the separation process. These assumptions are made to simplify the mathematical treatment; their validity will be discussed in conjunction with the model development.

The Cylindrical Section

Liquid particles in the incoming gas stream can be categorized, according to their size, in the following rough manner:

a. Particles of near molecular size.

b. Particles so large that they stay in suspension only with great difficulty.

c. Particles of intermediate size.

Category c is regarded as the design condition which will provide the greatest probability of efficient operation of this type of separation system.

Particles of the intermediate size range are assumed to be uniformly distributed in the gas and are assumed to have the properties of a continuum. No viscous interaction occurs in the particulate phase. Shear, of course, occurs in the gas phase as the individual particles move with a non-zero velocity relative to the gas. The resulting drag forces transfer momentum from the gas to the liquid droplet cloud, and are represented by F in the following equations.

Momentum transfer from the cloud to the gas is assumed not to occur (a violation of the continuum property). As the interparticle spacing decreases, this form of momentum exchange begins to occur (ref. 7). In this model, however, the gas simply acts as a free stream with the kinetic energy of the particles dissipated completely in their wakes.

Conservation of mass and momentum for the particulate phase is specified below in cylindrical coordinates (ref. 9).

$$\frac{\partial}{\partial r}(\rho ru) + \frac{\partial}{\partial z}(\rho rw) = 0 \tag{1}$$

$$u\frac{\partial u}{\partial r} + w\frac{\partial u}{\partial z} - \frac{v^2}{r} = -Fu \tag{2}$$

$$w\frac{\partial w}{\partial z} = g \tag{3}$$

Velocities u, v, and w are in the radial, azimuthal, and axial directions and correspond, respectively, to coordinates r, θ, and z, and F is used to represent momentum transfer from the gas to the liquid particles. Gravity forces are assumed to act only in the z-direction. The azimuthal velocity is $v = c/r$. All properties are constant in the azimuthal direction; hence, the θ-component momentum equation vanishes. No variation exists in w over a given cross-section normal to the axis, and the flow is steady.

A stream function, ψ, is now introduced such that

$$r\rho u = -\left(\frac{\partial \psi}{\partial z}\right)_r, \quad r\rho w = \left(\frac{\partial \psi}{\partial r}\right)_z \tag{4}$$

Equation (1) is automatically satisfied.

Changing independent variables from r and z to ψ and z gives

$$\left(\frac{\partial u}{\partial z}\right)_{\psi} + \frac{Fu}{w} = \frac{c^2}{wr^3} \tag{5}$$

where r is now a dependent variable.

Equation (3) can be integrated directly, with $w = w_o$ at $z = 0$, to obtain

$$w = \left(2gZ + w_o^2\right)^{1/2} \tag{6}$$

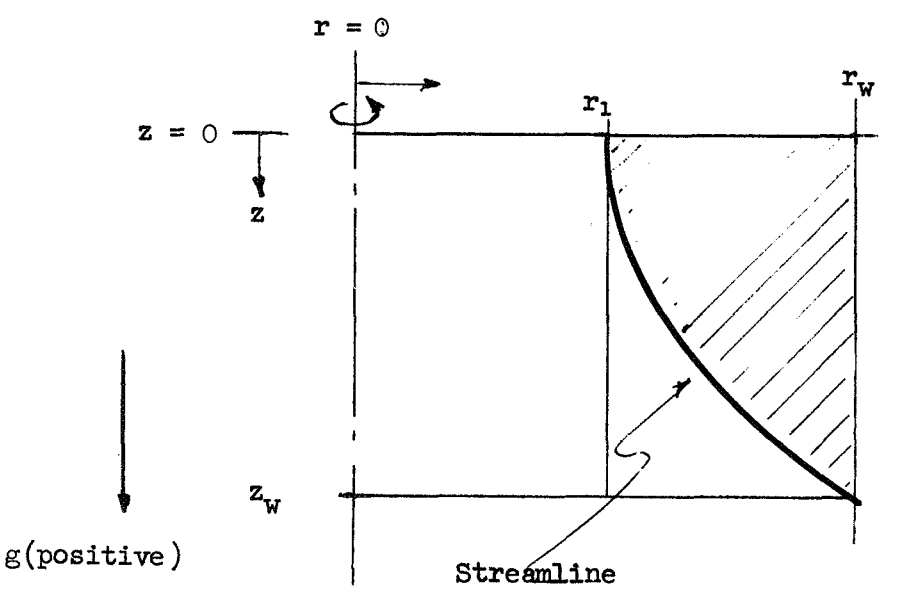
The relationship between r and z along a streamline is found by using equation (1)

$$\frac{u}{w} = \frac{-\left(\frac{\partial \psi}{\partial z}\right)_r}{\left(\frac{\partial \psi}{\partial n}\right)_z} = \left(\frac{\partial r}{\partial z}\right)_{\psi} \tag{7}$$

and using equation (7) in (5) gives

$$w\frac{d^2 r}{dz^2} + \left(\frac{g}{w} + F\right)\frac{dr}{dz} = \frac{c^2}{wr^3} \tag{8}$$

A typical streamline is shown in the sketch.



Equation (8) with (6) becomes, using the nondimensional definition $r_* = r/r_o$, $z_* = zF^2/g$,

$$\frac{d^2 r_*}{dz_*^2} + \left(\frac{1}{2z_* + A^2} + \sqrt{\frac{1}{2z_* + A^2}} \right) \frac{dr_*}{dz_*} + \frac{B^2}{r_*^3 (2z_* + A^2)} = 0 \tag{9}$$

where $A \equiv Fw_o/g$ and $B \equiv c/(Fr_o^2)$.

Since all the particles represented by the shaded region will impact the wall ($r = r_w$) in the interval $0 \le z \le z_w$, we can compute the flux of particles in this interval as

$$m = \int_{r_1}^{r_w} 2\pi \rho w r \, dr = \pi \rho w (r_w^2 - r_1^2) \tag{10}$$

Given r_w and m, for a given design condition, the radial coordinate r_1 can be calculated from equation (10). This coordinate marks the "critical" streamline; it is the lowest value of r which defines (at z = 0) a streamline that will intersect r_w in the interval $0 \le z \le z_w$. In other words, a streamline which intersects the plane z = 0 at any value of r less than r_1 will intersect the plane r_w at a value of z greater than z_w.

Equation (9) has been integrated numerically from $r_* = 1$ to $r_* = 3$. The value of Z_* at $r_* = 3$, denoted as $Z_*(3) = L$, is plotted in figure 3 against A with B as a parameter. To design the cylinder length (for the case $r_1/r_0 = 3$) one must extract the value of Z(3) from L by knowing the drag parameter F and the gravity acceleration g. These variables are also used in A and B so that an estimate of F is necessary to obtain a value of L from figure 71. Furthermore, at the larger values of A the curves are nearly linear and follow the relationship $L \sim A/B$. This indicates that the gravity acceleration and drag parameter have little influence on the length required for separation for values of A greater than, say, 1. But this is what one would expect since the value of A is proportional to w_o, the initial downward velocity of the particles. For values of A less than 1 the curves are not linear and gravity influence is present. An a priori estimate of F, however, is still necessary.

Further theoretical investigations appear to be required to clarify the appropriateness of the analytical model. One area of investigation is application of the drag parameter F to the downward motion of the two-phase mixture. In equation (3) the drag parameter F has not been applied, with the implicit assumption that the downward air flow does not influence the downward particle velocity. The validity of this assumption may require further investigation.

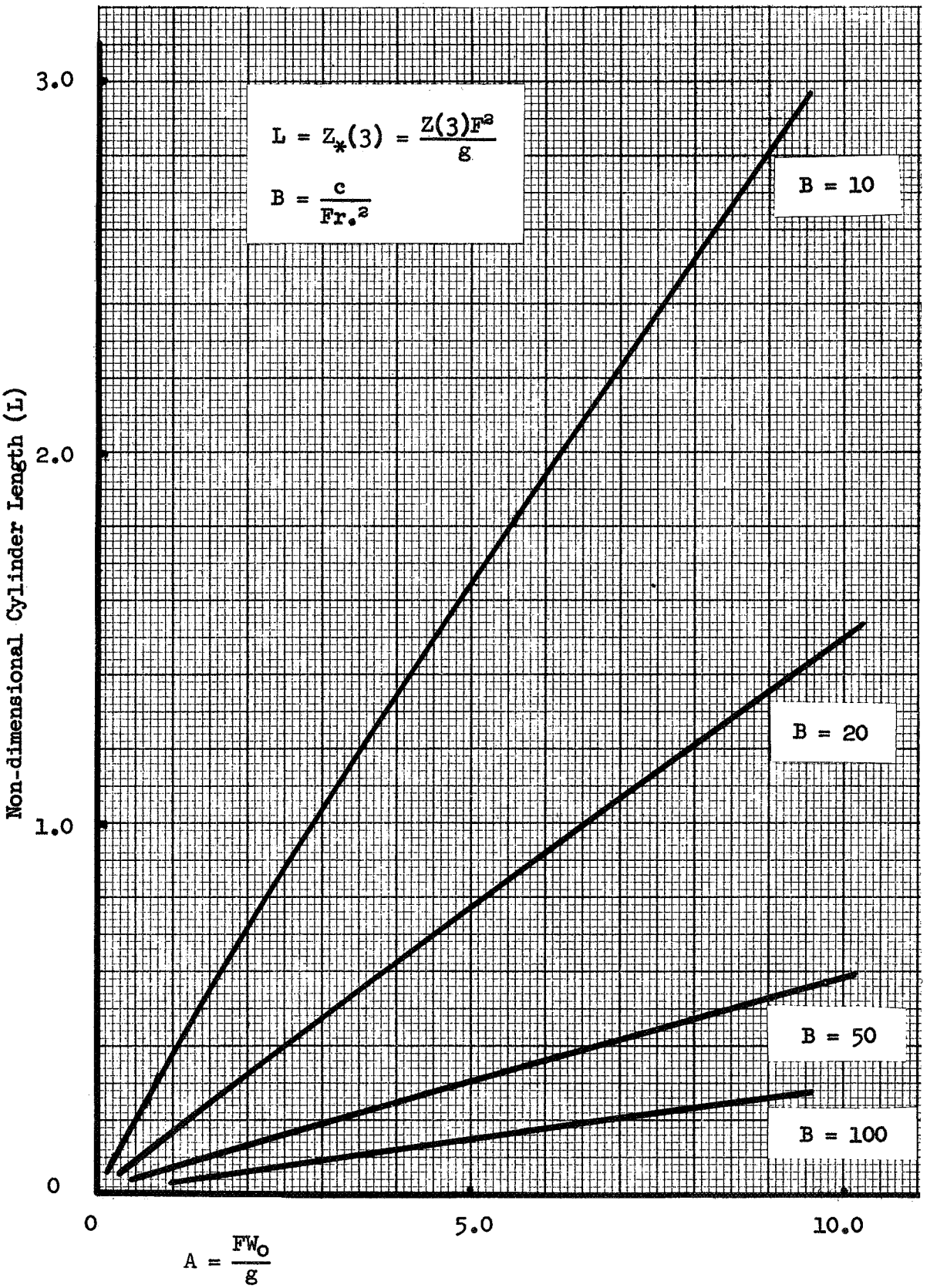


Figure 71. — Cylindrical Section Length

Particles in Suspension

The motion of small particles which are maintained in suspension is discussed in AMR 2, Section 1.5. The evolution is modeled by the general diffusion equation with inertial field (e.g., vortex or centrifugal acceleration) specification. The steady-flow equation is given by equation (24) of Section 1.5 in AMR 2, with the appropriate inclusion of the coriolis force for the rotating coordinate system.

The Conical Section

In the previous discussion we assumed that the liquid/gas mixture separates into a gas core and liquid film on the wall due to the swirling action of the fluid in the cylindrical container. We can now develop a model for the liquid film flow toward the apex of the attached conical section.

When fluid is admitted to the device tangentially we assume that a swirling, potential vortex flow field develops ($v \sim \frac{1}{r}$). This flow field contains a singularity at $r = 0$; the flow has a "hollow core" as in a tornado. Pressure in the fluid varies inversely as the square of the radial coordinate, all the way from the edge of the "hollow core" to the wall, since boundary layers do not sustain a significant pressure gradient normal to the surface. Outside the boundary layer the centrifugal acceleration balances the radial pressure gradient. Within the boundary layer, although the pressure gradient remains, the tangential velocity is slowed by viscous shear, and fluid is driven toward the apex of the cone.

Polhausen's momentum integral method has been used by Taylor (ref. 10), Cooke (ref. 11) and others to determine boundary layer thickness and velocities in conical swirling flows of a homogeneous incompressible fluid. Lawler and Ostrach (ref. 12) have commented on Taylor's solution in connection with the operation of vortex separators. They have demonstrated experimentally that a sufficiently strong swirling flow can force boundary layer fluid toward the vortex of a cone in a direction opposite to the gravity force. No explicit analytical solution including a body force was given, however, in reference 12.

In this presentation Taylor's solution is modified to include an axial body force. The results, applicable to flow in a vortex separator, are of importance to spacecraft life support processes which occur in a variable gravity environment.

Taylor's swirl problem. — An incompressible fluid enters a conical tube tangentially. The conical chamber, whose vertex angle is 2α, is so designed that the axial component of velocity is small compared to the swirl component. Except for a thin layer along the wall, the velocity is given by Ω/r where r is the distance from the axis and Ω is the circulation. The nomenclature is shown in figure 72.

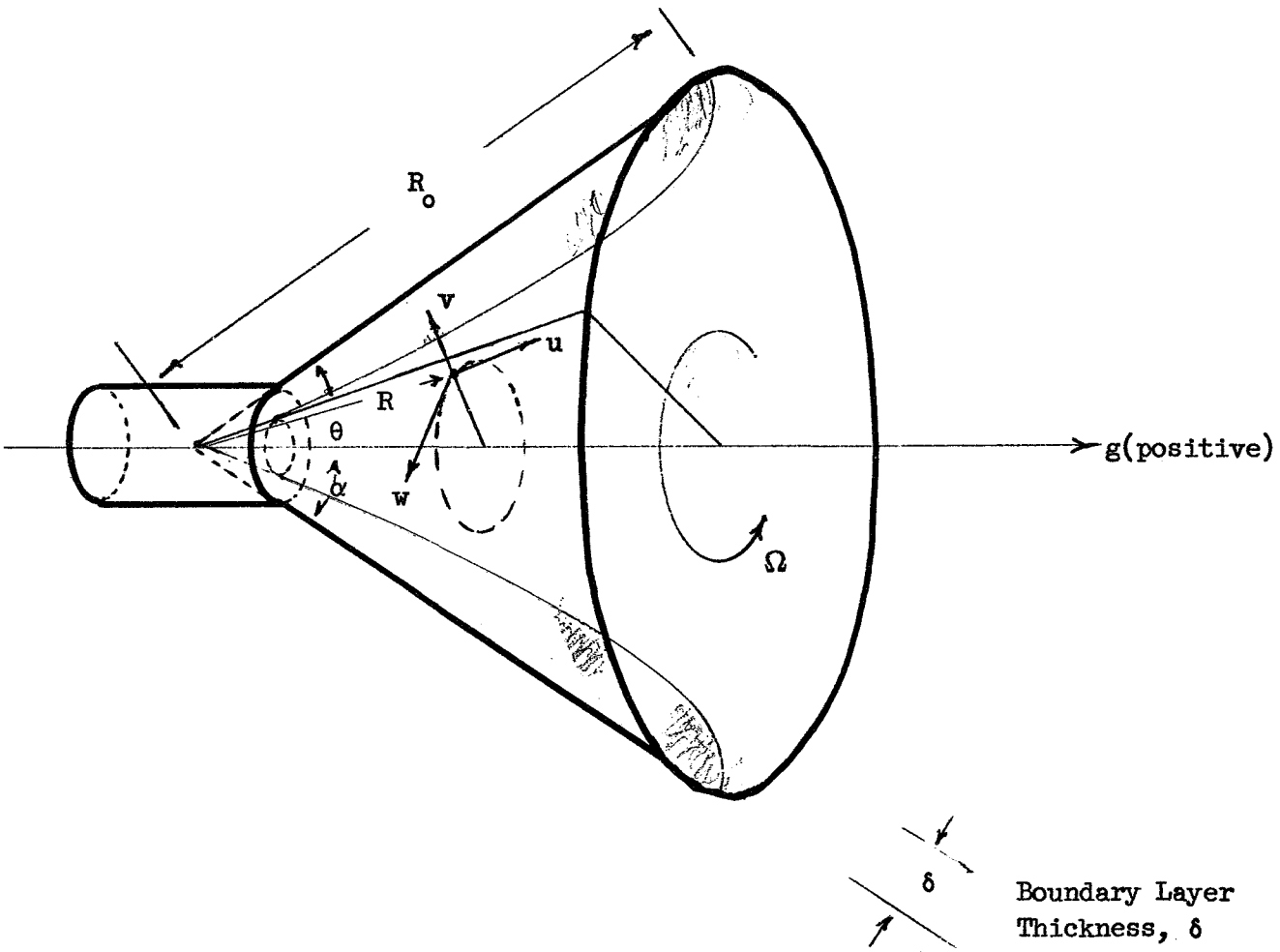


Figure 72. — Taylor's Swirl Problem Nomenclature

The equations of motion with the usual approximations for boundary layer flow are listed below, in spherical coordinates, with the origin at the vertex of the cone.

$$u\frac{\partial u}{\partial R}+\frac{v}{R}\frac{\partial u}{\partial \theta}-\frac{w^2}{R}=-\frac{1}{\rho}\frac{\partial p}{\partial R}+\frac{\nu}{R^2}\frac{\partial^2 u}{\partial \theta^2} \tag{11}$$

$$0=-\frac{1}{\rho R}\frac{\partial p}{\partial \theta} \tag{12}$$

$$u\frac{\partial w}{\partial R}+\frac{v}{R}\frac{\partial w}{\partial \theta}+\frac{wu}{R}=\frac{\nu}{R^2}\frac{\partial^2 w}{\partial \theta^2} \tag{13}$$

The continuity equation is

$$\frac{\partial u}{\partial R} + \frac{2u}{R} + \frac{1}{R}\frac{\partial v}{\partial \theta} = 0 \tag{14}$$

where

R = distance from the vertex of the cone along the conical surface

θ = the angle a radius vector makes with the axis

u = radial velocity

w = component of velocity perpendicular to axial planes

v = component of velocity perpendicular to R

p = pressure

ρ = density

ν = kinematic viscosity ($\nu = \mu / \rho$)

Outside the boundary layer $w = \Omega/R \sin\theta$, and the pressure is given by

$$\frac{P}{\rho} = -\frac{1}{2}\frac{\Omega^2}{R^2 \sin^2\theta} + \text{constant} \tag{15}$$

Taylor's solution demonstrates that, near the conical surface, where viscosity retards the fluid motion, the radial pressure gradient given by equation (15) cannot be balanced by the centrifugal acceleration and a boundary layer flow toward the apex occurs.

Inclusion of gravity force. — We depart slightly from Taylor's equations by including an axial body force which is positive in the direction from the apex to the large end of the cone. The component of this force normal to the wall is neglected, and only the fluid in the boundary layer is considered to be influenced by the body force. Such an assumption is approximately valid in a vortex separator where the boundary layer is comprised of fluid with a density greater than the fluid in the core. Equation (11) then becomes

$$u\frac{\partial u}{\partial R} + \frac{v}{R}\frac{\partial u}{\partial \theta} - \frac{w^2}{R} = -\frac{1}{\rho}\frac{\partial p}{\partial R} + \frac{\nu}{R^2}\frac{\partial^2 u}{\partial \theta^2} + g\cos\alpha \tag{16}$$

Equations (12), (13), and (14) are unchanged.

We assume that the boundary layer is contained entirely within the film of heavy fluid. Since the radial pressure gradient in the boundary layer is the dominant driving force, we must specify the circulation Ω for the heavy fluid in equation (15). Assuming that Ω_ℓ is known, the problem becomes one of relating Ω_ℓ and Ω_h. Lawler and Ostrach equate the shear stress at the interface to arrive at

$$\Omega_\ell \, \mu_\ell = \Omega_h \, \mu_h$$

where the subscripts ℓ and h stand for the light and heavy fluids. This statement is contradictory since the velocities have been assumed to be proportional to Ω/r in both fluids, implying slip at the interface.

Perhaps a better way to determine Ω_h is to ignore the boundary layers in the interface region and accept the interface slip implication. Equating pressures at the interface gives

$$\Omega_h = \sqrt{\Omega_\ell^2 \, \rho_\ell / \rho_h} \tag{17}$$

This is consistent with the usual assumption that the external flow field pressure is impressed upon the boundary layer. In the following equations Ω_h will be assumed whenever Ω appears.

We follow reference 10 by integrating equations (13) and (16) over the boundary layer thickness from $\theta = \alpha$ to $\theta = \alpha - \delta/R$. The resulting equations are:

$$2 \int_{\alpha - \delta/R}^{\alpha} u \frac{\partial u}{\partial R} \, d\theta + 2 \int \frac{u^2}{R} \, d\theta + \int \left(\frac{\Omega^2}{R^3 \sin^2 \alpha} - g \cos \alpha - \frac{w^2}{R} \right) d\theta = \frac{\nu}{R^2} \left[\frac{\partial u}{\partial \theta} \right]_{\theta = \alpha} \tag{18}$$

$$- \frac{\Omega}{R^2 \sin \theta} \int_{\alpha - \delta/R}^{\alpha} \left(R \frac{\partial u}{\partial R} + 2u \right) d\theta + \int \frac{\partial}{\partial R} (uw) \, d\theta + 3 \int \frac{uw}{R} \, d\theta = \frac{\nu}{R^2} \left(\frac{\partial w}{\partial \theta} \right)_{\theta = \alpha} \tag{19}$$

We use the same velocity distribution expressions satisfying the same boundary conditions as Taylor where the undetermined parameter E is proportional to the u-velocity and does not appear in the expression for w.

$$u = \frac{\Omega E}{R \sin \alpha} f(\eta) = \frac{\Omega E}{R \sin \alpha} (\eta - 2\eta^2 + \eta^3) \tag{20}$$

$$w = \frac{\Omega}{R \sin \alpha} \phi(\eta) = \frac{\Omega}{R \sin \alpha} (2\eta - \eta^2) \tag{21}$$

where

$$\eta = R(\alpha - \theta)/\delta$$

Substitution into equations (18) and (19) yields

$$\frac{\delta^2}{R^2}\left[\left(R\frac{dE^2}{dR} + \frac{RE^2}{2\delta^2}\frac{d\delta^2}{dR} - E^2\right)\int_o^1 f^2\, d\eta + K - \int_o^1 \phi^2\, d\eta\right] = -E\,\frac{\nu \sin\alpha}{\Omega}\left(\frac{df}{d\eta}\right)_{\eta=0} \tag{22}$$

$$\frac{1}{2}\frac{\delta^2}{R^2}\left(R\frac{dE^2}{dR} + \frac{RE^2}{\delta^2}\frac{d\delta^2}{dR}\right)\left(-\int_o^1 f\, d\eta + \int_o^1 f\phi\, d\eta\right) = -E\,\frac{\nu \sin\alpha}{\Omega}\left(\frac{d\phi}{d\eta}\right)_{\eta=0} \tag{23}$$

The nondimensional parameter K is a result of the introduction of the gravity force term and is defined as

$$K \equiv 1 - \left(gR^3 \sin^2\alpha \cos\alpha\right)/\Omega^2 \tag{24}$$

To nondimensionalize equations (22) and (23) introduce

$$\left.\begin{aligned} R_1 &= \frac{R}{R_o} \\ \delta_1 &= \frac{\delta}{R_o}\sqrt{\frac{\Omega}{\nu \sin\alpha}} \end{aligned}\right\} \tag{25}$$

We then arrive at two nonlinear ordinary differential equations with dependent variables E^2 and $E\delta_1^2$ and independent variable R_1:

$$\frac{dE^2}{dR_1} = -\frac{98(1-Fr\,R_1^3)}{R_1} + \frac{2E^2}{R_1} - 330\,\frac{E^2 R_1}{E\,\delta_1^2} \tag{26}$$

$$\frac{d}{dR_1}\left(E\delta_1^2\right) = \frac{49(1-Fr\,R_1^3)E\delta_1^2}{E^2 R_1} - \frac{E\delta_1^2}{R_1} + 285\,R_1 \tag{27}$$

These differ from Taylor's equations only in the term containing Fr. The factor Fr is a nondimensional relationship between the swirling inertial force and gravity force (a Froude number) and is defined as

$$Fr = 2.14\, g \cos\alpha\, R_o^3 \sin^2\alpha\,/\Omega^2 \tag{28}$$

When Fr = 0 we have Taylor's original pair of equations.

The numerical factor 2.14 comes from the terms

$$K - \int_0^1 \phi^2\, d\eta = K - .5333 \qquad \text{in equation (22)}$$

When divided by $\int_0^1 f^2\, d\eta = 0.009524$, this term becomes

$$\frac{49}{R}\left[\frac{K - .5333}{49(0.009524)}\right]$$

which is equivalent to the first term on the right-hand side of (27). The same applies for equation (26).

Numerical analysis and results. — Equations (25) and (26) have been integrated numerically starting with $E^2 = E\delta_1^2 = 0$ at $R_1 = 1$. Since both equations have a singularity at $R_1 = 1$, an initial approximation to the solution is formed in the immediate vicinity of $R_1 = 1$. The approximations are determined by setting $R_1 = 1 - \Delta$ and expanding the terms of equations (26) and (27) which contain the large numerical coefficients. Terms with Δ^2 and Δ^3 are neglected. The result is

$$\left.\begin{aligned} E^2 &= 19.1\Delta\,(1 - Fr) \\ E\delta_1^2 &= -80\Delta \end{aligned}\right\} \tag{29}$$

where the gravity field affects only the initial approximation for E^2. Numerical values have been obtained for E^2 and $E\delta_1^2$ over the range $0.999 < R_1 < 0.05$ using the fourth order Runge-Kutta method with automatic step size; equation (29) provided initial values for the range $1.0 < R_1 < 0.999$. A plot of δ_1 versus R_1 for selected Fr values is given in figure 73. The curve for Fr = 0 is in agreement with reference 10.

To determine the boundary layer mass flow rate we integrate the u-velocity over the boundary layer thickness:

$$m = 2\pi\rho R^2 \sin\alpha \int_{\theta=\alpha}^{\theta=\alpha-\delta/R} u\, d\theta$$

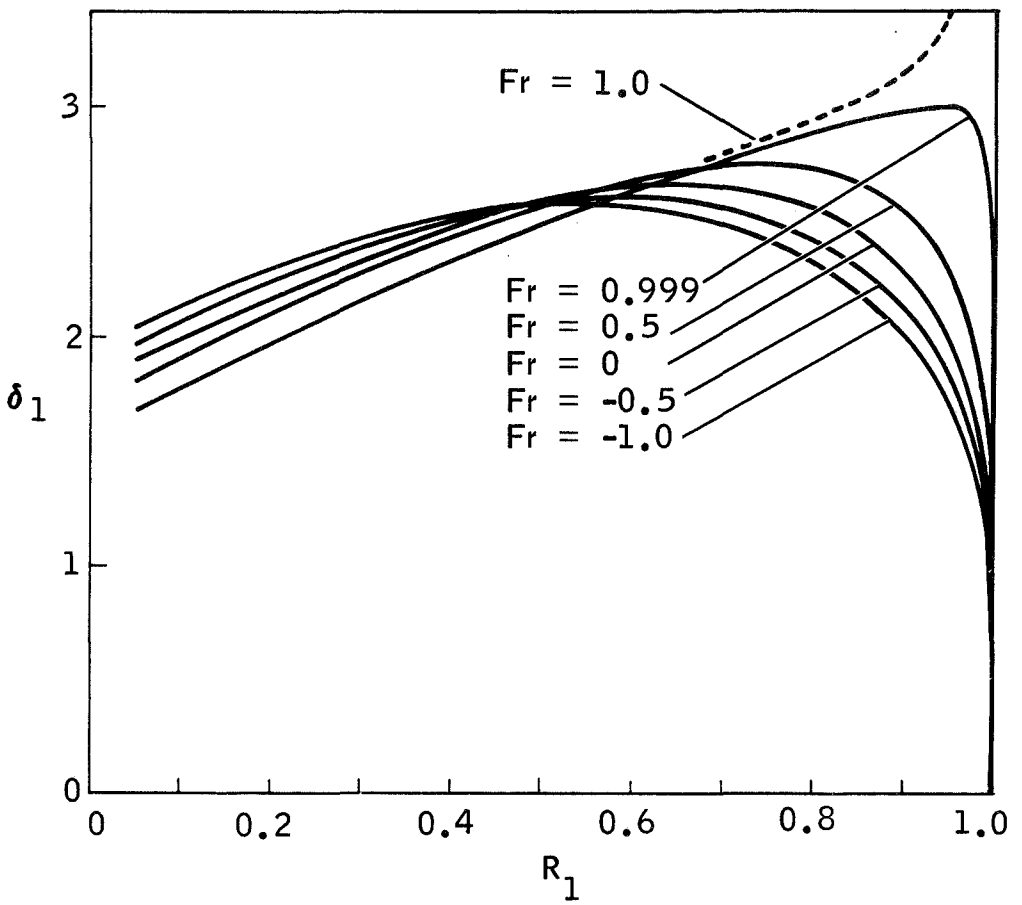


Figure 73. — Boundary Layer Thickness - Vortex Separation

using the relationships $d\theta = -(\delta/R)\, d\eta$,

$$\int_0^1 f(\eta)\, d\eta = \frac{1}{12}, \text{ and equation (25),}$$

we have

$$m = -\frac{\pi}{6} \rho_h R_o E \delta_1 \sqrt{\Omega \nu_h \sin\alpha} \tag{30}$$

A nondimensional flow rate is defined as

$$M \equiv m \left(-\frac{\pi}{6} \rho_h R_o \sqrt{\Omega \nu_h \sin\alpha}\right)^{-1} = E \delta_1$$

Values of $E \delta$ as a function of R_1 from the solution of equations (22) and (23) are plotted in figure 73.

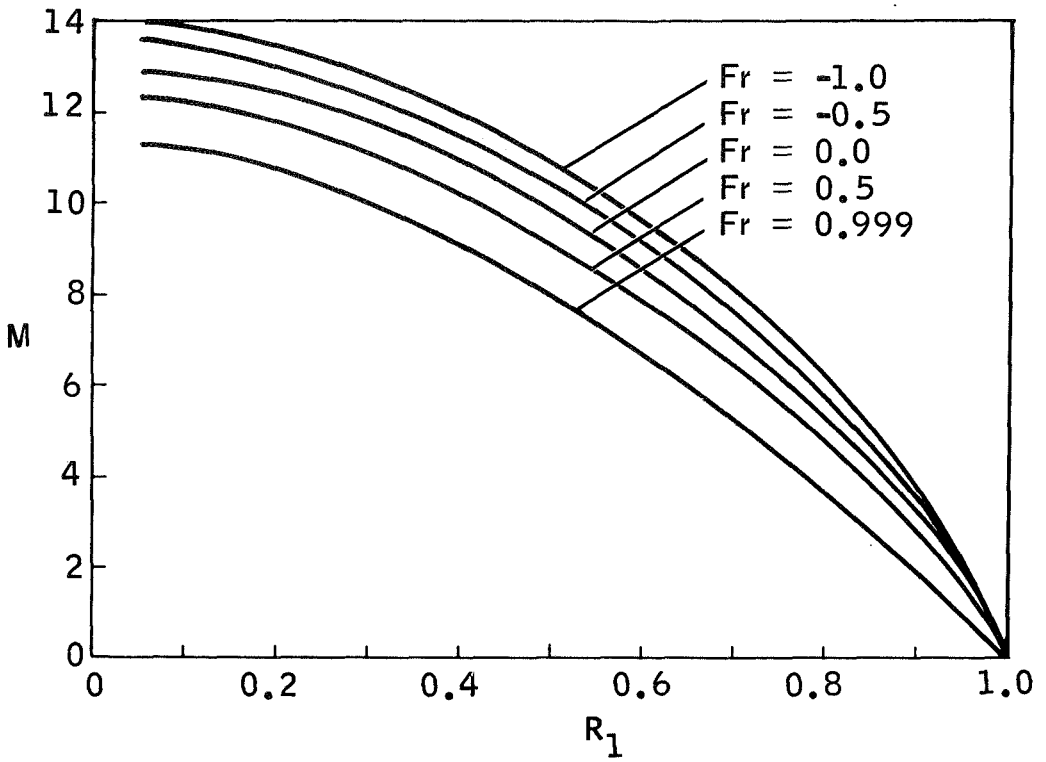


Figure 74. — Boundary Layer Mass Flow Rates - Vortex Separation

Equations (26) and (27) can be transformed with M and δ_1 as dependent variables into

$$\frac{dM}{dR_1} = 60 \frac{R_1}{\delta_1} \tag{31}$$

$$\frac{d\delta_1}{dR_1} = 225 \frac{R_1}{M} - \frac{\delta_1}{R_1} + 49 \frac{\delta_1^3}{M^2 R_1} (1 - Fr R_1^3) \tag{32}$$

At any point other than $R_1 = 1$ (where $\delta_1 = 0$) solutions cannot be obtained with the mass flow parameter M equal to zero. A condition of $M = 0$ in the range $0.05 < R_1 < 1.0$ indicates a flow reversal where the boundary layer fluid diverges from the zero flow point. At a value of $Fr = 1.0$ the flow "reversal" occurs at $R_1 = 1$ and a numerical solution cannot be obtained. At $Fr = 0.999$, however, δ_1 and M are shown in figures 73 and 74. The limiting condition for efficient operation of a vortex separator in an adverse gravity field is therefore taken to be $Fr = 1.0$.

THE COMPUTER PROGRAMS

Computer programs were not needed for the Case 1 system either for the model predictions or for the experimental data analysis. The analytical model was constructed by considering individual aspects of the droplet behavior on the screen which are not interdependent implicitly; thus, each phenomenon could be predicted explicitly using observable data and no iterative or repetitive computations were necessary to develop the predictive relationships.

The analytical model of the vortex separator, however, resulted in the specification of nonlinear ordinary differential equations which were integrated numerically. In these cases the equations were integrated with a fourth order Runge-Kutta routine featuring partial double precision, automatic step-size adjustment, and local Richardson extrapolation.

APPLICATION TO LSS DESIGNS

The generalized nature of the analytical models provides a relatively high probability that they can be directly applied to the development of several LSS design approaches. Table 23 identifies examples of the type of LSS equipment which, potentially at least, will be so designed that the information can be profitably applied in the analysis of primary or "on-design" modes of operation. Additionally, reference is shown with respect to the liquid/gas separation/transport functions associated with the mechanization of condensers/evaporators.

EXPERIMENTAL EVALUATION

Requirements

An experimental evaluation of the accuracy of the predictive aspects of the analytical model must include the following observations against a series of test conditions:

a. Droplet shapes and sizes, and stability during gas stream transport.

b. Gas pressure differences (losses).

c. Droplet impact reactions (screen).

d. Droplet flow patterns along separator surface.

e. Liquid film generation, transport, and outflow rate.

Table 23. Examples of LSS Equipment Designs for Which the Analytical Model has Relevance

Equipment Type by Degree of Relevance by Mode / LSS Function	Model Relevance		
	Phase Separation		Cond./Evap.
	A*	B	
Oxygen Supply & Recovery		11**, 22,23	4,7,8,9,10,12, 21,24,25,26,32, 36
CO_2 Removal		15,17	14,16,18,19
Water Reclamation	42,43, 45	38,39, 40,41	56,64,59(a) & (c)
Humidity Control	57(a)&(b), 58(a)&(b), 60	61	62,63
Sanitation & Hygiene	78,80, 81,82	66,67(b), 76,74, 76(a),79, 83,84	68,69

* Degree of relevance: A implies a high degree of relevance both as to similarity of the model to the equipment processes produced under the designated model combined with a high probability that the process will be extended into similar designs in updated systems, while B implies a lower degree of similarity and/or probability of extension to similar designs.

** Equipment type identified by LSS equipment reference number.

Experimental process variables should include:

a. Stream velocity.

b. Droplet size and velocity.

c. Droplet population density.

d. Screen mesh and installation angle.

The design of the experiments should be such that they include an examination of the potential effect on the model parameters of various alterations in the local inertial acceleration vector, especially with respect to their effects on the characteristics of the liquid layers and liquid transport characteristics.

Figure 75 illustrates the type of predictive data produced by the model(s) which will form the major guide to the design of the experiments which, in turn, will evaluate the analytical model(s).

Laboratory Experiments

The nature and magnitude of the forces involved which provide the separation and transport mechanisms for both Cases 1 and 2 are such that experimentation at 1g can be highly informative. Variations in the orientation of the systems to the gravitational vector are considered to be of greater potential value than variations produced by increasing the magnitude of the inertial acceleraton field forces.

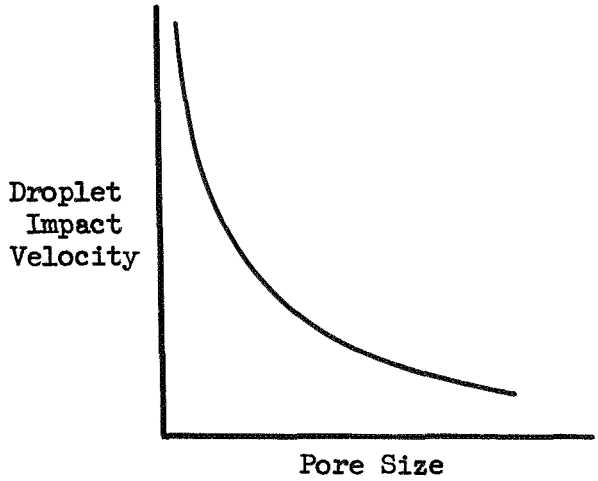
Reduced Gravity Experiments

Both the screen and vortex separation systems will require experimental evaluation under conditions where the gravity force is not the dominant mechanism. For the screen separator this applies particularly for the phenomenon of droplet motion parallel to the screen. In the vortex separator, low-g testing is necessary to isolate the effect of the radial pressure gradient.

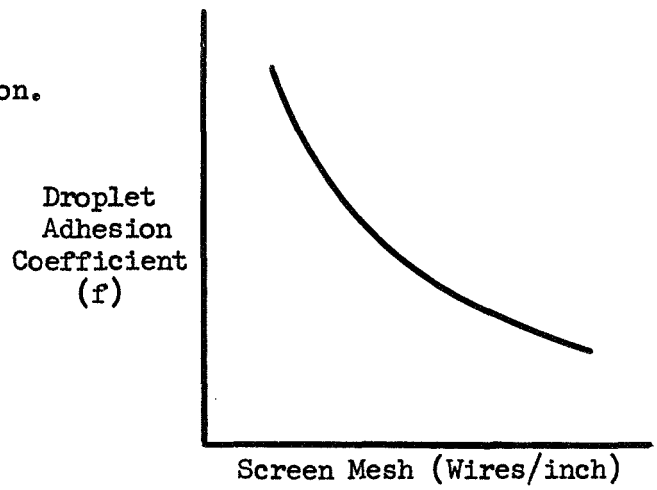
Description of the Case 1 Experiment

A decision was made at the outset of the analytical phase of the NAS1-8494 contract to forego the experimental evaluation of the model for Case 2 (vortex separation) due to the uncertainties relating to the potential yield of the experiment at least as conducted under laboratory conditions in an austere program.

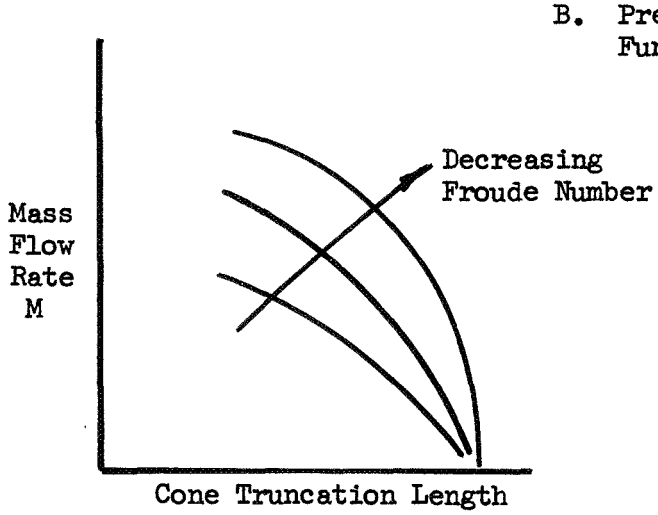
A laboratory experimental program was conducted to verify the predictions in the analytical model of the screen separation system. Data on the behavior of water droplets



A. Predicted Values of Droplet Velocity Producing Penetration.



B. Predicted Values of (f) as a Function of Screen Mesh



C. Predicted Discharge Rates as a Function of Cone Truncation Rates

Figure 75. — Characteristic Predictive Data

on Teflon-coated screens were obtained over a wide range of conditions. Both direct visual observations and high-speed photography were employed (ref. 13).

Major Goals

A major goal was to determine if the analytical predictions satisfactorily delineate the actual characteristics of the process of removing liquid droplets from a gas stream where the capture and subsequent removal transport is provided by inertial forces acting upon the droplet against the resistive forces of a slanted flat surface hydrophobic screen. Particular attention was focused on the effects of both variations in process conditions, particularly with respect to the gravitational vector, and in the configuration of the screen.

An additional goal was to examine various experimental test techniques, both for their applicability to laboratory testing and for their potential in the design of apparatus for experimental tests under reduced gravity.

Principal Observations

The experimental observations required included:

a. Gas pressure losses.

b. Droplet impact reactions.

c. Characteristics of the droplet transport along the slanted screen surface.

d. Characteristics of droplet breakthrough.

The experimental variables programmed against these observations included:

a. Air flow rate.

b. Orientation to the local gravity vector.

c. Droplet impact frequency.

d. Droplet size.

e. Droplet impact angle (screen angle).

f. Screen pore size.

Criteria for Test Model Design

The test model and its supporting apparatus were designed against the following criteria:

a. Air stream velocity controllable in a range from a minimum which produces virtually no effect on the dispersed droplet to a maximum which results in visually observable distortion of the dispersed droplet.

b. A replaceable and adjustable screen installation which provides the capability to vary the impact angle (screen slant) from a position normal to the droplet flight path, i.e., a 90-degree impact angle to an impact angle of approximately 150 degrees.

c. An air stream duct providing a means of photographing the droplet from its point of generation in one case to 1) final withdrawal from the duct, and another case to 2) its breakthrough at the downstream side of the screen.

d. A droplet generator capable of producing single droplets in a controlled range of sizes and propelling same along a horizontal or vertical duct with little or no aiding air flow.

e. Instrumentation to record the data required to define:

   1. Stream velocity.

   2. Gas pressure loss through the screen.

   3. Droplet shape, size, and impact configuration.

   4. Droplet transport characteristics along the surface of the screen.

   5. Characteristics of the breakthrough event.

f. Gravity effects on droplet behavior can be observed.

g. Maximum feasible utilization of previously developed test apparatus.

Test Apparatus

The concepts relative to test apparatus requirements as illustrated in ETP 4 were subsequently modified in response to interactions between the on-going maturation of the analytical and accompanying test design studies. The apparatus used in this experiment is shown schematically by figure 76 and pictorially by figure 77.

Air stream control assembly. — The air stream control assembly was a modification of that employed in Experimental Tests 2 and 3A and consisted of the following components:

a. Blower and inlet area control (Dayton, Model 20570).

b. Blower inlet plenum and flow-measurement orifice assembly.

c. Blower outlet to flow channel inlet adaptors and flexible duct.

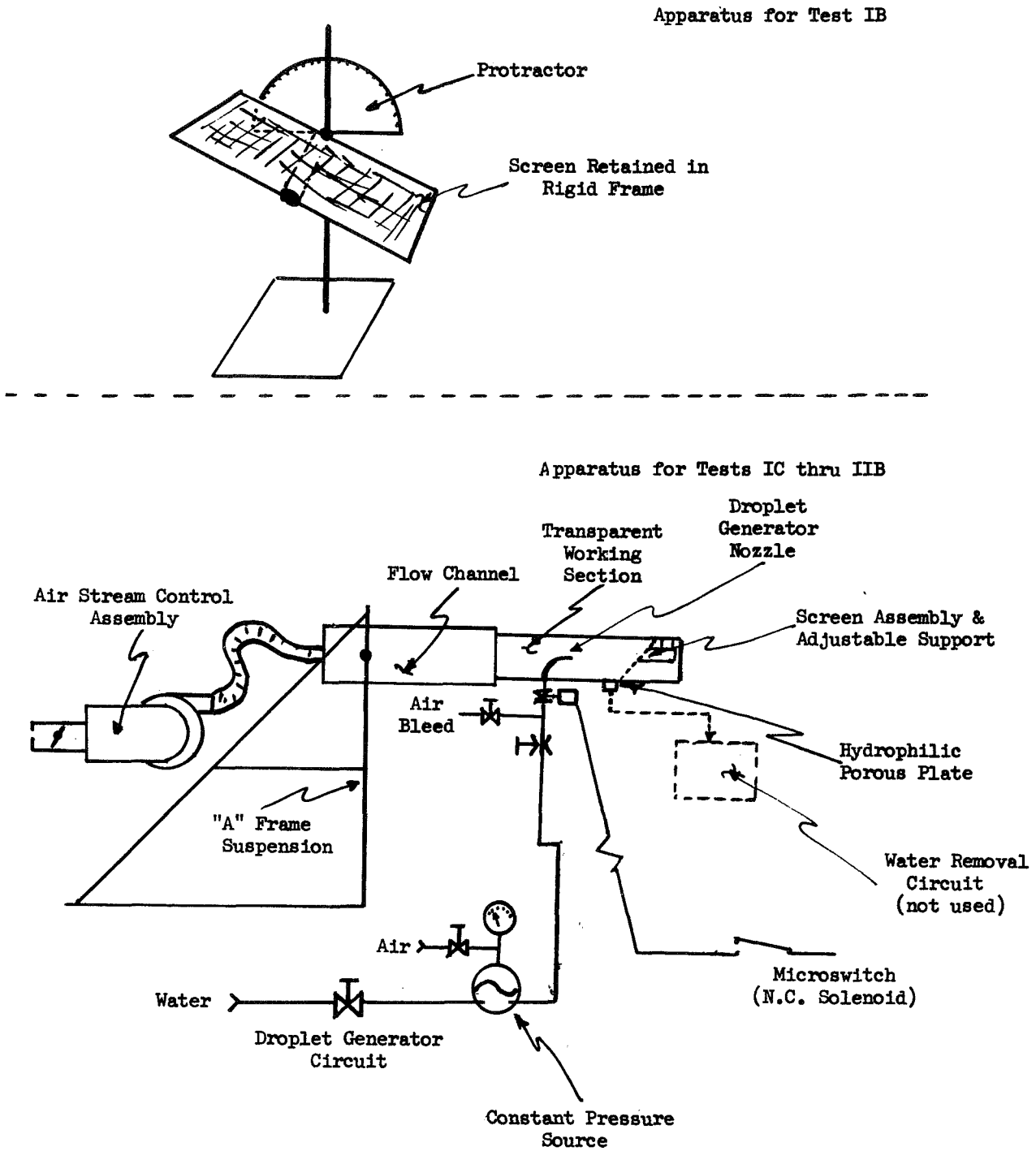


Figure 76. — Test Apparatus - Schematic

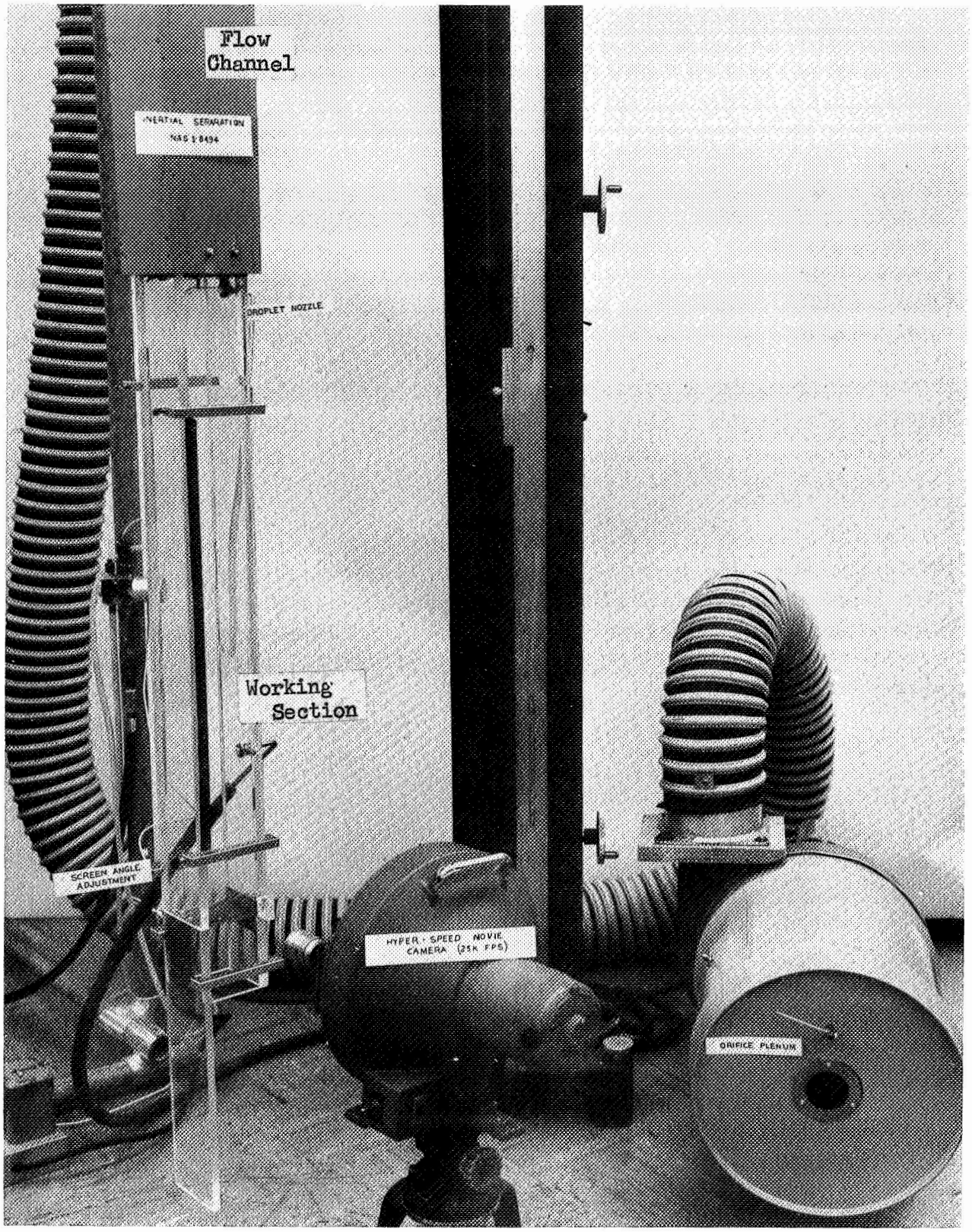


Figure 77. — Test Apparatus — Photograph

Flow channel and working section assembly. — (See figure 78.) The flow channel, approximately 36 inches long with a 4- by 4-inch interior cross section, was constructed of plywood and provided both a means of introducing the air stream to the working section and supporting the transparent working section. The working section, fabricated of 1/2-inch sheet lucite approximately 40 inches in length with a 3- by 3-inch interior cross section, was cantilever mounted from the exit section of the flow channel. A unique feature of the working section was the configuration of its "top" panel, which was constructed in two sections, and rather than being permanently attached as were the other three panels (sides), was held in place by specially constructued "C" clamps, allowing it to be positioned as desired along the longitudinal axis of the section. This configuration provided a means of both retaining the hydrophobic screen and adjusting its slant, i.e., droplet impact angle.

A porous plate (capillary) water removal assembly was incorporated into the working section to provide a capability for both high-density droplet flow and long-duration, uninterrupted data runs. However, the design of the test was such that neither condition was required; thus the unit was never activated following its initial checkout.

Screen assemblies. — The hydrophobic screen was stretched across the interior of the working section to produce an even, flat surface on which to impact the droplets. The screen was retained along two of its opposing sides, at the "bottom" panel surface by an adjustable plate acting to clamp the screen against the lucite panel and at the "top" panel surface by a clamping action provided by the butt joint between the two sections of the "top" panel.

Four square weave, stainless steel screens were employed, each of which had been coated with Dupont TFE Primer, 851-204 green, material 119-482-945. The original and resulting pore configurations were determined through analyses of microphotographs of the uncoated and coated screens as shown in figures 79, 80, and 81. A summary of these findings is given in table 24. The Teflon coating was applied with a paint spray gun operating on a pressure of 25 psi. The key to good quality coating can be summarized as follows:

a. Retain screen in a rigid frame to provide smooth, even surface.

b. Prepare the 851-204 primer as instructed by manufacturer.

c. Cover one side in one continuous operation, holding spray nozzle some 6 inches from screen (going back over the first pass coat for touch-up is not successful and causes blockage).

d. Immediately follow up the spray with a very low level air blast to blow away the excess coating and to prevent blockage.

e. Allow 10 to 15 minutes set time and repeat process for reverse side.

f. Oven cure as instructed by manufacturer.

g. Keep screen free from dust, hand soiling, water-borne residues, etc.

Droplet generator circuit. — The droplet generator circuit required an extensive program of experimental design to produce the final configuration illustrated by figures 76 and 78. The key elements of the circuit, and thus the implied design requirements, can be summarized as follows:

a. Constant pressure water source with pressure levels adjustable through a range of 40 to 100 psi. This is made possible by an air-charged accumulator of sufficient capacity that no single series of droplet flow demands would alter the selected pressure level.

b. A high-response, low-volume, batch-water metering circuit. This is made possible by an adjustable orifice, and "normally closed" high-response solenoid valve, small-diameter, low-capacitance tubing short coupled from solenoid to discharge nozzle, and microswitch.

c. A small-diameter, sharp-edged discharge nozzle.

Instrumentation. — The major instrumentation was the high-speed movie and film analyzer. The first series of runs was made employing the Bechman and Whitley DYNAFAX, Model C326-2, capable of up to 25,000 fps. However, the complexity of the procedures for its successful use led to a change to the Wollensak FASTAX high-speed 16mm camera, also capable of speeds up to 25,000 fps. The former provided a more economical approach in that no special operator was required, only a very short film roll was needed, and developing was simply accomplished and virtually immediate. However, timing of the droplet impact event, lighting, and camera start due to the very limited run time were critical and resulted in excessive equipment and procedural complexity. In addition, the FASTAX camera produced a somewhat superior picture quality. A Fairchild Mini-Rapid Film Processor was used to provide review of each test set prior to proceeding on through the sequence. The FASTAX was used from the fifteenth run of Test IIA and on. Figure 82 is the instrument schematic for test level II.

The timer/sequencer employed with the FASTAX camera produces a timing signal resulting in a series of marks on the film strip, thus providing a precise timing measurement from which velocity determinations can be made. Droplet size is determined from the notched wires installed immediately upstream of the screen.

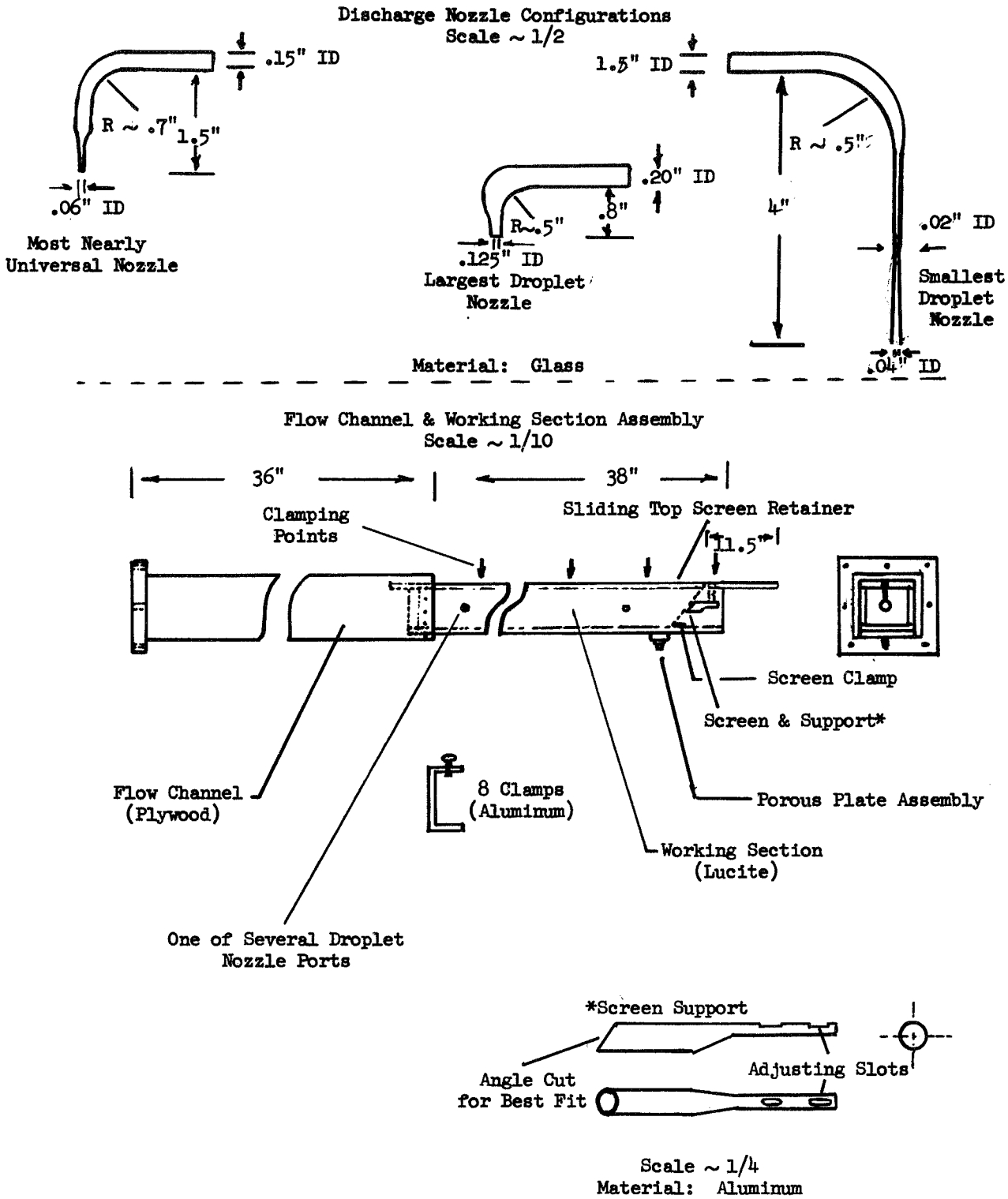
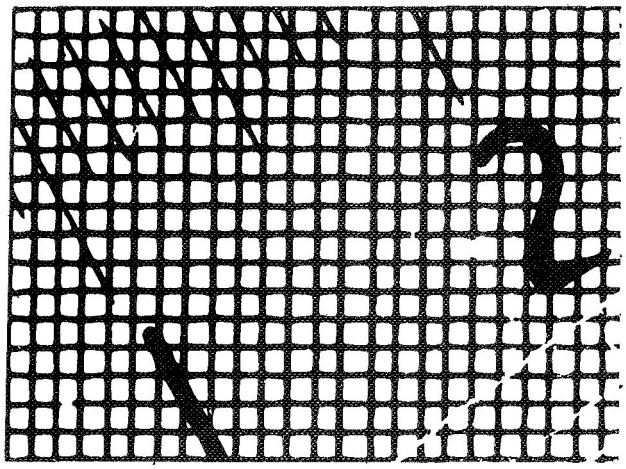
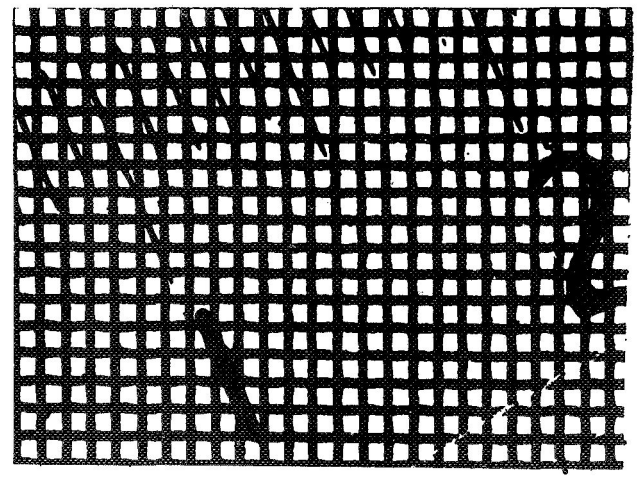


Figure 78. — Test Apparatus Drawing

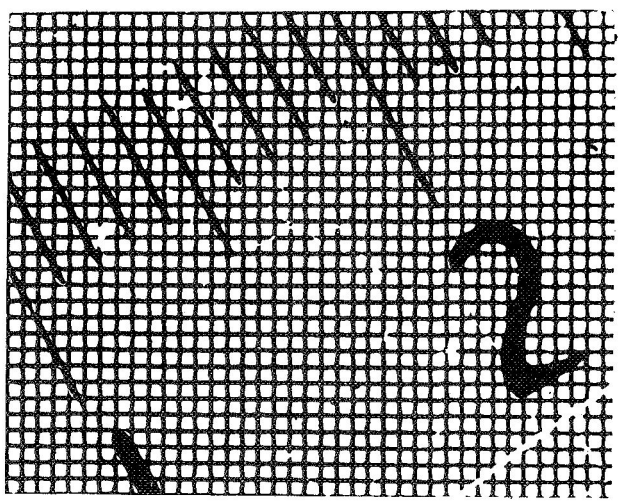


150 Mesh Uncoated - #105915B

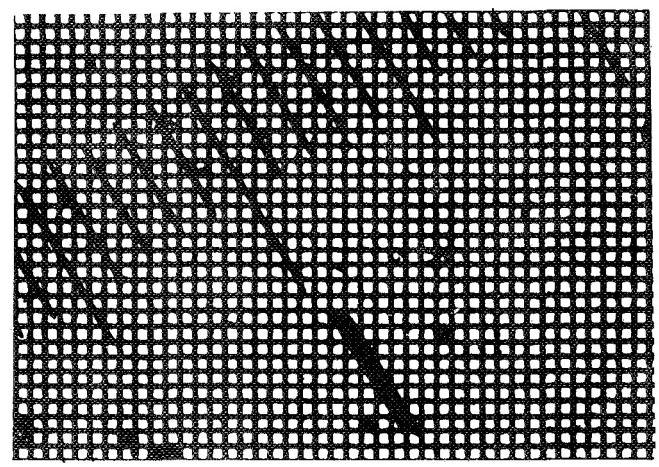


150 Mesh Coated* - #105999

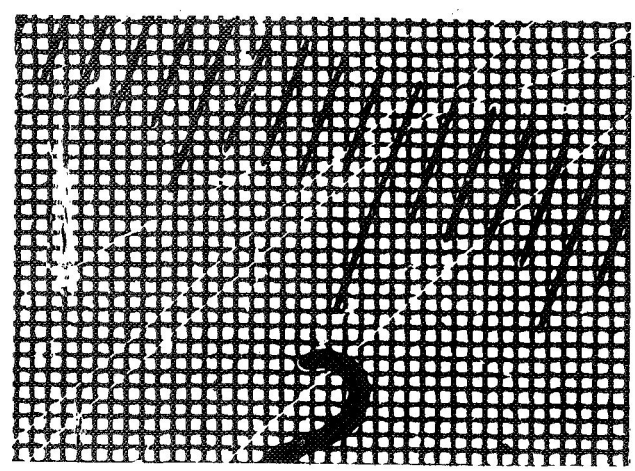
Photo Scale: Numbered Divisions are Tenths of Inches



250 Mesh Uncoated - #105917B



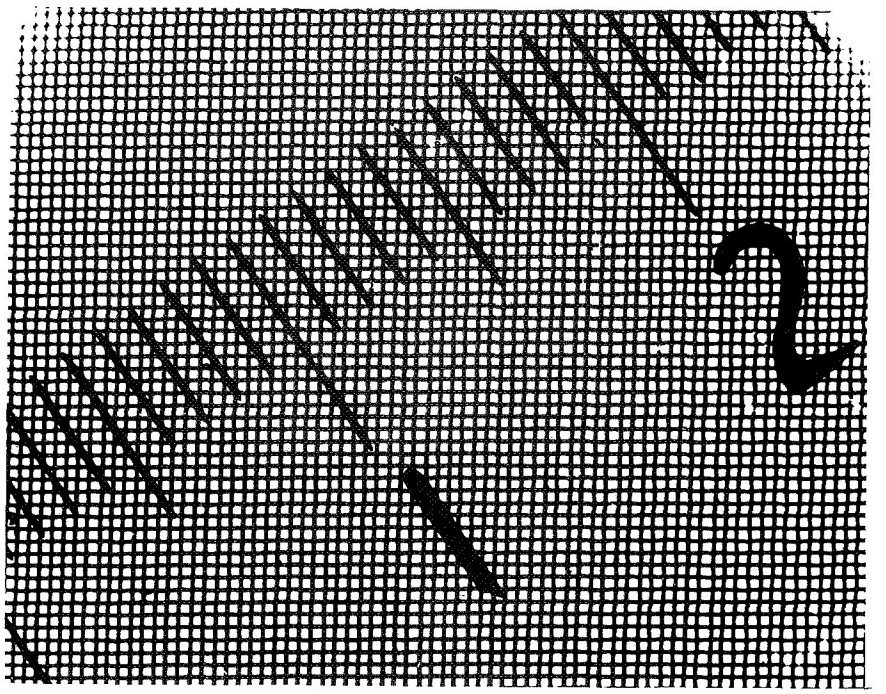
250 Mesh Coated(Initial) - #106002B



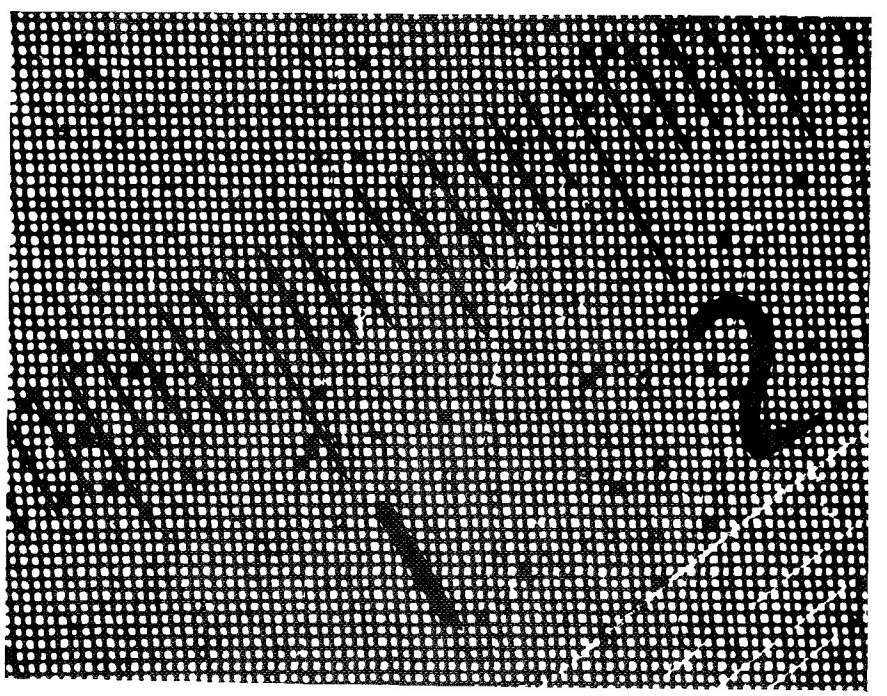
250 Mesh Coated(Improved) - #106606B

* Dupont TFE Primer-Green
851-204, Mat. #119-482-945,
GD Spec. 0-00109-2

Figure 79. — Microphotographs, Uncoated Versus Coated Screens

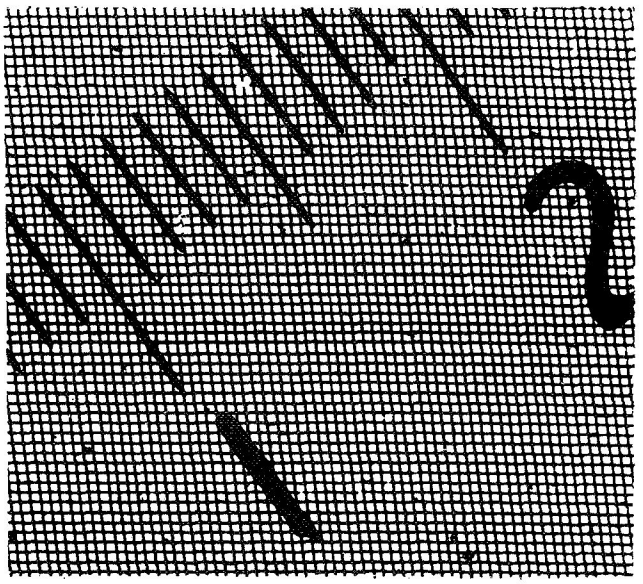


325 Mesh Uncoated - #105918B

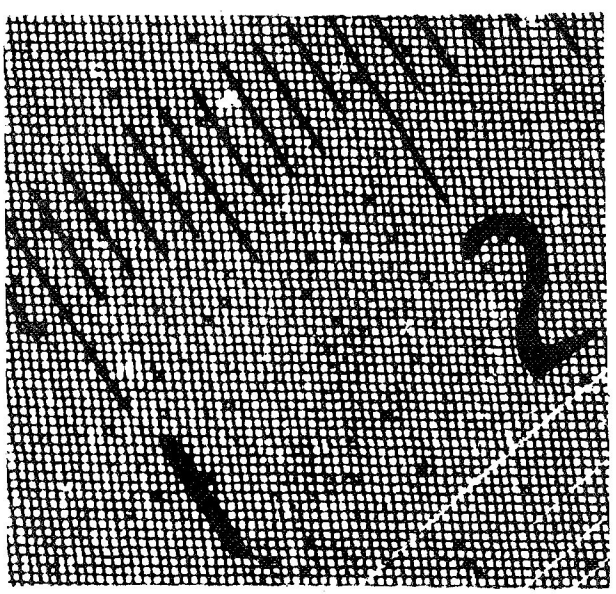


325 Mesh Coated - #106003B

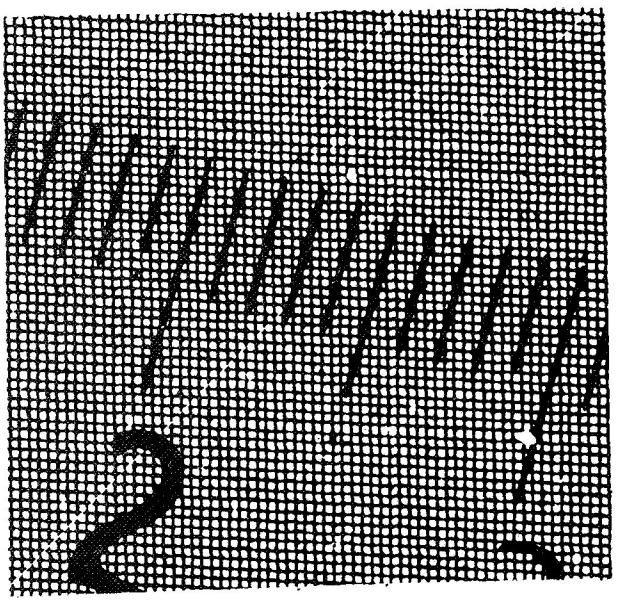
Figure 80. — Microphotographs, Uncoated Versus Coated Screens



400 Mesh Uncoated - #105919B



400 Mesh Coated (Initial) - #106004B



400 Mesh Coated (Improved) - #106605B

Figure 81. — Microphotographs, Uncoated Versus Coated Screens

Table 24. — Screen Pore Configuration Summary

Configuration Specifics / Screen Identity (wires/inch)	Uncoated Pore Size* (inches)	Coated Pore Size (inches)	Micro Photo Identity	Pore Configuration & Coating Quality
150 x 150	0.0050	0.0040	105 915B 105 999B	Square, uniform, no pores blocked.
250 x 250	0.0040	0.0025 0.0030**	105 917B 106 002B **106 606B	Square, generally uniform, 0.50% blocked. Improved, uniform and unblocked.
325 x 325	0.0030	0.0020	105 918B 106 003B	70% appear as 90° segments of circle, fairly uniform, 0.75% blocked.
400 x 400	0.0025	0.0015 0.0018**	105 919B 106 004B **106 605B	30% appear as 90° segments of circle, generally uniform, 0.60% blocked. Improved, open and unblocked.

*Side dimension obtained from scaled micro-photographs.

**Improved screen coating.

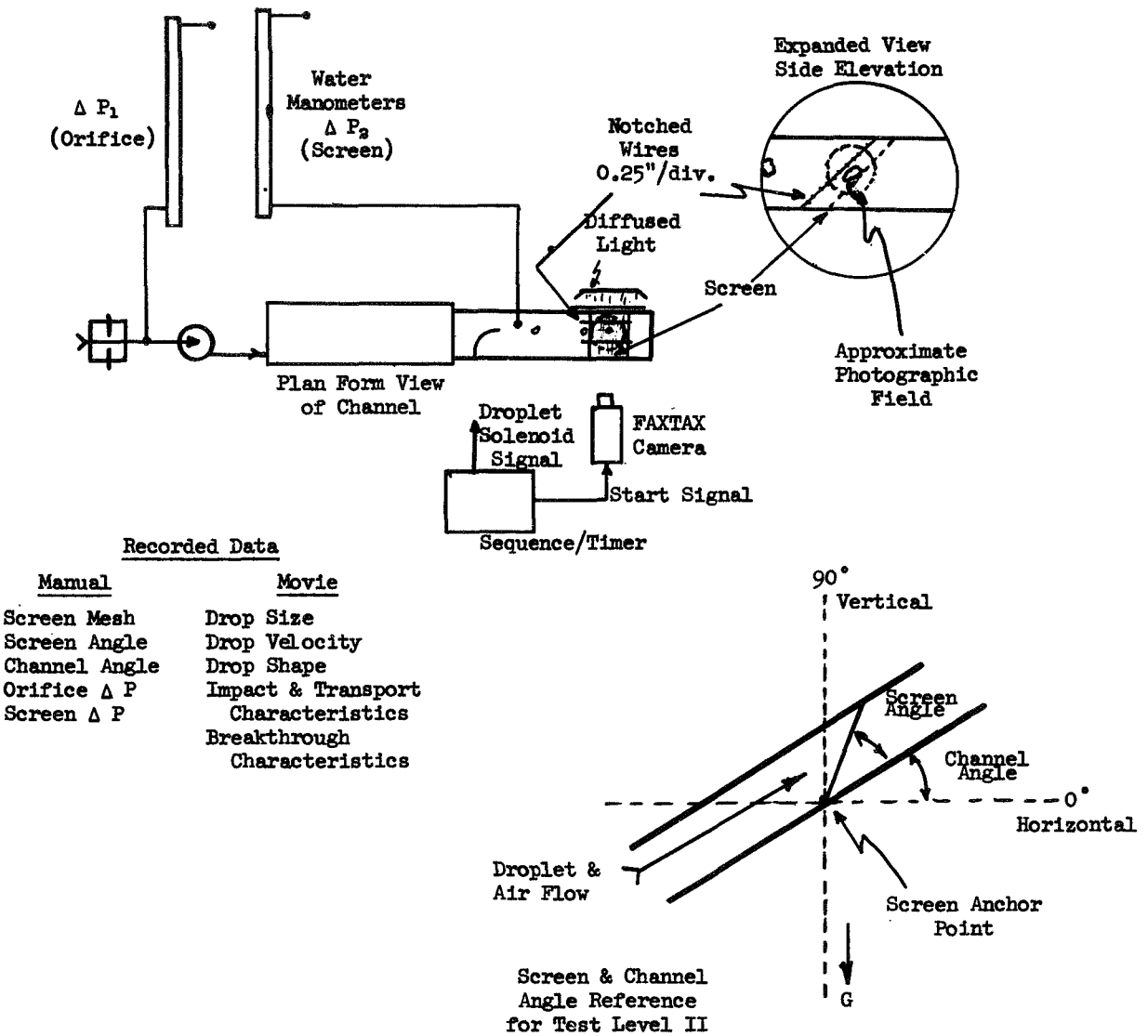


Figure 82. — Instrument Schematic, Test Level II

Test Procedures

The test procedures were developed from the following experiment design concepts.

Test level I - analytical component tests. — Four basic test sequences are required to gain information on the fundamental droplet forces expected. Each test should be performed in a duplicate way for each of three screens. These screens are square weave, Teflon coated, with the following rating in number of wires per inch - 150, 250, 325, and 400.

Test A - screen configuration: The equivalent round pore size, d, of the screens can be determined visually from enlarged photographs. The following formula can be used

$$d \sim \frac{4}{\pi}\left(\frac{1-n_1 d_1}{n}\right)^2 \tag{1}$$

where n_1 = number of wires per inch; d_1= coated wire diameter.

Test B - adhesion force test: Adhesion forces restraining drop motion parallel to the screens can be determined by placing a droplet of known size (volume) on a flat section of screen and tilting the screen at an angle with respect to the gravity vector. The angle for incipient motion is recorded. Adhesion force, f, and a friction coefficient, η, are unknown and can be determined by

$$f \sim \rho \lambda^2 g\,(\sin\theta - \eta\cos\theta) \tag{2}$$

A suggested method is to plot f versus η using the data obtained. The value of η for which all the ρ's are equal will determine both unknowns.

Test C - screen penetration test - static: Balance of capillary, gravity, and pressure forces can be determined by placing a drop on a screen normal to the gas flow and increasing the air flow until the drop penetrates the screen. At penetration, the gas flow ΔP across the screen is recorded. Data are taken for several drop sizes (volume). An unknown coefficient, α, can be determined by

$$\alpha = \frac{d}{\cos\psi}\left(\frac{\rho\lambda g}{\sigma} + \frac{4}{\lambda} + \frac{\Delta P}{\sigma} + \frac{c\rho u^2}{\sigma}\right) \tag{3}$$

Equation (3) is written for the gravity vector parallel to the air flow vector. The factor c is essentially a drag coefficient.

Test D - screen penetration - drop distance: The effect of velocity on droplet penetration can be verified by dropping liquid onto screens tilted at various angles to

the gravity vector. Impact velocity will be determined analytically. Dropping of a given size (volume) can be performed at increasing heights. The height at penetration should be recorded. This should be done for screens at angles of 0, 15, 30, 45, and 60 degrees to the horizontal. Velocities derived from the height data can be checked against the following formula:

$$v = (1/2\ \rho\ d)^{-1/2} \left(\alpha\ \sigma \cos\psi - \frac{4\sigma d}{\lambda} - \rho\lambda g d\right)^{1/2} \qquad (4)$$

Test Level II - analytical system tests. — Two basic tests are required in level II to evaluate the full analytical model. The phenomena of penetration and lateral motion of droplets can be considered separately in the two basic tests as they are separated in the analytical model. Primary emphasis should be placed on determining regions (in plots of the important parameters) where the different phenomena occur. Determination of gravity sensitivity is also a primary objective. The magnitude of the air flow required to produce a range of conditions bounding the transition point of retention/penetration must be experimentally determined in trial runs preceding the final test design.

Test A - vertical orientation: Penetration regions (in the range of variables) can be mapped by taking photographic data of droplets impacting a horizontal screen. Gas flow and droplet motion should be normal to the screen. Test should be run with flow up and flow down.

Test B - horizontal orientation: Regions for droplet motion (in either direction on the screen) can be mapped by taking photographic data of droplets and air flow moving horizontally and intersecting screens set at a given angle to the horizontal (probably $40 < \alpha < 80$ degrees). The angle can be determined in preliminary checks of available air speed and droplet release mechanics. The test should be run with flow left-to-right and right-to-left such that the effect of gravity will be opposite in the two cases.

Experiments in the design of the droplet generator were initiated on 13 January 1970 and, in the main, were concluded on 30 January 1970. System checkout, including examination of motion picture techniques, was initiated on 27 January 1970. Final system configuration for test level II was completed on 17 February 1970.

Test level I data runs were initiated on 3 February and, except for special runs required by uncertainties brought to light by level II tests, were completed on 10 February 1970.

Test level II data runs were initiated on 10 February and completed on 27 February 1970.

Test Data Summary

Manually recorded data. — The manually recorded unprocessed test data have been organized in tabular form and included herein as tables 25 through 30.

Table	Test	Test Title	Number of Test Points
—	Level I	Analytical Component Tests	496
—	A	Screen Configuration	--
25	B	Adhesion Force - Roll Angle	(60)
26	C	Screen Penetration - Δ P	(28)
27	D	Screen Penetration - Fall Distance	(398)
28	E	Screen Δ P	(10)
—	Level II	Analytical System Tests	64
29	A	Vertical Orientation	(25)
30	B	Horizontal Orientation	(39)
		Total Recorded Test Points	560

Photographically recorded data. — The principal source of information on droplet behavior in the level II tests is with the high-speed motion pictures. Runs 1 to 14 were photographed by the DYNAFAX camera and produced data of marginal quality. Runs 15 to 64 were photographed by the 16mm FASTAX high-speed camera and produced data of excellent quality and, prior to analysis at least, appears to be in an abundance and variety to form the basis for analysis far beyond the scope of the present contract. With but one exception each of the 64 level II test points (runs) were photographically recorded. The film identity for each run is given as part of the manually recorded data. Figure 83 illustrates the quality of the photographic data.

Critique of the Test Design

With the exception of the problems associated with the inherent difficulties with droplet generation and transport, the general approach to the test design appeared to be straightforward, tests were easy to manage, and construction costs were low. The approaches followed and the instrumentation information compiled can be recommended as a guide to future test designs for experimental studies involving film stability and transport phenomena.

Table 25. — Test IB - Adhesion Force Roll Angle

First Run 5 February 1970 - 42 Test Points

	θ* / Drop Size (cc)	Trials 1	2	3	4
Test Set #1 150 x 150	.01	24	32	30	34
	.03	30	34	21	
	.07	22	14	15	20
Test Set #2 250 x 250	.01	29	21	33	36
	.03	26	40	26	21
	.07	22	19	25	
Test Set #3 325 x 325	.01	38	35	28	31
	.03	17	27	20	23
	.07	18	20	20	21
Test Set #4 400 x 400	.01	43	38	39	44
	.03	41	36	30	39
	.07	24	26	25	

* Angle of screen from horizontal at which initial roll-off motion is observed.

Second Run 27 February 1970, Improved Quality Coating

	θ* / Drop Size (cc)	Trials 1	2	3
Test Set #1 250 x 250	.02	38.0	40.5	38.0
	.04	23.5	21.5	22.0
	.07	15.0	14.0	16.0
Test Set #2 400 x 400	.02	18.0	22.0	20.0
	.04	11.0	10.0	14.0
	.07	9.0	12.0	8.5

Note: A second run was conducted on 27 February using improved quality screens (more uniform coating). See "Second Run" data.

Table 26. — Test IC - Screen Penetration - ΔP

Date: 9 February 1970
28 Test Points

	Δ P* / Drop Volume (cc)	Trials						Comments
		1	2	3	4	5	6	
Test Set #1 150 x 150	.010	.079	.090	.064	.065			
	.025	.074	.050	.078	.070	.062	.082	
	.050	.071	.053	.049	.069	.053	.064	
Test Set #2 250 x 250	.020	.115	.105					Broke, then penetrated
	.050	.090						Broke up at .090 & penetrated at 0.147
Test Set #3 325 x 325	.020	.150	.170					Deformed at .013, part way thru at .150, split & small drops thru at .170
	.050	.117						Deformed at .100 & split at .117
	.100	.140						Deformed at .080 & split up at .140
Test Set #4 400 x 400	very large	.240	.160	.200				Some thru, some remained on screen, drop spreads over screen
	very small (.005)	.225	.210					

* Δ P at which penetration of screen begins.

Table 27. — Test ID - Screen Penetration - Fall Distance

Test Set #1; 150 x 150 Screen; 3 February 1970
97 Test Points

Screen Angle	Droplet Size (cc)	Trial Fall Distances (inches)
0°	.030	[2] 3 4 3 2 [1 2 2]
	.065	[1 2] 3 2 2 [1]
15°	.010	5 4 3 [2 1] 3* 2.5* [2.25]
	.030	6 5 4 3 [2* 1 2] 2.5 [2 2.5*]
	.065	5 4 3 [2 1 2] 3
30°	.010	5 4 [3 2] 3 [2.5 2.5 3] 3
	.030	6 5 4* 3 [2] 3 [2]
	.065	[2 3*] 4 [3*] 4 5
45°	.010	6 [5* 4] 6 [5]
	.030	[3 4] 5* 6 5* [4 3]
	.065	[2] 3 4 3 [2 2.5]
60°	.010	8* 7 [6] 7 [7 6]
	.030	8 [6] 7 [6 6.5] 7
	.065	[6] 8 [9] 9 8 7* [6 5]

Legend: [2] denotes no penetration at 2" fall distance.
3* denotes shear at 3" fall distance but no penetration.

Table 27. — Test ID - Screen Penetration - Fall Distance, Contd

Test Set #2; 250 x 250 Screen; 5 February 1970
104 Test Points

Screen Angle	Droplet Size (cc)	Trial Fall Distances (inches)
0°	.030	10 7 6 **4 5 6** 8 7 6 **5**
	.065	6 **4** 4 **3** 5 4 **4**
15°	.010	10 9 **8* 7*** 6 **7* 6* 5**
	.030	**3 4* 5* 6*** 7 8
	.070	7 6 5 4 **3 3 2**
30°	.010	**7*** 8 9 **8* 7* 7***
	.030	7 6 5 **4* 3**
	.070	**2 3** 4* 5 **3.5**
45°	.010	**10* 11 12* 13* 14* 15* 17*** 18 18
	.030	**9 10*** 10 9 8 **7*** 7 **7*** 6* **7 8* 9*** **8 9** 10
	.070	**4 5 6* 7* 8*** 9 **8**
60°	.030	16 15 **14* 13 13* 15* 16*** 16 15
	.070	**10 10 12 13*** 13 14 13 **12 12**

Legend: **2** denotes no penetration at 2" fall distance.
3* denotes shear at 3" fall distance but no penetration.

Table 27. — Test ID - Screen Penetration - Fall Distance, Contd

Test Set #3; 325 x 325 Screen; 4 February 1970
97 Test Points

Screen Angle	Droplet Size (cc)	Trial Fall Distances (inches)
0°	.030	[6] 7 [7] 8 6 [5 5]
	.065	6 5 [4] 4 [3 3]
15°	.030	9 [6 6 7] 8 7
	.065	5 [4 4 5] 6 6 5
30°	.010	16 [12] 13 13
	.030	9 8 [7] 6 [6 5 6] 7
	.065	[8] 9 8 7 6 5 [5 5 6 6] 7 7
45°	.010	22 [18] 20 18 16 [14 12 14]
	.030	[10 12*] 14 13 [12* 11* 10*]
	.065	10 [9* 8* 9 10 10*] 11 11
60°	.030	[12 14 20] 24 [22* 24*] 24 [26*] 26
	.065	[11 19* 19* 24* 24*] 30 28 [26* 28 28] [30 24] 26 [28] 28

Legend: [2] denotes no penetration at 2" fall distance.
3* denotes shear at 3" fall distance but no penetration.

Table 27. — Test ID - Screen Penetration - Fall Distance, Contd

Test Set #4; 400 x 400 Screen; 3 February 1970
106 Test Points

Screen Angle	Droplet Size (cc)	Trial Fall Distances (inches)
0°	.030	9 [6] 7 [6]
	.065	10 8 [6] 6 [5 5 6] 7 7
15°	.010	7* [6 7] 8* [7*] 8
	.030	9 [7] 8 [7* 6] 8
	.070	10 9 [4] 6 [5 4 5 6] 7 7
30°	.010	14 [10 10* 11 12*] 15 15 14 [13* 13]
	.030	[6] 10 [9 8*] 9 10 9* [8* 7* 7*]
	.065	[8] 9 8* [7 6 7 8] 9* 10
45°	.010	24 22 20 [18* 18* 16* 17*] 19 [19]
	.030	[10 12*] 13* 13* [12* 12] 14
	.065	12* [11 10 11 12 13] 14 13 12 [11]
60°	.030	[15 16* 17* 18* 24* 35*] 36 37 35 34
		[33] 33 32 [30 31] 32

Legend: [2] denotes no penetration at 2" fall distance.
3* denotes shear at 3" fall distance but no penetration.

Table 28. — Test IE - Screen ΔP

27 February 1970

Test Apparatus: Test Level II apparatus with screen assembly removed. Test screens taped across the exit end of the working section.

Sequence #1

250 x 250 Screen ~ Area = 7.92 in.^{2}

Orifice Δ P*	Screen Δ P
.1860	.0863
.1480	.0709
.0809	.0462
.0272	.0224
.0005	.0038

Sequence #2

400 x 400 Screen ~ Area = 8.07 in.^{2}

Orifice Δ P*	Screen Δ P
.1680	.1000
.1530	.0931
.1030	.0710
.0438	.0412
.0167	.0237

* 1.5" diameter orifice used throughout.

Table 29. — Test IIA - Vertical Orientation

	Run Date Feb. 1970	Run Sequence	Duct Angle	Screen Angle	Air Vel. Δ P **	Air Vel. In.Sec.	Screen Δ P	Comments
Screen Mesh = 250 x 250	24	31*	90°	120°	.0123	56	.0085	
	25	32	90	120	.0222	74	.0115	
		33	90	120	0	0	0	
		34	90	120	.0222	74	.0115	
		35	90	90	0	0	0	No penetration.
		36	90	90	0	0	0	Marginal penetration, spray.
		37	90	90	.0952		.0364	Penetrated.
		38	90	90	.156		.0528	Drop on back,no spray.
		39	90	90	.153		.052	Better qual. screen installed,bounced off.
		40	90	90	0	0	0	Bounced off, no penetration.
		41	90	90	0	0	0	Some spray, small drops on back.
		42	90	90	0	0	0	
		43	90	90	.169		.069	Drop hung on screen, 1 small drop on back.
		44	90	90	.191		.080	No film, drops .080-.150 diam. hung on front & would not blow off. New and clean screen did not hold drops larger than .020 diam.
	27	61	270	90	.0588		.0295	No penetration.
		62	270	90	.120		.0467	Penetration.
		63	270	90	.084		.036	No penetration.
Screen Mesh = 400 x 400	26	45	90	90	0	0	0	Marginal penetra., sm. drops on back(top).
		46	90	90	.189		.080	Some spray through.
		56	270	90	.0414		.0255	Penetration.
		57	270	90	0	0	0	No penetra. but appeared marginal.
		58	270	90	.0414		.0249	Incipient penetration.
		59	270	90	.043		.0248	Better qual.screen installed, no penetra.
		60	270	90	.150		.0573	Penetra.,drop on back.
		64	270	90	.179		.0922	Better qual. screen installed, borderline penetration only.

* Film reel (FASTAX 16 mm) number same as Run Sequence Number for Runs #15 and on.

** 1.5" diameter orifice used throughout Level II tests.

Table 30. — Test IIB - Horizontal Orientation

	Run Date Feb. 1970	Run Sequence	Duct Angle	Screen Angle	Air Vel. Δ P ***	Air Vel. In/Sec	Screen Δ P	Comments
Screen Mesh = 250 x 250	17	7(1)*	0°	120°	0	0	0	
		8(2)	0	120	.033	91	.0107	
	18	9(1)	0	120	.008	45	.007	Sequencing incorrect, film coverage poor.
		10(3)	0	120	.0212	72.5	.0147	Same as Run 9(1).
		11(4)	0	120	.0205	72	.0142	" "
		12(1)	0	120	.0242	77.5	.0142	" "
		13(2)	0	120	.0240	77.5	.0146	" "
		14(3)	0	120	.052	112	.022	Good film coverage.
	19	15**	0	120	.054	115	.022	FASTAX used for remainder of tests.
		16	0	120	.0098	50	.008	Film coverage excellent. 0.8 sec. delay between camera start & drop generation sig.
		17	0	120	.0229	76	.0128	
		18	0	120	.023	76	.013	
		19	0	120	.023	76	.013	Smaller droplet nozzle used.
		20	0	120	.023	76	.013	Small drops penetrated screen.
	20	21	0	120	.189	218	.0545	
		22	0	120	.210	230	.060	Smallest nozzle used in Runs 22 - 24.
		23	0	120	.111	167	.035	Penetrated screen.
		24	0	120	.110	167	.035	No penetration.
	24	25	0	120	.028	83.5	.0137	
		26	0	120	.028	83.5	.0137	
		27	180	120	.0246	78	.0129	Went thru screen and clung to back side.
		28	180	120	0	0	0	Same as Run 27.
		29	180	120	.066	128	.024	Penetration.
		30	180	120	.0047	34.5	.0054	Ran Down.
	26	49	180	120	0		0	Light spray, some hung on back.
		50	180	120	.0642		.0343	Two sm. sprays, 2 drops hung on back.
		51	180	120	.105		.0375	Small spray thru.
		52	180	120	.0492		.0222	Some thru spray, drop hung on front.
		53	180	120	.176		.054	Spray thru, drop on front.

* Film strip number for DYNAFAX (tests 1 - 14 only).
** Film number for FASTAX identical with Run Sequence number, #15 and on.
*** 1.5" diameter orifice used throughout Level II tests.

Table 30. — Test IIB - Horizontal Orientation, Contd

	Run Date Feb. 1970	Run Sequence	Duct Angle	Screen Angle	Air Vel. Δ P ***	Air Vel. In/Sec	Screen Δ P	Comments
Screen Mesh = 400 x 400	12	1(1)	0°	135°	.070	132	.040	
		2(2)	0	135	.070	132	.040	Instru. sequence incorrect, film coverage poor.
		3(3)	0	135	.042	102	.029	
		4(2)	0	135	.042	102	.029	
		5	0	135	.028	84	.023	
		6	0	135	.028	84	.023	Sequence problems, film coverage poor.
	26	47	0	120	.026		.017	Borderline penetra.
		48	0	120	0	0	0	Medium spray, drop hung on back.
		54	180	120	.194		.061	Small spray thru.
		55	180	120	0	0	0	Drops roll down front.

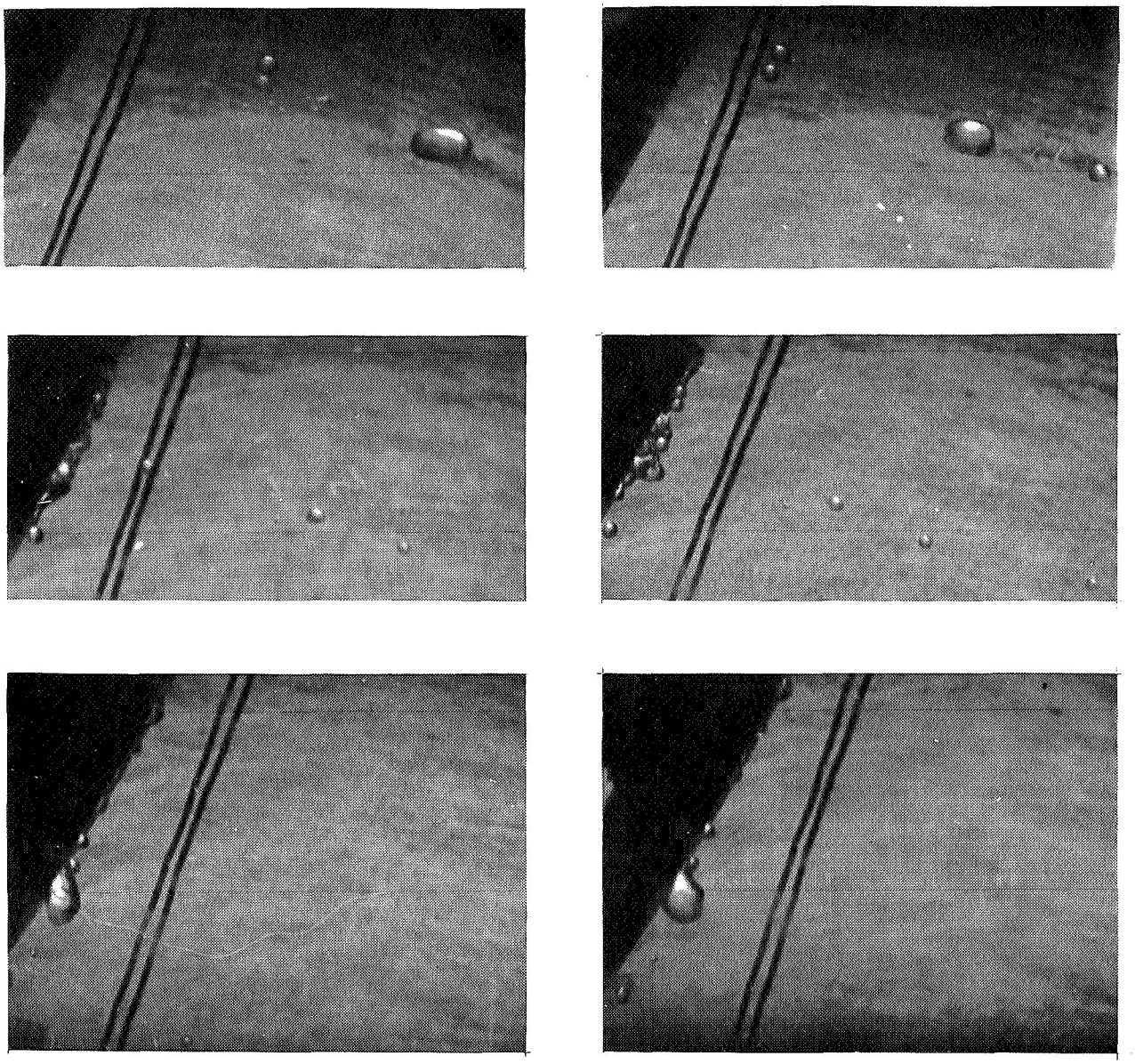
*** 1.5" diameter orifice used throughout Level II tests.

Instrumentation. — The extensive dependence on the analysis of movie films for an experiment involving such a large number of test points where the exact design of each subsequent set point in a series is dependent upon the characteristics of the preceding run results in an expensive and time-consuming program. If such a dependence exists for flight experiments, the use of "instant replay" TV might well be examined. The other instrumentation involved is entirely straightforward and simple.

Droplet generation. — The droplet generation system which finally evolved from the experimental design can provide some worthwhile starting points for future designs. The requirement for and attainment of the constant-pressure water source, low-capacitance "accumulator," and high-response control valve for precise metering demands are examples. Nozzle designs are also of interest, possibly leading to the investigation of variable nozzle configurations as an iris diaphragm or plug nozzle.

The requirement imposed by the test design criteria that the droplet generator be capable of sizing, ejecting, and propelling a single droplet was severe and led to extensive, time-consuming experimental design. Doing so, however, may have served to carry the design beyond the point of problems similar to those experienced with the nozzles employed in recent KC-135 low-gravity, flight trajectory tests.

Screen types, configurations, and materials. — The screen type and coating material selected for the experiments appeared satisfactory. The installation scheme which permitted easy screen angle changes was very satisfactory. For more complex



Test IIA - Run Sequence #47; Channel Orientation - Horizontal; Screen Angle - 120°; Channel Stream Velocity - 80"/sec; Screen - 400 x 400 Mesh.

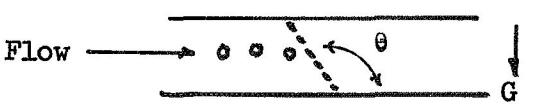


Figure 83. — Typical Droplet Behavior - Movie Frame Prints

test environments it is reasonable to suggest that the task of screen assembly change occasioned by inclusion of mesh size as an experimental variable could well be accomplished by a continuous belt or perhaps loop of screen made up of sections of different mesh. With such an approach, mesh size change could be effected by merely applying a specific number of turns to a reel.

A note of caution should be raised concerning the contamination effects of foreign materials on the screen. During the course of the tests, contaminants, most likely in the form of residuals from the evaporation of the tap water which was used in the droplet generation, significantly altered the characteristics of the screen. Such a problem raises two important points, namely, 1) that future R&D tests consider using contaminant-free water, and 2) that application of the screen separator as an operational system may be severely limited by this demonstrated sensitivity, possibly restricted to only those functions involving contaminant-free, water/gas streams.

A very important aspect of the success of a screen separator is the coating effectiveness of the screen as demonstrated by the very different results obtained with poorly coated as opposed to well-coated screens. Exacting methods of specifying and applying screen coating are needed.

Improved methods for keeping the screens flat should be devised so that visual and photographic inspection of both front and back of the screen is clearly available. This must allow visualization of the screen edge as a line not much thicker than the screen itself.

Procedures. — Design of future tests should attempt to reduce the number of test points required to obtain sufficient data to examine and update the model. This will be more easily accomplished for future tests as a result of the data provided by the tests reported herein than it was in the design of these tests, even with the two-stage design approach which was followed. In general, however, the procedures eventually employed were relatively simple to manage and should be considered as a starting point in the design of future tests.

CORRELATION OF ANALYTICAL AND EXPERIMENTAL OBSERVABLES

Correlation of the analytical models with experimental evidence is evaluated through the comparison of processed data with the predictive representations. The experimental data are processed to form significant parametric representations and are displayed in discrete form.

Predictive Data

Predictions for Case 1, the screen separation system, are listed in equation form in section headed "Case 1 — Hydrophobic Screen Liquid/Gas Separation." Because of the complexity of the system, verification was not accomplished by comparison of predictive and experimental data against a single criterion. Predictive data, therefore, are specifications of the expected trends of droplet behavior under isolated conditions. Each of the predictive equations will be separately discussed and related to the experimental results being presented.

Experimental Data

The following sections describe the individual test data obtained to verify the analytical model of the Screen Separation System and present some conclusions relating to each test. It can be noted that the test design did not include an explicit examination of the behavior of the droplet during its transport along the gas stream; rather it concentrated on the areas of major uncertainty, that of the behavior of the droplet during and immediately following its impact on the screen.

Droplet Adhesion

Adhesion forces tending to "stick" liquid droplets to surfaces were measured by placing water droplets of known sizes on several flat Teflon-coated square-weave wire screens. As the screens were tilted at angles θ to the horizontal, the angle was recorded when the gravity force just overcame the adhesion forces.

During the testing a screen change was made which showed that the previous screens were poorly coated with Teflon. Data from all tests are presented in figure 84. Approximately 50 data points were recorded. There were five drop sizes and four screens tested.

Drop volumes (cc): 0.01, 0.02, 0.03, 0.04, 0.07
Screens (all square weave): 150X, 250X, 325X, 400X

If an analogy is drawn between droplet "friction" and solid material friction, droplet motion should just occur when

$$F_a + \eta N = \left| F_g \cos (\beta - \theta) \right| \tag{1}$$

where η is a friction coefficient and N is the normal force. Since $\beta = 90$ degrees

$$f \approx \rho \lambda^2 g (\sin \theta - \eta \cos \theta) \tag{2}$$

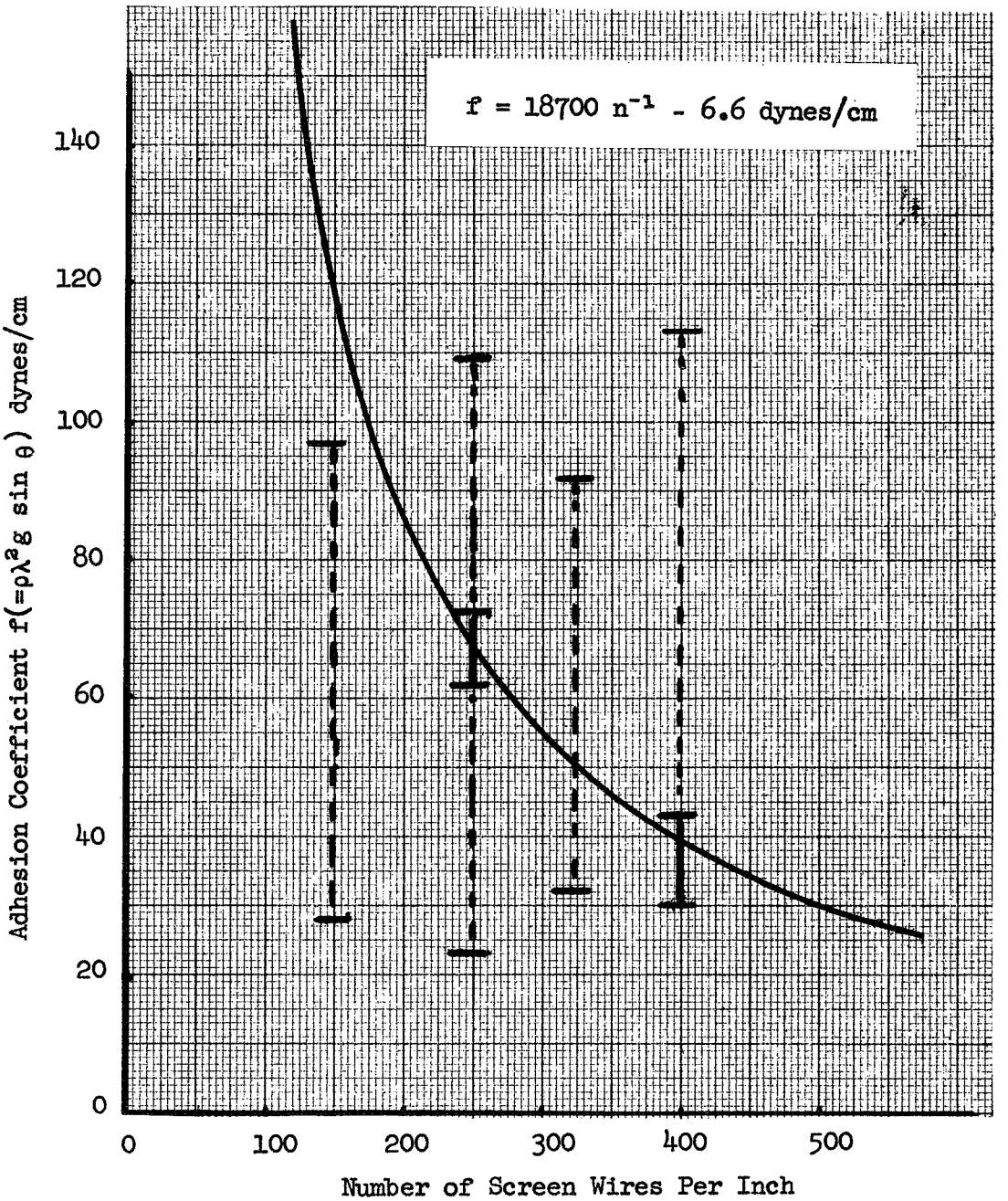


Figure 84. — Droplet Adhesion

for three-dimensional drops F_a is defined as:

$$F_a \equiv f \lambda$$

Examination of the first set of data for the screens which were poorly coated showed no apparent correlation. The data points were quite scattered and, although the proper trends were visible, repeatability was poor.

In reducing the second data set collected against improved screens (250 mesh and 400 mesh screens only) it was immediately apparent that $\eta \sim 0$ (see figures 6, 7, and 8 of reference 13). Also, f was seen to depend upon the screen mesh. The following relationship was found to best fit the second data set:

$$f = \rho \lambda^2 g \sin \theta = 18700\, n^{-1} - 6.6 \qquad (3)$$

where n is the number of screen wires per inch.

Figure 84 shows the data and the correlation with equation (3). Agreement is seen to be good for the second data set and poor for the first set. The curve shows that as the screens become more coarse, the effective friction increases sharply. Since there is an effective f for a plane, smooth surface, the curve should approach this value asymptotically as $\eta \to \infty$. This is not shown since, for the range of data taken, the simple expression (3) seems quite adequate.

Because $\eta \sim 0$, one can assume that the mechanical type of rolling friction which is proportional to the normal force is not the dominant phenomenon. Adhesion of the liquid to the material is clearly the most important consideration.

Pressure Loss in Flow-Through Screens

Screen pressure drop was measured and used directly in the predictive equations without attempting to verify this section of the analytical model. Since only single drop experiments were anticipated, the effective solidity due to residence of more than one droplet on the screen was not determined.

Coated screen pore sizes for the screens used in the test program were determined by microphotography. The hole-size measurement was used in place of the pore diameter, d, in analysis of data.

Penetration Due to Screen Pressure Drop

An attempt was made to isolate the effects of screen pressure drop on droplet penetration by placing water on a horizontal screen and increasing the air flow rate until

penetration occurred. Rather large drops were used (in comparison with the screen pore size).

Droplet volumes (cc): 0.01, 0.025, 0.05
Screens (all square weave): 150 x 150, 250 x250, 325 x325, 400 x 400
Pressure range: 4,800 to 17,000 dynes/cm^2

The test were only partially successful in that penetration usually was preceded by severe deformation and lateral motion of the liquid on the screen. As air drag on the initially spheroidal droplets increased, the liquid deformed into a pancake shape, sometimes with a pronounced center depression. Because of the deformed droplet shape, lateral motion on the screen occurred very easily.

Since the predominant mode of operation of a liquid/vapor separator will induce droplet motion by angling the stream to the air flow vector, the droplet deformation mode will generally not occur. The results of this test are therefore presented in terms of pressure drop across the screen and screen pore size, while parameters connected with the drop shape (e.g., drag coefficient and droplet internal pressure) are neglected. The predictive equation is

$$\Delta P = \alpha \sigma \left| \cos \Psi \right| / d \qquad (4)$$

Figure 85 shows a plot of pressure difference across the screen required for penetration (ΔP) versus screen pore diameter (d). Sixteen data points are included in the bar for d=-0.0102 cm (150 x 150 screen); fewer points are included in the other bars. Good correlation is achieved with α = 2.5, whereas Test I-D (13) showed that α is probably closer to 3.5. This discrepancy is attributed to the omission of gravity forces, drag forces, and droplet internal pressures in reduction of the test data. Because of the large drop deformations, these data are considered to be useful when correlated in the present way.

It can be concluded that for screens with a mesh as fine or finer than 250 x 250 (hole sizes smaller than 0.006 cm), droplet deformation will generally occur before penetration when droplet velocities are low. Since the deformation leads to lateral motion on the screen, large (> 0.01 cc volume) low-velocity drops on inclined screens are not likely to penetrate even at rather high values of screen pressure drops.

Penetration Due to Impact Velocity

Penetration of water droplets on screens was determined by dropping water particles from various heights onto Teflon-coated screens inclined at various angles. Approximately 400 data points were recorded over five screen angles, four droplet sizes, and four different screens:

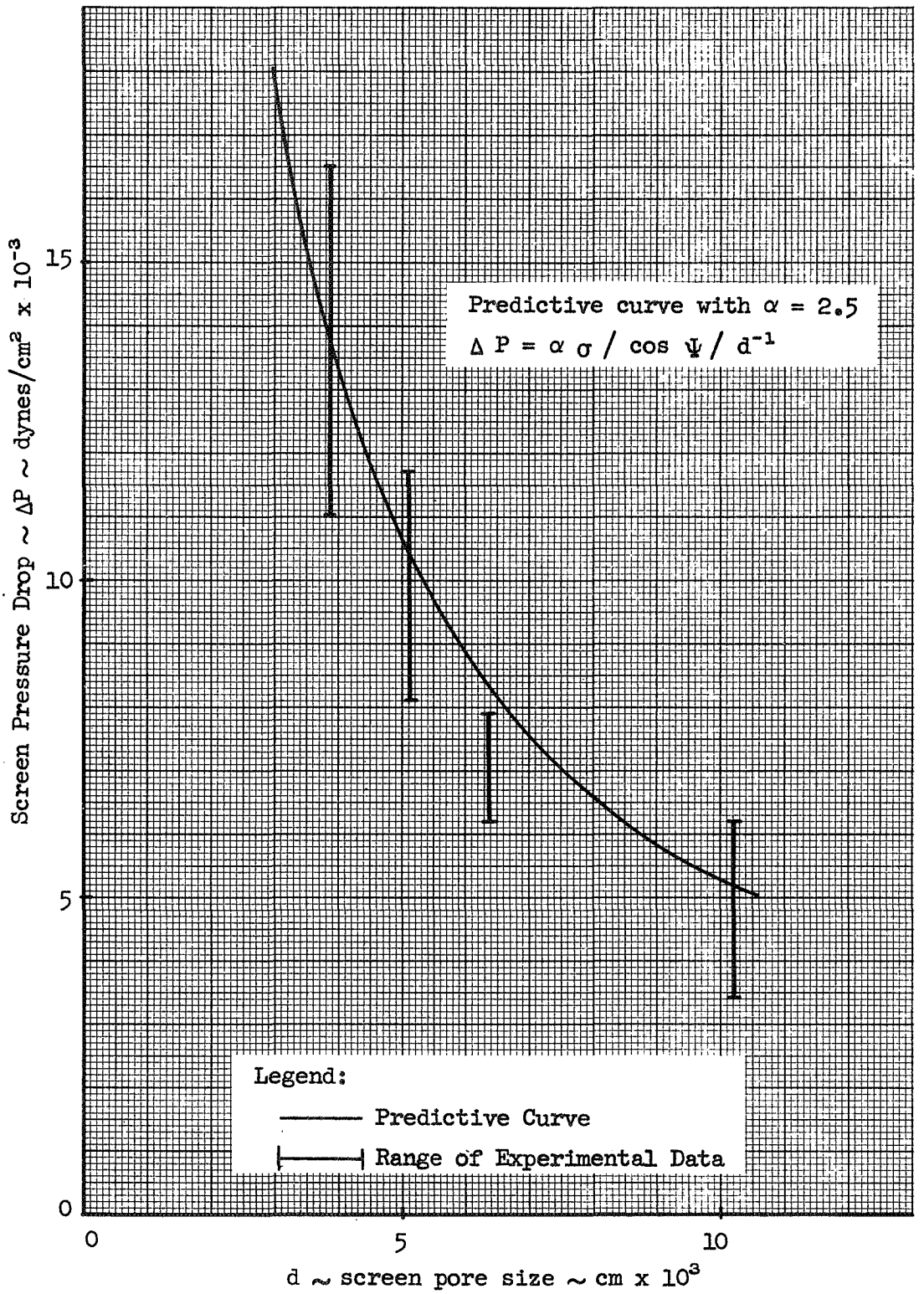


Figure 85. — Penetration Due to Screen Pressure Drop

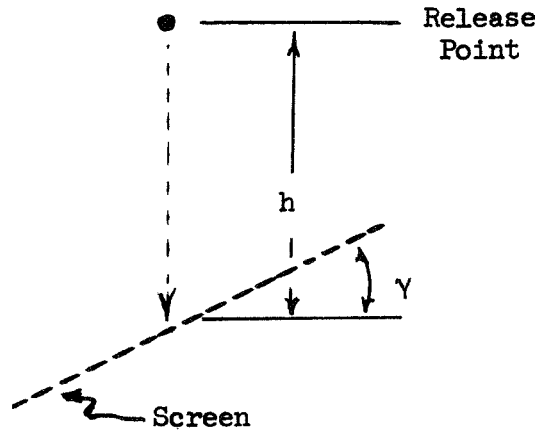
Screens (all square weave): 150 x 150, 250 x 250, 325 x 325, 400 x 400
Angles to the horizontal, γ (degrees): 0, 15, 30, 45, 60
Drop volumes (cc): 0.01, 0.03, 0.065, 0.07

Because there were no pressure forces on drag due to air flow, penetration should be governed by the following predictive equation:

$$(F_g + Fr)\ (\cos\ \gamma)\ \frac{nd^2}{\lambda^2} + F_c = F_{st} \tag{5}$$

Ignoring drag in the droplet fall and setting the deformation parameter D = 1.0,

$$v = \sqrt{2gh}$$



Equation (5) can be written

$$(\rho\lambda^3 g + \rho\lambda^2 g\ h)(\cos\gamma)\frac{d}{\lambda^2} + \frac{4\sigma d}{\lambda} = \alpha\sigma\cos\Psi \tag{6}$$

Since $h >> \lambda$ we have

$$h = \frac{\alpha\ \lambda\ \sigma\ \cos\ \Psi - 4\ \sigma\ d}{\rho\ g\ d\ \lambda\ \cos\gamma} \tag{7}$$

The following data were used:

ρ = 1.0 gm/cc
g = 980 cm/sec^2
σ = 72 dynes/cm
$|\cos\ \Psi|$ = 0.2924

Equation (6) then becomes

$$h = \frac{\alpha \lambda - 13.7\, d}{46.5\, d\lambda \cos \gamma}$$

or

$$h = \frac{\alpha - 13.7 \frac{d}{\lambda}}{46.5\, d \cos \gamma} \tag{8}$$

A preliminary determination of the value of the coefficient α yielded

$$\alpha \cong 3.5 \tag{9}$$

Over the range of most of the data

$$3.5 >> 13.7 \frac{d}{\lambda}$$

and equation (8) can be expressed in the approximate form

$$h = \frac{0.075}{d \cos \gamma} \tag{10}$$

Figure 86 shows the data ranges and a plot of equation (10). Disagreement for $h > 10$ cm is due to neglect of air drag on the falling droplets. Each data "bar" represents approximately 20 data points.

Several conclusions can be drawn. Most important is that equation (5) accurately predicts the droplet inertia required for penetration, under the test conditions, when $\alpha = 3.5$ and when the droplet deformation parameter, D, is equal to 1.0. Another important conclusion is that the droplet size is unimportant, over the range of data taken, for prediction of penetration. Droplet breakup upon impact was observed during Test I-D and is a strong function of droplet size. This phenomenon will be discussed later.

Penetration Under Combined Conditions

Penetration of droplets through Teflon-coated screens was tested with the combined effects of flow pressure drop across the screen, droplet impact, gravity, and air flow drag. Impact of the droplets was normal to the screen with the duct in a vertical position. Gravity acted for and against penetration as the tests were performed in the "flow-up" as well as "flow-down" mode.

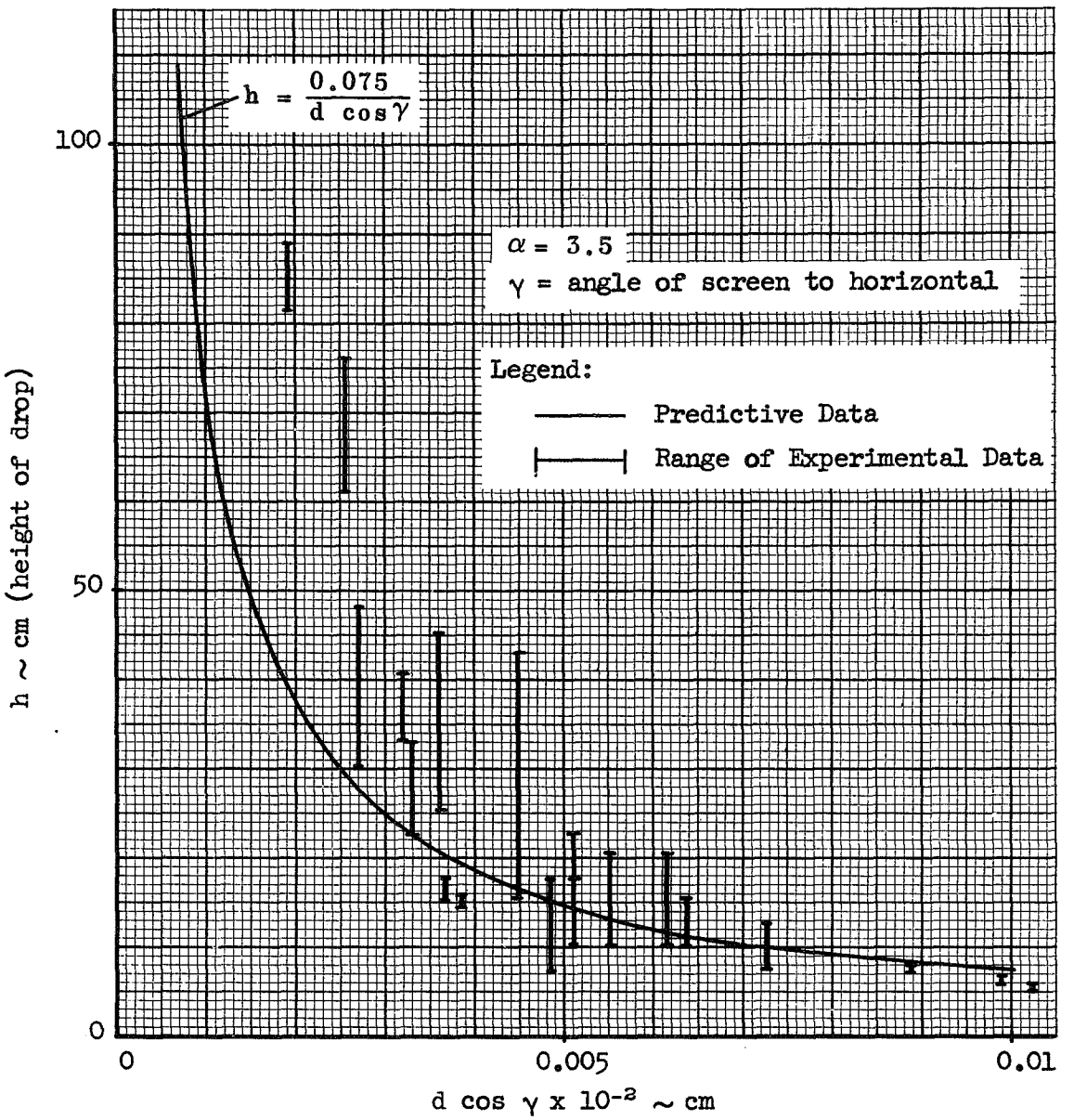


Figure 86. — Droplet Penetration Due to Impact

To observe droplet behavior accurately, high-speed motion pictures were taken in the period of interest, i.e., just before and just after impact. Pictures were taken through the clear duct wall so that the screens were seen from an edge view. Difficulty in keeping the screens flat, however, resulted in the small droplets "disappearing" into the folds of the screen. This problem was solved by pushing the screen from the downstream side with the flat face of a cylinder so that the extended surface was tight and quite flat. Good profile observations of droplet impact were then obtained.

This procedure had a serious drawback, however, which was not realized until the testing was completed. Because of the way that the screens were stretched, the down-

stream portion of the duct could not be photographed. Penetration determinations were thus made visually and not photographically, with attendant reduction in observational quality.

For the geometry of the test apparatus a penetration parameter, P_t, is defined,

$$P_t \equiv \pm \rho g \lambda + \rho(c u^2 + 1/2\ D\ v^2) + \frac{4\sigma}{\lambda} + \Delta P = \frac{\alpha \sigma \left|\cos \Psi\right|}{d} \tag{11}$$

with the following constant values used

ρ = 1 gm/cc

σ = 72 dynes/cm

$|\cos \Psi|$ = 0.2924

g = $\pm$ 980 cm/sec^2 (+ for flow down, -for flow up)

A sampling of the photographic data is presented in figure 87 where four data points are obtained from flow-up and four points from the downward flow setup. Three points represent visual (not photographic) cases of "penetration" and five points were noted for "no penetration."

Data shown in figure 87 are computed by setting the drag coefficient to equal 0.003. This low value is not consistent with the theoretical predictions and may be the result of the data reduction or data recording methods.

Best correlation was also obtained when the droplet deformation parameter, D, was equal to 1.0. This result, consistent with the previous penetration tests, suggests that the kinetic energy of impacting droplets is converted into pressure rather than lateral motion.

One phenomenon not previously discussed is the apparent ability of the liquid to sustain temporary forces sufficient to cause penetration without its actual occurrence. It is possible for surface forces in the screen pores to be overcome, allowing a finger of liquid to be extruded from the screen. If the forces are suddenly decreased, surface forces can cause the extrusion to return to the screen with no actual penetration.

Assuming that at the instant of droplet impact the fluid velocity in the screen pore of interest is the same as the impact velocity, then by conservation of momentum in a control volume through which the extruded liquid is moving we have

$$-\pi \sigma d = \int_V \frac{\partial}{\partial t} (\rho \underline{v})\, dV = \rho A\, \ell v'$$

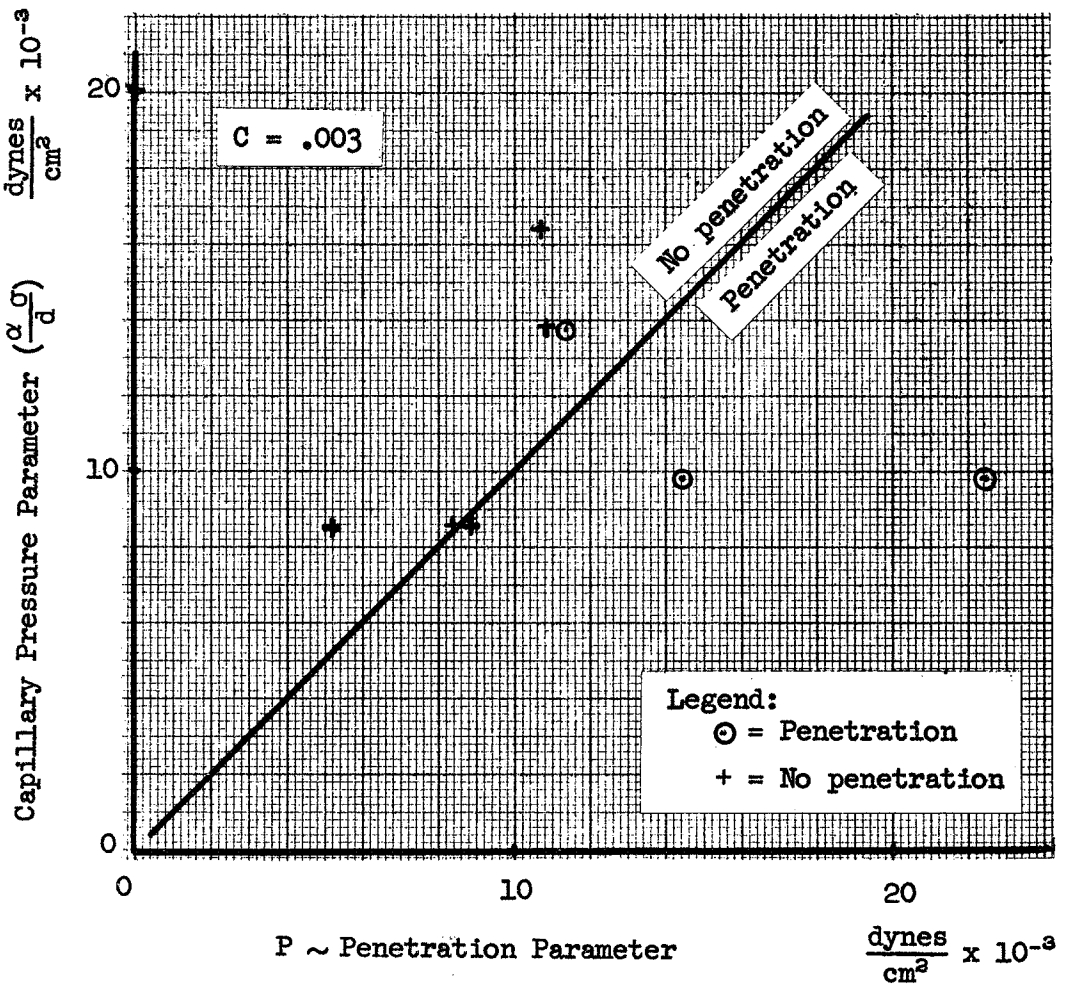
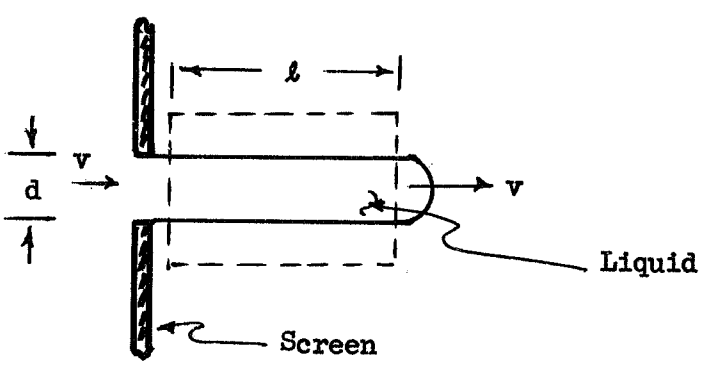


Figure 87. — Droplet Penetration



This defines the differential equation

$$\ell\,\ell'' = -\frac{4\sigma}{\rho d}\,,\quad \ell(o) = 0,\ \ell'(o) = v_{impact} \tag{12}$$

Define $\ell_* \equiv \ell/d$ and $t_* = t/\sqrt{\rho d^3/\sigma}$

Substituting into equation (12) results in the nondimensional equation

$$\ell_* \ell_*'' = -4 \tag{13a}$$

with boundary conditions

$$\ell_*(o) = 1/2, \quad \ell_*'(o) = v^i \sqrt{\rho d/\sigma} = v_*^i \tag{13b}$$

Equation (13a) has been integrated numerically for W = 0.5, 1.0, 2.0. The results in figure 88 show that a dimensionless initial velocity v_*^i between 2 and 5 probably is the critical region for detachment of the extended liquid. For Test II-A

$$30.8 \leq \frac{v^i}{v_*^i} \leq 43.6 \text{ cm/sec}$$

because of the different screens used. This indicates that further investigation into this phenomenon may be fruitful, especially if substantiated by experimental data. It also indicates that the extrusion phenomenon could be used to reduce data scatter.

Conclusions to be drawn from Test II-A are that, for the range of velocities, gravity, drop size, and screen mesh:

a. Gravity forces are not important to penetration.

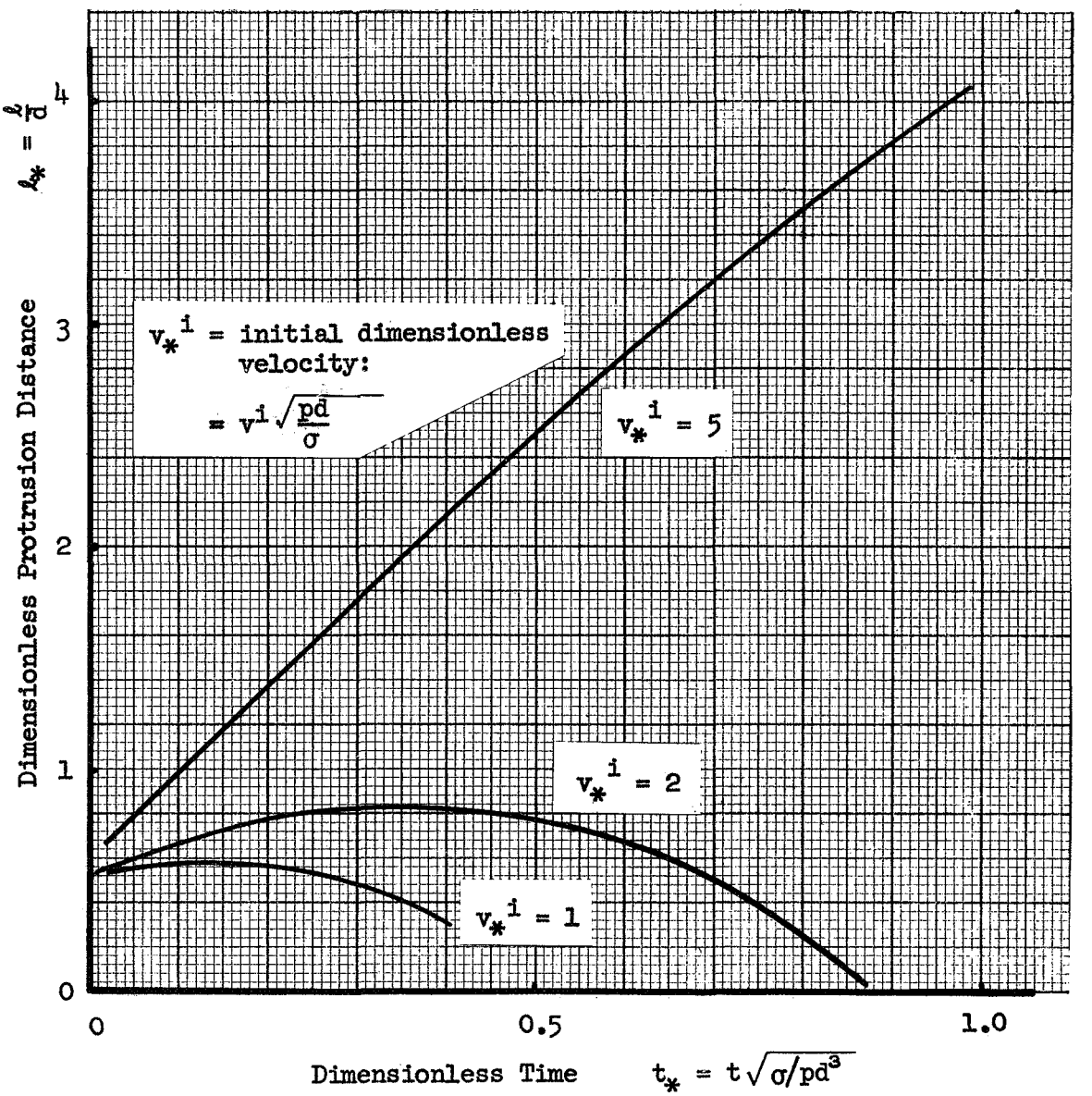
b. Penetration is not easily observed. High-magnification photography of the back of the screen would have been desirable in addition to the screen front face profile photographs obtained in this test sequence.

c. Drag forces on the impinging droplets either are not strong or the test data was inaccurate.

d. The deformation parameter for penetration is $D \approx 1.0$ for the range of screen angles examined, but is probably a function of the droplet-screen impact angle.

Droplet Movement Under Combined Conditions

Figure 83 is an example of the photographic data taken in this phase and subsequently analyzed to confirm and determine criteria for droplet motion parallel to the surface of hydrophobic screens. Three basic phenomena were investigated:



Solution of the Equation:

$\ell_* \ell_*'' = -4$, $\ell_*(0) = 1/2$, $\ell_*'(0) = v_*^i$

where $\ell_* = \ell/d$

and $\ell_*' = \frac{d\ell_*}{dt_*}$, $t_* = t\sqrt{\sigma/\rho d^3}$

[d = pore diameter
σ = surface tens. cof.
ρ = mass density
v^i = impact velocity]

Figure 88. — Impact Droplet Extrusion

a. Droplet deformation upon impact.

b. Air drag on droplets attached to the screens.

c. Influence of droplet velocity on initial movement parallel to screen (bounce or roll).

Droplet behavior upon impact with the screens can be estimated by a Weber number in the form

$$We = \rho \lambda \, u^2 \, (1 - \cos \theta)^2 / \sigma \tag{14}$$

Photographic data from eight different test conditions indicate that two basic phenomena occur as below when the droplets are stable just before impact:

a. Fragmentation: $We > 100$

b. Severe deformation: $We > 10$

Operation of a liquid/vapor separator is less efficient when the droplets deform. The photographic data indicate that when droplets deform, their residence time on the screen is often long enough so that they are impacted by subsequent drops. This perturbation to the deformed (usually oscillating) drop often results in fragmentation. The small fragments generally stick to the screen.

Air drag on attached droplets was studied by reviewing photographic data for drops stuck to the screens and drops slowly moving parallel to the screens. Cases where impact velocity was obviously influencing the droplet motion were not considered for this investigation.

A force comparison

$$f \lambda \lesseqgtr \left| \rho \lambda^3 \, g \cos (\beta - \theta_1) - c \lambda^2 \, \rho \, u^2 \cos \theta_2 \right| \tag{15}$$

was used to determine the appropriate value of C. Test results from II-A were used for f. Six data points for droplets that stuck, and moved with and against gravity, indicated that $C = 0.003$ was the best value for data correlation. The results here are consistent with the anomalous low C value obtained in Test II-A.

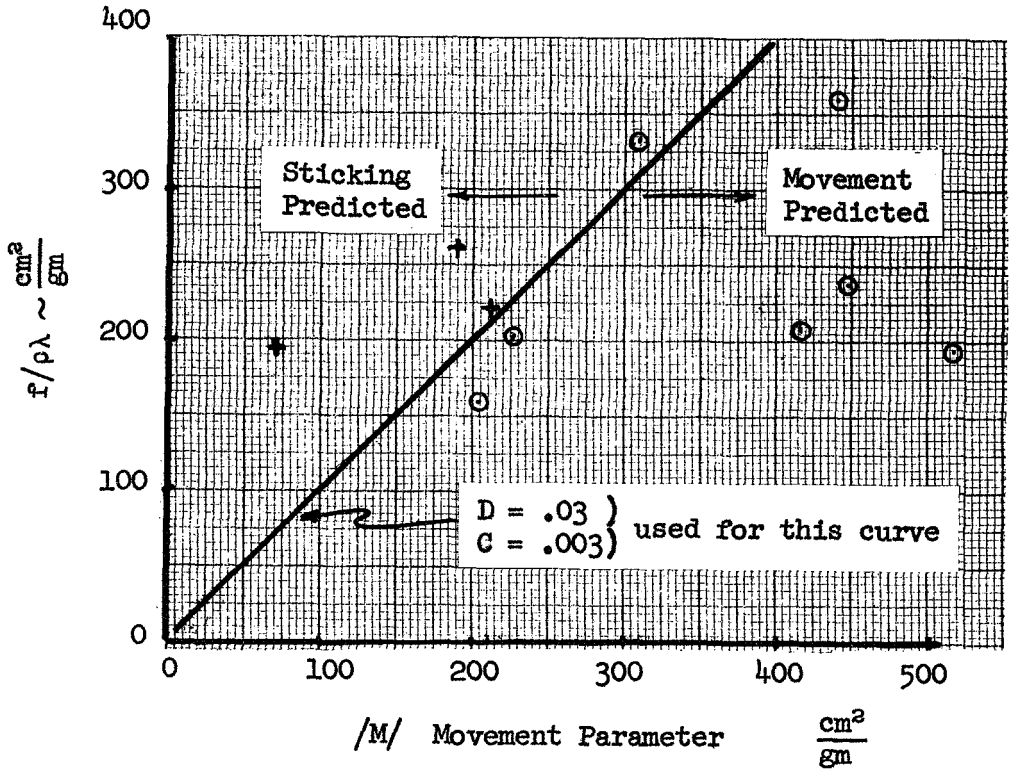
The point of incipient droplet motion after impact with the screens is determined by

$$f \lambda = \left| \rho \lambda^3 \, g \cos (\beta - \theta_1) - 1/2 D \lambda^2 \, \rho v^2 \cos \theta_1 - C \lambda^2 \rho u^2 \cos \theta_2 \right| \tag{16}$$

where D is a deformation energy factor, an attempt to account for loss of droplet kinetic energy upon impact. Figure 89 shows that with C = 0.003 and D = 0.03, a fair division of the data into regions of motion and nonmotion seems to be predictable.

A severe loss of kinetic energy is apparent in the majority of data analyzed. The droplets, in almost all cases, strike the screen, deform into a very flat, thin, pancake shape, and then collapse into spheroidal shapes as a result of surface tension forces. The deformation is usually oscillatory and generally persists for several cycles until it is damped by viscosity. Thus, for the range of impingement angles studied ($132 \geq \theta \geq 60$ degrees), only a very small portion (about 3%) of the droplet kinetic energy on impact was available for conversion into lateral motion.

Conclusions to be drawn from Test II-B are, in general, that droplet deformation should be suppressed when possible. The two main causes are high droplet velocity and large screen angle with the droplet incident path. By decreasing the screen angle, the large droplet velocities will be much less likely to cause droplet deformation and a larger fraction of kinetic energy can be converted to lateral droplet motion on the screen.



Legend:

⊙ = Movement

\+ = Sticking

The predictive equation is

$$f\lambda < \left| \rho \lambda^3 g \cos(\beta - \theta_1) - 1/2\, D \rho \lambda^2 v^2 \cos\theta_1 - c \lambda^2 \rho u^2 \cos\theta_2 \right|$$

Figure 89. — Droplet Movement on Screens

Confirmation of the gravity-sensitivity predictions is considered good, especially since the droplet motions investigated were both with and against the gravity vector. Gravity is quite important when D is low as was the case in these tests. For shallow screen angles and higher D values the gravity effect may easily be overcome by the inertia term $1/2\ D\ \lambda^2\ \rho\ v^2\ \cos\ \theta_1$.

Data Correlation

The experimental data were correlated by evaluation of the constants of proportionality and undetermined coefficients in the equations. Determination of the coefficients was performed by intuitively selecting a best fit of the test data to the predictive equations.

In general, the experiments verified the basic form of the predictive equations. The data were useful in completing unknown portions of the model and eliminating others.

Impact on the Analytical Model

Droplet motion on the screen was found to be almost exactly as predicted insofar as adhesion is concerned. The coefficient f was found to be a function of the screen mesh, as anticipated, and the normal force, as suspected, did not influence droplet motion.

Deformation and fragmentation occurred at Weber numbers somewhat higher than expected, but the Weber number does seem, as anticipated, to be a good indicator of these phenomena.

Initially, the drag force exerted by the air flow on the droplet was omitted from the analytical model. Testing showed its effect to be present, but not as significant as predicted.

Another unspecified phenomenon was the loss of kinetic energy of impacting drops due to deformation. Transference of all the energy available before impact into motion parallel to the screen does not occur. Addition of a correction factor was necessary to achieve proper correlation. In reality this factor is undoubtedly a function of the impact Weber number; however, no specific relationship has been derived here.

The following conclusions can be stated:

a. The factor n (number of screen pores covered by the droplet) can be algebraically eliminated from the predictive equations and is, therefore, not an important parameter.

b. Droplet size is not important in determining penetration due to impact.

c. Gravity forces are small by comparison with the other forces where droplet penetration is concerned.

d. Forces normal to the screen have a negligible effect on droplet resistance to lateral motion.

e. Screen coating is critical to the effectiveness of an operating separator.

f. Penetration and droplet sticking occurred frequently enough during these tests so that unqualified success of such a system cannot be assured.

Further improvements could be made by development of a droplet generator that would discharge single drops over a wider range of sizes and velocities than were available in these tests. In general, the droplet size for the combined effects tests was 0.1 → 0.4 cm in diameter. Smaller drops would have been desirable in certain situations. Droplet velocities ranged from 100 cm/sec to 250 cm/sec. Extension of this range from 0 to 500 cm/sec would have been useful.

Recommendation for Further Experimental Evaluation

Laboratory experiments. —

Screen separator: Further laboratory experiments at the level of the present tests are not suggested except as might be desirable to aid in the application of the present model to particularized equipment configurations such as that represented by the circular channel and conical screen. Additional testing might also be justified if the model were to be modified to include the mechanism of hydrophilic screen absorption of the separated liquid.

Vortex separator: Laboratory testing of the vortex separator would be useful and should be accomplished prior to low-gravity testing. The laboratory tests are useful in checkout of the analytical model and for determination of unforeseen testing difficulties and, as such, are highly recommended.

Reduced-gravity experiments. —

Screen separator: Laboratory testing has shown that the effect of gravity on droplet penetration through screens is negligible compared with the other forces involved. The following discussions, therefore, are limited to investigations of the effect of gravity on droplet motion along the screen surface.

Drop tower tests: The usually objectionable feature of short, low-g periods available during drop tower tests is not a problem for the screen separator. Sufficient duct length and air flow equipment could be a serious problem and could limit productive drop tower

tests to cases without air flow. Such data would be useful, and investigation into drop tower testing of this system is recommended.

KC-135: Aircraft tests for low-g conditions would be able to include the air flow requirement much more easily than the drop tower tests. From many points of view the aircraft is an ideal test bed for the screen experiments.

Orbital experiments: Most, if not all, the essential data concerning low-g effects on the screen separator can probably be obtained by means other than the orbital flights.

Vortex separator: Because of the steady-state nature of operation of the vortex separator system, long-term testing (several minutes) is required. Due to setup time and the desirability of changing flow conditions during the tests, orbital experiments are thought to be the only fully satisfactory way to evaluate this system.

REFERENCES

1. Burton, K.; Evans, E., Burnett, J.; Analytical Model Report 4 "Inertial Separation," 2nd Issue, NAS1-8494, March 1970.

2. Landau, L. D.; Lifshitz, E. M.: Fluid Mechanics. Addison Wesley, 1959.

3. Bradshaw, R. D.; et al.: Thermodynamic and Fluid Dynamic Studies of Cryogenic Propellants. GDC-ERR-AN-1333, Convair division of General Dynamics, December 1968.

4. Hollister, M. P.: LMSC A665481. 1964.

5. Olcott, T. M.; Lamparter, R. A.: Evaluation Testing of Zero Gravity Humidity Control System. NASA CR-66543, October 1967.

6. Smith, J. M.; Cima, R. M.; Li, Yi-Sheng: The Application of Hydrophilic and Hydrophobic Surfaces for Phase Separation in a Low-G Environment. Paper 16, Symposium for Fluid Mechanics and Heat Transfer Under Low Gravity, June 1965.

7. Serebryakov, V. N.: Control of the Dynamics of a Two-Phase Liquid-Gas Weightless Medium with the Aid of Surface Effects. Kosmicheskiye Issledovaniya, vol. 4, no. 5, 1966 (NASA TT F-469, May 1967).

8. Booth, F. W.: Research on a Zero Gravity Air Separator. NASA-LWP-458, August 1967.

9. Soo, S. I.: Fluid Dynamics of Multiphase Systems. Blaisdell Publishing Company, Massachusetts, 1967.

10. Taylor, G. I.: The Boundary Layer in the Converging Nozzle of a Swirl Atomizer. Quarterly Journal of Mechanics and Applied Mathematics, vol. 3, part II, 1950.

11. Cooke, J. C.: On Pohlhausen's Method with Application to a Swirl Problem of Taylor. Journal of Aeronautical Sciences, July 1952.

12. Lawler, M. T.; Ostrach, S.: A Study of Cyclonic Two-Fluid Separation. AFOSR 65-1523, June 1965.

13. Burnett, J. R.: Experimental Test Report 4A: Inertial Separation - Case 1, Screen. NAS1-8494, March 1970.

ANALYTICAL MODEL NO. 5 – "CONVECTION HEAT TRANSPORT"

The nomenclature used in the discussion of and the calculations for the convection heat transport model is listed in table 31.

DESCRIPTION OF THE MODEL

The analytical model which has been developed describes the characteristics of convective heat transport in a fluid stream (ref. 1). The design of the analytical system is such that a focus is placed on the change in these characteristics in the transition from stable to unstable conditions within the fluid stream. The effect of inertial acceleration is explicitly examined throughout.

The model considers the effects on the predicted behavior within the system resulting from variations in such parameters as:

a. Gravitational field strength and orientation (the local-g vector).

b. Stream velocity.

c. Heat input/output rate.

d. Fluid density.

e. Stream profile characteristics.

f. Duct dimensions.

Table 31. — Convection Heat Transport Model Nomenclature

d	duct height, plate separation
L	plate length
g	magnitude of inertial acceleration
x	flow direction
z	direction normal to flow
α	coefficient of thermal expansion
$\chi = \frac{K}{\rho c_p}$	thermometric conductivity
ν	kinematic viscosity
ΔT	temperature difference between plates
$\vec{\beta} = \nabla T_o$	initial temperature gradient
$\rho, p, \vec{v}, T$	instantaneous density, pressure, velocity, and temperature of air stream
$\rho_o, p_o, \vec{v}_o, T_o$	mean values of density, pressure, velocity, and temperature of air stream
u_o	stream velocity
$Re = \frac{u_o d}{\nu}$	Reynolds number
$Pr = \frac{\nu}{\chi}$	Prandtl number
$Gr = \frac{g\alpha d^3 \Delta T}{\nu^2}$	Grashof number
$R\ell = Pr \cdot Gr$	Rayleigh number

The model is principally designed to provide information in an area of the phenomena associated with convective heat transport where existing information is most wanting and, in many instances, an area of considerable concern to the equipment designer, namely, the conditions involved in the transition from convective heat transport to conductive heating and stream stratification under varying "gravitational environments." This model has relevance to the convective mechanisms of the humidification/dehumidification problem (Analytical Model No. 2) and the interaction of multicomponent diffusion and heat transfer characteristics. For instance, the behavior of the gas phase of this process will depend strongly on the convective stabilities or instabilities due to adverse temperature gradients. The present model will, therefore, aid in developing design criteria for processes requiring laminar flow or special heat transfer properties as does

the humidification/dehumidification process. The model should help in solutions to the design of such items as equipment packages as related to their thermal control and heating chambers such as might be found in waste management and oxygen recovery systems. The information made available through the exploitation of this model supplements that produced by Ballinger in an earlier phase of this program (ref. 2).

General Approach

Transition from thermal diffusion to convective thermal energy transport (when both processes are present) is dependent on the inertial field (e.g., gravity) by the character of natural convection. When forced fluid motion is not present and an adverse temperature gradient exists, the stability is determined by the Rayleigh number only; the transition is from thermal diffusion to natural convection. With forced fluid motion, the Reynolds number becomes important and the stability is associated with natural and forced convection exchange. In other words, instability occurs at the minimum temperature gradient at which a balance can be steadily maintained between the kinetic energy dissipated by viscosity (momentum) and the internal energy released by the buoyancy forces of the fluid.

The equations used to describe thermal instability are derived from the general Navier-Stokes equation, continuity equation, and the energy equation. These are

$$\frac{\partial \vec{v}}{\partial t} + (\vec{v} \cdot \nabla)\vec{v} = -\frac{1}{\rho}\nabla p + \nu \nabla^2 \vec{v} + \vec{g} \tag{1}$$

$$\nabla \cdot \vec{v} = 0 \tag{2}$$

$$\frac{\partial T}{\partial t} + \vec{v} \cdot \nabla T = \chi \nabla^2 T \tag{3}$$

where ρ, p, $\vec{v}$ and T are functions of location and time. The stability model is based on a perturbation analysis wherein these instantaneous variables are assumed to be in the form

$$\vec{v} = \vec{v}_o + \vec{v}'$$

$$p = p_o + p'$$

$$\rho = \rho_o + \rho'$$

$$T = T_o + \theta$$

where the variations (primed quantities) are assumed small compared with the time independent, mean quantities. ρ_o is assumed a constant since we are not assuming fluid columns of great height. The Boussinesq approximation is used for specifying ρ' is

$$\rho' = \left(\frac{\partial \rho_o}{\partial T}\right)_p \theta = -\rho_o \alpha \theta$$

where α is the coefficient of thermal expansion (volume). p_o is given by the hydrostatic equation, $p_o = \rho_o \vec{g} \cdot \vec{r}$ + constant. Therefore, the term $\frac{\nabla p}{\rho}$ in equation (1) can be written as

$$\frac{\nabla p}{\rho} = \frac{\nabla p_o}{\rho_o} + \frac{\nabla p'}{\rho_o} - \frac{\nabla p_o}{\rho_o^2}\rho' - \cancel{\frac{\nabla p' \rho'}{\rho_o^2}}^{0}$$

Second-order perturbation term

$$= \vec{g} + \frac{\nabla p'}{\rho_o} + \vec{g}\,\alpha\theta$$

The terms $(\vec{v}\cdot\nabla)\vec{v}$ and $\vec{v}\cdot\nabla T$ can be similarly simplified and after neglecting second-order perturbation terms and noting that the mean quantities satisfy steady-state equations (1) and (3), these equations reduce to

$$\frac{\partial \vec{v}'}{\partial t} + (\vec{v}_o \cdot \nabla)\vec{v}' + (\vec{v}' \cdot \nabla)\vec{v}_o = \frac{-\nabla p'}{\rho_o} + \vec{g}\,\alpha\theta + \nu\nabla^2\vec{v}' \tag{4}$$

$$\nabla \cdot \vec{v} = 0 \tag{5}$$

$$\frac{\partial \theta}{\partial t} + \vec{v}_o \cdot \nabla\theta + \vec{v}' \cdot \vec{\beta} = \chi\nabla^2\theta \tag{6}$$

where $\vec{\beta} = \nabla T_o$, the initial temperature gradient.

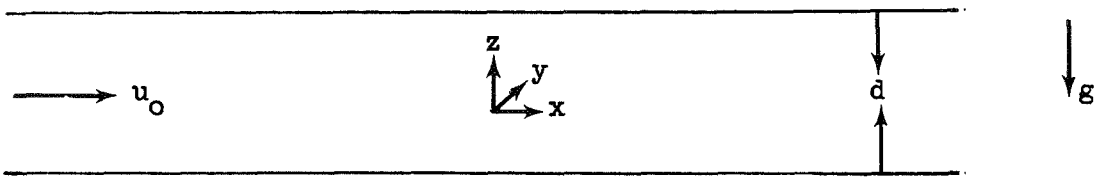
This general system of five linear perturbation equations is simplified by neglecting derivatives of the initial velocity, i.e., assumed $\vec{v}_o$ constant. The term $(\vec{v}\cdot\nabla)\vec{v}_o$ in equation (4) is, therefore, neglected. In addition, the pressure perturbation can be eliminated. Taking the curl of equation (4) once and twice yields

$$\frac{\partial \nabla}{\partial t} \times \vec{v}' + (\vec{v}_o \cdot \nabla)\nabla \times \vec{v}' = \alpha\nabla\theta \times \vec{g} + \nu\nabla^2(\nabla \times \vec{v}') \tag{7}$$

$$\frac{\partial}{\partial t}\nabla^2\vec{v}' + (\vec{v}_o \cdot \nabla)\nabla^2\vec{v}' = \nu\nabla^4\vec{v}' - \alpha\left[\vec{g}\nabla^2\theta - (\vec{g}\cdot\nabla)\nabla\theta\right] \tag{8}$$

The Model Defined

The problem to be considered is flow between two infinite parallel plates,



with a finite length, L, having an adverse temperature gradient.

Neglecting the gradient of the initial, steady-flow temperature in the x direction, only the z component of equation (8) is required. In addition

$$\vec{v}_o = v_x = u_o$$

$$\vec{g} = g_z = -g$$

Therefore, taking the z component of equation (8) and rewriting equation (6) we have,

$$\frac{\partial}{\partial t}\nabla^2 v_z' + u_o \frac{\partial}{\partial x}\nabla^2 v_z' = \nu \nabla^4 v_z' + g\alpha\left(\nabla^2 - \frac{\partial^2}{\partial z^2}\right)\theta \tag{9}$$

$$\frac{\partial \theta}{\partial t} + u_o \frac{\partial \theta}{\partial x} + v_z' \beta_z = \chi \nabla^2 \theta \tag{10}$$

where

$$\nabla^2 \equiv \left(\frac{\partial^2}{\partial x^2} + \frac{\partial^2}{\partial y^2} + \frac{\partial^2}{\partial z^2}\right)$$

$$\beta_z \equiv \frac{\partial T_o}{\partial z}$$

$T_o \equiv$ initial temperature field established by conduction only.

Stability is established by using a normal mode analysis and solving for the marginally stable state (ref. 3).

$$\frac{\partial \nabla^2}{\partial t} v_z' + u_o \frac{\partial}{\partial x}\nabla^2 v_z' = \nu \nabla^4 v_z' + g\alpha\left(\nabla^2 - \frac{\partial^2}{\partial z^2}\right)\theta \tag{11}$$

$$-\frac{1}{\beta_z}\frac{\partial\theta}{\partial t}-\frac{u_o}{\beta_z}\frac{\partial\theta}{\partial x}+\frac{\chi}{\beta_z}\nabla^2\theta=v_z' \tag{12}$$

Equations (11) and (12) may be solved for the temperature perturbation,

$$\left(\frac{\partial\nabla^2}{\partial t}+u_o\frac{\partial}{\partial x}\nabla^2-\nu\nabla^4\right)\left(\frac{\chi}{\beta_z}\nabla^2\theta-\frac{u_o}{\beta_z}\frac{\partial\theta}{\partial x}-\frac{1}{\beta_z}\frac{\partial\theta}{\partial t}\right)=g\alpha\left(\nabla^2-\frac{\partial^2}{\partial z^2}\right)\theta \tag{13}$$

The problem is that of uniform translation with diffusion of the perturbation quantity θ; therefore, a pseudo-time variable, characteristic time, is defined,

$$\frac{\partial}{\partial\eta}\equiv\frac{\partial}{\partial t}+\nu_o\frac{\partial}{\partial x}$$

Equation (13) becomes,

$$\left(\frac{\partial}{\partial\eta}\nabla^2-\nu\nabla^4\right)\left(\frac{\chi}{\beta_z}\nabla^2\theta-\frac{1}{\beta_z}\frac{\partial\theta}{\partial\eta}\right)=g\alpha\left(\nabla^2-\frac{\partial^2}{\partial z^2}\right)\theta \tag{14}$$

The normal mode analysis is used to reduce the partial differential equation to an ordinary sixth-order equation,

$$\theta=\theta(x)\,e^{i\frac{m\pi}{d}y}\sin\frac{n\pi z}{d}\,e^{p\eta}$$

$$m\geq 0;\ n=1,2,3,\ldots;\ p\geq 0$$

The z functional, $\sin\frac{n\pi z}{d}$, was determined by the boundary condition that $\theta=0$ at $z=0,\ d$. It is also necessary to assume that $\beta_z\equiv\beta(x)$ a function of x only.

Equation (14) becomes,

$$\left(p\frac{d^2}{dx^2}-pk^2-\nu\frac{d^4}{dx^4}+2\nu k^2\frac{d^2}{dx^2}-\nu k^4\right)\left(\frac{\chi}{\beta}\frac{d^2\theta}{dx^2}-\frac{1}{\beta}(\chi k^2+p)\theta\right)=g\alpha\left(\frac{d^2\theta}{dx^2}-k_y^2\theta\right) \tag{15}$$

where

$$k^2\equiv\frac{m^2\pi^2}{d^2}+\frac{n^2\pi^2}{d^2}$$

$$k_y^2 \equiv \frac{m^2 \pi^2}{d^2}$$

$$k_z^2 \equiv \frac{n^2 \pi^2}{d^2}$$

choose $\beta = \beta_o$ a constant,

$$\beta_o = -\frac{\Delta T_o}{d}$$

Equation (15) reduces to,

$$\frac{d^6\theta}{d\lambda^6} + A_4 \frac{d^4\theta}{d\lambda^4} + A_2 \frac{d^2\theta}{d\lambda^2} + A_o\, \theta = 0 \qquad (16)$$

where

$$A_4 = -\left[3a^2 + \sigma\, Re\, \epsilon\, (1+Pr)\right]$$

$$A_2 = 3a^4 + 2\,\sigma\, a^2\, Re\, \epsilon\,(1+Pr) + \sigma^2\, Re^2\, Pr\, \epsilon^2 - R\ell$$

$$A_o = -\left[a^6 + \sigma\, a^4\, Re\, \epsilon\,(1+Pr)\, \sigma^2\, a^2\, Re^2\, Pr\, \epsilon^2 - R\ell\, a_y^2\right]$$

$$\sigma \equiv p\frac{L}{u_o}$$

$$\lambda \equiv \frac{x}{d},\ 0 \le \lambda \le \frac{L}{d}$$

$$a^2 \equiv k^2 d^2$$

$$a_y^2 \equiv k_y^2\, d^2$$

$$Re \equiv \frac{u_o d}{\nu}\ \text{Reynolds number}$$

$$R\ell \equiv \frac{g\,\alpha\,(\Delta T)\, d^3}{\chi\,\nu}\ \text{Rayleigh number} \equiv Gr \cdot Pr$$

$$Pr \equiv \frac{\nu}{\chi}\ \text{Prandtl number}$$

$$\epsilon \equiv \frac{d}{L}\ \frac{\text{height}}{\text{length}}\ \text{ratio}$$

For marginal stability take θ periodic in λ,

$$\theta \sim \sin a_x \lambda \tag{17}$$

Equations (16) and (17) define the Rayleigh number in terms of other non-dimensional parameters,

$$R_\ell = \frac{a_T^2 \left\{ a_T^4 + \sigma \, Re \, \epsilon \left[(1+Pr) a_T^2 + \sigma \, Re \, \epsilon \, Pr \right] \right\}}{(a_T^2 - a_z^2)} \tag{18}$$

$$a_T^2 \equiv a_x^2 + a^2$$

$$a_z^2 \equiv k_z^2 d^2$$

The "σ" is a growth parameter that represents the change in the perturbation magnitude over one transit time (e^σ).

For Re = 0 or large $\frac{L}{d} \gg 1$ (which implies $\epsilon \to 0$), equation (18) is consistent with the equation for no flow stability (ref. 2). A plot of equation (18) for fixed Re, Pr, and ϵ is given in figure 90. The meaning of equation (18) and figure 90 is this: for all Rayleigh numbers less than that given by equation (18), disturbances with the wave number a_T will be stable. These disturbances will become marginally stable when the Rayleigh number equals the value given by equation (18); when it exceeds the value given by equation (18), the same disturbances will be unstable. The critical Rayleigh number, R_{ℓ_c}, for the onset of instability is, therefore, determined by finding the minimum value for Rayleigh number versus wave number (i.e., at $\frac{\partial R_\ell}{\partial a_T^2} = 0$).

$$\frac{\partial R_\ell}{\partial a_T^2} = \frac{2a_T^6 + \left(\sigma Re\epsilon(1+Pr) - 3a_z^2\right) a_T^4 - \left(2\sigma \, Re\epsilon(1+Pr) a_z^2\right) a_T^2 - \left(\sigma^2 Re^2 \epsilon^2 Pr a_z^2\right)}{\left(a_T^2 - a_z^2\right)^2}$$

At R_{ℓ_c},

$$2\tilde{a}_T^6 + \left(\sigma Re\epsilon\,(1+Pr) - 3a_z^2\right)\tilde{a}_T^4 - \left(2\sigma Re\epsilon(1+Pr) a_z^2\right)\tilde{a}_T^2 - (\sigma^2 Re\epsilon^2 Pr a_z^2) = 0 \tag{19}$$

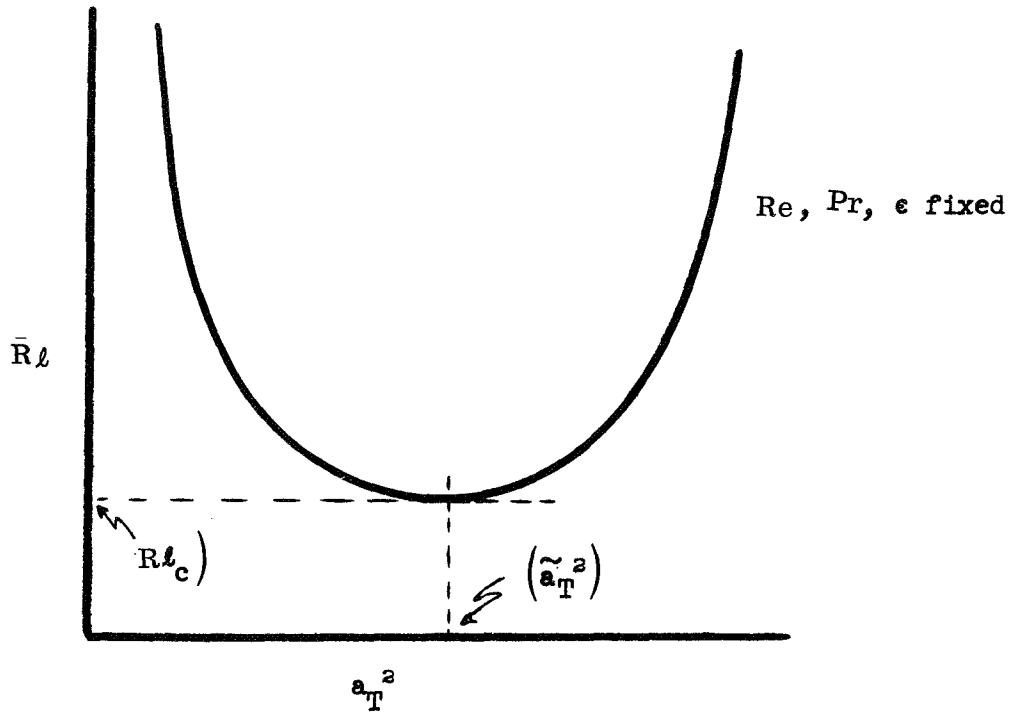


Figure 90.- Stability Defined-Critical Rayleigh Number

Using $\tilde{a}_T^2$, the real solution to equation (19), in equation (18) yields,

$$R\ell_c = \frac{\tilde{a}_T^2\left[\tilde{a}_T^4 + \sigma Re\epsilon\,(1+Pr)\,\tilde{a}_T^2 + \sigma^2 Re^2\epsilon^2 Pr\right]}{\left(\tilde{a}_T^2 - a_z^2\right)} \tag{20}$$

$R\ell_c = f(\sigma Re\epsilon)$ for constant Pr.

Figure 91 illustrates the dependence of critical Rayleigh number, the stable/unstable boundary, on the Reynolds number height-to-length ratio product.

The intercept of the curve is easily found by solving equation (19) for $\tilde{a}_T^2$ at Re = 0 and calculating $R\ell_c$ from equation (20). A value of $R\ell_c = 657$ is found. For the no-flow condition or infinite length section, the time for development of the instability is infinite; therefore, the critical Rayleigh number or adverse temperature gradient is low. As flow increases or the section length decreases, the time available for instability development is reduced and the critical Rayleigh number is increased.

The model has direct relevance to the diffusion/convection mechanisms described by analytical model 2, and thus should be explicitly treated in the future development of the two models.

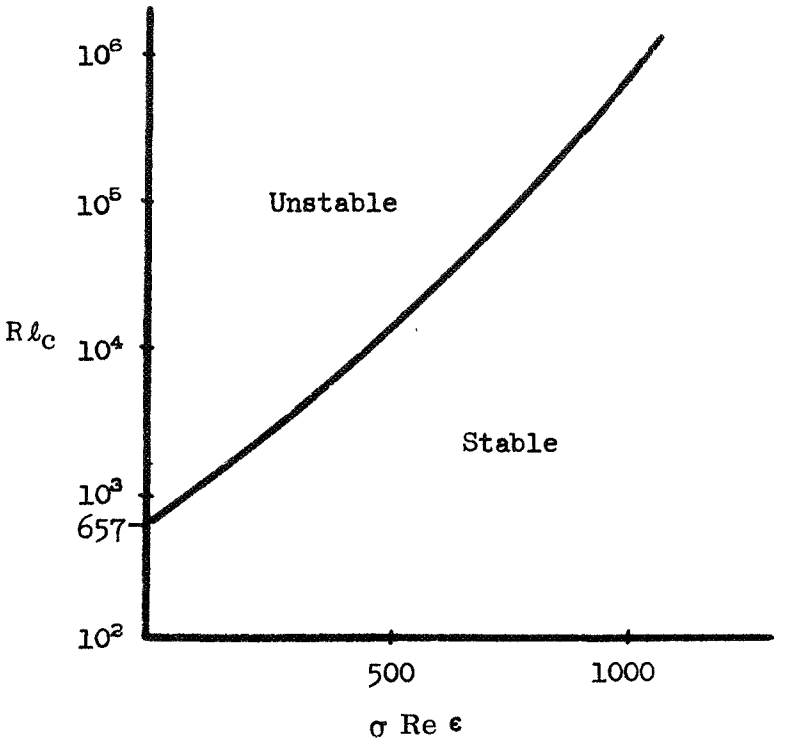


Figure 91. — Stability Boundary

Physical Description of Stability/Instability and Higher Order Transitions

The stability analysis developed in the previous section pertains to the boundary between forced convection/conduction heat transport and natural convection/forced convection heat transport. The forced convection is the primary flow in the system, figure 92. The natural convection is the secondary flow superimposed on the primary flow. The physical character of the stable/unstable boundary is the specification of the onset of laminar, steady (in time) secondary flow, natural convection, figure 93.

Both the stable forced convection and the unstable, laminar natural and forced convection are steady flows in time (no local time dependence). Region I (see figure 94) is defined as the stable forced convection/conduction flow region; Region II is defined as the unstable, but steady in time, laminar natural/forced convection flow region. The stability is only relevant to the ability of thermal diffusion (i.e., conduction) to satisfy the heat transport requirements in the adverse temperature gradient environment. When this is insufficient, then unstable convective or secondary flow appears to provide additional thermal energy transport.

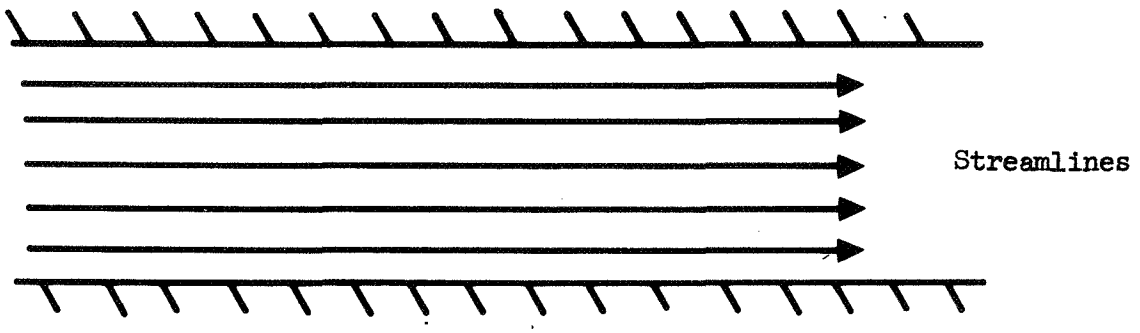


Figure 92. — Streamlines [for stable, forced convection primary flow (steady in time)]

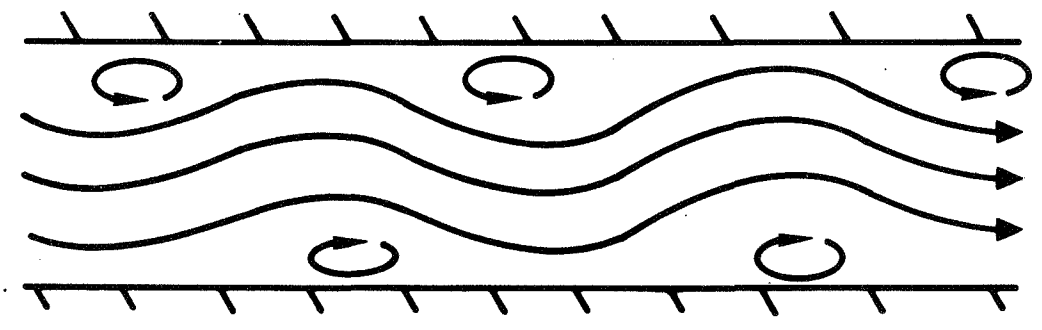
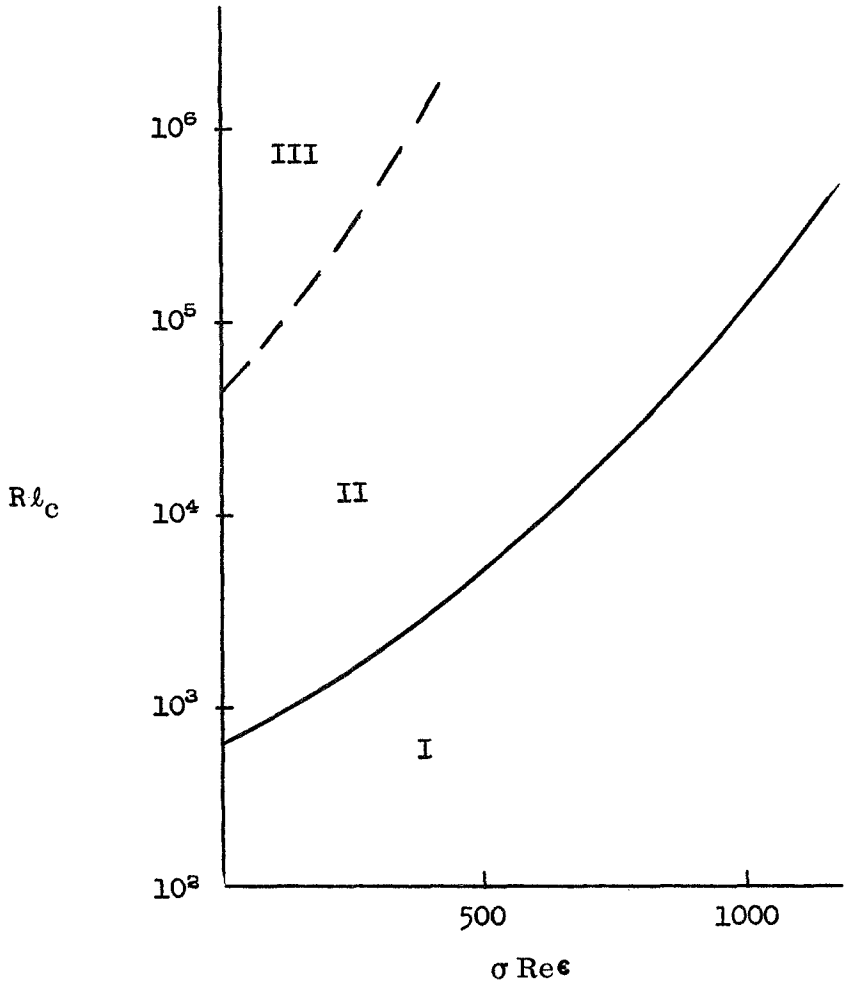


Figure 93. — Streamlines and Stationary Vortices [for unstable, natural and forced convection, primary plus secondary flow (steady in time)]

As the adverse temperature gradient increases, the vortex strength and distribution increases until the entire flow is populated with vortices and they begin to statistically become independent from the bulk fluid motion. At this point, a second transition occurs, the development of turbulent, unsteady natural and forced convection. Figure 95 illustrates the multiple vortices and their motion relative to the stationary observer (the vortices are convected past the observer yielding a local unsteady temporal character).

Region III is, therefore, defined as unstable, unsteady in time, turbulent natural and forced convection. The title turbulent is used since the demarcation from Region II to Region III specifies the onset or development of turbulent eddies and rapidly degenerates into developed turbulence.

The Rayleigh number ratio for specification of the Region I/II boundary and the Region II/III boundary should be essentially independent of Reynolds number provided the primary flow is well below the critical Reynolds number for laminar, turbulent transition. This is the situation for the major portion of the Region I/II boundary ($Re \lesssim 1000$). The implication is that the natural convection laminar-to-turbulent



Region	Flow Behavior		Heat Transfer Mechanism
	Spatial	Temporal	
I	Stable	Steady, laminar	Thermal conduction and forced convection
II	Unstable	Steady, laminar	Natural and forced convection
III	Unstable	Unsteady, turbulent	Natural and forced convection with turbulent eddy diffusion

Figure 94. — Stability Boundaries of Natural Convection/ Forced Convection System

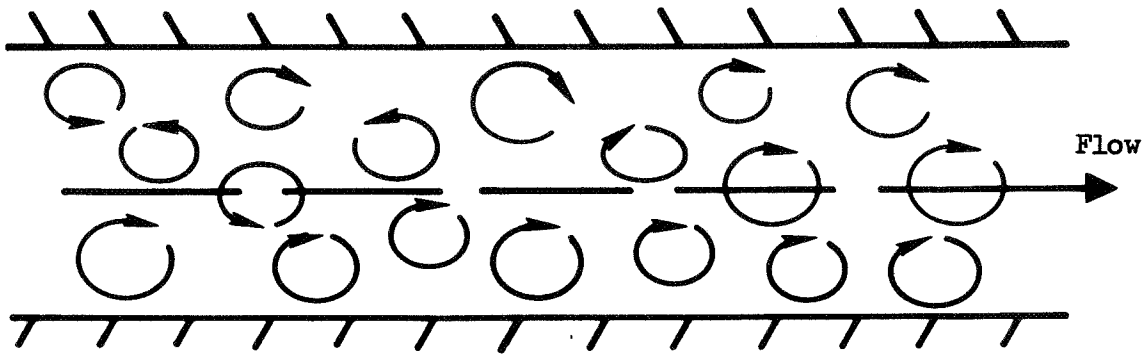


Figure 95. — Vortex Distribution (being convected past an observer illustrating unsteady, unstable, natural and forced convection)

transition is only a function of the adverse temperature gradient environment and that, for nearly uniform velocity profiles, the interior of the fluid is not mechanically coupled to the boundaries (e.g., entering laminar primary flow); therefore, thermal energy transport mechanisms occur freely including the laminar-to-turbulent natural convection of secondary flow transition. The time required for stability degeneration of the laminar natural convection and the turbulent natural convection are similar. This is to say that the shape of the Region I/II boundary is approximately the same as the Region II/II boundary only the intercept at $Re_\epsilon = 0$ is different (see figure 94). The result is a second transition curve, which is analytically similar to the Region I/II boundary (stable, unstable limit in figure 91) but displaced upward in Rayleigh number.

The preceding several paragraphs describe the three distinct regions on the plot of Reynolds number versus Rayleigh number (figure 94). These in turn are separated by two transition boundaries, one between stable and unstable laminar flow and the other between steady and unsteady flow. The Re = 0 intercept for the former curve has already been stated as $R\ell_c = 657$. The intercept for the turbulent transition has been experimentally found to be about 4×10^4 (ref. 4). The shape of the laminar-to-turbulent transition boundary is arbitrarily drawn based on the preceding similarity discussion.

The two transition intercept points (i.e., Re = 0) of figure 94 have been studied extensively, both analytically and experimentally (ref. 3, 4, 5). Below $R\ell = 657$, heat flows only by conduction (thermal diffusion). As the Rayleigh number is increased, convection currents are set into motion, and the overall unit conductance (heat transfer coefficient) increases. The motion is laminar but unstable until the Rayleigh number reaches about 4×10^4 where the particle motion becomes stochastic in time. In the laminar region the motion is cellular and looks somewhat like a honeycomb. These regions of local circular motion are commonly referred to as Benard cells and in the first instance after transition are hexagonal in shape. Further increase in $R\ell$ produces cells of smaller sizes and various shapes. A thorough treatment of this phenomenon is found in reference 3.

Because Region II is temporally stable, the insertion of a velocity-sensitive device into the flow stream will not produce a signal. Only methods using interferometry, contrast photography, or smoke streams are useful in visualizing the spatial distribution in the laminar Region II. In Region III, however, point source probes, such as hot-wire anemometers and thermistors, can be used to measure velocity or temperature fluctuations.

THE COMPUTER PROGRAM

A computer program was used for the numerical solutions required in the determination of $R\ell_c$ and the stability boundary. A CDC 6400 library routine, which finds roots to general polynomial equations, was used to find the real and physically reasonable root to equation (19). The result was used in equation (20) to specify the critical Rayleigh number.

It was not considered necessary or particularly relevant to attempt to construct a simulation model at this point at least.

APPLICATION TO LSS DESIGNS

The generalized nature of the analytical model provides a relatively high probability that the model can be directly applied to the development of several LSS design approaches. Table 32 identifies examples of the type of LSS equipment which, potentially at least, will be so designed that the model can be profitably applied in the analysis of primary or "on-design" modes of operation. However, because of the model being concerned with the transition between two operating regions, the model certainly has utility in the assessment of gravity effects on "off-design" or marginal performance conditions.

The major application of the analytical model will be in the design of those systems where heat transport by convective mechanisms is important. As has been pointed out previously, this model has a direct relevance to the diffusion/convection mechanisms treated in analytical model 2 and the humidification/dehumidification process. Most likely simultaneous consideration of the two models is needed to aid the designer of humidity-control equipment. In this problem the three parameters of importance will be mixture quality, temperature, and flow velocity. Simultaneous use of the two models would provide information concerning a prime variable, like heat transfer rate or condensation rate, by using temperature and velocity data in this model and quality and velocity data in model 2. In addition, both models predict medium behavior in reduced-gravity situations.

Table 32. — Examples of LSS Equipment Designs for which the Analytical Model has Relevance

Equipment Type by Degree of Relevance by Mode / LSS Function	Model Relevance		
	Primary Modes		Off-Design
	A*	B	
Oxygen Supply & Recovery		1**, 8, 4-10	21-36
Water Reclamation		40	46
Humidity Control		61-63	
Environmental Temperature Control	(***)	(***)	(***)
Sanitation & Hygiene	67,68, 70-73, 75		82

* Degree of relevance: A implies a high degree of relevance both as to similarity of the model to the equipment processes under design, combined with a high probability that the process will be extended into similar designs in updated systems; B implies a lower degree of similarity and/or probability of extension to similar designs.

** Equipment type identified by LSS equipment reference number.

*** Such items as cabin air temperature control including cabin air as a heat sink for equipment cooling are not covered under this contract.

EXPERIMENTAL EVALUATION

Requirements

An evaluation of the accuracy of the predictive aspects of the analytical model should include the following observations against each condition in a set of steady-state conditions:

a. Flow rate (mean velocity).

b. Temperature profile.

c. Velocity profile.

d. Locus of instability onset.

The design of the experiments should be such that they include an examination of the potential effect on the model parameters of various values of the local inertial acceleration vector, especially with respect to the effects on transitions from laminar to turbulent flow. Analysis of the experimental data may lead to altering and/or augmenting the analytical model in this area, especially with regard to arbitrarily chosen parameters in the marginal stability analysis.

Description of the Experiment

Major Goals

Primary. — To record the various flow patterns which develop in a ducted air stream due to an imposed temperature differential acting along the vertical axis of a horizontally oriented channel. The data collected against the observations are required in the evaluation and possible modification of an analytical model which has been developed to predict the stream characteristics operating in response to imposed heat loads.

Secondary. — To examine various experimental techniques, both for their applicability to laboratory test and for their potential in the design of apparatus and techniques for experimental tests to be performed under reduced gravity.

Principal Observations

Principal observations are as follows:

a. The experimental observations required for this evaluation were the characteristics of the stream flow patterns with respect to the degree of thermally induced (convection) turbulence present.

b. The experimental variables programmed against these observations included:

1. Air flow rate.

2. Temperature differential.

3. Channel orientation.

Criteria for Test Model Design

The test model and its supporting apparatus were designed under the following criteria:

a. A nonturbulent air stream be controllable in a range of channel velocities from essentially 0 to 4 ft/sec.

b. A temperature differential along the vertical axis of a horizontally oriented channel be controllable within a given area of the channel in a range of 0 to 50° C.

c. The temperature differential be attainable both positively and negatively with respect to the vertical axis.

d. The effect of the temperature differential on the flow patterns within the controlled area of the channel be measurable and recorded in real time and, insofar as practicable, be made visually observable.

e. The parameters defining channel flow conditions be accurately measured and precisely recorded.

f. Maximum utilization of previously employed test apparatus with minimum outlay for labor and material costs as dictated by the realities of the cost and schedule constraints imposed by the objectives of the NAS1-8494 contract.

Test Apparatus

The concepts relative to test apparatus requirements as illustrated in ETP 5 were only slightly modified by interactions between the on-going maturation of the analytical and accompanying test design studies. The apparatus used in this experiment is shown schematically by figure 96 and pictorially by figure 97.

Air stream control assembly. — The air stream control assembly, essentially unmodified from Test 2 and 3A, consisted of the following components:

a. Blower.

b. Plenum chamber.

c. Inclination pivot axis suspension.

d. Air flow control.

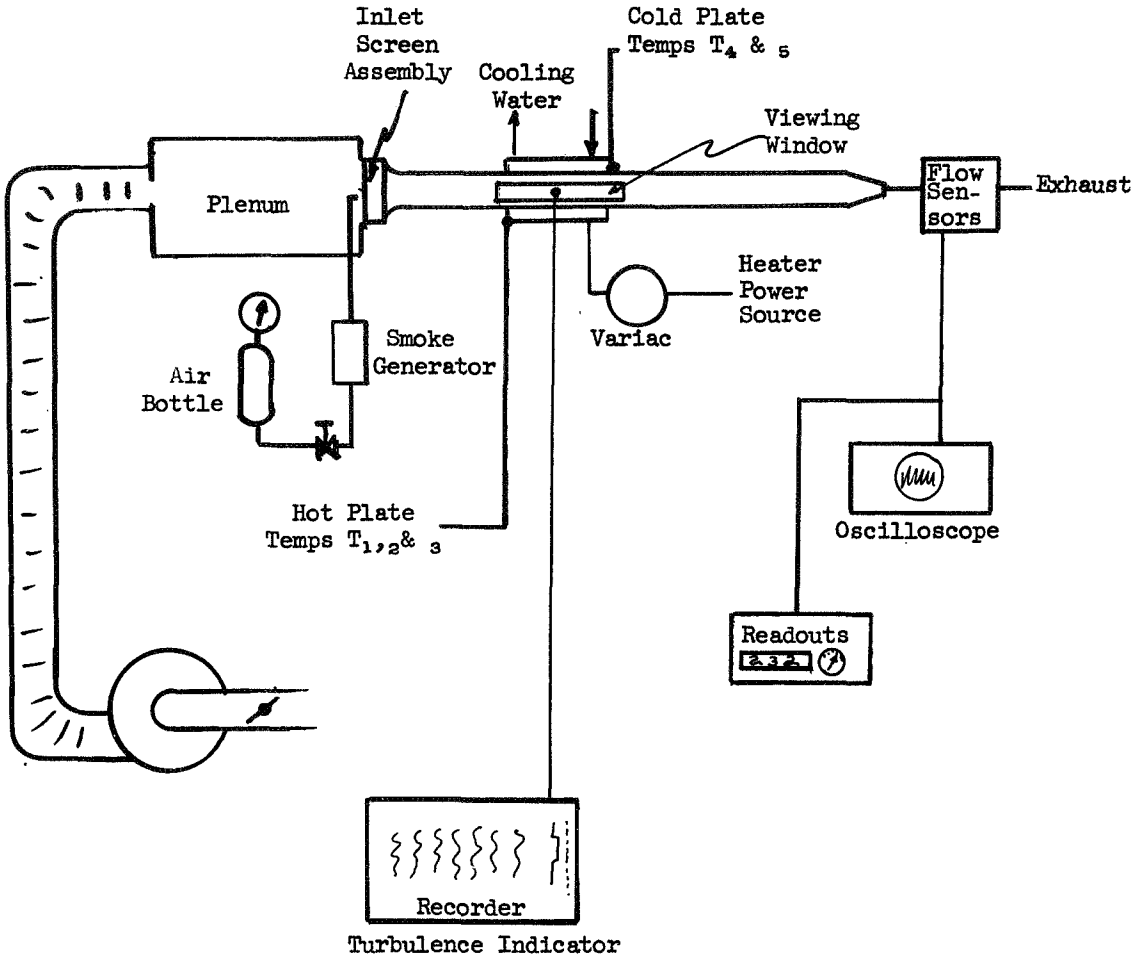
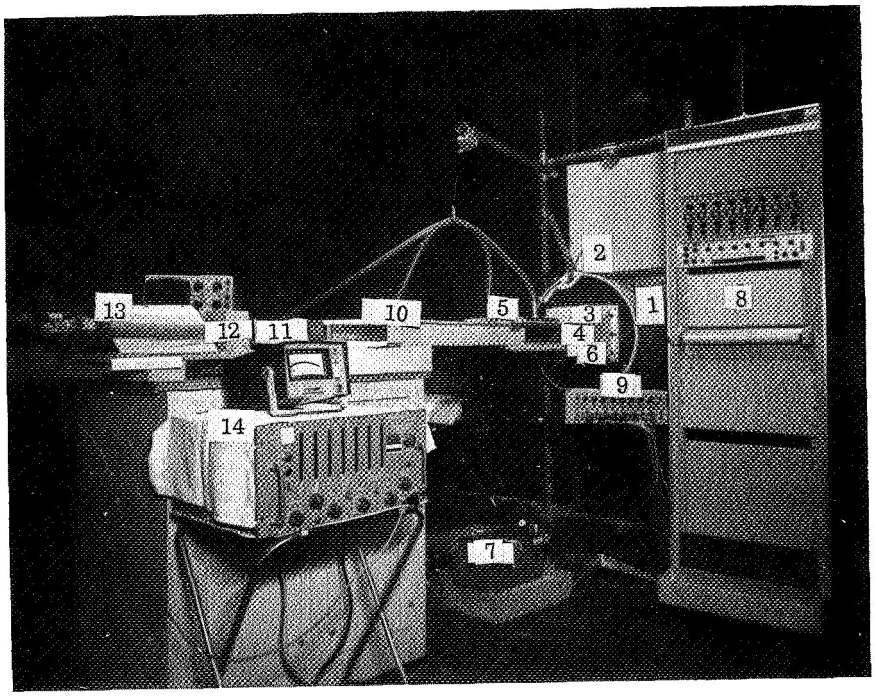


Figure 96. — Test Apparatus Schematic

The blower was a Dayton, Model 2C570, with a modified (restricted) single-side inlet.

The plenum chamber was fabricated from two metal drums attached end-to-end and coated with corrosion-resistant paint. The chamber volume was approximately 13.3 ft^3 over an inlet-to-outlet distance of approximately 5.7 feet. The exit end of the chamber was removable (typical drum top peripheral over center compression ring clamp). An adaptor section was incorporated into the exit end of the chamber to facilitate 1) channel inlet instrumentation mounting, 2) channel attachment, and 3) minimum disturbance in the transition from plenum to channel stream velocities.

The inclination pivot axis suspension was a simple double A-frame construction fabricated from 1.5-inch-diameter commercial pipe and Nu-Rail fittings. Air flow was provided in a controllable range from essentially 0 to 20 ft/sec in the 30 $in.^2$ cross section channel without exit flow meter impedance and 0 to 5 ft/sec with the exit impedance.



1. Plenum Chamber
2. Smoke Injector
3. Flow Channel Inlet
4. Viewing Window
5. Cold Plate and Cooling Water Well
6. Hot Plate with Heater and Insulation
7. Plate Temperature Readout
8. Turbulence Indicator Recorder
9. Turbulence Signal Amplifier
10. Lucite Converging Section
11. Flexible Duct Coupling
12. Stream Velocity Sensor Manifold
13. Stream Velocity Sensors
14. Stream Velocity Readouts

Note: Inlet screen assembly not installed.

Figure 97. — Test Apparatus Photograph

Flow channel and test section assembly. — The details of the flow channel and test section are illustrated by figure 98. The channel was constructed principally of plywood to take advantage of both its workability and low thermal conductivity. Its overall length was approximately 64 inches including the inlet screen assembly and the converging exit section. The channel cross section was approximately 10 by 12 inches at the inlet, 2.5 by 12 inches throughout the main section, and approximately 1-3/4 by 2-1/2 inches at the outlet of the converging exit section (inlet-to-instrumentation manifold). A flexible duct, coupling the channel exit and air flow transducer manifold, was fabricated from nonporous silicone sheeting to provide shock and vibration isolation between the two assemblies. The air flow transducer manifold was constructed of a block of hardwood approximately 3 by 4 by 3 inches through which three tubing runs of 17 inches each were extended in diverging directions. This configuration permitted a minimum flow disturbance at the inlet and in-line transducer installation without tubing bends while requiring minimum fittings and a minimal fabrication cost.

Initial exploratory runs indicated that stream turbulence was higher than desirable and operated to mask-off at least the initial indications of the convection phenomena. An inlet screen assembly was designed to minimize this interference. The effect of the installation is illustrated by figure 99.

The inlet screen assembly incorporated five stages of 15 by 15 mesh copper screen spaced approximately 1/2 inch apart. The channel inlet was constructed to provide a two-dimensional flow convergence over an 8-inch run. The configuration of the convergence was based on the curvature of a "30-degree elipse" tangentally intersecting the plane of the channel and the end plate of the screen assembly normal to its minor and major dimensions respectively. The converging section produced approximately a 4 to 1 reduction ratio with the 2-1/2- by 12-inch channel. The exit section was designed as a converging, transparent section to provide both a means of obtaining a reasonably uniform acceleration to that required by the channel flow measurement assembly and a potential means of lighting and observing the channel interior. The section was constructed of 1/2-inch lucite flat stock.

The test section incorporated two opposing metal plates installed normal to the vertical axis (i.e., top and bottom) each constructed of aluminum sheet stock 12 by 12 inches by 1/2 inch. One plate was heated with a 6-foot run of Cal-Cord heating tape #33725 (240 watts) attached to the exterior surface and insulated to ambient. The other plate was temperature stabilitized (cooled) with a controllable flow of water directed across its exterior surface through a well of approximately 1-inch depth.

A removable viewing window of approximately 2-1/2- by 12 inches was built into the channel wall to provide visual and photographic access to the test section.

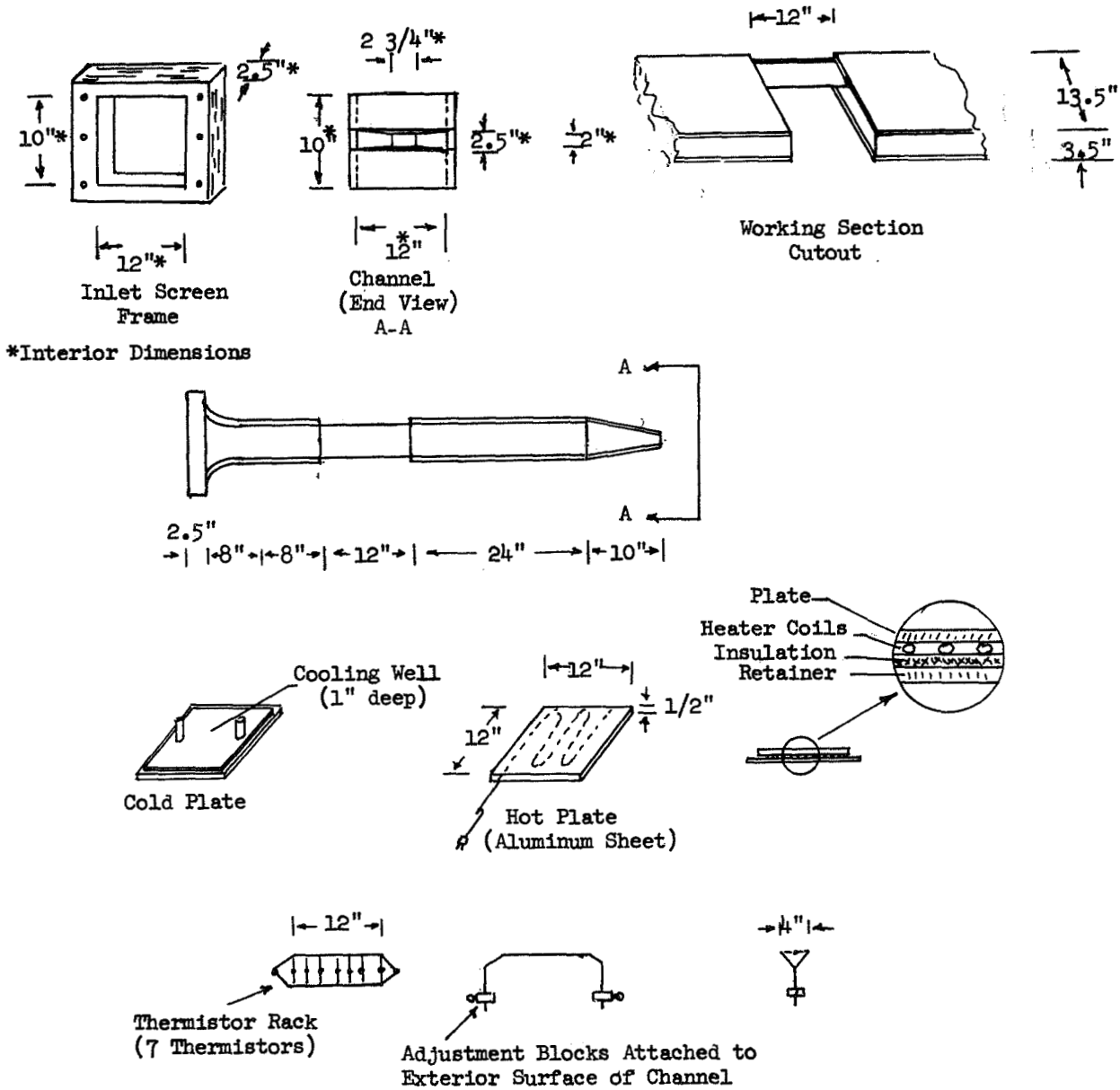


Figure 98. — Flow Channel and Test Section Components

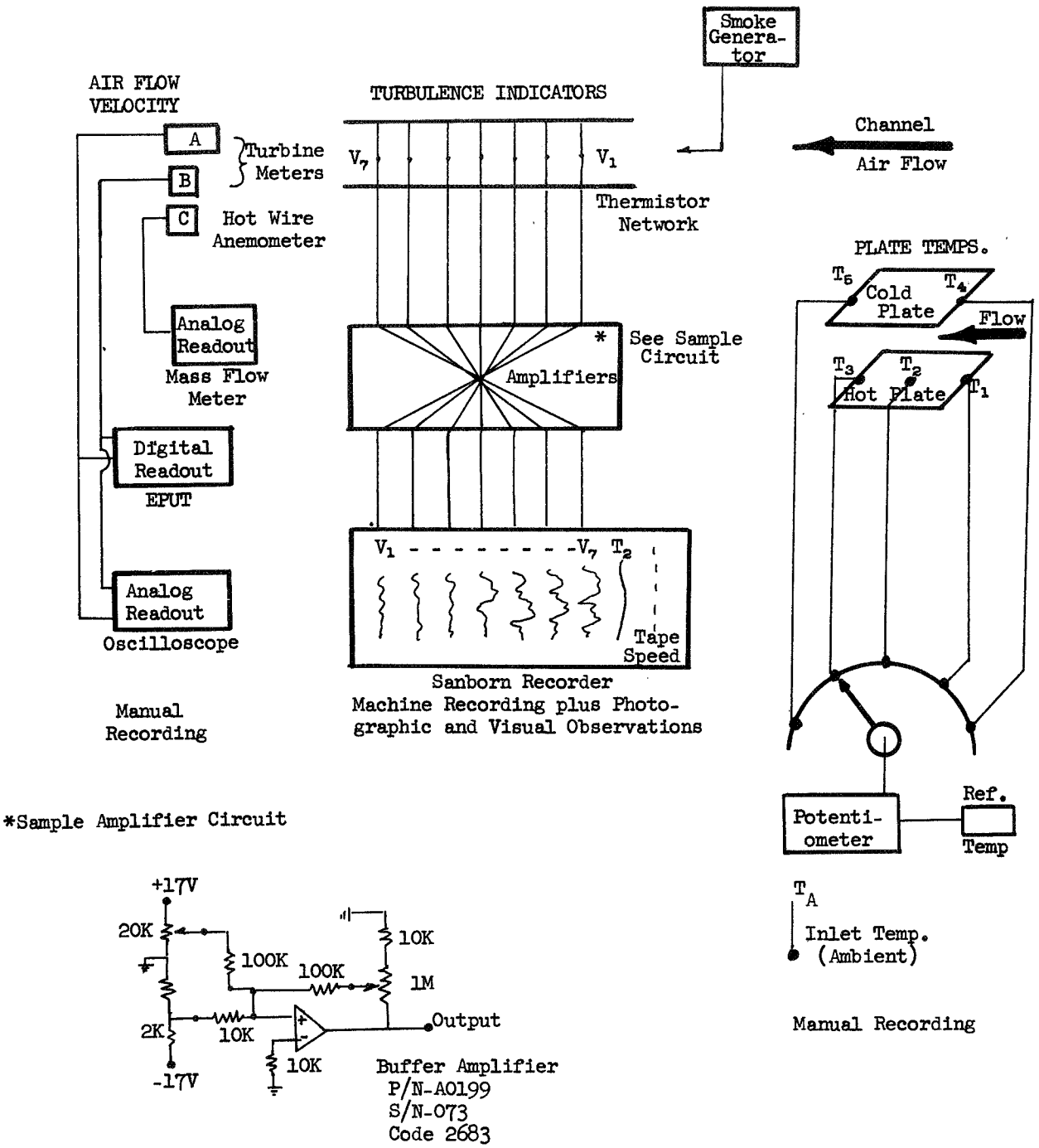


Figure 99. — Instrument Schematic

The interior surfaces of the channel, including the thermal plates, window, and all joints, were initially sanded and, following assembly, were joined and sealed internally and/or externally with Duxseal (putty).

Instrumentation. — As shown in figure 99, the major components of the instrument complex were:

a. Channel Air Flow Velocity Measurement (Manual Recording)

   1. Flow Transducers

      a) Turbine type - Flow Technology: FT-24M-GL #24001 ("A")

      b) Turbine type - Flow Technology: FT-12M-GL #22001 ("B")

      c) Hot wire anemometer - Technology Versatronics: MFG-10-12T #1441 ("C")

   2. Signal Converters - Data Readouts

      a) Type 545 oscilloscope - Tektronix #14773

      b) EPUT and timer - Beckman 7360R

      c) Mass flow meter - Technology Versatronics: MFG-10-12T #1441, 50-400 Hz (matched to transducer)

b. Plate Temperature (Manual Recording)

   1. Chromel-Alumel Thermocouples

      a) Cold plate - leading edge, trailing edge (2)

      b) Hot plate - leading and trailing edge, center (3)

   2. Potentiometer - Leeds & Northrup (plus ice bath reference)

c. Turbulence Indicator (Machine Recording)

   1. Thermistor network - VECO type 31A7, 1K (7)

   2. Signal amplifiers (bridge circuit control, see Schematic)

   3. Brush recorder - Sanborn 7700 series, 8 channel

d. Turbulence Visualization (Manual and Photographic Recording) (Smoke generator, nozzle, lighting, high-speed camera).

The turbulence-sensing thermistors were mounted in a rack so that they were evenly spaced fore to aft along the channel over a distance defined by the leading and trailing edge of the opposing hot and cold plates and in a plane parallel to surfaces of the plates. The location of the thermistors with respect to the distance between the plane of the

network and that of the hot plate was adjustable through a range of 1-1/2 inches from a point approximately 3/4 inch "above" the plate. The plane of the rack could also be canted with respect to the plane of the hot plate, making it possible to position the trailing edge thermistor approximately 1/2 inch "above or below" the leading-edge thermistor. The extremely fragile nature of the thermistor leads requires that they be structurally protected from all tension stress.

Smoke visualization was provided by metering bottled air through a smoke generator and driving the smoke through a nozzle located in the plenum approximately 3/4 inch upstream of the first stage of the inlet screen assembly. The location of the nozzle was adjustable. Smoking tobacco (cigarettes), a traditional fuel for high-performance smoke tunnels, was used for generator fuel thus providing a dense smoke made up of exceptionally low-mass particles.

Visual and photographic observations were accomplished through the viewing window with lighting access through the transparent panels of the converging exit section.

TEST PROCEDURES

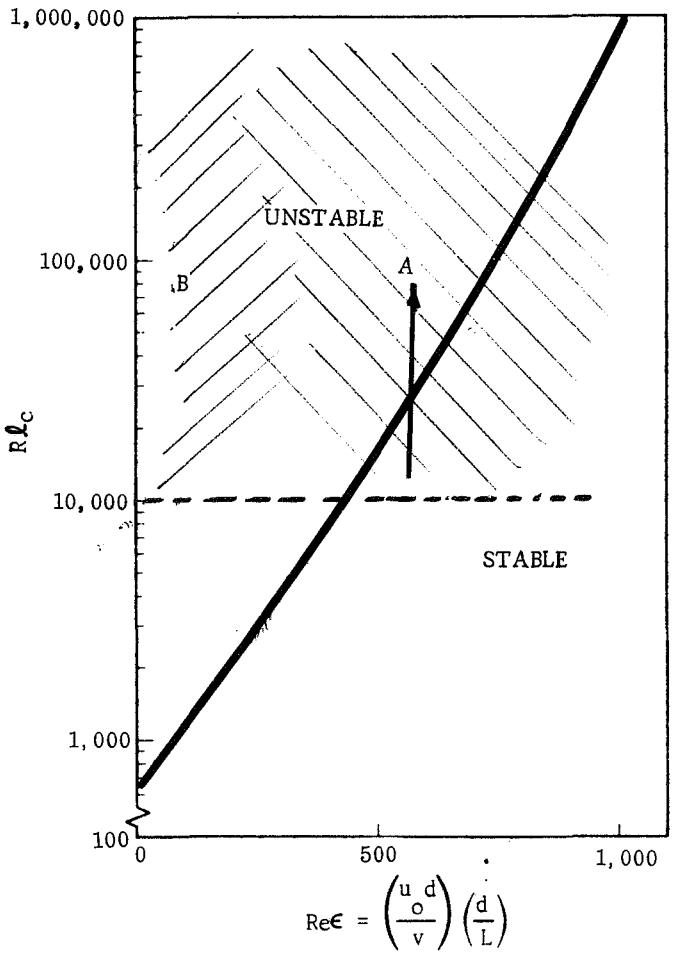
The concepts presented in the Test Plan (ETP 5, 19 September 1969) were found to be generally applicable throughout. The guidelines for the design of the experiment and formulation of the procedures are illustrated by figure 100.

An initial set of test procedures was developed from the guidelines implied by figure 100 and as organized by table 33. As a result of the information produced by the Trial Data Runs, a second set was formulated for the Formal Data Runs as shown in subsequent sections.

Similar tests were run against each of two channel orientations with respect to the local gravitational vector, specifically one set with the hot plate "below" the cold plate and one set "above" the cold plate.

Final assembly of the test apparatus was initiated on 19 February. The Exploratory Data Runs, including component checkout and calibration, were started on 25 February and extended through preliminary systems checks on 9 March. During this period minor system modifications were made including the addition of the inlet screen assembly and various instrument adjustments.

Trial Data Runs were initiated on 11 March. Formal Data Runs were initiated on 17 March and completed on 23 March.



Legend:
A = Region of Exploratory Test Runs
B = Region of Formal Data Runs

Notes:
1) The stability criteria model shown hereon was first published in AMR #5 as Figure 2, "Stability Boundary."
2) Channel height (h=2.5") limited testing capabilities less than 10^4. (h < 2" required for lower region).
3) Formal runs shifted to region "B" based on initial analysis of data indicating that the boundary might well be located at lower values of $Re\epsilon$ than initially predicted.

Figure 100. — Experiment Design Guidelines

Table 33. — Initial Trial Data Run Design

Δ Temp (°F) \ u_o (ft/sec)	.5	1	1.5	2	2.5	3	3.5	4
1	X	X	X	X	X	X		X
2.5								
5		X	X	X	X			
10		X	X	X	X	X		
25								
50			X	X	X	X	X	
100				X	X	X	X	X

NOTE: Run sequence establishes a ΔT as near as practicable to one of the values shown and then schedules the applicable range of air flows. All conditions data are manually recorded against each set point and in turn related to the strip chart recording.

Conditions data:

Temperature: T_1 & 2; $T_{3,4}$ & 5; T_A

Channel Stream Velocity: Sensor A, B, or C

Test Data Summary

Data were recorded against two sets of experiments, namely, Exploratory Data Runs and Formal Data Runs.

Exploratory data runs. — These runs were essentially instrumentation and test mode evaluation, system and procedure modification, and system calibration.

Resolution of test uncertainties and calibration: Several major questions concerning the capability of the experimental apparatus required resolution through exploratory runs and the analysis of data. These questions included:

a. Rate of hot plate temperature variation over time for each of the several candidate stream velocities.

b. Attainment and control over stream velocity.

c. Precision in control of ΔT especially at the lower values.

d. Capability of the thermistor circuits to provide a meaningful indication of the nature of the thermally induced stream turbulence.

e. Possibility of the elimination of the channel-induced turbulence or, if not, the possibility that indications of this turbulence be analytically isolated from the indications of the thermally induced turbulence.

f. Clarity with which the stability/instability transition characteristics can be observed.

Calibration and trial data: Calibration data for the turbulence indicator system (thermistors) are given by table 34 and figure 101. Flow meter calibration is given by figures 102 and 103.

A summary of the trial data runs of 12 March is recorded on table 35. Samples of the strip chart data relating to these runs are included as figure 104.

Following a series of exploratory runs which included those producing the sample data shown on table 35, it was determined that:

a. Temperature control of the hot plate, although somewhat marginal, was sufficient to perform the experiment especially with the T_2 data included as one channel of the strip chart recordings.

b. Stream velocities were controllable throughout the range required except that variations in the "quality" of the laboratory air due to the air conditioning cycle was suspected of imposing a periodic (1 to 2 minutes) alteration on the blower inlet and thus the observed flow patterns when operating and the very low stream velocities.

c. Following the installation of the inlet screen assembly, indicated turbulence was reduced by roughly two orders of magnitude to a sufficiently low level to be of little if any significance (see figure 105).

d. The stability/instability characteristics can undoubtedly be observed and the transition points identified, but most likely at a much lower channel stream velocity and at lower ΔTs than anticipated, probably in the range of $0 < \Delta T < 50°$ F and $0 < u_o < 1.5$ ft/sec.

Formal data runs. — These were the runs that produced the data against which the analytical model was evaluated. The experimental variables were channel stream velocity, temperature differential, and channel orientation to the gravity vector. Samples of the data collected during the formal data runs are presented in the following form:

a. Manually recorded data, table 36.

b. Machine-recorded data, figures 104 through 111.

c. Photographs of smoke streams, figure 112.

Table 34. — Thermistor Calibration Data

12 March 1970 AM

Velocity \ Thermister		1		2		3		4		5		6		7		Gain (mv/div)
Meter * Reading	ft/sec.	z.p. Volts	Output Volts	z.p. Volts	Output Volts	z.p. Volts	Output Volts	z.p. Volts	Output Volts	z.p. Volts	Output Volts	z.p. Volts	Output Volts	z.p. Volts	Output Volts	
A. T_2 = 67°F (initial), T_2 = 68°F (final)																
71A	0.852		1.70		1.65		1.70		1.45		1.50		1.55		1.60	100
54A	0.648		1.40		1.40		1.45		1.30		1.35		1.40		1.35	100
112A	1.34		1.95		1.90		2.10		1.75		1.90		1.85		1.90	100
180A	2.16	2.0	0.55	2.0	0.60	2.0	-0.10	2.0	0.25	2.0	0.45	2.0	-0.45	2.0	0.50	100
220A	2.64	2.0	0.85	2.0	0.85	2.0	0.05	2.0	0.45	2.0	0.65	2.0	-0.25	2.0	0.75	100
280A	3.36	2.0	1.10	2.0	1.20	2.0	0.45	2.0	0.75	2.0	1.00	2.0	0.05	2.0	1.10	100
312A	3.74	2.0	1.25	2.0	1.35	2.0	0.65	2.0	0.90	2.0	1.15	2.0	0.20	2.0	1.25	100
373A	4.48	2.0	1.55	2.0	6.65	2.0	0.95	2.0	1.20	2.0	1.50	2.0	0.50	2.0	1.50	100
93A	1.12	0	1.75	0	1.75	0	1.85	0	1.50	0	1.65	0	1.65	0	1.70	100
18C	0.072	0	0.32	0	0.25	0	0.20	0	0.13	0	0.13	0	0.05	0	0.05	50
49C	0.196	0	1.00	0	0.90	0	0.90	0	0.73	0	0.80	0	0.60	0	0.50	50
80C	0.320	1.0	0.40	1.0	0.33	1.0	-0.05	1.0	0.07	1.0	0.23	1.0	-0.32	1.0	-0.10	50
B. T_2 = 125°F (initial), T_2 = 126°F (final)																
61A	0.732	0	1.70	0	1.70	0	1.80	0	1.65	0	1.55	0	1.65	0	1.70	100
128A	1.54	0	2.30	0	2.30	0	2.45	0	2.10	0	2.10	0	2.15	0	2.15	100
90A	1.08	0	2.00	0	2.00	0	2.10	0	1.80	0	1.75	0	1.85	0	1.75	100
227A	2.72	2.0	1.00	2.0	1.05	2.0	0.35	2.0	8.50	2.0	0.80	2.0	0	2.0	0.85	100
187A	2.24	2.0	0.70	2.0	0.75	2.0	0.05	2.0	0.45	2.0	0.50	2.0	-0.30	2.0	0.55	100
276A	3.31	2.0	1.25	2.0	1.30	2.0	0.60	2.0	0.95	2.0	1.05	2.0	0.15	2.0	1.10	100
321A	3.85	2.0	1.50	2.0	1.55	2.0	0.85	2.0	1.20	2.0	1.25	2.0	0.40	2.0	1.30	100
91A	1.09	2.0	-0.10	2.0	-0.10	2.0	-0.85	2.0	-0.35	2.0	-0.30	2.0	-1.15	2.0	-0.25	100
90A	1.08	0	1.90	0	1.90	0	2.00	0	1.70	0	1.65	0	1.75	0	1.75	100
27C	0.11	0	0.63	0	0.65	0	0.23	0	0.40	0	0.25	0	0.50	0	0.20	50
52C	0.21	0	1.13	0	1.07	0	1.07	0	0.80	0	1.05	0	0.97	0	0.45	50
83C	0.33	1.0	0.50	1.0	0.55	1.0	0.15	1.0	0.45	1.0	0.35	1.0	-0.40	1.0	-0.35	50

* Meter reading for A in Hz, meter reading for C in %.

Note: Sudden decreases in output as flow increases may be due to various modes entering or leaving the area.

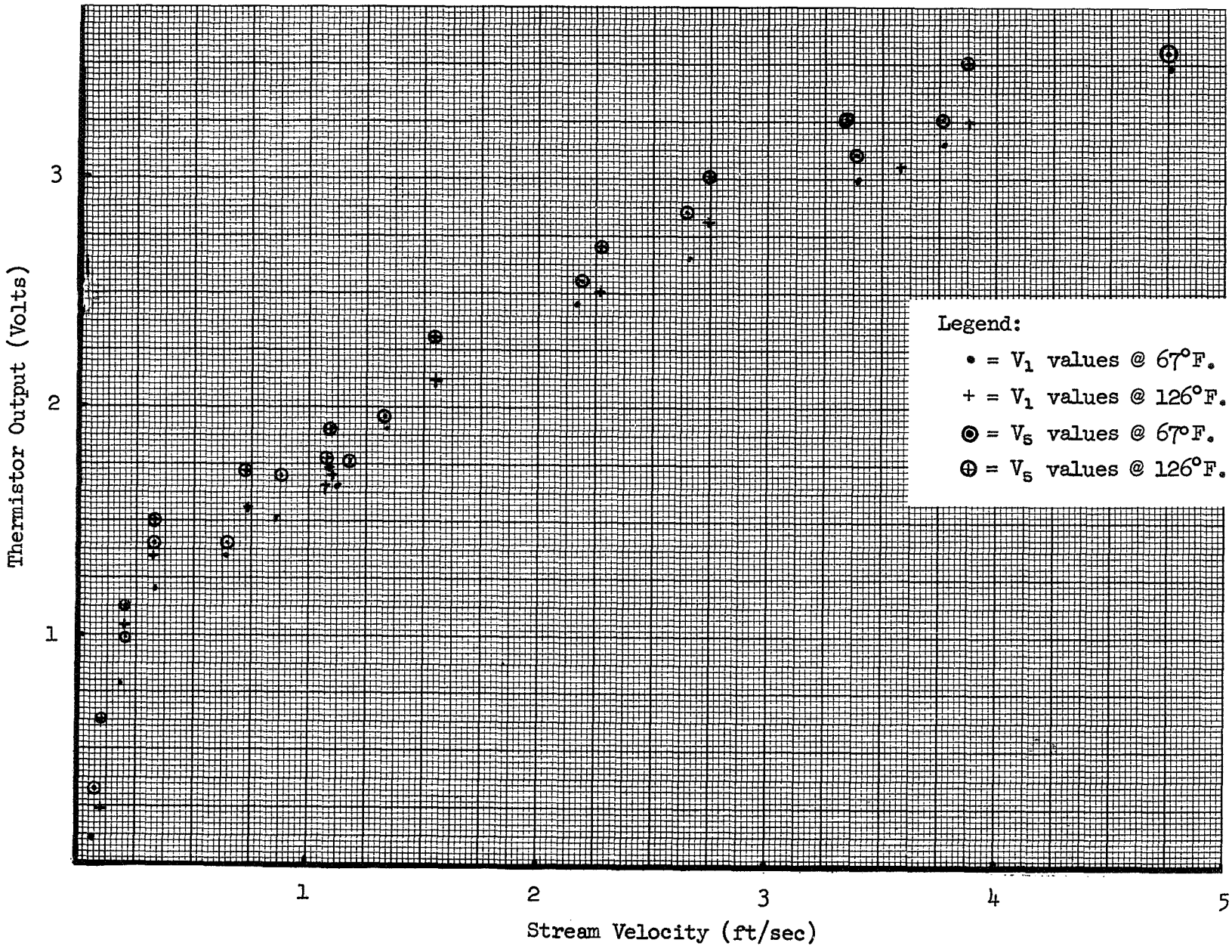


Figure 101. — Turbulence Indicator Calibration, V_1 and V_5

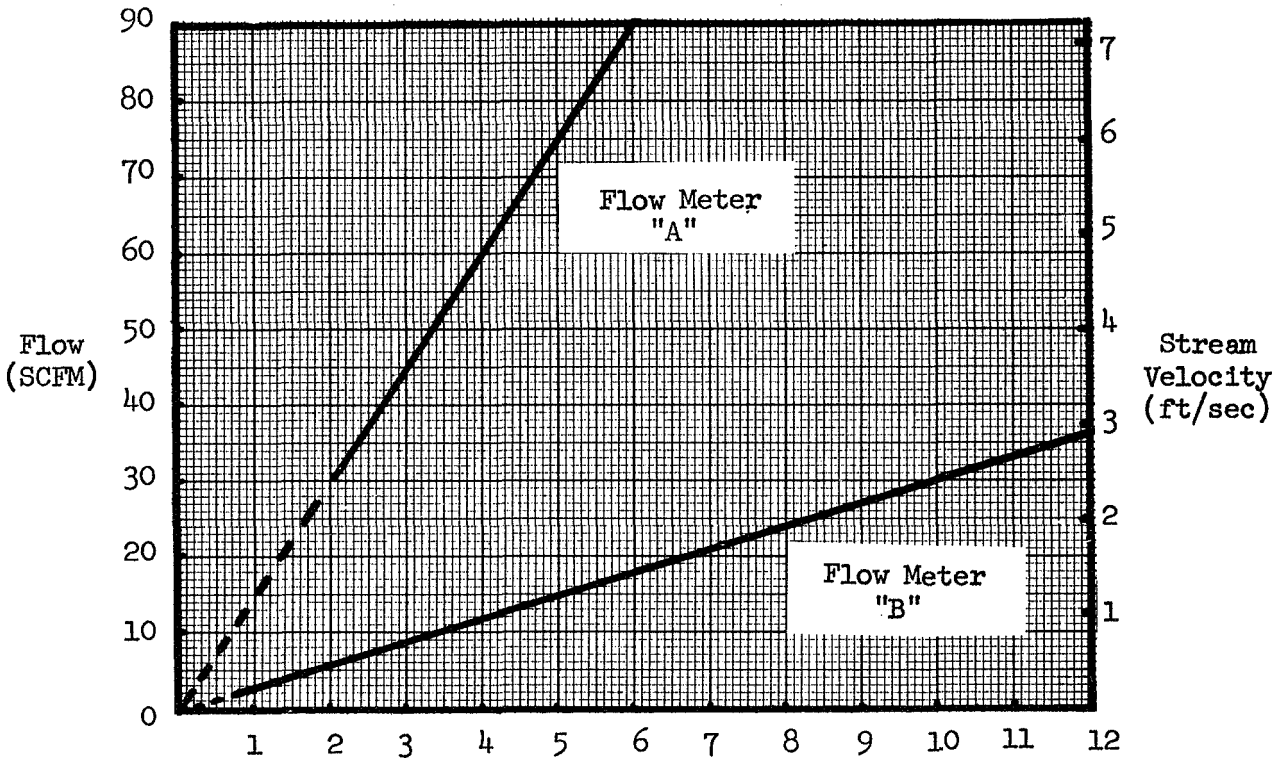


Figure 102. — Turbine Flow Meter Calibration

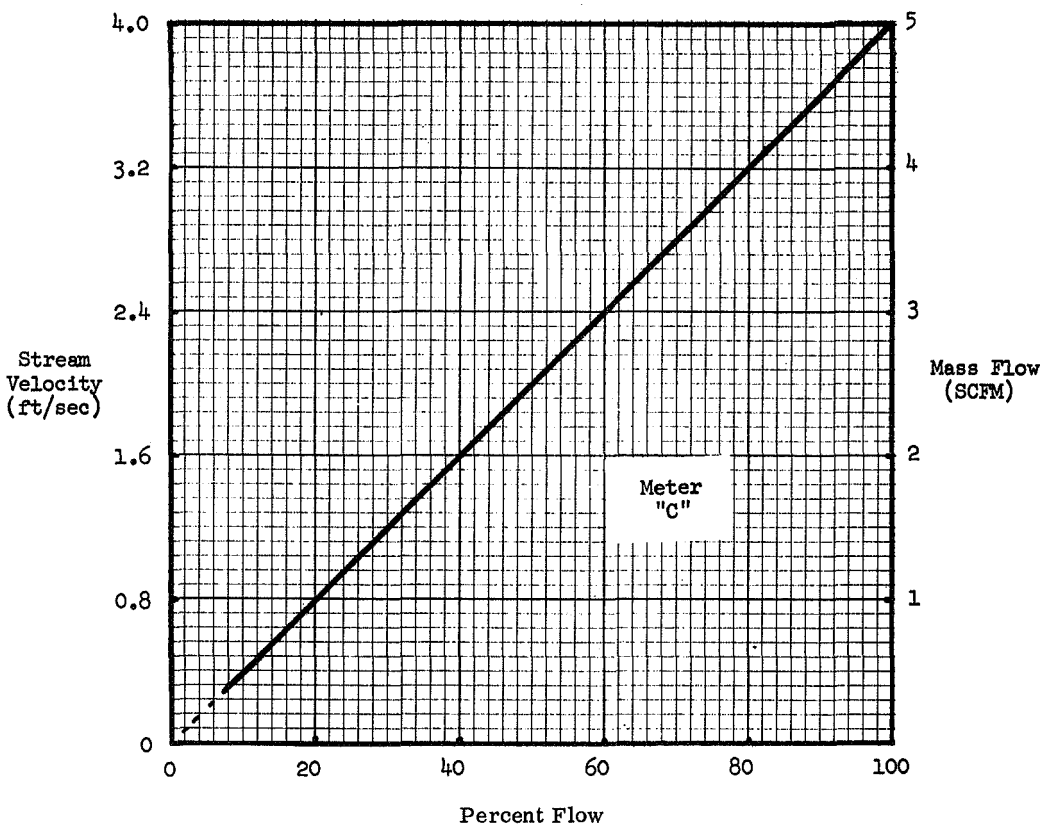


Figure 103. — Mass Flow Meter Calibration

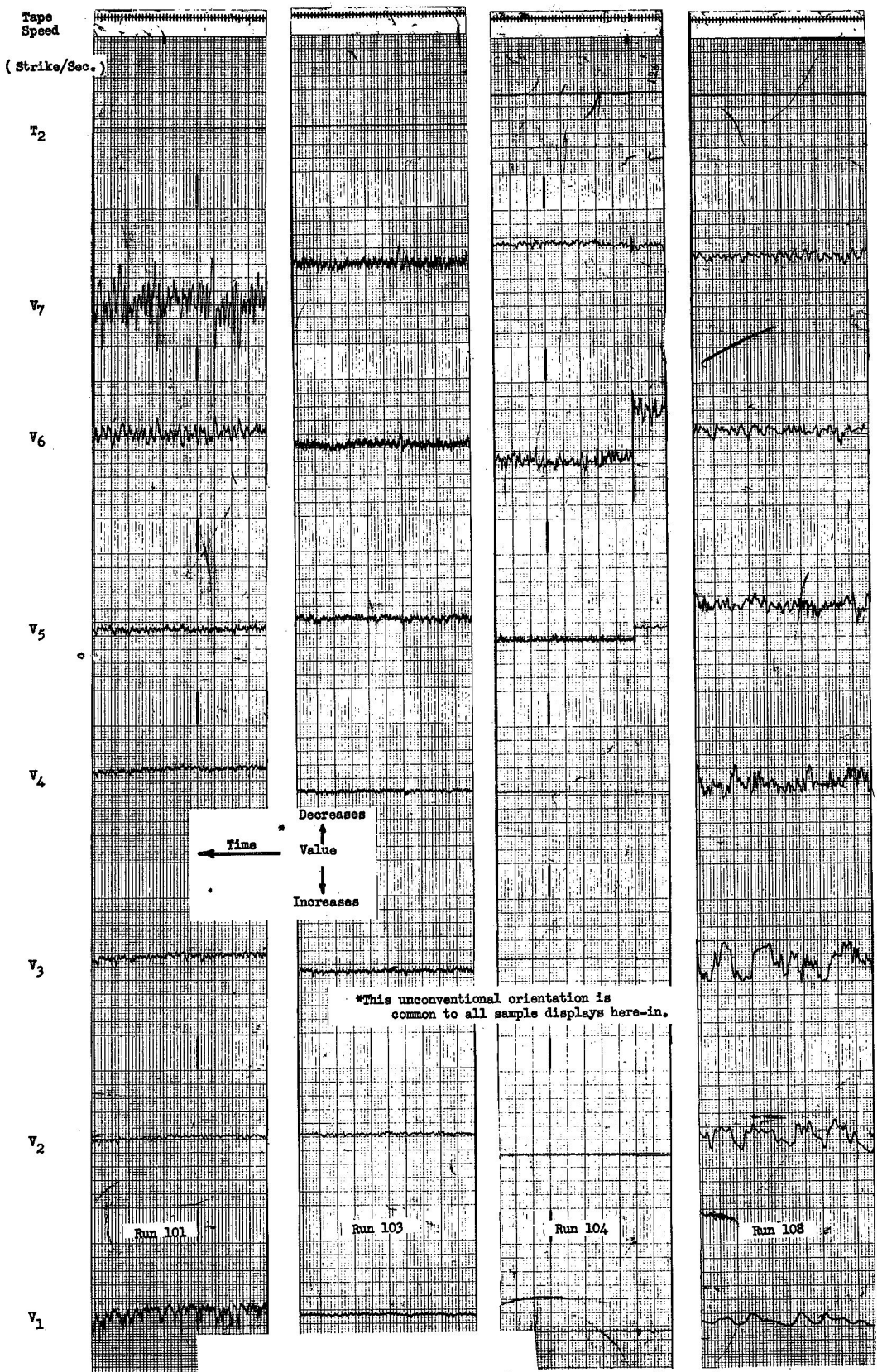


Figure 104. — Turbulence Indicator Data Samples

Table 35. — Trial Data Runs - Sample Data

12 March 1970

Data Ref.	Stream Velocity Measurement			T_2 (°F)	Turbulence Indicator Data								Comments
					Gain (mv/div)	Thermistor Output @ Zero Suppression (Volts/20)							
	$A_{(Hz)}$	$B_{(Hz)}$	$C_{(\%)}$			1	2	3	4	5	6	7	
101			80	68	10	.07	.07	.05	.06	.06	.04	.04	Plate roughness suspect on 1, 6, & 7.
102			39	"	"	.04	.037	.025	.027	.03	.02	.018	Variations on 1 only.
103	310			"	"	.17	.174	.122	.148	.153	.108	.162	Progressive amp and frequency, 1-7.
104			83	126	50	.05	.05	.05	.05	.05	.02	.05	Activity 5, 6, 7, and most 8.
105			56	"	"	"	"	"	"	"	.05	"	Added 4, dropped 5, 1 & 7 most.
106			36	"	"	0	0	0	0	0	0	0	Added 3, dropped 4, minimal.
107			22	"	"	"	"	"	"	"	"	"	3-7 increased, 2 VLF.
108			12	"	"	"	"	"	"	"	"	"	3 max. response,5 highest, all responding.
109			79	"	"	.6	.6	.6	.6	.6	.3	0	6 only.

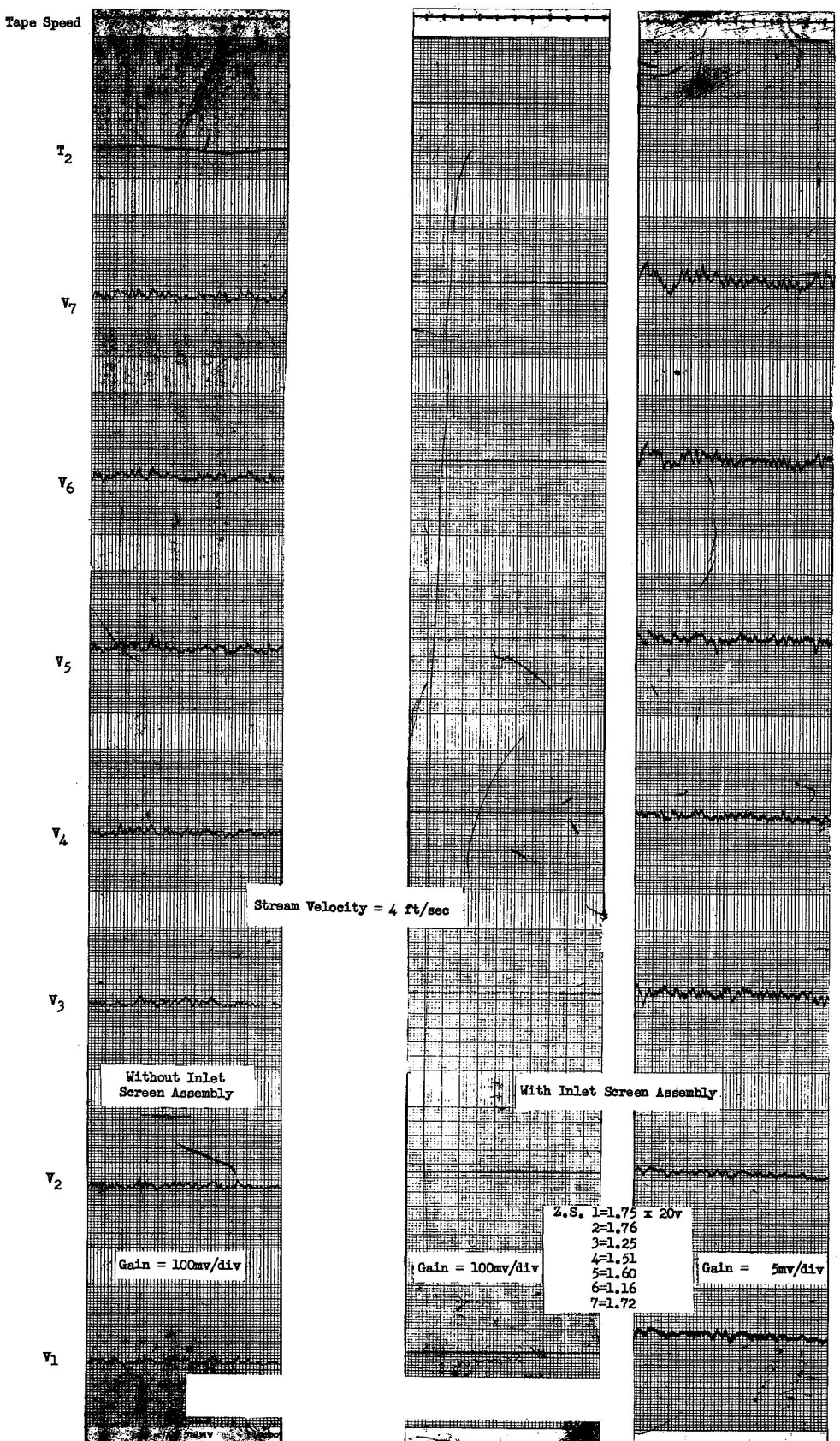


Figure 105. — Effect of Inlet Screen on Stream Turbulence

Table 36. -- Manually Recorded Data

Run No.	Stream Vel. Measurement		Temperatures			Turbulence Indicator Data								Comments
	Meter Read.	Vel. ft/sec	T_2	T_4	T_A	Gain mv/d	Zero Suppression (X20 Volts) 1	2	3	4	5	6	7	
156	7.8C	.031	75.5	68			.01	0	0	0	.0096	.006	.0098	Excessive activity on 1 due to sealant suspended in stream
161	69.2C	.276				5	.052	.046	.03	.035	.041	.028	.028	Excessive on 1 same as Run 156
164		0	75		75.5		0	0	0	0	0	0	0	Turn water off. Blow out residual from cold pl.
165		0					0	0	0	0	0	0	0	8 - amplifier introducing much noise. Possibly due to amp. instability. Terminate ~5:15 PM
198	31A	.37	126	67			.056	.055	.038	.047	.061	.042	.061	Slight on all chnls.
199	286A	3.43	126	66.5			.151	.155	.110	.132	.148	.102	.154	1 died out. Rest inc. slightly. Do not see any long term variations
201	17.5C	.07	129	66°	78.4		.006	.010	0	0	0	0	0	T4:40 A→ C Large on all h.f. on 1
202	40.5C	.16	131	66			.030	.025	.017	.023	.017	.012	.015	2 out, 3 small, rest larger
210						5	0	0	0	0	0	0	0	Thermistor vibration test
211						5	0	0	0	0	0	0	0	B1
218			116	65.5	75.5	20	0	0	0	0	0	0	0	T2:04
219			116.5	66		20	0	0	0	0	0	0	0	Blower on. Orifice closed. Slight breeze from A. Big. dec. on 2.

* Samples from Tables IV through IX of reference 6; runs correspond to those for the sample traces shown herein.

Table 36. — Manually Recorded Data, Contd

Run No.	Stream Vel. Measurement		Temperatures			Turbulence Indicator Data								Comments
	Meter Read.	Vel. ft/sec	T_2	T_4	T_A	Gain mv/d	Zero Suppression (X20 Volts) 1	2	3	4	5	6	7	
301	22c		144.7	63.0			0	0	0	0	0	0	0	1 died out, 2 slight action
302	36.5c						0	0	0	0	0	0	0	3,4 decreases, 2 out
309	19.5c						0	0	0	0	0	0	0	1 died down, others same
310	39c						0	0	0	0	0	0	0	1,2 out, 3 low freq.
P-1			155	88.5		20								Smoke - no air flow
P-5	13c	.052				20								
P-6	35c	.140	157	88.5		20								
342	3.5c	.014	138				-.008	-.009	-.009	-.009	-.009	-.007	0	Blower on, inlet closed, channel inverted
344	55.5c	.222					.042	.038	.026	.021	.010	0	0	Channel inverted
347	171A	2.05	140.7	63.8	72.5	5	.124	.125	.090	.108	.119	.076	.117	C→ A Channel inverted
349	83A	0.98					.087	.086	.062	.072	.081	.051	.079	High activity on V_1, long period variation. Channel inverted

* Samples from Tables IV through IX of reference 6; runs correspond to those for the sample traces shown herein.

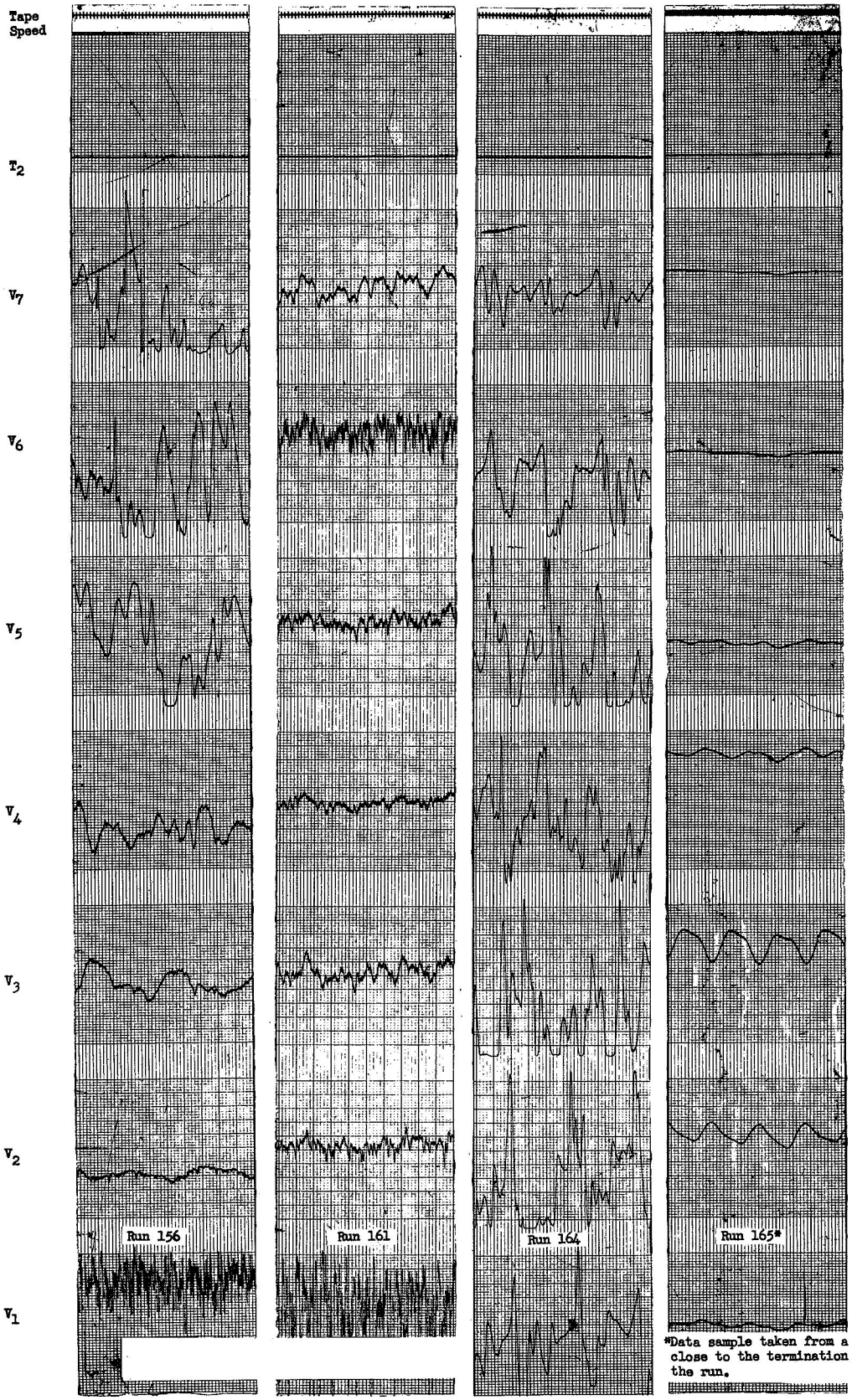


Figure 106. — Turbulence Indicator Data Samples Formal Data Runs 150-165

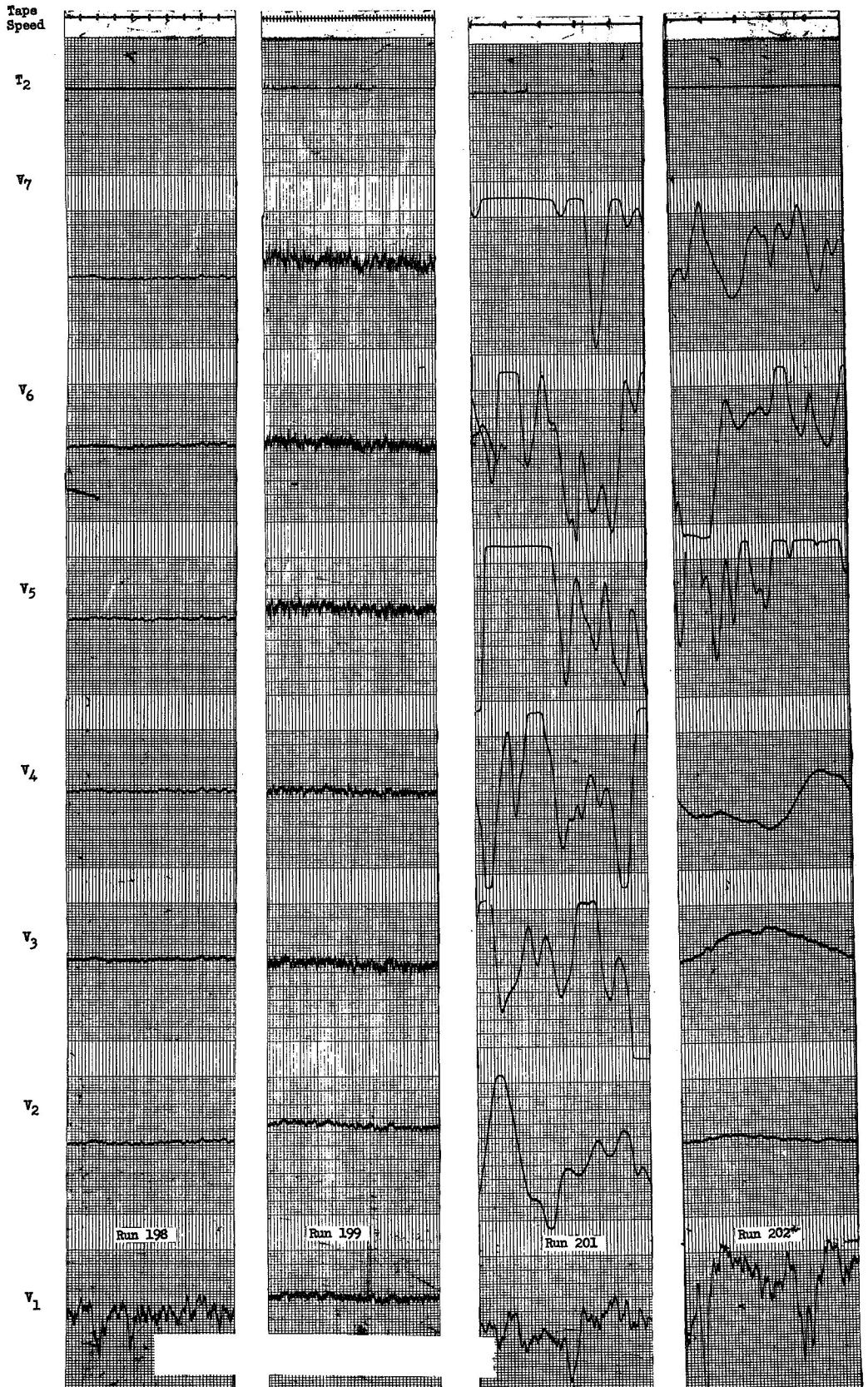


Figure 107. — Turbulence Indicator Data Samples

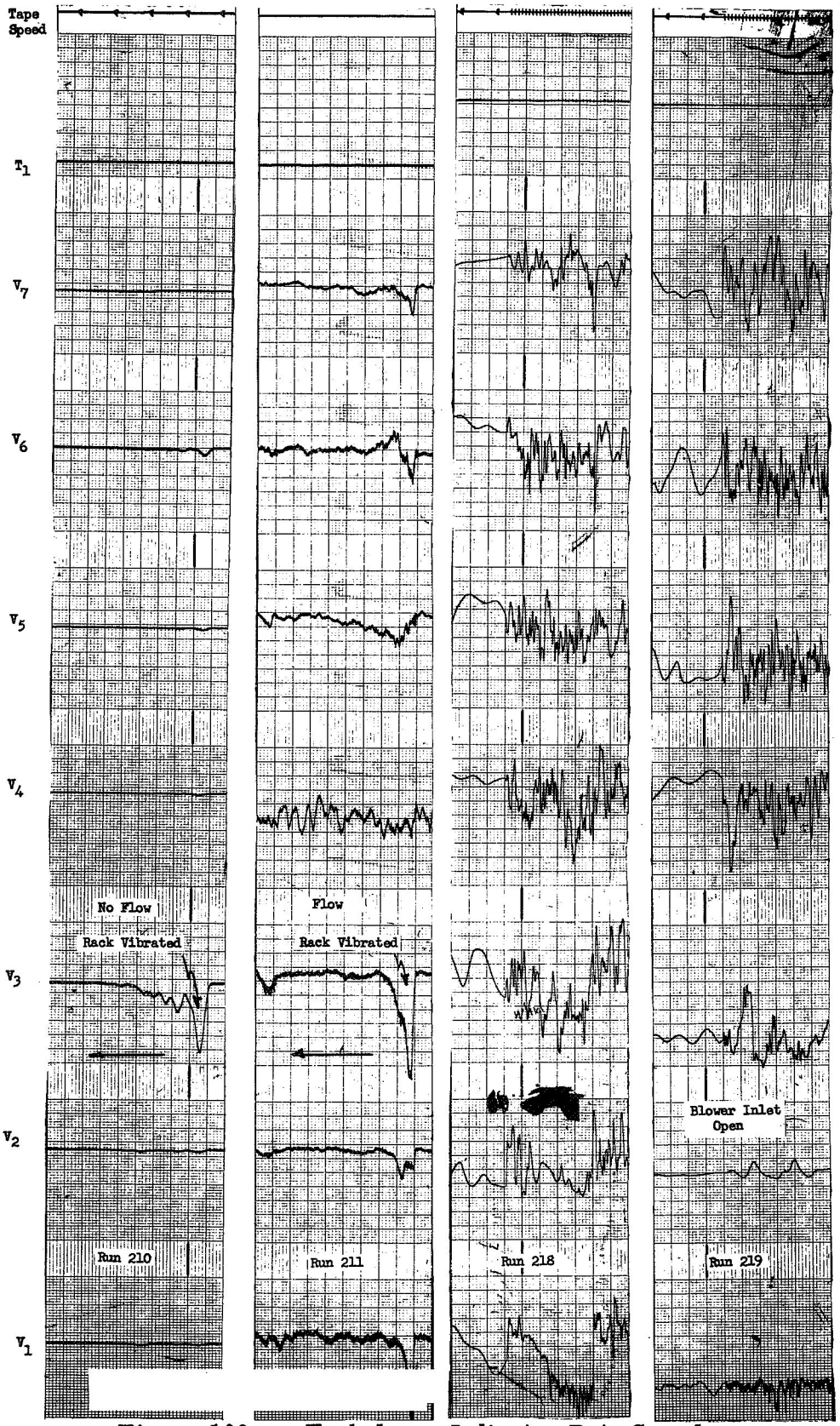


Figure 108. — Turbulence Indicator Data Samples

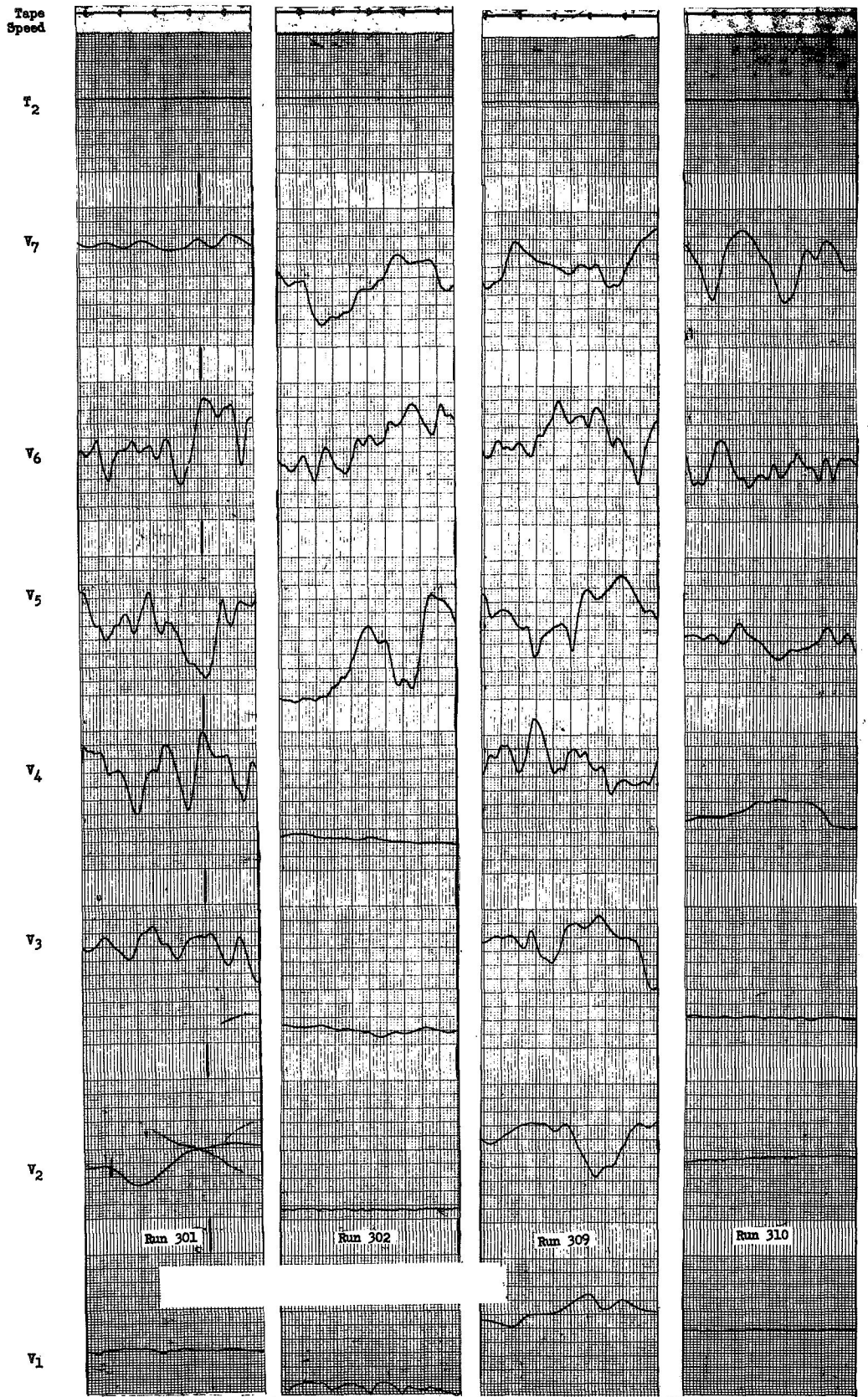


Figure 109. — Turbulence Indicator Data Samples

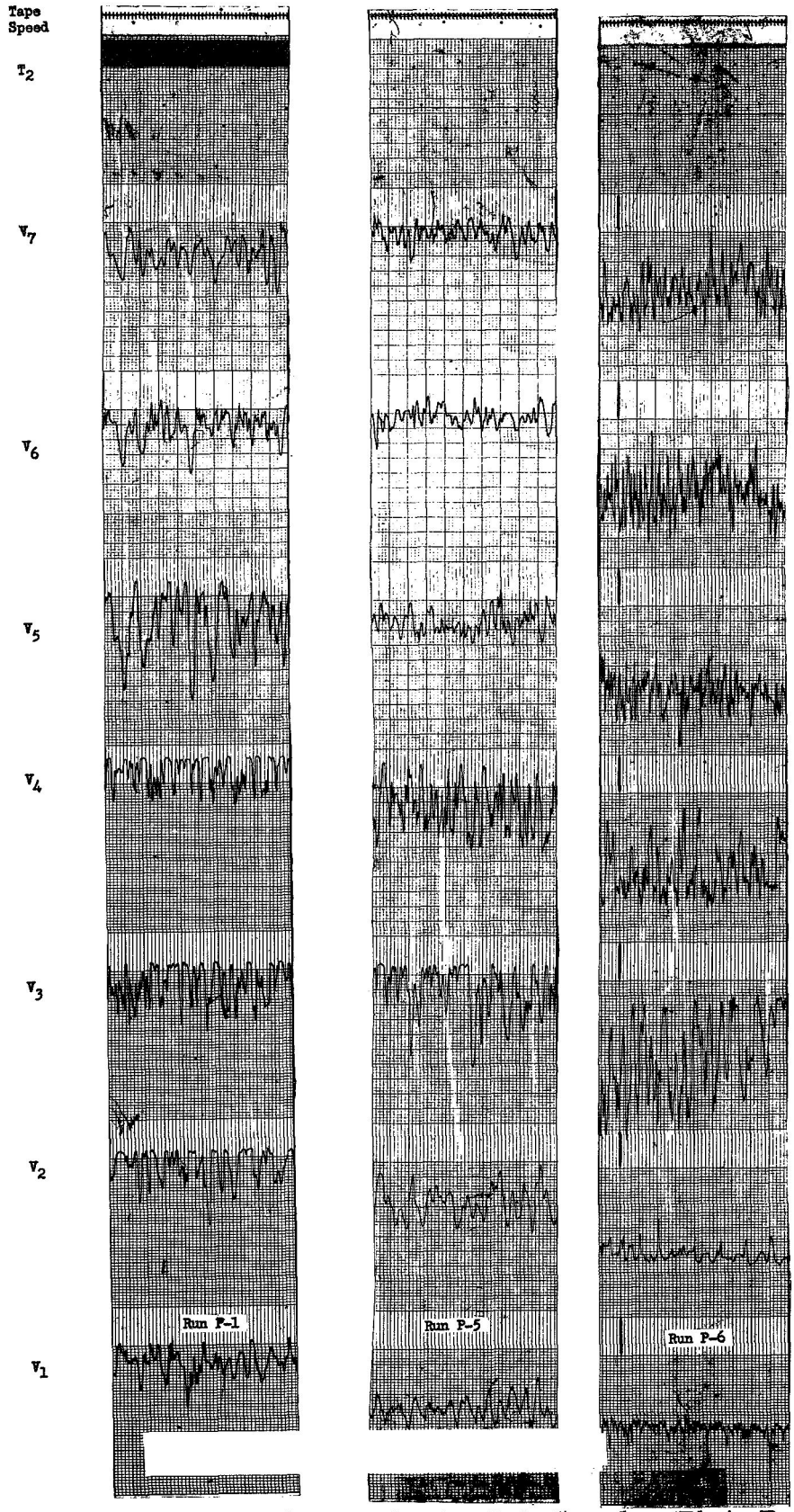


Figure 110. — Turbulence Indicator Data Samples (Photo Runs)

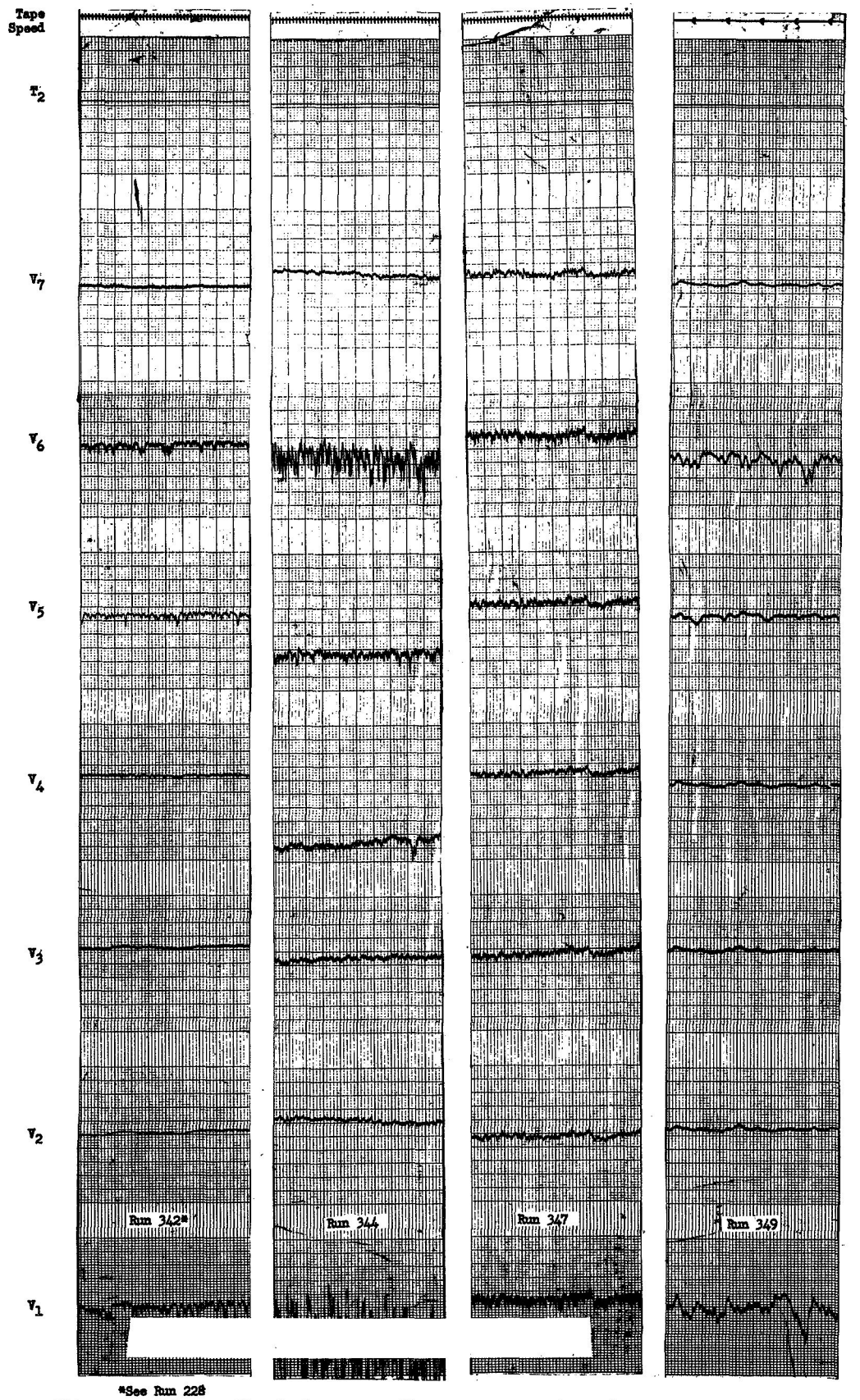
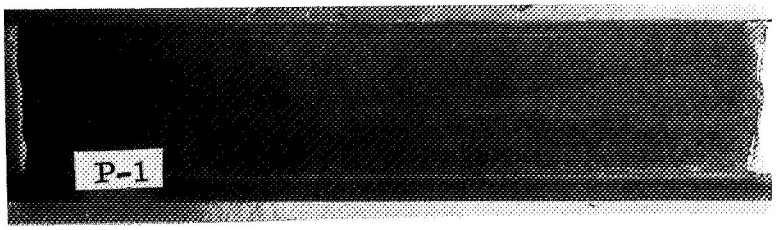
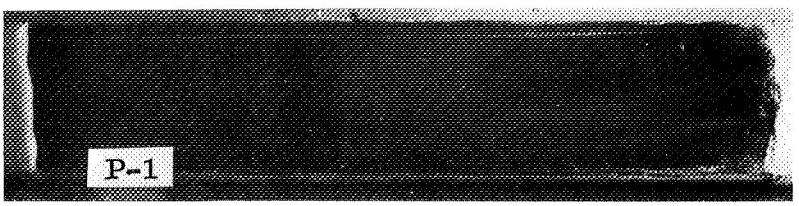


Figure 111. — Turbulence Indicator Data Samples (Inverted Channel)



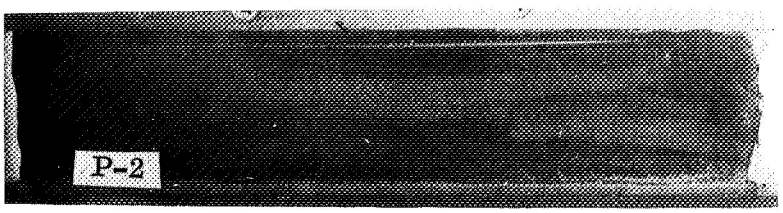
#106924B

Note: Refer to figure 110 for turbulence indicator traces for P-1 & P-5.

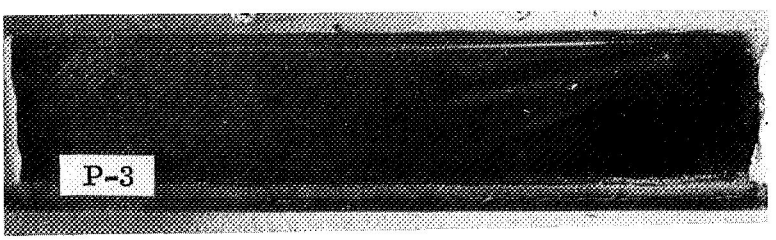


#106925B

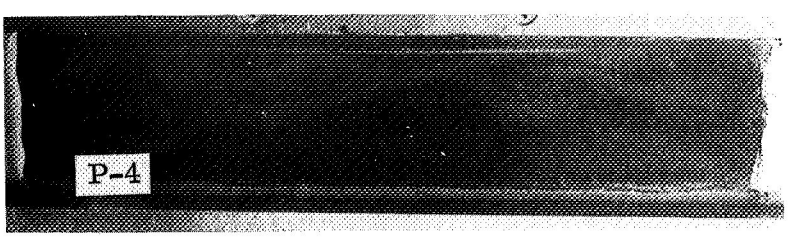
*Initial flow pattern not reflected by figure 110.



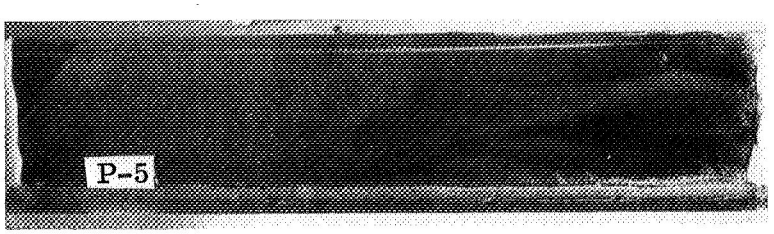
#106923B



#106922B



#106921B



#106920B

Figure 112. — Smoke Stream Visualization of Channel Flow

Critique of Test Design

With the exception of the initial uncertainties regarding approaches to the design of the turbulence indicators, the general approach to the test design appeared to be straight forward, tests were easy to manage, and construction costs were low. Many of the elements of the design should prove to be candidates for future test designs while attention to several of the less desirable aspects of the design should be of value in avoiding future problems.

Instrumentation. — The requirement for precise and accurate measurements of channel stream velocity, plate temperature, and turbulence velocites make this experiment a difficult one to instrument. The instrumentation which was employed in this first phase met both the primary and secondary requirements, specifically 1) to provide a means of collecting data to be used in evaluation of the analytical model, and 2) to provide a base of experience from which future tests can be designed. Relative to the latter, it is probable that if any major changes are indicated, they will involve augmentation of the thermistor turbulence sensors with a system providing a more explicit definition of the stream characteristics such as might be expected from such optical systems as the interferometer. Such a system would be an upgrading of the smoke visualization as employed. However, the thermistor/hot-wire anemometer sensing devices, as turbulence indicators, were very well suited to this experiment as they were sensitive to extremely small velocities (order of tenths ft/sec) and produced many millivolts of output voltage.

For future designs, stream velocity, temperature, and plate temperature measurements could well be merely improved versions of the initial phase designs. Attention must be directed to selecting measurement devices with low hysteresis characteristics. Specifically, the turbine meters required "starting" torques far in excess of running torques due to the inherently high induction drag associated with initial rotor armature acceleration. This was not unduly limiting with the larger meter ("A") which permitted sufficient channel flow to meet the starting requirements, but with the smaller turbine on the line, channel flow was so restricted that starting torques were not attainable and an auxiliary starter (vacuum cleaner inlet held close to the turbine exhaust) was required. The use of an axial blower instead of the industrial radial blower employed would reduce the rate of flow drop-off with increased channel resistance and thus potentially at least reduce the starting problems if such existed.

Process apparatus. — The experiment demonstrated the feasibility of constructing a simple and economical channel and stream control. Improvements in stream control at the $<<$ 1 ft/sec range will be required for more complete examination of the model, especially during low-gravity experiments. Such improvements should be simple to attain and indeed were considered attainable even in this first phase if such became necessary.

Channel leakage is an ever-present problem and of course was magnified by the decision to position the blower at the channel inlet rather than at the turbine meter and thus channel outlets. With the availability of higher performance equipment, consideration should be given to repositioning the blower.

Closer control of plate temperature is desirable and, although rejected for the current design due to cost and schedule constraints, should be considered for future designs.

A square cross-section (quadratic) converging inlet nozzle and graduated screen assembly would provide better flow stabilization than the simple design employed.

Procedures. — In general the procedure proved to be adequate and well organized, resulting in an economic and effective test.

The selection of set points and the range of velocity and temperature variables for this investigation were somewhat unsatisfactory. Originally, the velocity was expected to range up to 5 to 10 ft/sec, but meaningful measurements data were obtainable only in the range 0 to 0.5 ft/sec. However, in this range the velocity-sensing devices were the least accurate. This problem can be circumvented by changing the duct dimensions (decreasing height d) so as to increase velocity for the same flow. It would also have been desirable to measure plate temperatures more accurately than the $\pm 0.3°$ F obtainable with the standard thermocouple circuits employed.

Except for the additional procedures dictated by the improved instrumentation suggested herein, it is not clear that future test designs will require significantly different procedures.

Correlation of Analytical and Experimental Observables

Predictive Data

The primary variables in the analysis result from an inspection of equation (20). These are the Rayleigh and Reynolds numbers which in turn are simply related to the temperature difference across and the mean velocity through the duct. Since the stability boundary is strongly affected by the choice of the growth parameter, σ, it may be better to let it be a parameter. Figure 113, therefore, illustrates the type of predictive data that is characteristic of the analytical model for various values of σ. An additional curve (dotted) is drawn indicating the transition from Region II to III as previously discussed. It is this boundary that we expect to determine from the experimental test since only Region III provides temporal perturbation information. While the value of the $Re = 0$ intercept for this curve is well documented, its overall shape is intuitively constructed.

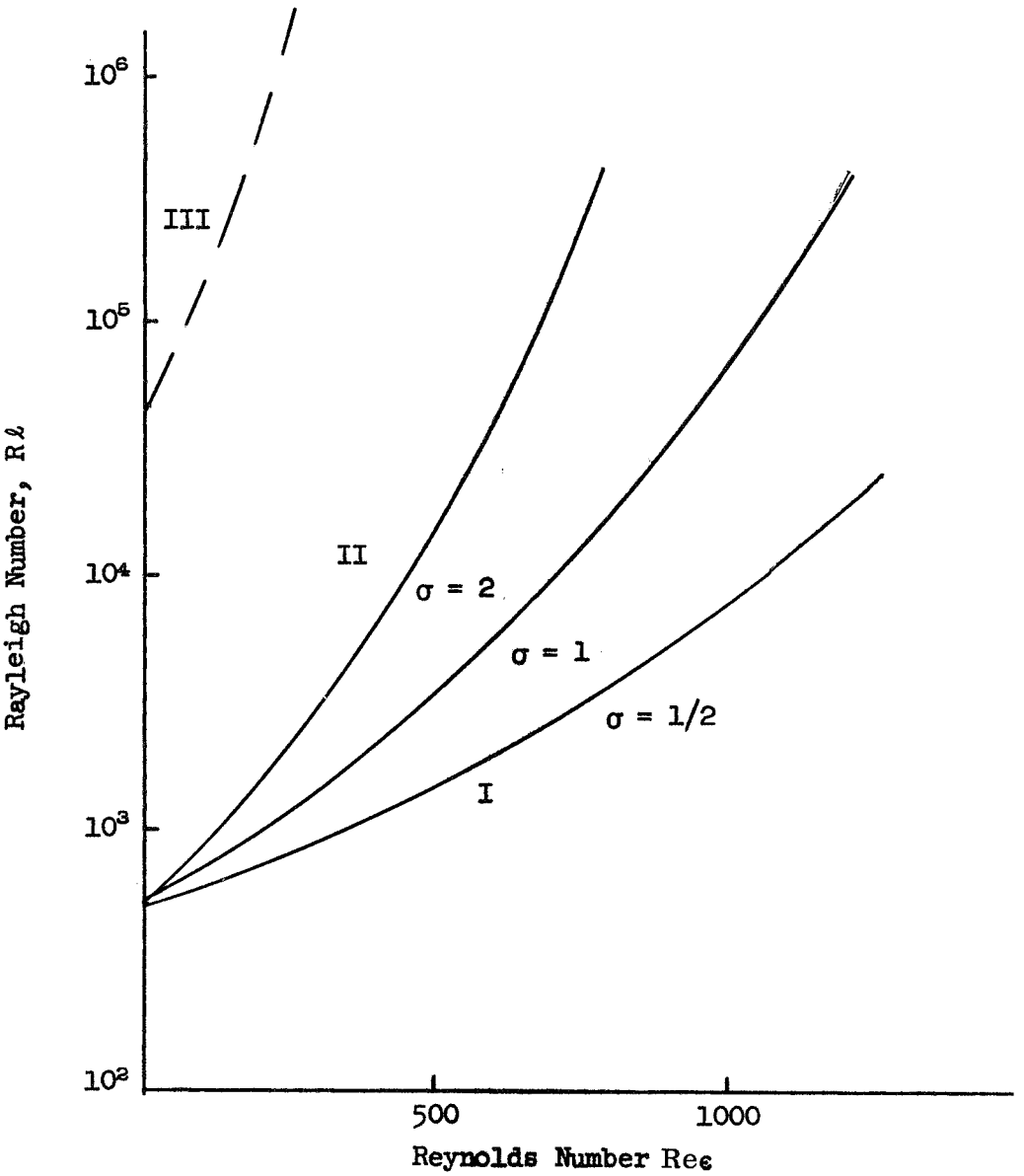


Figure 113. — Stability Boundaries

Experimental Data Analysis

A total of 45 runs were used in evaluation of the stability of the air stream for various conditions of velocity and temperature. These runs were taken with the duct in the horizontal, hot-plate-down configuration. Additional runs were made for the inverted channel but no instabilities were observed, which is to be expected. A complete listing of all runs is given in table 37, which includes data reference numbers, type of data taken, and conditions of experiments. Air velocities ranged from 0 to 4 ft/sec and temperature differences from 0 to 100° F. The raw data consisted of 1) air stream velocities using calibrated flow meters, 2) thermocouple and thermometer temperature measurements

Table 37. — Summary of Data Runs

Date	Data Ref. Numbers	Type of Data	Hot Plate Condition*	Cold Plate Condition*
3-17-70	150-165	Normal	Ambient	Water Cooled
3-18-70	170-207	Normal	78, 97 & 126 F°	Ambient
3-19-70	210-244	Normal	116° & 155°F	Water Cooled
3-20-70	P1 - P6	Photographs	155°F	Ambient
3-20-70	300-313	Thermistors Relocated	143°F	Water Cooled
3-23-70	340-350	Channel Inverted	138°F	Water Cooled
3-25-70	370-372	Normal	Ambient	Water Cooled

*Temperatures refer to approximate hot plate value during the run. Exact values are given on data sheets.

Ambient means plate temperature near that of room temperature.

Water Cooled means tap water was continuously passed through plate. Exact temperature is given on data sheets.

of the two plates, ambient and cold water both, and 3) strip chart recordings of thermistor outputs. These data can be found in reference 6.

The first step of the analysis was to reduce the velocity and temperature information to the two coordinate variables, Rayleigh and Reynolds numbers. This step is shown as table 38 with sample calculations given in appendix B of reference 1. Here, Re is given by $Re = d/\nu\, u_o$ and is not multiplied by the factor ϵ which will depend upon thermistor location. These ϵ values are calculated from the formula $\epsilon_i = L/x_i$ where x_i is the distance from the leading edge to the ith thermistor. After measuring x_i, the following values of ϵ_i were found.

Table 38. — Reduced Experimental Data

Ref. No.	u_o ft/s	Δ To °F	$Re = \frac{d}{\nu} u_o$	$Gr = \frac{gd^3 \alpha \Delta T_o}{\nu^2}$	$R\ell = Gr \cdot Pr$
155	0.016	7.5	19.7	13.2 x 10^4	10.1 x 10^4
156	0.031	7.5	38.3	13.2	10.1
157	0.054	7.5	66.6	13.2	10.1
158	0.076	7.5	93.8	13.2	10.1
159	0.124	7.5	153.0	13.2	10.1
160	0.204	7.5	251.8	13.2	10.1
161	0.276	7.5	340.6	13.2	10.1
162	0.324	7.5	399.9	13.2	10.1
172	0.014	5.5	17.3	9.7	7.4
173	0.030	5.5	37.0	9.7	7.4
174	0.044	4.5	54.3	7.9	6.0
175	0.098	4.0	120.9	7.0	5.4
176	0.236	4.0	291.3	7.0	5.4
180	0.014	16.0	17.3	28.2	21.4
181	0.034	14.5	42.0	25.5	19.4
182	0.058	16.2	71.6	28.5	21.7
183	0.084	19.0	103.7	33.4	25.4
184	0.122	18.2	150.8	32.0	24.3
185	0.224	18.2	276.5	32.0	24.3
186	2.56	20.5	3159.6	36.1	27.4
187	1.61	20.5	1987.1	36.1	27.4
188	0.78	20.5	962.7	36.1	27.4
189	0.47	20.5	590.1	36.1	27.4
197	1.16	59.5	1431.7	104.7	79.6
198	0.37	59.0	456.7	103.8	78.9
199	3.43	59.5	4322.3	104.7	79.6
200	0.48	60.7	952.4	106.9	81.2
201	0.07	63.0	86.4	110.9	84.3
202	0.16	65.0	197.5	114.4	87.0
203	0.23	64.2	283.9	113.0	85.9
204	0.32	65.0	374.5	114.4	87.0
220	2.82	49.5	3480.4	87.1	66.2
221	1.54	49.5	1900.7	87.1	66.2
222	1.12	49.5	1382.3	87.1	66.2
223	0.47	49.5	581.1	87.1	66.2
228	0.014	53.0	17.3	93.3	70.9
229	0.058	54.5	71.6	95.9	72.9
230	0.136	56.2	167.8	98.9	75.2
233	0.208	54.5	256.7	95.9	72.9
235	0.36	54.5	444.3	95.9	72.9
238	3.94	87.5	4862.8	154.0	117.1
239	3.58	90.7	4418.7	159.7	121.4
240	2.33	90.7	2875.6	159.7	121.4
241	1.20	95.5	481.0	168.1	127.7
242	0.5	97.5	617.1	171.6	130.4

$\epsilon_1 = 2.86$ $\epsilon_5 = 0.26$

$\epsilon_2 = 0.83$ $\epsilon_6 = 0.21$

$\epsilon_3 = 0.49$ $\epsilon_7 = 0.19$

$\epsilon_4 = 0.34$

The corresponding values of normalized Reynolds number Re_{ϵ_i} for the four thermistors that were considered in the stability analysis are shown in table 39. Only data from these thermistors were considered further since the first one and last two (i.e., 1, 6, and 7) thermistors frequently gave anomalous results. These could have arisen from sensor failure, sensor vibration, or later discovered channel leaks which were proximal to the thermistors in question. Only the four thermistors (2, 3, 4, and 5) directly over the plate were considered completely reliable.

Several hundred feet of strip chart recordings were taken. These were traces of local velocity fluctuations produced by spatial density variations due to the interaction of natural and forced convection. Obviously some way of reducing these velocity versus time records into stability data was needed. The determination of stability in this experiment was of necessity quite subjective. However, some guidelines were generally followed. At the usual amplifier gain setting, 5 mv/div, a free stream turbulence was noted to be no more than three or four chart divisions in amplitude. This value, incidentally, is extremely small compared to mean velocity and attests to the quality of the added flow-straightener section. If the amplitude of the variations during a run was of the same order of magnitude as the free stream turbulence, thermal stability was assumed for that channel. If the variations were greater than 100 times the free stream turbulence, the condition was considered to be unstable. Variations between these two conditions were considered to be marginally stable. In general, instabilities were much larger than noted above and the three states were fairly well defined.

Frequency information was not used in this analysis although it was obvious that a spectral analysis of the perturbations would yield valuable information concerning the energy makeup of the various turbulent eddies. Again, the frequency of the instability perturbations was considerably less than the free stream turbulence frequencies and aided the determination of the three states. It was fortuitous that the unstable amplitude was much greater and the frequency much less than that of the free stream turbulence.

The results of performing the above analysis on the strip chart data is shown in table 40. One of the three states is noted for each thermistor for each run. While conditions were tabulated for all seven sensors, only four thermistors (2, 3, 4, 5) were considered further. For unknown reasons data for runs 185 and 204 did not follow the general pattern and thus were not included in the data analysis.

Table 39. — Values of Normalized Reynolds Numbers

Ref. No. \ Thermistor	2	3	4	5
155	16.3	9.6	6.7	5.1
156	31.8	18.8	13.0	10.0
157	55.3	32.6	22.6	17.3
158	77.8	46.0	31.9	24.4
159	127.0	75.0	52.0	40.0
160	209.0	123.4	85.6	65.5
161	282.7	166.9	115.8	88.6
162	331.9	196.0	136.0	104.0
172	14.4	8.5	5.9	4.5
173	30.7	18.1	12.6	9.6
174	45.1	26.6	18.5	14.1
175	100.3	59.2	41.1	31.4
176	241.8	142.7	99.0	75.7
180	14.4	8.5	5.9	4.5
181	34.9	20.6	14.3	10.9
182	59.4	35.1	24.3	18.6
183	86.1	50.8	35.2	27.0
184	125.2	73.9	51.3	39.2
185	229.5	135.5	94.0	71.9
186	2622.5	1548.2	1074.3	821.5
187	1649.3	973.7	675.6	516.6
188	799.0	471.7	327.3	250.3
189	489.8	289.1	200.6	153.4
197	1188.3	701.5	486.8	372.2
198	379.1	223.8	155.3	118.7
199	3513.6	2074.3	1439.3	1100.7
200	790.5	466.7	323.8	247.6
201	71.7	42.3	29.4	22.5
202	163.9	96.8	67.1	51.5
203	235.6	139.1	96.5	73.8
204	310.8	183.5	127.3	97.4
220	2888.7	1705.4	1183.3	904.9
221	1577.6	931.3	646.2	494.2
222	1147.3	677.3	469.9	359.4
223	482.3	284.8	197.6	151.1
228	14.4	8.5	5.9	4.5
229	59.4	35.1	24.3	18.6
230	139.3	82.2	57.0	43.6
233	213.0	125.8	87.3	66.7
235	368.8	217.7	151.1	115.5
238	4036.1	2382.8	1653.1	1264.3
239	3667.5	2165.2	1502.4	1148.9
240	2386.8	1489.0	977.7	747.7
241	399.2	235.6	163.5	125.1
242	512.2	302.4	209.8	160.5

Table 40. — Thermistor Condition Matrix

Run Ref. No. \ Thermistor	1	2	3	4	5	6	7
155	hfn	U	U	U	U	U	U
156	"	S	MS	U	U	U	U
157	"	S	S	S	S	S	S
158	"	S	S	S	S	hfn	S
159	"	S	S	S	S	"	S
160	"	S	S	S	S	"	S
161	"	S	S	S	S	S	S
162	"	S	S	S	S	S	S
172	"	U	U	U	U	MS	MS
173	"	S	S	U	U	U	S
174	"	S	S	S	S	S	S
175	"	S	S	S	S	S	S
176	"	S	S	S	S	S	S
180	"	U	U	U	U	U	U
181	"	U	U	U	U	U	U
182	"	S	MS	U	U	U	U
183	"	S	S	MS	MS	MS	U
184	"	S	S	S	MS	S	MS
185*	"	MS	U	U	U	U	U
186	S	S	S	S	S	S	S
187	S	S	S	S	S	S	S
188	S	S	S	S	S	S	S
189	MS	S	S	S	S	S	S
197	hfn	S	S	S	S	S	S
198	"	S	S	S	S	S	S
199	S	S	S	S	S	S	S
200	hfn	S	S	S	S	S	S
201	U	U	U	U	U	U	U
202	hfn	S	MS	U	U	U	U
203	"	S	S	U	U	U	U
204*	"	S	U	MS	S	MS	U
220	S	S	S	S	S	S	S
221	hfn	S	S	S	S	hfn	S
222	"	S	S	S	S	"	hfn
223	"	S	S	S	S	"	S
228	U	U	U	U	U	U	U
229	U	U	U	U	U	U	U
230	hfn	S	S	MS	U	U	U
233	"	S	S	MS	U	U	U
235	"	S	S	S	S	S	S
238	S	S	S	S	S	S	S
239	S	S	S	S	S	S	S

Table 40. Thermistor Condition Matrix, Contd

Run Ref. No. \ Thermistor	1	2	3	4	5	6	7
240	S	S	S	S	S	S	S
241	S	S	S	S	S	S	U
242	S	S	S	S	S	MS	U
243	hfn	S	U	U	U	U	U

Legend:

U - Unstable
S - Stable
MS - Marginally stable
} See text for definition of these terms.

hfn - High frequency noise due to factors other than convective phenomena.

* Data may be in error.

The information in table 40 was then translated to semi-log graph paper as shown in figures 114 through 117. The coordinate variables on these charts are temperature difference and velocity. These charts include only those points within the velocity range 0 to 0.6 ft/sec as it was soon determined that the majority of the transition points occurred at very low velocities at least for the temperature range tested.

Data Correlation

The principal element of the data correlation is a comparison with the predicted stability boundary, figure 113. However, this comparison must be made with the previous discussion of the stability/instability and higher order transitions in mind since what was being measured was the Region II to III transition which inferentially relates to the Region I to II transition. First the four figures 114 through 117 were superimposed as in figure 118. This chart represents the most important results of the experiment for it shows how the transition boundary is a function of distance along the channel. It clearly indicates that at a constant velocity, a greater temperature difference is required to produce turbulence for points nearer the leading edge. In other words, the upstream is not affected by downstream turbulence. This is the identical behavior expected for the Region I to II stability boundary and adds further proof that the two stability curves are parallel as has been hypothesized.

In order to further compare the predicted and experimental data, the four curves of figure 118 were plotted on the nondimensional coordinates of Rayleigh and normalized Reynolds numbers. This conversion is shown in figure 119. The curve for each thermistor (2, 3, 4, 5) was transferred to the new coordinates by computing the appropriate

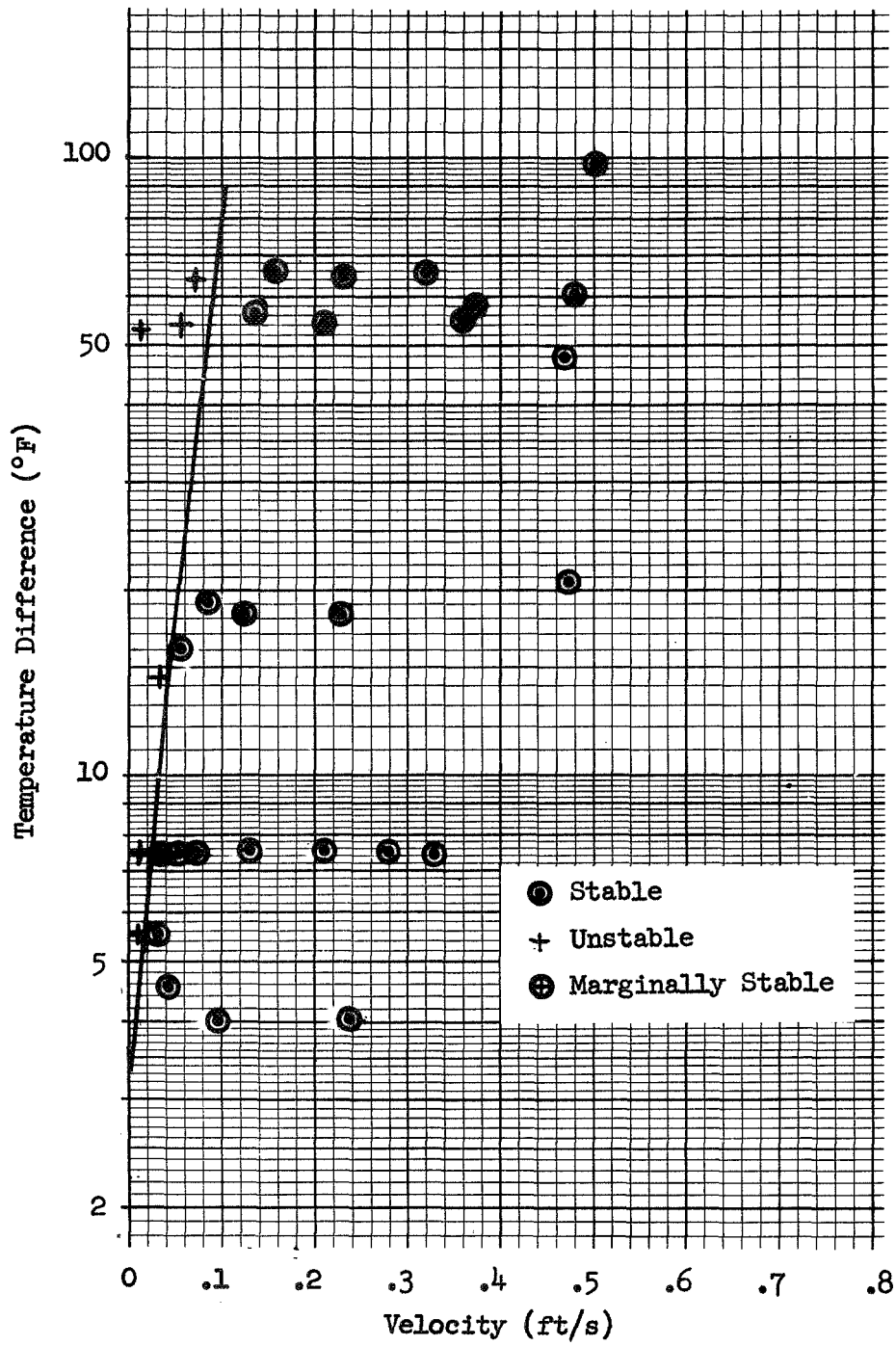


Figure 114. — Experimentally Determined Stability Boundary for Thermistor 2

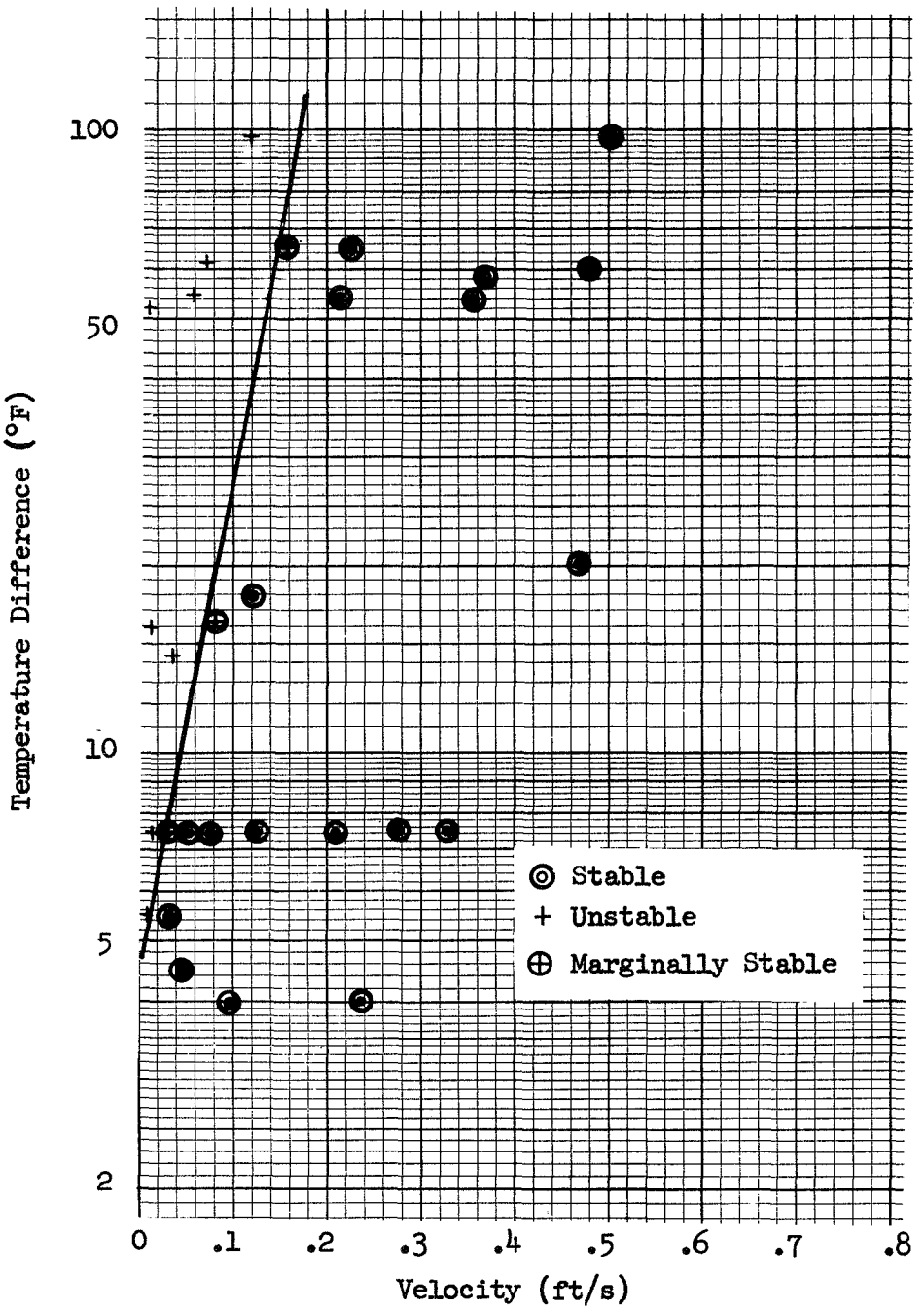


Figure 115. — Experimentally Determined Stability Boundary for Thermistor 3

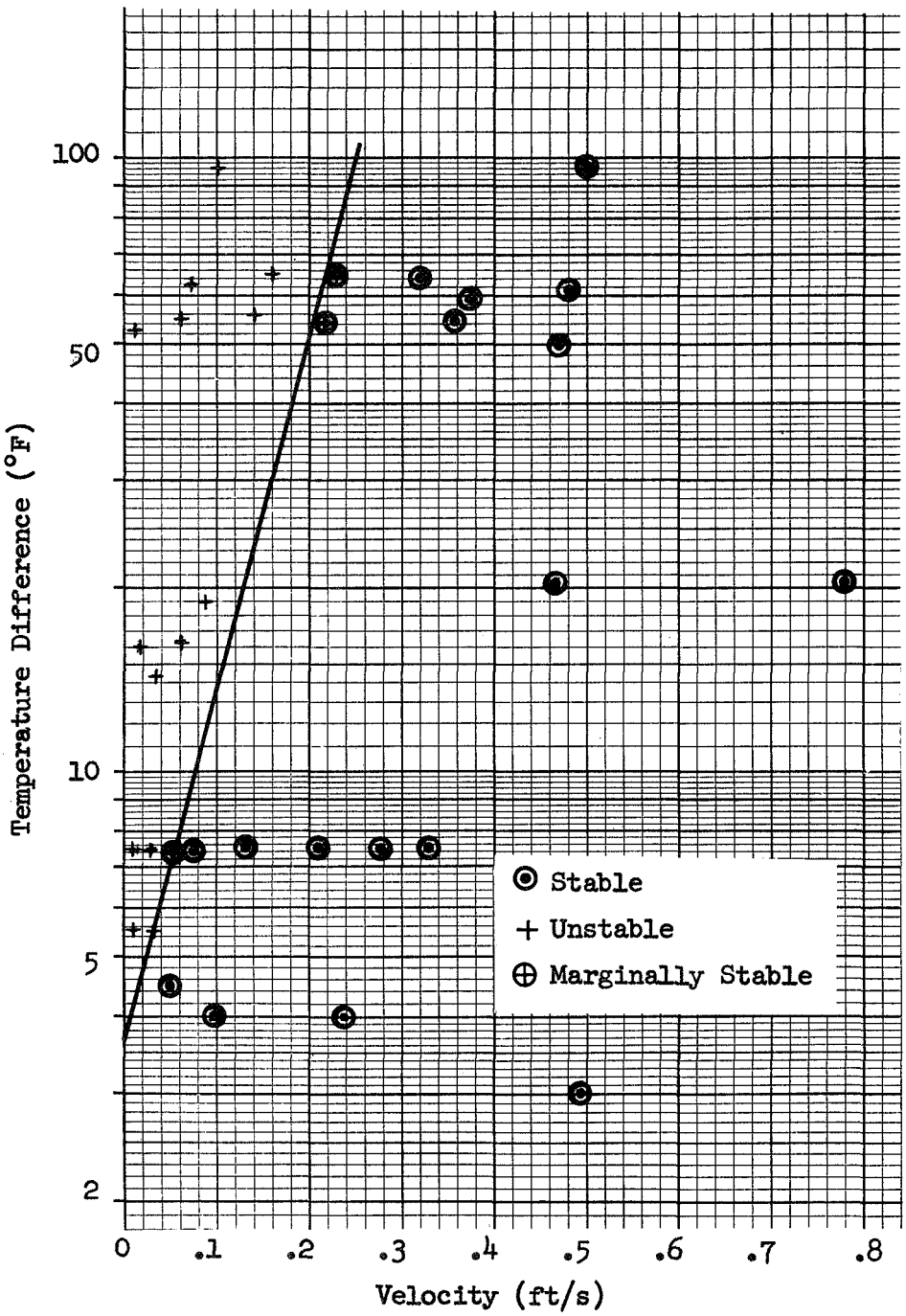


Figure 116. — Experimentally Determined Stability Boundary for Thermistor 4

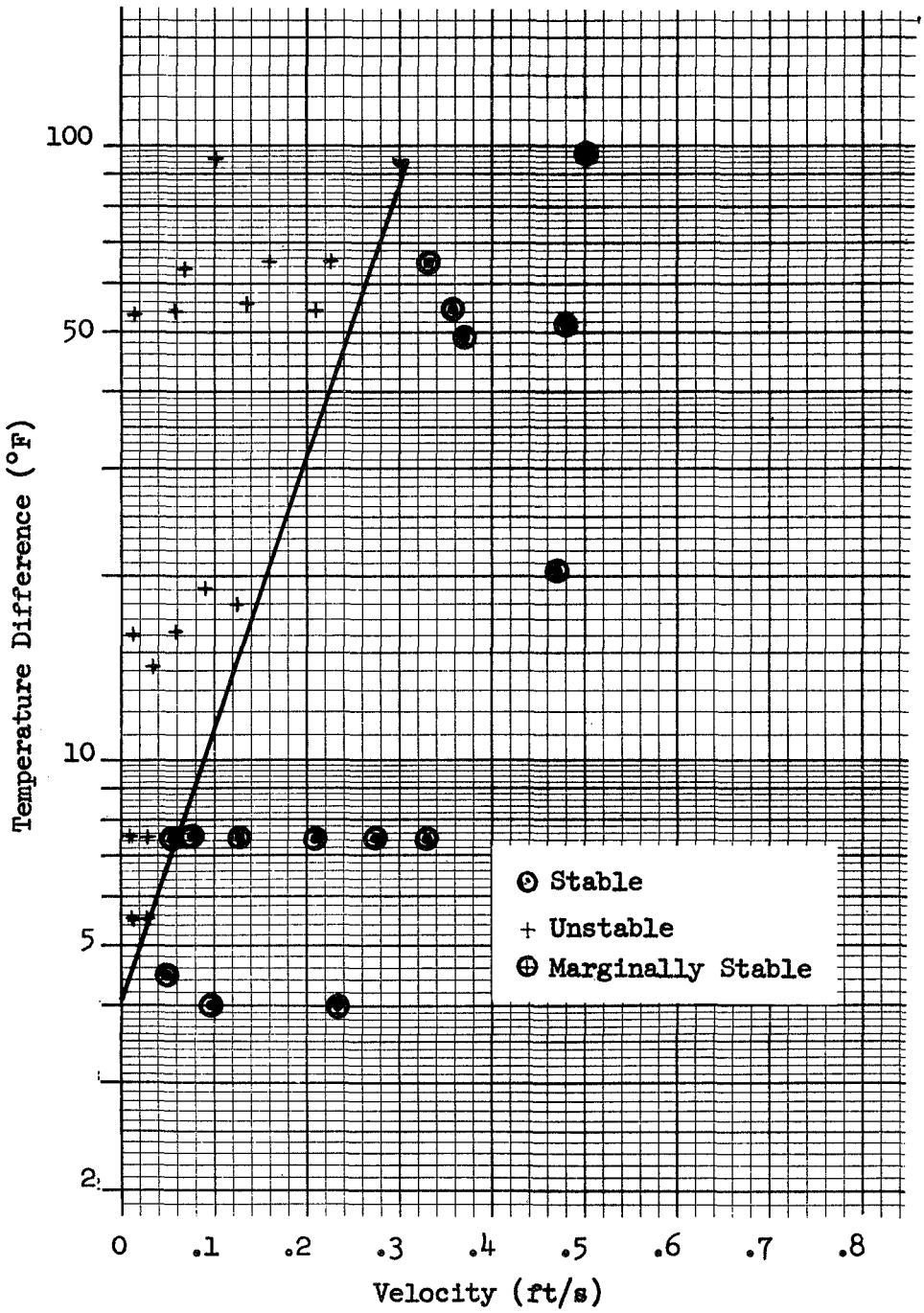


Figure 117. — Experimentally Determined Stability Boundary for Thermistor 5

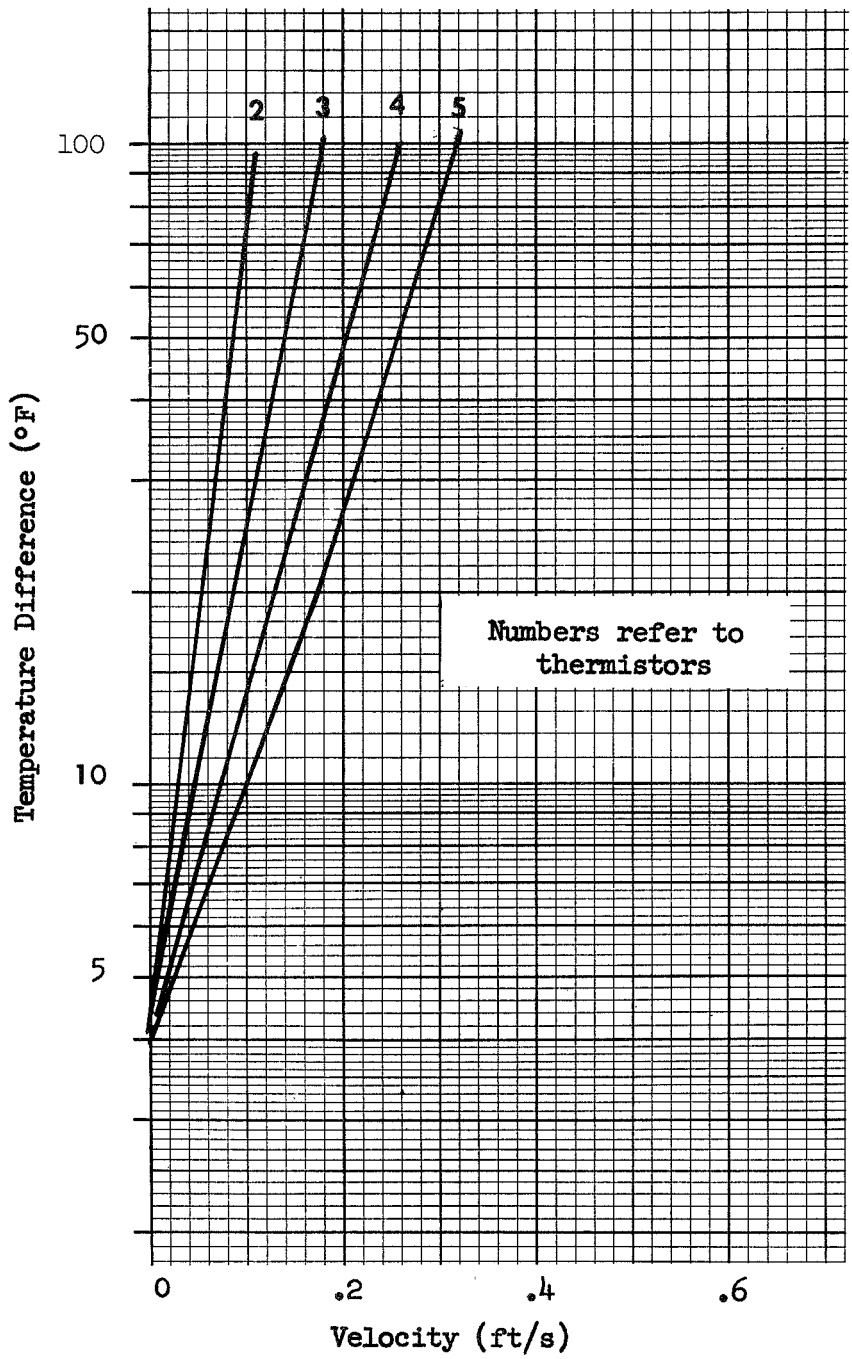


Figure 118. — Composite Stability Boundaries

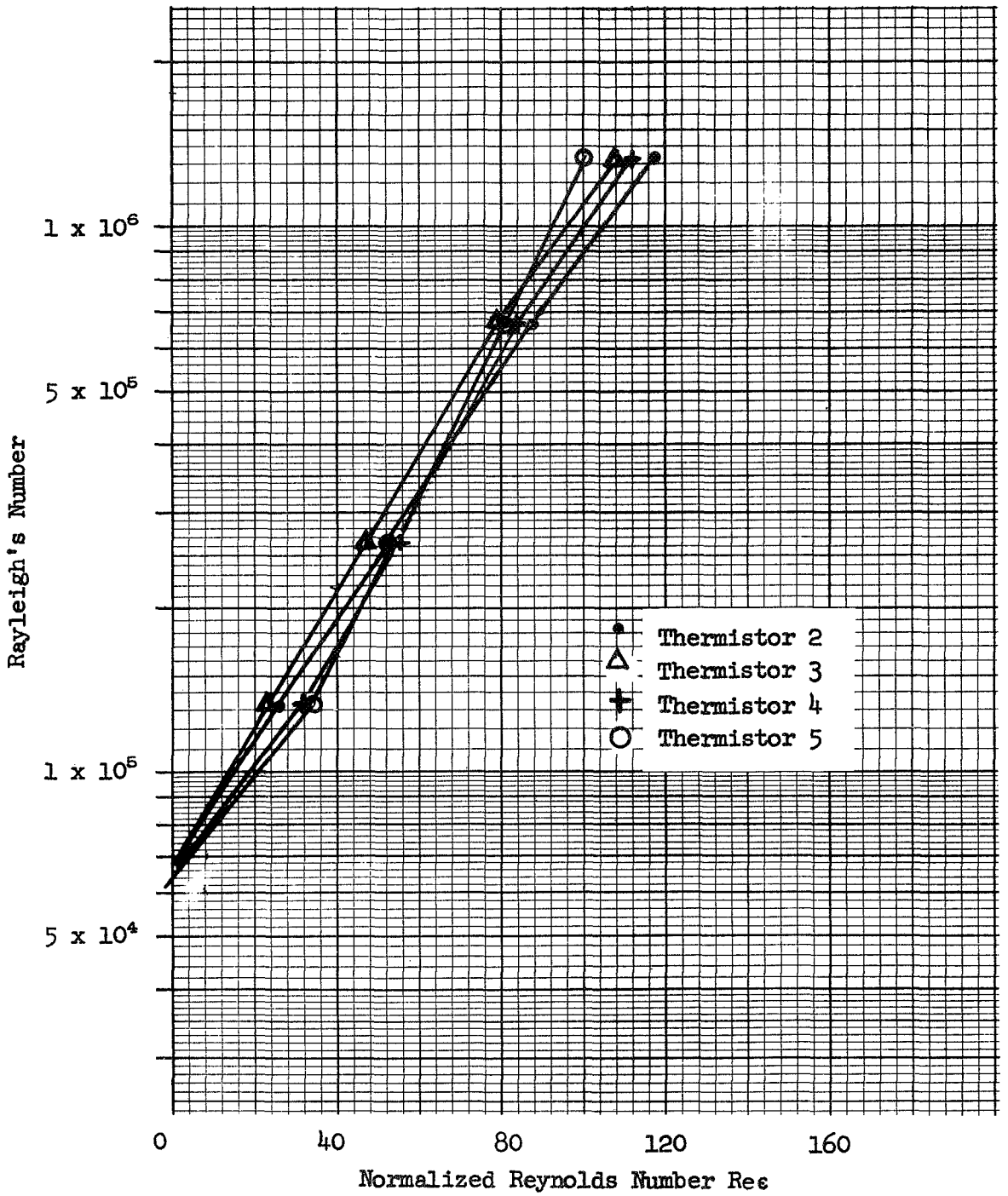


Figure 119. — Composite Stability Boundaries (Rayleigh vs Normalized Reynolds Number)

Re_ϵ value (see table 39) for that sensor along with the corresponding Rayleighs. Actually, only four points for each curve of figure 118 were transformed as indicated in figure 119. The four normalized curves all lie in a fairly narrow region which attests to the basic validity of the experimental information.

The $Re_\epsilon = 0$ intercept values of $Ra \sim 6 \times 10^4$ agree very well with other independent measurements (ref. 4). Of course, these data are the most unreliable since the temperature and velocity measurements in this region are probably not too accurate. However, since all four intercept extrapolations gave essentially the same value, it can be assumed fairly valid.

Since we are assuming that the two transition boundaries are parallel, the principal element of the data correlation now is to determine the value of the parameter σ for this condition. Figure 120 shows the superposition of the experimental results taken from figure 119 and several transition boundaries. The latter were calculated from equations (19) and (20). It appears that the line for $\sigma = 3$ gives the best fit under the stated parallel assumption.

The direct verification of the functional nature of the ϵ parameter (d/L) adds significantly to the confidence in the parallel hypothesis; the growth parameter σ, which represents the perturbation amplification during one transit time, is not analytically predictable. However, experimental correlation indicates a value of order 3 or a perturbation growth of order e^3 ($\sim$ 20:1) which is not unreasonable. Future experiments should include the observation of the dependent or independent nature of σ on geometry and the two region transitions. The fact that the functional dependence of Rayleigh number for the Region II to III transition on $\sigma\, Re_\epsilon$ (with σ fixed at its correlative value) is appropriately represented by equation (20) indicates that the physical hypothesis behind the thesis of the higher order transitions is reasonable.

Results of the Experimental Evaluation

The execution of the experiment, analysis of the data, and examination of the correlation between predictive and experimental results has led to a major reconsideration of the nature of convective heat transport. More importantly, recognizing the existence of the two transition boundaries is considered to be significant to the design of life support equipment and further development of the analytical model.

Critique of the Experimental Design Concept

The analytical model as currently formulated deals with the transition from thermal diffusion/forced convection to natural convection/forced-convection heat transfer or, in the terms of the graphical representation of the model, transition from Region I to II.

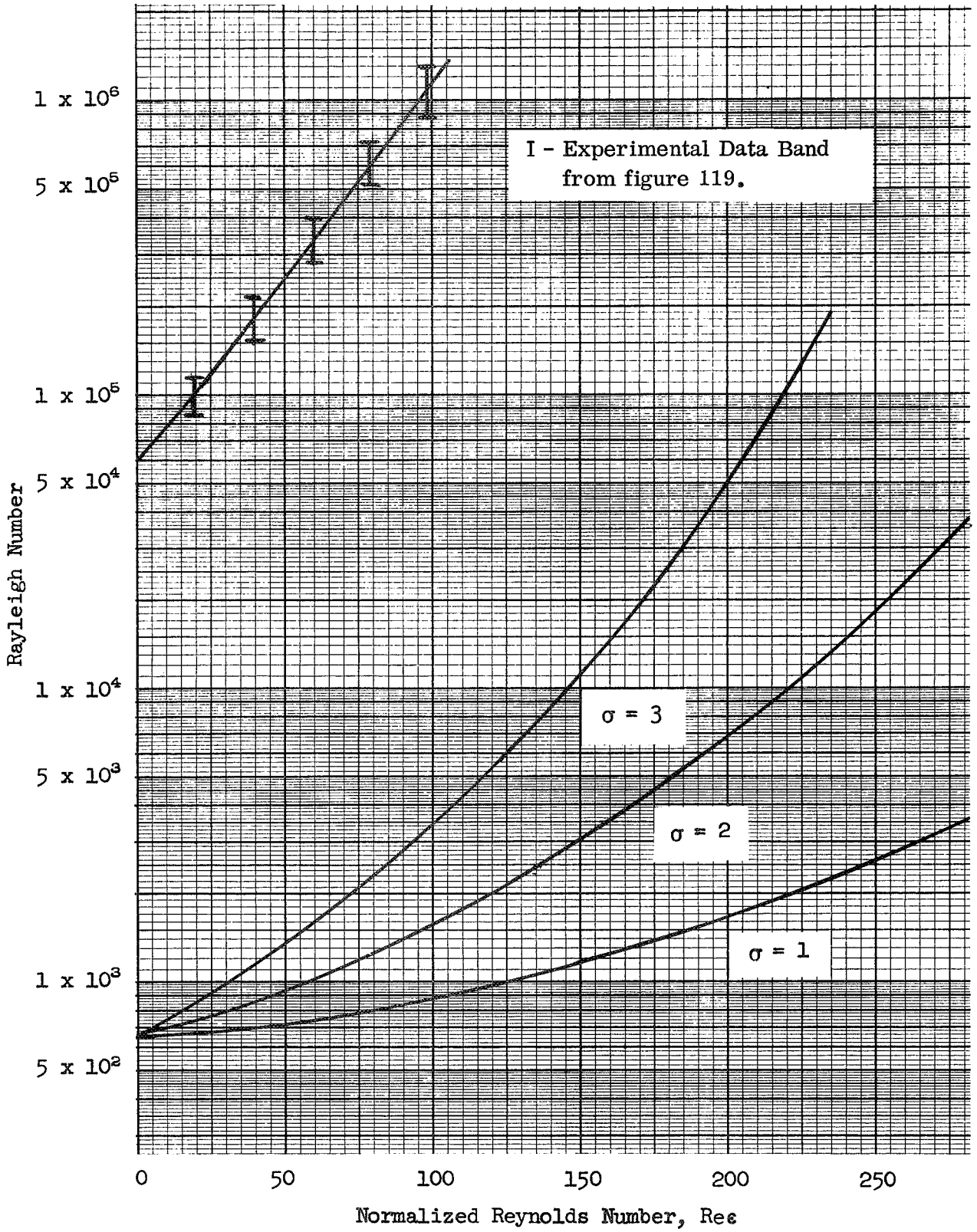


Figure 120. — Correlation of Experimental and Predictive Data

The experimental design on the other hand restricted the primary observations (that of the measurement of the velocity variations operating in a plane parallel to the surraces of the hot and cold plates) to the phenomena involved in the system of laminar-to-turbulent natural/forced convection as illustrated graphically by the transition from Region II to III. The secondary observations, however, made possible by smoke visualization provided a tool for at least a qualitative examination of both transitions. The degree to which the design of the turbulence-sensing assembly restricted the observations was not fully appreciated until well into the experiment schedule and at a point where analysis of data was in progress. As previously indicated, this restriction produced an additional insight into the larger problem of heat transport phenomena in a moving stream. However, without being fully aware of the nature of this restriction during the major portion of the allotted schedule, the test resulted in unnecessarily limiting the exploitation of the potentials of the smoke visualization for definitions of the transition from Region I to II.

Impact on the Analytical Model

The experimental observations suggest no corrective change of the basic analytical model and have inferentially at least substantiated its validity. However, the observations strongly suggest expanding the scope of the model to include the transition from Region II to III. In so doing, the entire spectrum of operating conditions would then be covered, making it possible to more completely and accurately determine the heat transport effects. At the present time analytical developments in the area of the turbulent transition are fragmentary at best, and the task may prove to be extensive. Preliminary indications from the analysis of the laboratory data are that such a model is both feasible and attainable. Reduced-gravity experiments should add significantly to such a development.

Recommendations for Further Experimental Evaluation

Laboratory Experiments

The nature and magnitude of the forces involved which provide the convection heat transport mechanisms are such that experimentation at both 1g and higher can be informative, especially under variations in the orientation of the systems to the gravitational vector. However, the practicality of the higher g tests is not established at this point in the study.

The experiments conducted in this phase of the program provided valuable insights into the solution of design problems for future experiments. However, the approaches to obtaining quantitative measurements data relating to transition from Region I to II have not been fully examined. Prior to the final design of experiments for reduced

gravity, sufficient laboratory experimental work should be undertaken to assure equal confidence with that which now characterizes the designs for investigation of the transition from Region II to III.

Reduced-Gravity Experiments

The model will require further experimental evaluation under conditions where the values associated with the local-gravity vector are sufficiently low to observe the transport behavior when its mechanisms can be dominated by other than the effects of density differences in the fluid stream.

The KC-135 aircraft low-g flight trajectories could be of value in the continued evaluation of the model, if sufficient isolation from airframe vibration could be achieved. These flights, although short in time for each trajectory and thus limiting with respect to determining steady-state conditions, would provide sufficient time to observe the initial changes taking place in the steam profiles with changes in the g level. It is possible that observations throughout the trajectory, both during the transitional stages where increasing and decreasing inertial acceleration forces are seen, as well as during the steady-state low-g phase, could provide some useful data against the analytical model. While the KC-135 may provide sufficient experiment time at a sufficiently low- and stable-g level to be of some value, the long duration tests made possible by the manned orbital station are ultimately required and thus should be considered the prime source of data. Other ground-based facilities, such as the drop tower, are of marginal value at best due to short observation times and the relatively complex nature of the experimental apparatus.

REFERENCES

1. Heppner, D.; Evans, E.; Burnett, J.: Analytical Model Report 5, "Convection Heat Transport." Second Issue, NAS1-8494, April 1970.
2. Ballinger, J.; et al: Study of Zero Gravity Capabilities of Life Support Systems Components. Final report NAS1-6939, NASA-CR-66534, GDC-DBD67-004, Convair division of General Dynamics, February 1968.
3. Chandrasekhar, S.: Hydrogynamic and Hydromagnetic Stability. Oxford, 1961.
4. Kreith, F.: Heat Transfer. International, Scranton, Pa, 1962.
5. Landau, L. D.; Lifshitz, E. M.: Fluid Mechanics. Pergamon Press, London, 1959.
6. Burnett, J.: Experimental Test Report, Test 5, "Convection Heat Transport." NAS1-8494, March 1970.

ANALYTICAL MODEL NO. 6 — "FLOW REGIME CHARACTERISTICS"

The initial steps in the development of an analytical model have been formulated which describe the significant phenomena involved in two-phase flow. The new approach can be developed with sufficient rigor to provide a means of determining the two-phase transport characteristics with a certainty approaching that traditionally associated with "Newtonian fluids."

The majority of the work accomplished during this phase of the analysis has been centered in the examination of two-phase flow as represented by the traditional Baker "flow maps." The extensions are primarily associated with the changes in flow characteristics resulting from variations in the local inertial acceleration field forces (ref. 1).

The current version of the model is primarily oriented to the qualitative prediction of transport characteristics of two-phase fluid flow in a closed conduit of circular cross section. Although two-phase flow can be either adiabatic or diabatic flow, only adiabatic flow has been examined. The principal reason behind imposing this limitation on this phase of study was to reduce the experimental complexity. The major emphasis is on momentum effects rather than the phase-change kinetics. Transport characteristics and phase separation are dependent on knowledge of the spatial distribution of phases, i.e., flow regime.

The model considers the efects on the predicted behavior in each of several flow regimes resulting from variations in such operating parameters as:

a. Gravitational field strength and orientation.

b. Liquid characteristics as influenced by

    1. Mass density.

    2. Dynamic viscosity.

    3. Surface tension.

c. Gas/liquid mass ratio.

d. Duct diameter.

The model is so designed as to be of potential value in the development or analysis of LSS equipments where two-phase fluid flow phenomena can be expected. The major area for application in the on-design condition is primarily with the sanitation and hygiene subsystems and in the initial delivery circuit of subcritical cryogenics. However, there are many areas throughout the full range of subsystems where two-phase fluid flow can develop and require management at least temporarily. Such is the potential

with many of the subsystems employing mass or, in some cases, surface effects liquid/gas separation devices.

DESCRIPTION OF THE MODEL

Identification of the Flow Regimes

The flow regimes as they are manifested under normal gravitational forces are illustrated by observing vertical and horizontal flow sections. The flow, when vertically oriented and directed upward, progressively moves through the following flow regimes when the mass velocity of the liquid is held constant and the gas mass velocity is increased: bubble, slug, foam, semi-annular or wave, annular, dispersed annular, and mist. For horizontal flow, which is selectively gravity-sensitive to stratification, the regimes are bubble, plug, stratified, slug, spray annular, and mist. A visual representation of the flow regimes for both conditions is presented in figure 121 and 122. In the traditional Baker plots (ref. 2), the flow regimes are defined for horizontal flow in the air/water system as shown by figure 123.

Characteristics of Two-Phase Flow

Two-phase flow is characterized by individual phase properties, e.g., velocity, mass flow, and density. This implies that the equational degrees of freedom are doubled. To investigate a two-phase transport process, it is necessary to eliminate three-flow ambiguities:

a. Gas/liquid spatial distribution (flow regime).

b. Velocity inhomogenieties and interphase momentum exchange between phases (gas/liquid relative velocity-slip and "drag").

c. Interphase energy transport (heat transfer and mass exchange).

Items "b" and "c" are dependent on "a," flow regime. Intuitively, interphase exchange processes (b, c) are facilitated when phases are uniformly mixed (foam, mist, bubble flow) and inhibited when separated (annular or separate phase flow).

Not only are interphase exchange equations dependent on flow regime specification but the overall, mean mass transport equations are affected. Reference 3 contains an investigation relative to the limiting conditions of total spatial homogeneity to totally separate phase or annular flow and the effects on velocity, thermal inhomogeneities, i.e., slip ratio, interphase equilibrium. Flow regime knowledge greater than that

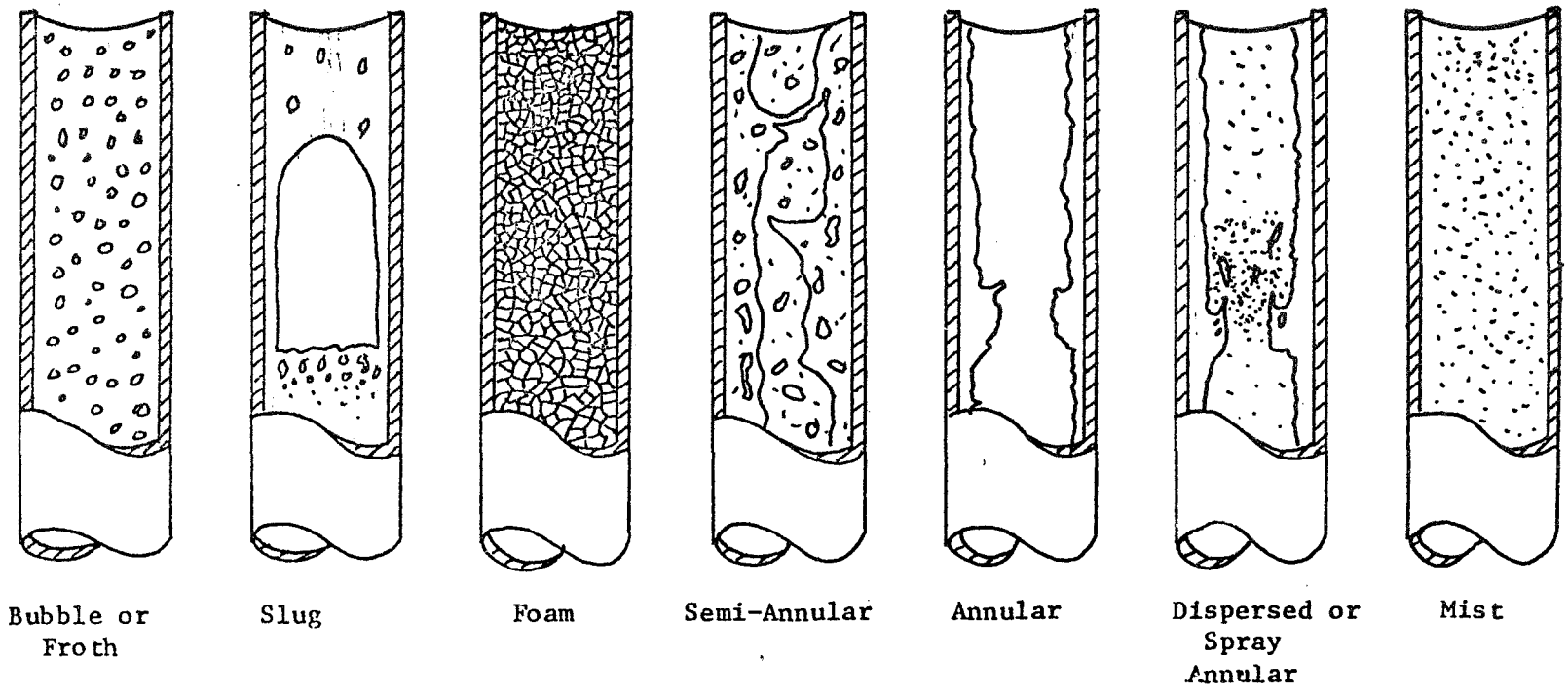


Figure 121. — Two-Phase Flow Patterns - Vertical

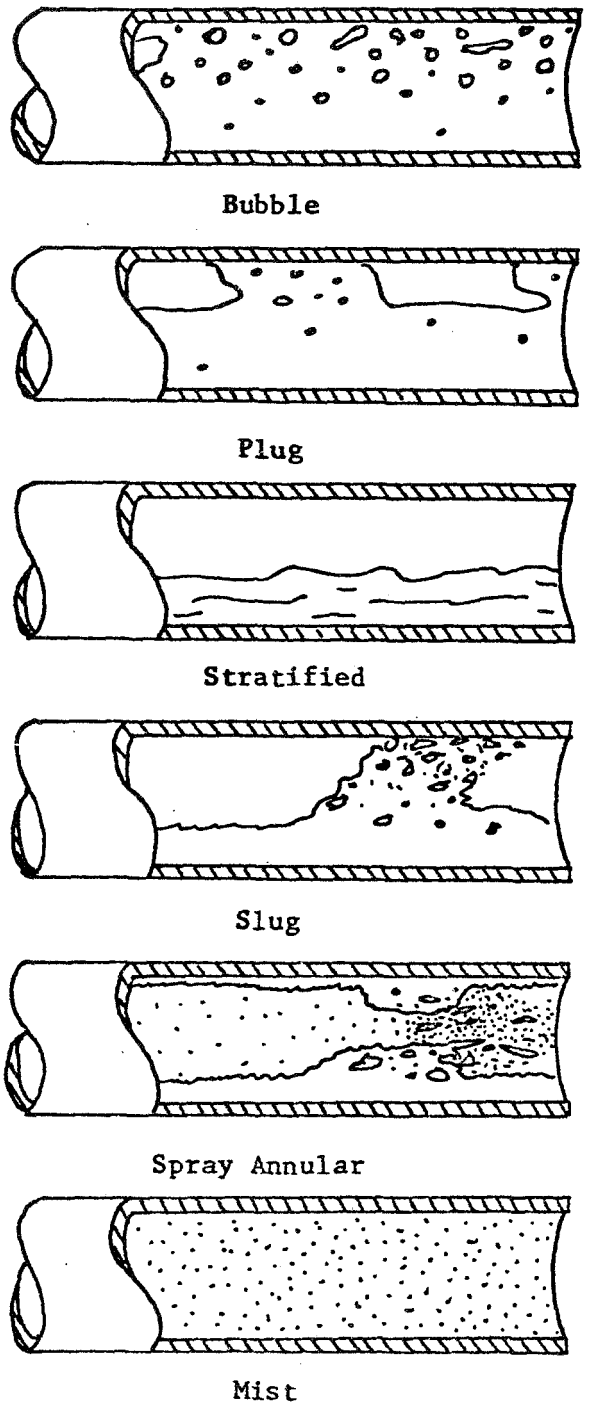
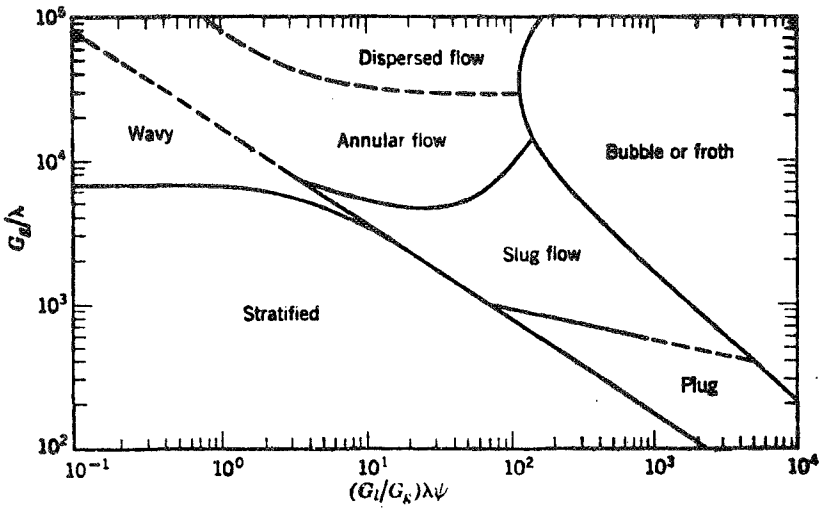


Figure 122. — Two-Phase Flow Patterns - Horizontal



$$\lambda = \left[\frac{\rho_g}{.075} \cdot \frac{\rho_\ell}{62.3}\right]^{1/2}$$

$$\psi = \frac{73}{\sigma}\left[\mu_\ell\left(\frac{62.3}{\rho_\ell}\right)^2\right]^{1/3}$$

μ_ℓ = centipoises

σ = dynes/cm

ρ = lb/ft^3

G_g/λ = $lb_m/hr.\ ft^2$

Figure 123. — Baker Flow Correlation

currently available must be developed to adequately analyze and design for two-phase flow processes. As an initial step, flow regime parametric topologies have been constructed in an attempt to meet this requirement. Both vertical and horizontal orientations were used. The crude method of spatial orientation is not satisfactory to investigate the effect of inertial fields; it only serves to increase or decrease the relative gas velocity. As is observed in the vertical position, major counter or cocurrent boundary layer flows exist as a result of gravity; this greatly affects pressure gradients and interphase momentum exchange. In low-g, the effects would be absent and new forces are apparent, e.g., surface tension

The forces acting in two-phase flow are, 1) pressure gradient, 2) body force (density times gravity, electrical field, magnetic field), 3) interphase viscous interaction, 4) interphase surface tension effects, 5) external viscous or wall shear stress. In normal gravity, forces 3 and 4 are dominated to a greater or lesser extent by forces 1, 2, and 5. Except for totally separate flow, the interphase shear stress (combination of forces 3 and 4) is dominated by flow turbulence and becomes important in the viscous subrange of turbulence in determining drop configuration. The turbulent effect on drop size and mixing is greatly affected by inertial or body forces and fluid vorticity, e.g., stratified and annular flow. It is apparent that the force complementation is very complicated and subtle, and that inertial fields play a significant role in the overall balance regardless of spatial orientation of the flow channel.

The classifcal Baker correlation illustrated in figure 123 presents little in the way of total parametric understanding. Approaches have been suggested for expanding the parameter dimensionality of the correlation to include the classical fluid mechanics dimensionless force ratios, e.g., Reynolds number, Froude number, Weber number, Bond number, etc. An example is the simple analysis of Quandt (ref. 4).

This particular analysis contains a major anachronism; that is, the fluid inertia and turbulence are neglected, although subtly and inaccurately represented by the pressure force. The merit, however, of the study is that it illustrates an informative empirical approach. Inclusion of turbulent and fluid inertia effects is necessary. The approach will not be fruitful until low-g data are obtained to fully eliminate the gravity field dependence and an inertial force spectrum is provided.

Spatial distribution of phases is determined by the balance of the homogenizing or mixing effect of turbulence against the separating effect of body forces and fluid vorticity.

Description of turbulence properties is extremely difficult and only slightly approachable in fully developed turbulence (macroscopic environment statistically coupled to fluid interior). To develop a methodology for parametric evaluation of flow regime, the scaling analysis of fully developed turbulence should be employed. It is emphasized, however, that in many situations the turbulence is only slightly developed if at all, e.g., slug, plug, and bubble flows.

References 5 and 6 contain extensive descriptions of turbulence scaling theory. The important parameters characterizing the flow are:

ϵ ≡ the dissipation or rate of energy transfer from large eddies to small eddies and eventually to the microscopic or viscous subrange eddies where the energy is converted to heat.

Re ≡ Reynolds number characterizes the "extent" or number of "degrees" of freedom (eddies) of the turbulent flow.

λ ≡ Kolmogorov length, the distance over which viscosity acts, the viscous subscale, the scale of the smallest eddy, etc.

ν ≡ the kinematic viscosity.

ρ ≡ the density.

u ≡ bulk velocity.

ℓ ≡ scale of large eddies (e.g., tube cross-sectional diameter).

σ ≡ surface tension of liquid.

$$\epsilon \sim \frac{u^3}{\ell} \ \mathrm{cm^2/sec^3} \tag{1}$$

$$\mathrm{Re} \sim \frac{u\ell}{\nu} \tag{2}$$

$$\lambda \sim \ell \mathrm{Re}^{-3/4} \ \mathrm{cm} \tag{3}$$

For two-phase flow, a set of parameters for each phase is defined:

Gas	Liquid
$\epsilon_g \sim \frac{u_g^3}{\alpha D}$	$\epsilon_\ell \sim \frac{u_\ell^3}{(1-\alpha)D}$
$Re_g \sim \frac{u_g \alpha D}{\nu_g}$	$Re_\ell \sim \frac{u_\ell (1-\alpha) D}{\nu_\ell}$
$\lambda_g \sim \alpha D Re_g^{-3/4}$	$\lambda_\ell \sim (1-\alpha) D Re_\ell^{-3/4}$

where

$\alpha \equiv$ void fraction (volume fraction of gas)

$D \equiv$ tube diameter

subscripts ℓ, g = liquid and gas properties

The largest size that a gas bubble, in the liquid phase, can attain is expressed by the surface tension traction greater than the viscous shear stress.

$$\frac{2\sigma}{R_{B_g}} > \rho_\ell \nu_\ell \frac{u_\ell}{\lambda_\ell}, \quad R_B = \text{bubble radius}$$

$$R_{B_g} < \frac{2\sigma (1-\alpha) D Re_\ell^{-3/4}}{\rho_\ell \nu_\ell u_\ell} \tag{4}$$

Similarly, for liquid drops in the gas phase,

$$R_{B_\ell} < \frac{2\sigma\alpha D Re_g^{-3/4}}{\rho_g \nu_g u_g} \tag{5}$$

Criteria (4) and (5) represent the turbulence limits on phase size.

The actual distribution is represented by the comparison of the turbulent eddy diffusion (mixing) with the separation effect of the body force or secondary rotation and vorticity.

The turbulent diffusion is modeled by the diffusion law,

$$D_E \nabla C > C b \vec{f} \tag{6}$$

D_E = turbulent diffusion constant

C = concentration of species

b = mobility

$\vec{f}$ = body force, e.g., gravity (g)

∇ = gradient operator

The diffusion constant for statistically independent and isotropic systems is proportional to the kinetic or statistical energy; therefore, the turbulent eddy diffusion constant is scaled by the dissipation

$$D_E \sim \frac{D \epsilon}{u} b$$

Equation (6) is scaled by,

$$D \frac{\epsilon b}{u} \left(\frac{C}{D}\right) > CD g_r$$

$$\frac{\epsilon}{u} > g_r \tag{7}$$

g_r = gravity component normal to flow direction

Using equation (1), equation (7) becomes

$$\frac{u^2}{Dg_r} > 1 \tag{8}$$

The left-hand side is the classical Froude number; therefore, the balance of gravity against turbulent eddy diffusion is represented by the Froude number for each phase.

$$Fr_g \equiv \frac{u_g^2}{\alpha D g_r} > 1$$

$$Fr_{\ell} \equiv \frac{u_{\ell}^2}{(1-\alpha)Dg_r} > 1$$

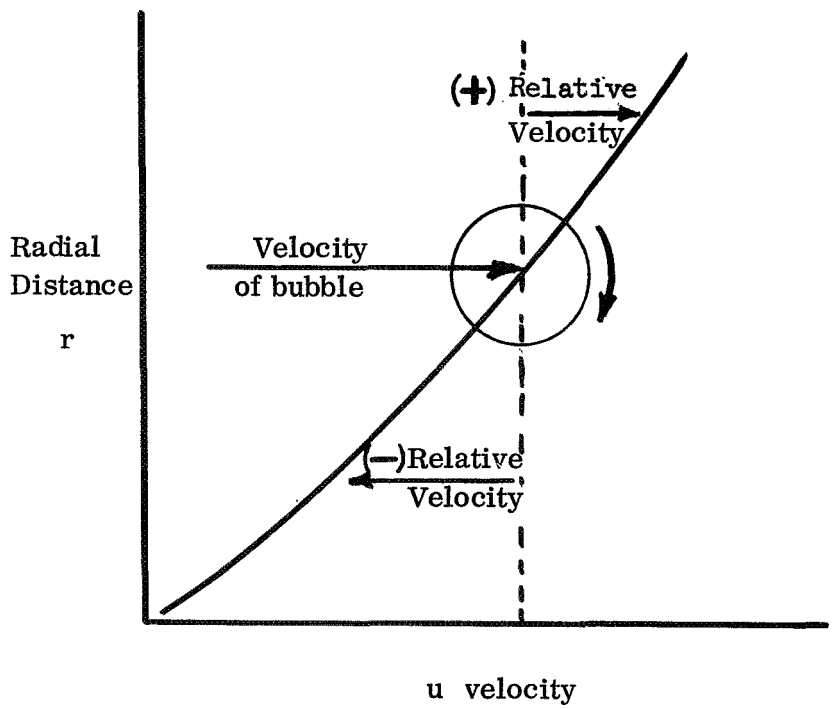
Some function of the Froude numbers should define the stratified flow condition, e.g.,

$$Fr_g + Fr_{\ell} < 1 \tag{8a}$$

Slug, plug, bubble or froth, and mist flow conditions are conditions determined by large Froude numbers and the criteria (4) and (5) which were previously described. Entrainment of gas bubbles in the liquid phase or liquid droplets in the gas phase (for pseudo-stratified condition) is also determined by the conditions (4) and (5).

The most difficult aspect of the flow regime character to specify is the annular or separate phase flow for large Froude numbers. Here, the secondary flow (rotational) and fluid vorticity create centrifugal separation which is balanced against turbulence and, a lesser extent, body force or gravity.

Consider the following simple model: bubble placed in a velocity gradient rotates because of the moment induced by the different relative velocities on either side of the body.



The angular velocity "ω" is proportional to $\frac{\partial u}{\partial r}$

$$\omega \sim \frac{\partial u}{\partial r}$$

Since the fluid in the vicinity of body is also in rotation, there is a centrifugal acceleration and force induced by the rotation,

$$f_\omega \sim u \left|\frac{\partial u}{\partial r}\right| \sim (\vec{\omega} \times \vec{v}) \tag{9}$$

For cylindrical flow channels $\partial u/\partial r$ is the shear stress on the fluid; therefore, the force, f_ω, acts in the radial direction and causes the lighter fluid to move to the center and the heavy fluid to separate to the exterior, i.e., annular flow.

Equation (9) is used in equation (6) to determine the balance between the homogenizing effect of turbulence and the separation due to fluid shear.

$$\frac{D \epsilon b}{u} \frac{C}{D} > Cbu \left|\frac{\partial u}{\partial r}\right|$$

$$\frac{u}{D} > \left|\frac{\partial u}{\partial r}\right| \tag{10}$$

The shear stress is given by,

$$\left|\frac{\partial u}{\partial r}\right| \sim \frac{-\Delta P/\rho + g_Z L}{\nu}$$

where

$g_Z \equiv$ axial component of inertial (gravity) field

$L \equiv$ axial length parameter

$\Delta P \equiv$ pressure drop over L

Equation (10) becomes,

$$\frac{u}{D} > \frac{-\Delta P/\rho + g_Z L}{\nu} \tag{11}$$

It is evident from equation (11) that the effect of gravity is not eliminated by orienting the flow section vertically. Equation (11) represents the boundary between a mixed or dispersed (bubbles, etc.) flow regime and annular flow. The boundary for annular and stratified flow is represented by (also annular to slug or plug flow boundaries in the vertical position)

$$u\left|\frac{\partial u}{\partial r}\right| > g_r \tag{12}$$

$$\frac{u(-\Delta P/\rho + g_Z L)}{\nu} > g_r \tag{13}$$

The super-position and projection of equations (4), (5), (8), (11), and (13) provide a method of determining flow regime topologies. It is evident that these equations represent the interference between turbulent mixing, inertial fields (gravity), and fluid vorticity or shear separation effects; the many combinations of which create the complicated and subtle world of two-phase flow observations.

When gravity is decreased by orders of magnitude, one may expect it to disappear as a significant force and total interphase shear stress effects will become more important than has previously been observed. The complex and unsteady characteristics of the gravity-controlled regimes will be minimized.

It was not necessary or advantageous to develop a computer program for this phase of the study.

APPLICATION TO LSS DESIGNS

The generalized nature of the analytical model which most likely can be developed following the analysis of experimental data obtained under low gravity provides a relatively high probability that the model can be directly applied to the development of several LSS design approaches. Table 41 identifies examples of the type of LSS equipment which, potentially at least, will be so designed that the model can be profitably applied to the analysis of primary or "on-design" modes of operation. However, possibly one of the major applications of the model may be in the analysis of the behavior of two-phase flow which might exist when systems operate under "off-design" conditions. Such conditions have existed when an excessive entrainment of gas has resulted from separator malfunction or inefficiency but operation is still possible due to the existence of "down-stream" secondary modes of separation or the ability of the system to ingest the excessive gas. In the early phases of a system design study, the model might be employed in the comparative analysis of competing designs, one or more of which are

either designed for two-phase transport or have the potential for formation of a two-phase condition under off-design conditions.

The most likely application of the model(s) for design analysis and synthesis involves 1) those functions employing transport of subcritically stored cryogenics, and 2) the majority of the principal sanitation and hygiene functions as currently conceived. The latter have been continuously troublesome, both analytically and operationally, with designs intuitively determined in most cases.

Table 41. — Examples of LSS Equipment Designs for which the Analytical Model has Relevance

Equipment Type by Degree of Relevance by Mode / LSS Function	Model Relevance			
	On-Design		Off-Design	
	A*	B	A	B
Oxygen Supply & Recovery		3**	11,12	8,10,22, 23,24,27, 28,32
CO_2 Removal	16		15	17,18,19
Water Reclamation			38,39,40, 41,43,45, 47,48	46,49,50, 51,52,53
Humidity Control***	58(a)		57(a),(b) 59(b),60	58(b) 61,62,63
Sanitation & Hygiene	78,80, 81,82	74,79	68,69 76(a),83	

*Degree of relevance: "A" implies a high degree of relevance both as to similarity of the model to the equipment processes produced under the designated mode combined with a high probability that the process will be extended into similar designs in updated systems, while "B" implies a lower degree of similarity and/or probability of extension to similar designs.

**Equipment type identified by LSS equipment reference number.

***Many areas of the humidity control function were not included in the equipments for analysis, thus the paucity of entries, especially in the off-design mode.

EXPERIMENTAL EVALUATION

Requirements

It has been determined during the course of this study that the experiments which must be conducted in the examination of the characteristics of two-phase flow, will be called upon to perform a multiple role, including:

a. Determination of the feasibility and applicability of the approach which has been suggested for the development of an analytical model describing the dynamic, spatial properties of the two-phase flow.

b. Production of empirical data which can be utilized in the continued development of the suggested analytical model.

c. Investigation of approaches to the design of experiments to obtain the required data, with special emphasis on those to be conducted under low gravity.

Potentials of Laboratory Experiments

It is believed that the role of laboratory experiments conducted prior to the low-gravity experiments can best serve to determine appropriate approaches to test design for the low-g experiments. Evaluation of the effectiveness of the experiment design approaches can logically be accomplished by comparisons of the experimental data with that implied by the Baker flow correlation.

Potentials of the Experiments Under Reduced Gravity

It is considered vital to the development of the suggested analytical approach that experiments be conducted under reduced gravity, preferably at more than one level. Experiment design concepts developed in the laboratory phase will be significant in the design of the low-g experiments.

Description of the Experiments

Laboratory experiments have been conducted which have produced significant information relative to the requirements discussed in the previous section (ref. 7).

Experimental Test Summary

An experimental test was designed to investigate the characteristics of two-phase adiabatic flow regimes with special emphasis on the effects of variations in the quality of the mixed-phase fluid, the orientation of the direction of flow with respect to the

gravitational vector, and the physical characteristics of the liquid. The primary objectives of the experimental investigation were:

a. The evaluation of test design concepts developed during the course of this study.

b. Determination of definitions of flow regime characteristics somewhat beyond those presented in the open literature, especially relating to the effects of:

   1. Orientation of direction of flow with respect to the gravitational vector.

   2. Differences in the physical characteristics of fluids.

Two fluid systems were investigated, namely glycol/air and water/air. Principal instrumentation for the determination of the flow characteristics was provided by 1) high-speed movie photography and film analysis, correlated with various flow, pressure, and temperature measurements, and 2) visual observations relating the observed characteristics to those identified by the existing analytical descriptions. In excess of 350 flow conditions were monitored against five working section flow "angles" and the two fluid systems. Data have been collected in the form of motion pictures, still photographs, narrative descriptions, numerical data, and brush recordings.

Major Goals

Primary. — To record the various flow patterns that develop in the transport of a liquid/gas mixture for various mixture ratios and momentum transport forces, with special emphasis placed on the effect of orientation to the local gravity vector.

Secondary. — To accumulate information helpful to the design of the future experiments required under reduced gravity.

Principal Observations

The experimental observations which were required included:

a. Gas pressure drop.

b. Two-phase flow pattern.

The experimental variables to be programmed against these observations included:

a. Liquid flow rate.

b. Air flow rate.

c. Working section orientation to the gravity vector.

d. Liquid physical characteristics.

Criteria for Test Model Design

The test model and its supporting apparatus were designed under the following criteria:

a. Two-phase adiabatic flow through a closed duct of circular cross section be visually observable and photographically recordable.

b. The liquid/gas ratio of the two-phase flow be controllable through a range sufficient to evaluate the analytical model, particularly as applied to the identification of flow regimes to the extent determined practicable.

c. The effect of changes in liquid characteristics be determinable.

d. The principal transport forces be determinable.

e. The effects of the local gravitational forces be demonstratable.

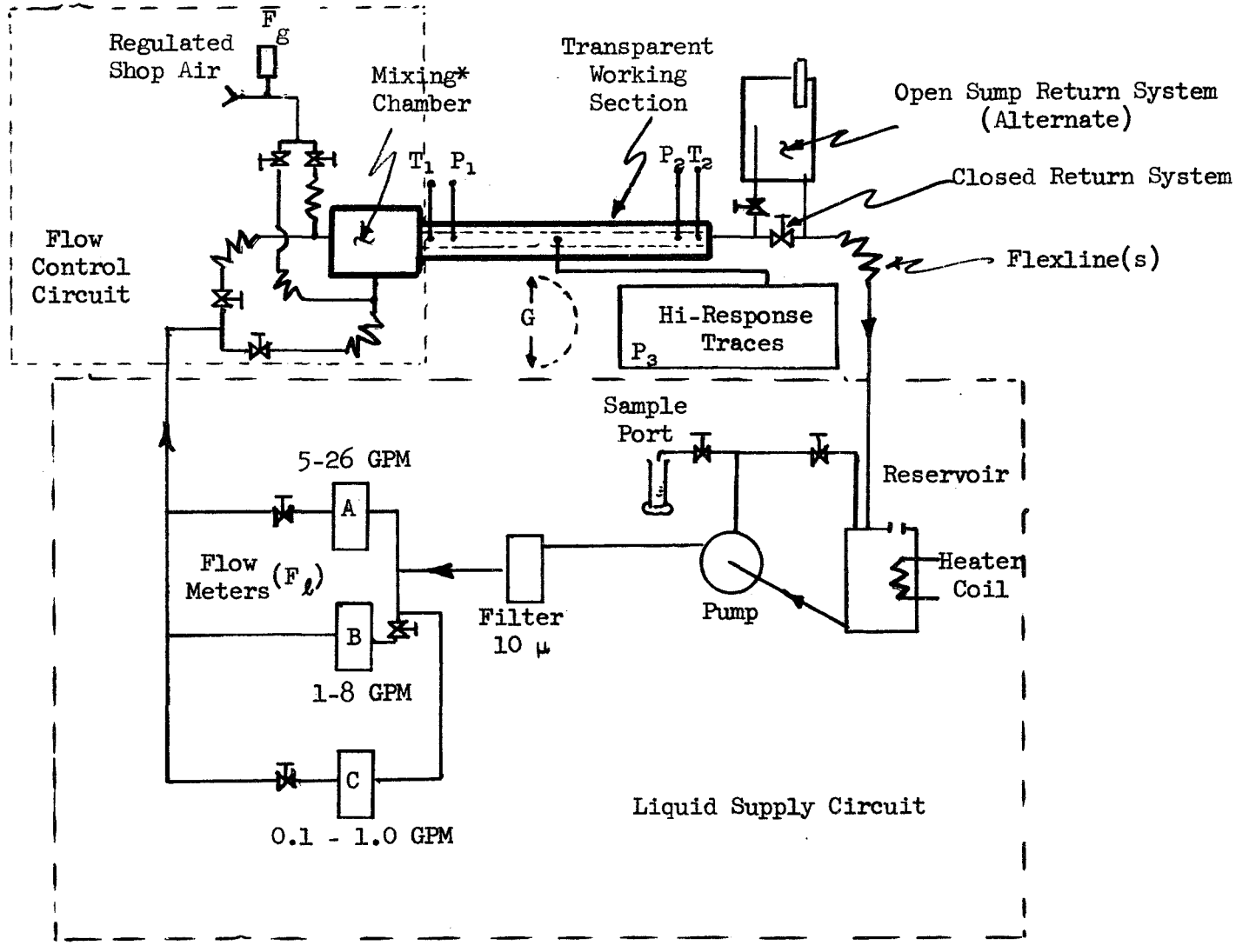
f. Economy of construction, simplicity of test procedures, and schedule be compatible with NAS1-8494 objectives.

Test Apparatus

The concepts relative to test apparatus requirements as illustrated in ETP 6 were only slightly modified by interactions between the on-going maturation of the analytical and accompanying test design studies. The apparatus used in this experiment is shown schematically by figure 124 and pictorially by figure 125.

Liquid supply circuit. — The liquid supply circuit was initially designed for test 2 and subsequently modified for use in test 3A in keeping with the requirement for demonstratable potential for experiment integration. As shown in the schematic, the circuit is composed of a centrifugal pump, 10-micron filter, a bank of flow meters, reservoir, valving, and several minor subcircuits for venting, sample, and other test support functions. Circuit flow capacity was adequate to provide the maximum flow required of the experiment, approximately 20 gal/min under a 5-psi line loss. Two return systems were provided; one comprised merely of a length of 1-inch transparent plastic tubing, and the other adding a vented sump immediately downstream of the working section outlet.

Flow-control circuit. — The flow-control circuit was designed to provide experimental flexibility with respect to control of the characteristics of the two-phase mixing to achieve as much of the full range of the predicted flow regimes as is economically practicable. Valving for air and liquid flow provided for various liquid/gas ratios at each of the two inlets to the mixing chamber. An air flow measurement was also provided. Liquid inlet line size was primarily 1-inch diameter, providing an ID ranging from 3/4 to 7/8 inch. Air inlet line size was primarily 1/4- to 3/8-inch ID.



*Variation of the flow control circuit is indicated by Figure 126, where single inlet flange replaces dual inlet mixing box.

Figure 124. — Test 6 Apparatus Schematic

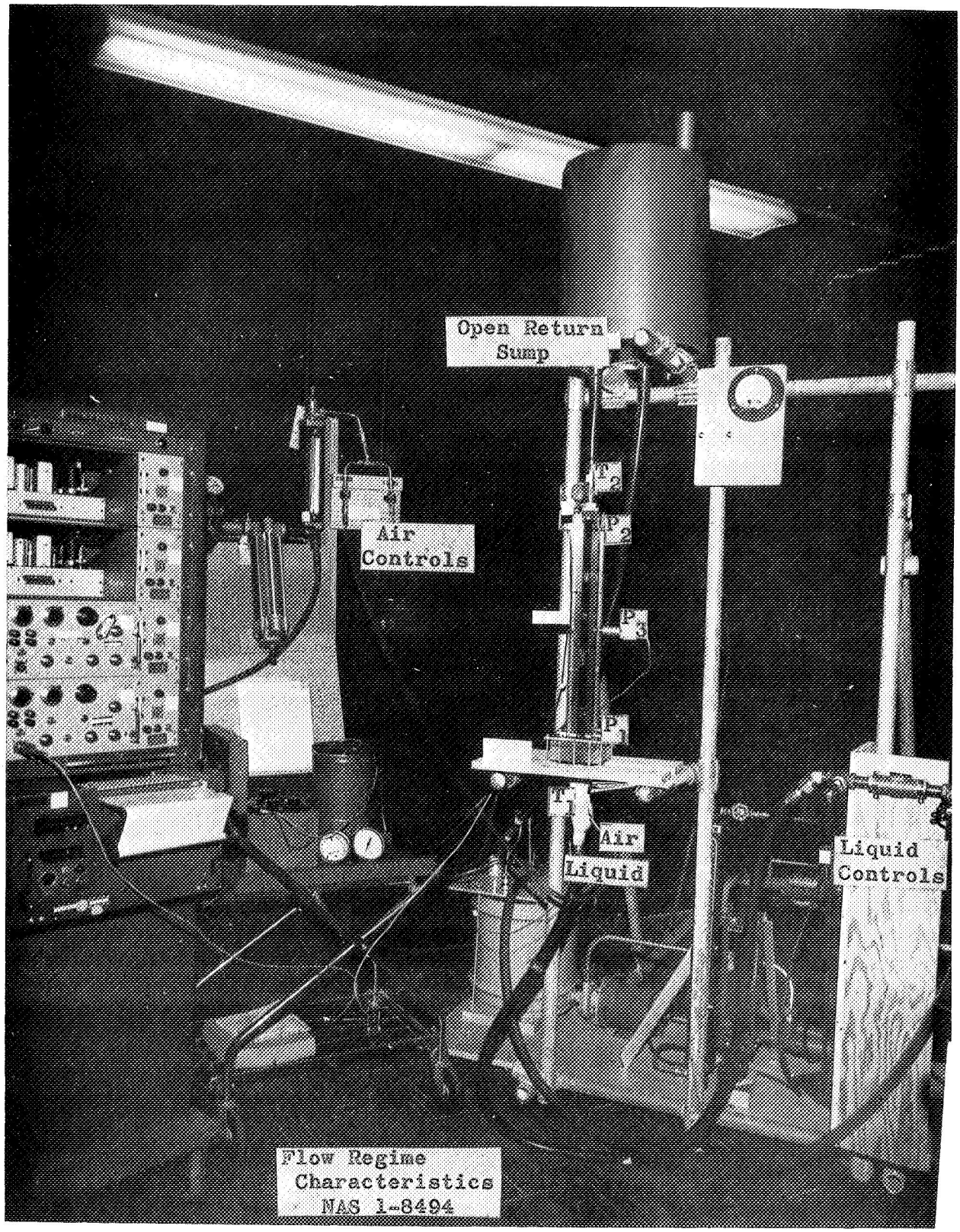


Figure 125. — Test Apparatus Photograph

The mixing chamber was constructed of 1/2-inch sheet lucite, providing a 3- by 3- by 6-inch working section inlet. A 5- by 5-inch mounting flange was attached to the oulet end of the chamber to facilitate removal and replacement of mounting with the working section. The two individually controlled inlets feeding into the transparent chamber, one parallel with and one normal to the duct axis, were designed to provide a convenient and repeatable means of manual control of the experimental variables involved, especially as required under alterations in the orientation to the gravity vector. A means for altering this basic inlet system (as experiments might dictate) was provided by a flange to replace the dual inlet mixing chamber. Additionally, a length of stainless steel tubing, roughly the length of the working section and of the same ID, was provided.

Working section. — As shown in figure 126, the working section was constructed from a solid block of lucite which, prior to sectioning and polishing, was 4- by 4- by 24-inches. A hole was drilled along the longitudinal center line of the block which, when polished, provided a circular cross section with a 1-inch diameter. The block was cut into three 8-inch sections to reduce the complexity of the drilling task. Following drilling and initial polishing, the sections were solvent joined, and the final internal and external polishing continued until sufficient optical clarity was attained as demonstrated by a series of trial motion picture runs. A 5- by 5- by 1/2-inch lucite plate was attached to the end of the working section to provide a mounting surface for the mixing chamber.

Flex line sections approximately 5 feet each for the mixing chamber inlets and 8 feet for the duct outlet made it possible to position the working section throughout the 180-degree range indicated.

The test model was mounted on an adjustable framework of 1.5-inch commercial pipe and Nu-Rail fittings as shown in figure 125.

Instrumentation. — As shown in figure 127, the major components of the instrumentation employed for the data runs against each of the measurements requirements included:

a. Fluid flow measurements (Rotameters A, B, and C).
    1. Liquid flow (0.25 to 30 gal/min).
    2. Air flow (0.25 to 20 scfm).
b. Working section pressure measurements.
    1. Working section internal pressure and transport pressure loss, P_1 and P_2.
    2. Flow regime pressure map, P_3.

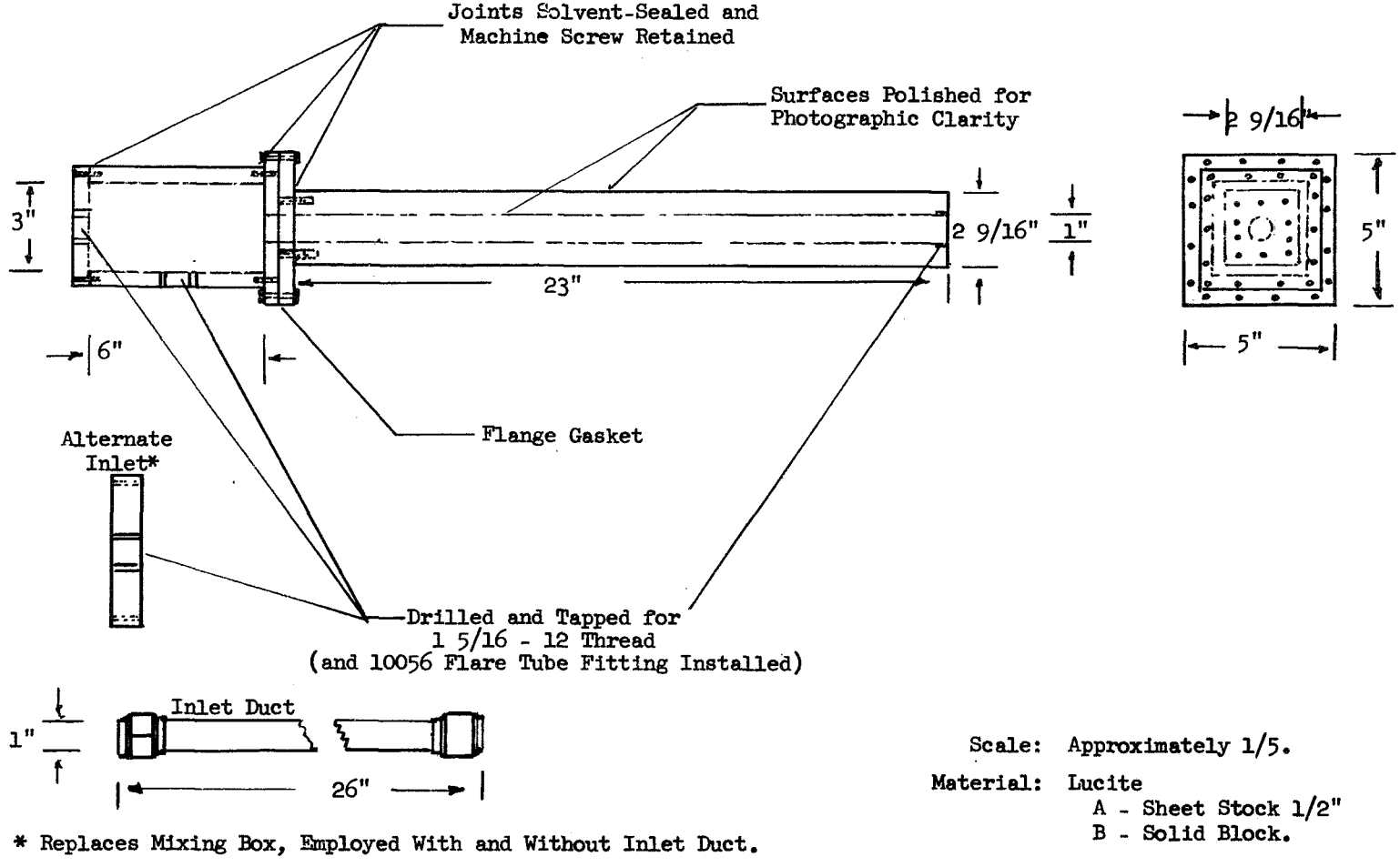
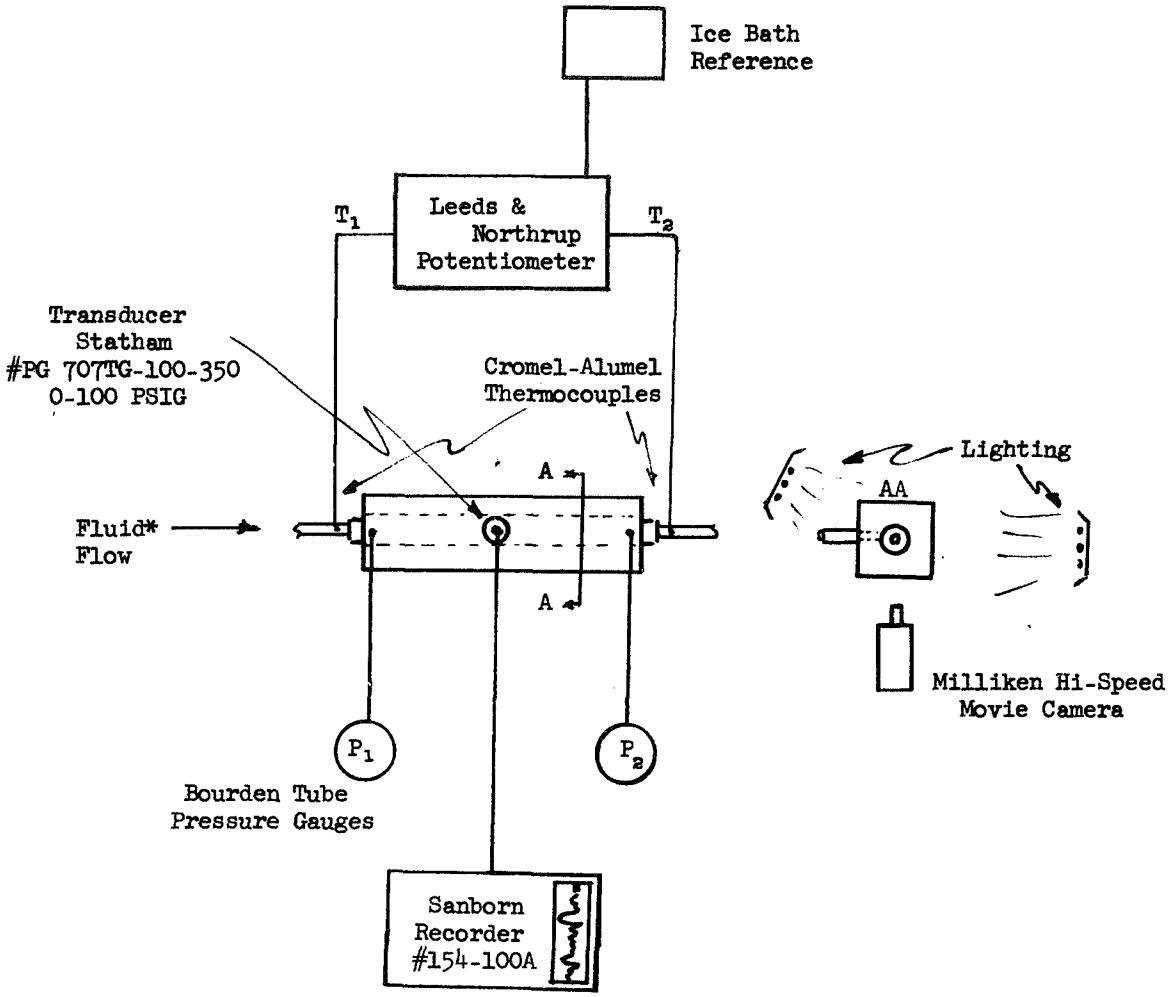


Figure 126. — Working Section Drawing



*Fluid flow measurement instrumentation shown on figure 124.

Figure 127. — Instrumentation Schematic

c. Working section temperature measurements (thermocouple).

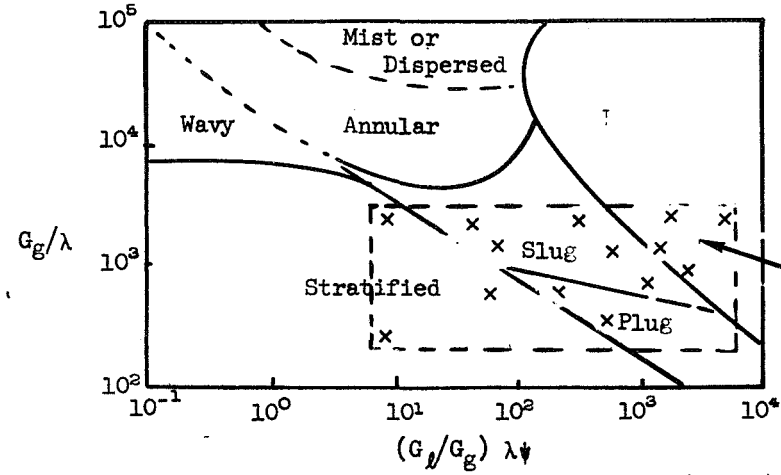
   1. Inlet fluid, T_1.

   2. Outlet fluid, T_2.

d. Flow pattern recording by Milliken, DB-4 pin registered, high-speed 16mm camera.

Test Procedures

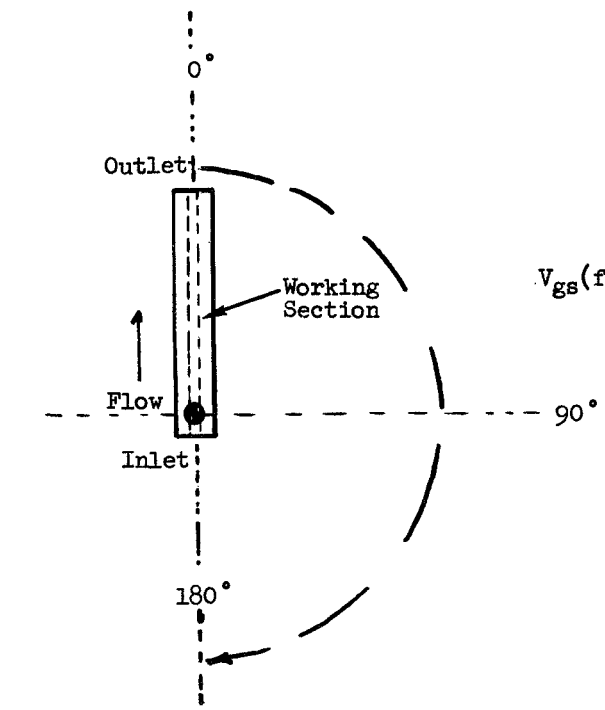
The test protocol developed from the guidelines shown on figure 128 is indicated by tables 42 and 43 and generally provides for establishing various combinations of input variables and recording the resulting flow patterns. The test protocol as implied by the format of the example data sheet was devised first by determining the various valve combinations which tended to produce observable differences in flow patterns. This



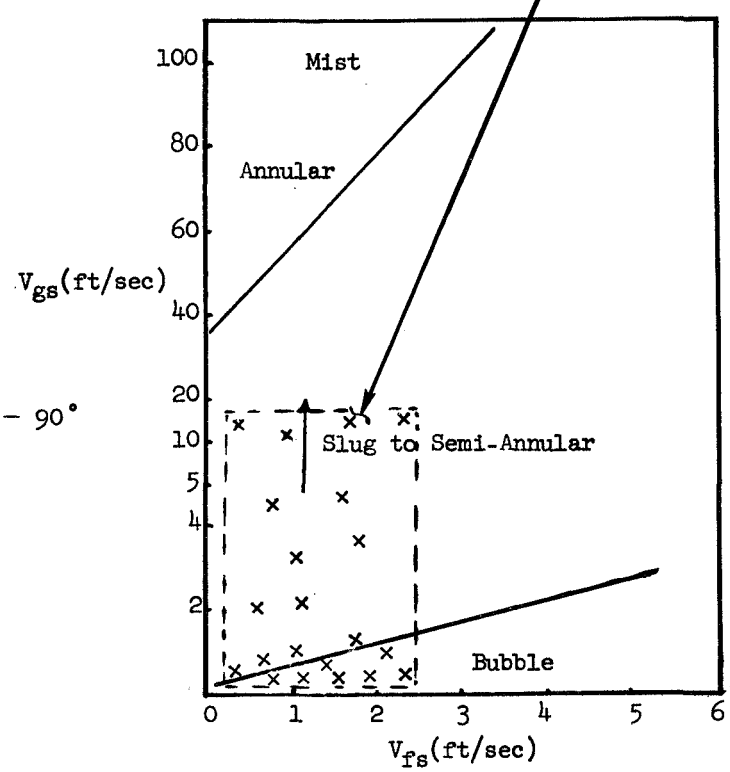
A. Baker Flow Correlation, Horizontal (Water)

Refer to Page 1-5 of AMR #6, 2 Sept. 1969.

\pproximate area of exploration by Test Design, Typical Test Points Shown.



C. Working Section Orientation



B. Rosenham Flow Map, Vertical (Water)

Figure 128. — Test Protocol Guidelines

Table 42. — Valve Position Combinations Selected for Vertical Orientation

Liquid (L) \ Air (A)	0	1	2	3	4	5	6	7	8	9
1	1 * 0	**1 1**	1 2	1 3	1 4	**1 5**	1 6	1 7	1 8	1 9
2	2 0	2 1	**2 2**	2 3	**2 4**	2 5	**2 6**	2 7	2 8	**2 9**
3	3 0	**3 1**	3 2	3 3	3 4	3 5	3 6	3 7	3 8	3 9
4	**4 0**	4 1	**4 2**	4 3	**4 4**	4 5	**4 6**	4 7	4 8	**4 9**
5	5 0	**5 1**	5 2	**5 3**	5 4	5 5	5 6	5 7	5 8	5 9
6	6 0	6 1	**6 2**	6 3	6 4	6 5	6 6	**6 7**	6 8	6 9
7	**7 0**	**7 1**	7 2	**7 3**	7 4	**7 5**	7 6	7 7	7 8	**7 9**

* Upper left is row number, lower right is column number.
Selected combinations shown in heavy outline.

resulted in the selections shown in table 44. All possible combinations (liquid/air) of these positions were listed as shown in table 42, a simplistic adaptation of the "Latin Square" typically employed for the design of tests. Selection of the combinations to include against any working section was determined by choosing a set of data points from the two flow-correlation plots as shown in figure 128 and translating to specific valve positions and so indicating on the appropriate "Latin Square."

Experimental investigation indicated that five working section orientations would adequately cover the full angular range, namely, 0, 45, 90, 135, and 180 degrees. Additionally, it was determined that these five orientations produced two basic sets of flow patterns characteristic of the vertical and horizontal flows. From this, two series of flows scheduled, namely, one for the vertical (0 and 180 degrees) and one for the nonvertical (45, 90, and 135 degrees).

Table 43. — Valve Position Combinations Selected for Horizontal Orientation

Liquid (L) \ Air (A)	0	1	2	3	4	5	6	7	8	9
1	1.0	1.1	1.2	1.3	1.4	1.5	1.6	1.7	1.8	1.9
2	2.0	2.1	2.2	2.3	2.4	2.5	2.6	2.7	2.8	2.9
3	3.0	3.1	3.2	3.3	3.4	3.5	3.6	3.7	3.8	3.9
4	4.0	4.1	4.2	4.3	4.4	4.5	4.6	4.7	4.8	4.9
5	5.0	5.1	5.2	5.3	5.4	5.5	5.6	5.7	5.8	5.9
6	6.0	6.1	6.2	6.3	6.4	6.5	6.6	6.7	6.8	6.9
7	7.0	7.1	7.2	7.3	7.4	7.5	7.6	7.7	7.8	7.9

Experimentation also indicated that the flow characteristics being observed might be significantly altered by pressure pulse feedback resulting from excessive slugging in the return line to the reservoir, identified as the "closed return system." To evaluate this, a vented sump was designed for installation immediately downstream of the working section outlet and was designated the "open return system." Comparative tests were scheduled against all working section positions but only the 0-degree position was executed as a result of 1) the relatively small difference observed, 2) the readily identifiable characteristics of the differences observed, and 3) the difficulty in positioning the open sump for the remaining positions.

Each set of conditions to be run against each working section position was identified as a "test set" and subsequently assigned a number. Each valve position combination was identified as a "subset" and assigned a number corresponding to the sequence of execution. The result of this system of identification is illustrated by the data sheet format.

Two sets of data were recorded against each of the two liquid/air systems, namely, 1) the "manual" data runs which recorded operating conditions and written descriptions of the observed flow patterns against all scheduled data points, and 2) the movie runs made against significant flow combinations identified as a result of the previous "manual" data runs.

Table 44. — Candidate Valve Positions

Valve Position Number		Flow	Meter Reading	
Liquid	1	0.5 (GPM)	B = 10 (glycol)	C = 26 (water)
	2	1.0	17	54
	3	2.0	30	B = 26
	4	4.0	57	50
	5	6.0	84	75
	6	8.0	A = 32	100
	7	12.0	48	A = 46
Air	0	0.10 (SCFM)	#1 = 0.11	
	1	0.25	0.26	
	2	0.50	0.52	
	3	1.0	1.02	
	4	1.5	1.54	
	5	2.0	2.05	
	6	2.5	2.55	
	7	3.0	3.05	
	8	3.5	3.56	
	9	4.0	4.08	

Note: A decision was made to run all tests at identical rotometer readings for both glycol and water in hopes of providing a more visually observable comparison of the differences in flow characteristics brought about by the differences in the physical characteristics of the two liquids. This decision in effect resulted in operating both systems at essentially identical "pumping power" levels rather than identical flow rates.

Data was manually and machine recorded with the former documented on test run data sheets. Following the manual runs, a set of conditions was chosen for motion picture recording. The criterion for selection of the movie runs was adequate documentation of all significantly different flow patterns; the constraint was cost and schedule.

Experimental tests in the completion of the apparatus design were initiated on 14 January 1970 and completed on 2 February 1970. Formal data runs were initiated on 3 February and completed on 12 February 1970.

Summary of Test Data

Data were recorded against two sets of experiments, namely:

a. Exploratory data runs — essentially instrumentation and test mode evaluation, modification, and calibration.

b. Formal data runs — the major experimental variables were mass flow rate, liquid/air ratio, liquid characteristics, and working section orientation to the gravity vector.

Exploratory data runs. — Exploratory data runs were made for instrument calibration and for procedure and equipment trials.

Calibration: Instrumentation calibration is shown by figures 129, 130, and 131 for flowmeters and P_3 recordings. Liquid characteristics were assumed to be identical with those for ET 3-A which were determined by laboratory test to be:

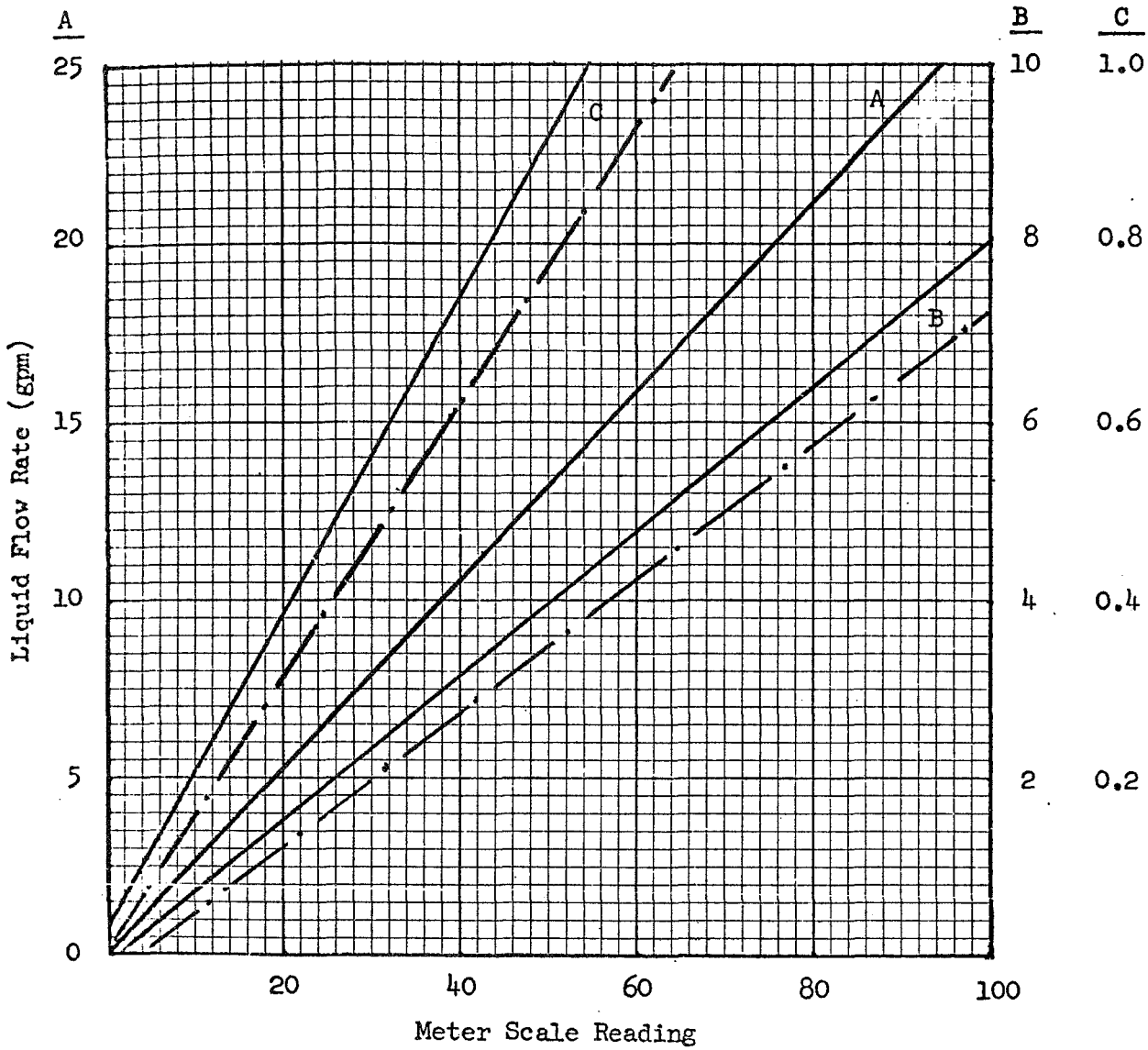
a. Propylene Glycol

   1. Viscosity (ASTM-D445-65) 21.1 CS @ 95° F.
   2. Surface tension (ASTM-D1331-56) 35.4 dynes/cm @ 92° F.
   3. Density (gms/ml) = 1.027 @ 70° F.; 1.014 @ 100° F.

b. Water

   1. Viscosity - 0.94 CS @ 75° F.
   2. Surface tension - 64.1 dynes/dm @ 73° F.
   3. Density (gms/ml) = 0.9979 @ 70° F; 0.9931 @ 100° F.

Trial data runs: Several sets of trial data runs were performed to evaluate and select the final test procedures, protocol, and equipment configuration. Following initial checkout and adjustment of apparatus, a systematic trial run was conducted to aid in finalizing the design of the tests.



Legend:

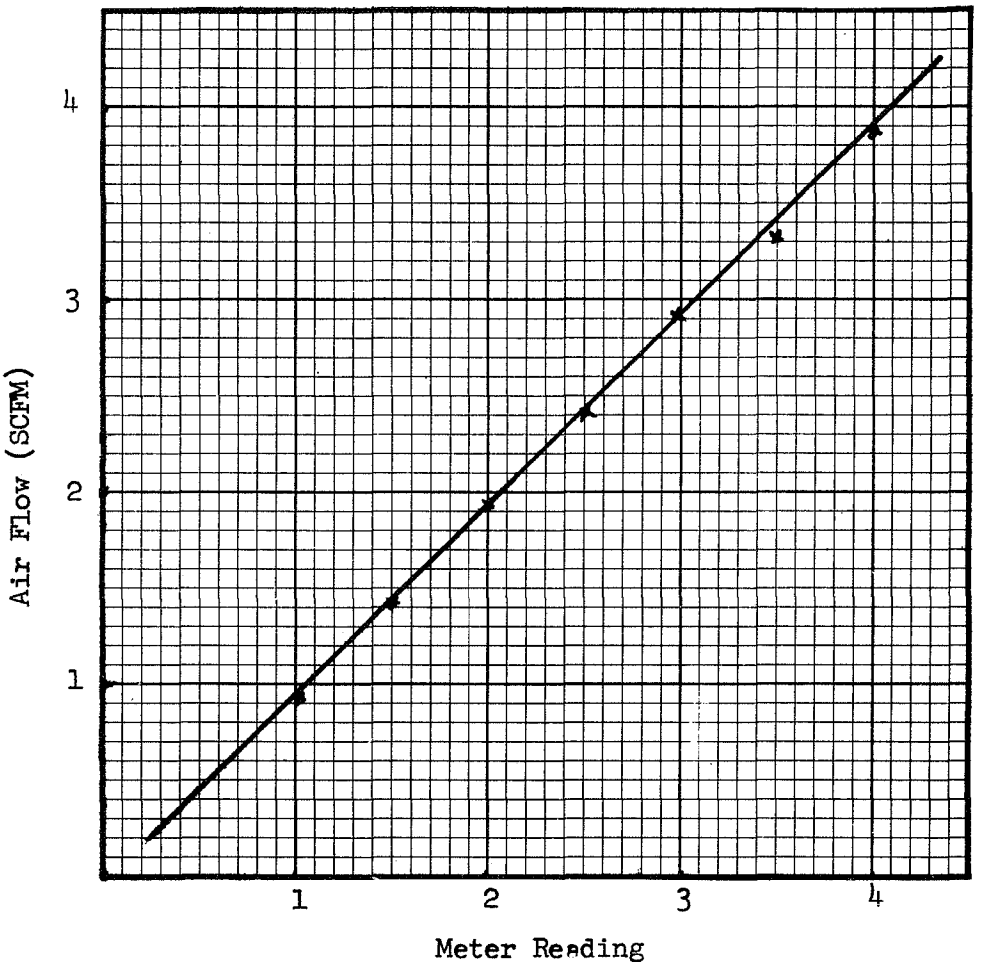
Water ————————

Glycol —— · (B & C only) ——·——

Note: 1. Water @ 69°F.

2. Letter designations identify corresponding graph scale and flow meter shown in System Schematic.

Figure 129. — Flow Meter Calibration, Liquid



Calibrated by Standards Lab, 09-15-69

Figure 130. — Flow Meter Calibration, Air

A series of trial data runs was made to resolve the following questions relative to the design of the formal tests:

a. Which inlet configuration(s) should be selected?

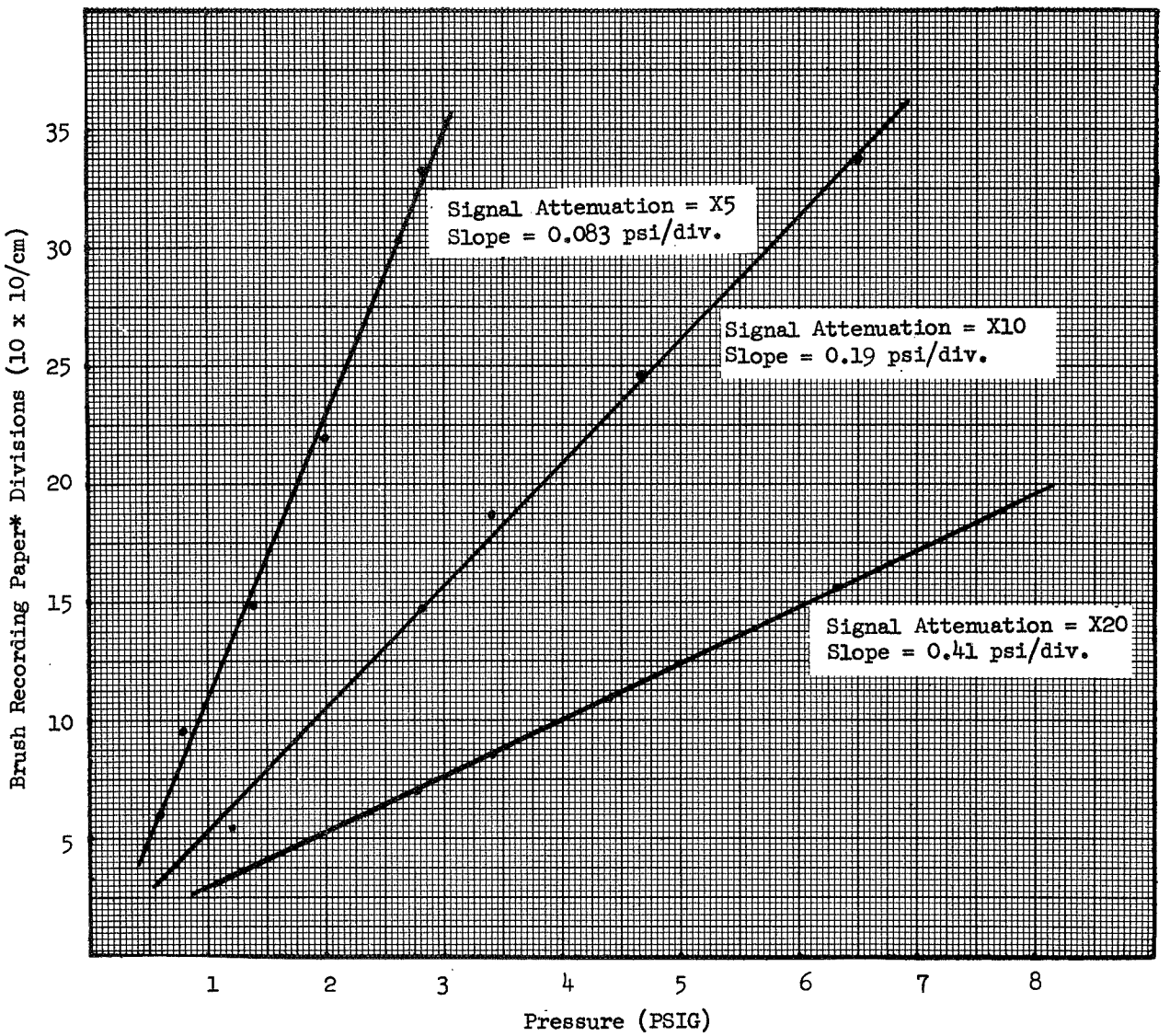
b. What working section angles should be included?

c. What minimum air flow set point should be selected?

d. What are the effects of alterations in outlet (return line) configuration? Are changes needed and, if so, what should they be?

e. Is it possible to visually identify flow regimes predicted and document the difference in characteristics of similar regimes for various test conditions?

f. Is the test manageable?



* Sanborn Permapaper - 4 Channel, P/N 651-54.

Figure 131. — Pressure Transducer (P_3) Calibration

To make these determinations, sample set points were adopted as shown in table 45.

Table 45. — Set Point Schedule for Trial Data Runs

Set Point	Liquid	Gas
1.1*	B-10	0.21
1.5	10	1.93
1.9	10	3.91
4.1	56	0.21
4.4	56	1.46
4.9	56	3.91
7.1	A-48	0.21
7.3	48	0.97
7.6	48	2.42
7.9	48	3.91

*Refer to Candidate Valve Positions, table 44.

Several runs were made in both the horizontal and vertical positions, employing several inlet configurations. These were compared to each other and to previous runs with the dual inlet mixing chamber in terms of effect on flow characteristics in the working section. The criterion for evaluation was the degree of correspondence to the flow regime pictorial models. The inlet configurations included:

a. Liquid/air injector, 90-degree elbow and inlet duct.

b. Liquid/air injector, no elbow, inlet duct.

c. Liquid/air injector, no elbow, no inlet duct.

It was abundantly clear that the single inlet without mixing chamber was preferable to the dual inlet and mixing chamber, at least for the 1g laboratory tests. It was equally clear that, although the inlet duct resulted in slightly less disturbance in the immediate vicinity of the inlet to the working section, it was not sufficiently superior to overcome the difficulty associated with physically managing the longer inlet, especially during angle changes.

Comparison of pressure data and observed flow patterns indicated that the test should be run at 0, 45, 90, 135, and 180 degrees.

Experiments showed that most, if not all, stable (non-oscillatory) slug flow for the vertical case occurred at air flows less than the minimum accurate set point for flowmeter 1, and that 0.1 scfm, the minimum measurable, should be scheduled and that further experiments should be performed at less than measurable flows.

Insofar as could be determined without high-speed movie data, flow regimes could be both identified and characterized through visual observation.

The test proved to be manageable except that the effect of variations in the outlet return line caused very significant alterations in the nature and magnitude of the feedback to the working section due to slugging in bends and rises. Investigations into the differences produced by an "open" return system demonstrated that the open sump outlet provided some reduction in feedback but not sufficient to warrant the additional system complexity. (See test M1A and M1 on page 360.)

A series of flow conditions was scheduled to investigate the differences which might be observable in the flow characteristics for water/air system flow regimes where flows are scheduled by:

a. Rotometer readings identical to those for the glycol/air system tests.

b. Rotometer readings producing flow velocities identical to those for the glycol/air system tests.

The runs were made with the working section in the 0-degree (vertical) position. A summary of these tests is given in table 46. Samples of the P_3 traces referred to in table 46 are included. Following review of these data, a decision was reached to conduct subsequent tests with identical rotometer readings for liquid flow to provide a means of comparing the total effects of the change in fluid characteristics, i.e., propylene glycol versus water.

Formal data runs. — Formal data runs are presented for the glycol/air system and for the water/air system.

Glycol/air system data: Data presented for this system was recorded manually and by motion pictures.

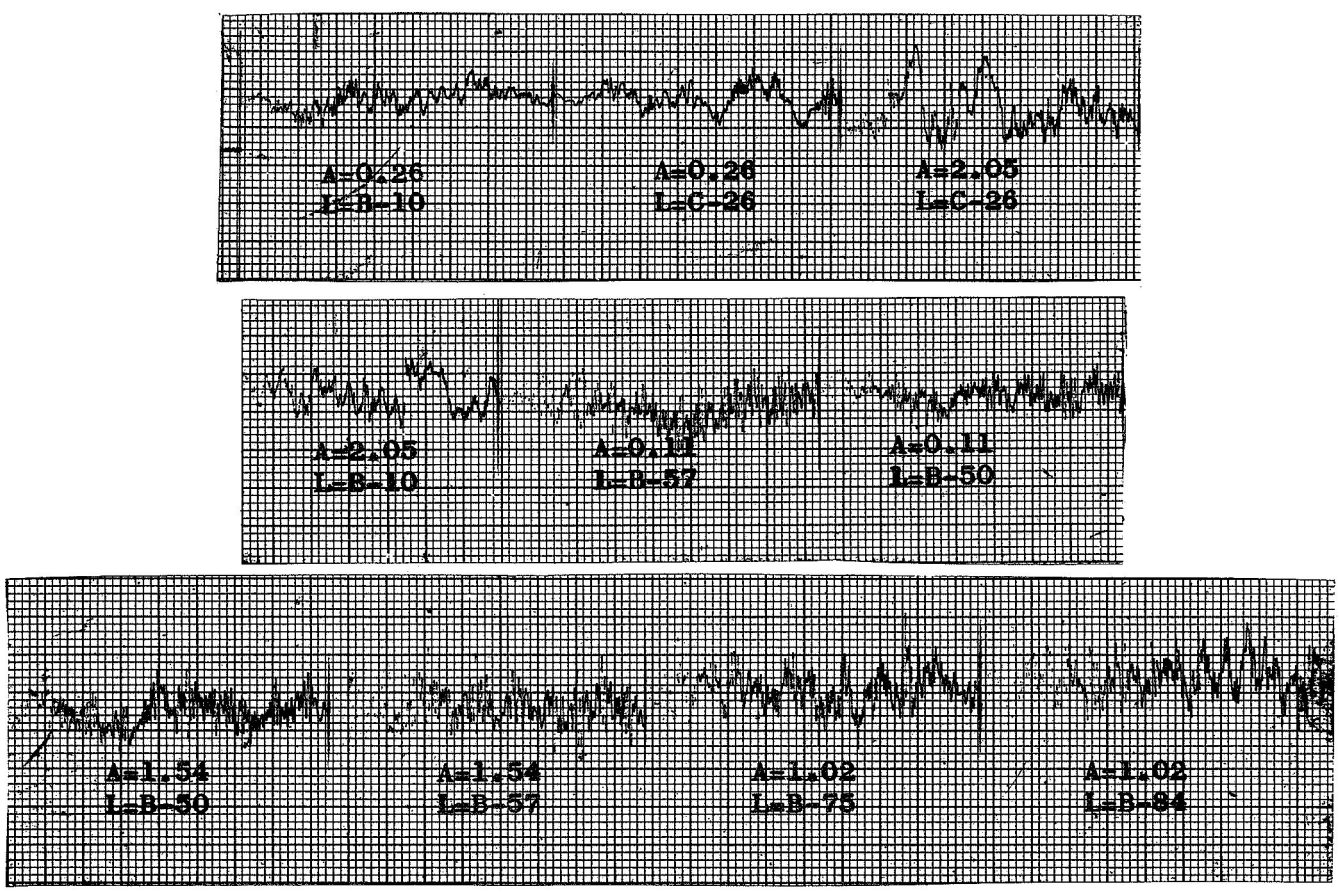
a. Manual Data Runs. The data recorded against this category are true copies of the original data sheets and are shown on table 47. A total of 135 flow conditions was scheduled against six sets of tests.

b. Movie Runs. A total of 42 flow conditions against five sets of tests was selected from the manual data runs as producing observable differences in flow pattern characteristics. The movie runs are identified and manually recorded data are summarized on table 48. Figure 132 is an example of the movie data obtained.

Table 46. — Comparative Tests - Identical Readings Versus Identical Flows

Valve Schedule	Liquid Rotometer Reading	P_1*	P_2*	P_3**	Observable Change in Characteristics
1.1	B-10	1.5	1.9	6	
	C-26	1.4	1.8	8	Very slight
1.5	B-10	1.2	1.8	10	
	C-26	1.3	1.8	12	Very slight
4.0	B-57	1.2	1.4	11 (P_3 VHF)	
	B-50	1.5	1.8	7	None
4.4	B-57	1.9	2.3	11 (P_3 VHF)	
	B-50	1.9	2.2	11	Slight, if any
5.3	B-84	2.2	2.6	12	
	B-75	2.1	2.5	15	Increased oscillation

*PSIG, ** Grid divisions, attenuation = x5.



Note: Run at 25 mm/sec, attenuation = x5. P_3 traces for table 46.

Table 47. — Glycol/Air System Manual Data Runs

Date: 2-3-70, Clock Hours: 1000

Test Set No. 5 Angle 180° Return Configuration Closed Fluid System Glycol

Sub Set	Valve* Sched.	Pres.(PSIG)			Temp.(°F)		Regime	Comments	Photo Select.
		** P_1	** P_2	*** P_3	T_1	T_2			
1	1.0	1.3	1.0				"Strat."/annu.	Straight down one side, smooth.	
2	1.1	1.3	1.0		101	101	" "	Thinner, sensitive to vertical.	
3	1.5	1.4	1.0				" "	Increasing ripple.	
4	2.2	1.4	1.0				Annu./"Strat."	Annular portion increasing, surface rough.	
5	2.4	1.4	1.0				" "	Less stratified, roughness increasing.	
6	2.6	1.4	1.0				" "	Beginning to form waves.	
7	2.9	1.4	1.0		102	103	" "	Still rougher.	X
8	3.1	1.4	1.0				Annular	Smooth (inlet vorticity).	
9	4.0	1.4	1.0				Strat./annu.	Vorticity high, annu. last 25%.	
10	4.2	1.4	1.0	1			" "	P_3 (starts) decreased annular.	
11	4.4	1.8	1.4	5			Annular	Outlet plugging.	
12	4.6	2.2	1.8	7			"	Increased outlet plugging.	
13	4.9	2.6	2.4	10			Spray/annular	Outlet choke feedback, oscillatory.	X
14	5.1	1.4	1.0	1	102	103	Stratified	Vorticity, full 360° in w.s.	
15	5.3	2.0	1.6	2			Annular		
16	6.2	2.0	1.6	>1			Annu./strat.	Smooth	
17	6.7	4.2	4.0				Spray/annular		
18	7.0	1.5	1.6				Bubble		
19	7.1	2.3	2.2				Semi-annular or bubble annular.		
20	7.3	3.6	3.4		101	101	" " "	"	X
21	7.5	5.2	4.6				Spray annular or semi-annular		
22	7.9	-	-	-	Overloaded return system.				

Baseline Pressure Readings (Liquid Only) Static: P_1 0 P_2 0.1 ; Flow: P_1 < 0 P_2 0 (@ 4)

* Valve positions scheduled for vertical (0° & 180°); first digit for liquid, second digit for air.

** PSIG

*** Grid divisions on trace paper, P_3 signal attenuation = X10.

Table 47. — Glycol/Air System Manual Data Runs, Contd

Date: 2-3-70 , Clock Hours: 1300

Test Set No. 4 Angle 135° Return Configuration _____ Fluid System Glycol

Sub Set	Valve* Sched.	Pres.(PSIG) ** P_1	** P_2	*** P_3	Temp.(°F) T_1	T_2	Regime	Comments	Photo Select.
1	1.0	2.0	1.0				Stratified	Smooth	
2	1.1	)							
3	1.3	)							
4	1.5	)	Not performed				"Identical"	to 90°	
5	1.7	)							
6	1.9	2.0	1.0	3			Stratified	Roughened.	
7	3.2	2.1	1.0	1			"	Inlet annular for 6" → strat. smooth.	
8	3.4	2.3	1.1	8			"	Increase to 8".	
9	3.6	2.5	1.4	8			"	Annular spray inlet → wavy strat. - outlet surge.	
10	3.9	2.7	1.6	10			"	Same - outlet feedback at inlet.	
11	4.2	2.3	1.2	3			Sp. ann./strat.	Some feedback, strat. for last 50%. Smooth.	
12	4.5	3.2	2.2				" " "	Sp. annu., 6" to strat., slight wave (outlet slugging)	
13	4.7	3.8	2.8	9			" " "	Sp. annu. 30%, last 30% strat., fairly smooth(slugging)	
14	5.1	2.4	1.3	0			Annu./strat.	Inlet annu. plus vorticity, strat. start middle.	
15	5.3	3.1	2.0	2			" "	Some spray inlet - no vorticity, 75% strat.	
16	5.5	3.6	2.9	5			Sp. annu./strat.	Last 40% strat. and spray.	
17	5.9	5.8	4.0	10			Sp. annu./strat.	Strat., last 30% rough.	
18	6.3	4.0	3.0	2	94	94	" " "	Strat., last 30% very rough and spray.	
19	6.6	5.1	4.7	5			" " "	Strat., last 10% very rough and spray.	
20	7.0	3.4	2.4				Stratified	Rough full length of w.s.	
21	7.2	4.4	2.6	2			Sp. annu./strat.	Strat. 30% rough.	
22	7.7	7.0	6.0	8	96	97	Sp. annu.	Slight strat. at outlet.	
23	7.9	---	---	---	overload		return system	---	

Baseline Pressure Readings (Liquid Only) Static: P_1 0 P_2 -.4 ; Flow: P_1 0.5 P_2 -0.1 (@ 4)

* Valve positions scheduled for "horizontal" (45°, 90°, & 135°); first digit for liquid, second digit for air.

** PSIG

*** Grid divisions on trace paper, P_3 signal attenuation = X10.

Table 47. — Glycol/Air System Manual Data Runs, Contd

Date: 2-3-70 , Clock Hours: 1400

Test Set No. 3 Angle 90° Return Configuration Closed Fluid System Glycol

Sub Set	Valve* Sched.	Pres.(PSIG) ** P_1	** P_2	*** P_3	Temp.(°F) T_1	T_2	Regime	Comments	Photo Select.
1	1.0	1.7	1.6				Stratified/slug	Slug frequency = 6 sec., long wave strat.	
2	1.1	1.7	1.5				" "	Slug frequency = 7-8 sec., long wave strat.	
3	1.3	1.7	1.6	1.5			" "	Slug frequency = 8 sec., wave 3-6/w.s. (hi-vel.)	
4	1.5	1.7	1.6	3			Stratified	6-8 waves/w.s., 2 crests together form slug and 90%.	X
5	1.7	1.7	1.6	3			"	Wave frequency increase, no slug.	
6	1.9	1.7	1.6	3			"	Approx. 15 crests/w.s., no slug.	X
7	3.2	1.8	1.6				Strat./slug	Wave and plug 2-3 sec. apart.	
8	3.4	1.9	1.8	10/3*			" "	Large - small slug more frequent.	X
9	3.6	2.1	1.9	8/3			Slug		
10	3.9	2.3	2.2	14			Spray/stratified		X
11	4.2	1.9	1.8	3			Slug	Fully developed, 50%-60% liquid.	
12	4.5	2.8	2.8	12			Strat./slug	Liquid thin at inlet to a high of 60% @ 3/4 & 50% out.	X
13	4.7	3.4	3.1	15			Stratified	50% liquid spray at liquid surface.	X
14	5.1	2.0	1.8	2			Strat./slug	1.5 waves/w.s.	
15	5.3	3.0	2.8	6				Same, higher velocity.	X
16	5.5	4.1	3.8	7			Strat./slug	Same, higher velocity/inlet = sp. annu.	
17	5.9	5.3	5.2	17			Sp. annu./strat.sp.	Violent.	X
18	6.3	4.0	3.8	4			" " " "	Some slugging.	
19	6.6	6.2	5.9	8			" " " "	Strat. only last 25%, much spray.	X
20	7.0	3.1	2.9	2			Bubble		
21	7.2	4.5	4.1	3			"	Liquid wedge, thin at inlet.	
22	7.7	8	7.7		97	98	Spray/bubble	Bubble last 25%.	X
23	7.9	---	---	---	-- overloaded return system --			---	

Baseline Pressure Readings (Liquid Only) Static: P_1 0 P_2 0 ; Flow: P_1 0.6 P_2 0.4 (@ 4)

* Valve positions scheduled for "horizontal" (45°, 90°, & 135°); first digit for liquid, second digit for air.

** PSIG

*** Grid divisions on trace paper, P_3 signal attenuation = X10.

* 10 big slug; 3 on small or more.

Table 47. — Glycol/Air System Manual Data Runs, Contd

Date: 2-4-70, Clock Hours: 0900

Test Set No. 2 Angle 45° Return Configuration Closed Fluid System Glycol

Sub Set	Valve* Sched.	Pres.(PSIG)			Temp.(°F)		Regime	Comments	Photo Select.
		** P_1	** P_2	*** P_3	T_1	T_2			
1	1.0	2.2	2.2				Plug	3 plug/w.s. - some back sliding, smooth.	X
2	1.1	2.1	2.0				"	Same but great air volume.	
3	1.3	2.0	2.0				Slug	Inlet oscillations, slug forms and accelerates.	X
4	1.5	2.0	2.0	5			"	Turbulent throughout.	
5	1.7	1.9	2.1	6			"	Lower liquid density ~ 25%.	X
6	1.9	2.0	2.1	6	86	85	"	Increased oscillation, feedback for 1-6 is minimal.	
7	3.2	2.3	2.2	5			"	Oscillation, turbulent 4-5cy/ws, liquid 40%-60%.	
8	3.4	2.3	2.2	6			"	Same, less dense.	
9	3.6	2.4	2.3	8			"	Less oscillation, greater vel. slug.	X
10	3.9	2.6	2.5	10			"	Much less oscillation, low density.	
11	4.2	2.6	2.3	3			"	Wave freq. high, bubble, inlet = 70%, outlet = 40%.	X
12	4.5	3.4	3.1	10			Sp.annu./slug-strat.	Beginning to get violent feedback.	
13	4.7	4.0	3.6	15			Sp.an/slug(alternat.)	Change from mixed regime to alternating regime.	X
14	5.1	2.8	2.7	2	93	93	Bubble/plug	Primarily bubble	
15	5.3	3.7	3.2	4			" "	Less dense, increased velocity.	
16	5.5	4.6	4.2	8			" "	Less dense, increased velocity.	
17	5.9	---	---	---	---	---	---	---	
18	6.3	4.9	4.4	5			Bubble annu./slug	Inlet 40% bubble annu., last 60% decreasing vol. slug.	
19	6.6	6.8	6.4	7			" " "	75% bubble.	X
20	7.0	4.3	3.8	2			Bubble		
21	7.2	5.3	4.8	3			Bubble/strat.		X
22	7.7	8.5	8.0	6			Not apparent	Too violent outlet (< 7.7).	
23	7.9	---	---	---	---	---	---	---	

Baseline Pressure Readings (Liquid Only) Static: P_1 2.2 P_2 2.2 ; Flow: P_1 1.9 P_2 1.5 (@ 4)

* Valve positions scheduled for "horizontal" (45°, 90°, & 135°); first digit for liquid, second digit for air.

** PSIG

*** Grid divisions on trace paper, P_3 signal attenuation = X10.

Table 47. — Glycol/Air System Manual Data Runs, Contd

Date: 2-4-70 , Clock Hours: 1000

Test Set No. 1 Angle 0° Return Configuration Closed Fluid System Glycol

Sub Set	Valve* Sched.	Pres.(PSIG)			Temp.(°F)		Regime	Comments	Photo Select.
		** P_1	** P_2	*** P_3	T_1	T_2			
1	1.0	2.7	2.3	3			Slug	3cy/w.s. oscillations, amp = 15% of w.s.	X
2	1.1	2.6	2.2	3			"	Same, more violent - amp = 30% w.s.	
3	1.5	2.4	2.2	5			Annu./plug	Oscillations 3-4cy/w.s.	X
4	2.2	2.5	2.3	4			Sp. annu./plug	Oscillations, 6-8cy/w.s.	X
5	2.4	2.5	2.3	7			" " "	Oscillations, changes amplitude greater.	
6	2.6	2.5	2.3	7			" " "	Same, lower density (liquid).	
7	2.9	2.6	2.4	5			" " "	Lower amplitude, greater frequency.	X
8	3.1	2.8	2.4	3			Semi-annular	Oscillatory, 3cy/w.s., high amp.-low frequency.	
9	4.0	2.7	2.6	1			" "	No oscillation, bubble, smooth.	
10	4.2	2.7	2.6	2			" "	Some oscillation, lower density (liquid).	X
11	4.4	3.4	3.0	6			Spray annular	Very low density, 1cy/w.s.(entire), some feedback.	X
12	4.6	4.2	3.7	9			" "	Oscillation in w.s. identical to that in return.	
13	4.9	4.9	4.3	12			" "	Oscillation in w.s. identical to that in return.	X
14	5.1	3.4	2.8	2	97	96	Dispersed annular	No oscillations.	
15	5.3	3.8	3.2	5			" "	Slight oscillation appearing.	X
16	6.2	4.0	3.4	2			Semi-annular	Bubble travelling in center of duct.	X
17	6.7	7.8	7.2	10			Annular	Feedback and oscillation.	X
18	7.0	4.2	3.4	3			Bubble	Dispersed at inlet, coalesced in center at outlet.	
19	7.1	4.6	3.8	3			"	Same, less dense.	
20	7.3	6.4	5.8	5			"	Very dispersed, lower density.	
21	7.5	8.3	7.6	8			Spray annular		X
22	7.9	9.2	8.6	12	97	97	Spray	Violent feedback.	

Baseline Pressure Readings (Liquid Only) Static: P_1 3.3 P_2 2.6 ; Flow: P_1 2.1 P_2 1.4 (@ 4)

* Valve positions scheduled for vertical (0° & 180°); first digit for liquid, second digit for air.

** PSIG

*** Grid divisions on trace paper, P_3 signal attenuation = X10.

Table 47. — Glycol/Air System Manual Data Runs, Contd

Date: 2-4-70 , Clock Hours: 1300

Test Set No. 1A Angle 0° Return Configuration Open Fluid System Glycol

Sub Set	Valve* Sched.	Pres.(PSIG)			Temp.(°F)		Regime	Comments	Photo Select.
		** P_1	** P_2	*** P_3	T_1	T_2			
1	1.0	2.5	2.2				Slug	Oscillatory, 3 cycles/w.s.	X
2	1.1	2.3	2.0				"	Oscillatory, higher amplitude.	
3	1.5	2.0	2.0				Annu./plug	Oscillatory, very low liquid density.	X
4	2.2	2.2	2.0				" "	High amplitude cycle.	X
5	2.4	2.2	2.0				" "	Lower density, oscillatory.	
6	2.6	2.2	2.0	7			" "		
7	2.9	2.2	2.0	3			Dispersed annu.	High freq., low amp, steady state oscillation.	X
8	3.1	2.6	2.2	2			Bubble/annu.-plug		
9	4.0	2.6	2.6	2			Bubble/semi-annu.	No oscillation.	
10	4.2	2.9	2.5	3			Sp. annu.	Oscillation low amplitude.	X
11	4.4	2.9	2.5	7			Disp. annu.	Whole section oscillation.	X
12	4.6	3.0	2.6	13			" "	Increased oscillation.	
13	4.9	3.2	2.8	15			" "	Oscillation same.	X
14	5.1	3.3	2.8	2			Semi-annu.	Half wave oscillation only.	
15	5.3	3.2	2.7	4			" "	Same, less dense.	X
16	6.2	3.6	3.0	3			" "	Smooth (beginning to cavitate pump).	X
17	6.7	4.3	3.7	15			Sp. annu.	Relatively smooth.	X
18	7.0						)		
19	7.1						Overload drain line from		
20	7.3						sump causing sump loading		
21	7.5						and pump cavitation.		
22	7.9						)		

Baseline Pressure Readings (Liquid Only) Static: P_1 3.3 P_2 2.6 ; Flow: P_1 3.5 P_2 2.8 (@ 4)

* Valve positions scheduled for vertical (0° & 180°); first digit for liquid, second digit for air.

** PSIG

*** Grid divisions on trace paper, P_3 signal attenuation = X10.

Table 48. — Movie Data Summary - Glycol/Air System

Date: 6 February 1970 Equipment: Milliken @ 128 FPS

Test Set: #M-1A (0°)(Open Return)

Sub Set	Valve Comb.	Pres.* P_1	Pres.* P_2	Temp. T_1	Temp. T_2
1	1.0	1.5	2.0	95	93
3	1.5				
4	2.2				
7	2.9	1.5	2.1	96	96
10	4.2	1.9	2.3		
11	4.4				
13	4.9	2.1	2.3	96	96
15	5.3	2.1	2.3		
16	6.2	2.6	2.8		
17	6.7	3.1	3.5	95	96

* Static: $P_1 = 2.3$; $P_2 = 2.3$

Test Set: #M-1 (0°)(Closed Return)

Sub Set	Valve Comb.	Pres. P_1	Pres. P_2	Temp. T_1	Temp. T_2
1	1.0	1.75	2.0	94	95
3	1.5	1.4	1.8		
4	2.2	1.5	1.9		
7	2.9	1.5	2.0		
10	4.2	2.0	2.4	95	96
11	4.4	3.3	2.8		
13	4.9	4.0	4.4		
15	5.3	3.0	3.2	99	99
16	6.2	3.1	3.3		
17	6.7	7.2	7.4		
21	7.5	8.2	8.4	96	95

Test Set: #M-2 (45°)

Sub Set	Valve Comb.	Pres.* P_1	Pres.* P_2	Temp. T_1	Temp. T_2
1	1.0	1.2	1.2		
3	1.3	1.2	1.5		
5	1.7				
9	3.6	1.9	2.2		
11	4.2	2.0	2.2	91	90
13	4.7				
19	6.6	7.2	7.0		
21	7.2	5.4	5.4	92	92

* Static: $P_1 = 1.1$; $P_2 = 1.2$

Test Set: #M-3 (90°)

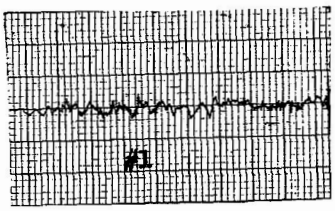
Sub Set	Valve Comb.	Pres.* P_1	Pres.* P_2	Temp. T_1	Temp. T_2
4	1.5				
6	1.9	1.2	1.4		
8	3.4	1.7+	1.8		
10	3.9	2.2	2.6		
12	4.5	2.8	2.8		
13	4.7	3.2	3.6	93	93
15	5.3	2.9	3.0		
17	5.9	5.7	5.8		
19	6.6	6.3	6.4	93	95
22	7.7	8.8	8.8	95	96

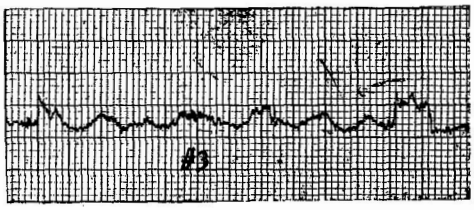
* Static: $P_1 = 0$; $P_2 = \sim -1$

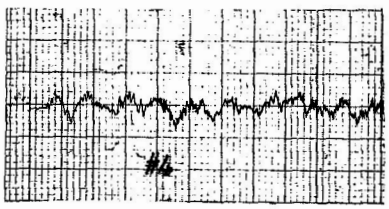
Set Set: #M-5 (180°)

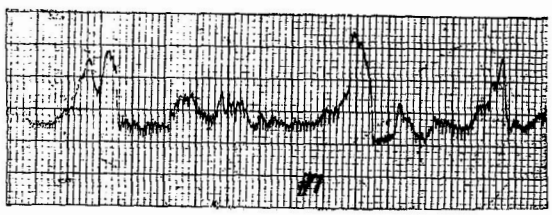
Sub Set	Valve Comb.	Pres.* P_1	Pres.* P_2	Temp. T_1	Temp. T_2
7	2.9	2.0	1.2		
13	4.9	4.2	3.6		
20	7.3	6.2	5.9	91	92

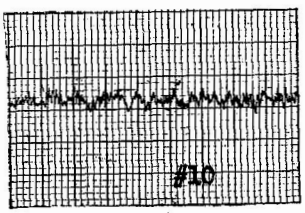
* Static: $P_1 = 1.0$; $P_2 = 0.4$ (least flow to clear duct).

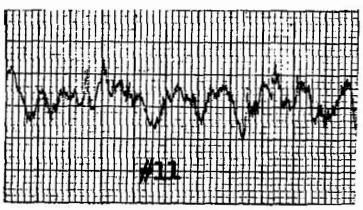


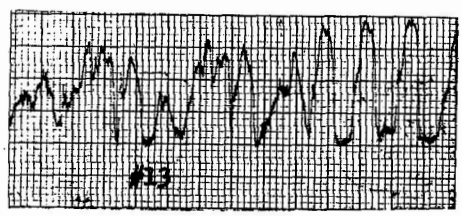


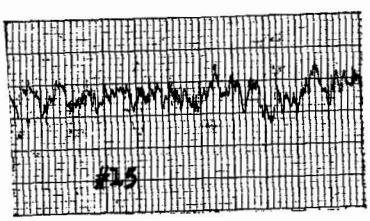


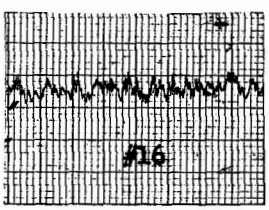


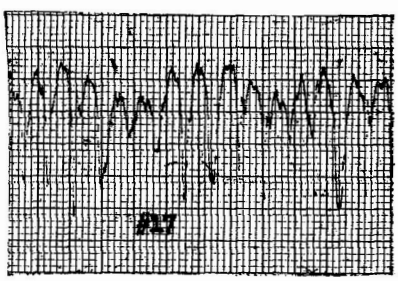


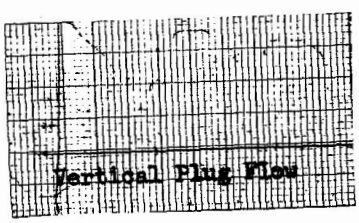






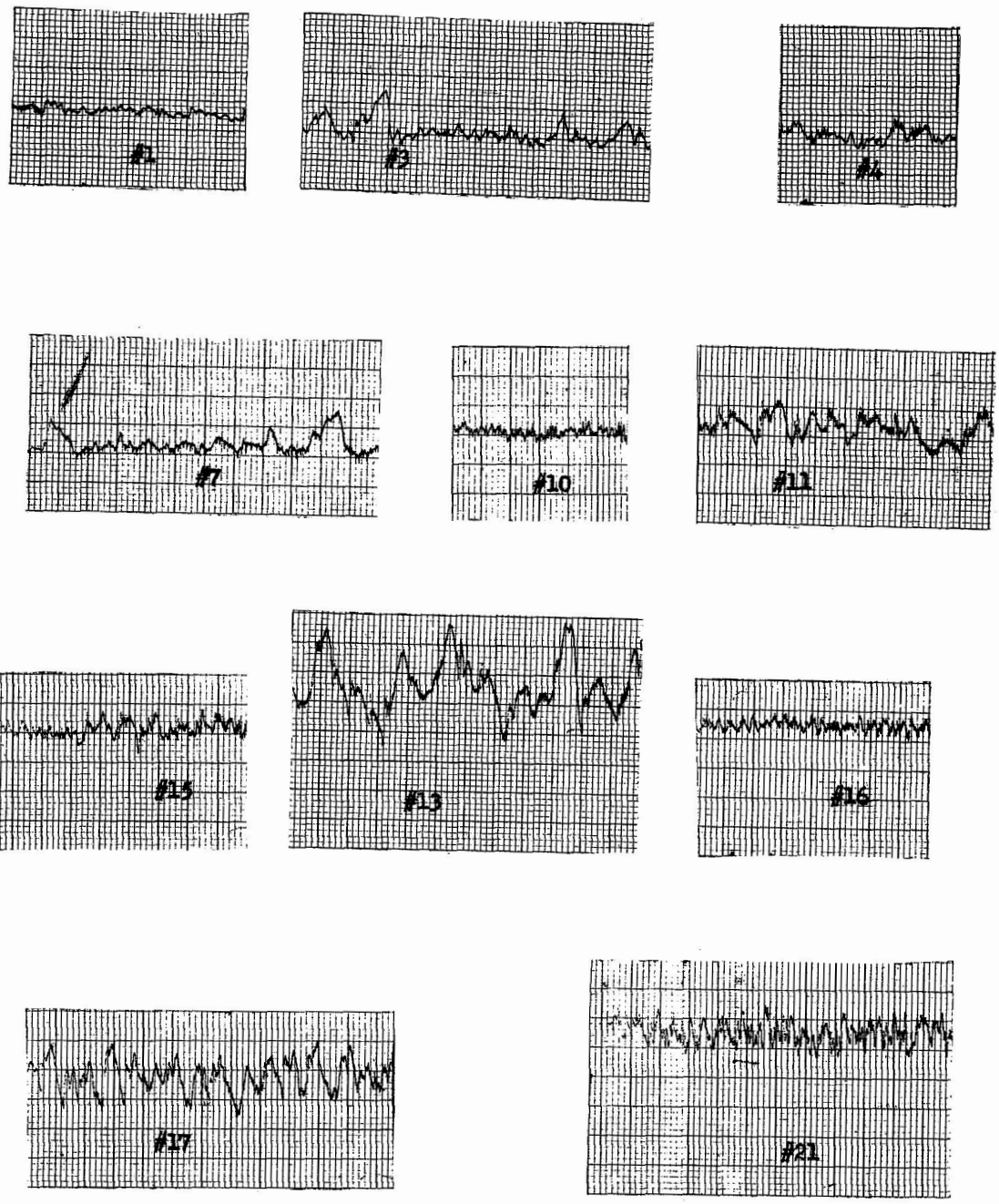






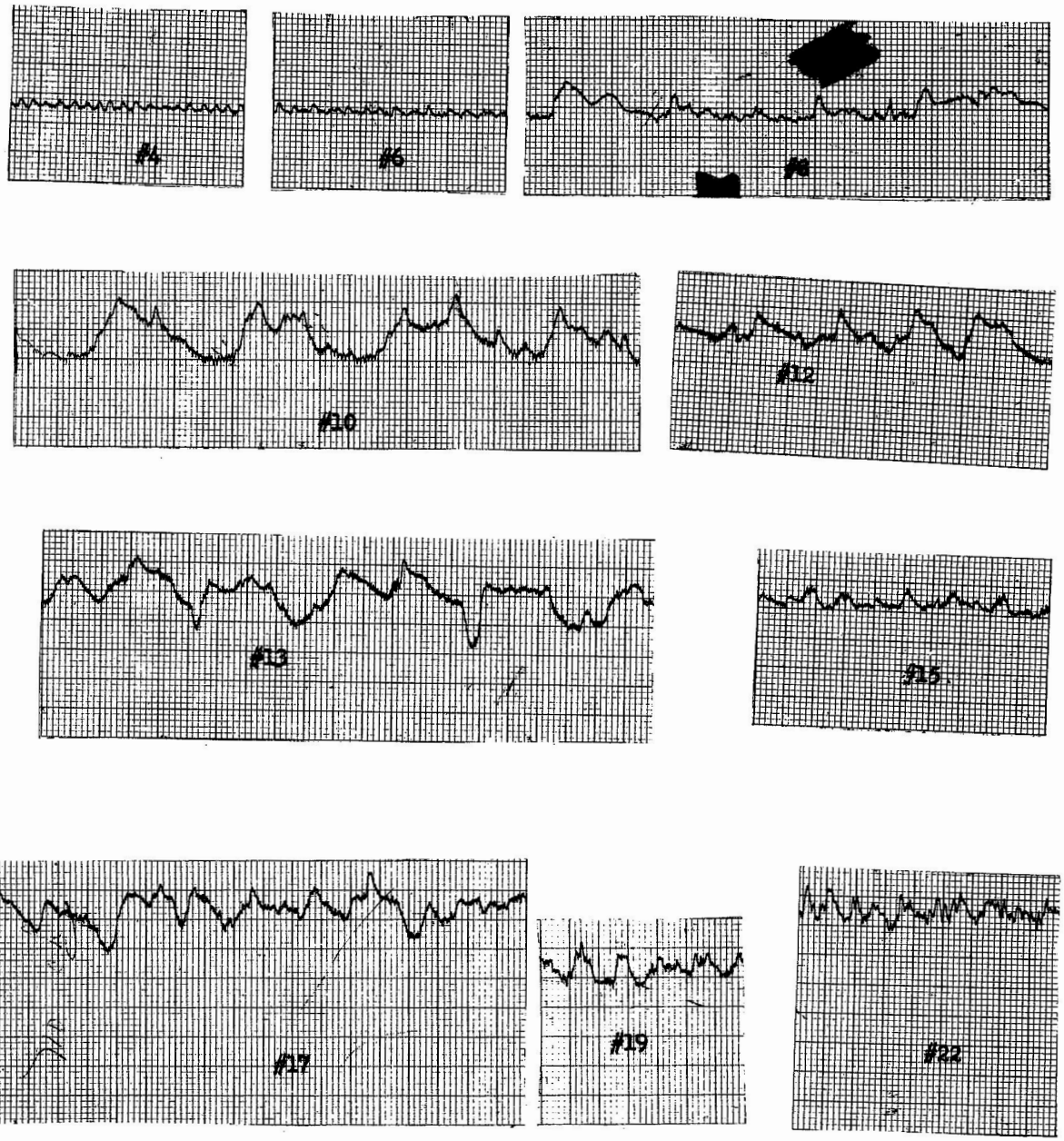
P_3 traces for Movie Run M-1A - Glycol/Air

Signal attenuation = X10, speed = 25 mm/sec. 6 February 1970



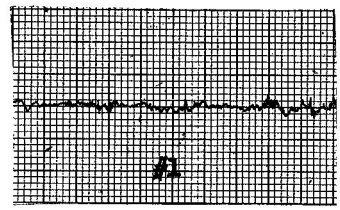
P_3 traces for Movie Run M-1 - Glycol/Air

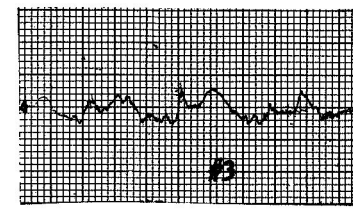
Signal attenuation = X10, speed = 25 mm/sec. 6 February 1970

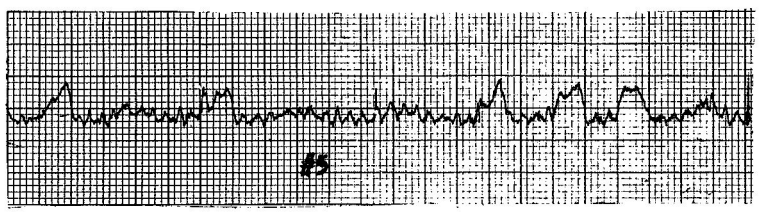


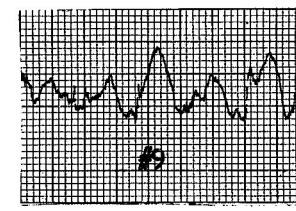
P_3 traces for Movie Run M-3 - Glycol/Air

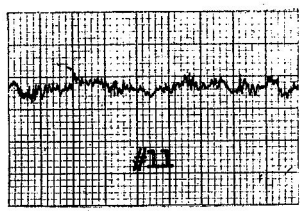
Signal attenuation = X10, speed = 25 mm/sec. 6 February 1970

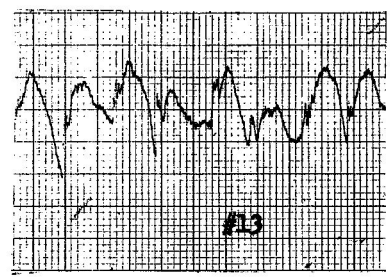


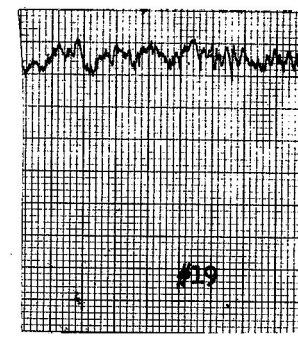


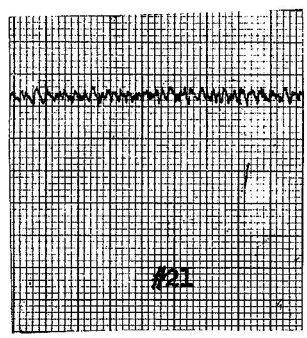




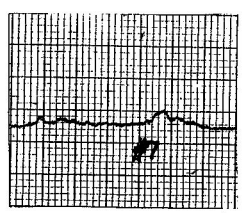


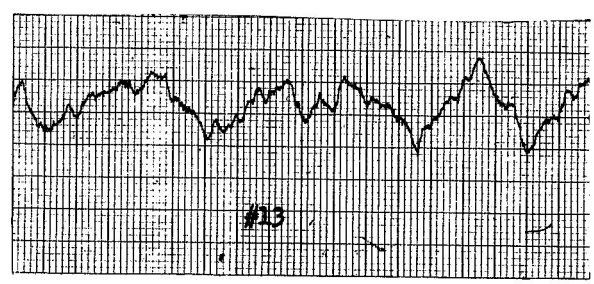


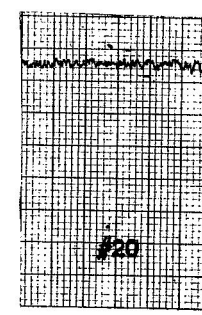




P_3 traces for Movie Run M-2
signal attenuation = X10, speed = 25 mm/sec
6 February 1970







P_3 traces for Movie Run M-5, attenuation = X10, 25 mm/sec. 6 February 1970

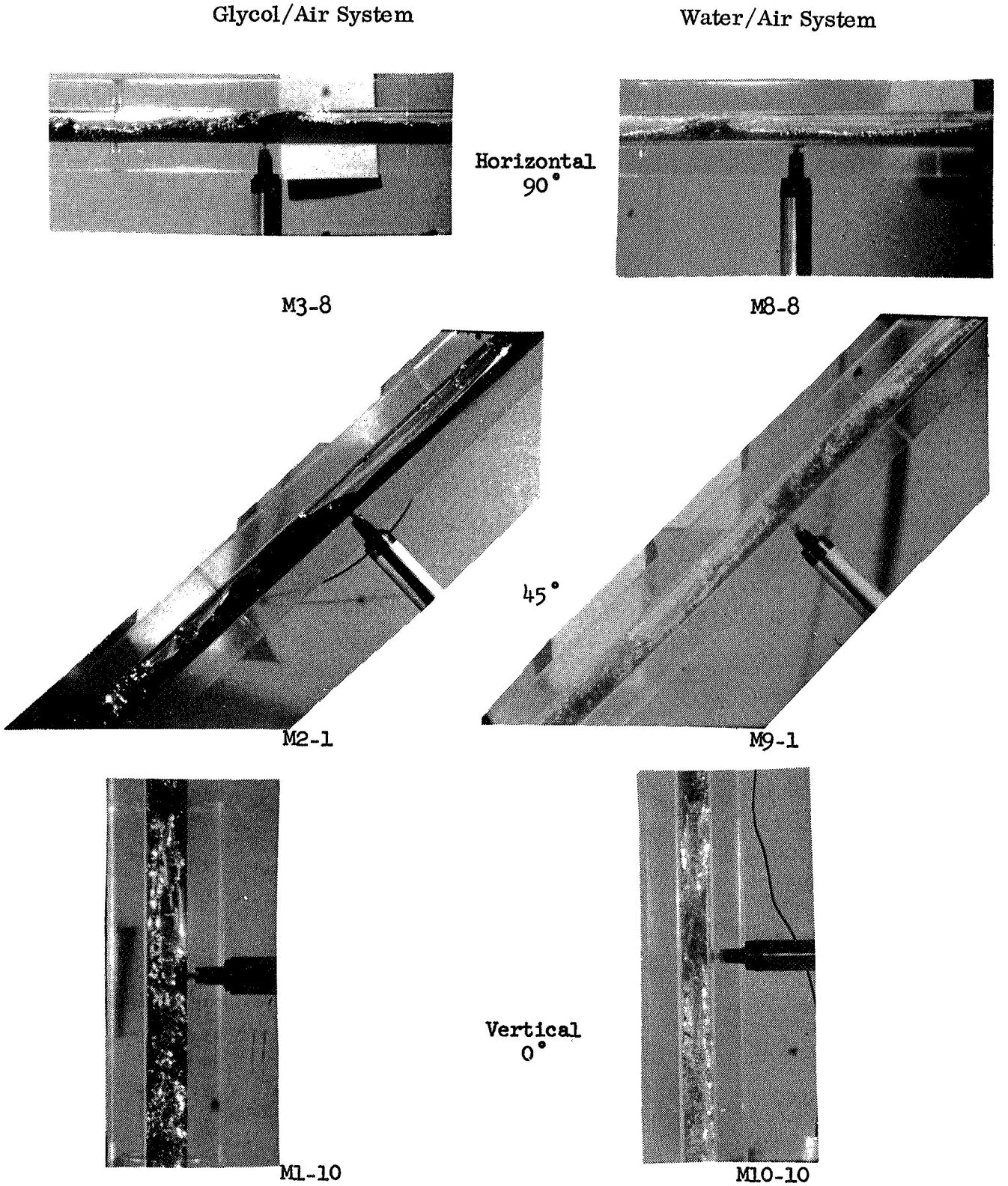


Figure 132. — Observed Flow Regimes - Sample Frames from Movie Data

Water/air system data: Data presented for this system was recorded manually and by motion pictures.

a. Manual Data Runs. The data recorded against this category are true copies of the original data sheets and are shown on table 49. A total of 113 flow conditions was scheduled against five test sets.

b. Movie Runs. A total of 35 flow conditions against four test sets was selected from the manual data runs as producing observable differences in flow pattern characteristics and was recorded on high-speed movie film.

The movie runs are identified and the manually recorded data are summarized on table 50.

Trace selections and documentation groupings are indicated in table 51, which identifies the trace recordings that appear subsequent to that table.

Critique of the Test Design

With the exception of the initial uncertainties regarding the requirements for inlet mixture control and the problems inherent in reducing outlet system feedback, the general approach to the test design appeared to be straightforward, tests were easy to manage, and construction costs were low. The approaches followed can be recommended as a guide to future test designs for experimental studies involving flow regime determinations for adiabatic two-phase flow.

Instrumentation

The pressure and high-speed motion picture data combined with visual observations are adequate for the qualitative determinations of flow characteristics required by the scope of this phase of the analytical model development program. However, for subsequent experiments where more precise data are required, quantitative flow pattern data should be provided. A system similar to the shadowgraph photocell arrangement used for film profile measurements for experiment 3A should prove satisfactory. Additionally, photographic and/or TV monitoring could well include at least two views around the flow duct, i.e., at points 90 degrees apart around the viewing section. This might be accomplished with a single camera and mirrors. Shadowgraph techniques should be examined, but it does not appear that results would warrant the additional complexity.

The conventional bourdon tube pressure gauges were generally unsatisfactory, especially in view of the continual change in working section orientation which changed the static head on the guages and periodically introduced varying amounts of air in the gauge lead lines, adding to the column effect. Pressure tranducers similar to the P_3 sensor should prove to be far superior.

Table 49. — Water/Air System Manual Data Runs

Date: 2-9-70 , Clock Hours: 1300

Test Set No. 6 Angle 180° Return Configuration Closed Fluid System Water

Sub Set	Valve* Sched.	Pres.(PSIG)			Temp.(°F)		Regime	Comments	Photo Select.
		** P_1	** P_2	*** P_3	T_1	T_2			
1	1.0	1.3	0.9	1			Annular	Smooth, even.	
2	1.1	1.3	0.9	1			"	"	
3	1.5	1.5	1.0	2			"	Starting to become wavy.	
4	2.2	1.3	0.9	2	68	68	"	" "	
5	2.4	1.4	1.0	3			"	Waves increasing.	
6	2.6	1.5	1.0	3			Spray annular		
7	2.9	1.7	1.1	2			" "	Increased spray (no return surge or feedback).	
8	3.1	1.4	1.0	1			Strat./sp. annu.	Inlet vorticity, stratified to annular.	
9	4.0	1.2	0.7	1			Stratified	" " " " (more pronounced)	
10	4.2	1.5	1.0	2			Spray/annular		
11	4.4	2.0	1.5	6			" "		
12	4.6	2.5 ±.5	2.0 ±.2	7			" "	Outlet slugging.	
13	4.9	3.0 ±.1	2.5 ±.4	13			" "		
14	5.1	1.5	1.1	1			" "	Smooth.	
15	5.3	2.0	1.6	3			" "	Slightly wavy.	
16	6.2	2.0	1.5	1			" "		
17	6.7	4.4	4.0	5			Sp./annu. → Mist	Outlet slugging.	
18	7.0	1.5	1.7	3			Strat./spray	H.F. on P_3, strat. at inlet.	
19	7.1	2.0	1.9	2			Disp. annu./sp.annu.		
20	7.3	3.5	3.2	3			Spray annu.		
21	7.5	4.8	4.6	3	75	75	" "	Outlet slugging moderate, H.F on P_3.	
22	7.9	7.3	7.1	5			Spray	Relatively smooth return.	

Baseline Pressure Readings (Liquid Only) Static: P_1 0 P_2 0 ; Flow: P_1 0 P_2 0 (@ 4)

* Valve positions scheduled for vertical (0° & 180°); first digit for liquid, second digit for air.

** PSIG

*** Grid divisions on trace paper, signal attenuation = X10.

Table 49. — Water/Air System Manual Data Runs, Contd

Date: 2-9-70 , Clock Hours: 1400

Test Set No. 7 Angle 135° Return Configuration Closed Fluid System Water

Sub Set	Valve* Sched.	Pres.(PSIG) ** P_1	** P_2	*** P_3	Temp.(°F) T_1	T_2	Regime	Comments	Photo Select.
1	1.0	1.0	0.6	2			Stratified		
2	1.1	1.0	0.6	2			"		
3	1.3	1.0	0.6	4			"		
4	1.5	1.0	0.6	5			"		
5	1.7	1.0	0.6	6			Strat./spray	Surface breaking up into spray.	
6	1.9	1.1	0.8	5			" "	Spray very large percentage of flow at outlet.	
7	3.2	1.0	0.7	3			Stratified	Smooth - some spray at inlet.	
8	3.4	1.1	0.8	8			"	Spray at surface.	
9	3.6	1.2	1.0	15			"	Wavy, spray at inlet.	
10	3.9	1.5	1.2	11			Sp. annu./strat.	Sp. annu. at inlet to strat., last 75%.	
11	4.2	1.2	0.8	5			" " "	Similar to 10 except lower vel., thicker layer.	
12	4.5	2.0	1.4	16	78	78	" " "	Some slug flow.	
13	4.7	2.0 ±.5	1.8 ±.2	18			" " "	50% sp. annu. at inlet.	
14	5.1	1.1	0.8	2			Stratified	Wavy.	
15	5.3	1.8	1.5	6			"	Spray at surface - large drop breaking.	
16	5.5	3.0 ±.5	2.8 ±.2	16			Sp. annu./strat.	75% sp. annu., nearly slug flow.	
17	5.9	3.8 ±.4	3.4 ±.2	21			" " "	75% sp. annu., mist-like.	
18	6.3	2.1	2.0	7			Stratified	Wavy.	
19	6.6	3.5	3.3	14			Sp. annu./strat.	50% stratified.	
20	7.0	1.5	1.3	< 1			Annular	Vorticity.	
21	7.2	2.2	2.2	6			Annu./strat.	50% stratified.	
22	7.7	5.7	5.6	13			Sp. annu.		
23	7.9	6.7	6.5	12			Sp. annu./M		

Baseline Pressure Readings (Liquid Only) Static: P_1 _____ P_2 _____; Flow: P_1 -0.1 P_2 -0.2 (@ 4)

* Valve positions scheduled for "horizontal" (45°, 90°, & 135°); first digit for liquid, second digit for air.

** PSIG

*** Grid divisions on trace paper, signal attenuation = X5.

Table 49. — Water/Air System Manual Data Runs, Contd

Date: 2-9-70 , Clock Hours: 1500

Test Set No. 8 Angle 90° Return Configuration Closed Fluid System Water

Sub Set	Valve* Sched.	Pres.(PSIG) ** P_1	** P_2	*** P_3	Temp.(°F) T_1	T_2	Regime	Comments	Photo Select.
1	1.0	1.0	1.2	3			Strat./plug	Plug/2 sec - wavy.	
2	1.1	1.1	1.2	3			" "	Plug/4 sec - wavy.	
3	1.3	1.2	1.2	6			" "	Very thin strat. - wave build to plug/6 sec.	
4	1.5	1.1	1.2	10			Strat./slug	Wave form long wave length.	
5	1.7	1.0	1.2	10			Stratified	Wave form long wave length.	
6	1.9	1.0	1.2	9			"	Wavy.	
7	3.2	1.1	1.3	5			Strat./slug	Wavy, build up to slug.	
8	3.4	1.2	1.4	8			Stratified	Very wavy - regular smooth.	
9	3.6	1.2	1.5	13			"	Very wavy but some breakoff at surface.	
10	3.9	1.5	1.8	11			"	Foam or mist at surface.	
11	4.2	1.2	1.4	4			Stratified	Wavy, regular.	
12	4.5	2.0 ±.5	2.2	17			Strat./slug		
13	4.7	2.2	2.6	18			Strat./slug	Very rough and breakoff at surface.	
14	5.1	1.1	1.3	3			Stratified	Wavy - regular and smooth.	
15	5.3	1.8	2.0	8			"	Wavy - very broken at surface.	
16	5.5	3.5	3.8	13			Sp.annu./strat.	20% at inlet sp. annu. - very broken spray.	
17	5.9	3.5	4.0	25			" " "	50% " " " " " "	
18	6.3	2.2	2.5	7			" " "	30% sp. annu., lots of spray.	
19	6.6	3.5	4.0	15			" " "	50% sp. annu., increased spray.	
20	7.0	1.6	1.8	3			Strat./slug	Very rough at surface - wavy.	
21	7.2	2.2	2.6	7			Sp. annu./strat.	20% sp. annu., lots of spray VHF at P_3.	
22	7.7	5.7	6.2	11			Sp. annu.	60% " " " "	
23	7.9	7.0	7.2	12	83	84	" "	80% " " rought outlet.	

Baseline Pressure Readings (Liquid Only) Static: P_1_____ P_2_____; Flow: P_1 -0.1 P_2 -0.1 (@ 4)

* Valve positions scheduled for "horizontal" (45°, 90°, & 135°); first digit for liquid, second digit for air.

** PSIG

*** Grid divisions on trace paper, signal attenuation = X5.

Table 49. — Water/Air System Manual Data Runs, Contd

Date: 2-10-70 , Clock Hours: 0830

Test Set No. 9 Angle 45° Return Configuration Closed Fluid System Water

Sub Set	Valve* Sched.	Pres.(PSIG) ** P_1	** P_2	*** P_3	Temp.(°F) T_1	T_2	Regime	Comments	Photo Select.
1	1.0	1.5	2.0	2			Plug	Regular, classical regime.	
2	1.1	1.4	1.8	5			"	Higher frequency plug movement, smaller plugs.	
3	1.3	1.2	1.8	7			"	Highly oscillatory.	
4	1.5	1.2	1.8	7			Plug/slug	Highly oscillatory, foamy (regime unclear).	
5	1.7	1.2	1.8	9			Strat./slug	Foamy - breakup.	
6	1.9	1.2	1.8	12			" "	Foamy - breakup, very turbulent.	
7	3.2	1.5	1.9	8			Plug	Highly oscillatory - low amplitude, regular.	
8	3.4	1.5	2.0	12			Plug/slug	Mixed characteristics.	
9	3.6	1.5	2.1	14			Slug	Much sloshing.	
10	3.9	1.8	2.2	18			Slug	Much sloshing.	
11	4.2	1.7	2.1	6			Strat./slug	Most strat. very high wave, low wave length.	
12	4.5	2.2	2.6	10			" "	" " "	
13	4.7	2.5	2.9	15			" "		
14	5.1	1.5	1.8	3			Strat./plug	Regime unclear, smooth.	
15	5.3	1.9	2.3	5			Strat.	Very wavy.	
16	5.5	2.8	3.2	10			Sp. annu./strat.	50% sp. annu.	
17	5.9	4.0	4.6	18			Sp.annu./strat/slug	Very broken.	
18	6.3	2.5	2.8	7			" " " "		
19	6.6	3.7	4.3	11			" " " "	60% sp. annu.	
20	7.0	1.5	1.8	4			Bubble/strat.		
21	7.2	2.6	3.0	4			" "		
22	7.7	5.5	6.2	10			Sp.annu./strat.	Sp. annu. 75%.	
23	7.9	6.8	7.6	12	75	75	Spray - mist		

Baseline Pressure Readings (Liquid Only) Static: P_1 _____ P_2 _____; Flow: P_1 -0.1 P_2 -0.2 (@ 4)

* Valve positions scheduled for "horizontal" (45°, 90°, & 135°); first digit for liquid, second digit for air.

** PSIG

*** Grid divisions on trace paper, signal attenuation = X5.

Table 49. — Water/Air System Manual Data Runs, Contd

Date: 2-10-70 , Clock Hours: 1100

Test Set No. 10 Angle 0° Return Configuration Closed Fluid System Water

Sub Set	Valve* Sched.	Pres.(PSIG) ** P_1	** P_2	*** P_3	Temp.(°F) T_1	T_2	Regime	Comments	Photo Select.
1	1.0	1.7	2.2	3			Slug	Oscillatory, liquid plugs bubble as drop back.	
2	1.1	1.4	2.1	4			"	Oscillatory, semi-annular drop back.	
3	1.5	1.2	2.0	10			Sp. annu./slug	Highly oscillatory.	
4	2.2	1.4	2.1	8			Sp. annular	Highly oscillatory.	
5	2.4	1.4	2.1	10			Sp. annular	Highly oscillatory.	
6	2.6	1.4	2.1	9			Sp. annular	Highly oscillatory.	
7	2.9	1.4	2.1	11			Sp. annu./mist	Oscillatory high frequency, low amplitude.	
8	3.1	1.7	2.2	4			Disp. annu.	Oscillatory.	
9	4.0	1.2	1.6	3			Bubble	No observable oscillation.	
10	4.2	1.9	2.3	5			Disp. annu.	Oscillatory.	
11	4.4	2.0	2.6	10			Sp. annu.	Oscillatory.	
12	4.6	2.4	2.9	13			" "	Oscillatory.	
13	4.9	3.0	3.4	26			" "	Very thin broken annular film, little oscillation.	
14	5.1	1.8	2.1	4			Sp.annu./bubble	Nearly bubble.	
15	5.3	2.2	2.7	10			Disp. annu.	Some oscillation.	
16	6.2	2.2	2.7	6			" "	Very little observable oscillation.	
17	6.7	4.3	4.9	13			M/sp. annu.		
18	7.0	1.5	1.7	8			Bubble	P_3 VHF.	
19	7.1	2.2	2.5	6			"	Larger bubbles.	
20	7.3	3.3	3.8	8			Bubble/sp. annu.	No observable oscillations.	
21	7.5	4.8	5.4	11			Foam/M	Foam is questionable description.	
22	7.9	6.7	7.5	12	79	79	Foam/M	Foam accurate.	

Baseline Pressure Readings (Liquid Only) Static: P_1 _____ P_2 _____; Flow: P_1 -0.2 P_2 -0.2 (@ 4)

* Valve positions scheduled for vertical (0° & 180°); first digit for liquid, second digit for air.

** PSIG

*** Grid divisions on trace paper., signal attenuation = X5.

Table 50. — Movie Data Summary - Water/Air System

Date: 10 February 1970
Return Configuration: Closed

Equipment: Milliken @ 128 FPS
P_3 Signal Attenuation = X5

Test Set: #M-10 @ 0° Vertical

Sub* Set	Valve Comb.	Pressure P_1**	P_2**	P_3***
1	1.0	1.7	2.0	6
3	1.5	1.2	1.9	12
4	2.2	1.5	1.9	10
7	2.9	1.5	2.0	10
10	4.2	1.9	2.2	13
11	4.4	2.1	2.4	13
13	4.9	2.9	3.3	21
15	5.3	2.2	2.6	14
16	6.2	2.3	2.5	9
17	6.7	4.2	4.6	24
21	7.5	4.9	5.2	13
22	7.9	7.0	7.4	14

*Refers to Vertical Flow Schedule.
**PSIG, P_1=-0.1; P_2=-0.4 @ 4
***Grid divisions on trace paper,
T_1 = 80°F; T_2 = 80°F.

Test Set: #M-9 @ 45°

Sub* Set	Valve Comb.	Pressure P_1	P_2	P_3
1	1.0	1.4	1.9	5
3	1.3	1.2	1.7	12
5	1.7	1.3	1.7	13
9	3.6	1.5	2.0	20
11	4.2	1.7	2.1	9
13	4.7	2.3	2.8	25
19	6.6	3.8	4.2	15
21	7.2	2.4	2.8	8
23	7.9	6.7	7.5	11

*Refers to horizontal flow schedule.
T_1 = 82°F; T_2 = 82°F

Test Set: M-6 @ 180°

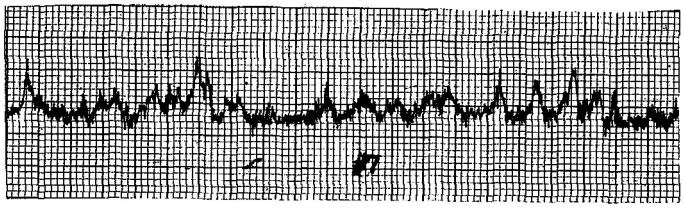
Sub* Set	Valve Comb.	Pressure P_1	P_2	P_3
7	2.9	2.0	2.1	7
13	4.9	3.2	2.5	21
20	7.3	3.6	2.9	5
22	7.9	7.6	6.9	14

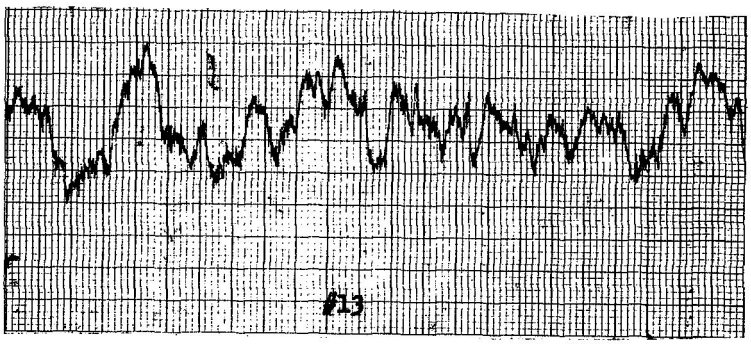
*Refers to vertical flow schedule.

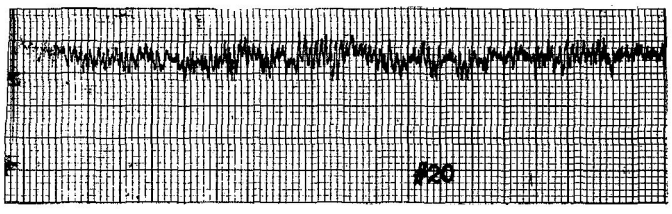
Test Set: M-8 @ 90°

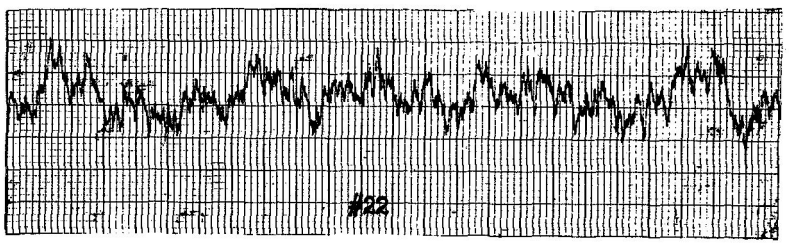
Sub* Set	Valve Comb.	Pressure P_1	P_2	P_3
4	1.5	1.2	1.3	6
6	1.9	1.2	1.3	8
8	3.4	1.4	1.4	9
10	3.9	1.9	1.9	14
12	4.5	2.1	2.1	11
13	4.7	2.5	2.5	24
15	5.3	2.0	2.0	6
17	5.9	3.8	3.8	16
19	6.6	4.0	4.0	12
22	7.7	6.5	6.5	11

*Refers to horizontal flow schedule
T_1 = 84°F; T_2 = 84°F.

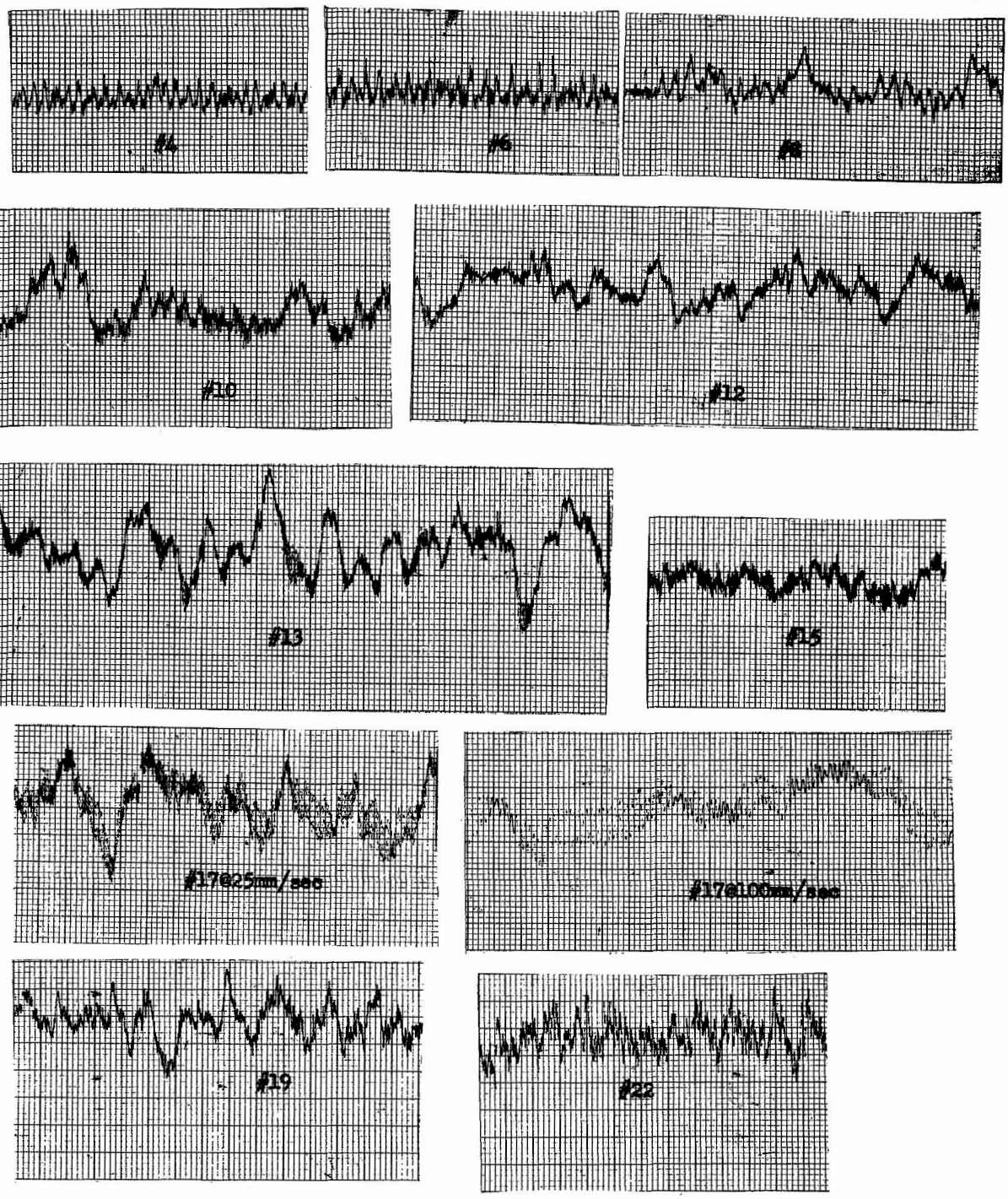




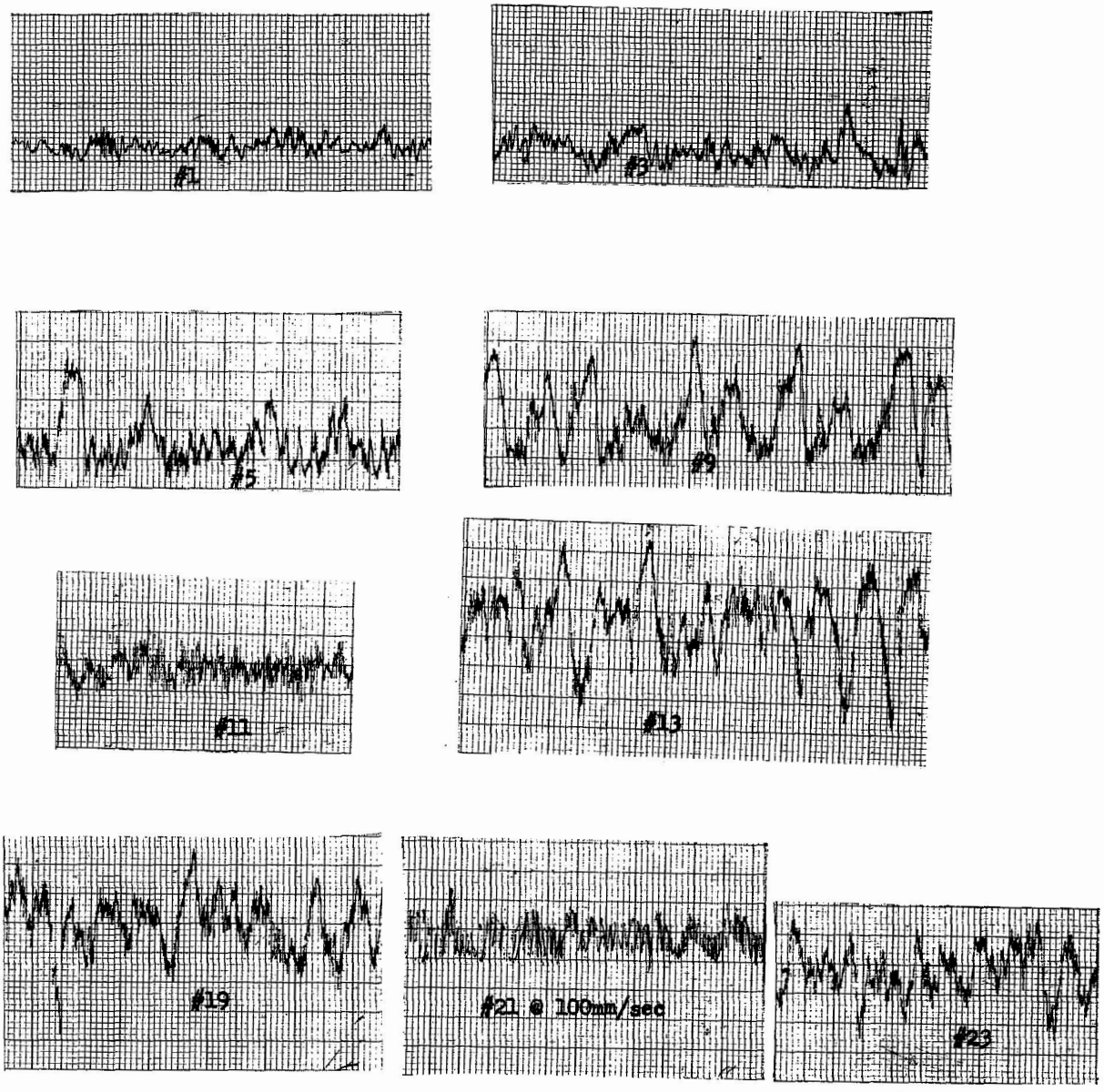




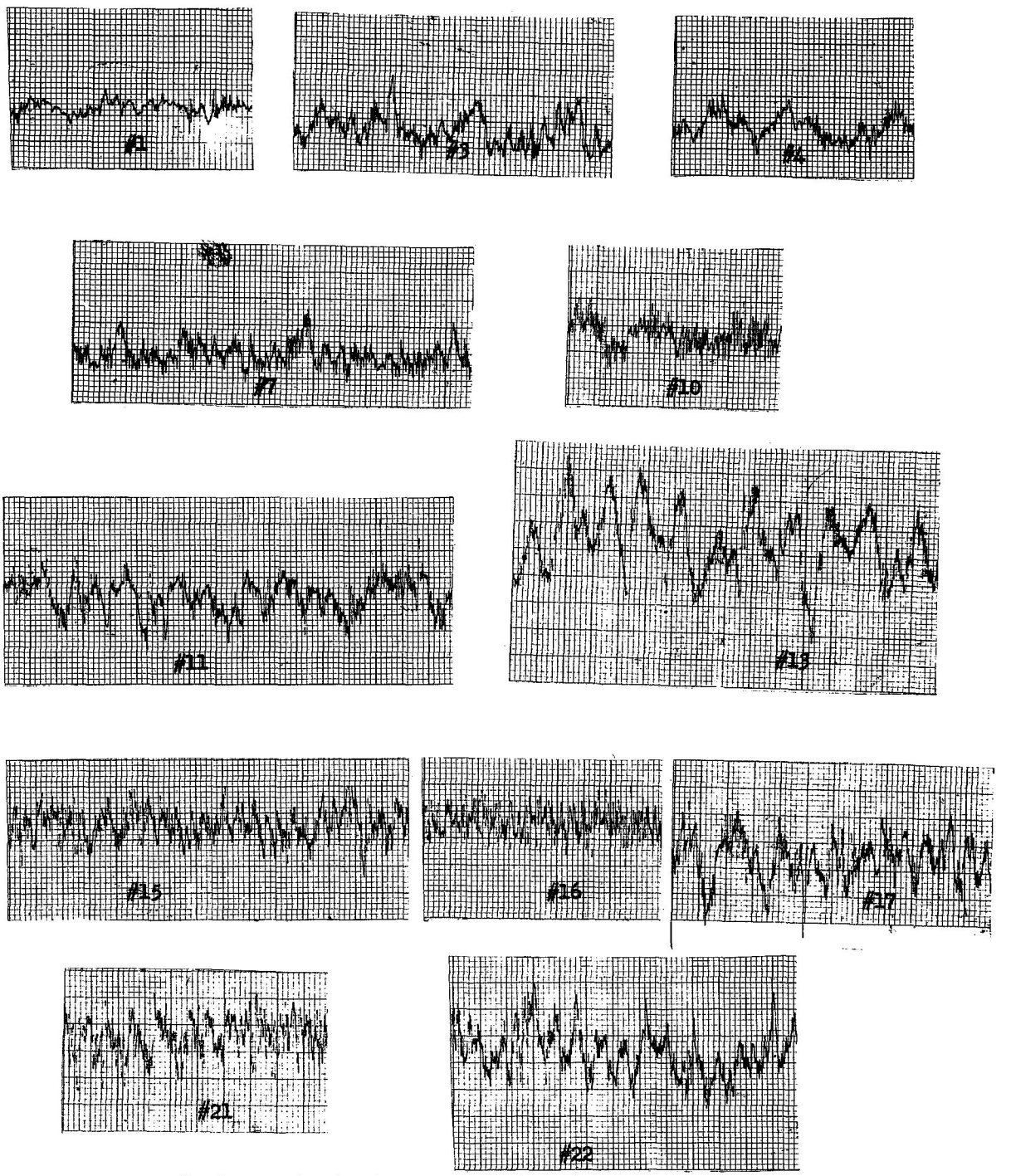
P_3 Traces for Movie Run M-6; 10 February 1970
Water-Air System; Signal Attenuation = X5;
Trace Speed = 25 mm/sec.



P_3 Traces for Movie Run M-8; 10 February 1970
Water-Air System; Signal Attenuation = X5;
Trace Speed = 25 mm/sec.



P_3 Traces for Movie Run M-9; 10 February 1970
Water-Air System; Signal Attenuation = X5;
Trace Speed = 25 mm/sec.



P_3 Traces for Movie Run M-10; 10 February 1970
Water-Air System; Signal Attenuation = X5;
Trace Speed = 25 mm/sec.

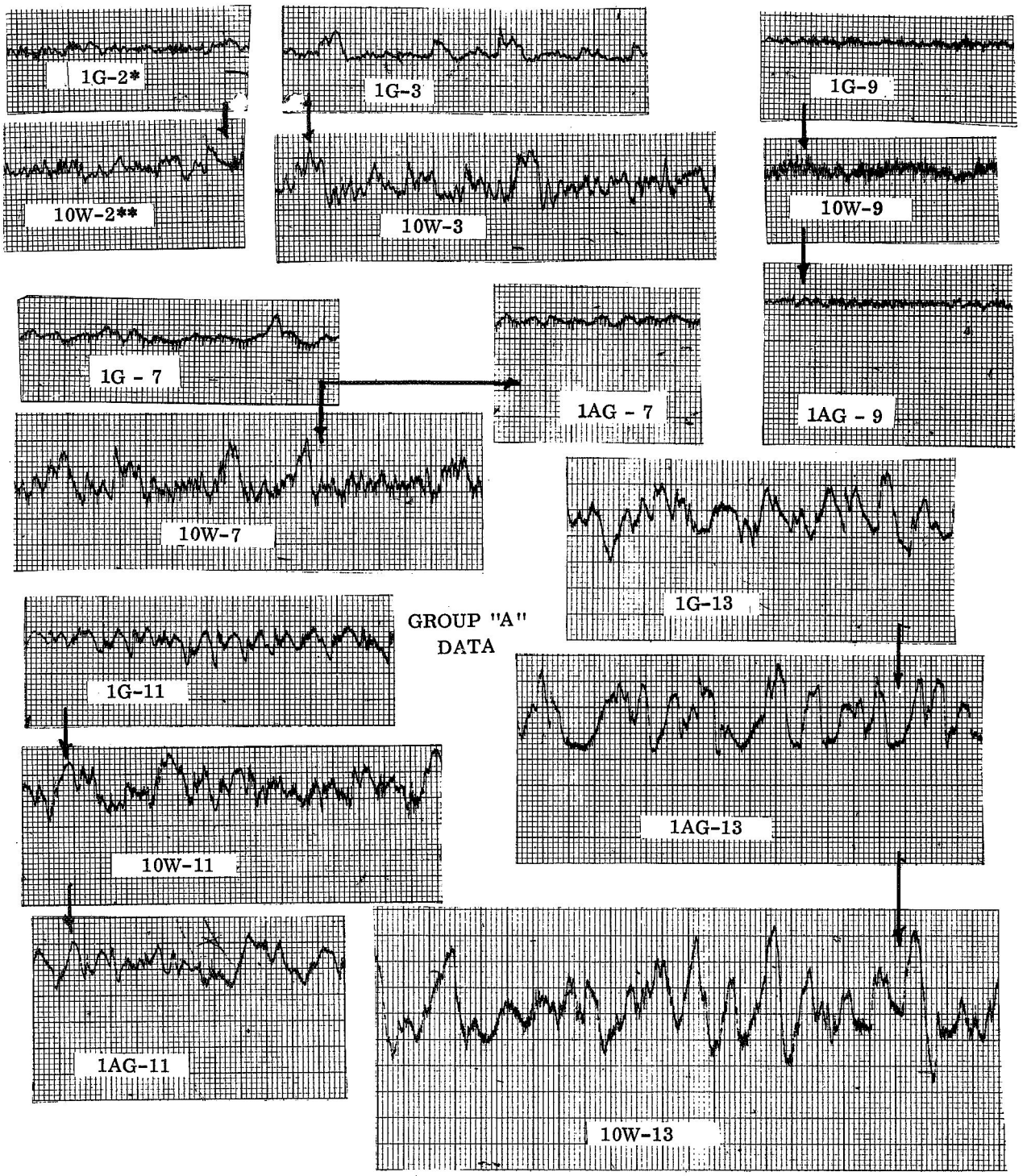
Table 51. — (Part 1) P_3 Trace Selections and Documentation Groupings

Q/L_1;L_2/ss / θ	1.1 G	1.1 W	1.3 G	1.3 W	1.5 G	1.5 W	1.9 G	1.9 W	2.9 G	2.9 W	3.2 G	3.2 W	3.6 G	3.6 W	3.9 G	3.9 W	4.0 G	4.0 W	4.2 G	4.2 W	4.4 G	4.4 W	4.7 G	4.7 W	4.9 G	4.9 W	Test Set* G	Test Set* W
0°(Closed)	2	2			3	3			7	7	Group "A" Data						9	9			11	11			13	13	1	10
0°(Open)									7								9				11				13		1A	(None)
45°	1	2	3				6	6			7	7			10	10			11	11			13	13			2	9
90°	2	2	3	3			6	6			7	7			10	10			11	11			13	13			3	8
135°	"C"	2	"D"	3			"E" 6	6			"F" 7	7			"G" 10	10			"H" 11	11			"I" 13	13			4	7
180°	2	2							7	7			"P"				9	9			11	11			13	13	5	6

Q/L_1;L_2/ss / θ	5.1 G	5.1 W	5.9 G	5.9 W	6.2 G	6.2 W	6.6 G	6.6 W	6.7 G	6.7 W	7.0 G	7.0 W	7.2 G	7.2 W	7.3 G	7.3 W	7.5 G	7.5 W	7.7 G	7.7 W	7.9 G	7.9 W			Test Set* G	Test Set* W
0°(Closed)					16	16			17	17	18	18	"B"				21	21			22	22			1	10
0°(Open)					16				17																1A	(None)
45°	14	14	17				19	19			20		21	21					22	22					2	9
	"J"		"K"				"L"						"M"						"N"							
90°	14	14	17	17			19	19					21	21					22	22		23			3	8
135°	14	14	17	17			19	19					21	22					22	22	"O"	23			4	7
180°					16	16			17	17	18	18			20	20	"P"(cont.)				22	22			5	6

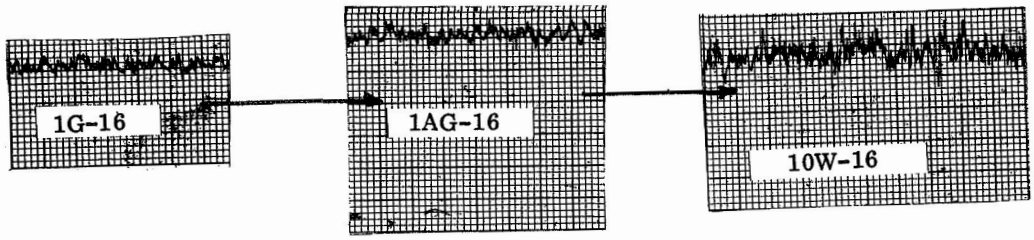
* See Test Data Sheets.

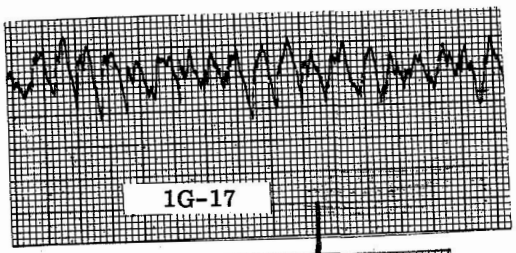
Legend: θ = Working Section Angle.
Q = Implied Two-Phase Quality, Notations Actually Indicate Valve Schedule for Liquid/Air.
L = Liquid; L_1 = Glycol (G); L_2 = Water (W).
ss = Sub Set of Test Set.

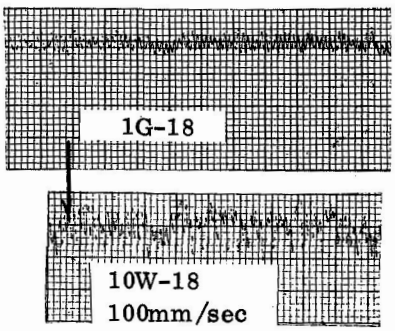


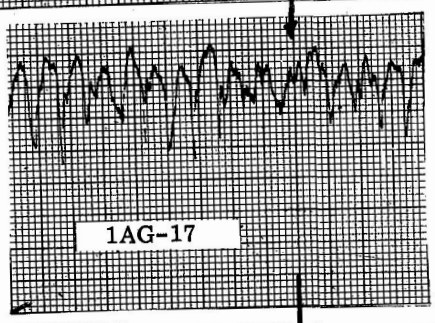
* P_3 Trace for Test Set #1 (Glycol-Air System) Sub Set #2. Signal Attenuation for All Glycol Tests = X10.

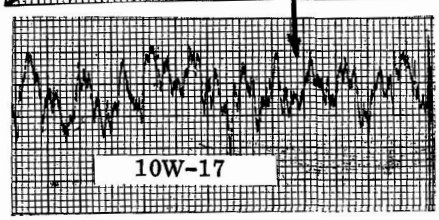
** P_3 Trace for Test Set #10 (Water-Air System) Sub Set #2. Signal Attenuation for All Water Tests = X5 except that TS #6 (180°) is at X10.


1G-16
1AG-16
10W-16

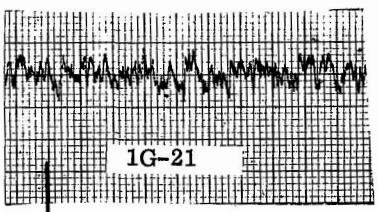

1G-17

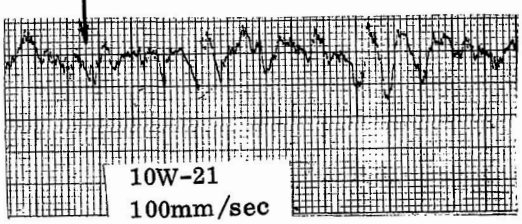

1G-18
10W-18
100mm/sec

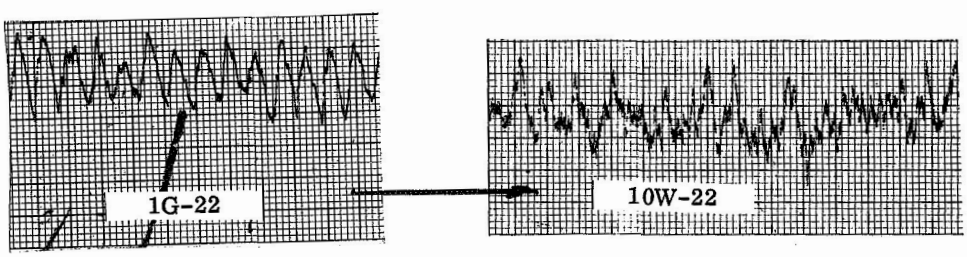

1AG-17

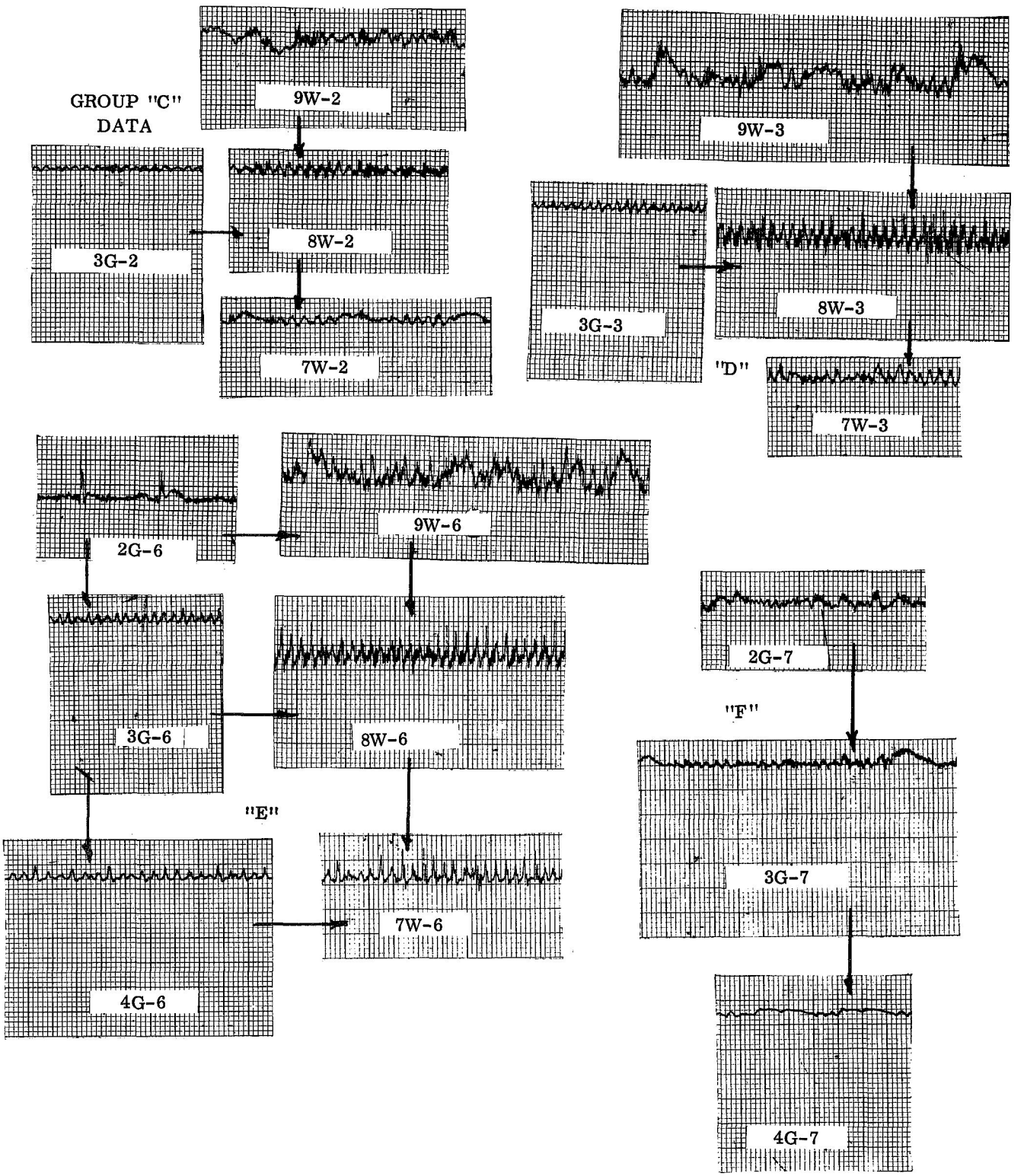

10W-17

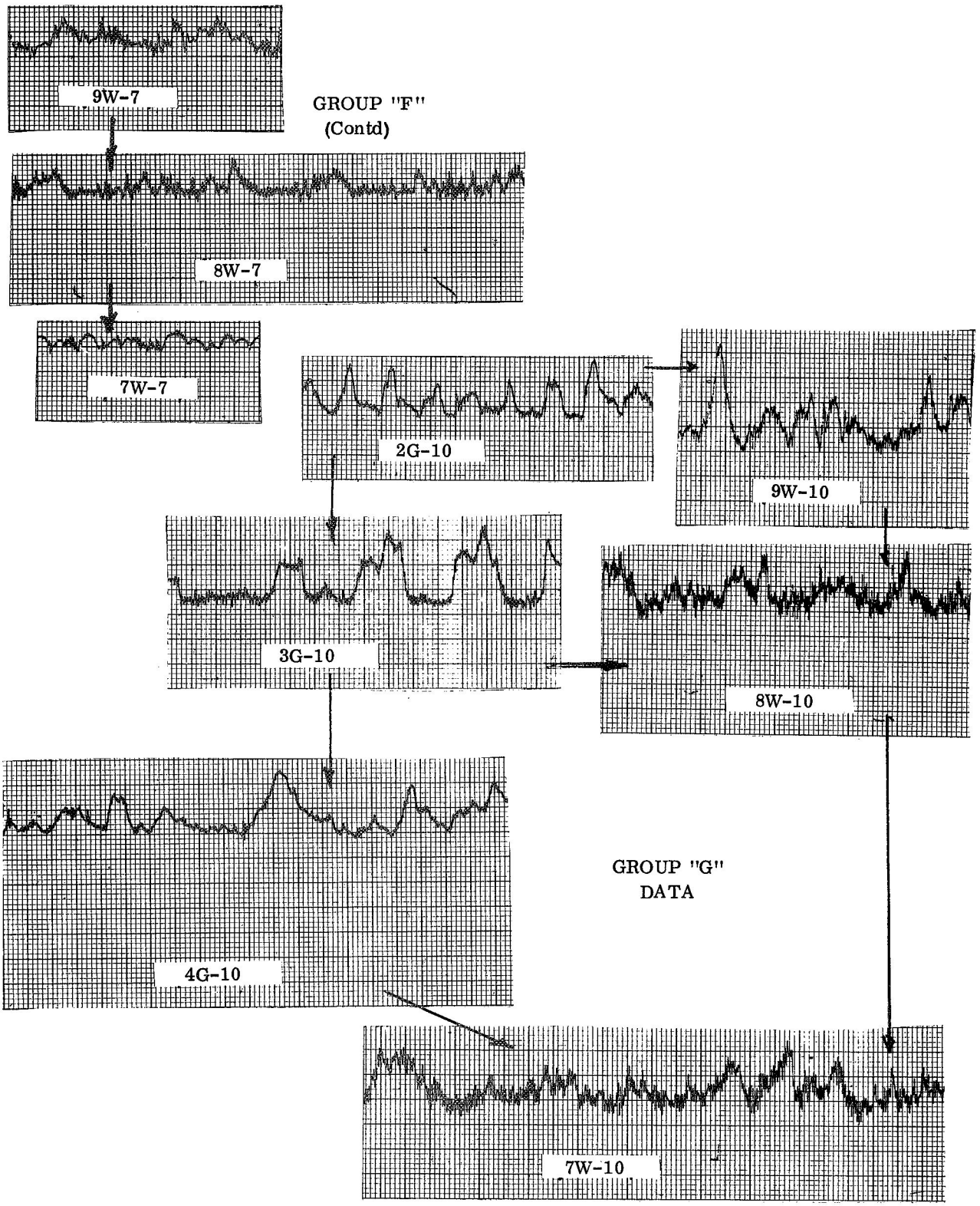
GROUP "B" DATA

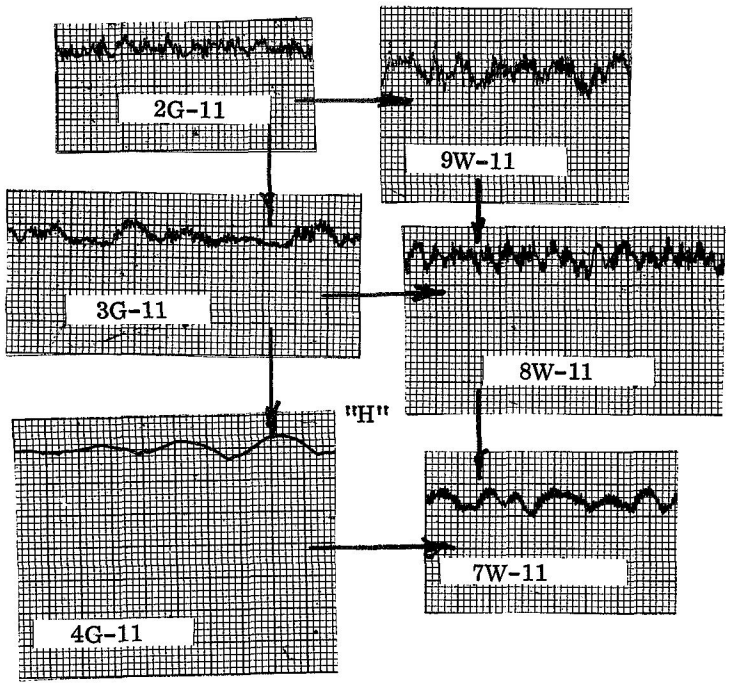

1G-21

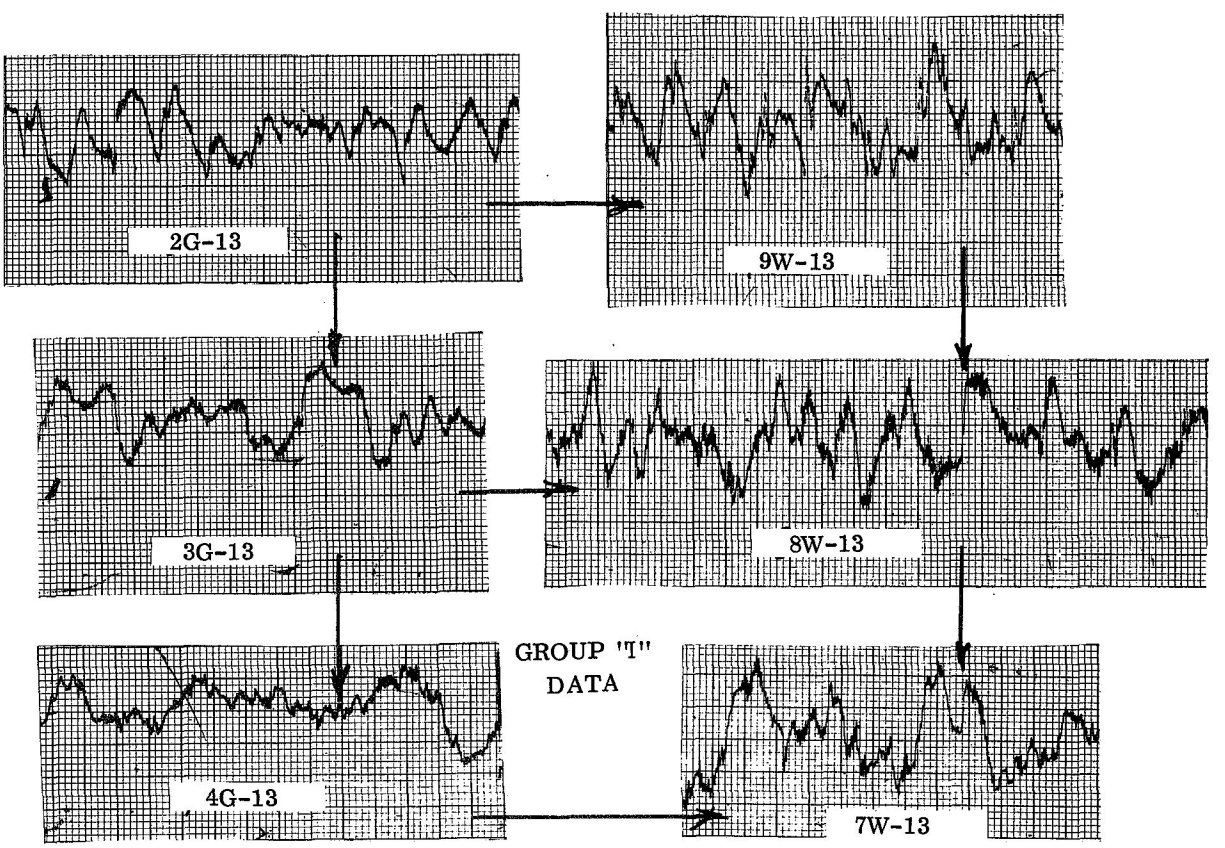

10W-21
100mm/sec

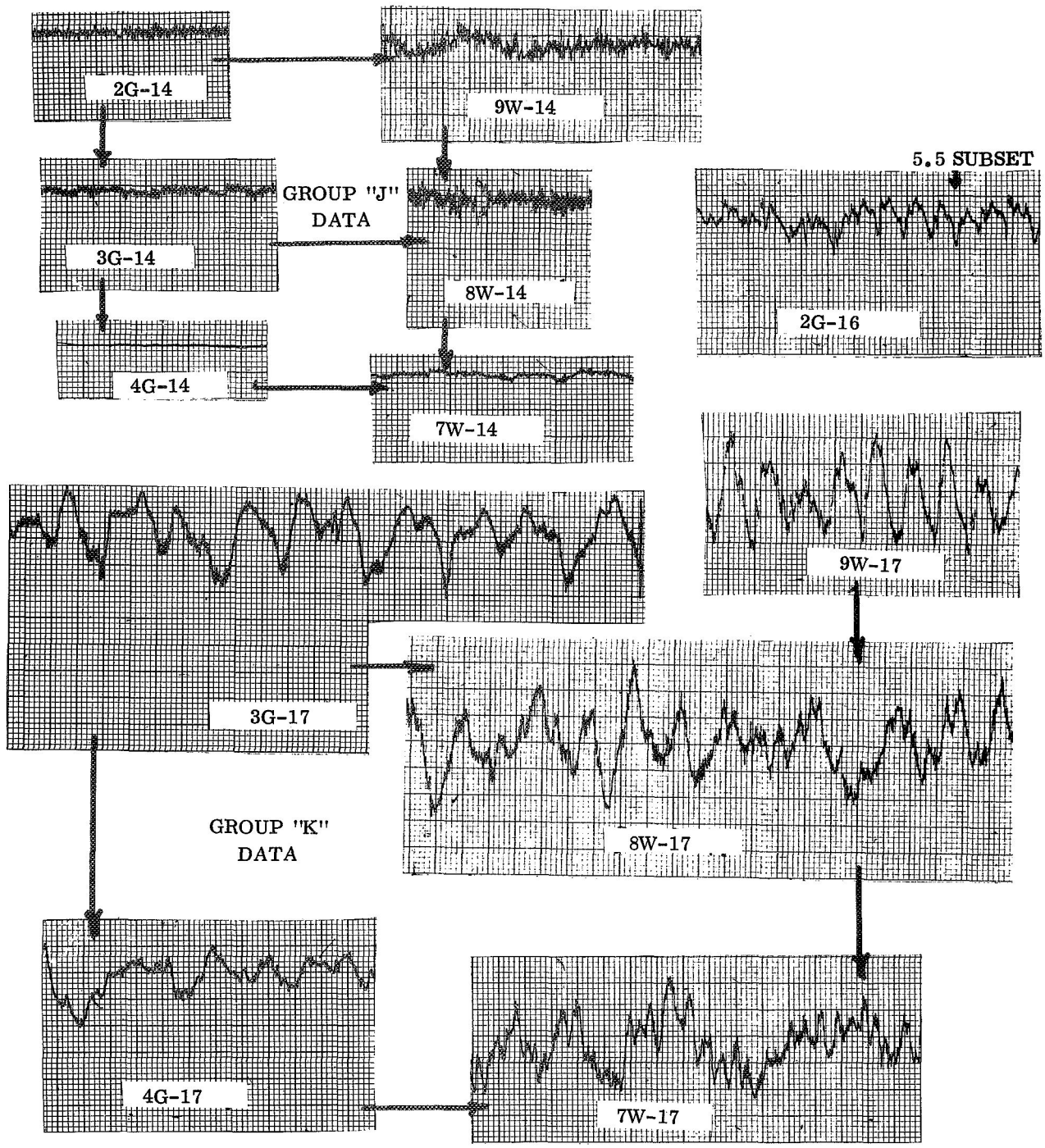

1G-22
10W-22

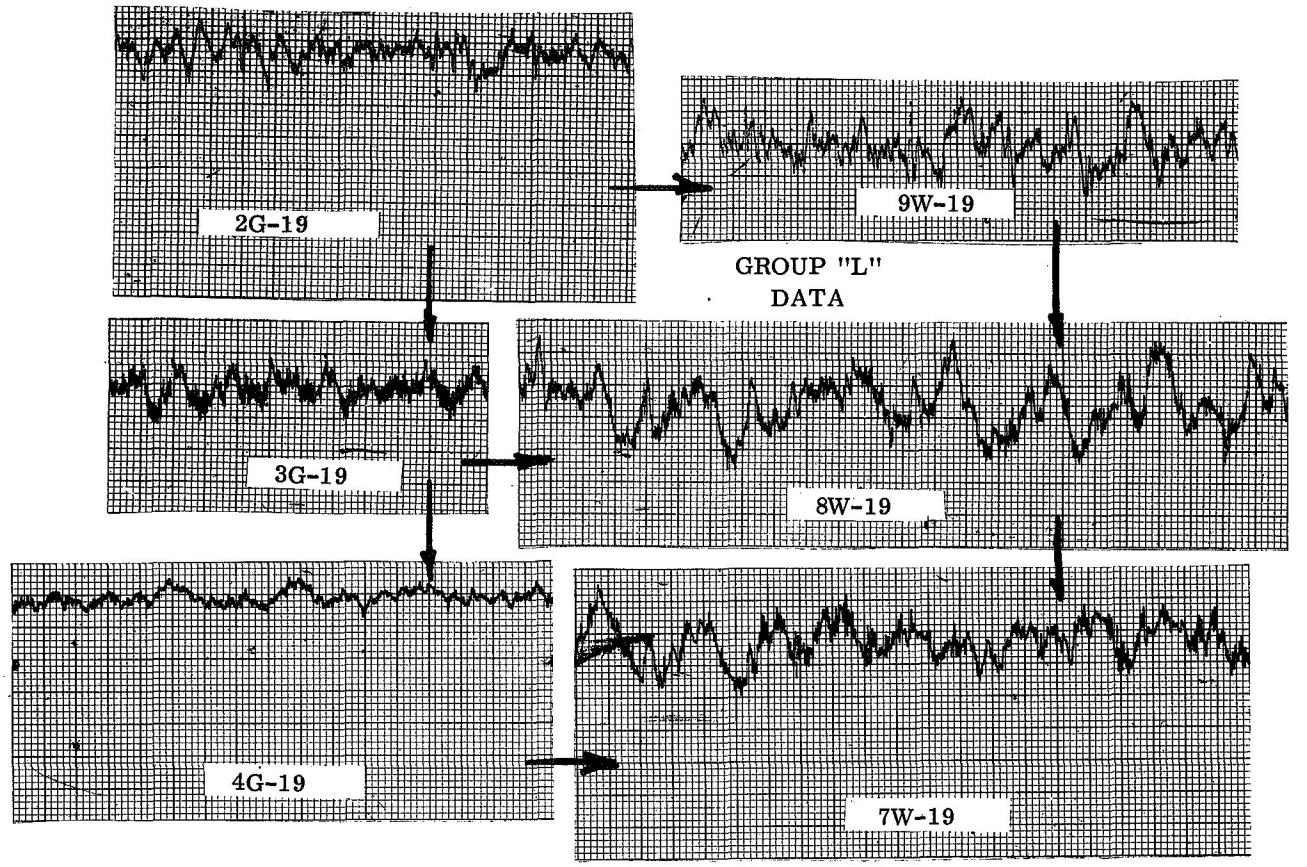

GROUP "C"
DATA
9W-2
3G-2
8W-2
7W-2
9W-3
3G-3
8W-3
"D"
7W-3
2G-6
9W-6
3G-6
8W-6
"E"
7W-6
4G-6
2G-7
"F"
3G-7
4G-7

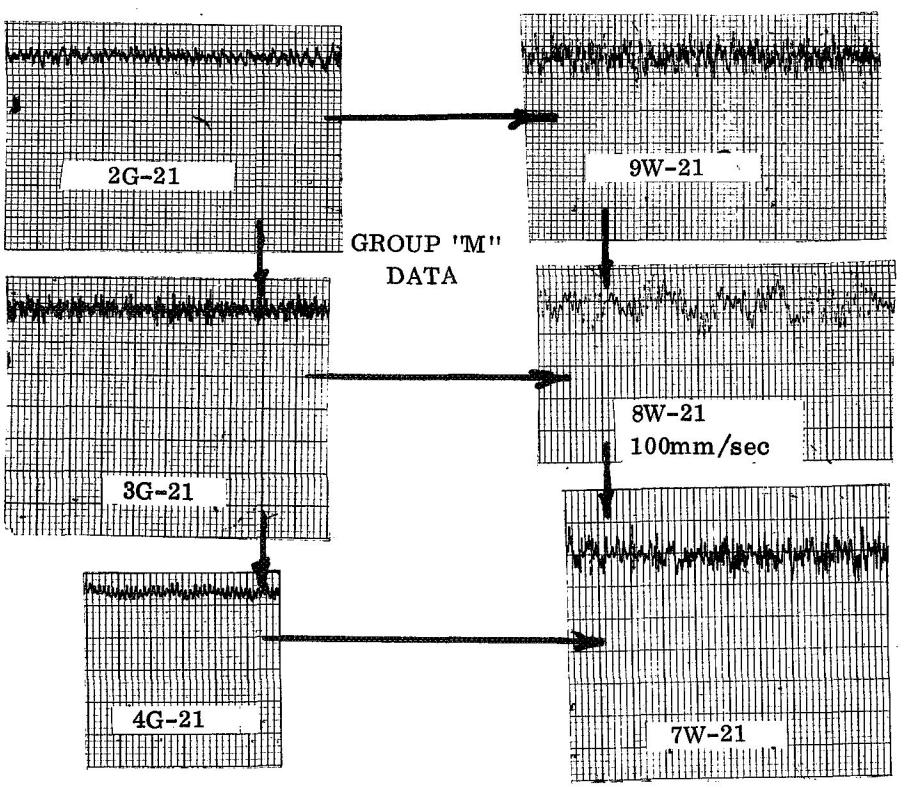

9W-7
GROUP "F"
(Contd)
8W-7
7W-7
2G-10
9W-10
3G-10
8W-10
GROUP "G"
DATA
4G-10
7W-10

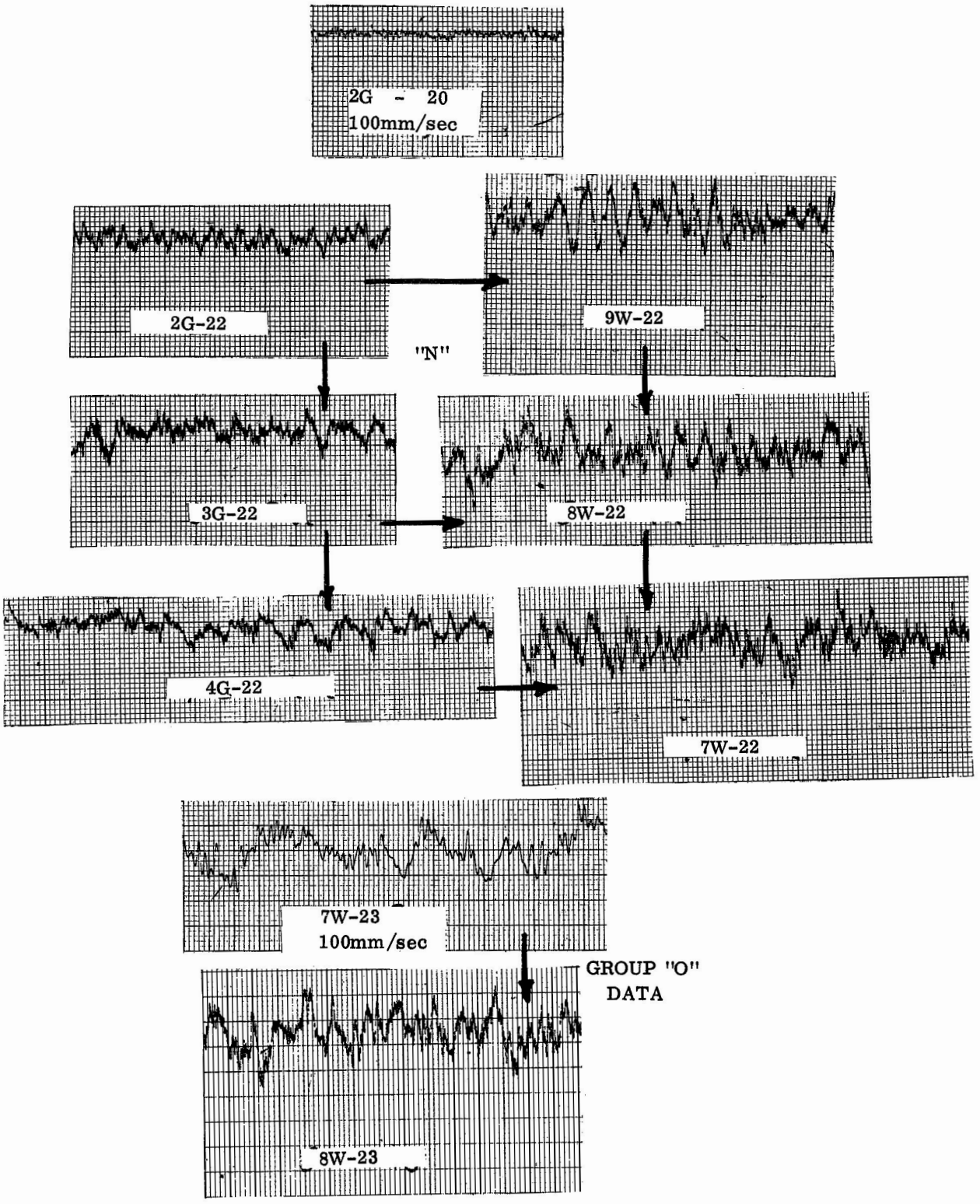

2G-11
9W-11
3G-11
8W-11
"H"
7W-11
4G-11

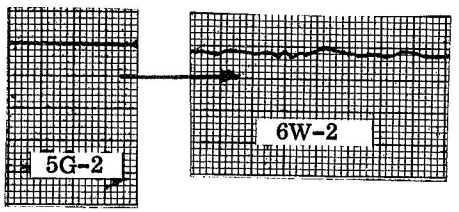

2G-13
9W-13
3G-13
8W-13
GROUP "I"
DATA
4G-13
7W-13

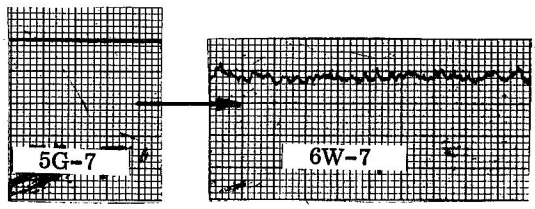

2G-14
9W-14
5.5 SUBSET
GROUP "J"
DATA
3G-14
8W-14
2G-16
4G-14
7W-14
9W-17
3G-17
8W-17
GROUP "K"
DATA
4G-17
7W-17

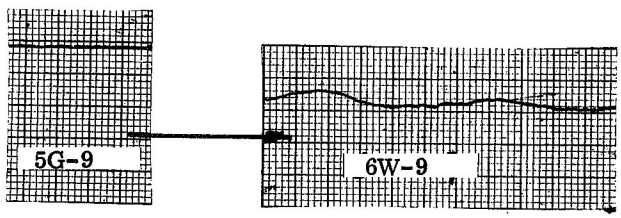

2G-19
9W-19
GROUP "L"
DATA
3G-19
8W-19
4G-19
7W-19

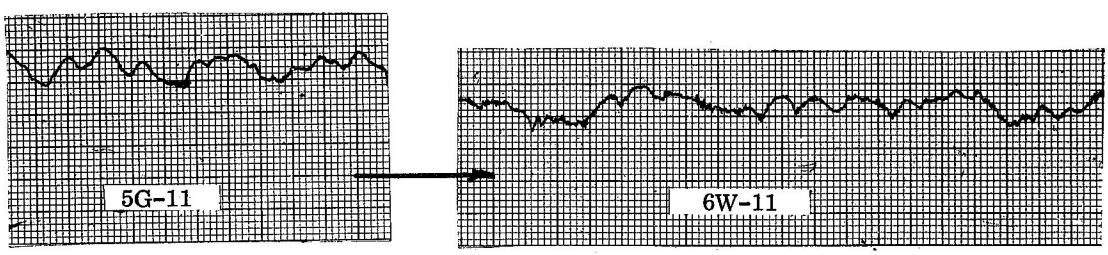

2G-21
9W-21
GROUP "M"
DATA
8W-21
100mm/sec
3G-21
4G-21
7W-21

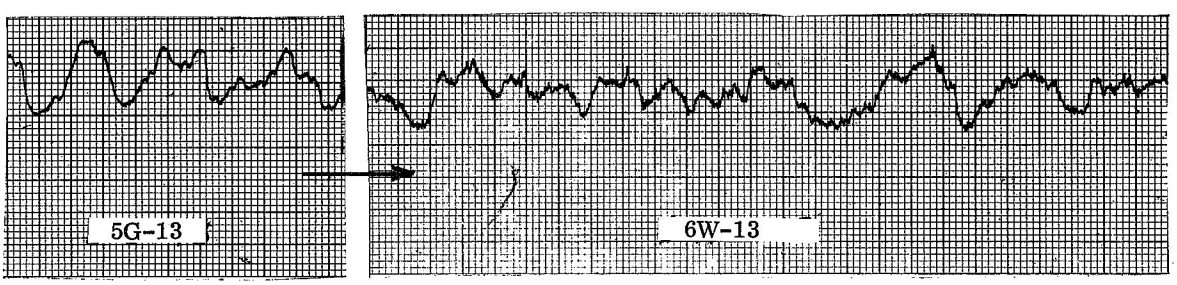

2G - 20
100mm/sec
2G-22
"N"
9W-22
3G-22
8W-22
4G-22
7W-22
7W-23
100mm/sec
GROUP "O"
DATA
8W-23



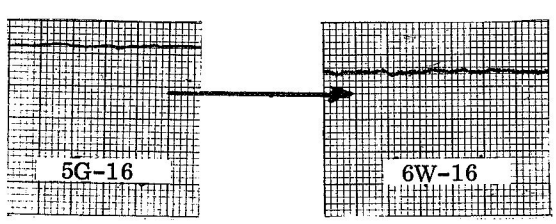


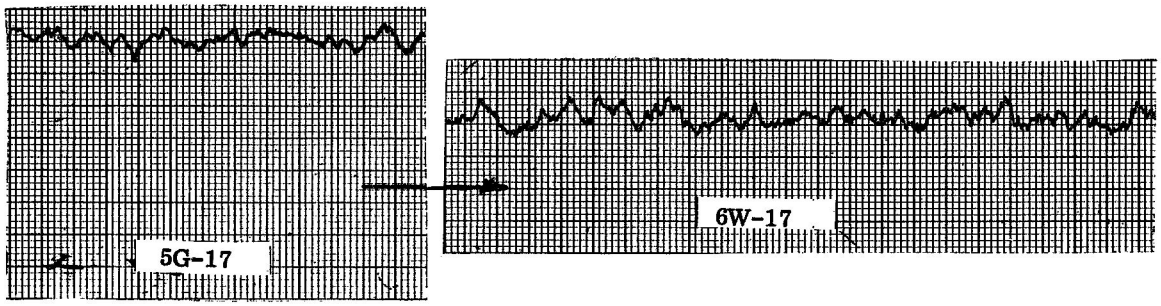


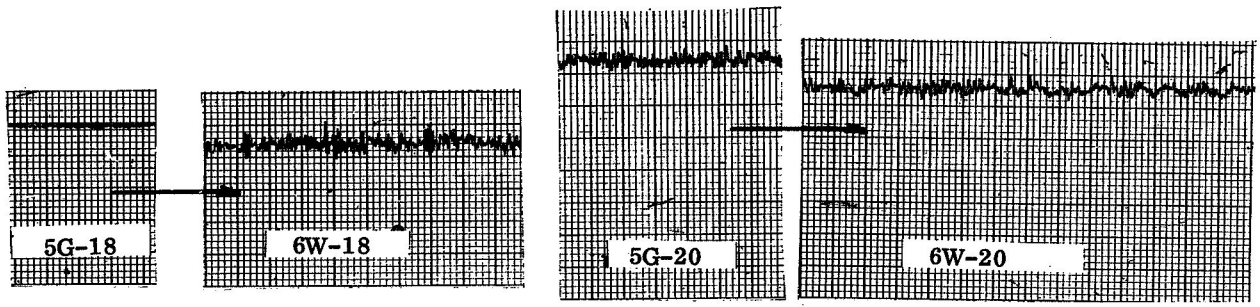




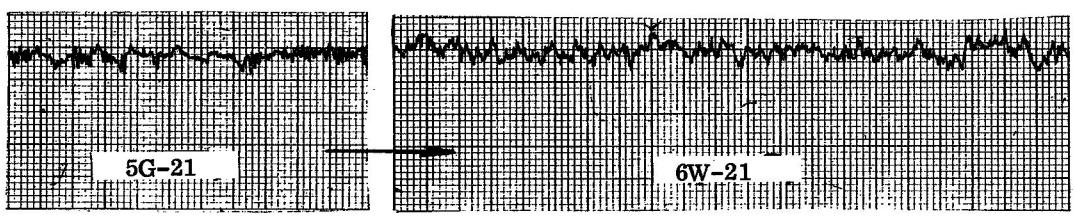
GROUP "P"
DATA







GROUP "P"
(Contd)



The thermocouple attachments external to the inlet and outlet tubing (thermally insulated) proved effective.

Measurements for gas flow should be available in the range of 0.01 to 0.10 to provide precise data for the low range of the slug flow regime.

Process Apparatus

As was experimentally demonstrated, there appears to be little or no value in more than a simple liquid/air mixing duct directly upstream of the working section inlet. However, it is believed that consideration should be given to increasing the effective length of the observable flow section, possibly by a combination of a reduced duct diameter and increased length. Doing so should more adequately display mixed regime patterns and establish more accurate measurements of wave lengths and wave form patterns. A more manageable "open sump" return should be developed to minimize feedback effects. Optical qualities of the working section were excellent.

Procedures

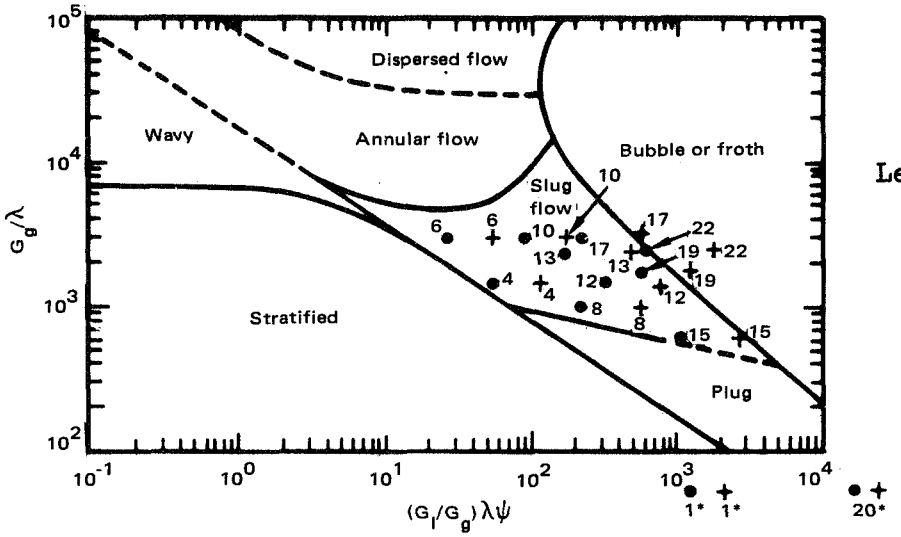
The procedures proved to be adequate and well organized resulting in an economic and effective test, particularly in the definition and execution of the rather extensive motion picture runs.

Future tests might well profit from further investigation into the merits of scheduling identical flow rates for all liquids in addition to the "similar transport power" scheduling chosen for this series as a simplifying technique.

Correlation of Predictive and Experimental Data

Figure 133 illustrates the validity of the flow regime boundaries within the domain defined by the fluid characteristics and "quality" of the two-phase fluid as established by the Baker correlation map. Some apparently significant variations in the locations of the experimental data points with respect to the regime boundaries as given by the Baker correlation were present.

Some question might be raised concerning the accuracy of the locations of regime boundaries if the regime identities assigned to the experimental observations are in keeping with those defined by Baker. If the regime identities listed on the test data sheets (ref. 7) are reasonable, the demonstrated repeatability of the flow patterns strongly suggests that the boundaries might be more accurate if shifted downward with respect to values of G_g/λ, i.e., to lower val ues and to the right with respect to values



Sub** Set	$(G_l/G_g)\ \lambda\psi$		G_g/λ ($lbs_m/hr\text{-}ft^2$)	Dominant Regime***	
	Glycol	Water		Glycol (+)	Water(•)
1	2,100	1,018	73*	Slug	Plug
4	105	54	1,460	Strat.	Slug
6	55	27	2,920	Strat.	Strat.
8	529	209	1,095	Slug	Strat.
10	189	78	2,920	Strat.	Strat.
12	839	300	1,460	Slug	Slug
13	560	200	2,190	Strat.	Slug
15	2,515	915	730	Slug	Strat.
17	630	229	2,920	Ann./Strat.	Sp.Ann.
19	1,342	462	1,825	Ann./Strat.	Sp.Ann.
20	51,000	17,000	73*	Bubble/Plug	Slug
22	1,679	570	2,190	Spray	Sp.Ann.

* Actually falls below abscissa.
** Test Sets #M-3, #3, (Glycol-Air); #M-8, #8 (Water-Air)
*** Regime identities may not be exact, additional study of movie and P_3 data should be undertaken.

Figure 133. — Experimental Data Correlation, Horizontal Flow

of $(G_\ell/G_g)\lambda\Psi$, i.e., to higher values. However, the general correlation is considered adequate to demonstrate that a controllable and valid experiment has been designed. Possibly the most significant point is that identification of the regime is both very difficult, as in most cases patterns relating to two or more regimes were mingled in the same flow condition, and further (as pointed out by the analytical approach presented in the section titled "Characteristics of Two-Phase Flow" may be of minor importance when the more rigorous analytical model is developed.

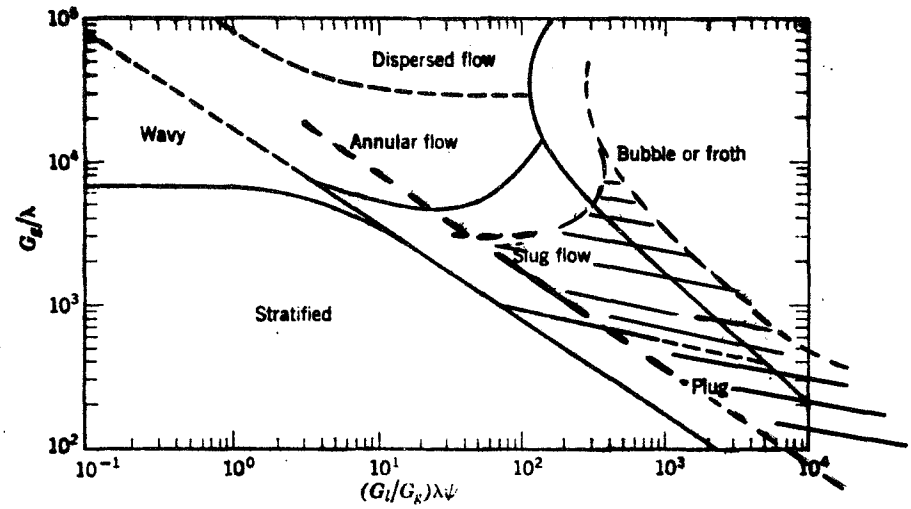
The limitation of the graphical representation as presented implies that the indicated boundaries sharply divide one set of flow characteristics from another. As might be expected, observation of these characteristics immediately provides ample evidence that no such sharply defined transition takes place, rather the transition is accompanied by a gradual change in characteristics typically passing through a region where the characteristics appear to define the simultaneous existence of two or more regimes.

One area of difference between the predicted and the observed flow which may prove to be significant, particularly in light of the suggested approach to the development of the analytical model, is that of the bubble flow regime. The traditional representation, as illustrated by figures 121 and 122, indicates that the bubbles are dispersed across the stream for vertical flow and partially stratified for horizontal flow. As indicated by the newly developed analytical approach, the experimental evidence was that the bubbles were concentrated in and traveled uniformly along the centerline of the flow channel whenever any significant level of liquid flow was present.

Effects of Fluid Physical Properties

Figure 134 illustrates the effects of alterations in the physical characteristics of the fluid (kinematic viscosity for glycol apparoximately 21 times that of water, surface tension $\sim 1/2$, and density $\sim$ equal). In the first instance again as suggested by the new model, the apparent effect was to shift the regime boundaries with respect to the abscissa to coincide with higher values for the ratio of the liquid/gas characteristics, specifically $(G_\ell/G_g)\lambda\Psi$. The second illustration photographically documents the flow pattern differences accompanying the change in fluid as viewed for each of three channel orientations.

Examination of the pressure variations along the flow channel as implied by the characteristics of the P_3 traces (samples of which are shown herein) indicates rather clearly that the magnitude of the variation is much higher ($\sim$2 times) for the more viscous fluid while the frequence of the variation is significantly lower ($\sim$1/3) for the horizontal flow. These characteristics represent the mechanical or physical system response to the flow of an "elastic," oscillating, and often turbulent two-phase fluid.



Baker Flow Correlation

Shift in regime boundaries suggested by the experimental data for a change from the water-air system to the glycol-air system resulting in an increase in viscosity by a factor of 20 and a decrease in surface tension by a factor of 2.

	Propylene Glycol	Water
Viscosity (CS)	21.1	0.94
Surface Tension (dynes/cm)	35.4	64.1
Density (gms/ml)	1.014	0.9931

Note: Values for typical temperatures experienced, see test data sheets for details.

Figure 134. — Effects of Fluid Properties

Effects of Flow Channel Orientation

Orientation of the direction of flow with respect to the gravitational vector demonstrated that there are marked similarities in the flow patterns regardless of the orientation. One of the major changes which appear is related to the magnitude of the mass flows required to produce the characteristic regimes for comparative values of two-phase quality. In that the range of mass flow attainable with the experiment apparatus was restricted, more different patterns could be attained at some channel angles than at others. For instance, the vertical down position operated in only two distinguishable regimes, namely variations in annular flow patterns and mist. On the other hand, the horizontal position progressed through plug, stratified, slug, and spray annular regimes in response to identical mass flow rates as the vertical down.

An example of the change in the characteristics of flow patterns for identical fluid mass flow rates can be observed in comparing three such conditions at horizontal, vertical up, and vertical down for the water/air system. Such a comparison is provided by table 52. It is shown that slug flow for horizontal is comparable to the oscillating spray-annular pattern for the upward flow, while the vertical down flow drops out the oscillatory and unidirectional slugging present with the other two directions. Although the amplitude and wave pattern of the pressure profiles are similar for the horizontal and vertical, the frequencies for the horizontal are significantly higher.

Characteristics of the Pressure Profile

The pressure profile data, listed as P_3 and recorded both by stripchart and by manual entries in the test report (ref. 7), are helpful in describing the dynamic nature of the two phase flow. Entries under columns 6 and 7 of table 52 illustrate both the similarities and differences which characterize the regimes resulting from identical mass flow rates in each of three flow directions. Column 6 indicates that a pressure variation exists in the basic flow pattern for all three (0.4 psi) but that the vertical up and horizontal, responding to the "resistive" gravitational force, produce an overlay variation in the form of an oscillatory flow pattern (slug). The oscillatory flow for the vertical up is gross and visually apparent as an actual momentary reversal in direction of a portion of the ongoing mass flow. This characteristic is far more subtle with the horizontal flow and appears as an accelerating slug moving very rapidly through the slower moving stratified flow pattern. The P_3 values, especially for frequency, illustrate this operational difference.

Figure 135 illustrates several interesting facets of the significance of the pressure profile. Perhaps the most obvious is the probable cyclic nature of pressure characteristics with increase values of the familiar $(G_\ell/G_g)\lambda\Psi$ of the Baker correlation.

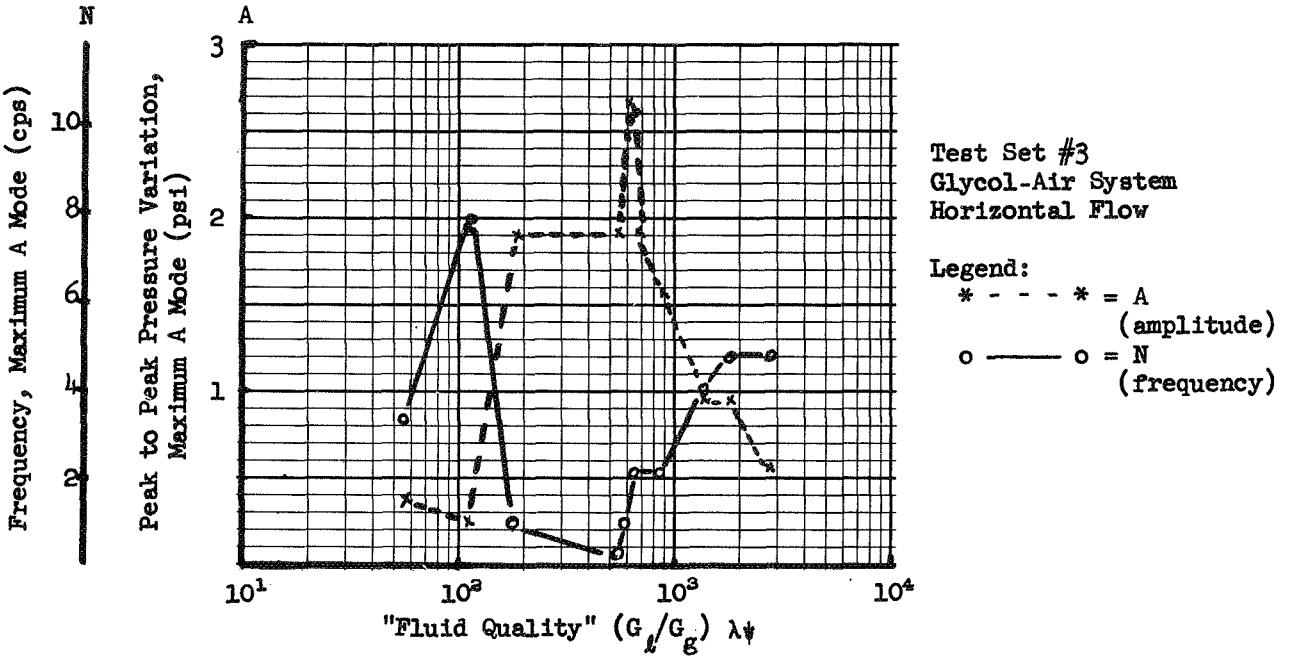
Table 52. — Comparison of Flow Characteristics for Identical Mass Flow Rates in Each of Three Flow Directions for the Water/Air System

Test Set	Sub Set	Valve Sched.	Flow Direct.	ΔP (psi)	P_s Variations		Regime	Characteristics
					Amp (psi)	Freq cps-t_1		
8	4	1.5	→	~ 0	0.8** / 0.4	15-1*** 15-0.08 (1st 2 of 3 modes)	Slug	Liquid-air interface for strat. flow segment is wavy, 1.3 crests/ft of duct, slug frequency ≅ 0.13/sec.
10	3	1.5	↑	0.8	0.8 / 0.4	5-1.50 5-0.24 (1st 2 of 3 modes)	Spray Annular and Slug	Up-down oscillations; slug up, annular runback, 1.3 slugs/ft. of duct.
6	3	1.5	↓	0.5	0.4	15 cps (single mode)	Annular	Generally uniform with slightly wavy interface.

* Pages 4-28, 30, & 32 of ref. 7

** Peak to peak pressure for major mode/secondary mode.

***Indicates 15 cps for major mode with 4-sec interval between major mode groupings (slug).



Sub Set	$(G_\ell/G_g)\ \lambda\psi$	Pressure Pulse			Regime	Observed Characteristics
		Amp*	Freq**	Back-Ground***		
6	55	0.38	3.5	10	Strat.	Very wavy
4	105	0.25	8.0	11	Strat.	Slug & wavy
10	189	1.90	1.0	3	Strat.	Much spray
8	529	1.90	0.3	8	Slug	
13	560	2.68	0.6	1	Strat.	Much spray
17	630	1.90	2.2	4	Sp.Ann.	Rough
12	839	1.52	2.2	2	Slug	
19	1,342	0.95	4.0	7	Sp.Ann.	
22	1,679	0.95	5.0	6	Spray	
15	2,515	0.57	5.0	5	Slug	

* Average amplitude of maximum amplitude mode, psi.
** Average frequency of maximum amplitude mode, cps.
*** Rank order of "degree" of pressure fluctuations for modes other than maximum amplitude.

Figure 135. — Effects of the Liquid/Gas Mass Ratio on Pressure Profile Characteristics

The underlying mechanism being observed is undoubtedly the "elastic" or compressibility characteristics which produced a combination of factors associated with each flow pattern operating in the sample series. These factors include the configuration of the liquid/gas interface, the average and local velocity differences, and the general degree of flow stability attained.

Figure 136 is a somewhat more simplistic attempt to graphically determine the nature of the relationship between "fluid quality" and the magnitude of the accompanying pressure variation.

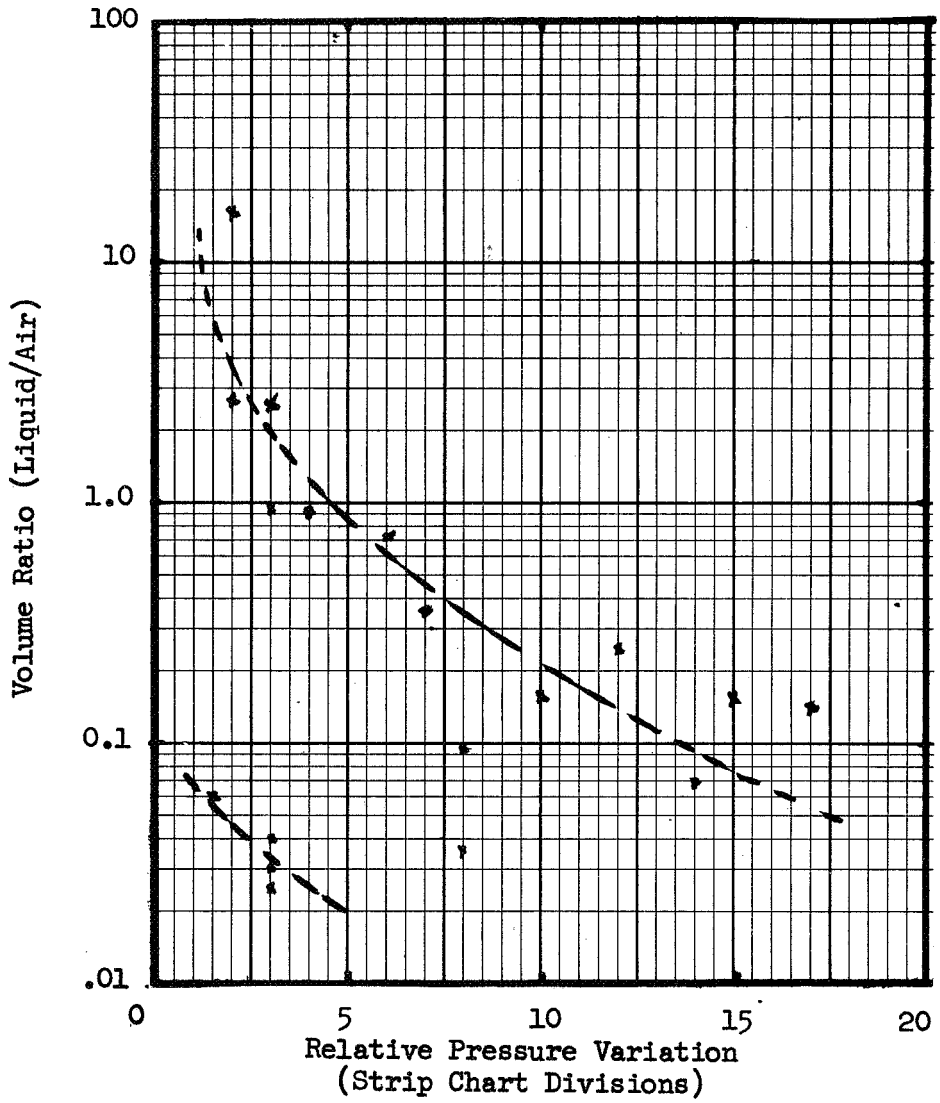


Figure 136. — Correlation of the Liquid/Gas Volume Ratio with the Magnitude of the Maximum Variation within the Pressure Profile

Although there is excessive scatter in the data as plotted, there appears to be a general overall tendency at least for an increasing pressure variation with an increasing percentage of air in the two-phase fluid makeup. Some of the scatter and apparent deviations could well be associated with the combination of the differences in the resonant characteristics of various liquid/air ratios, the mass flow rates, and the dynamics of the physical system. Additionally, it can be postulated, as suggested by the two subjectively constructed broken line curves, that the data represent at least two groupings, each reflecting a different set of compressibility and resonant characteristics.

Qualitative Correlation of the Analytical Model and Experimental Evidence

Experimental observations indicate several areas of correlation with the analytical development presented. The most obvious is the stratified flow regime boundary which is a function of the sum of the gas and liquid Froude numbers illustrated by equation (8a).

A more subtle evidence is the balance between the separating effect of vorticity (total fluid shear stress) and gravity represented by equation (13). When the flow section was oriented vertically downward ($g_Z > 0$), only annular and mist flows were observed which the inequality (13) suggests. On the other hand, when oriented vertically upward ($g_Z > 0$), additional flow regimes of slug and plug flow were apparent which are violationsof inequality (13), again consistent.

For horizontal orientations, the change in fluid viscosity upward caused a shift in the flow regime boundaries to the higher abscissa values. Equation (13) predicts this event.

The nature of the separation due to vorticity and total fluid shear stress is illustrated by the observations of the bubble flow regime. The bubbles are concentrated along the center of the flow tube. However, the size of the bubbles is the result of turbulence, equation (4), which prevents agglomeration. When the turbulence reaches a sufficient magnitude, the fluid becomes more homogeneous; however, the bubbles break up and mist or dispersed flow occurs, equations (1 to 11).

These observational consistencies demonstrate the potentialities of the analytical approach and the physical content and insight into the basic kinematics of the flow regime structure.

Significance of Motion Picture Data

The importance of the real-time recording of experimental observations by motion picture coverage cannot be over emphasized. The two-phase flow study is totally dependent on a combination of visual observations and analysis. Since the study is necessarily still in its embryonic stage, with low-g testing yet to come, the immortality

of the experiment is assured by motion picture recording. Establishing the relevance of future data to the recently completed testing is facilitated by actual comparison with the movies.

From a physical point of view, the "flow regime" is a time-averaged or expectation property of two-phase flow. The discrete time representation of still photography does not provide a representation for the dynamic statistical character of two-phase flow. This additional dimensionality is essential for experimental correlation and must be included in and compared with data from future tests.

REFERENCES

1. Evans, E.; Burnett, J.: Analytical Model Report No. 6 Flow Regime Characteristics. Second issue, Convair division of General Dynamics, February 1970.

2. Baker, O.: Simultaneous Flow of Oil and Gas. Oil and Gas J., 53, 185-190, July 1954.

3. Evans, E.: An Investigation of the Effects of Spatial, Thermal, and Velocity Inhomogeneities on Two-Phase, Single-Component Cryogenic Choked Flow. Advances in Cryogenic Engineering, vol. 14, p. 283, Plenum Press, 1969.

4. Quandt, E.: Analysis of Gas-Liquid Flow Patterns. Chemical Engineering Progress Symposium Series (Heat Transfer, Boston), 61, 128-135, 1965.

5. Landau, L. D.; Lifshitz, E. M.: Fluid Mechanics, vol. 6 of Course of Theoretical Physics, Pergamon Press, Addison-Wesley 1959, p. 116.

6. Hinze, J. O.: Turbulence, McGraw Hill, N.Y. 1959.

7. Burnett, J.: Experimental Test Report No. 6 — "Flow Regime Characteristics." Convair division of General Dynamics, 12 February 1970.

DESIGN PARMETRICS

The primary objective of the NASA-LRC life support system (LSS) gravity-sensitivity assessment program, of which the NAS1-8494 is the second contract in an on-going series, is the development of an informational base available to and readily usable by the designer of LSS and components. The primary function of the NAS1-8494 contract is the development of a set of analytical models. These models have been so designed as to form the basis from which virtually all gravity-sensitive processes of LSS equipments can be analyzed and their equipment designs configured.

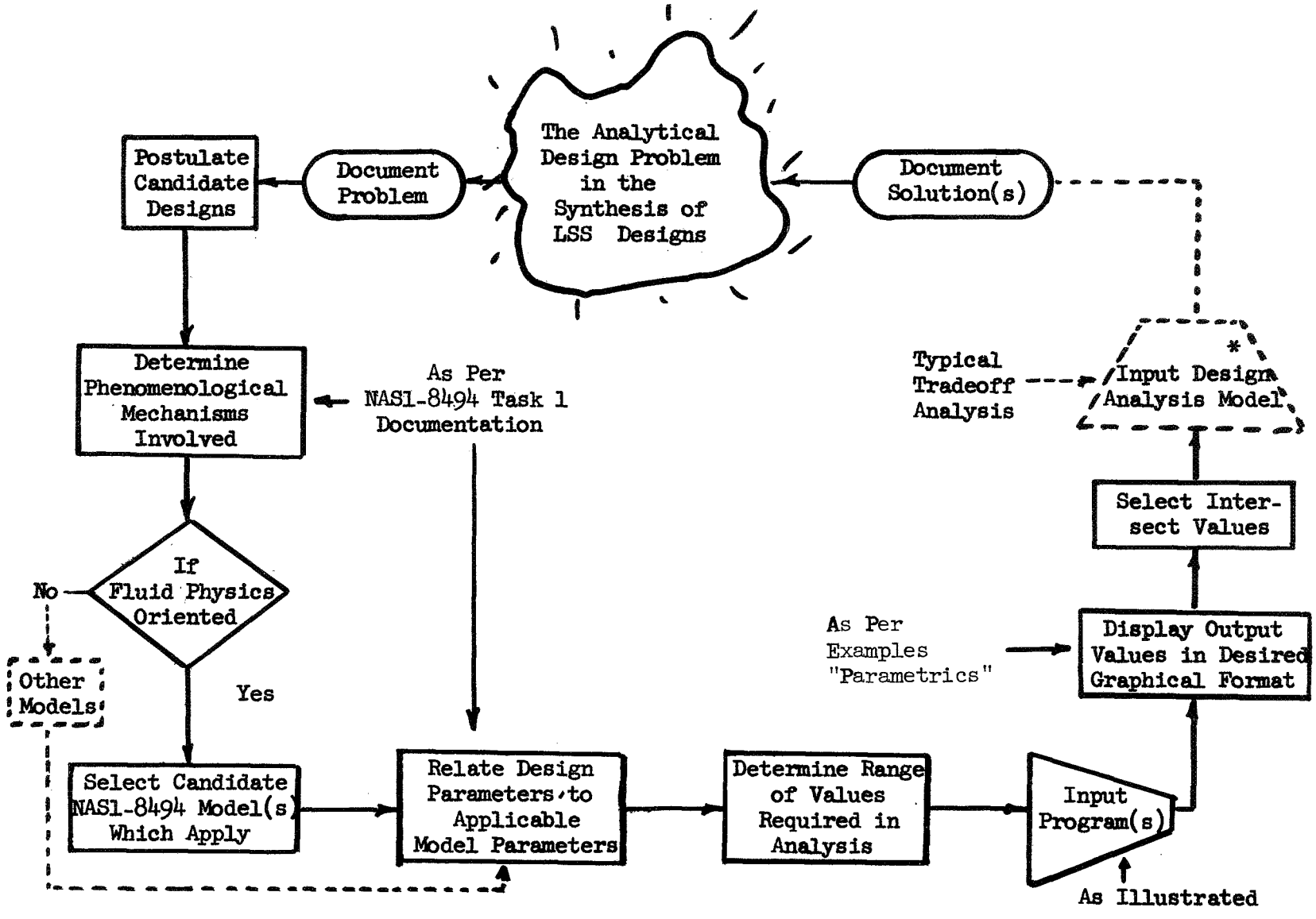
A typical method of organizing and relating the predictive data made available through the use of such analytical models as those being developed is the graphical representation of the quantitative relationship between parameters of the process as described by the model and a parameter of the design under study. Although it is both technically impossible to produce a set of mature design parametrics until the analytical models on which they are based have been fully matured through the experimental tests of ensuing programs, and operationally impractical except as part of an actual design program, an example can be constructed to illustrate their format and potential utility on the solutions of a design problem.

Figure 137 illustrates a typical approach in the utilization of the analytical models in the solution of design problems, i.e., analysis as a part of design synthesis.

ANALYTICAL MODEL NO. 1 — "NUCLEATE BOILING"

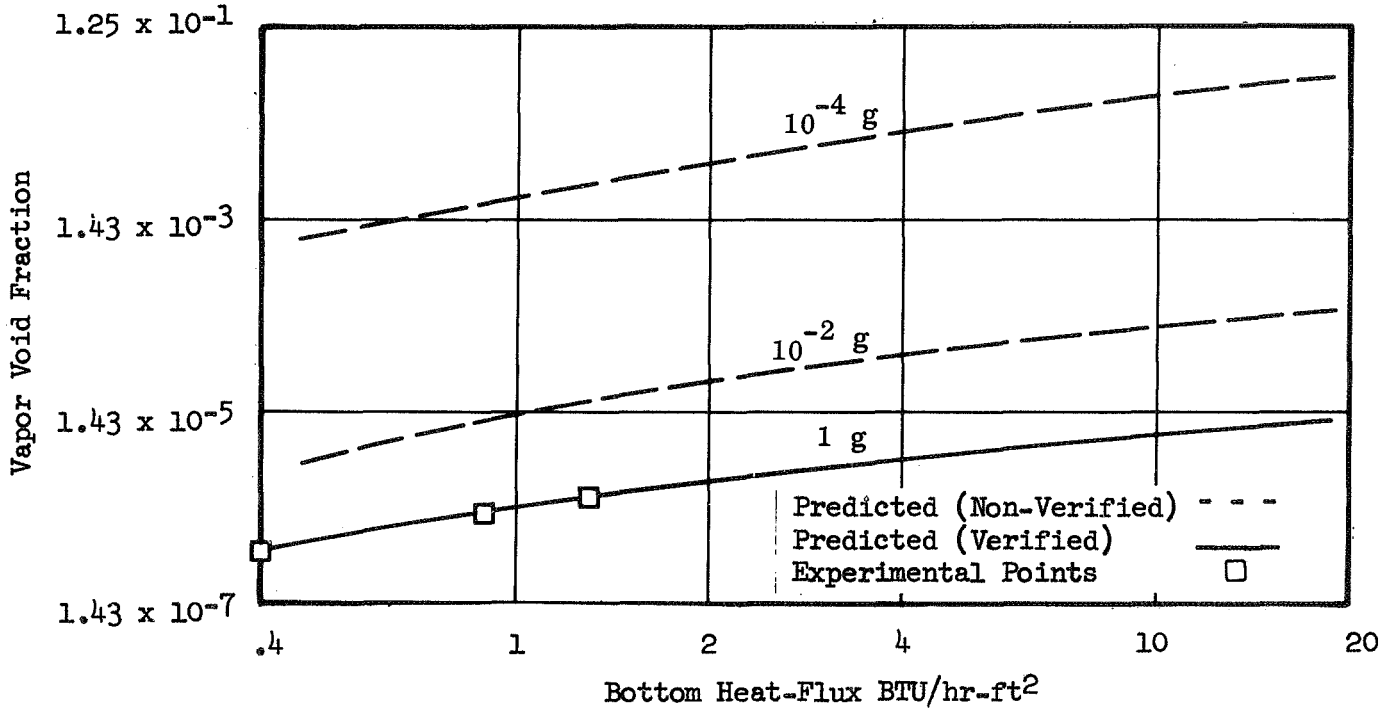
Figure 138 is a typical development which might be of interest to the design of a storage vessel and venting system. The data for the 1g case have been validated by experimental test while the data for the low-gravity cases represent unvalidated predictions.

The development of design parametric data relating to the overall phenomenological system involved might well require input data from sources other than from the model developed herein. For the example design parametric, input data pertaining to bubble departure from the heated surface must be obtained from the literature since the program simulates only the bubble trajectory after the bubble leaves the surface. These data include bubble size, departure frequency, and fraction of energy input going into latent heat. These variables are discussed by Tong (ref. 4), Keshock (ref. 5), and others. The physical characteristics of the problem are input taking advantage of the degeneracy factor for symmetric problems. The acceleration field for the problem is defined. Bubble size and frequency from the literature define the evolution rate for a given wall



* Not a NAS1-8494 Model.

Figure 137. — Typical Utilization of NAS1-8494 Analytical Models



Note: Data are based on the following conditions:

1. Nucleation site density = $1/ft^2$
2. Fluid = Freon 11
3. Vapor-free pool depth = 7 ft

Figure 138. — Example Design Parametric - Void Fraction Versus Heat Flux

heat flux. Conservatively assuming all energy, Q, goes to latent heating, i.e., bubble evolution, the number of sites, N, is defined from the frequency and size data.

$$Q = \lambda \rho_g \sum_n f_n (4/3 \pi R_b^3)$$

The free variable in this expression is the number of sites selected per unit area. The output from EVOLVE gives the void fraction; thus, with liquid height and container geometry, the void vapor entrained can be determined.

There are many areas where information from the analytical model described herein can be related to specific design parameters. The tabulation presented in the section titled "APPLICATION TO LSS DESIGN STUDIES" (for the nucleate boiling model) indicates the machine processes for each LSS function where such considerations could logically appear. For example, figure 138 could well be one of several applicable to Oxygen Supply (3), CO_2 Removal (17), Water Reclamation (47), and Waste Management (74). Other interests might relate the alterations imposed by variations in pressure, liquid characteristics, etc.

ANALYTICAL MODEL NO. 2 — "DIFFUSION/CONVECTION"

Figure 139 is a typical plot of parametric data for the dehumidification process which has been compiled from a procedure similar to that illustrated by figure 138. The dependent variable is the mass velocity of moist air through the unit and the water removal rate is specified for flow area in the channel for a range of channel heights. This type of data is easily obtained from the computer model.

In that the diffusion process can be considered gravity independent, it can be assumed at this point that the data could be used for both 1g and low-g design. The model has utility in the design of any life support process where the convective diffusion mechanism exists.

There are many areas where information from the analytical model described herein can be related to specific design parameters. The tabulation presented in the section titled "APPLICATION TO LSS DESIGNS" (for diffusion convection) indicates the machine processes for each LSS function where such considerations could logically appear. For example, figure 139 could well be one of several applicable to interests other than that illustrated, namely, the channel height (h). These could well be any of the several parameters handled directly or indirectly by the computer program; for example, plate temperature, inlet-outlet concentration, and stream inlet temperature. Such considerations form the major inputs to the design analysis of the typical aerospace condensing/humidifying porous plate heat exchanger.

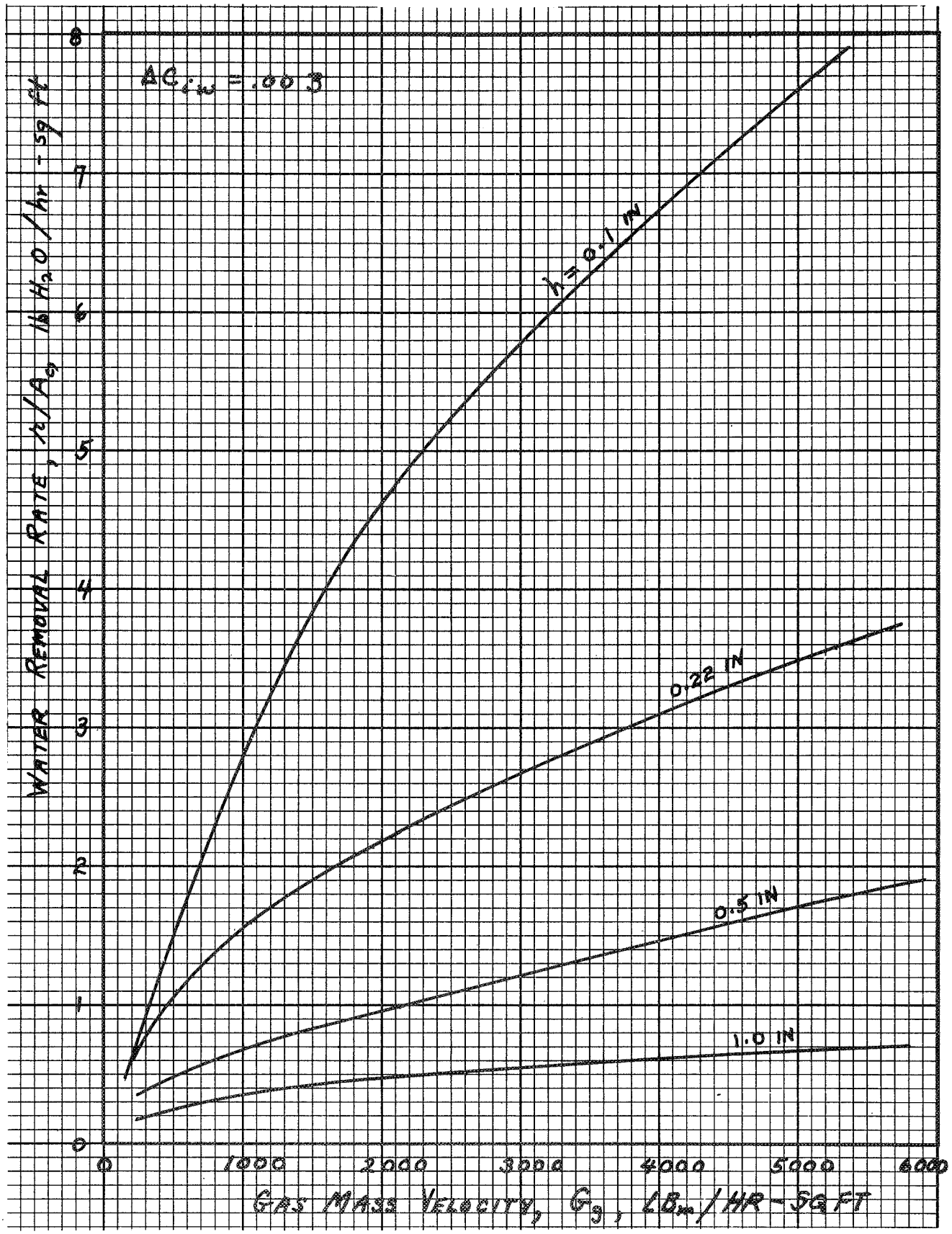


Figure 139. — Parametric Design Data for Dehumidification Process

ANALYTICAL MODEL NO. 3 — "FILM STABILITY AND TRANSPORT"

Figure 140 is a typical plot of potential value in the design of systems transporting liquid films. In this instance, the designer may choose to specify the film thickness which is expected within his hardware configuration, and he may ask the question, is the mass flow rate resulting in this interface velocity stable for the range of g-levels to be experienced? Program RECRIT was used to develop this parametric data plot. The plot is dependent on fluid properties and g-level. This model has potential for any application of film flow on a surface, be it condensing, evaporating, or adiabatic.

There are many areas where information from the analytical model described herein can be related to specific design parameters. The tabulation presented in the section headed "APPLICATION TO LSS DESIGNS" (for film stability and transport) indicates the machine processes for each LSS function where such considerations could logically appear. For example figure 140 could well be one of several applicable variables other than that illustrated. Other parameters treated in the model are fluid surface tension. With interface velocity defined, program SHEAR results can be used to determine characteristics of the gas phase flow. These are important considerations in any life support system where film drag by a second phase is a design objective.

ANALYTICAL MODEL NO. 4 — "INERTIAL SEPARATION"

Much of the predictive data from which the laboratory experiments (at 1g) relating to the screen separator were designed are directly applicable to equipment design solutions. There are, however, several cases where the data are not in an easily interpreted format for design use. One representative example is the information relative to penetration due to droplet impact where the data presentation was explicitly related to test design and only inferentially related to equipment design.

Figure 86 has shown droplet drop height, h, and a screen inclination angle, γ, neither of which are germane to an operating system and thus not likely to be recognizable by the designer as relevant to his decisions. The predictive equation used to correlate the data, however, was derived from the appropriate design equation listed below.

$$Fr \sin(\theta_1) \frac{nd^2}{\lambda^2} + F_c \leq F_{st}$$

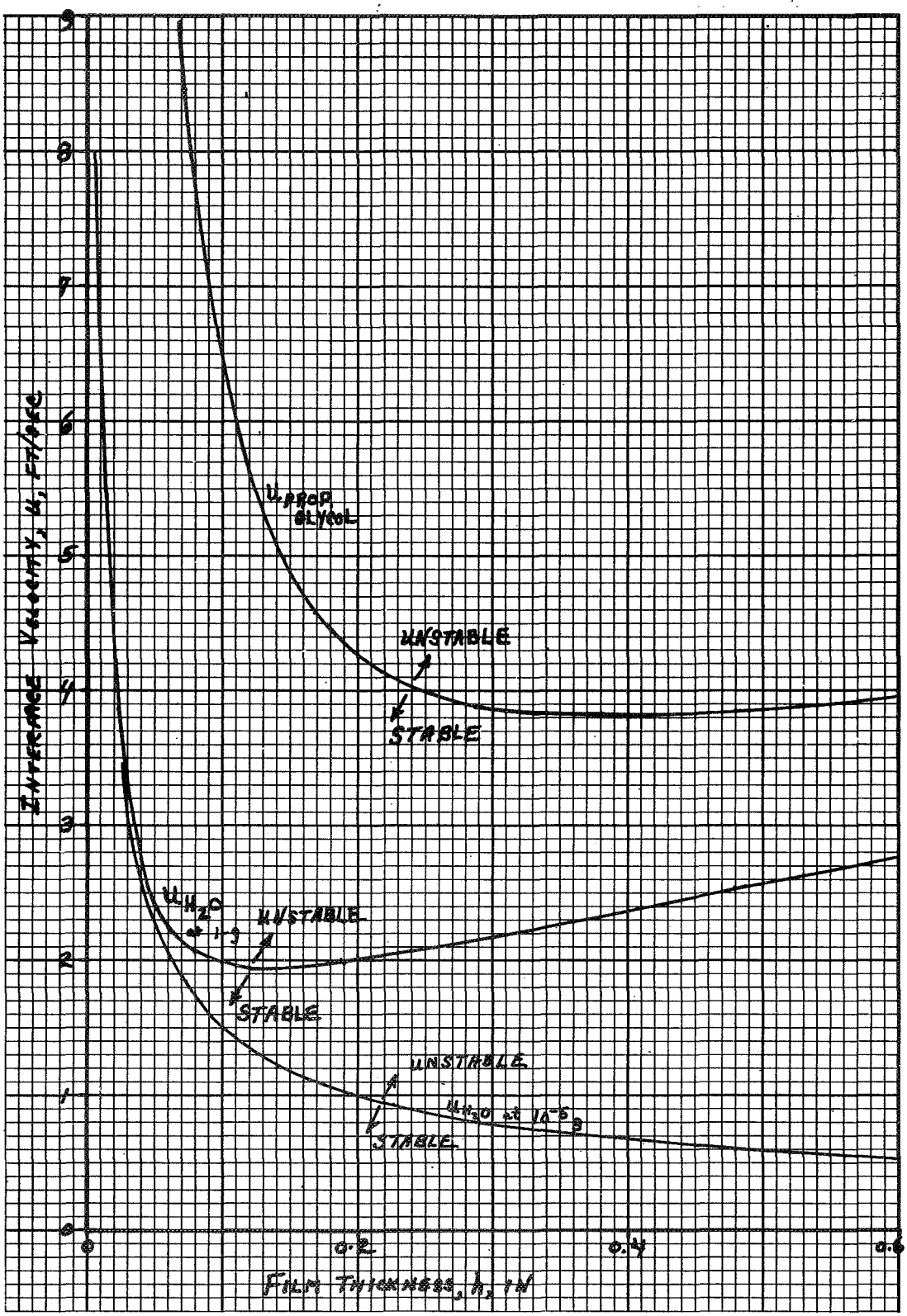


Figure 140. — Predesign Representation for Gravity Field Effect on Interface Velocity

For cases such as the test described where gravity forces are dominated by the impact inertia of the droplet, the design parametric curve will be as shown in figure 141. Thus by knowing the droplet velocity and assuming a droplet impact angle, a screen material can be chosen which will avoid penetration.

Additionally, certain design recommendations can be formulated now:

a. Choose the screen with the smallest pore size attainable, consistent with allowable duct pressure drop.

b. Incline the screen to the air flow and droplet impact vector with the shallowest angle possible.

c. Coat the screen with a good nonwetting substance (such as Teflon) in such a way so that the coating is uniform and complete and no screen pores are blocked.

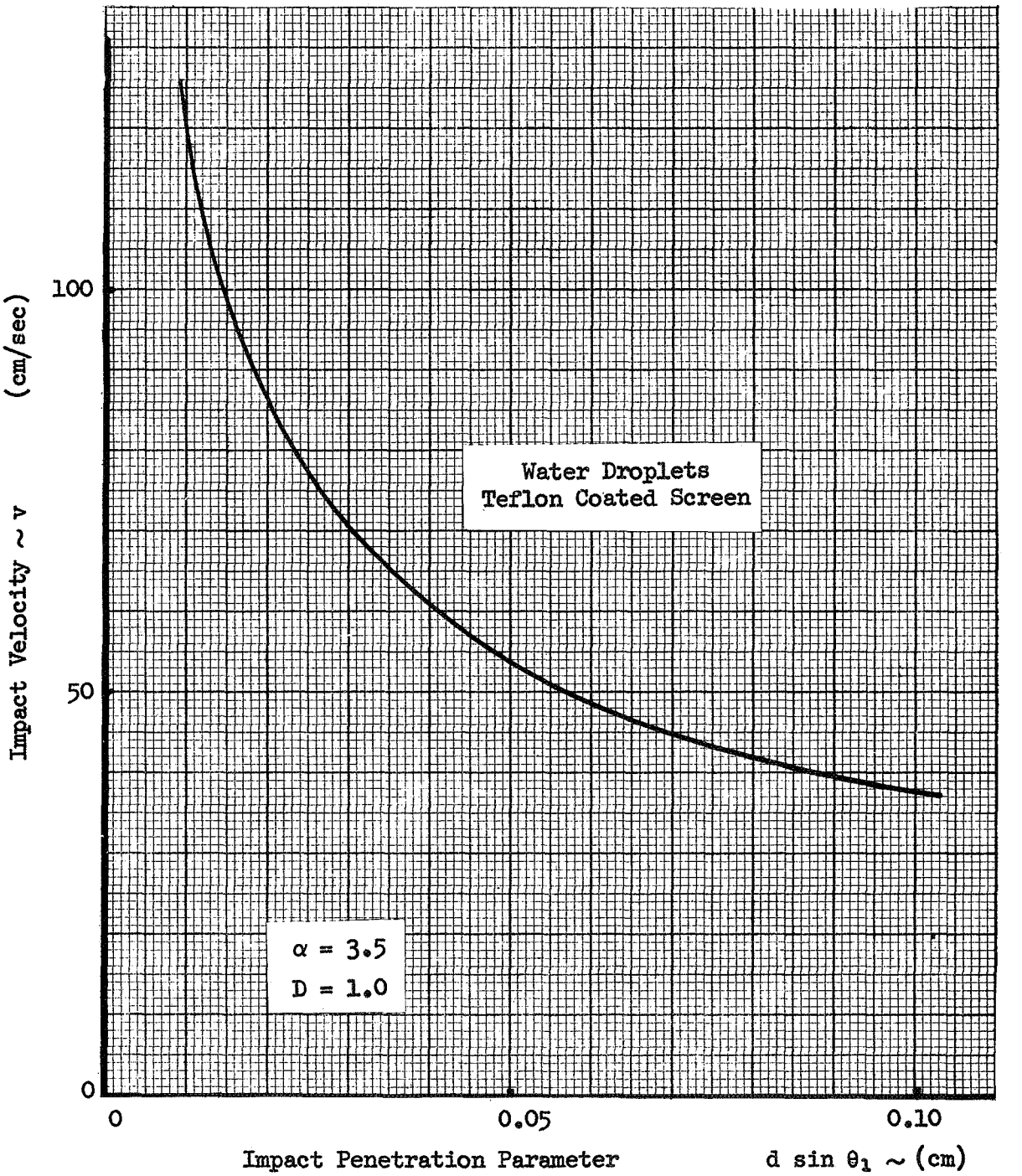
ANALYTICAL MODEL NO. 5 — "CONVECTION HEAT TRANSPORT"

Figure 142 is a typical plot of parametric data for the convective heat transport process. Here the designer may be operating at a set point, A, in the normal gravity environment. The convective heat transfer is unstable but laminar. If the g-level is reduced to one tenth the previous value, this set point changes to B by virtue of the linear dependence of $R\ell$ on g. Point B now is stable with a concomitant reduction in the heat transfer coefficient. Processes requiring certain heat transfer rates will alter those rates, depending on the g-level, by shifting to various regions of convective-mechanism interactions. It can also be seen that increasing the flow (to point C) will have a similar effect on the stability of the convection.

ANALYTICAL MODEL NO. 6 — "FLOW REGIME CHARACTERISTICS"

Previous examples have indicated typical approachs in the utilization of the analytical models in the solution of design problems. Due to the embryonic state of the proposed analytical model, it is difficult to provide a specific example of its application in numerical form. However, a sample design problem illustrates the methodology involved in the application of the analytical development.

Consider the problem area of liquid/gas separation by screen separators. To facilitate the separation process, it is necessary to establish the characteristic dimension (size) of each phase and its spatial distribution (location in the conduit or tube cross



Equation - $(F_v \sin \theta_1) \frac{nd^2}{\lambda^2} + F_c \leq F_{st}$

Figure 141. — Effects of Droplet Velocity on Penetration

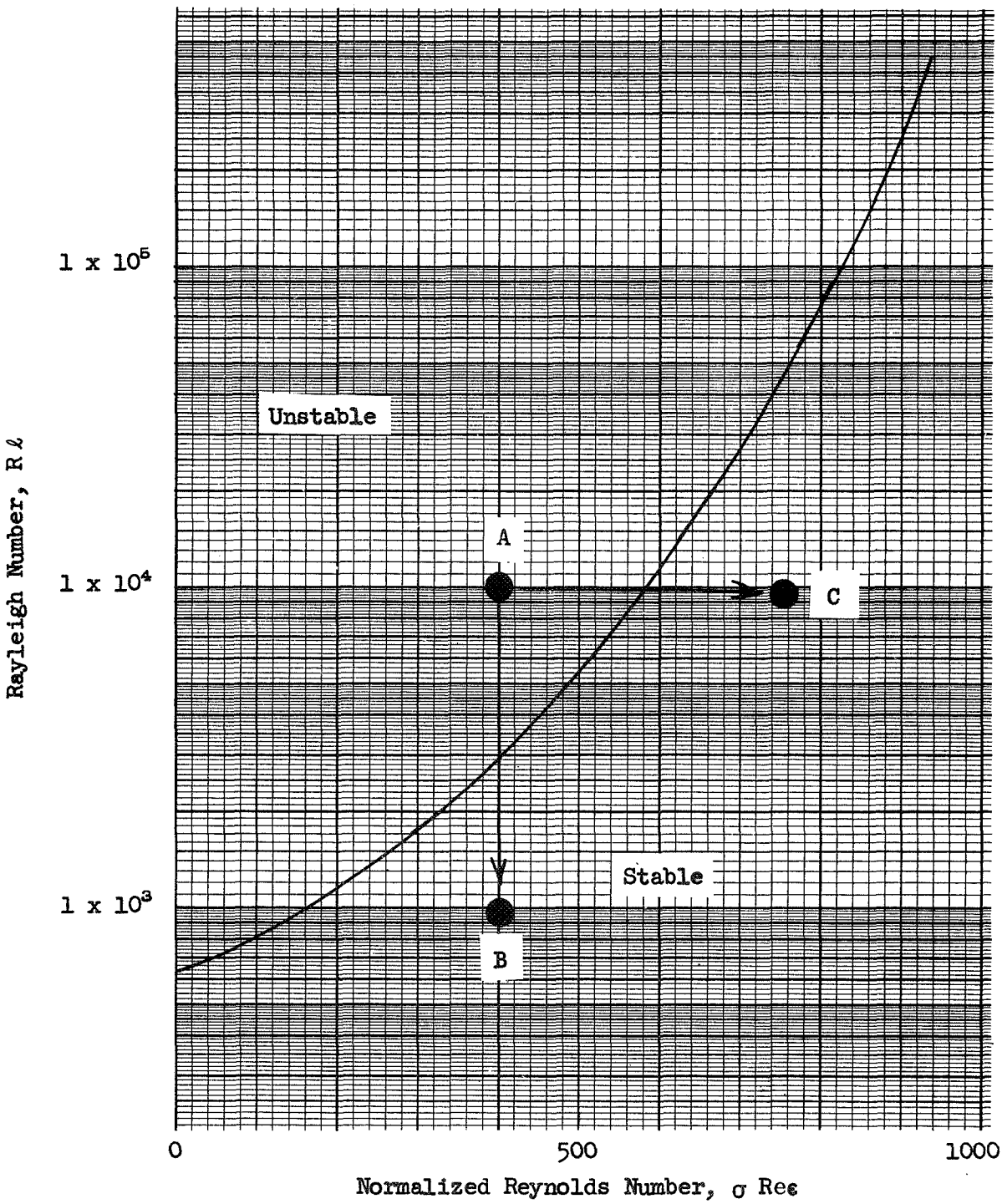


Figure 142. — Typical Design Parametric

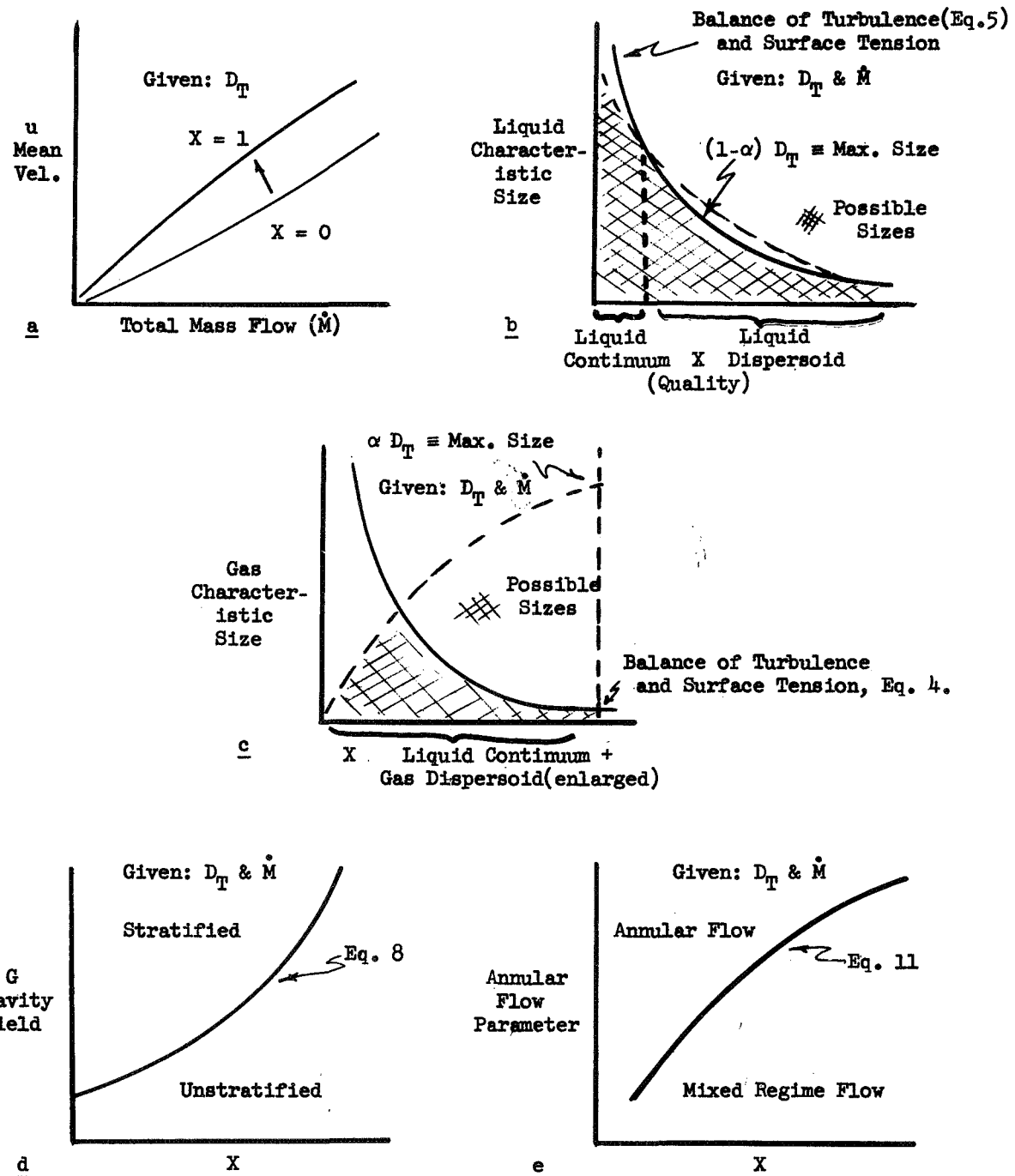


Figure 143. — Example Design Parametrics

section) which will dictate the screen mesh and orientation. In general, the designer knows the following a priori information:

a. Total mass flow range ($\dot{M}$).

b. Percent of gas, liquid or some type of quality range (X).

c. The inertial acceleration or gravity range (g).

Items a and b are represented by figure 143a for a fixed tube diameter.

Liquid, gas continuum, dispersoid relations are represented by figures 143b and 143c which result from the turbulent shear-surface tension balance, equations (4) and (5) in the section that discusses analytical model 6. Using equations (8) and (11), the spatial distribution is established based on the two figures 143d and 143e for stratified, annular, mixed-flow balances.

A set of conditions on characteristic sizes and distribution can be generated for varying tube diameters which change the velocity conditions. From this, the optimum diameter and screen characteristics can be determined using the results from analytical model 4.

REQUIREMENTS BEYOND THE SCOPE OF THE NAS1-8494 MOD 1 CONTRACT

The primary objective of the Mod 1 version of the NAS1-8494 contract was the initiation of the development and experimental evaluation of a set of analytical models which, when fully developed, will be of value to the designer of life support systems. With the conclusion of the Mod 1 tasks, the analytical models have been formulated and the first phase of their experimental evaluation and subsequent correction has been completed. It is necessary at this point to define the tasks which must be undertaken to meet the requirements for completing the evaluation and maturation of the models.

GENERAL REQUIREMENTS

It has become clear during the course of the program, especially in light of the experimental evidence, that requirements for evaluation and maturation of the models include both analytical and experimental tasks. Further, the evidence shows that in most cases the continuing requirements call for investigations which are direct extensions and refinements of the type of work already performed.

In general, the requirements are based on the necessity of 1) evaluating the accuracy of the predictive aspects of the analytical models under low-g, and 2) augmenting the development of the models where uncertainties and/or uncompleted areas exist. A prime example of the former can be seen with Analytical Model No. 1 – "Nucleate Boiling," where the model has been rather fully developed both with respect to total coverage and to detail, while the most obvious example of the latter is seen with Analytical Model No. 6 — "Flow Regime Characteristics." Model 6 has initiated the development of a method for describing the dynamic aspects of the two-phase process and thus has opened the way for the development of a more useful design tool. However, the continued development of the model is totally dependent upon the analysis of experimental data obtained under low gravity. Once this has been accomplished, the 1g and zero-g data can be compared to provide the basis for the continued analytical development.

For the most part, the other models require work at some combination of the two areas of interest within the range of the extremes required by Models 1 and 6.

Certain additional areas of investigation should be included in the on-going tasks which are over and above those introduced during the Mod 1 phase of the contract. These "new" areas of investigation exist as a result of several factors including 1) arbitrary limitations in the Mod 1 tasks, 2) increased understanding of the problem and/or phenomenological behavior under study, and 3) the unique characteristics of the low-g environment. The inclusion of these new areas will influence the scope and

significance of both the experimental and analytical work. These new areas are highlighted in the following paragraphs.

NEW AREAS FOR INVESTIGATION

ANALYTICAL MODEL NO. 1 — "NUCLEATE BOILING"

Experimental

The major new area of interest which should be included in the low-gravity experiments involves the effects of temperature fields on bubble motion. Observations of the phenoma were made in the laboratory tests, but specific measurements data were not considered as practicable due to the overwhelming influence of the buoyancy effects.

Where these effects are not dominant, the temperature field effects should prove to be significant and a major source of interest, particularly in view of its potential as a mechanism for control of the two-phase distribution.

Analytical

An additional analytical task might well involve the integration of the program EVOLVE with others relating to such facets of the overall phenomenological system as the characteristics of the formation and release of bubbles at the nucleation site.

ANALYTICAL MODEL NO. 2 — "DIFFUSION CONVECTION"

Experimental

The mechanisms of the dehumidification/humidification process are exceptions in the total group of processes under investigation for they are not considered to be "gravity sensitive." On the other hand, the liquid-transfer systems which interface with the dehumidification/humidification process are potentially at least affected by variations in the acceleration field. From this point of view, it is logical, although not mandatory, that experiments involving the interface be included in the low-g work. The most relevant approach would combine the interests of this experiment with those of other experiments in the series, particularly Models 3b, 4, and possibly 5.

Analytical

The "supra-efficiency anomaly" will require full resolution prior to designing flight experiments if such are to be undertaken. The resolution will undoubtedly require both analytical and experimental investigation, but the initial tasks must be oriented to an analysis of the experiment design and the theoretical aspects of the problem.

ANALYTICAL MODEL NO. 3 — "FILM STABILITY AND TRANSPORT"

Experimental

The major area for investigation which was not included in the Mod 1 tasks involves the conical surface system identified as Model 3b. The experiment should include at least two cone angles and be operated both with and without a condensation feed system. It is quite possible that, following the low-g experiments, specific laboratory experiments could be of value in augmenting the low-g data. As with the experiments against Model 1, the effects of temperature gradients on transport are an added area for investigation.

Analytical

Perhaps the major area for further analytical investigation is the development of a more appropriate criterion for stability determinations. The R criterion, the ratio of downstream wave height (h_2) to upstream wave height (h_1) where $h_2/h_1 > 1.2$ = unstable, was found difficult if not impracticable, to apply at least for the highly viscous liquid (glycol)/air system.

An initial estimate is that a wave frequency parameter rather than wave height might be more descriptive of the real world process and likewise more accurately applied.

ANALYTICAL MODEL NO. 4 — "INERTIAL SEPARATION"

Experimental

As with Model 3, the most obvious area for examination under low gravity is that of the conical or vortex separation system, identified as Model 4b. Although evaluation of the analytical model describing vortex separation could have profited, at least marginally, from the laboratory experiments, it is the low-g environment which offers

the major potential. This experiment should include several cone angles as well as variations on the inlet conditions. The major interest of the experiment would be in obtaining at least inferential data relative to the nature and influence of the boundary layer on the mass flow rate of the system.

There are essentially no new areas of interest to be introduced into the experiments required for the evaluation of Model 4a. Rather, as with most of the experiments, the changes will be associated with test design improvements suggested by the laboratory experiments.

Analytical

There is some evidence that, as more is learned of the basic mechanisms involved in the capture and transport of liquid droplets away from a ducted air stream, the development of an analytical model presenting the process as a continuous and interdependent series of events may be potentially feasible and of value to the design task.

ANALYTICAL MODEL NO. 5 — "CONVECTION HEAT TRANSPORT"

Experimental

Few if any new areas for experimental investigation are anticipated at this point unless possibly application of the experiments to other fluids than air. However, it is clear that additional data in the low flow/low ΔT areas are most desirable, especially if accompanied by interferometer "photography."

Analytical

One of the primary areas to be investigated is the integration of selected elements of the diffusion convection model with those of the convection heat transport model. In effect, this would represent the next step in orienting the basic analytical work to the design task.

ANALYTICAL MODEL NO. 6 — "FLOW REGIME CHARACTERISTICS"

Experimental

Along with the refinements suggested by the information made available through the laboratory experiments, the practicality and information yield from including the examination of a liquid/liquid and/or plastic/liquid system should be considered. The priority

of such a requirement has not been established at this point but should be prior to fixing the flight experiment design.

Analytical

The remaining analytical requirements against this model are extensive as previously stated. Such will involve expanding and translating the preliminary set of parametric topologies into a unified analytical system which will clearly describe the dynamic characteristics of two-phase flow.

DEFINITION OF A PROGRAM TO COMPLETE THE DEVELOPMENT OF THE ANALYTICAL MODELS

The Mod 1 contract work statement required that the program to complete the development of the analytical models be outlined with sufficient detail to facilitate decisions concerning subsequent courses of action. The principal tasks in the remaining program are those dealing with:

a. Program planning.

b. Apparatus and experiment design.

c. Apparatus development tests.

d. Equipment fabrication and checkout.

e. Flight qualification tests.

f. Flight and simulated flight experiments.

g. Data acquisition.

h. Analytical model update.

Experiments will be performed through a limited number of laboratory tests, a significant number of ground-based reduced-gravity tests principally through KC-135 flights, and a final set through orbital space vehicle flights.

INTERACTIONS WITH OTHER NASA PROGRAMS

In the course of the execution of the Mod 1 objectives, inputs have been made to and received from other NASA programs. These programs are primarily involved in producing definitions of experiments for applications in various manned orbital space vehicles for R&D. Major areas of interaction were:

a. Definition of NAS1-8494 experiments and preliminary concepts of integrated experiment package designs supplied to McDonnell Douglas for integration with the requirements for the NASA-LRC biotechnology laboratory, NAS1-9248 (ref. 6).

b. Preliminary definitions of the types of experiments which could profit from the capabilities of a space station internal centrifuge provided to the study team for NAS1-7309 and NAS1-8751.

c. Definition of selected nonintegrated experiments package design concepts supplied to Convair for integration with the requirements for the NASA-MSFC experiment module, NAS8-25051 (ref. 7).

d. Review of Apollo Block II systems to determine potentials for obtaining data relevant to the evaluation of the six analytical models.

e. Review of NASA-MSFC propellant transfer experiment being proposed for the orbital workshop and inputs relevant to the design alterations and data of interest to the NAS1-8494 objectives.

Efficient exploitation of the potentials provided by the several NASA programs which relate to requirements for space experiments in the areas of interest for NAS1-8494 strongly suggests continuing efforts to assure that the various study and planning activities are fully integrated.

EXPERIMENTAL PROGRAM SUMMARY

LABORATORY TESTS

The laboratory tests will be primarily those associated with reducing uncertainties relating to design alternatives and to certain phenomenological behavior as a part of the development of the various flight experiment packages. Although it became apparent that additional refinements of the Mod 1 tests would yield meaningful and desirable data, the requirement to conduct tests at reduced gravity very significantly reduces the potential of such data. Additionally, obtaining such data would do little to reduce the dependency on and complexity of the reduced-gravity experiments. It is considered that a more effective definition of additional laboratory requirements can be made following evaluation of the reduced-gravity experiments.

One exception to this might be the experimental investigation of Model 4b, vortex inertial separation. Original plans did not call for laboratory experiments against this model due to the complexity of the experiment and the low probability of obtaining a significant yield under normal gravitational conditions. The secondary objective of the experiments, that of providing information concerning the design of low-gravity experiments, was not considered sufficiently important to include it in the schedule. At the conclusion of the other experiments, it has become clear that their yield in this area may well have been underestimated. Thus, it may be well to schedule a brief but formalized laboratory experiment as a prelude to the design of the apparatus and procedures for the low-gravity experiments against Model 4b.

In a contrary vein, a laboratory experiment was initially scheduled against Model 3b, film transport on conical surfaces. However, the experiment was eliminated from the schedule following further analysis of the test design in view of the data being produced by its companion experiment, Model 3a - flat surfaces. Confidence at this time, relative to the correctness of this decision, is greater than that for not including the Model 4b experiment in the Mod 1 test program.

GROUND-BASED REDUCED-GRAVITY EXPERIMENTS

The facilities referred to in this category include drop towers, balloons, drops, KC-135 low-g trajectory flights, rocket flights, and to a lesser degree unmanned orbital space vehicles. Characterization of these facilities is summarized by table 53. All of these facilities can be shown to hold potentials in the evaluation of the analytical models. However, when the exploratory, i.e., nondeterministic, nature of the experiments is considered along with the relatively long duration of the observations involved, it becomes apparent that 1) in-progress observation and analysis must be available, 2) equipments and procedures must be sufficiently flexible to permit in-progress alterations based on the on-going analysis, and 3) sufficient dwell-time at the low-g level must be available to permit adjustment of variables and/or process stabilization.

As demonstrated by the Mod 1 laboratory experiments, the stabilization following an alteration of a major variable can run from a minimum of 5 to 10 seconds for thin film stabilization for certain limiting configurations of Model 3 to a high of 10 to 20 minutes for certain observations included in Model 5.

In establishing priorities with respect to the low-g facilities, it must be remembered that for the most part the NAS1-8494 objects relate to rather complex systems of phenomena rather than single phenomenon or a phenomenological system of minimal complexity, as has traditionally been the case with experiments typically scheduled for these facilities.

Tower and Balloon Drops

Although tower and tethered balloon drops are relatively attractive from an economic standpoint and inherently allow for repeated drop cycles although at a fairly low frequency, the limitations relative to package size, instrument complexity, and dwell-time all but eliminate them as strong candidates for exploitation.

Table 53. — Ground-Based Reduced-Gravity Test Facilities*

Facility Type	sec	g	lb**	Comment
Laboratory Drop	1/2	10^{-3}	20	Should be considered for exploratory investigations.
Laboratory Pop-up	1-1/2	10^{-3}	20	Launching acceleration may disturb the experiment.
Tower Drop	2	10^{-3}	200	Streamlined capsule can handle compact experiments.
Tower Drop	2	10^{-6}	100	"Box-in-Box" system provides low residual g.
Ground Facility Drop	4	10^{-7}	300	Driven outer box provides low residual g.
Ground Facility Pop-up	10	10^{-7}	300	Launching acceleration may disturb the experiment.
Sky Drop — Helicopter	6	10^{-4}	100	Pre-release acceleration effect may persist during trajectory.
Sky Drop — Tether Balloon	3	10^{-5}	100	Developmental.
Sky Drop — Free Balloon	20	10^{-3}	200	Developmental.
Aircraft (Tethered Capsule)	32	10^{-2}	1000	Random acceleration continues during trajectory.
Aircraft (Free Capsule)	10	10^{-5}	100	Pre-release acceleration effects may persist during trajectory approximately 10% yield.
Ballistic Vehicle	60	10^{-6}	20	"Small" rocket propulsion required.
Ballistic Vehicle	600	10^{-7}	300	ICBM class vehicle required for boost.
Ballistic Vehicle	6000+	10^{-8}	20	Orbital booster required.

*Adapted from reference 1, page 74.

**Approximate allowable weight of test specimen.

Rockets

Rocket flights are available which can accommodate essentially any package size and instrument complexity which might be required. The dwell-time at low-g could undoubtedly handle at least 75 percent of the process stability requirements of the six experiment groupings. However, the cost of experiment recovery and rescheduling a sufficient number of flights to assure success in the experimental process would be excessive. The rocket trajectory is far better suited for a specific inquiry into a specific aspect of a process rather than observations depending on a series of conditionally adjusted events in a "nondeterminable" series.

Unmanned Satellites

The unmanned satellite overcomes many of the disadvantages of the rocket trajectory, including provisions for in-progress adjustment and/or alteration of the experiment. However, the complexity of such a system to accommodate more than a fraction of the experimental requirements of the NAS1-8494 contract presents an essentially prohibitive task, both from the point of cost, schedule, and technological state-of-the art, particularly the latter.

KC-135 Flights

The KC-135 provides a very significant potential in two areas of the remaining program to complete the evaluation of the analytical models; namely, 1) the primary objective, that of procurement of experimental data for direct evaluation of the models, and 2) the evaluation and/or flight qualification of experiment packages scheduled for manned space flight vehicle installation. In addition, it is considered, in light of the experimental evidence to date, that at least the screen separation portion of Model 4 (4a) could be completely and perhaps ideally satisfied by the aircraft low-g trajectory. The reason for this is centered in the fact that the process being observed is inherently discontinuous with the initiation of each observed event fully controllable and the time span for each event very low, being in the range of <0.1 to 0.5 second. In addition, observations are not critically dependent on extremely low-g levels, as might be the case for some experiment designs. The experimental examination of this process, like all others in this series, is investigative, therefore subject to continual in-progress alteration. These characteristics are precisely those best satisfied by the aircraft facility. Additionally, the g-profile of the trajectory provides a variation in g-level which can be viewed as being somewhat analogous to the potentials of the space station internal centrifuge and which can be significant for a majority of the experiments.

It is reasonable to assume that each experiment package destined for application in manned space vehicles is a candidate for evaluation and/or flight qualification in the aircraft facility.

MANNED ORBITAL-FLIGHT EXPERIMENTS

With the possible exception of the diffusion convection elements of Model 2 and Model 3a in its entirety, the major elements of each experiment are candidates for inclusion in the manned orbital-space-flight experiment programs. As discussed in some detail in the previous sections specifically dealing with each individual analytical model, the capability to observe the behavior of the system under various levels of reduced gravity should be exploited where available. As briefly noted, the KC-135 trajectory may provide an initial view for certain high-response processes. However, the internal centrifuge mounted in a space station complex or an equivalent platform is required to provide steady-state operation at any desired point in a wide range of low-g levels (ref. 8).

FLIGHT-EXPERIMENT-PACKAGE DESIGN CONCEPTS

Although it is not possible within the scope of the Mod 1 study to specifically define the flight-experiment packages which should be considered for development, sufficient information is available to produce a set of design concepts which define the population from which the eventual designs will most logically emerge.

It is reasonable to assume that various configurations of each of two basic types of packages provide the greatest probability of correctly characterizing this population.

Characterization of Package

The two basic types of packages can be characterized as follows:

Type 1 — Integrated Experiment Package

a. Primary application — manned orbital spacecraft.

b. Expected configurations — prototype, flight, qualified.

c. Developmental test facilities potentially involved — laboratory, KC-135.

d. Degree of integration (portion of total model coverage per package) — 30 to 70%

Type 2 — Nonintegrated Experiment Package

a. Primary application — workshop, KC-135.

b. Expected configurations — experimental, prototype, flight qualified.

c. Development test facilities potentially involved — laboratory, KC-135, limited drop facilities.

d. Degree of integration (total/package) — 20%.

Preliminary Design Concepts for Type 1 Experiment Packages

Figure 144 illustrates an approach to the integration of all required functions into two experiment packages. The design and installation concepts are illustrated by figures 145 and 146. Power requirements for each of the two packages should be no more than 600 watts (peak) and 250 watts (time averaged) divided between fan, heater, and instrument (continuously regulated ac-dc power). Heat transport, cabin vent, and space vent interconnects would be required. Both photographic and numerical data would be produced with the latter requiring ground and/or on-board processing of 10 to 20 parameters per experiment mode with data channel sampling of at least 5 channels per scan at a rate of 2 to 0.03 scans/sec. Data are combinations of digital and analog.

General Instrumentation Requirements

The instrument requirements common to both Type 1 packages include:

a. Two-phase interaction dynamics — high-speed movie camera and/or TV monitor.

b. Air flow measurement and indicators — hot-wire anemometer, mass flow meter.

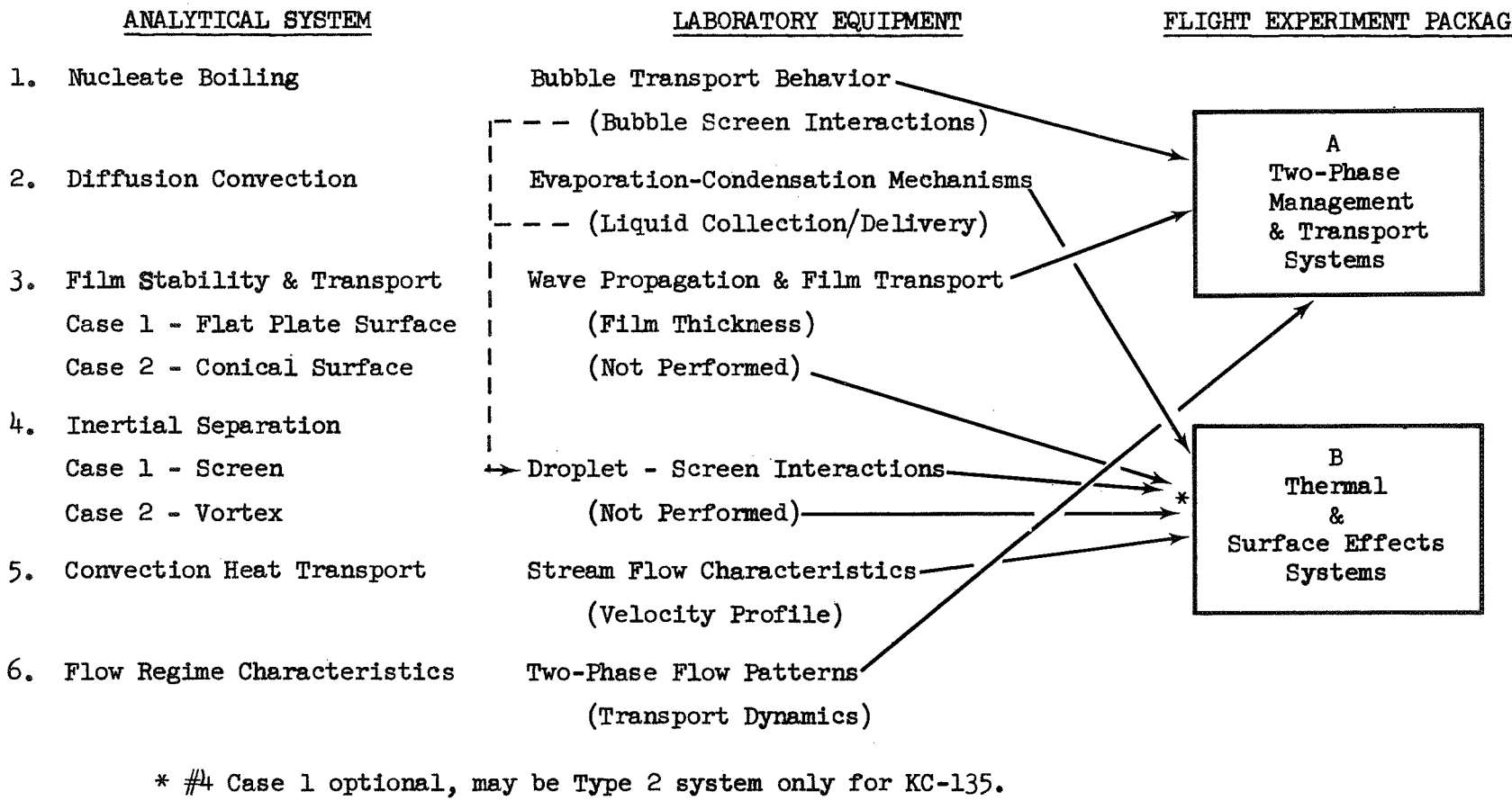
c. Liquid flow measurement and indicators — turbine meter.

d. Temperature measurement and indicator — mechanical/electrical transducer.

e. Signal conditioning and amplification — thermocouples, thermistors.

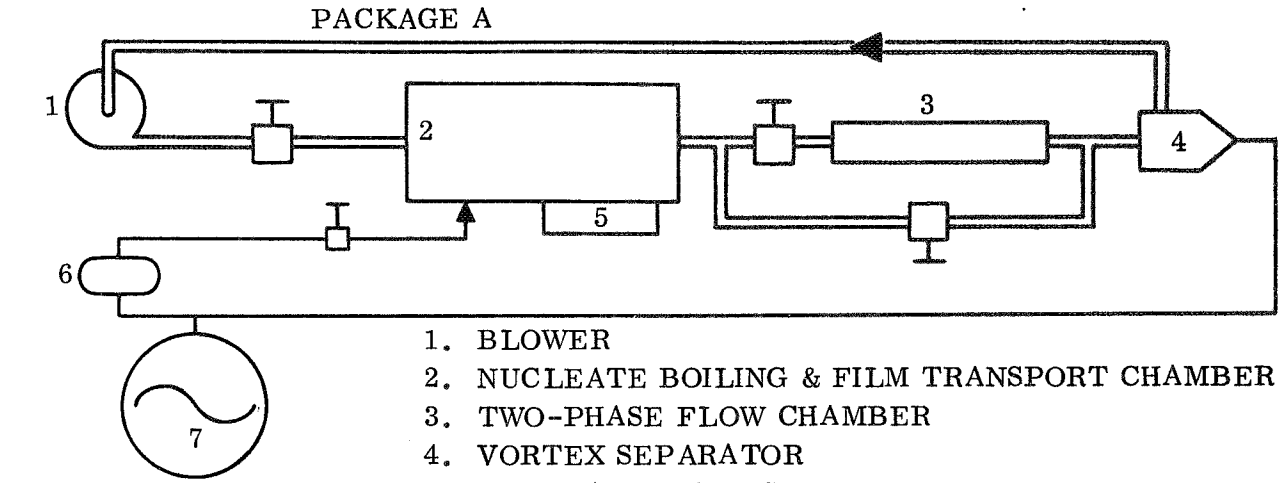
Package A. — Two-phase interactions and mass ratios — photocell and signal processor.

Package B. — Temperature profile dynamics — interferometer; and for the humidity concentration field — piezoelectric sorption or photocell.

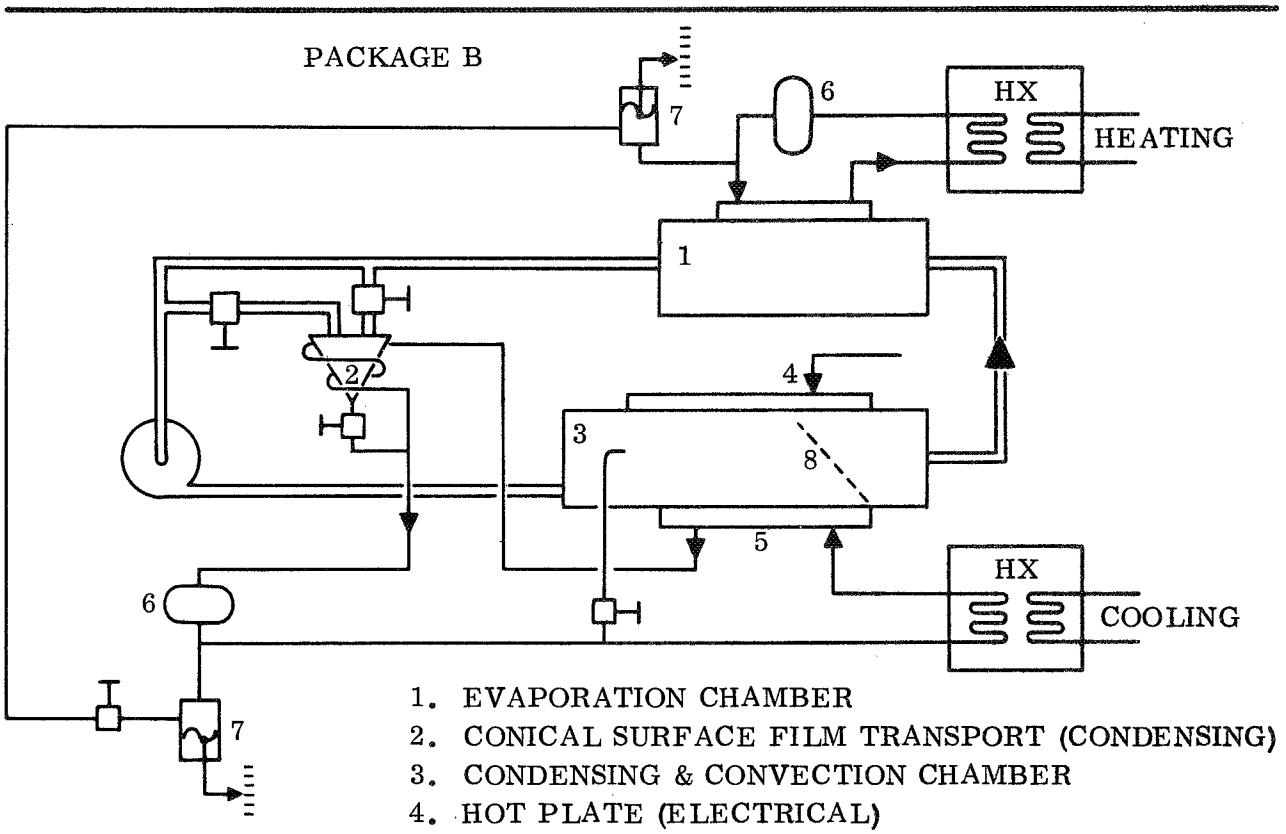


* #4 Case 1 optional, may be Type 2 system only for KC-135.

Figure 144. — Integration Concepts Relative to Flight Experiment Package Type 1 Designs



1. BLOWER
2. NUCLEATE BOILING & FILM TRANSPORT CHAMBER
3. TWO-PHASE FLOW CHAMBER
4. VORTEX SEPARATOR
5. NUCLEATION SITES
6. WATER PUMP
7. RESERVOIR



1. EVAPORATION CHAMBER
2. CONICAL SURFACE FILM TRANSPORT (CONDENSING)
3. CONDENSING & CONVECTION CHAMBER
4. HOT PLATE (ELECTRICAL)
5. COLD PLATE (POROUS)
6. WATER PUMP
7. RESERVOIRS
8. ADJUSTABLE HYDROPHOBIC SCREEN (OPTIONAL)

Figure 145. — Design Concepts for Type 1 Flight Packages



Figure 146. — Swing-out Module Installation Package

Installation Concepts

The swing-out module (ref. 9), shown in figure 146, provides both the access and manipulative flexibility required by the investigative nature of the experiment. In addition, it permits the extremely high-density packaging required to attain the highly integrated design in the space constrained environment. The installation weight of the packages should be in the range of 200 to 350 pounds for an envelope of 2.5 by 3 by 6 feet.

PROGRAM TASK SUMMARY

Figure 147 suggests a schedule appropriate to the execution of the continuing program.

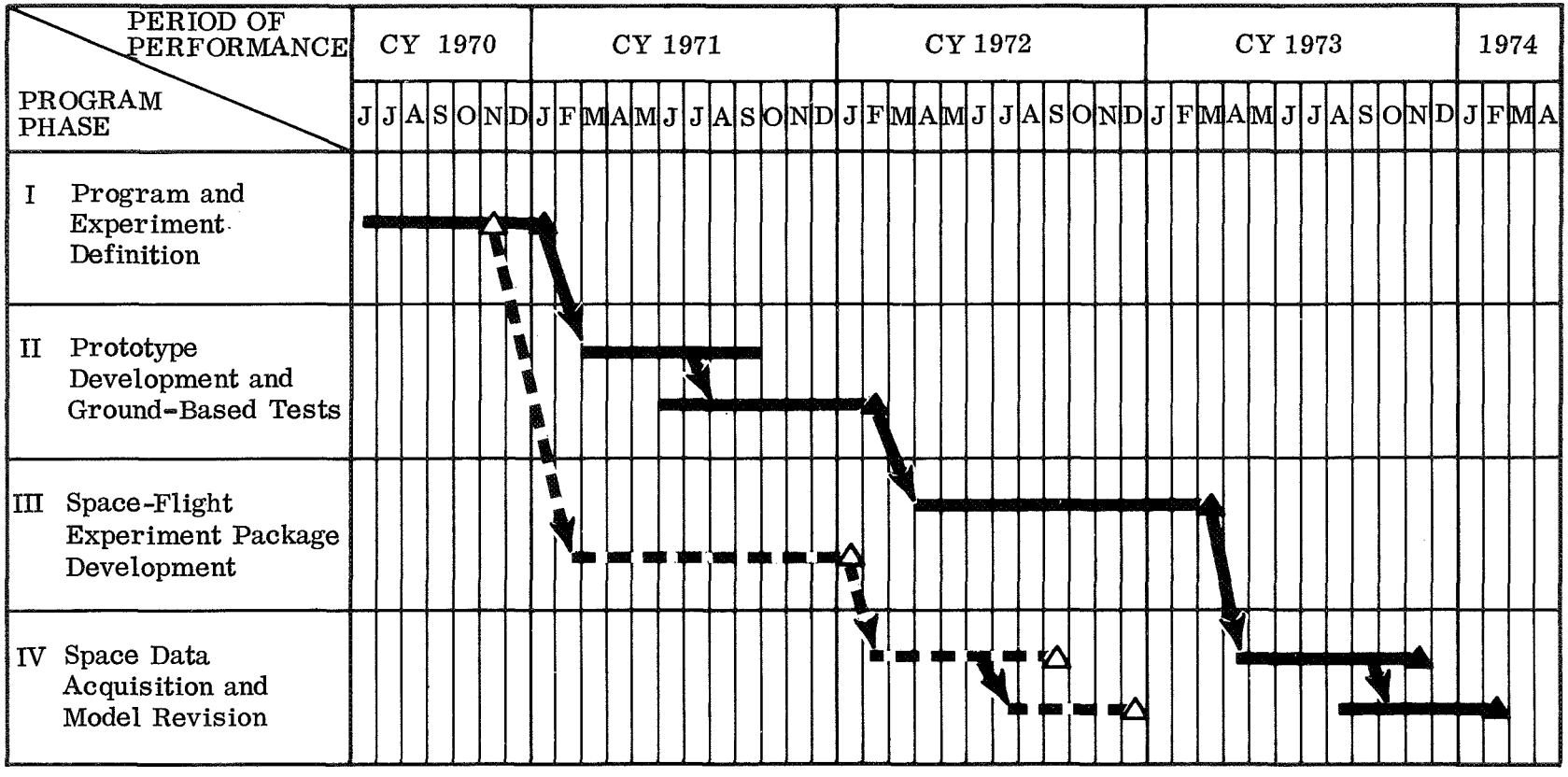
PROGRAM AND EXPERIMENT DEFINITION — PHASE I

A program planning and experiment definition phase is required to reevaluate and detail the recommendations being made by the Mod 1 contract. A degree of detail and specificity is required sufficient to permit timely decisions concerning immediate and definitive steps in the execution of the on-going program. The information should be so oriented that an optimum selection of alternatives can be made against a set of explicitly stated criteria which include such elements as NASA program cost, data yield potential, schedule feasibility, and data acquisition probability. Determination of the optimum course of action is a classic example of what has become to be known as "decision under uncertainty" and as such the determination should be made with the aid of an evaluation or decision model which fully and explicitly treats at least the major elements of such a decision process (ref. 10).

PROTOTYPE DEVELOPMENT AND GROUND-BASED TESTS — PHASE II

This phase of the program will develop and test prototypes of both Types 1 and 2 experiment packages for reduced-gravity applications. In addition, certain experimental models will be developed and experiments conducted as an aid to the design task. It is at this point that specific and detail integration of the equipment designs and schedules with those of the actual facilities to be employed is initiated and carried forward throughout the remainder of the program. Documentation of experiment procedures and flight-crew training programs also emerge during this phase of development.

LEGEND:
SPACE STATION EXPERIMENTS (PRIMARY R&D PATH)
WORK SHOP EXPERIMENTS (SECONDARY CONCURRENT PATH)



Note:

1. Schedule is compatible with mission schedules as indicated by references 11 and 12.
2. Workshop experiments do not replace space station experiments but could alter and possibly reduce the magnitude of the space station experiments.

Figure 147. — Program Schedule

The experiment packages prototypes will be evaluated in a combination of reduced and/or 1g facilities. For example, if a Type 2 design is contemplated for the inertial separation — Case 1 screen experiment and its ultimate reduced-gravity test facility is established as the KC-135, a prototype of this package would be developed and tested in the laboratory in preparation for final development and flight testing under Phase III. A Type 1 experiment package destined for ultimate application in a manned orbital spacecraft could be developed as a prototype with evaluation tests conducted both in the laboratory and under reduced gravity, including the KC-135 facility.

SPACEFLIGHT EXPERIMENT PACKAGE DEVELOPMENT — PHASE III

Tasks in this phase of the program would be centered in the translation of information produced in the previous phase, as a result of prototype development and evaluation testing, into flight-qualified operational hardware. If the prototype evaluation tests of the previous phase, particularly those involving the KC-135 facility, were not fully adequate for flight qualification of the operational models, the KC-135 might again be required, at least on a limited basis. At this point in the program, there should be but minimal uncertainty relative to both the expected performance of operational equipment and the data yield from the experiments to be subsequently performed aboard the orbital vehicle. In addition, it could be expected that the package layout and installation design were as close to optimum as feasibly attainable.

With proper attention to the design of both the experimental and evaluation tests for Phases II and III and the subsequent analysis of data, it can be expected that a significant advance in the maturity of the analytical models will have been attained prior to the space flight experiments.

It is in this phase that design and schedule integration becomes most critical, and flight-crew training is underway.

SPACE DATA ACQUISITION AND MODEL UPDATE — PHASE IV

Previous phases have defined the program, developed the experiment packages as an integrated function in a specifically scheduled space vehicle, and have initiated the working agreements relative to data acquisition from both prelaunch and postlaunch operations. Undoubtedly, the most effective method of obtaining these data is for an explicitly created interface of contractor data processing equipment and/or personnel with the NASA counterparts at the ground monitoring facility(s).

Data analysis and model updating will be a similar task to that of the Mod 1 contract.

It can be anticipated that problems will exist in carrying continuity of both analytical objectives and methods throughout the several phases of the contract. Special attention must be given to the importance of maintaining adequate continuity throughout.

GENERAL REFERENCES

These general references are those called out consecutively by number in the portions of this report entitled "INTRODUCTION," "SELECTION OF ANALYTICAL SYSTEMS," "DESIGN PARAMETERS," "REQUIREMENTS BEYOND THE SCOPE OF THE NAS1-8494 CONTRACT," and "DEFINITION OF A PROGRAM TO COMPLETE THE DEVELOPMENT OF THE ANALYTICAL MODELS."

1. Ballinger, J.C.; et al.: Study of Zero Gravity Capabilities of Life Support System Components and Processes. NASA-CR-66534, February 1968, GDC-DBD67-004, Convair division of General Dynamics.

2. Donlan, C. J.; et al.: The Needs and Requirements for a Manned Space Station. NASA, November 1966.

3. Anon.: Tradeoff Study and Conceptual Designs of Regenerative Advanced Integrated Life Support Systems. NASA-LRC, RFD-L-8360, September 1967, and Anon.: Trade-Off Study and Conceptual Designs of Regenerative Advanced Integrated Life Support Systems (AILSS). Final Report, NAS1-7905, HSD-UAC, July 1969.

4. Tong, L.S.: Boil Heat Transfer and Two-Phase Flow. John Wiley & Sons, Inc., New York, 1965.

5. Keshock, E.G.; Siegel, R.: Forces Acting on Bubbles in Nucleate Boiling Under Normal and Reduced-Gravity Condition. NASA-TN-D-2299, 1964.

6. Anon.: Requirements Study for a Biotechnology Laboratory for Manned Earth Orbiting Missions. NASA-LRC, McDonnell-Douglas, NAS1-9248, June 1970.

7. Anon.: Candidate Experiment Program for Manned Space Stations. MSFC-NHB. 7150.XX, September 1969.

8. Stumm, J.E.: The Orbital Research Centrifuge. NASA-CR-66830, GDC-DCL69-002, Convair division of General Dynamics, NAS1-8751, July 1969.

9. Burnett, J.R.: Development of the Swing-Out Module. GDC-ERR-AN-1118, Convair division of General Dynamics, October 1967.

10. Drake, G. L.; Burnett, J. R.: Selection of an Oxygen Regenerating System to Meet the Demands of a Multi-Mission Program. Society of Automative Engineers Tech. Paper 670849, October 1967.

11. Mueller, G.E.: An Integrated Space Program for the Next Generation. Astronautics and Aeronautics, January 1970, pp. 30-51.

12. Anon.: Program in Perspective — Manned Space Flight. Space/Aeronautics, January 1970, pp. 33-42.

APPENDIX A

GENERAL BIBLIOGRAPHY

The documents included in this category were selected from the NAS1-8494 Mod 1 literature search and are representative of the many reports influencing this study but not specifically referenced in the text.

Anon.: Evaluation and Application of Data from Low-Gravity Orbital Experiment. NAS8-21291, GDC-584-4-264 (Third Quarterly Progress Report), Convair division of General Dynamics, December 1968, pp. 2-10 through 2-50.

Booth, Franklin W.: A Liquid/Liquid Mixing Device for Zero Gravity Applications. LWP-657, NASA-LRC, 11 September 1968.

Booth, Franklin W.: A Porous Plant Air/Water Separator for the Integrated Life Support System Dehumidification Subsystem. LWP-630, NASA-LRC, 1 August 1968.

Boyd, 1/Lt. Cecil S. An Investigation of Boiling Water in a Porous Material as a Means of Separating Liquid and Vapor in Zero Gravity. Thesis, USAF Institute of Technology, AD 618022, 1965.

Bradshaw, R.D.; et al.: Evaluation and Application of Data from Low-Gravity Orbital Experiment. NAS8-21291, GDC-584-4-412 (Phase I Report), Convair division of General Dynamics, 1 November 1969.

Burnett, J.R.: Experimental Test Report — NAS1-8494, Test No. 1, Nucleate Boiling. Convair division of General Dynamics, 3 September 1969.

Clifton, J.V.; et al.: Motion of a Bubble in a Rotating Liquid. ERR-FW-699, Fort Worth Division of General Dynamics Corporation, 31 December 1967.

Cochran, Thomas H.; Aydelott, John C.: Effects of Fluid Properties and Gravity Level of Boiling in the Discrete Bubble Region. NASA TN D-4070, August 1967.

Cochran, Thomas H.; et al.: Experimental Investigation of Nucleate Boiling Bubble Dynamics in Normal and Zero Gravities. NASA TN D-4301, 1968.

Coe, C. S.; et al.: Analytical Methods for Space Vehicle Atmospheric Control Processes. Technical Report ASD-TR-61-162, Part II, November 1962.

APPENDIX A

Cohan, H.; Rogers, M. (editors): Fluid Mechanics and Heat Transfer Under Low Gravity. Proceedings of a Symposium held at Palo Alto, Calif., 24-25 June 1965, sponsored by USAF Office of Scientific Research and Lockheed Missiles & Space Company.

Elikan, Leonard (editor): Aerospace Life Support. Chemical Engineering Progress Symposium Series, no. 63, vol. 62, Published by American Institute of Chemical Engineers, 345 East 47 Street, New York City 10017, 1966.

Evans, R. G.; et al.: Pressure Wave Propagation in Adiabatic Two-Phase Flow. DSR 74629-2 Contract MOHV 3963 (15) MIT May 1968.

Fowkes, Frederick M. (Symp. Chairman): Contact Angle, Wettability, and Adhesion. The Kendall Award Symposium sponsored by the Division of Colloid and Surface Chemistry at the 144th Meeting of the American Chemical Society, Los Angeles, 2-3 April 1963, Advances in Chemistry Series 43, American Chemical Society, Washington, D.D., 1964.

Gouse, S. W., Jr.: An Introduction to Two-Phase Gas-Liquid Flow. 8734-3, MIT Engineering Projects Laboratory, June 1964.

Gronner, A. D.: Methods of Gaging Fluids Under Zero-G Conditions. AIAA Paper 65-365, AIAA Second Annual Meeting, San Francisco, 26-29 July 1965.

Howell, John R.; Siegel, Robert: Activation, Growth, and Detachment of Boiling Bubbles in Water from Artificial Nucleation Sites of Known Geometry and Size. NASA TN D-4101, 1967.

Ingebo, Robert D.: Drag Coefficients for Droplets and Solid Spheres in Clouds Accelerating in Airstreams. National Advisory Committee for Aeronautics, Technical Note 3672, Washington, September 1956.

Jagow, R. B.: Zero Gravity Evaluation of a Hydrophobic/Hydrophilic Water Separator. NASA CR-66828, July 1969.

Knapp, Karl K.: Zero-G Liquid Studies: Critical State and Liquid Drop Dynamics. EOS Report 7170, Electro-Optical Systems, Inc., 2 November 1967.

APPENDIX A

Kneisel, K. M.: The Marker-and-Cell Method (MAC), Thermodynamic Studies of Cryogenic Propellant Management. GDC-ERR-AN-1144, Convair division of General Dynamics, December 1967.

McCunney, S.; Burnett, J.: Liquid/Gas Separation Mechanisms. 64-26231, NAS1-2934, Convair division of General Dynamics, 13 September 1965.

McCunney, S. J.: Strode, C. D.: Zero-G Compatibility of Life Support Systems. GDC-ERR-AN-892, Convair division of General Dynamics, 1 April 1966.

Olcott, Thomas M.; Lamparter, Richard A.: Evaluation Testing of Zero Gravity Humidity Control System. NAS1-5622, Lockheed Missiles & Space Company, Sunnyvale, Calif., 25 October 1967.

Otto, E. W.: Static and Dynamic Behavior of the Liquid-Vapor Interface During Weightlessness. NASA TM X-52016, April 1964.

Perkins, Clay K.; Merino, Fred: Liquid Sensors for Zero Gravity. International Measurements Congress, Warsaw, Poland, 3-8 July 1967, USA-233, Convair division of General Dynamics.

Rayleigh, Lord B.: Scientific Pakers. vol. vi, pp. 432-446, Cambridge, England, 1920.

Siegel, Robert: Nucleate and Film Boiling in Reduced Gravity from Horizontal and Vertical Wires. NASA TR R-216, 1965.

Swalley, Frank E.; et al.: Saturn V Low-Gravity Fluid Mechanics Problems and Their Investigation by Full-Scale Orbital Experiment. Symposium on Fluid Mechanics and Heat Transfer Under Low-Gravitational Conditions, 24-25 June 1965, Palo Alto, Calif.

APPENDIX B

A CLASSIFICATION SYSTEM FOR ANALYTICAL AND COMPUTER MODELS FOR THE NAS1-8494 CONTRACT

A classification system to describe the analytical and computer models (ref. B1, B2) in terms relating to contract objectives has been developed in an attempt to provide an aid to:

a. Communications and general understanding.

b. A uniform framework through which an assessment of the relative value of the models can be undertaken.

c. A uniform framework through which alterations to the models can be described and evaluated.

The classification system utilizes alphanumeric designates. The primary or dominant characteristic, identified by a Roman numeral, refers to the degree of mathematical sophistication of the analytical model, i.e., a characteristic involving several factors including:

a. Complexity of the system being modeled (phenomenological or mathematical in this case) relative to number of elements (extent of substructure), significance of interactions, number and variability of the driving functions, etc.

b. Degree to which the model precisely describes the system, i.e., degree of detail and absence of simplifying assumptions.

The secondary characteristic, identified by a capital letter, refers to the completeness, degree of detail, and size of the computer model involved.

The tertiary characteristic, identified by an Arabic numeral, refers to the degree to which the model or element of the model developed under this contract contributes to the analytical literature or state-of-the-art.

The quarternary characteristic, identified by a lower case letter, indicates the degree to which the model is directly relatable to the macro or engineering system in question, in this case an LSS process.

The definitions of the classification categories are:

APPENDIX B

DEGREE OF MATHEMATICAL SOPHISTICATION

I. The model precisely describes a highly complex and dynamic phenomenological system involving a multiplicity of highly interactive, discontinuous variables which are described by higher order, partial differential equations. Solutions are attainable by numerical methods.

II. The model grossly describes a highly complex system through approximate descriptions attained by lower order, linearized, differential equations. Solutions for the resulting ordinary differential equations are analytical or numerical.

III. The model precisely describes a moderately complex system in which interactions of variables are minimal and essentially linear. Ordinary differential equations and numerical solutions apply.

IV. The model adequately describes a relatively simple system through simplified lower order, linear, ordinary differential equations, or a complex set of algebraic relationships.

COMPUTER MODEL SOPHISTICATION

A. Computer model is complex, highly detailed, and complete in description of the micro-structure of the phenomenological system.

Computer storage capacity requirements are large, generally in excess of 120 K.

The ratios of computer run time to system real time are very high, ranging from 10 to 1 to $\gg$ 10 to 1.

Practicality of use usually requires extensive dependence on a broad range of computer system software.

B. Computer model grossly describes the process. Relatively few assumptions are required and the description is moderately complex and detailed.

Ratios of computer run time to system real time are only moderately high, generally in a range of less than 10 to 1 to as low as 1 to 1. Moderate utilization of computer storage and computational capacity, generally in the range of 80 to 90 K.

Moderate requirements for computer system software.

C. Computer model concisely and adequately describes the process although many simplfying assumptions are present.

Computer run time ratios are low. Computer storage and computer system software requirements are relatively low.

D. Computer model is highly simplified and standard computer system software can often provide the major portion of the computational task.

DEVELOPMENT CONTRIBUTION

1. Provides an analytical tool where none has existed, at least in the open literature.

2. Augments an analytical tool previously existing in the open literature and, in so doing, significantly increases its utility.

3. An analytical tool previously existing in the open literature with no significant changes required.

LSS PROCESS SIMULATION

a. The model provides a basis for direct simulation of a set of phenomenological processes which combine to produce an LSS function or "macro system."

b. The model provides the basis for direct simulation of a set of phenomenological processes which combine to produce the sub- or microstructure of a typical LSS function.

c. The model provides the basis for describing the characteristics of certain mechanisms operating within a selected element or substructure of an LSS process.

d. The model describes phenomenological processes only indirectly related to LSS processes.

APPENDIX B

REFERENCES

B1. Savas, E. S.: Computer Control of Industrial Processes. Chapter 3 of Mathematical Models, pp. 39-77, McGraw-Hill, 1965.

B2. Janes, M. L.; et al: Analog and Digital Computer Methods in Engineering Analysis. International Textbook Company, 1965.

LIBRARY CARD ABSTRACT

CONVAIR DIVISION OF GENERAL DYNAMICS, FINAL TECHNICAL REPORT, GRAVITY-SENSITIVITY ASSESSMENT CRITERIA "The Life Support System Zero-G Study," by J. R. Burnett, E. A. Evans, and K. D. Burton, June 1970.

This report documents the first phase of the analytical and experimental work being conducted in the synthesis of the six analytical models relating to gravity-sensitive phenomena involved in life support systems typical of the near-term future.

The six models are:

1. Nucleate Boiling.
2. Diffusion Convection.
3. Film Stability and Transport.
4. Inertial Separation.
5. Convection Heat Transport.
6. Flow Regime Characteristics.